

STEM Project

Salt Tectonics Early Movement in the Dutch Offshore

by Renaud Bouroullec, Sander Osinga, Susanne Nelskamp, Tanya Goldberg,
Mart Zijp, Geert de Bruin, Roel Verreussel, Nico Janssen, Alexander Houben,
Susan Kerstholt-Boegehold, Tom van Hoof, Stefan Peeters and Madelaine Halter

TNO Report 2017

STEM Project

Salt Tectonics Early Movement: Impact on Triassic and Jurassic Stratigraphy and on Petroleum Systems in the Dutch Offshore.

16.11.2017

Authors:

Renaud Bouroullec, Sander Osinga, Susanne Nelskamp, Tanya Goldberg, Mart Zijp, Geert de Bruin, Roel Verreussel, Nico Janssen, Alexander Houben, Susan Kerstholt-Boegehold, Tom van Hoof, Stefan Peeters and Madelaine Halter

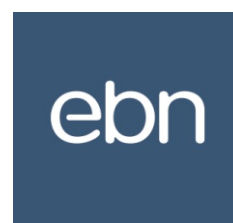
Sponsors: EBN B.V., Spectrum, Sterling Resources, Wintershall Noordzee B.
Project name: STEM
Project number: TNO 2017 R11242

All rights reserved

No part of this publication may be reproduced and/or published by print, photoprint, microfilm or any other means without the previous written consent of TNO.

In case this report was drafted on instructions, the rights and obligations of contracting parties are subject to either the General Terms and Conditions for commissions to TNO, or the relevant agreement concluded between the contracting parties. Submitting the report to inspection, the parties who have a direct interest is permitted.

© 2017 TNO



The Triassic structural evolution of the Central and Northern Dutch offshore is investigated in the STEM Project. This research focuses on the early salt tectonic events and their expression at different locations in the basin. This research topic was previously understudied in the Dutch sector where more attention was paid regarding the Jurassic and Cretaceous salt tectonic events. The main aim of this project is to provide insights on the location, geometry and kinematics of individual salt systems, such as salt welds, allochthonous salt systems, growth fault/raft systems and collapse salt bodies, and to build a comprehensive structural evolution of the study area during the Triassic. This research was carried out at two scales of investigation: 1) at a regional scale that covers the A, B, D, E, F, G and part of L and M blocks; and 2) at a block scale through three case studies. This project used a multidisciplinary approach by combining seismic-based structural analysis, 2D structural restoration, palynological analysis and geochemical analysis. The first two techniques were used to understand the salt tectonics of individual salt systems and of basin, while the latter two techniques were used to distinguishing between in-situ Triassic salt and remobilized Permian salt at selected locations.

The geochemical study reveals that Permian and Triassic salts can be dated with S-isotope stratigraphy and therefore can geochemically be distinguished from each others. This results opens up a new avenue for future research, with the aim at developing a new tool for Permian and Triassic salt dating. The palynological analysis did not allow for discrimination of Permian and Triassic salt due to the limited recovery of pollen and spores, especially in cutting samples. The discovery of rich Permian palynomorph assemblages in black stringers in the Zechstein has relevance to petroleum geology as it explains the provenance of the well preserved Permian palynomorphs that are found in great abundance in the Jurassic and which have excellent preservation and display bright fluorescence. This indicates low thermal maturity and possibly the presence of oil in the black stringers.

The structural analysis carried out using seismic and structural restoration techniques reveals that salt tectonics started during the Early Triassic but only as isolated minibasins in northern part of the Dutch sector (Block A). The first strong evidence of significant salt tectonic activity occurred during the Middle Triassic with salt pillowing, diapirism, growth faulting, rafting and thrusting. During the Late Triassic salt tectonic activity increased as indicated by continued diapic growth, which is locally affected by shortening due to continued updip growth fault/rafting activity. During the same period a few isolated allochthonous salt sheets were emplaced but were loaded and rapidly deflated. Four turtle structures are identified and show different timing of inversion, from the Middle Triassic to the Late Jurassic, but similar timing of cessation, during the Early Cretaceous. Growth fault/raft systems are clearly proven for the first time in the Dutch sector with up to 12 km of translation deduced from structural restoration. Extruded salt sheets developed in the rift basins but have not been observed on the surrounding platforms, which is

likely due to the presence of squeezed pre-existing salt bodies in the central part of the basin. The salt body shortening is due to updip thin-skin extension as a triggering phenomena for active upward salt migration and extrusion at the free surface.

The detailed tectonostratigraphic analysis carried in the three case studies were also successful.

1) For the first case study (blocks F17/F18), an allochthonous salt system was emplaced during the Late Triassic in the southern part of block F17. It came from the southwestern part of the Block 17/southeastern part of Block F16 and was later welded out during the Upper Jurassic.

2) For the second case study (blocks L05/L06/L08/L09), two growth fault/raft systems and three allochthonous salt systems are identified. The two growth fault raft systems are located to the east in the M04/L06 and M07/L08 areas with direction of raft translation from east to west. The M07/L08 growth fault/raft system encompasses the fat sand play system. The three allochthonous salt systems are located westward and downdip of the growth fault raft systems and are related to shortening of pre-existing diapir. One of these allochthonous salt system is a stepped counterregional salt system, the first ever identified in the Dutch sector.

3) For the third case study (Blocks F10/F11), the western part of the Dutch Central Graben in the F11 block is likely not a welded out allochthonous salt system, such as proposed as the beginning of the study, but rather an unusually shaped rim syncline related to complex salt withdrawal from the basin axis to the western basin margin.

The regional structural analysis shows that basin was composed of three distinctive zones during the Middle and Late Triassic. An outer zone predominately affected by extensional thin-skin tectonics; an inner zone affected by contractional tectonics; and a middle zone, located between the previous two zones, which is a transitional zone with the presence of collapsed salt structures and allochthonous salt sheets. A new conceptual regional kinematic model of the Triassic is proposed that details successive events such as 1) the salt diapirism at the onset of the Middle Triassic, around the depositional time of the Röt Formation; 2) shortening of these salt diapirs due to concentric gravitational gliding around the Triassic basin margins; and 3) local extrusion of allochthonous salt sheets associated with this shortening of salt diapirs.

The STEM Project provides a new structural framework for the Triassic in the Dutch offshore and successfully reached the proposed goals. The results indicate that salt tectonics played a strong role in shaping the basin and specific structures as early as the Middle Triassic. The implications of this research are far reaching in regards of the petroleum geology of the study area and specifically the implication on Triassic/Jurassic reservoir characterization and hydrocarbon maturity and migration modelling in the vicinity of salt structures.

Management summary	1		
Content	3		
1 - Introduction	7		
1.1 Research goals	7		
1.2 Objectives	7		
1.3 Study area	7		
1.4 Stratigraphic interval of interest	7		
1.5 STEM project research team	8		
1.6 Acknowledgments	8		
2 - Geological setting	9		
2.1 Overview of the tectonic evolution of the study area and greater North Sea Region during the Mesozoic	11		
A) Permian	12		
B) Early Triassic	12		
C) Middle Triassic	12		
D) Late Triassic	13		
E) Early Jurassic	13		
F) Middle Jurassic	14		
G) Late Jurassic to Early Cretaceous	15		
H) Mid- to Late Cretaceous	16		
2.2 Overview of structural elements affecting the study area since the Triassic	16		
A) Main structural elements	16		
B) Strike slip deformation	18		
C) Rifting	19		
D) Salt tectonics	20		
3 - Data and Methodology	25		
3.1 Database	27		
3.2 Palynology	29		
A) Principles and application	29		
B) Workflow	30		
C) Reworking and caving	30		
D) Material	31		
3.3 Petrography and geochemistry	32		
3.4 Seismic interpretation	34		
3.5 Structural restoration	36		
4 - Results	37		
4.1 Palynology, petrography and geochemistry	39		
4.2 Regional structural analysis	49		
A) Zechstein and Lower Germanic Trias Groups Triassic mapping	49		
B) Growth fault/raft system	53		
C) Collapse structures	53		
		C) In situ Upper Triassic salt detachments	59
4.3 Case studies structural analysis	61		
A) Case study 1: F17-F18 blocks	63		
B) Case study 2: L05-L06-L08-L09 blocks	73		
C) Case study 3: F10-F11 blocks	81		
4.3 Structural restorations	91		
A) Structural restoration 1: F17-F18	94		
B) Structural restoration 2: L05-L06-L08-L09	100		
C) Structural restoration 3: F10-F11	105		
5 - Discussion	115		
5.1 Main lessons learned from the structural restorations	117		
5.2 Salt systems kinematics	123		
A) Timing of salt tectonics in the Dutch offshore	123		
B) Updip growth faulting/rafting versus downdip contraction	124		
C) Collapse structures in the Dutch offshore	125		
D) Growth fault/raft systems versus collapse structures	125		
5.3 Allochthonous salt systems	126		
5.4 Basin-scale salt tectonic model for the Triassic	127		
5.5 Impact of Triassic salt tectonics on petroleum systems in the Dutch offshore	131		
Conclusions	135		
Future work	136		
References	137		
Appendixes	140		
A1 Structural restorations (Poster format)			
A2 MSc. Report - Stefan Peeters			

Recommendations on reading and accessing information in this report:

- 1) The report is built in a graphically heaving format with some figures that, locally, display small fonts and graphic detail. For full appreciation of these graphics we recommend to use the digital version of this report in which the high resolution graphics are preserved and accessible.
- 2) There is a lot of cross referencing between chapters to avoid repetitions of figures and the reader will often require to turn few pages back and forth to follow some of the discussions.
- 3) The structural restoration results are displayed as single pages in the Appendixes. These documents may be printed as standalone A0 format posters.

INTRODUCTION 1

Recent TNO research projects (Bouroullec et al. 2015 and 2016) revealed that possible salt extrusions may have occurred in the Dutch subsurface during the Triassic. The present report discusses the research results of the STEM Project that focuses on the early salt tectonics in the Dutch offshore. Several facts triggered this research, such as:

- Early salt tectonics, and its implication, is not fully understood in the Dutch Offshore due to the complexity of salt features and the successive erosional event that affected the area during the Jurassic and Cretaceous.
- Salt was actively moving during the Triassic and numerous structures have not yet been studied, nor integrated into a regional model.
- Modern salt tectonic and tectonostratigraphic concepts have been under-used when studying the Permo-Triassic in the Dutch offshore

1.1 Research goals

- To better understand the origin, timing and structural styles of early (pre-Jurassic) salt tectonics in the Dutch offshore.
- To apply modern salt tectonics knowledge and concepts for investigating pre-Jurassic salt tectonics in the Dutch offshore.
- To evaluate the extent and impact of early salt movements (pre-Jurassic) on the Dutch Offshore basins and platforms.

1.2 Objectives

The main objective of this project is to study, at regional and local scales, salt tectonic features and their evolution, and to build more robust salt tectonic models. This is realized by:

- Studying regionally the Permian and Triassic stratigraphic intervals in regards to the salt systems that were active contemporaneously. This includes mapping and analyzing syn-depositional, faults growth fault/raft systems, salt pillows, diapirs, walls and welds.
- Carrying three tectonostratigraphic case studies to characterize several salt systems
- Modelling the structural evolution of key locations by using 2D structural restoration techniques.
- Evaluating if biostratigraphic and geochemical analysis can help distinguishing between in-situ Triassic and remobilized Permian salt in selected areas.

1.3 Study area

This research project focuses on the salt tectonics in the Dutch offshore using two scales of investigation, 1) at a regional scale and 2) at the block scale through three case studies (Figure 1.1). The regional analysis covers the A, B, D, E, F, G and part of L and M blocks. This area encompasses three basins, namely the Dutch Central Graben, the Step Graben and the Terschelling Basin, and five platform areas, namely the Cleaver Bank Platform (CBP), the Central Offshore Platform (COP), Friesland Platform (FP), Ameland Platform (AP) and Schill Grund Platform (SGP) (Fig. 1.1). The case studies areas are (Fig. 1.1):

- Case study 1: F17 and F18 blocks
- Case study 2: L05, L06, L08 and L09 blocks
- Case study 3: F10 and F11 blocks

1.4 Stratigraphic interval of interest

The Permian and Triassic intervals are the main focus of this project, however the Jurassic and Cretaceous intervals were also analysed to better capture the entire salt tectonic evolution of some salt features that were investigated. The Zechstein Group was interpreted and mapped using 2D and 3D seismic data and wells data. The Lower Triassic, that correspond to the Lower Germanic Trias Group, was characterized and mapped regionally as a single individual unit while the Middle/Upper Triassic, that corresponds to the Upper Germanic Trias Group, was mapped as multiple units depending on the case study or the level of investigation regarding specific features. The Jurassic interval was investigated specifically in the third case study (blocks F10 and F11) in addition to the older intervals.

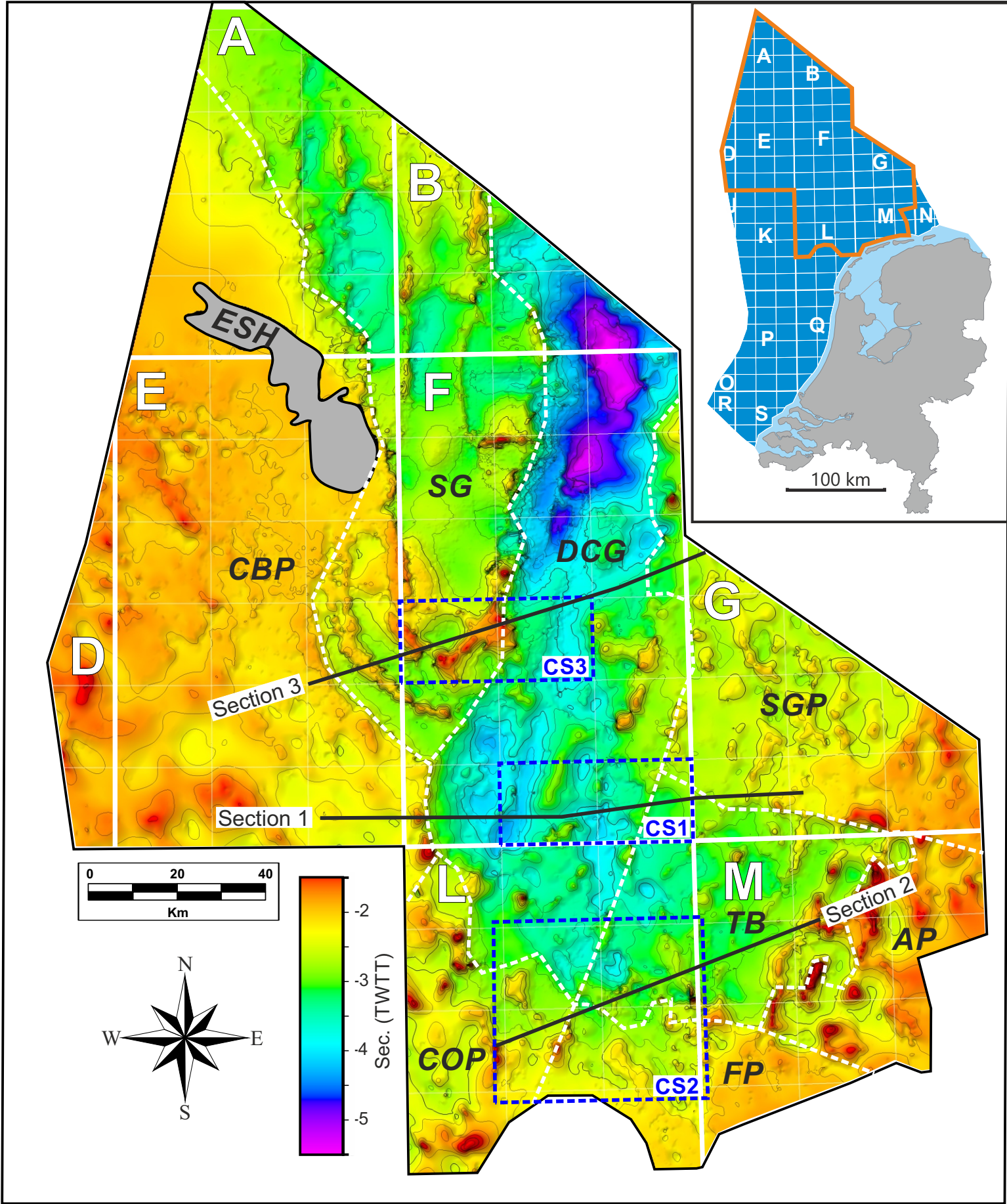


Figure 1.1: Base map of the project study area. Insert map shows the position of the study area within the Dutch offshore. Dashed white lines delineate the main structural provinces: **AP** = Ameland Platform; **CBP** = Cleaver Bank Platform; **COP** = Central Offshore Platform; **DCG** = Dutch Central Graben; **ESH** = Elbow Spit High; **FP** = Friesland Platform; **SG** = Step Graben; **SGP** = Schill Grund Platform; **TB** = Terschelling Basin. The three case study areas (CS1-3) are shown as dashed blue boxes (CS1 for F17/F18 blocks; CS2 for L05, L06, L08 and L09 blocks; and CS3 for F10 and F11 blocks). The position of the three structurally restored 2D sections are shown as black lines. The background map is the time structure map of the top Zechstein surface.

1.5 Project team

	Position	Role
Renaud Bouroullec	Senior Geologist	Lead Scientist: Seismic interpretation, structural analysis, palinspastic restoration, integration and reporting
Sander Osinga	Geologist	Structural geology, palinspastic restoration and reporting
Susanne Neldskamp	Geologist	Structural geology, palinspastic restorationand reporting
Tanya Goldberg	Geologist	Geochemistry and reporting
Mart Zijp	Geologist	Structural Geology, seismic interpretation
Geert de Bruin	Geologist	Structural Geology, seismic interpretation
Roel Verreussel	Senior Geologist	Biostratigraphic analysis and reporting
Nico Janssen	Analyst	Biostratigraphic analysis
Susan Kerstholt-Boegehold	Analyst	Biostratigraphic analysis
Tom van Hoof	Geologist	Reporting
Stefan Peeters	MSc Student (UU)	Internship project at TNO (Appendix A3)
Madelaine Halter	Manager	Project management

1.6 Acknowledgments

We would like to thank all the industry sponsors for their support for this project and for the valuable discussions we had during the various meetings, lectures, poster sessions and the field trip. We would especially like to thank Fred Kluin (Wintershall), Martin Wilpshaar (Wintershall/TNO), Jeroen Kneepkens (Wintershall), Henk van Lochem (Wintershall), Elavarasan Selvaraj (Wintershall), Ruud Lambert (Wintershall), Marten ter Borgh (EBN), Marloes Kortekaas (EBN), Eveline Rosendaal (EBN), Phil Mollicone (ONE B.V./Sterling Resources), Hugh Riches (ONE B.V./Sterling Resources) and Kim Gunn Maver (Spectrum) for their active roles in this project. We would also like to thank the field trip leaders Dirk Radies and Klaus-Werner Tietze for organizing and leading an interesting trip in Germany.

We would also like to thank the colleagues involved in the previous FOCUS and COMMA Projects, from which many results were instrumental for the STEM Project. Thanks to Kees Geel, Rader Abdul Fattah, Thijs Boxem and Dirk Munsterman. Thanks to Bruno Vendeville for providing material for the salt tectonics course offered to STEM sponsors and TNO colleagues.

GEOLOGICAL SETTING

2

2 - Geological Setting

The geological setting of the study area is complex since it involves several extensional, compressional and strike-slip deformation phases during the Paleozoic, Mesozoic and Cenozoic (Figure 2.1). In this chapter we summarize key published geological information regarding the Southern Permian Basin tectonic and stratigraphy evolution during the Permian and Mesozoic. The second part of this chapter summarizes the existing knowledge regarding specific structural geology topics relevant to this project, namely the strike slip deformation, the Mesozoic rifting and more prominently the salt tectonics.

2.1 Overview of the tectonic evolution of the study area and greater North Sea Region during the Mesozoic

The Mesozoic tectonic evolution of the studied part of the Dutch offshore has been summarized in several publications (Herngreen and Wong, 1989; van Adrichem et al., 1997; de Jager, 2007; Geluk, 2007; Wong, 2007; Rosendaal et al., 2014). It is important to place this tectonic evolution into a larger regional west-European context and various key publications are instrumental in that respect (e.g. the extensive work of Ziegler; the Millennium and Southern Permian Basin atlases). During the Triassic and Jurassic the structural setting of the Netherlands changed from a single extensional basinal configuration (the Southern Permian Basin) to a series of smaller, fault-bounded basins and highs (De Jager, 2007). Two main tectonic events shaped the North Sea Basin during the Mesozoic: 1) the break-up of Pangea and the associated rifting during most of the Mesozoic, and 2) the closure of the Tethys Ocean/Alpine collision and the associated inversion tectonics during the late Mesozoic (culminating later during the Cenozoic). A brief summary of the tectonic activity during the Mesozoic is presented below, with information regarding the overall North Sea region as well as specific information regarding the study area.

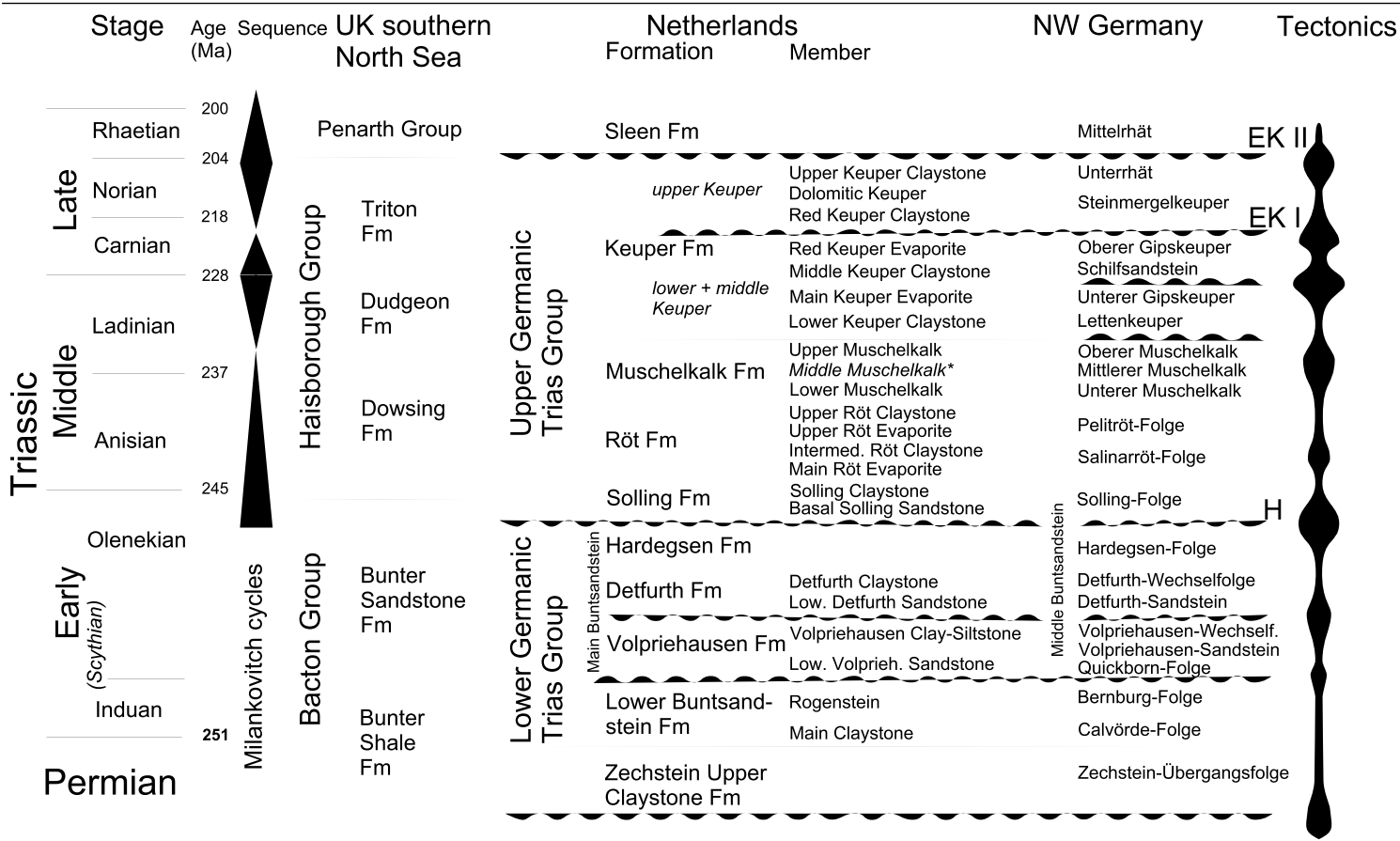


Table 1.1: Stratigraphic subdivision of the Triassic in the Netherlands and adjacent countries.From Geluk M.C. (2007).

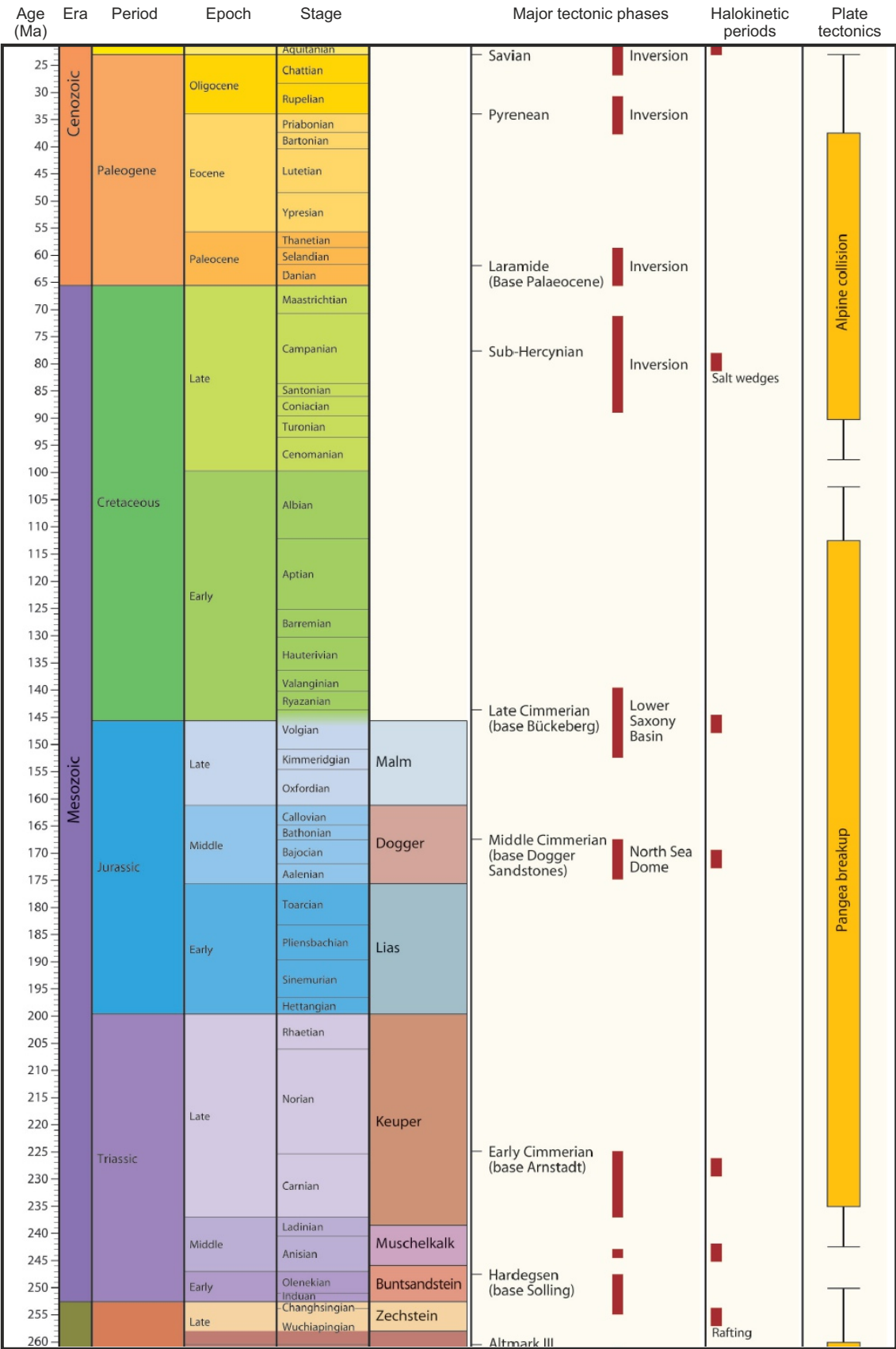


Figure 2.1: Main tectonic episodes and halokinetic episodes during the Mesozoic and Paleogene in the Southern Permian Basin (Pharaoh et al., 2010).

2 - Geological Setting

A) Permian

The Permian stratigraphic interval was deposited after the Variscan Orogeny and is composed of the Rotliegend and Zechstein Groups. The Early Permian stratigraphic interval is only deposited in the northwestern part of the study area (Lower Rotliegend, De Bruin et al, 2005) but is missing in a large part of the Dutch sector. The Middle Permian Upper Rotliegend Group and the Late Permian Zechstein Group, are often unconformable with the Carboniferous strata. The Upper Rotliegend is a productive sandy reservoir interval while the Zechstein is composed mainly of marine evaporites, carbonates and few clastic deposits. The Zechstein Group, which often forms a good seal for hydrocarbons, is composed of five evaporite cycles (Formation Z1-Z5) (Van Adrichem Boogaert and Kouwe, 1994). The depositional thickness of the Zechstein Group is between 50 m to 1200 m in the northern Dutch Offshore. Ten Veen et al. (2012) indicate a depositional Z2-Z4 salt thickness between 500 to 900, with the thickest zone located in the northeastern part of the study area (Blocks B and F, Figure 1.1)

B) Early Triassic

The start of rifting during the Early Triassic was related to the break-up of Pangea in the proto-Atlantic between Greenland and the Fennoscandia High (Lott et al., 2010). The southward propagation of the rift system toward the North Sea can be traced down into the northern part of the study area, breaching the Mid North Sea–Ringkøbing-Fyn High, with more prominent extensional faulting in the Northern part of the North Sea than in the study area (Ziegler, 1990b; Roberts et al., 1995; Coward et al., 2003).

Farther south, into the study area as well as in the North German Basin, the subsidence (mainly thermal in origin) was uniform, with Buntsandstein reflectors apparently unaffected by syn-depositional faulting (Ziegler, 1990a; Hoffmann & Stiewe, 1994; Geluk, 2007). The Dutch Central Graben subsided faster during the Buntsandstein depositional cycle than the platform areas (Terschelling and Vlieland basins) but not as rapidly as the Horn and Glückstadt Grabens further to the east (Fig. 2.2 A-C)

C) Middle Triassic

In response to continued thermal subsidence, the Muschelkalk strata were deposited over a wider area than the Buntsandstein series and onlap onto paleo-highs such as the London-Brabant and Bohemian massifs (Pharaoh et al., 2010). Differential subsidence of the Central, Horn and Glückstadt grabens is reflected in synsedimentary faulting and increased thicknesses of Muschelkalk strata compared to areas outside the grabens (Fig. 2.2 D-F, Geluk, 2007).

Triassic sequences thicken into the newly-formed Dutch Central Graben and Broad Fourteens Basin (Fig. 2.2). The Zechstein salt was mobilized at this time with piercing salt domes and rim-synclines developing in later stages (De Jager, 2007).

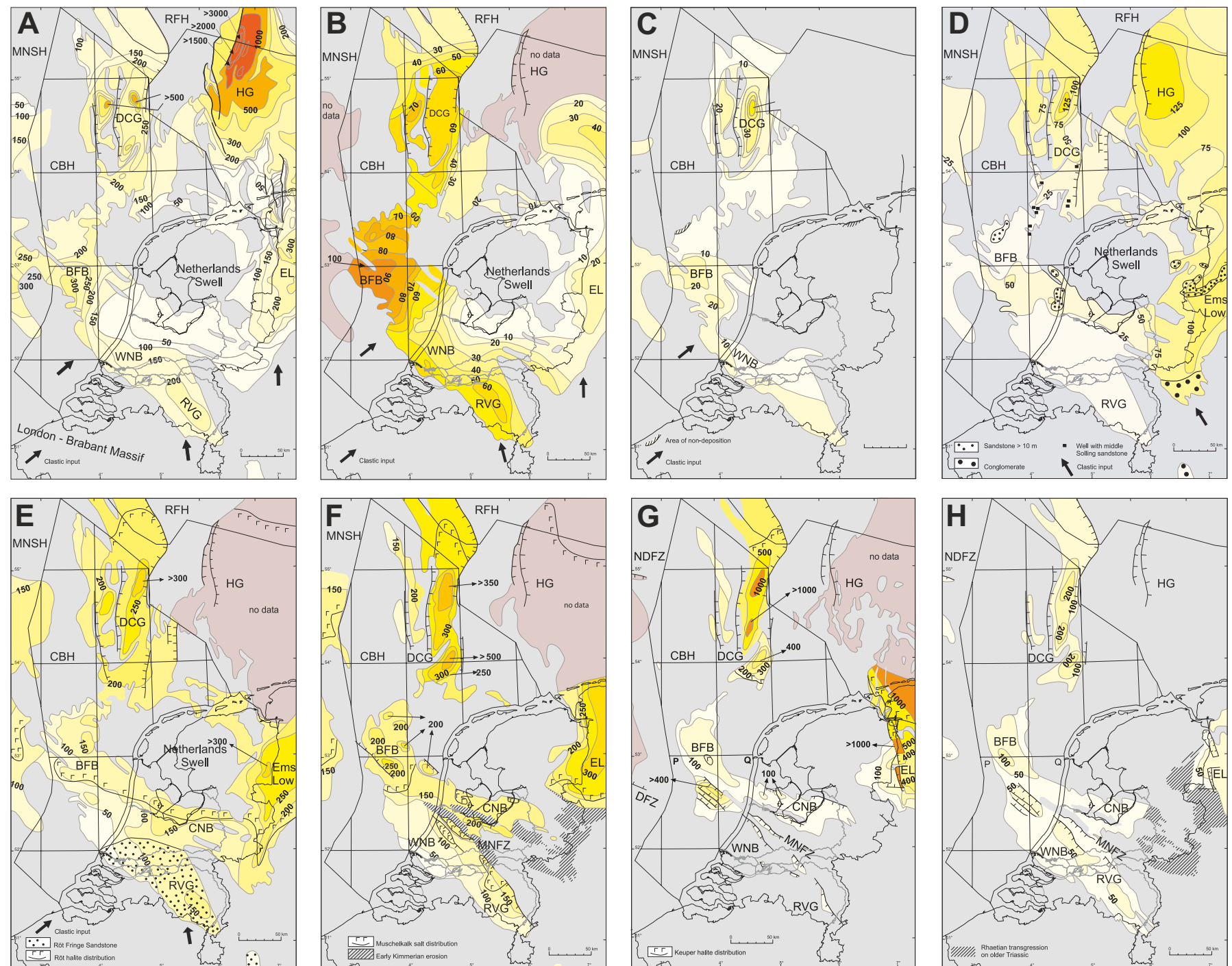


Figure 2.2: Isopach maps (in meters) of the Triassic units. A) the Main Buntsandstein Subgroup; B) Lower Volpriehausen Sandstone; C) the Lower Detfurth Sandstone; D) the Solling Formation; E) the Röt Formation; F) the Muschelkalk Formation; G) the lower and middle Keuper; and H) the upper Keuper. From Geluk (2007).

2 - Geological Setting

D) Late Triassic

The North Atlantic rift system propagated southward into the Central Atlantic area. Contemporaneous uplift of the flanks of the rift is indicated by the increased clastic influx into the Southern Permian Basin from northern sources (Ziegler, 1988 and 1990a). In response to continued counter-clockwise rotation of Pangea, the Southern Permian Basin moved to latitudes of 30 to 40 degree N by Late Triassic times. In the Southern North Sea, the direction of extension was E-W during the Late Triassic (Pharaoh et al. 2010). The North Sea, Horn and Glückstadt grabens remained active during this period, with very minor associated volcanic activity (Ziegler, 1990a).

Stratigraphic sequences deposited during this period thicken northwards into the Dutch Central Graben and Broad Fourteens Basins, the only regions with active faulting (Fig. 2.2, G-H). The faults affecting the Upper Triassic were produced by dextral transtension (Van Hoorn, 1987). The increased sediment loading upon the thick Zechstein salt in the northern Dutch offshore sector, triggered piercing of salt diapirs and the development of rim-synclines (Pharaoh et al., 2010). It is important to notice that some salt structures extruded onto the basin floor to form large allochthonous overhangs overlapped by uppermost Triassic deposits (Krzywiec, 2004).

E) Early Jurassic

The North Atlantic rift propagated southwards into the Central Atlantic, with crustal separation achieved toward the end of the Early Jurassic. There seems to have been very little Early Jurassic rifting in the northern North Sea. The palaeogeography indicates infilling of the passively subsiding Triassic–Lower Jurassic rift (Coward et al., 2003). Continued regional thermal subsidence of the Northern and Southern Permian basins during the Rhaetian and Hettangian, combined with a eustatic sea-level rise, controlled the development of a wide, open-marine basin. Clastics were shed into this broad, regionally subsiding basin from the Fennoscandian Shield, East European Platform and Bohemian Massif. Stagnant-water stratification led to the deposition of the Posidonia Shale Formation during the Toarcian, the principal source rock for the oil provinces of the southern North Sea and northern Germany (Ziegler, 1990a).

The Lower Jurassic series was later deeply truncated in the central North Sea during Mid- to Late Jurassic times. Nevertheless, it appears that the Early Jurassic was a period of relative tectonic quiescence, with faulting largely restricted to the Dutch Central Graben and locally to the Broad Fourteens Basin. The Cleaver Bank and Schill Grund Platforms remained stable areas during much of the Early Jurassic and probably accumulated sediments hundreds of metres thick (Pharaoh et al., 2010).

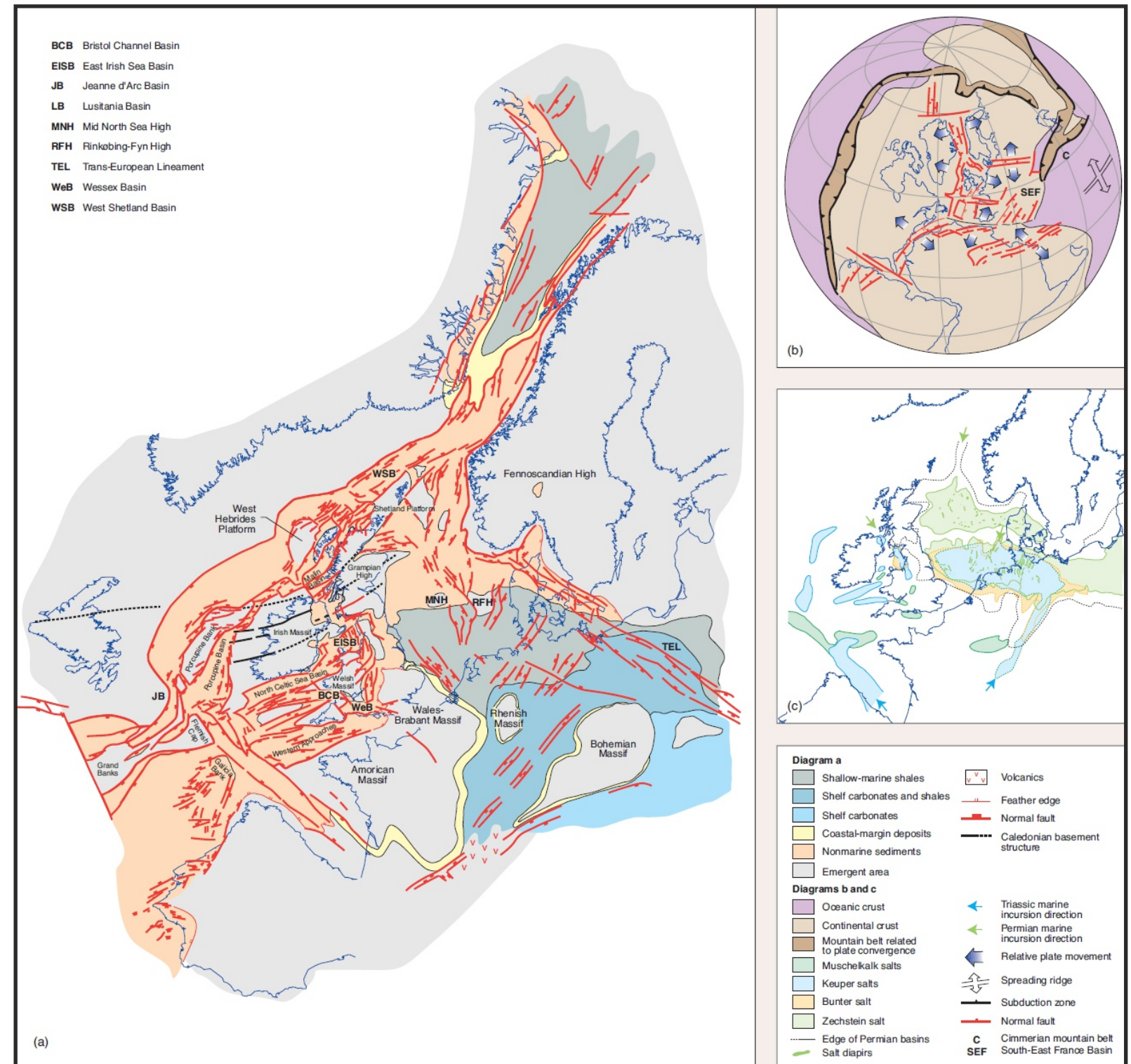


Figure 2.3: Triassic times in the North Sea Region. a) Palinspastic maps. b) Global views. c) Distribution of the basins and structures. From Coward *et al.*, 2003.

2 - Geological Setting

F) Middle Jurassic

The most important event during this period is the uplift of the central North Sea area that started towards the end of the Aalenian, presumably in response to the impingement of a transient mantle plume on the lithosphere, which continued during the Bajocian and Bathonian (Ziegler, 1990a; Underhill & Partington, 1993; Surlyk & Ineson, 2003). Development of this large thermal dome (700 × 1000 km), caused deep truncation of Lower Jurassic and even Triassic sediments and the development of the regional Mid Cimmerian Unconformity (also referred as the Intra-Aalenian Unconformity by Underhill and Partington, 1993) in the central North Sea area (Fig. 2.4). This regional uplift closed the existing seaway, separating the Arctic Seas from the Tethys and Atlantic Oceans (Ziegler, 1988 and 1990a). Crustal extension across the North Sea rift system persisted during the uplift of this thermal dome as shown by continued fault-controlled subsidence of the Viking Graben, the subsidence of deep half-grabens containing continental series in the Central Graben, and continued tectonic activity in the array of transtensional basins along the southern margin of the Southern Permian Basin (Ziegler, 1990a). Three major rift systems were active in the Netherlands during Mid to Late Jurassic (Figs. 2.4, 2.5 and 2.6): 1) the N-S oriented Dutch Central Graben-Vlieland Basin system, 2) the E-W oriented Lower Saxony Basin system, and 3) the NW-SE oriented Ruhr Valley Graben, West and Central Netherlands Basins, and Broad Fourteens Basin (extending to the UK to the Sole Pit Basin).

By late Mid-Jurassic times, the Central North Sea Dome had subsided sufficiently for open-marine conditions to be restored in the North Sea. Sedimentation resumed variably during the Callovian or Late Jurassic in areas uplifted during Mid-Jurassic times (Ziegler 1990a).

It is important to notice that the London-Brabant Massif was also uplifted during Mid-Jurassic times, its Triassic and Upper Paleozoic cover was removed to expose the Lower Carboniferous core. Fission-track data suggest that a thickness of 3000 m of sediments was removed (Van den Haute & Vercoutere, 1990).

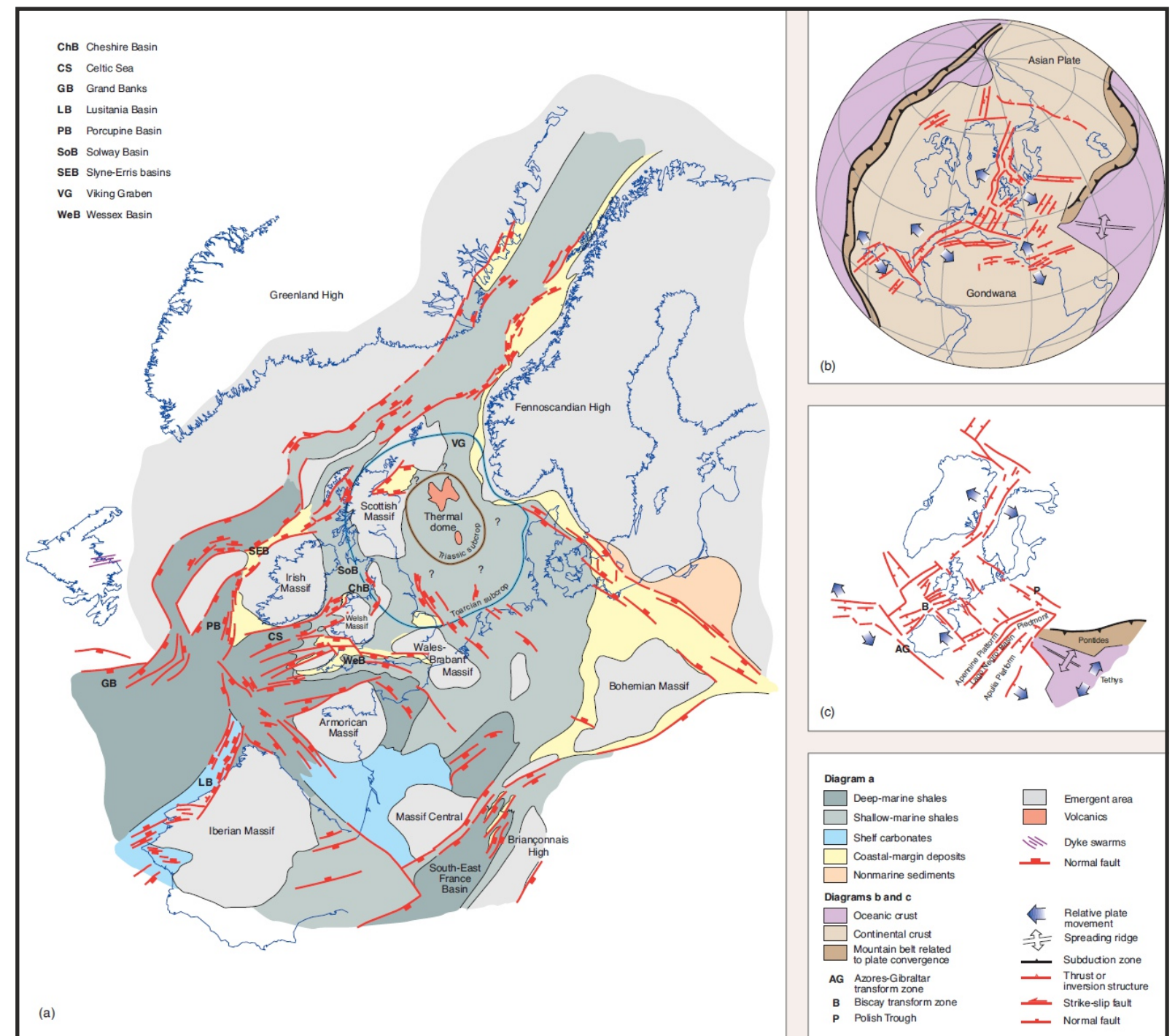


Figure 2.4: Mid-Jurassic times in the North Sea Region. a) Palinspastic maps. b) Global views. c) Distribution of the basins and structures. From Coward *et al.*, 2003.

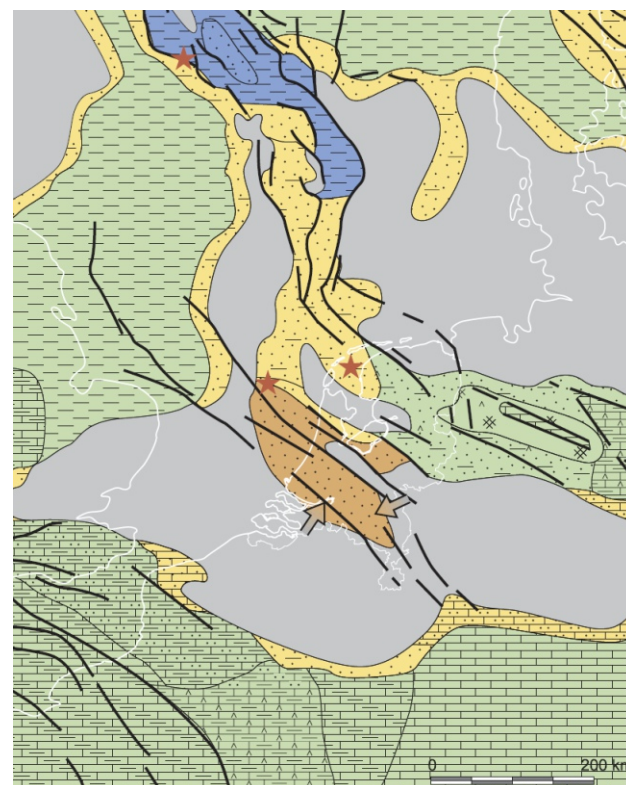


Figure 2.5: Paleogeographic map of the Netherlands and adjacent areas during the Kimmeridgian-Tithonian (after Ziegler, 1990; modified by Wong, 2007).

G) Late Jurassic to Early Cretaceous

Accelerated crustal extension across the North Sea rift system resulting in NW trending transtensional basins to form along the southern margin of the Southern Permian Basin (Figures 2.4, 2.5 and 2.6). This rifting phase allowed large areas to be exposed and subsequently eroded. During the Late Jurassic and Early Cretaceous transtensional subsidence occurred within northwest-oriented basins but also transpressional uplift of narrow highs along the southern margin of the Southern Permian Basin. The main tectonic elements of the Dutch sub-surface developed during the Late Jurassic and Early Cretaceous, comprising the late Cimmerian rift pulses. Extensional faulting and subsidence accelerated in the northerly trending Dutch Central Graben (Heybroek, 1975; Schroot, 1991).

An eustatic sea-level lowstand at the Jurassic-Cretaceous transition, combined with stress-induced deflection of the lithosphere, led to earliest Cretaceous emergence and erosion of large parts of western and central Europe (Ziegler, 1990a). Crustal extension across the North Sea graben system gradually decreased during the Early Cretaceous and essentially ended during the Aptian to Albian (Ziegler, 1990a; Torsvik *et al.*, 2002; Coward *et al.*, 2003).

In the Dutch sector, thick fluvio-lacustrine to shallow-marine sequences accumulated in the Dutch Central Graben during Late Jurassic and Early Cretaceous times. Volgian to Ryazanian shales are kerogenous in the northern Dutch Central Graben (Herngreen & Wong, 1989). In the southern part of the graben, the provenance of clastic sediments was the Cleaver Bank-Broad Fourteens High, which was uplifted during Callovian times. Adjacent highs such as the Friesland Platform were uplifted and eroded at the same time. The Schill Grund Platform formed a stable platform area on the eastern flank of the Dutch Central Graben.

The Step Graben and Terschelling Basin subsided more slowly than the Dutch Central Graben during the Late Jurassic and accumulated thinner sequences. Salt walls developed along the main bounding faults of the Dutch Central Graben. Late Jurassic uplift of the Friesland Platform resulted in erosion down to Lower Triassic and, locally, to Zechstein levels.

Basin-controlling faults accommodated the east-west extension in the Dutch Central Graben. However, due to the complex reactivation history, unambiguous evidence of dextral transtensional displacement is only available locally, for example, in the Rifgronden Fault Zone between the Terschelling Basin and the Schill Grund Platform (De Jager, 2007).

During Callovian to Oxfordian times, the uplift of structural highs such as the Broad Fourteens and Friesland highs shed clastics into the adjacent rapidly subsiding basins. The Zuidwal alkaline volcanic complex (Kimmeridgian) developed during the late Kimmerian rifting phase. In the Terschelling Basin, tectonic events were slightly delayed compared to the Dutch Central Graben; uplift occurred before the end of the Mid-Jurassic and a thin, younger, Upper Jurassic sequence rests on the Triassic, whereas the Lower Cretaceous sequence is thicker than in the Central Graben.

The Cleaver Bank and Schill Grund Platforms, which were structural highs during much of Triassic to Early Jurassic times, were uplifted and eroded during the mid- to late Kimmerian rifting phases. Upper Jurassic and Lower Cretaceous syn-rift strata are consequently missing from these highs, where Triassic and Permian strata are unconformably overlain by thin post-rift Lower Cretaceous and thicker Upper Cretaceous rocks (De Jager, 2007). Hundreds of metres of Triassic to Middle Jurassic sediments were probably removed from these highs. The thick Rijnland Group (latest Ryazanian to Albian) succession, comprising mainly fine-grained clastics, was subsequently deposited across a large open-marine basin. (Pharaoh *et al.*, 2010).

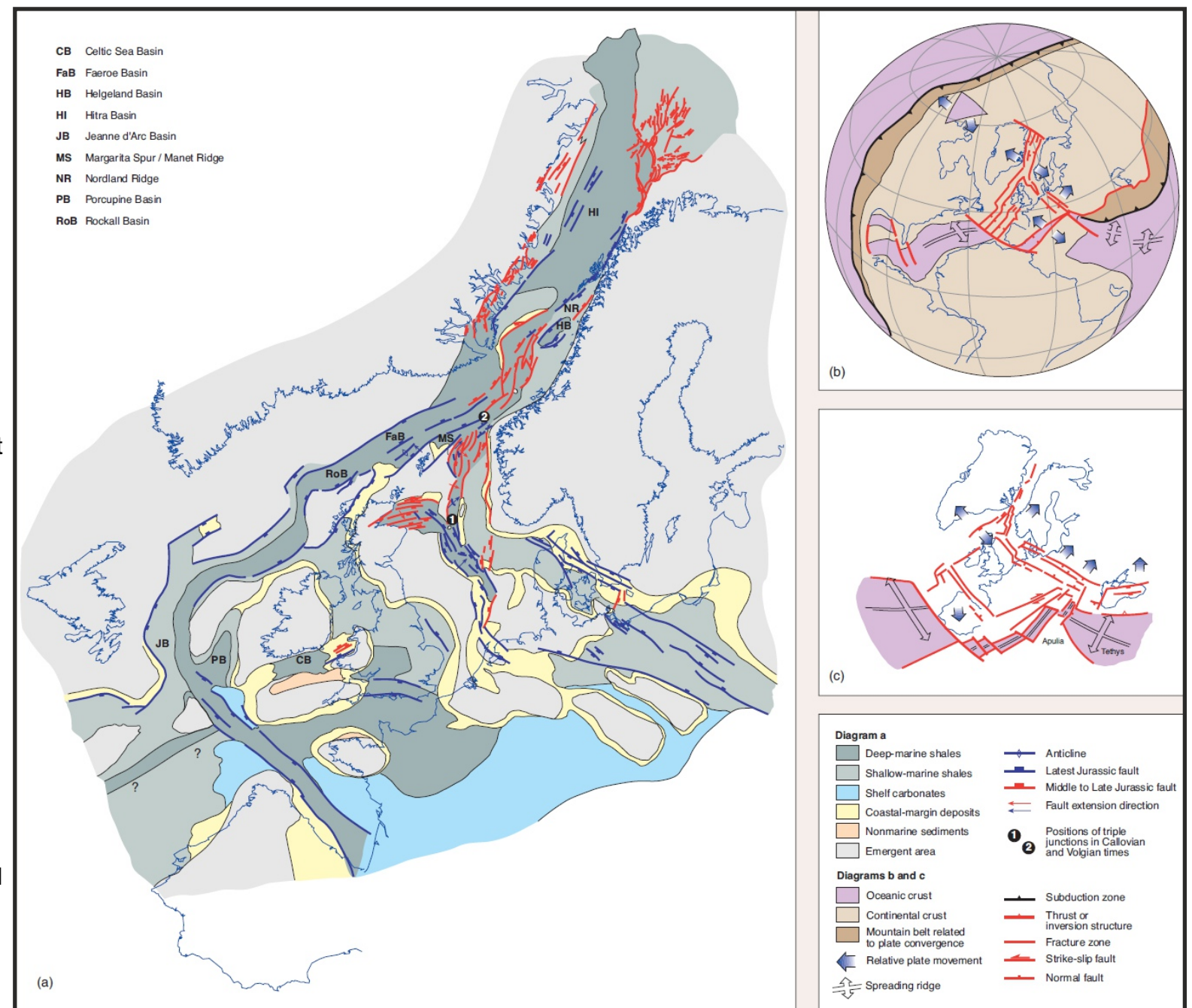


Figure 2.6: Late Jurassic times in the North Sea Region. a) Palinspastic maps. b) Global views. c) Distribution of the basins and main structures. From Coward *et al.*, 2003.

H) Mid- to Late Cretaceous

The North Sea rift system became inactive and the North Atlantic Ocean started to open with rifting concentrated on areas between Europe and Greenland (Ziegler 1988 and 1990a). The Neo Tethys Ocean opened to the south of Europe during the Mid-Cretaceous and starting to close during the Late Cretaceous due to the convergence between the African and Eurasian plates (Ziegler, 1990a).

Regional thermal subsidence of the North Sea Basin started during the Hauterivian and Barremian in combination with gradually rising sea levels, and by Aptian-Albian times the southern Permian Basin was a vast shallow-marine basin. Transgression and thermal subsidence occurred during the Albian to Turonian. During the Late Cretaceous, this basin further expanded to reach its maximum extent in response to thermal subsidence and sea-level rise to about 100-200 m above the present-day level. The Upper Cretaceous Chalk series is up to 2000 m thick in the basin (Ziegler, 1990a).

In the southern Permian Basin, inversion tectonics due to the Alpine collision affected basement blocks during the late Turonian and intensified during the Senonian and the Paleocene (Ziegler, 1990a). This inversion was heterogeneous with strain localized in narrow zones separated by undeformed regions (Pharaoh *et al.*, 2010). Inversion also produced decoupling on Zechstein salt and thin-skinned tectonics. The NW trend of early inverted basins and transpressional fault reactivation indicates N to NE oriented compressional stresses (Kley & Voigt, 2008).

2.2 Overview of structural elements affecting the study area since the Triassic

A) Main structural elements

The study area is composed of three main basins (DCG, TB and SG) and five platforms (CBP, COP, FP, AP and SGP) (Fig. 2.7). All these structural provinces have been affected by large-scale tectonics events such as the Triassic-Jurassic rifting or the Alpine orogeny. However, these provinces have also various and specific geological characteristics and structural architectures due to local parameters such as the original Zechstein salt thickness, the amount of erosion related to the main tectonic and eustatic events, or the type of structural reactivation on pre-existing structures. Below is a short description of each key structural element in the study area (Fig. 2.7).

Basin 1: Dutch Central Graben (DCG): The Dutch Central Graben is a SSW/NNE trending aborted rift that spans from the northern part of the L block to the eastern part of the B block in the Dutch offshore. The DCG extends to the NNE into Germany and is connected farther to the north to the Tail End Graben in the Danish western offshore. This rift system is believed to have initiated from the Early Triassic (Geluk, 2005) due to over thickened stratigraphy in the DCG region during this period (Figure 2.2). Clear evidence of differential subsidence along the rift structure are observed during the Upper Triassic, as early as the Anisian (245 to 237 Ma) and continued intermittently throughout the Upper Triassic and Jurassic (Geluk, 2007). During this period basement faults triggered widespread remobilization of ductile Zechstein salt.

Basin 2: Terschelling Basin (TB): The TB is overall a rectangular-shape basin that formed during the Later Jurassic on the SE side of the DCG. This basin is bounded on its northern, eastern, and southern sides by platforms, respectively the Schill Grund, the Ameland and the Friesland Platforms, and is connected on its western side to the southern part of the DCG. Its

initiation started 155 My ago during the Late Kimmeridgian (Late Jurassic), with the deposition of continental deposits of the Main Frieze Front Formation (Munsterman *et al.*, 2012; Bouroullec *et al.*, 2016; Bouroullec *et al.*, in press). The basin widened during the Upper Jurassic with the final deposition of the Scruff Greensand Formation that spilled over the basin limits. The TB is bounded to its northern and southern side by large faults systems, respectively the Rifgronden and Hantum fault zones. Salt tectonics also play a significant role in the development of the TB and will be discussed in this report in relation to the second case study (Chapter 4.3 and 4.4).

Basin 3: Step Graben (SG): The SG is a N-S oriented terrace-like structure located along the northwestern part of the DCG (Kombrink *et al.*, 2012). During the main phase of rifting it accommodated Upper Jurassic deposition but in a more limited fashion than the DCG. The SG likely accommodated Lower and Middle Jurassic sediments, which were subsequently eroded by the Mid-Kimmerian thermal uplift or during the rifting- and orogen-related uplifts. The SG tectono-stratigraphic style is situated halfway between the Terschelling Basin and the Schill Grund Platform, which accumulated respectively more and less Upper Jurassic sediments.

Platform 1: Cleaver Bank Platform (CBP): The CBP borders to SG and the DCG to its east and the COP to the south. It extends to the west to the UK sector where it corresponds to the Anglo-Dutch Basin. The CBP was a relatively stable area during the Mesozoic and was the place of substantial erosion during the Early Cretaceous with Jurassic, Triassic and locally Permian strata being eroded. During the Lower Triassic, large swells (low amplitude basins) formed on the CBP with relatively thin deposits (e.g. 50 m of Main Bundstanein Formation, Geluk, 2007).

Platform 2: Central Offshore Platform (COP): This platform separates the southern part of the DCG from the Broad Fourteens Basin to the south. This area was possibly flooded during the Upper Jurassic, linking the two basins, but later erosion may have erased any traces of such physiographic connection.

Platform 3: Friesland Platform (FP): This large platform is located mainly in the Dutch onshore and extends north westward to the southern edge of the TB. It transitions westward to the Vriesland Basin that accumulated moderate amount of Middle and Upper Jurassic sediments. Toward the northeast, the FP holds thick Triassic strata (up to 800 m).

Platform 4: Ameland Platform (AP): This platform is located to the east of the TB and transitions southward to the FP (separated by the Hantum Fault Zone) and northward to the SGP (separated by the Rifgronden Fault Zone). No Jurassic strata are observed on this platform where Lower Cretaceous directly overlies Triassic and Zechstein strata.

Platform 5: Schill Grund Platform (SGP): This platform bounds the DCG on its eastern side and the TB on its northern side. Locally, Upper Jurassic sediments are still present in this platform in zones preserved from Lower Cretaceous erosion. Everywhere else the Cretaceous lies over Triassic or Zechstein strata with the SGP. To the north this platform extends into the German offshore area.

2 - Geological Setting

Other important structural features:

Elbow Spit High (ESH): This structural high is located above an early Devonian plutonic body on which the Carboniferous thins and is partially eroded. The Cretaceous overlies locally directly the Devonian and the Carboniferous.

Hantum Fault Zone (HFZ): The HFZ trends ESE-WNW between the northwestern part of the FP and the southern margin of the TB. This fault zone extends to the northwest to the southern part of the DCG where it splits into several faults. Toward the SE, this fault zone extends onshore and forms the northwest limit of the Friesland Platform

Rifgronden Fault Zone (RFZ): The RFZ separates the SGP to the TB and HP and roughly parallels the HFZ. This fault zone holds shorter fault segments than the HFZ, and shows an echelon-type geometry. The RFZ was active from Late Jurassic to Paleogene with thicker strata on the TB side during the Late Jurassic and Early Cretaceous, while the Upper Cretaceous and Paleogene strata thicken toward the platforms rather than the TB.

Triassic growth faults (the Fat Sand story): Thin-skinned growth faulting during the Triassic has been observed in the Dutch offshore by a few authors (Geluk et al., 2007; ten Veen et al., 2012; de Jager, 2012; Bouroullec et al., 2016) and elsewhere in the North Sea (Petersen et al., 1992; Penge et al., 1993; 1999; Stewart and Clark, 1999). The publication by de Jager (2012) shows that, locally, overthickened sandy strata of the Solling Formation (Upper Triassic), named the Fat Sands, were deposited on the downthrown side of a large listric growth fault. The conceptual restoration model proposed by de Jager (2012) indicates some limited rafting similar to the classic cases of gravitational gliding observed along the south Atlantic margins (Cobbold and Szatmari, 1991; Rouby et al., 2002 and 2003) (Figs. 2.16 and 2.17).

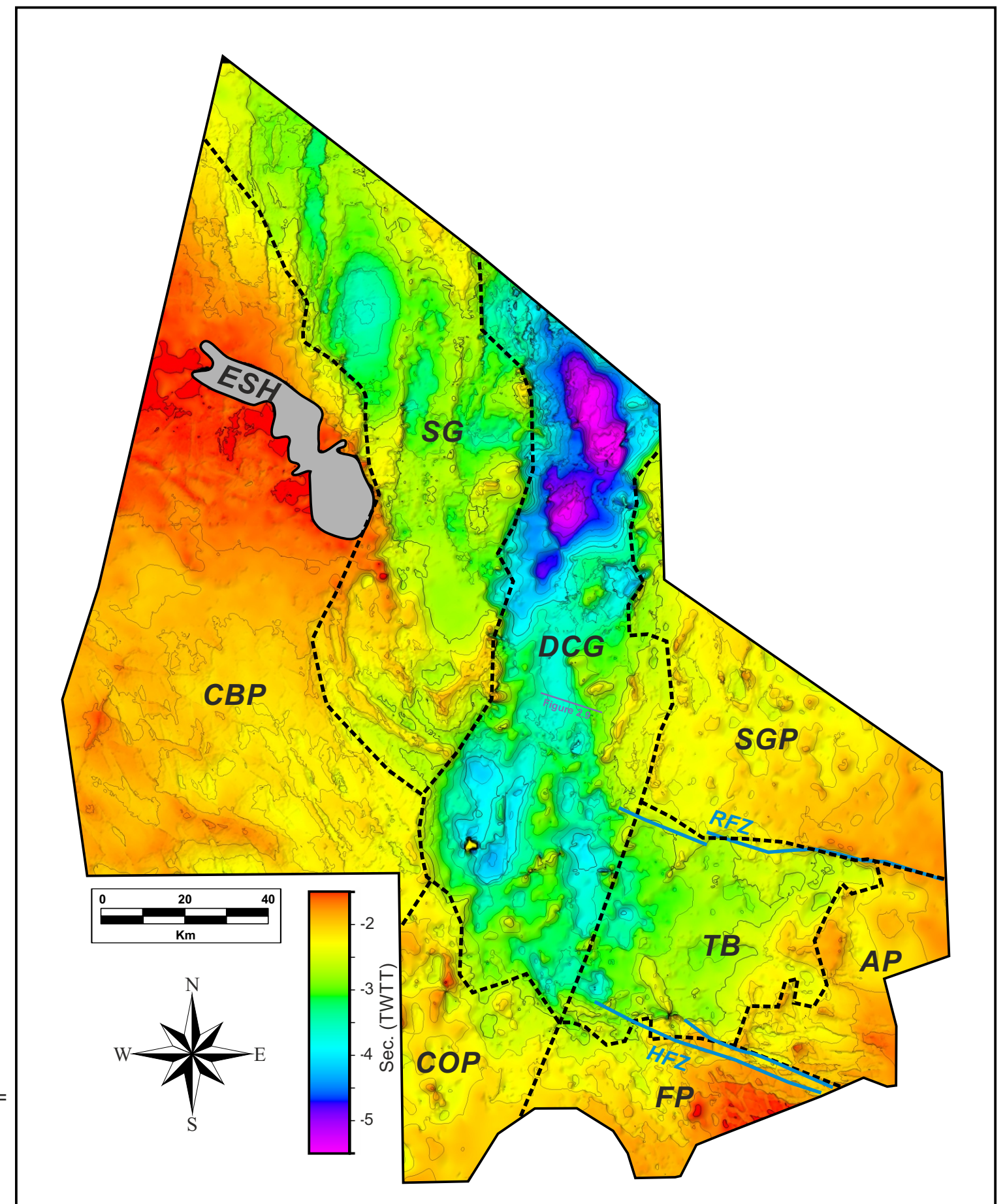


Figure 2.7: Structural elements in the study area. Base map is the time structure map of the base Zechstein obtained in the regional study. See text for comments regarding the structural elements. **AP** = Ameland Platform; **CBP** = Cleaver Bank Platform; **COP** = Central Offshore Platform; **DCG** = Dutch Central Graben; **ESH** = Elbow Spit High; **FP** = Friesland Platform; **SG** = Step Graben; **SGP** = Schill Grund Platform; **TB** = Terschelling Basin.

2 - Geological Setting

B) Strike slip deformation

Although often overlooked, several strike-slip fault systems have been recognized in the Dutch subsurface. This section summarizes some of the previous work that has been published on strike-slip tectonics in the Dutch subsurface.

The dominant NW-SE fault set in the Netherlands such as the Hantum and Rifgronden Fault Zones, probably dates back to the Caledonian orogeny when Laurentia and Avalonia collided (De Jager, 2007). Several of this early NW-SE faults were reactivated during the Permian (George and Berry, 1993 and 1997; Glennie, 1998; De Jager, 2007) as well as less prominent conjugate NE-SW to NNE-SSW oriented fault set which is the second most common fault set in the Dutch subsurface (Ziegler, 1988 and 1990a and b). Reactivation of some of these NW-SE oriented structures also occurred during the Meso-Cenozoic.

In the study area the Rifgronden and Hantum Fault Zones are present. The Rifgronden Fault Zone is a WNW-ESE trending fault zone is the northern margin of the Terschelling Basin. This fault zone shows dextral offsets (De Jager 2007). The Hantum Fault Zone is a WNW-ESE oriented fault zone is the southern boundary of the Terschelling Basin. The Hantum Fault Zone extends southeastward and forms the western boundary of the Lauwerszee Trough. In the study area faults in the Hantum Fault Zone show vertical offsets at the base of the Zechstein Group of up to 1500 m (De Jager 2007). Different phases of fault activation and reactivation were identified. The old Hantum Fault Zone have been active since the Late Carboniferous, and was reactivated multiple times during the Triassic and Late Jurassic. The Rifgronden Fault zone may be a similar repeatedly reactivated fault zone (De Jager 2007).

The MSc research by Stefan Peeters was carried out as part of the STEM Project. Figures 2.8 and 2.9 show some of the results obtained during this research. The full MSc report can be found in Appendix 2.

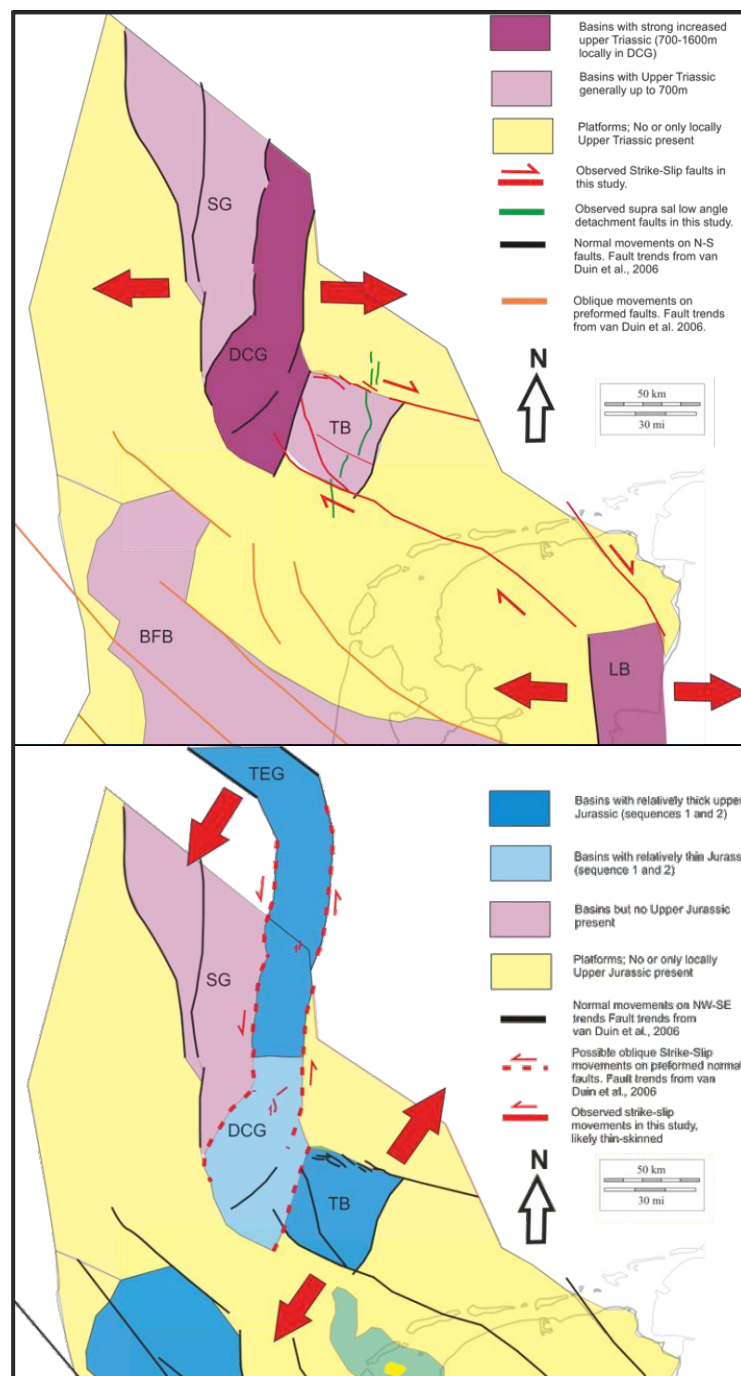


Figure 2.8: Schematic maps of the A) Middle/Late Triassic and B) Late Jurassic/Early Cretaceous (Peeters et al., 2016).

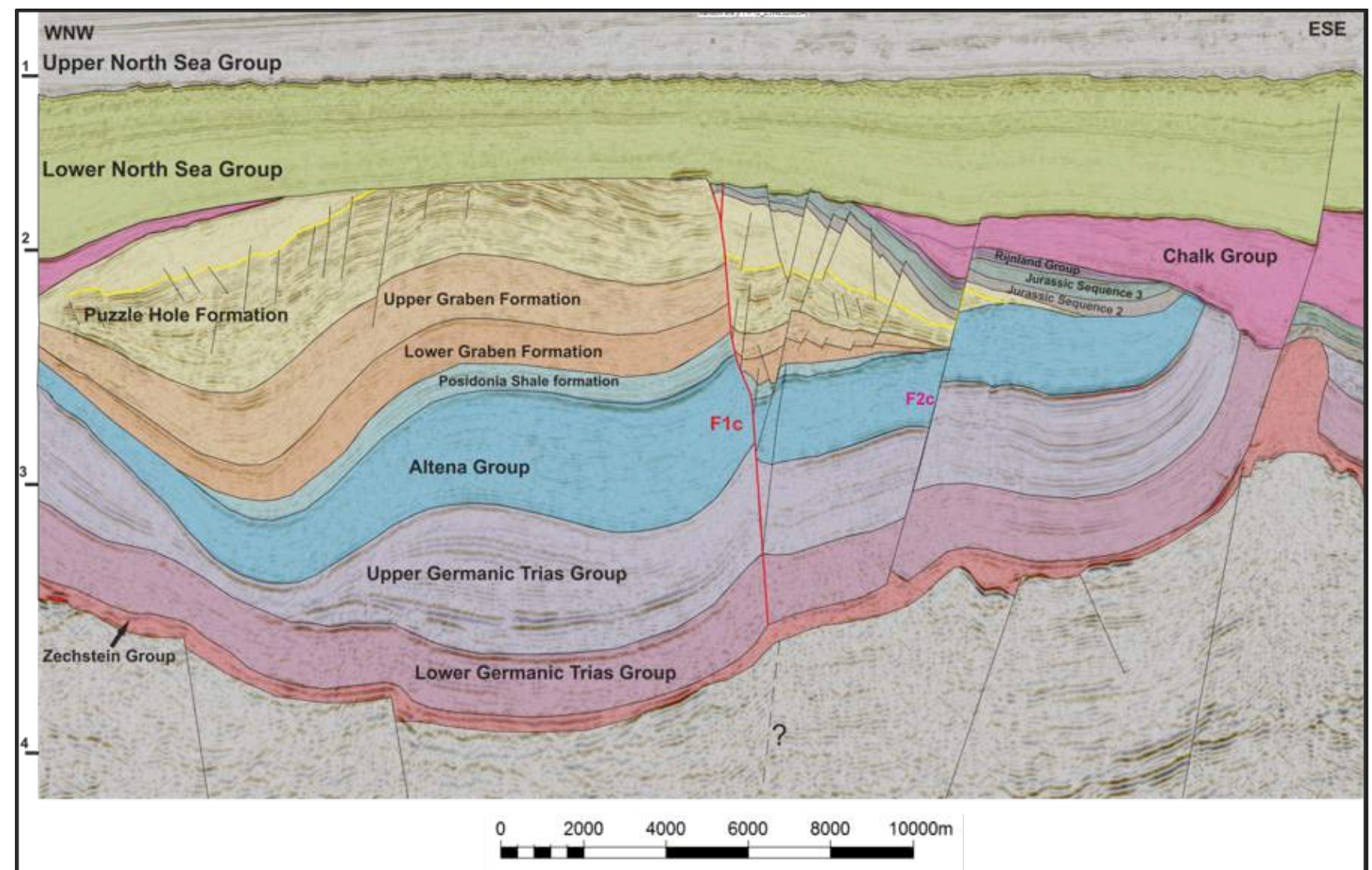


Figure 2.9: Interpreted seismic section across the Dutch Central Graben showing a strike-slip fault (F1c) (Peeters et al., 2016). See Figure 2.7 for location.

C) Rifting

Active rifting started in the north of the study area in the **Early Triassic** (e.g. Central and Horn Grabens) but only reached the study area in the Mid-Triassic (Fig. 2.10). The Dutch Central Graben subsided slightly faster than adjacent platforms (Terschelling and Vlieland Basins) but not as rapidly as the Grabens farther east in Germany and Denmark. No rift-shoulder uplift has been documented during this period.

During the **Mid-Triassic** the Dutch Central Graben and the Broad Fourteens Basin started to subside with Zechstein salt becoming mobile along bounding faults (Remmelts, 1995).

During the **Late Triassic** the differential subsidence persisted between the basins and their shoulders. Locally, transtentional dextral strike slip structures (including flower structures) are involved (Van Hoom, 1987). Zechstein salt was also mobilized during this period.

Rifting was still possibly active during the **Early Jurassic** in the Dutch Central Graben but little evidence of active faulting is observed in the Southern Permian Basin, especially in the study area where tectonic activity is focused in the Dutch Central Graben.

The rift evolution during the **Mid-Jurassic** is broadly unknown due to the Central North Sea-related uplift that eroded all of the Middle Jurassic deposits in the study area. The erosion locally denudated the Dutch Central Graben down to the Carboniferous level such as in the northern part of the Cleaver Bank High. The exact amount of eroded strata on the eastern shoulder of the Dutch Central Graben is unknown. The Step Graben and the Terschelling Basin were also uplifted and erosion cut down to Lower Jurassic and Triassic levels (Van Hoorn, 1987). The Horn Graben became inactive during the Middle Jurassic.

The rifting during the **Late Jurassic** and Early Cretaceous is dominantly expressed as wrench tectonics with NW-oriented transtensional basin subsidence and transpressional uplift of narrow zones. The main rifting pulses (Kimmerian rift pulses) in the study area occurred during this period. The Schill Grund Platform was a stable platform area and the Step Graben and Terschelling Basin subsided but relatively less than the Dutch Central Graben. Late Jurassic uplift of the Friesland Platform resulted in erosion down to Lower Triassic and, locally, to Zechstein levels. There are evidences of local dextral transtensional displacement in the Rifgronden Fault Zone between the Terschelling Basin and the Schill Grund Platform (De Jager, 2007). The Zuidwal alkaline

volcanic complex (Kimmeridgian) developed during the late Kimmerian rifting phase. In the Terschelling Basin, tectonic events were slightly delayed relative to the Dutch Central Graben; uplift occurred before the end of the Mid-Jurassic and a thin, younger, Upper Jurassic sequence rests on the Triassic, whereas the Lower Cretaceous sequence is thicker than in the Dutch Central Graben (Doornenbal and Stevenson, 2010). The Cleaver Bank and Schill Grund Platforms were uplifted and eroded during the mid- to late Kimmerian rifting phases. Therefore, Upper Jurassic and Lower Cretaceous strata are often missing on these highs, where Triassic and Permian strata are unconformably overlain by thin post-rift Lower Cretaceous and thicker Upper Cretaceous rocks (De Jager, 2007).

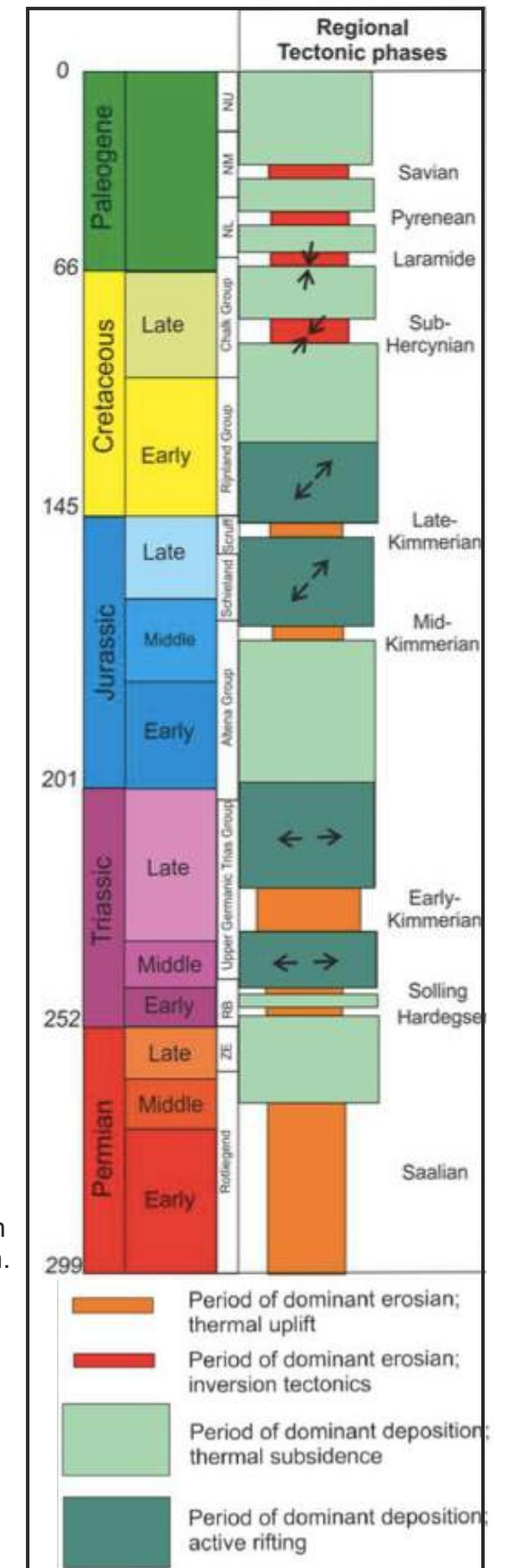


Figure 2.10: Main Tectonic phases in the Dutch offshore since the Permian. The black arrows indicate the direction of extension and contraction. Note the shift of extensional trend from E-W during the Triassic to NE-SW during the Middle Jurassic to Early Cretaceous. (Compiled from data the SPBA, Peeters et al., 2016).

2 - Geological Setting

D) Salt tectonics

The presence of Zechstein salt that was deposited during the Late Permian had a pronounced influence on the subsequent evolution of the North Sea Basin, beginning with its effects on Triassic sedimentation patterns.

The partitioning of the Southern Permian Basin into several basins and highs during the Triassic and Jurassic was accentuated by the intense salt tectonics, primarily along fault-bounded basin margins (Wong, 2007). Basin compartmentalization and minibasin formation were associated with salt withdrawal in much of the Dutch Central Graben. These basins are often bounded by listric growth faults. Mid-Triassic minibasins subsided into the Zechstein salt over much of the central North Sea.

Differential loading was important for minibasin development near sediment entry points, and thin-skinned extension on the platforms was balanced by basement extension in the central axis of the basin. Along the edges of the Triassic fault basins, the faults are commonly soft-linked and offset through the Zechstein salt (Pharaoh et al., 2010).

Locally, salt tectonics started in the North Sea during the Permian (Stewart, 2007) but it became widespread during the early Triassic with the formation of minibasins (sometime in the form of pods) and rafts (Stewart and Clark, 1999; Penge et al. 1999). In the Dutch subsurface, such Early Triassic structures have not been described and salt tectonics is often proposed as being active from the Middle onward (Geluk, 2007).

During the Mid-Triassic, thin-skinned normal faults formed on autochthonous Zechstein salt and large salt swells formed. Piercing salt bodies and rim-synclines developed later (Jager, 2007). With increased differential subsidence between the subsiding basins and their shoulders, salt bodies increasingly mobilized upward from the previously formed salt swells and initiated large rim-synclines. In the study area the salt bodies are located mainly along the basin margin and a few in the basin itself. The salt bodies are either salt diapirs or salt walls with a SSW/NNE preferential orientation.

Several key publications regarding salt tectonics in the Southern Permian Basin shed some lights on its complex evolution.

In Bouroullec et al. (2016) the impact of salt tectonics on Upper Jurassic depositional systems in the DCG, the TB and the surrounding platforms is discussed in detail. The salt played a strong role on controlling not only the differential depositional thickness but also the sediment pathways and preservation around the rift basins. Korosi (2016) analyzed the marginal depositional setting along the northern part of the DCG and shows that active salt structure along the basin controlled the sediment pathways and the amount of confinement and erosion of continental and shallow water depositional systems along the basin margins.

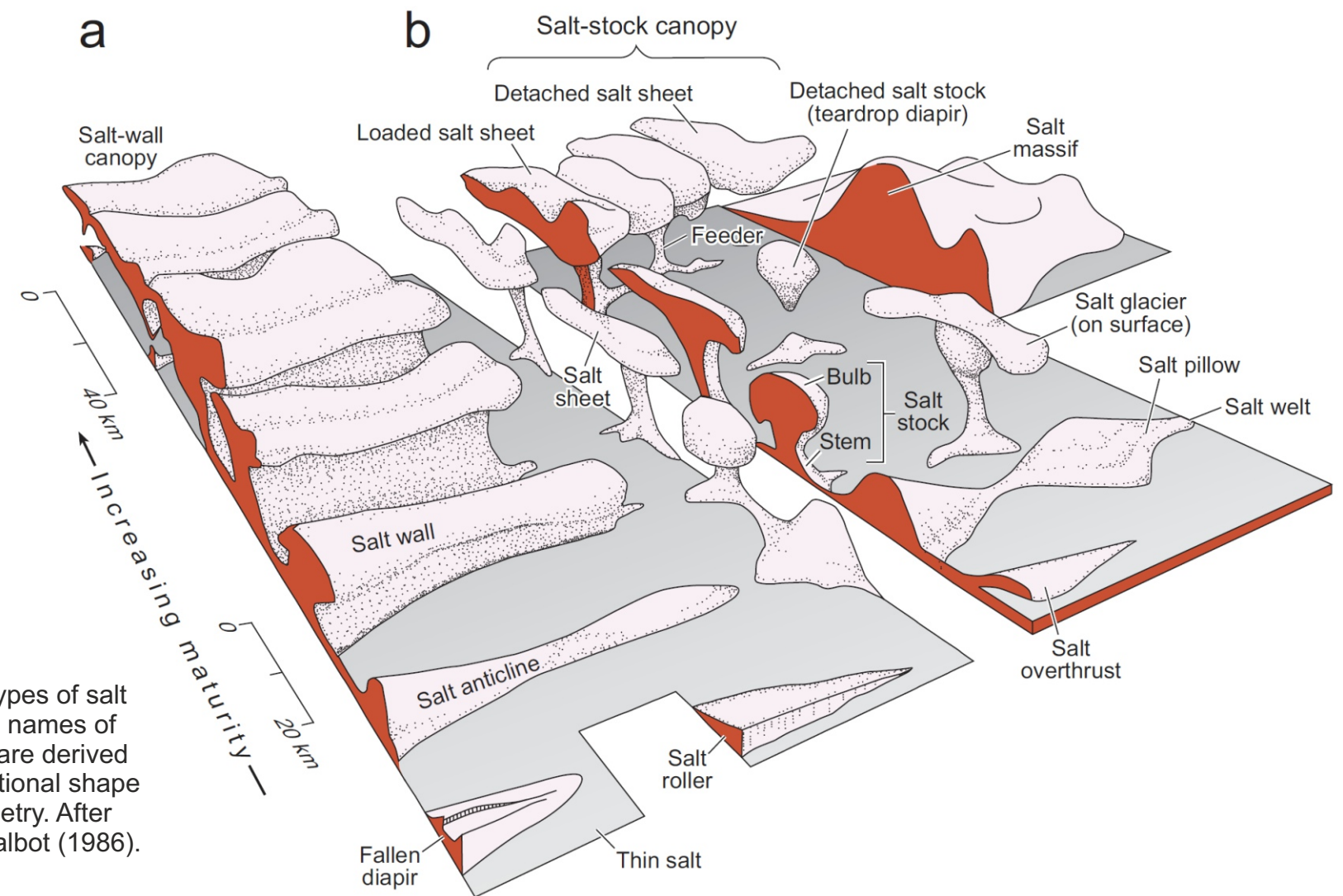


Figure 2.11: Types of salt structures. The names of salt structures are derived from cross-sectional shape and map geometry. After Jackson and Talbot (1986).

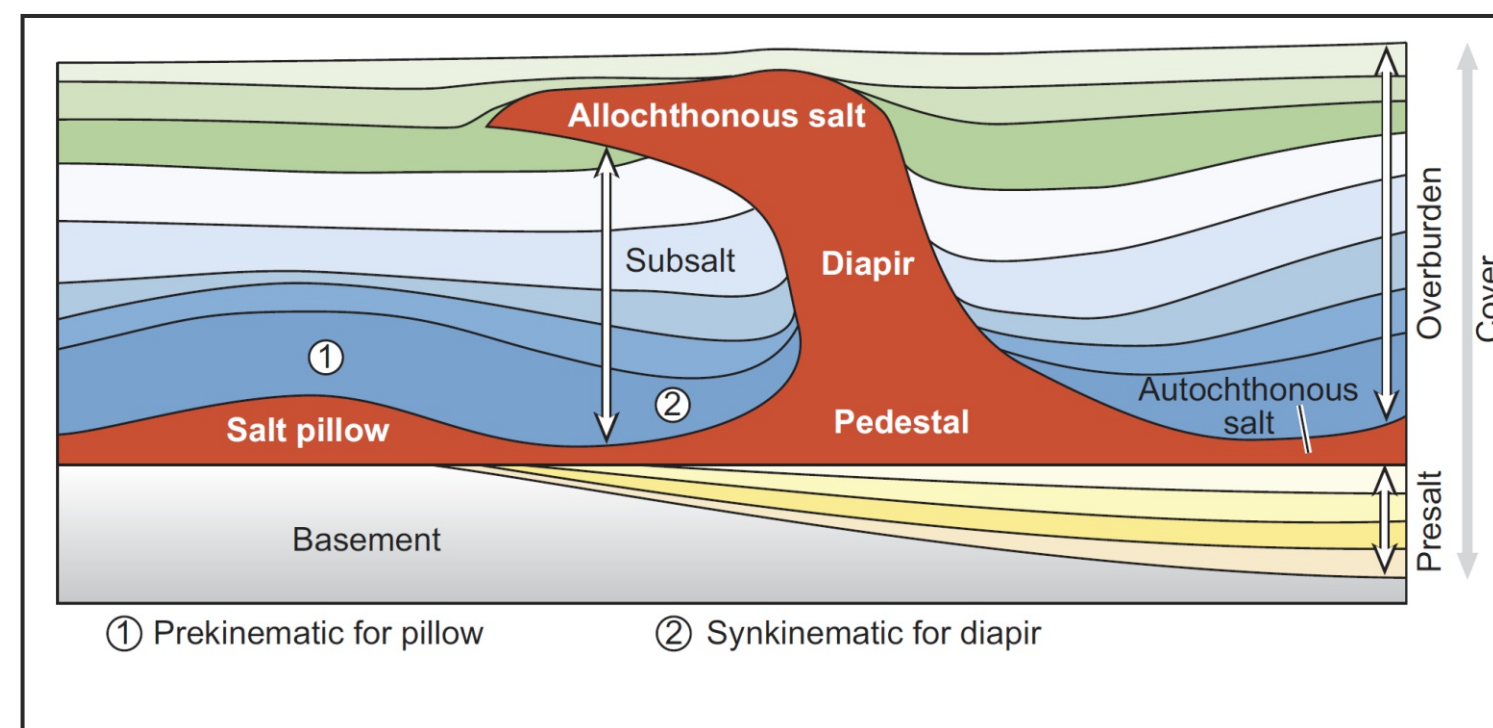


Figure 2.12: Basic tectonostratigraphic elements of a salt system. The lowermost overburden layer maintains constant thickness above the salt pillow, making it prekinematic with respect to the onset of salt flow in that structure. The same layer thins against the diapir flank and is thus synkinematic for that structure (Jackson and Hudec, 2017).

2 - Geological Setting

Salt tectonics glossary

(based on Bouroullec and Weimer, 2017; Jackson and Hudec, 2017)

Autochthonous salt (Figures 2.12 and 2.13)

A salt layer, surface (weld) or body resting in the original stratigraphic position. Also referred to “mother salt.

Allochthonous salt (Figure 2.12)

A sheet like salt body remobilized upward and emplaced within stratigraphically younger strata.

Basement

In salt tectonics, basement loosely refers to presalt rocks underlying the source layer.

Cap rock

In salt tectonics, a dissolution residue composed predominantly of anhydrite, gypsum, or calcite above a salt body. Cap rock forms at the crest of a diapir as halite dissolves and the residue is chemically altered.

Collapse structure

A graben-like depocenter associated with a deepsalt layer or diapir that reflect salt withdrawal or dissolution.

Expulsion rollover (Figure 2.20)

A tectono-stratigraphic feature that forms over a flat layer of salt. This feature forms by a succession of basinward shifting depocenters that follow basinward spreading salt, giving the overall feature a progradational geometry.

Growth fault/raft systems (Figures 2.16 and 2.17)

Association of updip growth faulting, detaching on sub-horizontal autochthonous or allochthonous salt layer, and downdip raft(s). The two features are separated by troughlike depocenters of younger synkinematic strata.

Minibasin

Small intrasalt basin largely surrounded by and subsiding into relatively thick allochthonous or autochthonous salt.

Postkinematic (Figure 2.12)

Occurring after salt flow, or other deformation, has ceased. The postkinematic sedimentary interval overlies the synkinematic interval. The postkinematic interval has regional dip, but strata do not deflect over individual structures (except compactionally induced drape). Basal postkinematic strata can onlap or truncate an underlying, uneven, deformed surface. Compare with prekinematic.

Prekinematic (Figure 2.12)

Occurring before salt flow, or other deformation, begins. The prekinematic sedimentary interval is isopachous (or changes thickness at regional rates) above local structures. The prekinematic interval underlies any synkinematic interval and records sedimentation before salt flow, or other visible deformation, began. Compare with postkinematic.

Raft

(a) Fault block that has extensionally separated from its original footwall and lies entirely on a décollement, which typically consists of thin salt. Rafts form by extreme extension over autochthonous or allochthonous salt. Rafts are separated by troughlike depocenters of younger, synkinematic strata. (Burlot 1975; Duval et al. 1990). (b) Blocks of nonhalite rock within salt structures. These blocks, also known as stringers or floaters, most commonly consist of strata originally interbedded within salt (Talbot and Jackson 1987a)

Roho

A salt system that soles onto a shallow salt nappe and has updip extensional and downdip contractional structures. A roho system is characterized by large listric basinward-dipping growth faults that sole into a horizontal flat salt weld and are balanced by reverse faulting in the down dip area (Schuster, 1995).

Salt body

General term referring to any individual salt feature. A salt body can autochthonous (e.g. salt roller) or allochthonous (e.g. salt stock). An autochthonous salt body is composed of a salt stem and salt bulb. A salt body can be partially or completely welded out.

Salt canopy (Figure 2.11)

A composite salt structure formed by partial or complete coalescence of salt bodies or salt sheets.

Salt diapir (Figures 2.11, 2.12 and 2.13)

A mass of salt that has flowed ductilely and appears to have discordantly pierced or intruded the overburden. Alternative definition: A relatively mobile mass of salt that intrudes into preexisting rocks. Salt diapirs commonly intrude vertically through denser rocks because of buoyancy forces associated with the relatively low-density salt.

Salt pillow (Figure 2.11)

A subcircular upwelling of salt that has a concordant overburden (Trusheim, 1960).

Salt roller (Figure 2.11)

A low-amplitude, asymmetric salt structure composed of two flanks, a gently dipping flank with a conformable stratigraphic contact with the overburden, and a steeply dipping flank with a normal-faulted contact with the

overburden (Bally, 1981).

Salt sheet (Figure 2.11)

A subhorizontal salt body that originally forms, by salt expansion at or near the seafloor, from a salt-diapir configuration.

Salt stem (or feeder) (Figure 2.11)

The narrow part of salt body connecting the source salt to the allochthonous salt body.

Salt stock (Figures 2.11 and 2.13)

A mushroom/bubble-shaped salt body that can have various shapes but own a deep feeder underneath connected to the mother salt (autochthonous salt) and a larger salt volume upward.

Salt tongue

A unconformable salt body that intrude obliquely into the overburden at the basinward limit of the salt layer. This term often refers to salt that is overthrusting the distal sediments at the basinward limit of the salt tectonic system.

Salt suture

Limit of precursor salt bodies within the canopy are called suture.

Salt system

The term “salt system” was defined by Jackson et al. (1994) as a system comprising a source salt layer and its overburden and subsalt strata. In the present study, an “allochthonous salt system” is defined as a group of structures that comprises (1) an allochthonous salt body (or genetically linked allochthonous salt bodies), (2) a source salt (autochthonous or deeper allochthonous salt layer), (3) salt-related stratigraphic forms, and (4) genetically-related faults and folds.

Salt wall (Figure 2.14)

An elongate upwelling of diapiric salt that forms in parallel, sinuous rows (Trusheim, 1960).

Salt weld (Figures 2.18 and 2.19)

A thin or narrow salt interval that form when a salt layer becomes very thin due to salt movement, dissolution or removal by faulting, and when the overburden and the underlying sub-salt strata become effectively welded together. Salt welds may also develop in the vertical direction by putting the sides of a former diapir in contact.

Turtle structure (Figures 2.14 and 2.15)

Mounded strata between salt diapirs, typically having a flat base and rounded crest. The sedimentary sequence is thick in its core and thins laterally. The anticline may or may not be cored by a low salt pillow. The turtle structure forms between diapirs whose flanks subside because of regional extension (see diapir fall) or between salt structures whose withdrawal basins migrate and widen through time (Trusheim 1960).

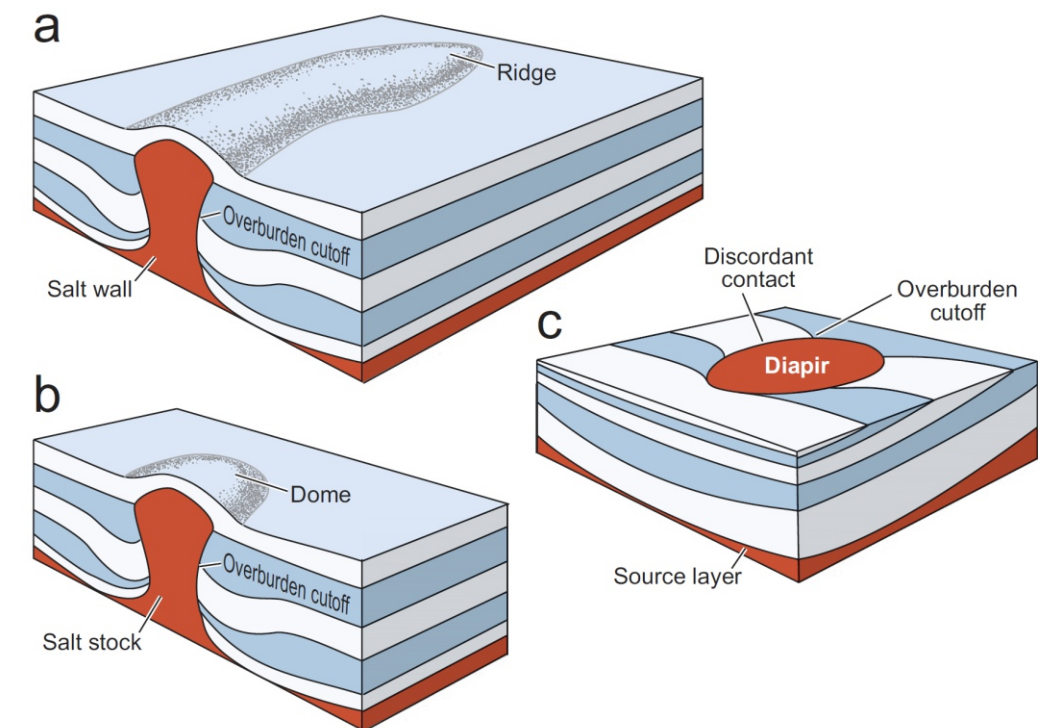


Figure 2.13: All diapirs, whether they are salt stocks, salt walls, or salt sheets have discordant contacts against their overburden (Jackson and Hudec, 2017).

2 - Geological Setting

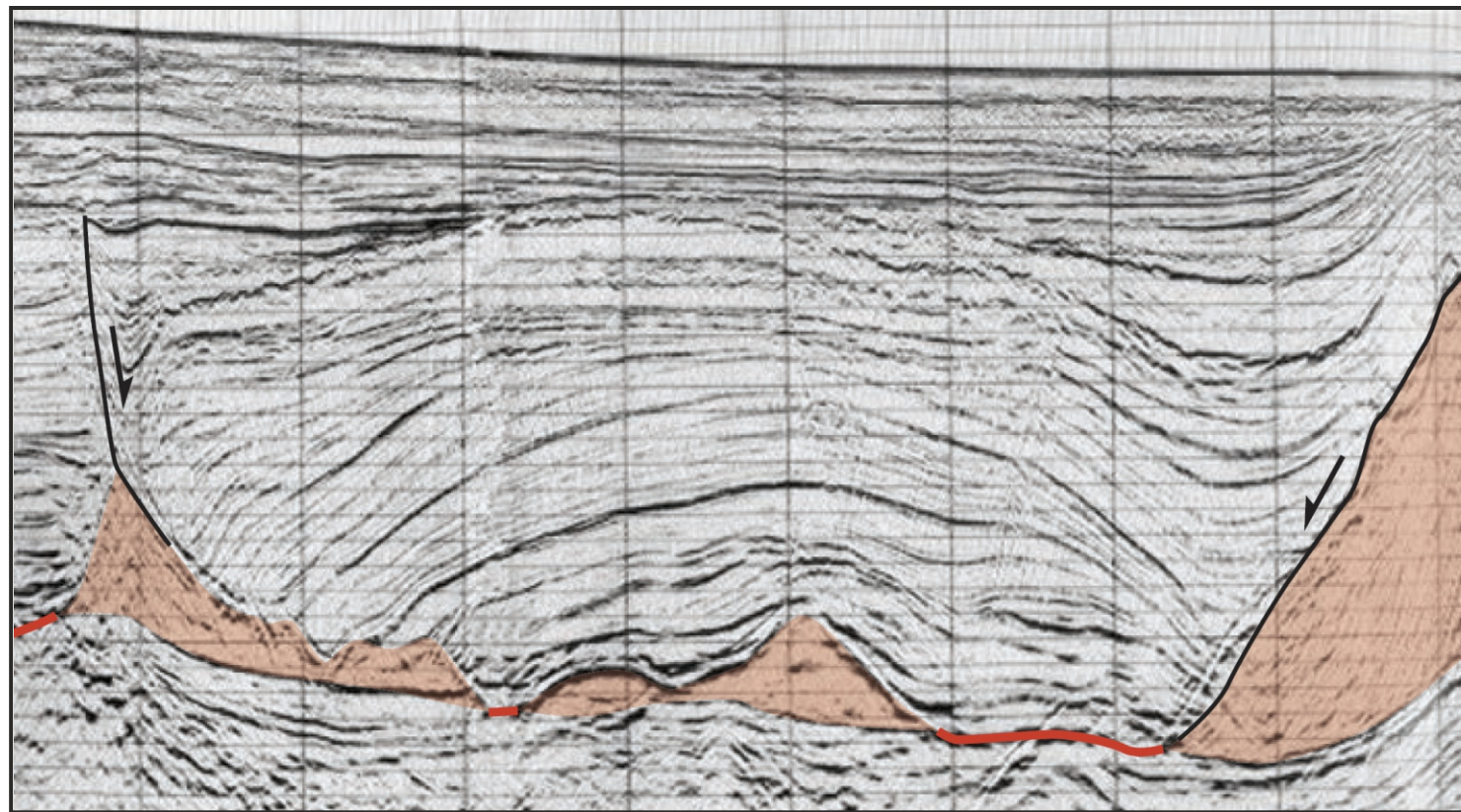


Figure 2.14: Example of a turtle structure in offshore Brazil. A salt anticline is bounded by extensional rollovers and salt diapirs on both sides. Salt welds shown as red lines and salt as orange polygons. After Schlumberger and TGS-NOPEC (2000).

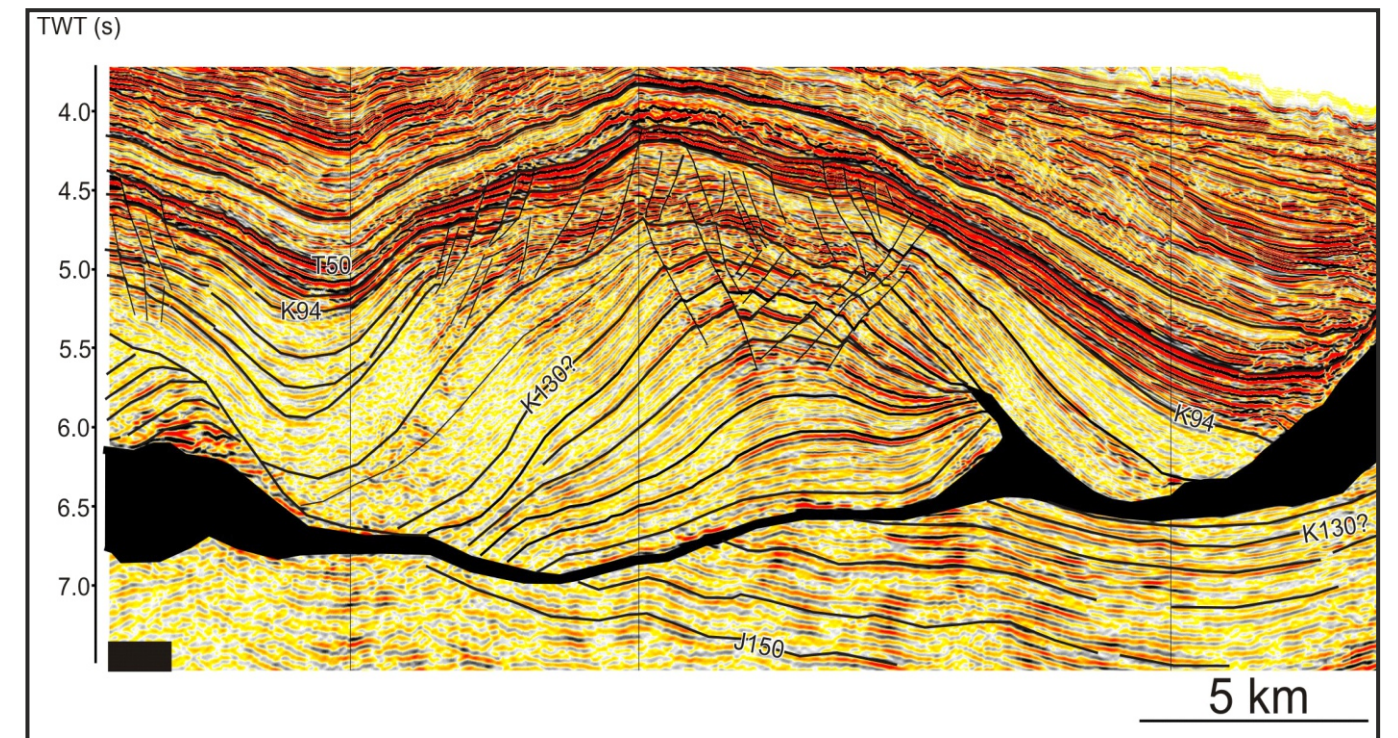


Figure 2.15: Example of a turtle structure Nova Scotia. Salt shown as black polygons. Canada-Nova Scotia Offshore Petroleum Board. callforbids@cnsopb.ns.ca

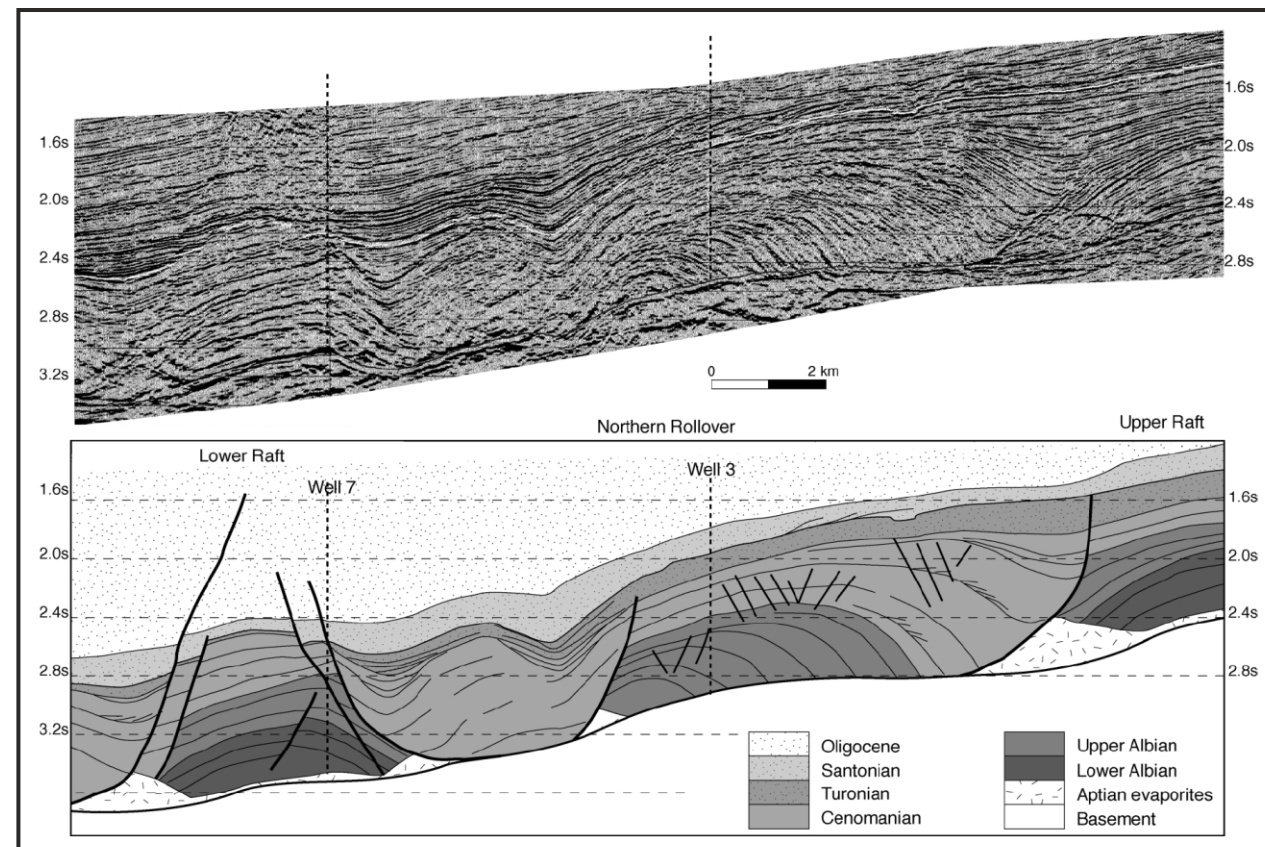


Figure 2.16: Growth fault/raft system in the Congo Cabinda Basin (Rouby et al., 2002). Note that the Lower Albian is missing in the central part of the section due to rafting of blocks along the basal detachment formed by the Aptian salt. See Figure 2.16 for kinematic model.

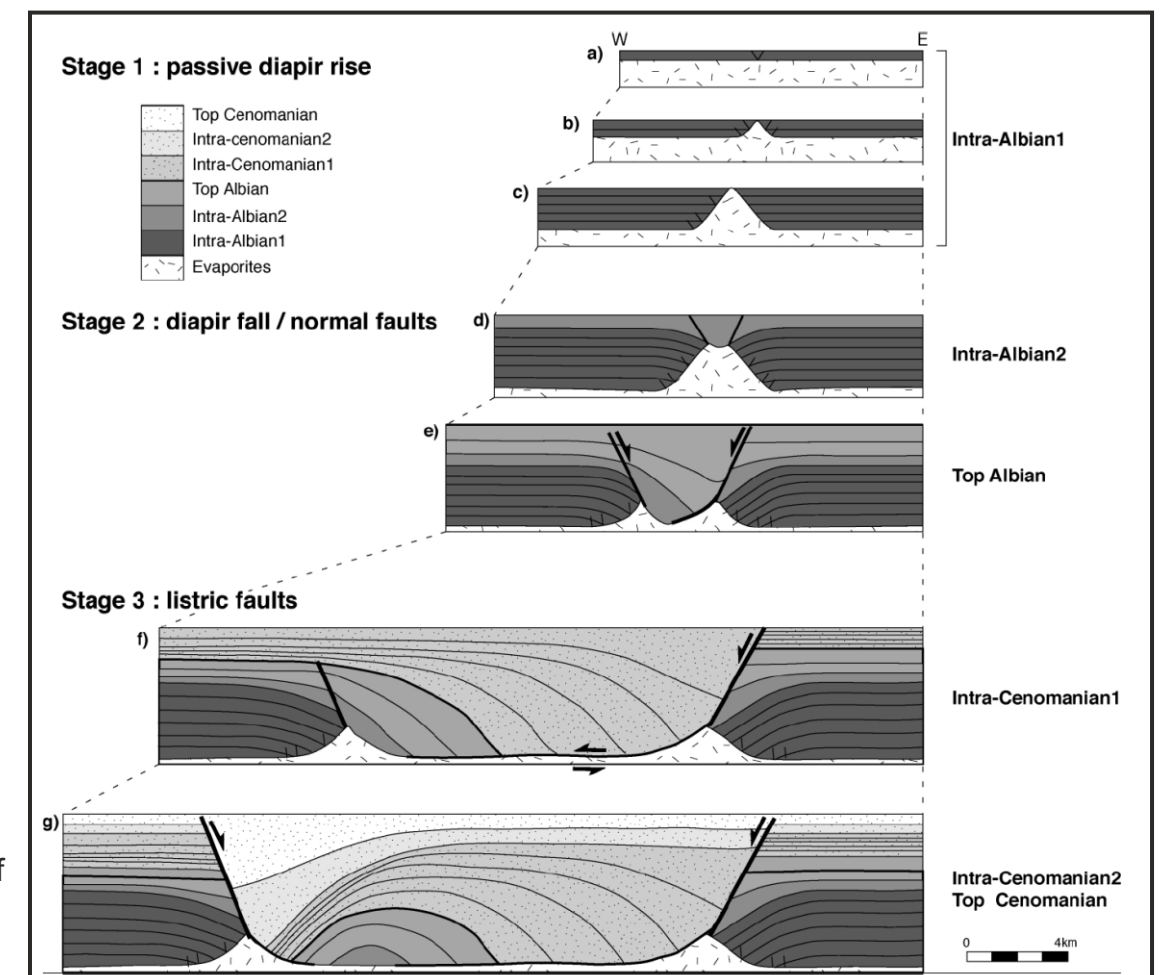


Figure 2.17: Evolution of a raft/listric fault system (Rouby et al., 2002).

2 - Geological Setting

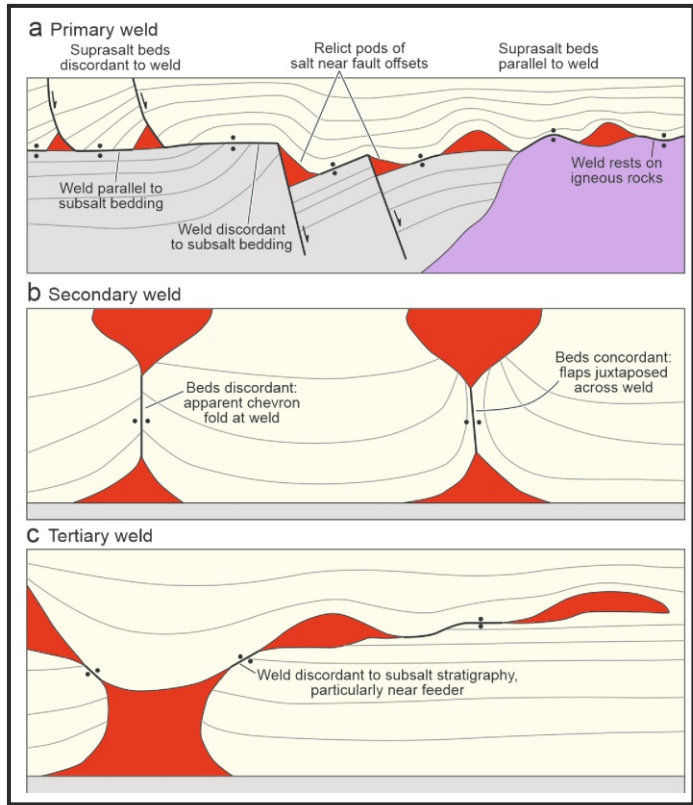


Figure 2.17: Structural style and juxtapositions vary across primary, secondary, and tertiary welds. (Jackson and Hudec, 2017).

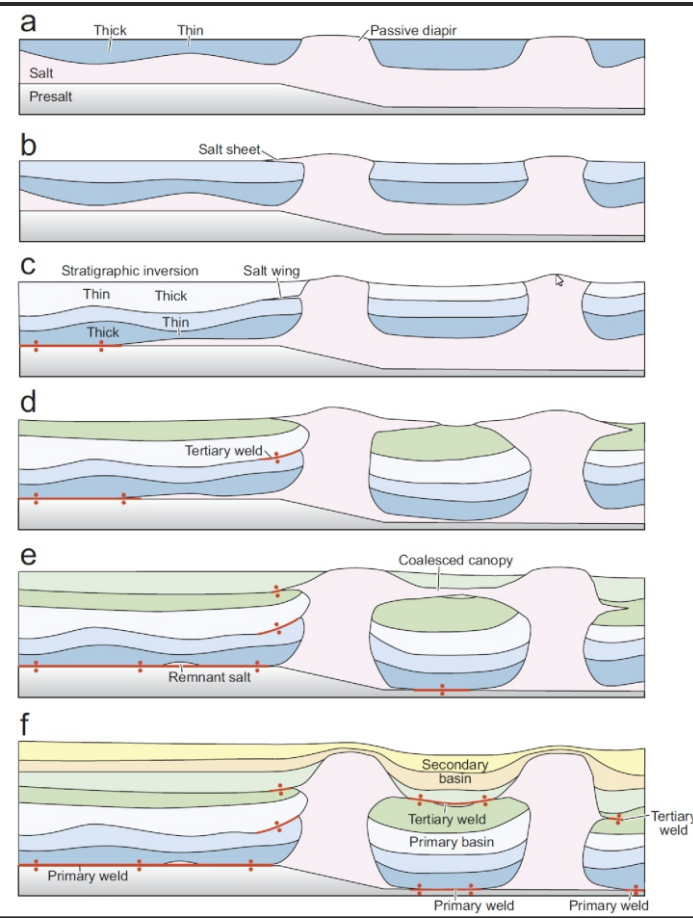
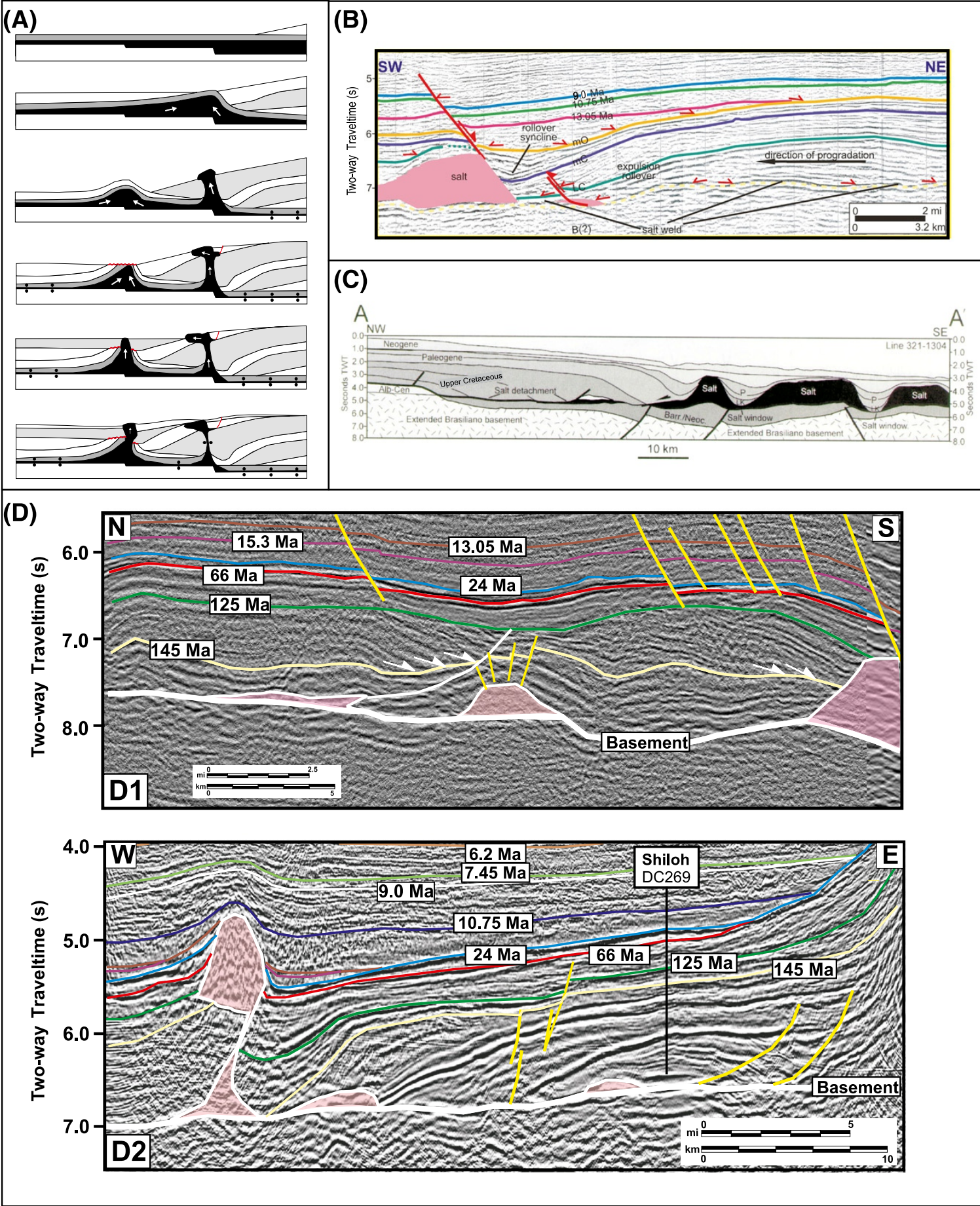


Figure 2.19: Vertical sedimentary loading onto flat-lying salt forms primary welds in autochthonous salt below primary basins. Tertiary salt welds form by evacuation of salt wings and parts of a salt canopy (Jackson and Hudec, 2017).

Figure 2.20: Profiles illustrating expulsion rollovers. (A) Kinematic model of an expulsion rollover from physical analog modeling (after Ge et al., 1997). Autochthonous salt is shown in black, prekinematic interval is shown in dark grey, and synkinematic intervals are shown in white and light grey. Faults are shown in red. (B) Seismic profile showing an expulsion rollover in the eastern DeSoto Canyon (DC) area in the Deep Gulf of Mexico, after Pyles et al. (2001). Salt is shown in pink, and faults are shown as red lines. Reproduced with the permission of the Gulf Coast Section SEPM Foundation, and any other use requires their permission, and Schlumberger. © Seismic profile of the Campos Basin, Brazil, showing an expulsion rollover (Cobbold et al., 2001). Autochthonous salt is shown in black. (D) Seismic profiles showing expulsion rollover in the Deep Gulf of Mexico. The autochthonous and allochthonous salt bodies are shown as transparent pink polygons with white outlines. The faults are shown as yellow lines. Profile D1 shows the base Cretaceous through top Barremian strata thickening southward and downlapping onto the 145 Ma surface. Profile D2 shows an expulsion rollover associated with the Shiloh discovery. For more details of the Shiloh (DC 269) discovery. From Bouroullec et al. (2017).



METHODOLOGY 3

3.1 Methodology - Database

Several analytical techniques were used in the STEM project: 1) A regional 2D seismic interpretation; 2) 3D seismic interpretation for three case studies; 3) a palynological analysis, 4) a geochemical analysis and 5) 2D structural restoration of three sections.

The database used in this project consist of well data, 2D and 2D seismic data, core and cutting samples.

Well data

- 543 wells were loaded in the petrel project with many used for the regional seismic interpretation (Phase 1 of the project).
- 5 wells were used for palynological and 5 wells for geochemical/petrographical analysis (Table 3.1)
- 54 wells were used for the 3D case studies (Table 3.1)
- 37 wells were used for the structural restorations (Table 3.1)

Core and cutting samples

- Five wells were sampled for the palynological analysis that focused on the Zechstein Group and the Röt Formation (Table 3.1)
- Two wells with cores were used for petrographic analysis and three wells with cuttings for geochemical analysis (Table 3.1.1)

Seismic data

- 11 2-D and 28 3-D seismic surveys were used for the regional seismic interpretation (Phase 1) (Table 3.2)
- Three 3-D seismic surveys were used for the case studies (Phase 2). We would like to thank:
 - 1) Sterling Resources, Wintershall and EBN for providing access to the F17-F18 PSDM survey;
 - 2) Wintershall and EBN for providing the merged L06-L08 survey; and
 - 3) EBN, Wintershall, Rosewood, ENGIE, Taqa Offshore for providing the reprocessed F10F11F14_2016 survey.
- Twelve 3-D seismic surveys were used to create the three 2-D seismic sections used for the structural restorations (Phase 3). We would like to thank Spectrum for providing 2D seismic sections from the DEF 3D survey.

Well	Palynological analysis	Geochemical and petrographical analysis	Case study			Structural restoration		
			F10/F11	L06/L08	F17/F18	F10/F11	L06/L08	F17/F18
A18-02-S1	Core - 5 samples							
E01-02								
E09-02								
E12-01								
E12-03								
E12-04-S2								
E18-03								
F07-02								
F08-02								
F09-01								
F09-02								
F09-03								
F10-01								
F10-02								
F10-03								
F11-01								
F11-02								
F11-03								
G07-02								
F16-02								
F16-04								
F17-01-S2								
F17-02								
F17-03								
F17-04								
F17-05								
F17-06								
F17-07								
F17-09								
F17-10								
F17-11								
F17-12								
F18-01								
F18-02								
F18-04								
F18-06								
F18-08								
F18-09	Cuttings - 17 s.							
F18-10								
F19-02								

Table 3.1.1: Well database and associated activity

Well	Palynological analysis	Geochemical and petrographical analysis	Case study			Structural restoration		
			F17/F18	L06/L08	F10/F11	F17/F18	L06/L08	F10/F11
G10-01	Core - 4 samples							
G16-06								
K13-02	Core - 17 samples							
L05-01								
L05-02								
L05-07								
L05-09								
L05-10								
L05-12								
L05-C-02-S1								
L06-01								
L06-02								
L06-03								
L06-04								
L06-05								
L06-07								
L06-08								
L07-06								
L07-09								
L08-01								
L08-02								
L08-03								
L08-04								
L08-05								
L08-06								
L08-07								
L08-09								
L08-10								
L08-11								
L08-12								
L08-P-01-S1								
L09-02								
L09-04								
L09-07								
M04-01								
M04-02								
M04-03								
M04-04								
M04-05-S1								
TWR-480	Core - 7 samples							

Seismic surveys		Regional				Case studies			
		Base ZE	Top ZE	Top RB	Features	F17/F18	L06/L08	F10/F11	Restoration
2D	NSR - 2D lines 2016								
	A15_Z2WES1988B								
	A_B_E_F_ABT-91								
	A_B_E_F_NSR08								
	F01_F04_Z2ARC1988C								
	SNST-83								
	SNST-87								
	B16_B17_A15_B13_F02_Z2NAM1990A								
	B17_B14_Z2WES1985C								
	E03_F01_F014_B17_Z2ARC1988C								
	F13_Z2CGG1985A								
	A08_09								
3D	A15_								
	B_Blocks_Z3FUG-2002A								
	M01								
	M02								
	M04_Z3NAM1991D								
	M05								
	M07_M08_M05								
	M07-L09								
	E12_E09_Z3PET1993A								
	E14_E15								
	E18_F16-Z3WIN1997A								
	E18_F16_Z3WIN1997A								
	F08_F09_Z3OXY1994A								
	F09								
	F10_Z3PET1994B								
	F16								
	F11F12_Z3WES2003A								
	F13_F14								
	F17_F18								
	F18_G16								
	L01_L02								
	L03_L02								
	L05								
	L05_L04								
	L06_Z3WIN2005B								
	L06_L05								
	L07L08_Z3WIN1995A								
	L08								
	L09								
	L12_L09_L15								
	L11								
	L06-big_2005								
	L06_Z3WIN2005B								
	L04								
	F17-F18_PSDM								

Table 3.1.2: Seismic database and associated activity

3.2 Methodology - Palynology

A) Principles and application

Palynologists study acid-resistant organic matter from sedimentary rocks. Organic matter is classified into palynomorphs, organic microfossils within a certain size range, and palynodebris, all other organic material such as plant-tissue, wood fragments, structureless organic matter, and so on. The combination of palynomorphs and palynodebris is called palynofacies. Within the

palynomorph category, two groups are considered the most important: the dinoflagellate cysts, or dinocysts, and the pollen and spores, or sporomorphs. Because palynology straddles both the marine and the terrestrial realm, it is ideally suited for the study of shallow- to non-marine sedimentary rocks.

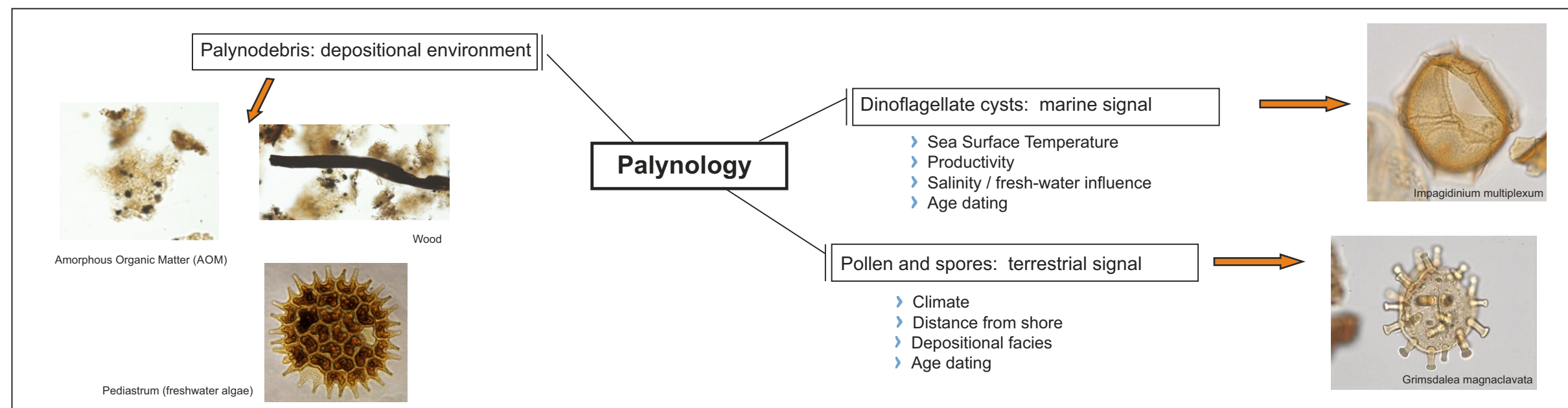


Figure 3.2.1: Principles and application of palynological analysis.

B) Workflow

The organic matter is extracted from the rock by a standard laboratory processing procedure. During the first step, the sedimentary rock is crushed and treated with HCl to digest the carbonate. After that, the mineral bonds of the silicates are destroyed by applying HF, which releases the acid-resistant organic matter. The organic residue is then concentrated by sieving over a 7 micron mesh. The organic matter particles larger than 7 micron are brought on a glass slide, fixed by a mounting medium such as glycerine jelly, and covered by a thin glass cover slip.

The result is called a palynological preparation or slide. Its content is studied using a transmitted light microscope with magnifications varying between 100 and 1000 microns. The microfossils such as dinoflagellate cysts and pollen and spores are identified on species level and counted. The occurrences of the different species are displayed on distribution charts. These charts are the basic modules for the age and palaeoenvironmental interpretation.

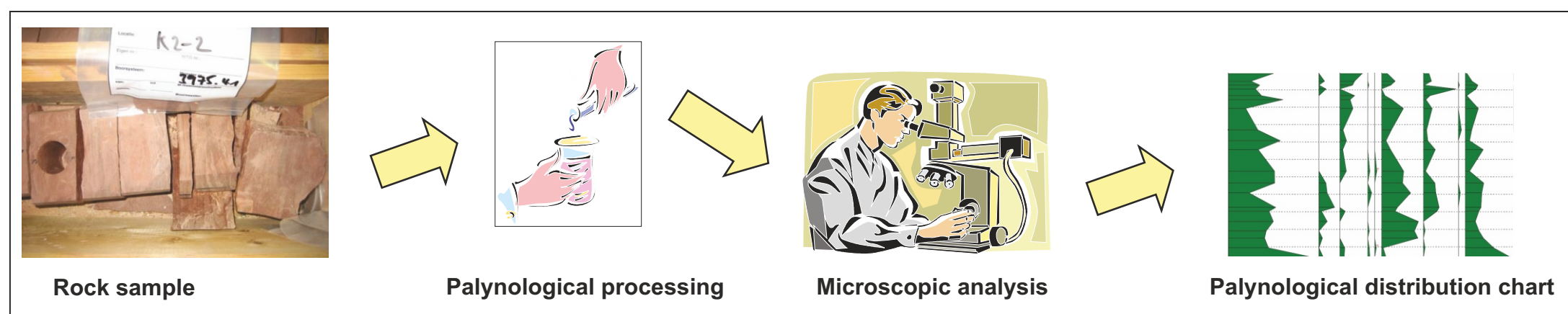


Figure 3.2.2: Typical workflow for palynological analysis: sample selection, processing, microscopy and distribution charts.

C) Reworking and caving

Fossils, like palynomorphs, typically occur in specific stratigraphic intervals. For example fossil remains of dinosaurs may occur in the Jurassic and the Cretaceous, but not in the Paleogene, because dinosaurs became extinct at the Cretaceous-Paleogene boundary.

Reworking refers to fossils that first have been eroded from old layers and subsequently deposited in younger layers (Figs. 3.2.3 and 3.2.4). When, for instance, dinosaur bones occur in Paleogene strata, then these occurrences are due to reworking. In the case of dinosaur bones, the chances of fossil bones surviving erosion is quite unlikely, but small palynomorphs are less

vulnerable and therefore easily reworked into younger sediments.

Caving is a phenomenon that is related to the process of taking cuttings samples during drilling (Figs. 3.2.5 and 3.2.6). When a well is drilled, mud flows down the drill string to the drill bit. The rotating drill bit produces clippings when cutting through the rock layers. The drill clippings, or cuttings, are taken up hole by the drill mud and are successively collected in troughs. During the way up the borehole, pieces from the side of the hole break off (cave) and are also taken up in the mud flow. These pieces from younger layers then end up in the cuttings sample from an older layer. Only the well transects that are sealed off by a casing cannot contribute to the mud flow.

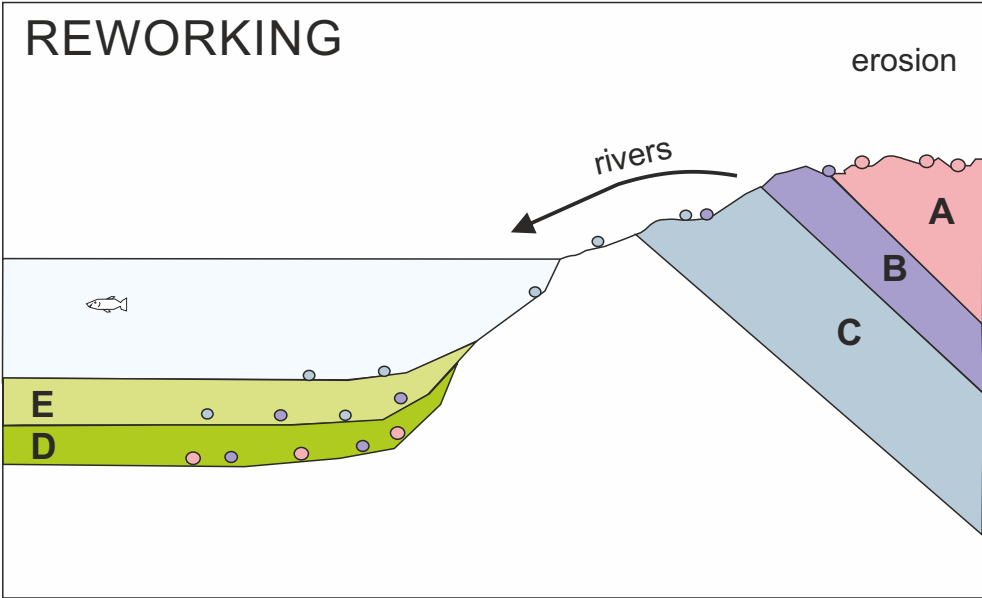


Figure 3.2.3: Reworking explained: old strata A, B and C are eroded and material from it is transported by rivers into the sea. In the sea, the reworked material from A, B and C becomes incorporated in the younger sediment layers D and E.

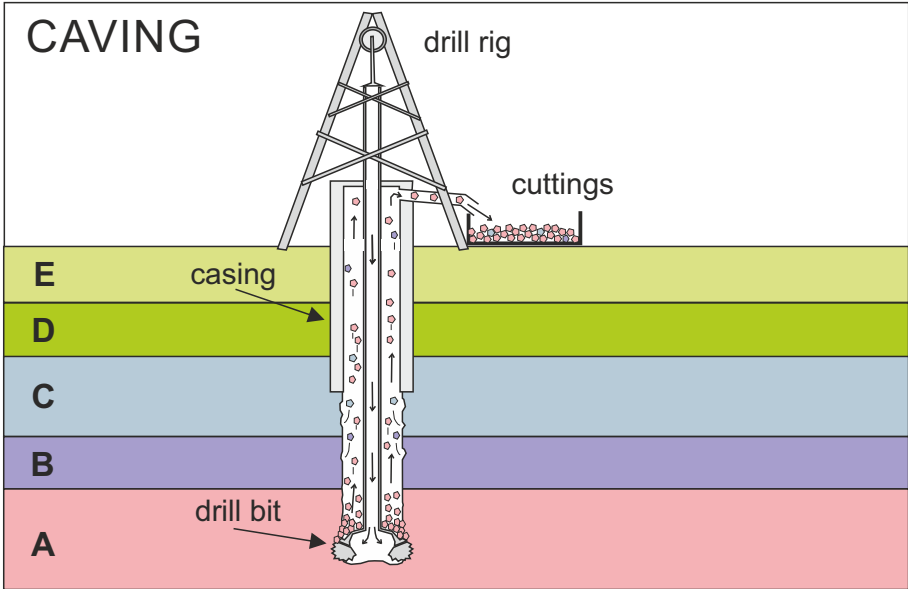


Figure 3.2.5: Caving explained: the drill bit cuts clippings from layer A, which are taken up by the mud stream. During its way up hole, the drill mud picks up pieces of younger layers B and C from the wall of the borehole. Layers D and E are sealed off from the mud stream by a casing.

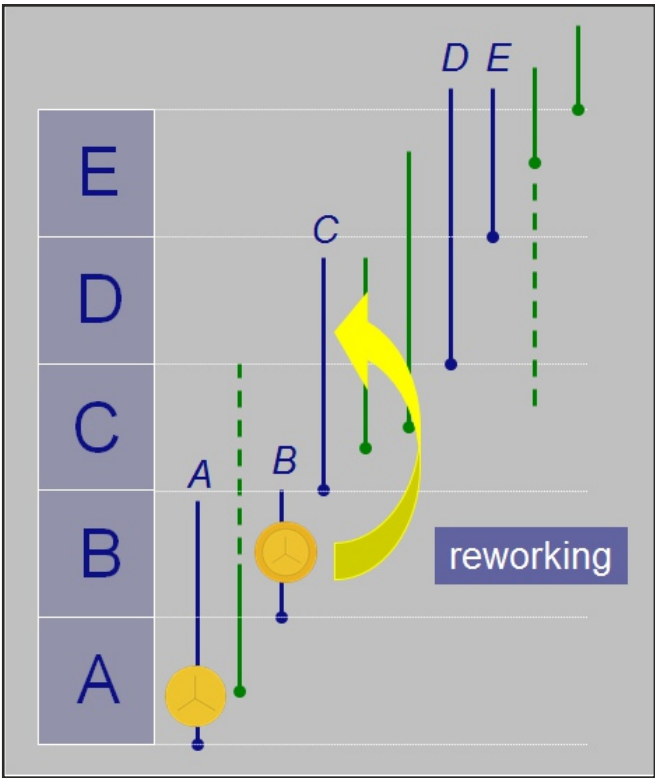


Figure 3.2.4: Reworking explained: pollen and spores with a stratigraphic range limited to layers A or B, end up in younger layers D and E via erosion and transport by rivers.

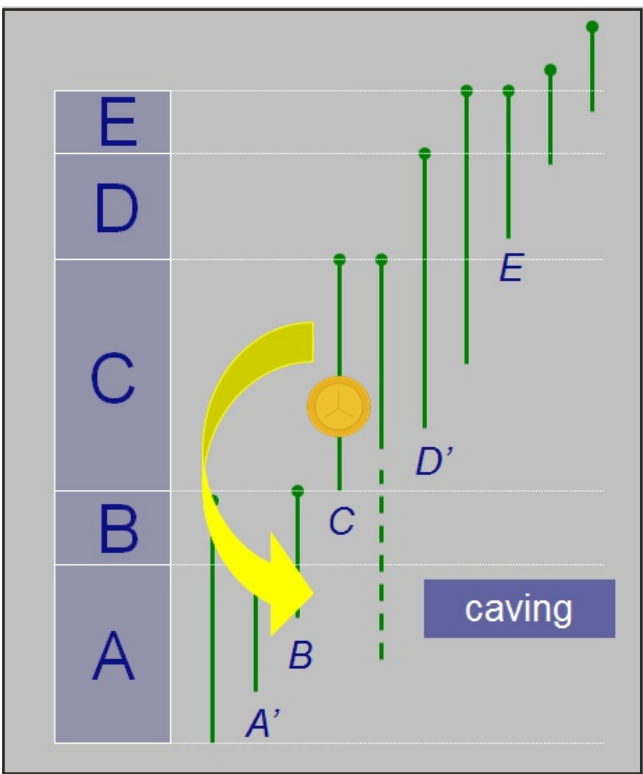


Figure 3.2.6: Caving explained: cuttings samples from layer A are contaminated by palynomorphs from layer C.

D) Material

In the Triassic, three sizable salt layers occur: the Main Röt Evaporite, the Middle Muschelkalk and the Main Keuper Evaporite Members (Fig. 3.2.7). An inventory into the availability of core material indicated that only the Röt Evaporite was sufficiently suited for the reference study. Seventeen (17) core samples from the Röt Evaporite and adjacent units of offshore well K13-02 were selected for palynological analyses (Table 3.1.1). Seven (7) core samples from the Main Röt Evaporite Member of onshore well TWR-480 were selected for palynological analyses (Table 3.2.1). The Permian Zechstein is considered for this study as one single salt body. However,

within the Zechstein salt, black shale stringers occur. It was suspected that the black stringers would yield different results than the samples consisting of halite. Therefore, the halite and black stringers were sampled and analysed separately. Five (5) core samples from the Zechstein of well A18-02-S1 and four (4) core samples from the Zechstein of well G10-01 were selected for palynological analyses (Table 3.2.1). A feasibility study was undertaken to evaluate if biostratigraphic information can be used to discriminate between Permian and Triassic evaporites. For the feasibility study, only one well was sampled. Seventeen (17) cuttings samples from the presumed Triassic Röt Evaporite of well F18-09-S1 were selected for palynological analyses (Table 3.2.1).

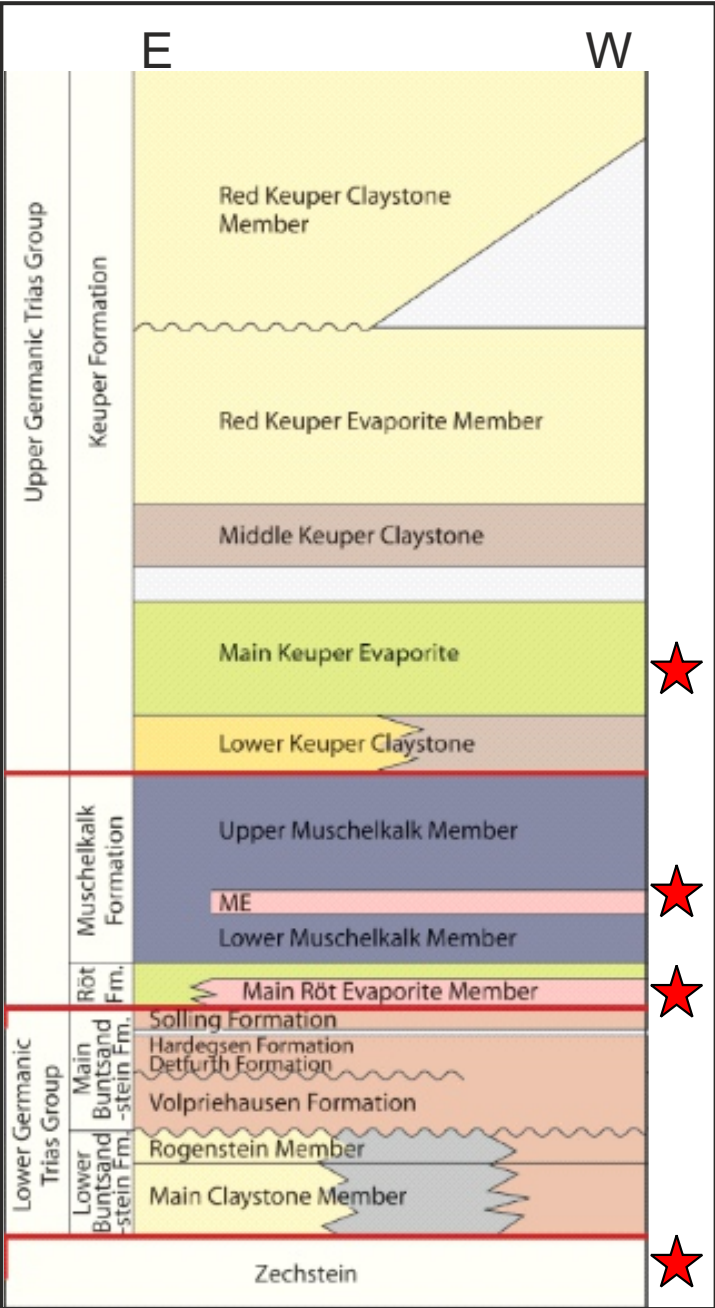


Figure 3.2.7: Permian and Triassic in situ salt layers. Modified from Bachmaan et al. (2010).

	Depth (m)	Type	Lithostratigraphy	Lithology
K13-02	1286.6	Core	Röt Claystone Member	mixed siliciclastic/evaporitic
	1288.1	Core	Main Röt Evaporite Member	mixed siliciclastic/evaporitic
	1288.9	Core	Main Röt Evaporite Member	mixed siliciclastic/evaporitic
	1290.25	Core	Main Röt Evaporite Member	mixed siliciclastic/evaporitic
	1292.8	Core	Main Röt Evaporite Member	mixed siliciclastic/evaporitic
	1293.4	Core	Main Röt Evaporite Member	mixed siliciclastic/evaporitic
	1294.4	Core	Main Röt Evaporite Member	mixed siliciclastic/evaporitic
	1294.75	Core	Main Röt Evaporite Member	mixed siliciclastic/evaporitic
	1296.3	Core	Main Röt Evaporite Member	mixed siliciclastic/evaporitic
	1299.6	Core	Main Röt Evaporite Member	cauliflower evaporitic
	1300.4	Core	Solling Claystone Member	laminated carbonate
	1302.4	Core	Solling Claystone Member	mixed siliciclastic/evaporitic
	1302.8	Core	Solling Claystone Member	mixed siliciclastic/evaporitic
	1326.4	Core	Hardegen Member	red claystone
	1444.3	Core	Lower Volprieausen Sst Mb	red claystone
	1476.5	Core	Rogenstein Member	red claystone
	1492.8	Core	Rogenstein Member	red claystone
TWR-480	429.5	Core	Main Röt Evaporite Member	halite
	440.65	Core	Main Röt Evaporite Member	shale
	447.1	Core	Main Röt Evaporite Member	shale
	448.45	Core	Main Röt Evaporite Member	halite
	455.3	Core	Main Röt Evaporite Member	halite
	468.6	Core	Main Röt Evaporite Member	halite
	479.5	Core	Main Röt Evaporite Member	shale
G10-01	2664.1	Core	Zechstein Group	black stringer
	2666.2	Core	Zechstein Group	black stringer
	2668.1	Core	Zechstein Group	black stringer
	2679.05	Core	Zechstein Group	anhydrite
A18-02-S1	2067.2	Core	Zechstein Group	black stringer
	2072.7	Core	Zechstein Group	black stringer
	2112.1	Core	Zechstein Group	dolomite
	2120.6	Core	Zechstein Group	halite
	2127.0	Core	Zechstein Group	halite
F18-09-S2	3220	cuttings sample	Red Keuper Claystone Member	
	3240	cuttings sample	Red Keuper Claystone Member	
	3540	cuttings sample	Main Keuper Evaporite Member	
	3590	cuttings sample	Main Keuper Evaporite Member	
	3780	cuttings sample	Lower Keuper Claystone Member	
	3800	cuttings sample	Lower Keuper Claystone Member	
	3830	cuttings sample	Muschelkalk Claystone member	
	3880	cuttings sample	Muschelkalk Claystone member	
	3890	cuttings sample	Muschelkalk Evaporite Member	
	3975	cuttings sample	Muschelkalk Evaporite Member	
	3995	cuttings sample	Muschelkalk Evaporite Member	
	4015	cuttings sample	Main Röt Evaporite Member	
	4250	cuttings sample	Main Röt Evaporite Member	
	4310	cuttings sample	Solling Claystone Member	
	4320	cuttings sample	Solling Claystone Member	
	4350	cuttings sample	Solling Claystone Member	
	4440	cuttings sample	Volprieausen Clay Member	

Table 3.2.1: Selected core and cutting samples. The lithostratigraphic assignments are adopted from NLOG. All depths are in core depth (m) except for well F18-09-S2 that are measured depths.

The aim of this study was to distinguish between depositional and remobilized intra-Triassic salt (autochthonous vs allochthonous). Autochthonous salts represent the in situ depositional salt layers, which can be the Zechstein Group or the Triassic Main Röt Evaporite, Middle Muschelkalk, Main Keuper Evaporite and Red Keuper Evaporite Members (Figure 3.2.7). Allochthonous salts on the other hand are upward remobilized Zechstein salts forming intrusive and extrusive salt sheets. Salt of different ages may be stacked upon each other or one can even find older (Zechstein) salts on top of Triassic salts. To understand the timing and magnitude of salt

A) Literature study

A literature study was performed to investigate the differences in the salt deposits and to identify adequate techniques to distinguish between the Zechstein and Triassic salts. The possible techniques included mineralogical characterisation, chemical composition (major, minor and trace elements) and isotopic compositions (S and Sr isotopes).

The literature study indicated that the mineralogy can be quite similar in all deposits and therefore not diagnostic for a particular age of the deposit (e.g., Zhang et al., 2013, Sonderholm, 1987). The literature lacked a good understanding and reference data of element compositions and their ratios. For this reason we abstained from using element compositions. For S and Sr isotope study global Sr and S isotope records were assessed, which gave a good indication for a large shift in the isotope composition of both elements during the Permo-Triassic (Fig. 3.3.1).

Variation in the strontium isotope ratios of Sr ($^{87}\text{Sr}/^{86}\text{Sr}$) through time is related to two main Sr sources, being the continental (preferentially ^{87}Sr) and the magmatic source (preferentially ^{86}Sr). From Middle to Late Permian extreme continental aridity and minimised runoff led to a low $^{87}\text{Sr}/^{86}\text{Sr}$ ratio (Martin & Macdougall, 1995). From the Permian/Triassic global $^{87}\text{Sr}/^{86}\text{Sr}$ values the Sr pool progressively received more of the radiogenic ^{87}Sr due to increased weathering from the continent and increased riverine Sr flux (Dudas, et al., 2017).

The $\delta^{34}\text{S}$ composition of sulphur in sulphate-containing rocks (such as anhydrite, gypsum, barite and carbonate) reflects the S-isotope composition of marine SO_4^{2-} (Paytan et al. 1998; Kampschulte & Strauss, 2004). Due to the long residence time of sulphate in the ocean, its concentration and S-isotopic composition do not differ in different marine water bodies. Due to the long residence time of sulphate the concentration and isotopic composition is identical in the present oceans. The variation of the global $\delta^{34}\text{S}$ values through time are driven by changes in the exogenic sulphur cycle. Partitioning of S into different sinks and sources is related to the rates of influx of continental S to the oceans, the precipitation of evaporites, sulphate reduction, sulphide formation, and a minor input of magmatic and volcanic S (e.g., Veizer et al., 1980, Claypool et al., 1980, Canfield & Farquhar, 2012). The large shift towards high S-isotope values with the onset of the Triassic is thought to have been related to the preferential removal of light S in form of sulphide (mainly pyrite) from the oceanic pool (e.g. Newton et al., 2004).

A reference section was compiled from available literature data for the S-isotope curve. Figure 3.3.2 displays the 10 Ma moving average for evaporite sulphur and trace sulphur in carbonates. The moving average generally gives a better indication of the global S curve, whereas single values show a spread (Fig. 3.3.1). The main reason for the spread is that exact dates are often not achieved for evaporites and carbonates. Considering that the data was compiled from different locations erroneous ages are probable. Further, in strongly evaporative environments the isotope signature can deviate up to 4 per mill (Raab & Spiro, 1991). There is some discrepancy between carbonates and evaporite $\delta^{34}\text{S}$ values in the isotope record. In carbonates, S is a trace constituent, which makes the S isotope composition easier to become altered from the global seawater signature by local biogeochemical processes (Marenco et al., 2008). Furthermore sulphate

movement the aim of this task was to assess the age of the salt deposits in wells that cut through the case study areas. The composite logs show Triassic salt intervals but the question is whether these intervals have been assigned to the right age. Salt dating is not straightforward and has rarely been attempted. The task proposed in this study was therefore mainly designed as a proof of concept. This analysis was carried out in three steps, 1) as a literature study to build knowledge, 2) a petrographical study, and 3) geochemical analysis.

extraction from carbonates is prone to contamination if not performed correctly (Goldberg et al., 2011).

The light coloured rectangles are data from Zechstein and Triassic evaporite deposits in NW Europe (Fig. 3.3.2). Zechstein evaporites have relatively low S-isotope values of between 10 and 13 ‰ in W. Poland (Peryt et al., 2010), which corresponds with the world average. Very high S isotope values of between 27 and 32 ‰ were recorded in the Main Röt Evaporite from Dutch, German and Polish locations (Kovalevych et al., 2002). A shift to extremely high values with the onset of Triassic was also recorded in other deposits (Marenco et al., 2008). Keuper evaporites from the Lorraine Basin contain sulphur with values of 15 to 17 ‰ (Fanlo & Ayora, 1998), which deviates somewhat from the world record that shows higher values of between 17 and 20 ‰.

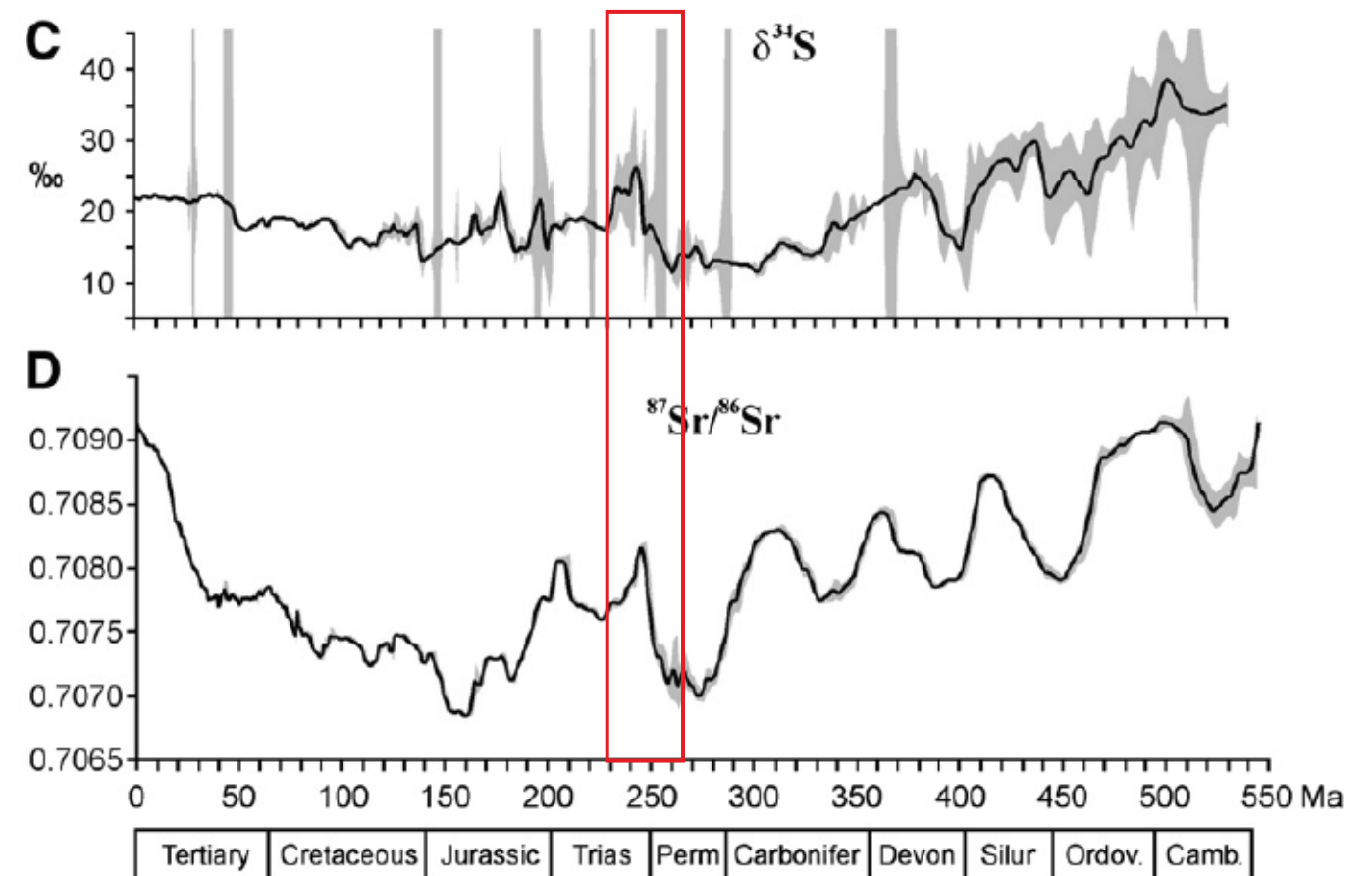


Figure 3.3.1: Compilations of Phanerozoic global seawater $\delta^{34}\text{S}$ and $^{87}\text{Sr}/^{86}\text{Sr}$ curves, modified after Prokoph et al. (2008). Red square indicates the time period studied in this project.

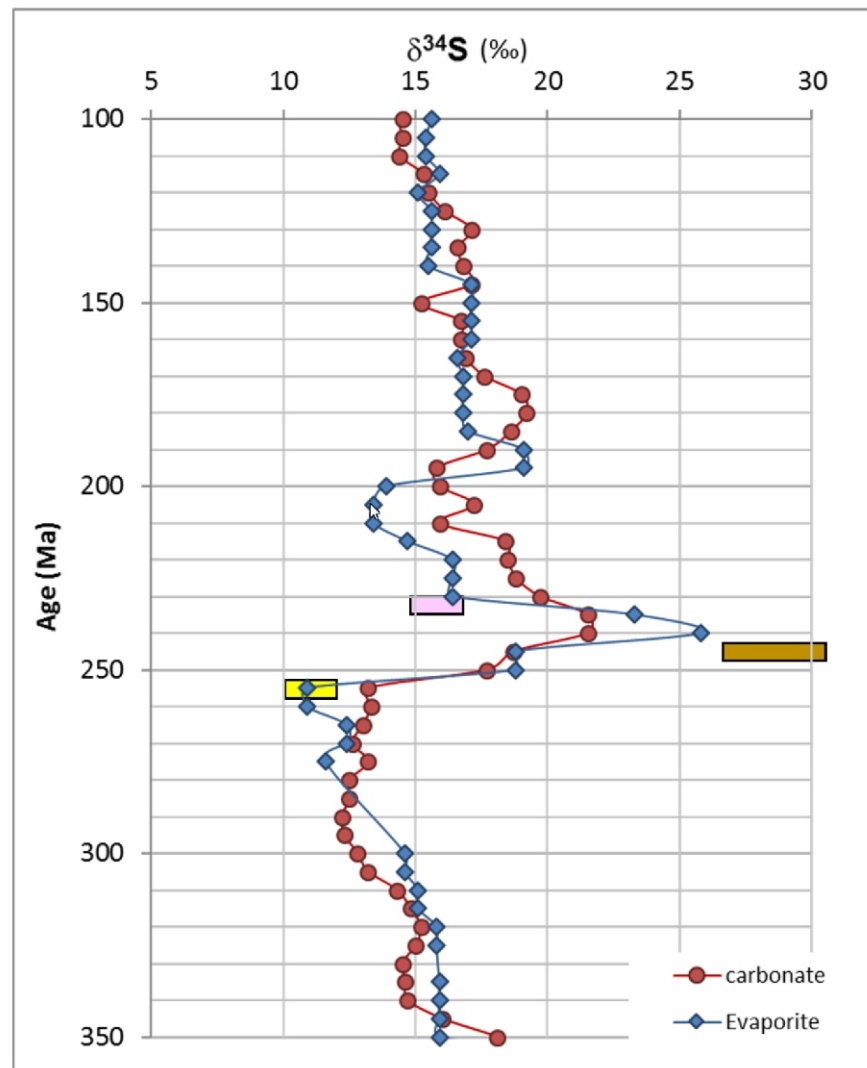


Figure 3.3.2: Ten Million year-moving average of the S-isotope values in evaporites (circles) and carbonates (diamonds) compiled from Prokoph (2008). Blue boxes span the range of $\delta^{34}\text{S}$ measured in evaporites European sections, compiled from Kovalevych et al. (2002) Peryt et al., (2010) and Fanlo & Ayora, 1998.

Keuper Evaporite
Röt Evaporites
Zechstein Evaporites

B) Geochemistry

Samples were collected from two reference cores (Well TWR-480 and K13-02). For the case studies only cuttings samples were available. Cuttings were collected from wells L09-04, F18-09-02 and F17-02. Thin sections were prepared from the core samples and from some of the washed cuttings to better understand the mineralogy (see Table 3.1.1).

Two different methods were used for S-isotope analyses. The first method was used on samples that contained pure anhydrite and/or gypsum minerals. For core samples the anhydrite and gypsum were microdrilled. For cuttings samples the anhydrite was picked under the binocular and hand powdered with a pestle and mortar. The second method was used on halite samples. In reference core TWR-480 pure halite was crushed and subsequently dissolved in de-ionised water. The unwashed, halite-rich cuttings from well F18-09-02 were directly dissolved in de-ionised water. After dissolution the samples were filtered through a 0.45 μm nitrate cellulose filter to remove any particles. The solutes were acidified with HCl to pH 2 and heated. BaSO_4 was precipitated with $\text{BaCl}_2 \cdot 2\text{H}_2\text{O}$ and filtered out. The rock powders and precipitates were measured on an EA-IRMS at Iso-Analytical Limited for their S-isotope composition. Reproducibility on $\delta^{34}\text{S}$ was better than ± 0.2 ‰.

C) Petrography

Optical microscopy analyses on thin-sections was performed to identify the lithology, mineralogy and porosity. Thin sections were prepared from the core samples of two reference cores (Well TWR-480 and K13-02) and from washed cuttings from wells F18-09-02 and F17-02. In total, 11 thin-sections were prepared. The rock material was impregnated in blue-dyed epoxy resin. The thin-sections were analysed on a Leitz optical microscope under plain (transmittent) and polarised light. This allowed for identification of mineral phases, lithology and texture (see Fig. 3.3.3). Mineral paragenesis was determined by assessing crystal habit. The volume percentages represent only a rough estimate of the actual lithology and mineralogy. The identification of clay mineralogy could not be achieved with the optical microscope due to the micro to nano-scale of the mostly detrital clay minerals and would require either scanning electron microscopy or XRD.

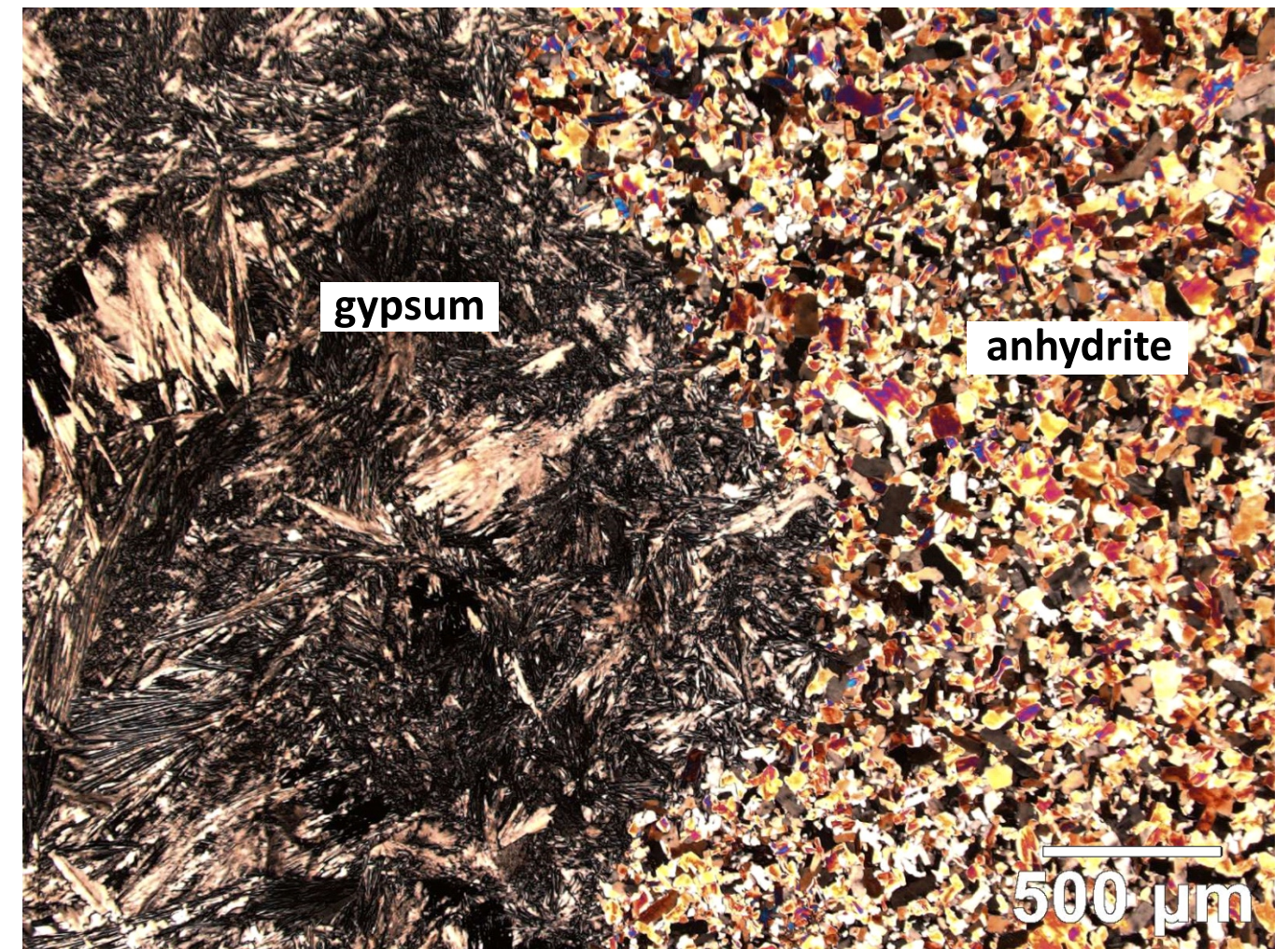


Figure 3.3.3: Well TWR-480 core piece from 438.8 under crossed polarised light. Needle-shaped gypsum crystals precipitated on the left side and anhydrite on the right.

An extensive database of 2D and 3D seismic data was used in this project (Table 3.1.2). The seismic interpretation was performed for three of the project 's phases (Table 3.4.1).

Phase 1: A regional mapping of the base and top Zechstein as well as the top Lower Triassic was performed. This was carried out using all publically available 2D and 3D seismic data in the study area (see Figs.3.4.1 and 3.4.2A and B). Time structure and time thickness maps for both the Zechstein and Lower Triassic were constructed. During this phase of the project other features were also identified and mapped, including salt features such as pillows, rollers, diapirs, welds and walls, as well as growth faults, rafts and collapse structures. The salt bodies were mapped using multi-z technique that allows to interpret salt bodies geometry even in the case of shallow salt bodies with overhangs.

Phase 2: Three case studies were carried out using primarily 3D-seismic data. For each case study multiple key horizons were mapped in 3D as well as key faults and salt bodies (carried out using multi-z technique) (Figure 3.4.2C). Time structure and time thickness maps were produce for each key horizon and intervals.

Phase 3: For the structural restoration, additional 2D and 3D seismic interpretation was carried out to create robust 2D interpreted seismic sections that were later used for the 2D structural restoration procedure. For each section a series of horizons were interpreted as well as faults and salt features.

Note that in addition to the interpretation of key horizons and structures, stratal terminations were identified and mapped in the Mesozoic section. These include truncations, onlaps and downlaps, which are represented as black half arrows on the interpreted seismic panels.

	Phase 1	Phase 2		
		CS 2.1	CS 2.2	CS 2.3
Base autochthonous salt	X	X	X	X
Top autochthonous salt	X	X	X	X
Multi-Z allochthonous salt	X	X		X
Top Lower Triassic (RB)	X	X		X
Top Volpriehausen Fm			X	
Base Muschelkalk Evaporite Mb		X	X	
Base Altena Gp or Top U. Jura		X	X	X
Base Kimmeridge Clay Fm.				X
Base Seq 2 (Up. Juras)				X
Base Seq 3 (Up. Juras)				X
Base Rijnland Gp				X
Base Chalk Gp				X
Salt welds		X	X	X
Faults		X	X	X
Time thickness maps		5	6	9

Table 3.4.1: Seismic interpretation carried out in project's phases 2 and 3.

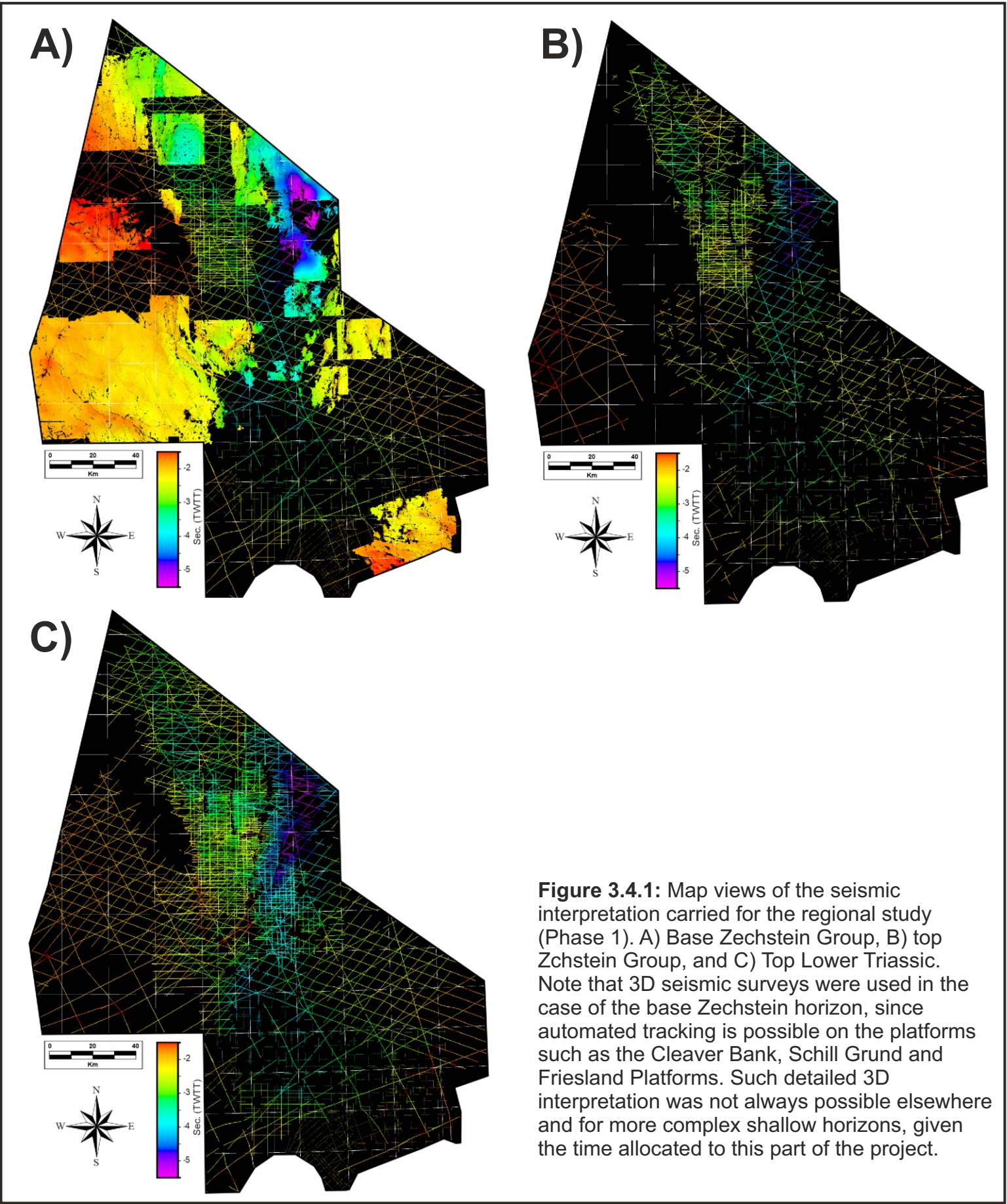


Figure 3.4.1: Map views of the seismic interpretation carried for the regional study (Phase 1). A) Base Zechstein Group, B) top Zchstein Group, and C) Top Lower Triassic. Note that 3D seismic surveys were used in the case of the base Zechstein horizon, since automated tracking is possible on the platforms such as the Cleaver Bank, Schill Grund and Friesland Platforms. Such detailed 3D interpretation was not always possible elsewhere and for more complex shallow horizons, given the time allocated to this part of the project.

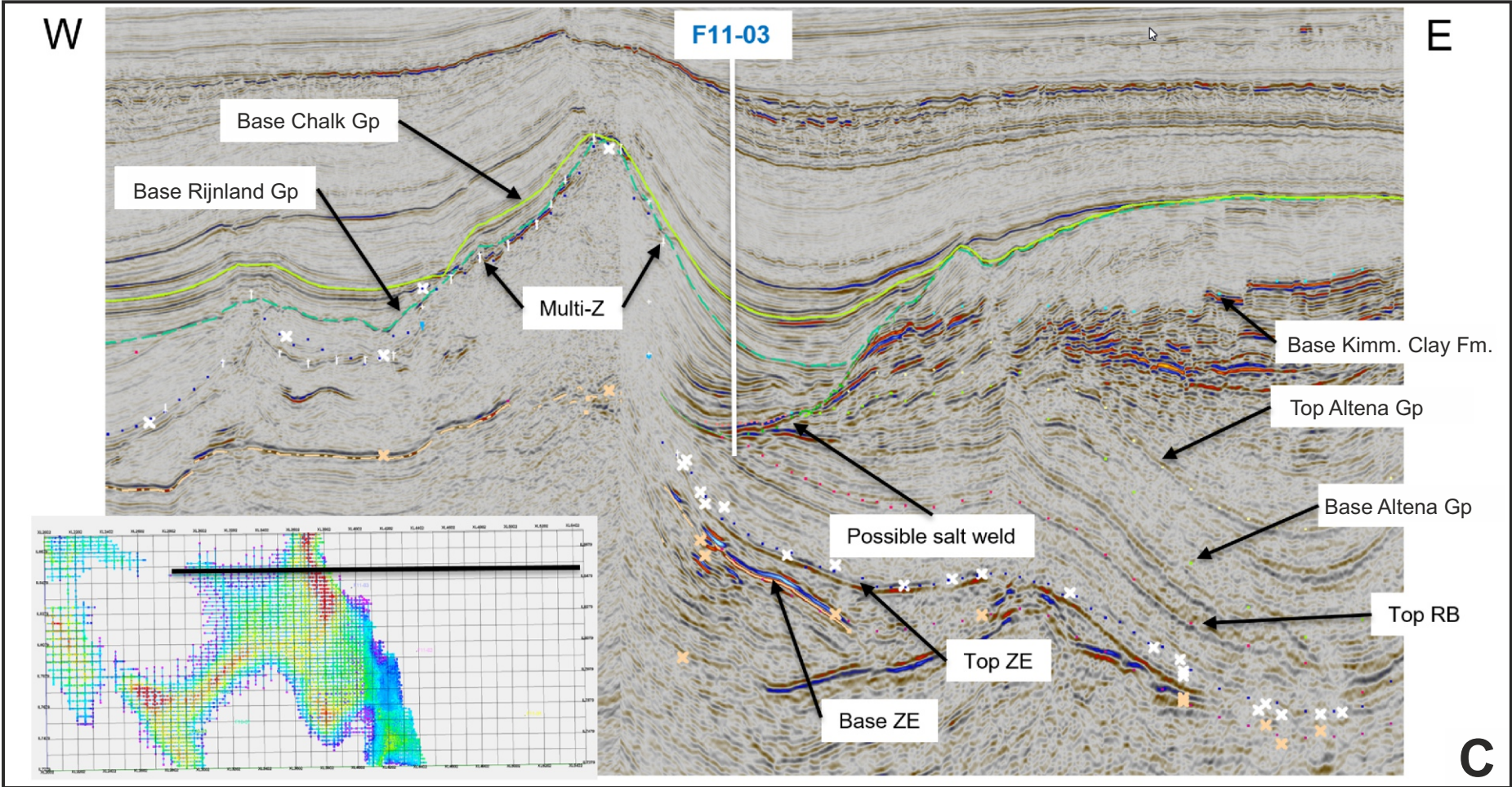
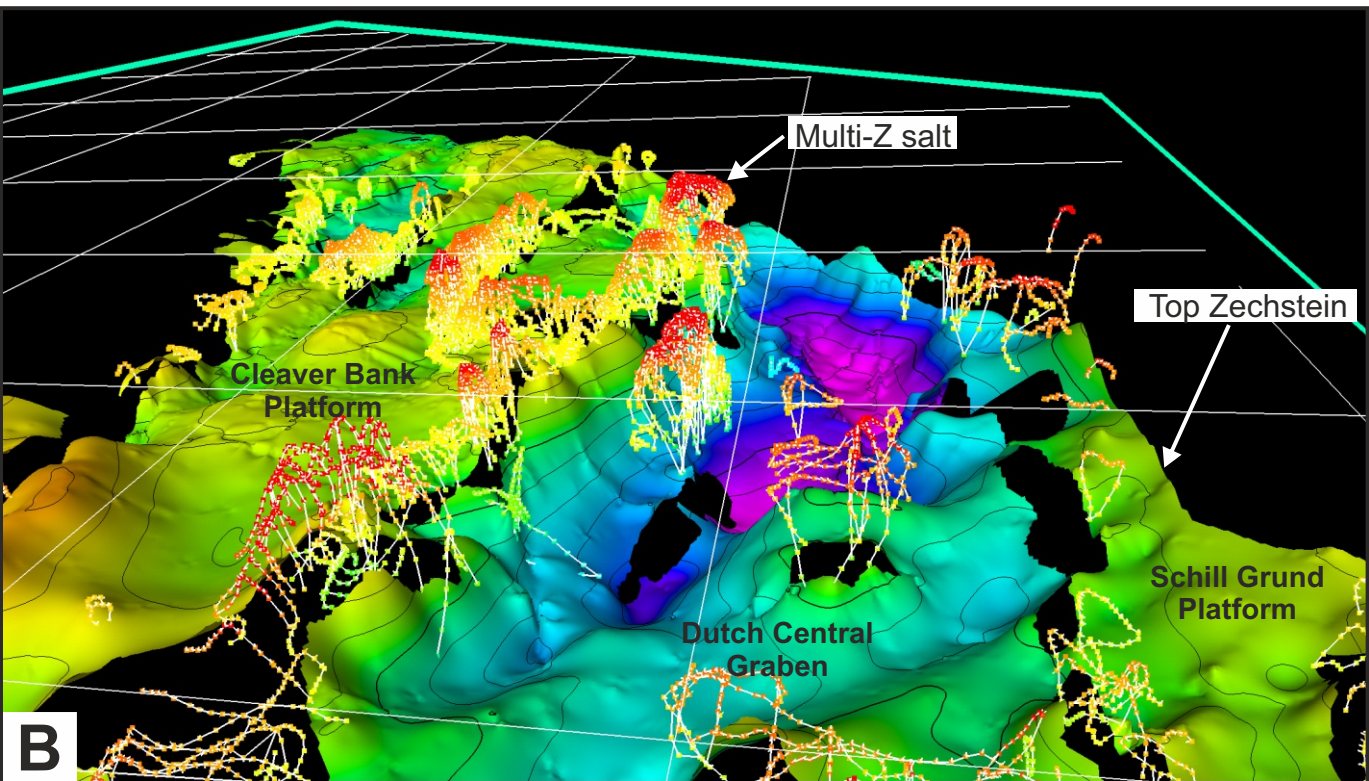
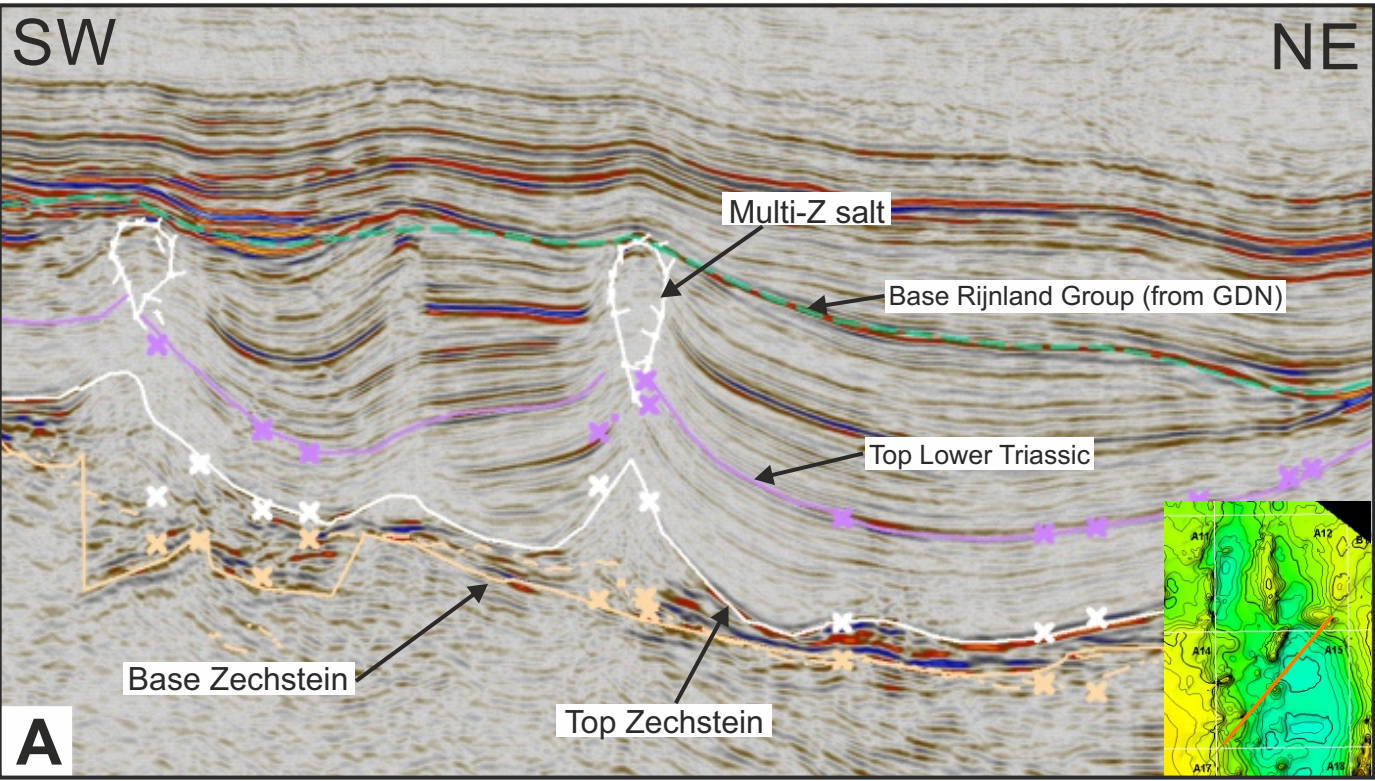


Figure 3.4.2: The seismic interpretation was carried out at different level of detail for the regional study (A and B) and the case studies ©.

A) Example of a 2-D seismic interpretation carried out in Phase 1 of the project. Some shallow horizons, such as the base Rijnland Group, displayed in most of the seismic examples shown in this report are from the Dutch Geological Survey mapping team. Those horizons are used to support the seismic interpretation carried out in this project.

B) Perspective view of the top Zechstein surface and the top shallow salt bodies (multi-z mesh) interpreted during Phase 1. In some areas the multi-z interpretation was difficult due to lack of 3D seismic data coverage or due to seismic data quality. The eastern part of the DCG and the Schill Grund Platform were especially difficult to interpret.

C) Example of an E-W interpreted seismic section from Phase 2 (case studies). All horizon displayed here were specifically interpreted for this project. See Chapter 4 for additional information regarding this section.

Three 2D structural restorations have been carried out for this project, one per case study. Once a 2D section was selected for the structural reconstruction, the seismic data was imported into Move2D software (Midland Valley Ltd.) and the horizons were interpreted.

A) Data preparation

When necessary, the 2D sections were extended further than originally planned to include additional key structural features (e.g. in the second case study). Depth-converted seismic data was used when available (e.g. in the first case study: F17/F18) . If only data in time domain was available, additional 2D sections were used to tie neighbouring wells to the focus 2D line. The wells were used to create simple, linearly depth-dependent velocity profiles for each formation. These were used for the time-to-depth conversion. Subsequently, the interpreted horizons were cleaned up (mainly around and below salt structures) and the basement was simplified to consist of mostly horsts and grabens without much small topography within each structural block. The resulting sections are considered to be the best interpreted depth section using all data available. These sections were the starting point for the subsequent restorations.

B) Restoration procedure

The structural reconstruction workflow consists of a number of steps, which were repeated for each formation:

1) Decompaction

In order to appropriately model deformation and decompaction of rocks, rock properties were assigned to every interval of the model. These properties were based on lithological information from the Terschelling basin (Verweij, 2009) and Cleaverbank Platform (Fattah, 2012), using the standardized lithologies defined in Tables 3.5.1 and 3.5.2.

For all post-Permian intervals a Sclater-Christie compaction curve was applied (Sclater and Christie, 1980). Salt is assumed to be incompressible and assigned a decompaction value of 0. Sclater-Christie decompaction curve assumes that porosity decreases with increasing depth and can be represented by:

$$f = f_0 \exp(-cy)$$

Where *f* = Present-day porosity at depth; *f*₀ = Porosity at the surface; *c* = Porosity-depth coefficient (km⁻¹); *y* = depth (m).

Lithology	Initial porosity	Decompaction factor (km ⁻¹)	Density (kg/m ³)
Sandstone	0.49	0.27	2650
Shale	0.63	0.51	2720
Chalk	0.70	0.71	2200
Salt	0.00	0.00	2200
Marl	0.50	0.50	2700

Table 3.5.1: Standardized rock properties for all relevant rock type (van Widen et al., in press)

2) Salt movement, fault movement and addition of eroded strata

Although this step contains three processes, they are often intertwined, and do not necessarily occur in the same order each time, or even at the same time everywhere in the section. Whenever possible, the seismic data was used to infer the timing of events and the amount and extent of erosion. Salt was typically moved as a result of geometrical constraints (passive salt movement), except in cases where a salt welds indicated the presence of salt or where a certain structural model was tested.

3) Unfolding

After the uppermost formation was judged to have been restored in terms of erosion and fault movement, the section was unfolded to achieve a flat topography. Typically, the unfolding was performed separately for each structural element, so that the unfolding algorithm could be chosen based on the expected driving force (i.e. flexural slip unfolding for tectonically driven folds and vertical simple shear for salt-driven uplift).

4) Additional notes on the reconstruction

- In the process of restoration, intervals were backstripped, moving from young to older intervals. As a response the underlying rocks decompaction, the section is adjusted isostatically. Due to the limited extent of the sections, applying Airy isostasy would lead to exaggerated local uplift. It was therefore decided to apply a section-wide uplift based on the expected depositional depth of the uppermost formation after each backstripping step.
- When needed, jagged/wiggly lines were smoothed to represent a more geometrically likely scenario. This holds especially for older (Late Jurassic and Triassic) formations, which were subjected to the largest amount of restoration steps.

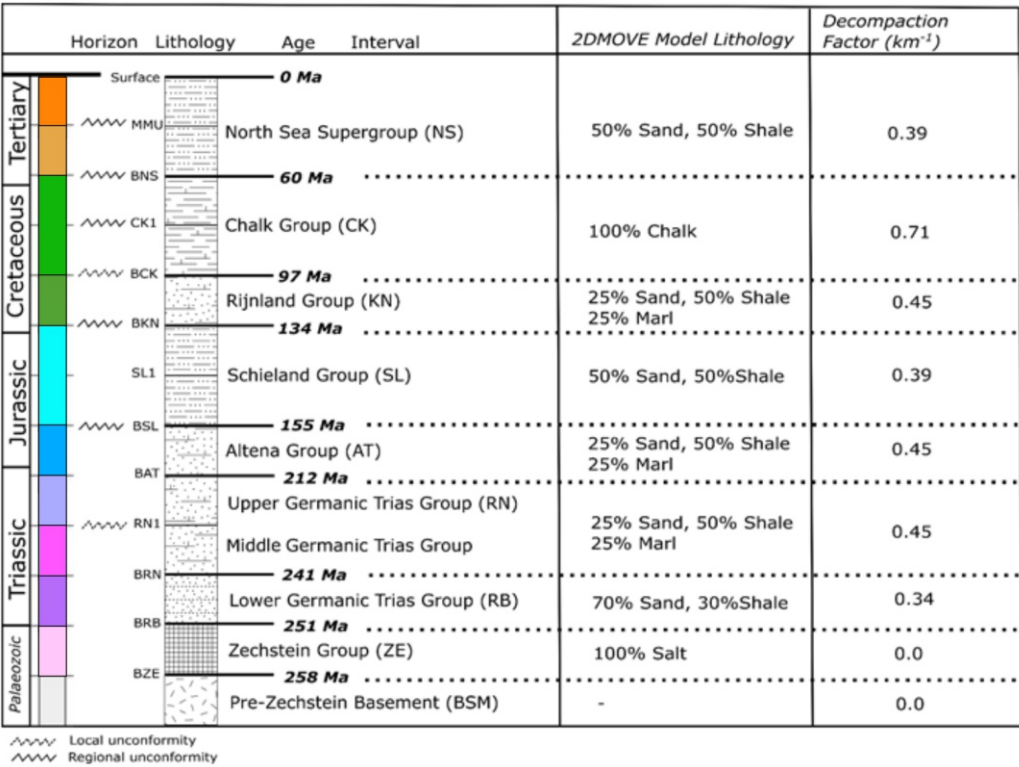


Table 3.5.2: Restoration model stratigraphy including lithologies and decompaction factors (van Winden et al, in press).

RESULTS

PALYNOLOGY, PETROGRAPHY and GEOCHEMISTRY

4.1

4.1 Results - Palynology

The main research question of the STEM project is to unravel the timing and magnitude of salt movement and its effect on sediment dispersal and deposition. To answer this question it is imperative to be able to assess the age of the - remobilized - salt at critical locations. However, dating salt units is challenging, as salt is generally barren of microfossils and not unique in its chemical expression. Nevertheless, a palynological and geochemical study was conducted to in an attempt to characterise and distinguish the Triassic and Permian salt units, based on geochemical and/or palynological parameters (Figs. 4.1.1 to 4.1.3)

For the method to be developed, a boundary condition was that the method should be applicable for cuttings samples. This chapter describes and discusses the results of the palynological study. The results of the geochemical study are described further in this Chapter 4.1

A) Approach

To develop the aforementioned method, a two-phased approach was necessary:

- 1) The first phase consisted of a reference study. A standard needed to be developed for the main salt units. Therefore, cores from known salt layers were analysed for palynology, in order to 'fingerprint' these layers on palynological characteristics.
- 2) The second phase consisted of a feasibility study. From the first STEM case study, the F17-F18 area, a well with an enigmatic salt body was selected to test the applicability of the palynological fingerprinting method on cuttings samples.

B) Results of Phase 1 (regional study)

1) A palynological reference for the Zechstein salt.

The halite and presumed dolomitic core samples from the Zechstein of well A18-02-S1 were all barren of palynomorphs. The core samples from the black stringers of well A18-02-S1 yielded Permian pollen and spores (Fig. 4.1.2). These included *Lueckisporites virkkiae*, *Scutasporites unicus* and *Vittatina* spp. The pollen and spores were dark-coloured, compared to the pollen and spores encountered in well G10-01 (Fig. 4.1.2). The anhydrite core samples from the Zechstein of well G10-01 was barren in palynomorphs. The core samples from the black stringers of well G10-01 yielded rich and well-preserved Permian pollen and spores (Fig. 4.1.2) including *Vittatina* spp, *Klausipollenites schaubergeri*, and *Lueckisporites virkkiae*. The well-preserved pollen and spores were also studied using incident ultra-violet light. The pollen and spore specimens displayed a surprisingly bright fluorescence, which would be generally interpreted as thermally immature organic matter. Note that in one sample (G10-01; sample 2666.2m), next to the Permian palynomorphs, also Jurassic pollen and spores were encountered. Contamination from the laboratory processing can never be excluded, but it most likely that the Jurassic palynomorphs are actually encased in the specific black stringer at that depth.

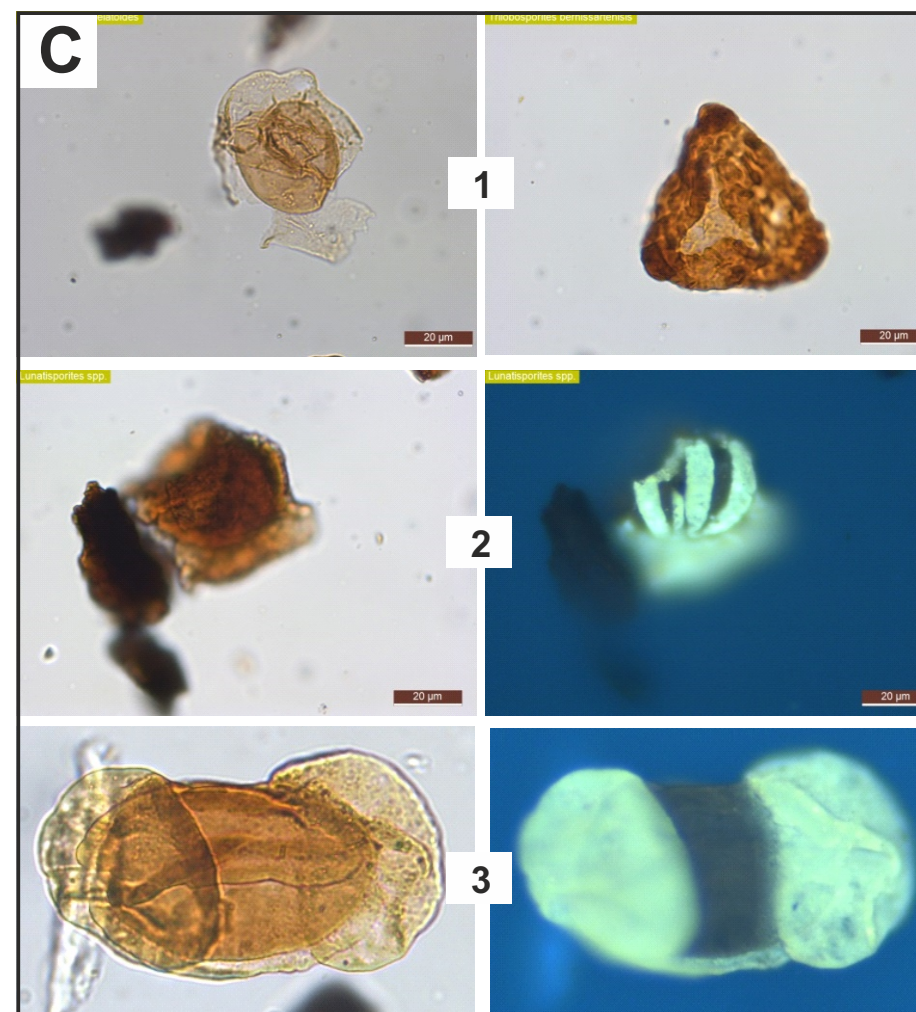
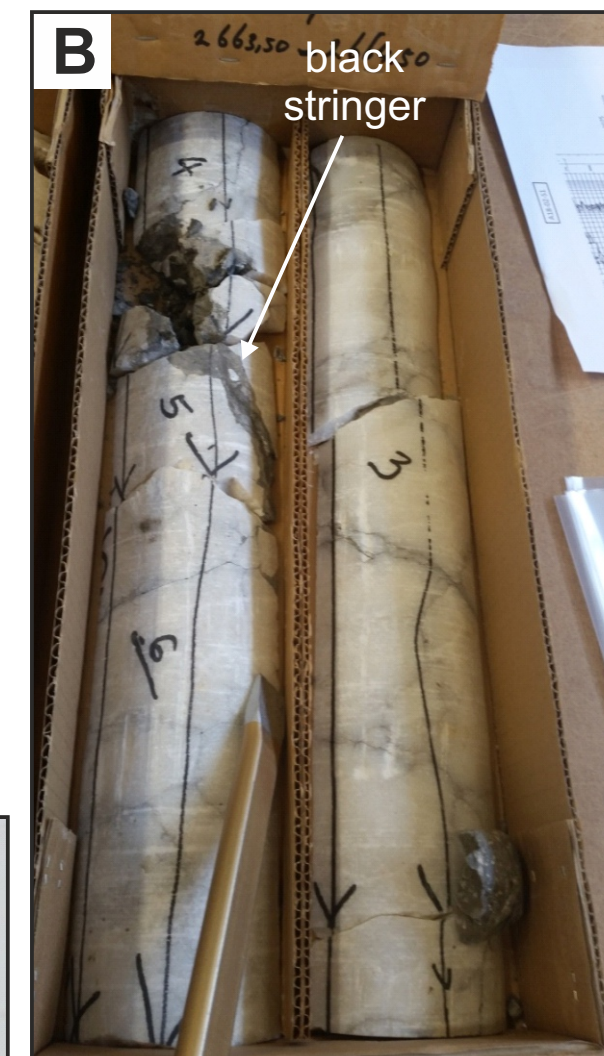
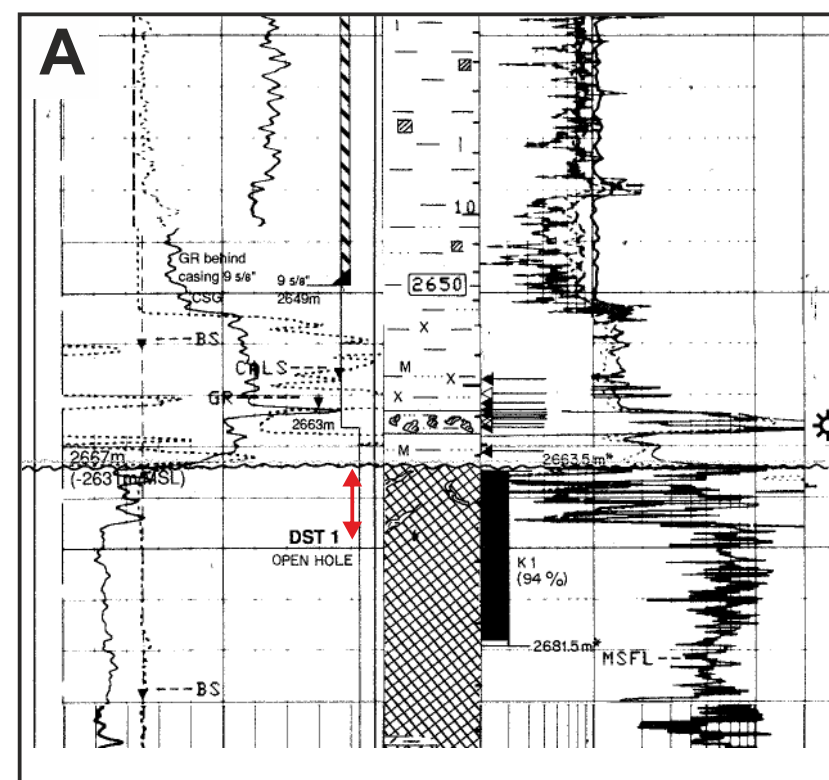


Figure 4.1.1: Palynological results from core samples of the Zechstein Group of well G10-01.

A) Composite log showing the position of the core (black rectangle) and the part studied (red arrow).

B) Photo of one of the cored section studied. Note the black stringers that yielded Permian pollen and spores with excellent preservation.

C) Microscope images of several pollens and spores. Note the bright fluorescence observed in the Permian pollen and spores under incident UV light. (1) Jurassic and Cretaceous pollen and spores from the black stringer sampled at 2666.2 m. (2) Permian pollen from black stringer sampled at 266.2 m. (3) Permian pollen from black stringer sampled at 2664.1 m

4.1 Results - Palynology

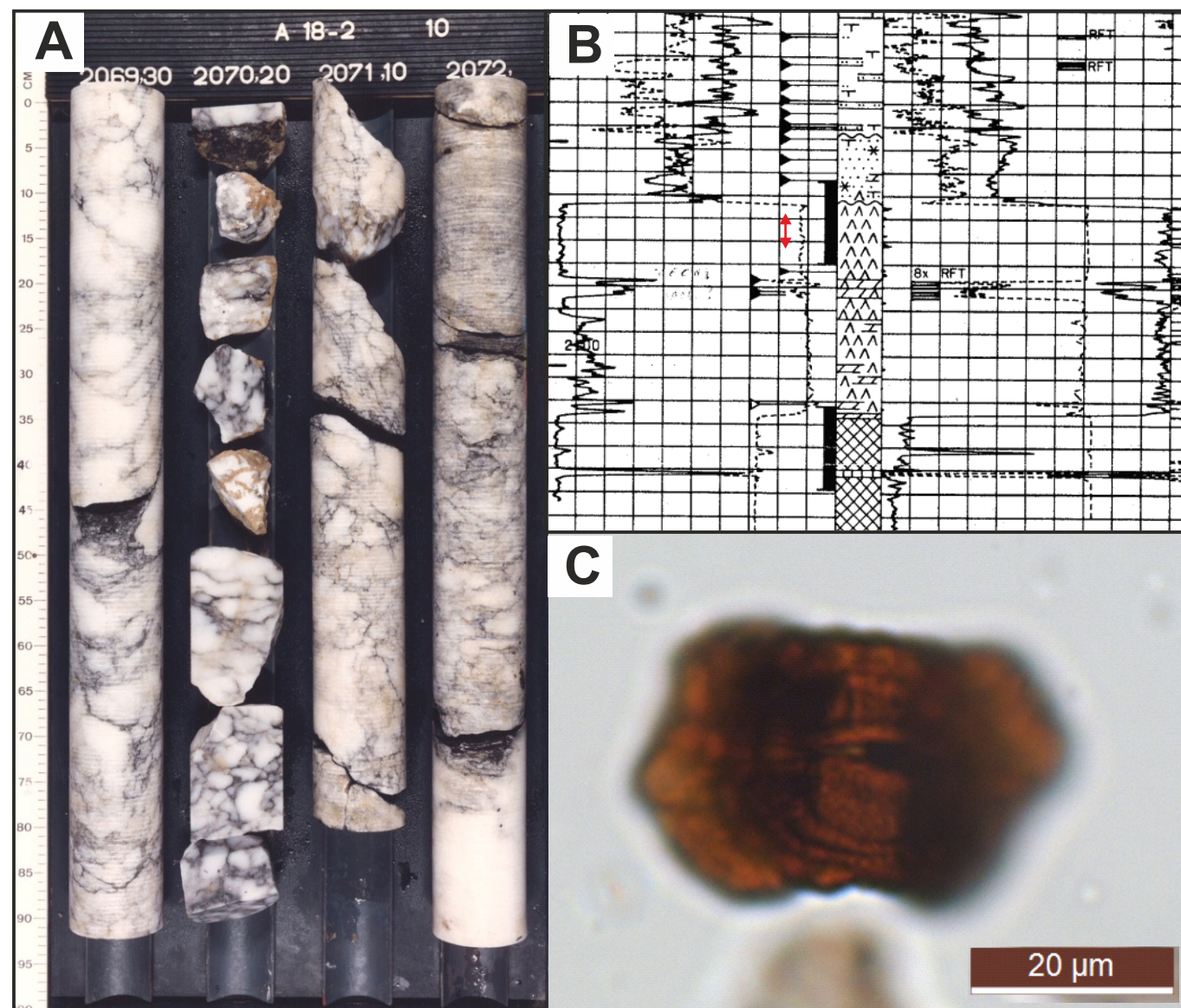


Figure 4.1.2: Palynological results from core samples of the Zechstein Group of well A18-02-S1. The black stringers yielded Permian pollen and spores that have dark colours. **A)** Photo of one of the cored section studied. Note the black stringers that yielded Permian pollen and spores with excellent preservation. **B)** Composite log showing the position of the core (black rectangle) and the part studied (red arrow). **C)** Microscope images of a Permian pollen from a black stringer sampled (2072.2 m).

2) A palynological reference for the Main Röt Evaporite Member.

The halite core samples from the Main Röt Evaporite Member of well K13-02 were all barren. The core samples from the Main Röt Evaporite Member of well K13-02 that contained siliclastic material, all yielded Triassic palynomorphs (Fig. 4.1.3). These included *Triadispora* spp., *Aratrisporites* sp., *Kuglerina meieri* and *Angustisulcites* sp. However, the richness and diversity of the assemblages was low. The samples from red-coloured Solling, Hardegsen and Rogenstein Members were all barren. The halite core samples from the Main Röt Evaporite Member of well TWR-480 were all barren. The core samples from the shales of the Main Röt Evaporite Member of well TWR-480 yielded very rare and poorly preserved Triassic palynomorphs including *Angustisulcites grandis* and *Striatoabietites balmei*.

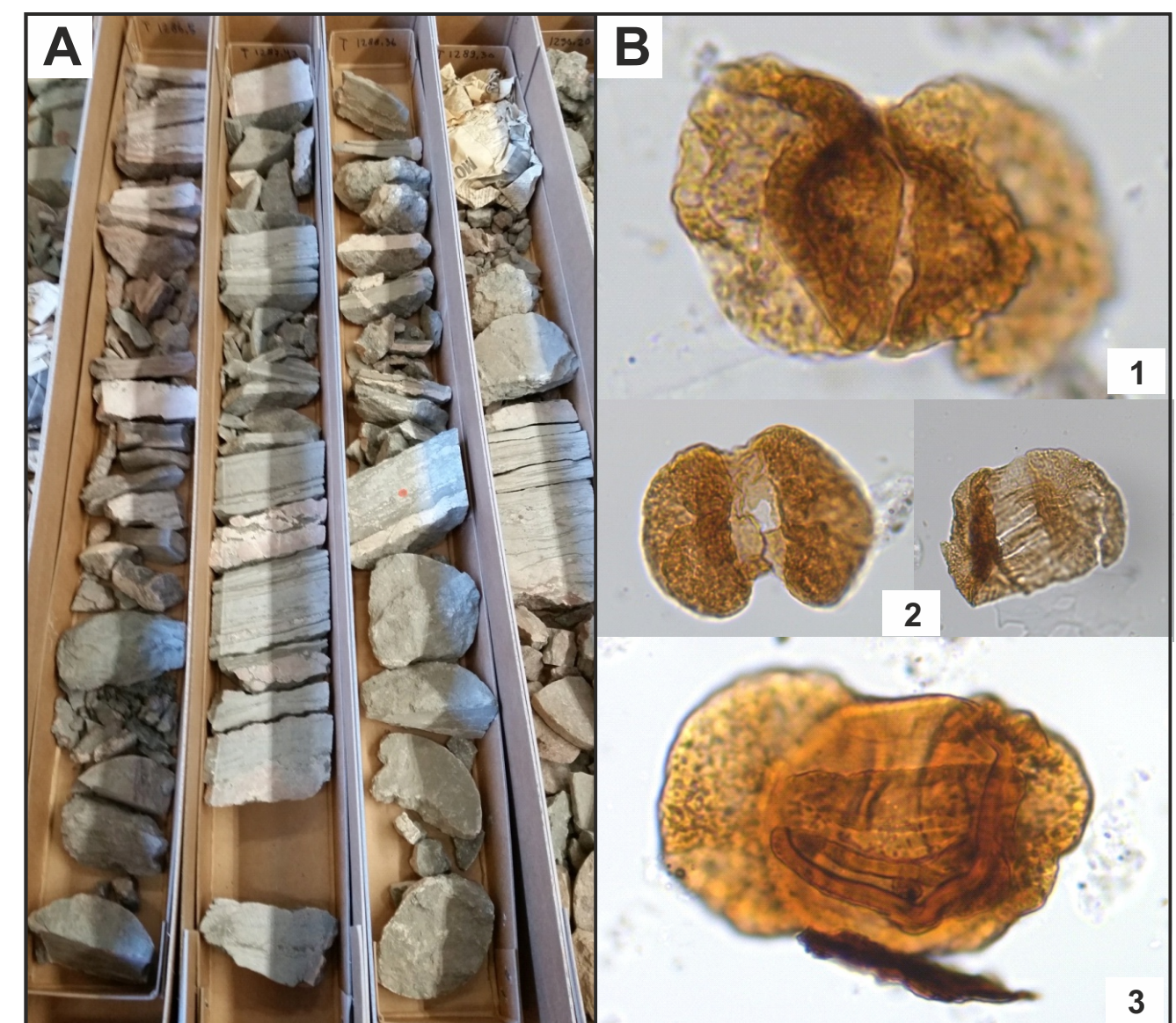


Figure 4.1.3: Palynological results from core samples of the Main Röt Evaporite Member and surrounding layers of well K13-02. The marly and mixed facies samples of the Main Röt Evaporite Member all yielded Triassic pollen and spores, albeit in relatively poor and low diversity assemblages. The samples from the red-coloured Solling, Hardegsen and Rogenstein Members were barren. **A)** Photos of one of the cored section studied. **B)** Microscope images of pollens and spores from (1) the Top Main Röt Evaporite Shaly/marly facies sampled at 1288.1 m; (2) the mixed facies sampled at 1296.4 m; and (3) the base of the Main Röt Evaporite Member sampled at 1300.4 m.

C) Results of Phase 2 (case studies)

The palynological analyses on cuttings samples from the Triassic, including salt from the Muschelkalk Evaporite and the Main Röt Evaporite Member, were disappointing. All samples yielded very poor to barren assemblages, with no conclusive age derivations.

4.1 Results - Petrography

Thin section descriptions are shown in Figures 4.1.4 to 4.1.7. Thin section analyses shows that core samples consist mainly of anhydrite, halite and gypsum with minor carbonate, detrital clay and litho-clasts. Halite is a major component (Fig. 4.1.4A) but it can only be seen in the core samples as the cuttings have to be pre-washed. In core material from well TWR-480 minor hematite (<0.3%) co-occurs with siliciclastic material. For most of the samples, the reddish part is composed of micro-carbonate, disseminated in a halite matrix. The pinkish color of the evaporites is due to Fe and other elements in the halite/gypsum matrix. Rare carbonate microcrystals (non-idiomorph) are disseminated in the gypsum matrix. Clay- and silt bands with quartz grains were observed that contain ca. 50% anhydrite. Mica, being mostly biotite, is common. In core K13-02 carbonate (presumably calcite) seems to have formed either syndepositionally post-anhydrite or was secondarily (diagenetically) dissolved and reprecipitated. Observations of straight carbonate edges point to a pre-anhydrite formation, supporting the second explanation (Fig. 4.1.5). Micritic carbonate patches are also present that contain some quartz, silt, clay, mica and on rare occasions microfauna.

Cuttings samples from F18-09-02 consisted mostly of halite before washing. The remaining material from well F18-09-02 consists of haematitic claystone/siltstone, micritic carbonate and anhydrite (< 5%) that is commonly interlayered with clay (Fig. 4.1.2.6). Several cuttings fragments contain considerable amounts of anhydrite (~25%) and some dolomite cement. Well F17-02 cuttings contain mostly siltstones and sandstones, with common anhydrite, gypsum and clay. Anhydrite and gypsum make up 15 to 20% of the washed material. Occasionally carbonate precipitated in the siltstones (Fig. 4.1.7). The red-brownish color is due to minor haematitic staining. Thin sections were not acquired from well L09-04. Macroscopic observations point to large amounts of halite with minor siliciclastic components.

The results show that the evaporative sulphur minerals anhydrite and gypsum are common both in the reference core as in the picked cuttings to be able to perform S-isotope analyses. The cuttings samples for well L09-4 were not acquired because the salt intervals consisted to a large amount of halite that was dissolved during washing. For these samples halite needs to be dissolved and sulphate reprecipitated for S-analyses. Sr is a minor constituent of carbonates and a low trace element in anhydrite. Carbonates are rare to non-existent both in cores and in the cuttings and thus insufficient to perform Sr analyses. For Sr extraction from anhydrite a lengthy extraction and measurement procedure is required that exceeds the timing and budget of the STEM project.

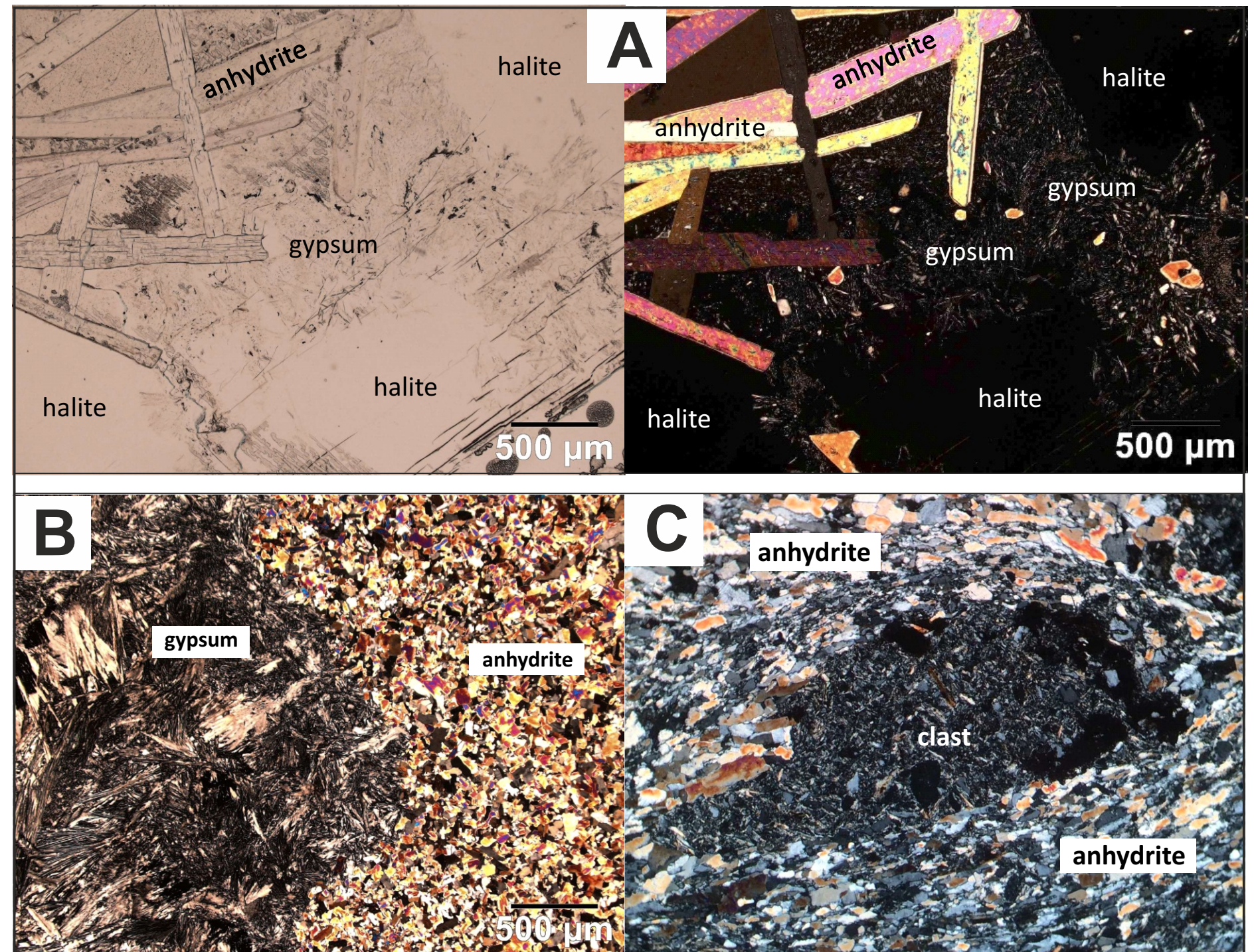


Figure 4.1.4: Thin section photography of Main Röt Evaporite Member core samples from well TWR-480.

A) Plain (left) and crossed polarised (right) light images from a sample at 414.8 m. The majority of crystals are halite. Large anhydrite crystals build up ca. 5% of the section. They are partially surrounded by gypsum in halite matrix.

B) Crossed polarised light image of sample 438.8 m. Needle-shaped gypsum crystals precipitated on the left side and anhydrite on the right.

C) Crossed polarised light image of a sample at 484.9 m. A lithic fragment consisting of quartz, clay and mica minerals is imbedded in an anhydrite matrix. This sample is mostly composed of anhydrite (85%), interlayered with silt/clay.

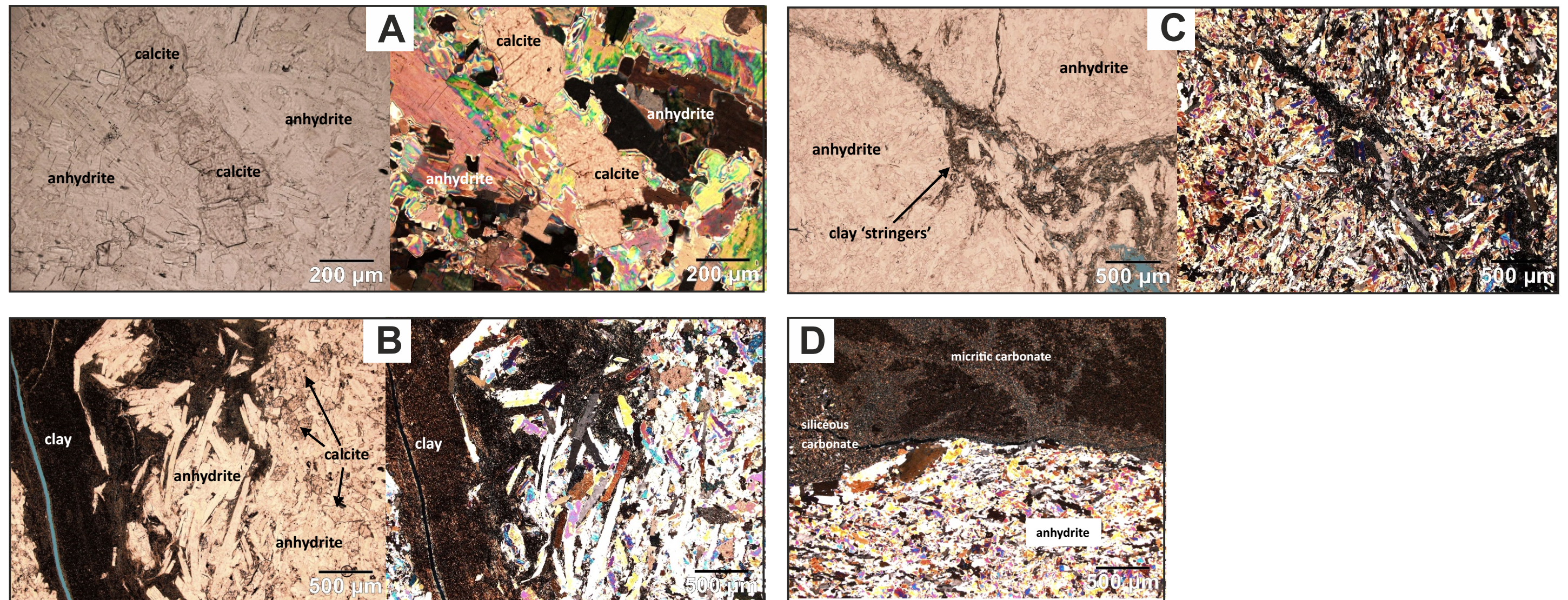


Figure 4.1.5: Thin section photography of core samples from well K13-02. **A)** Plain (left) and crossed polarised (right) light images of Main Röt Evaporite Member sampled at 1292.8 m, composed of anhydrite (80%) and carbonate (15%). **B)** Plain (left) and crossed polarised (right) light images of Main Röt Evaporite Member sampled at 1291.9 m, composed of anhydrite (70%), carbonate (20 – 25%) and clay 'stringers' with minor hematite staining (~10%). **C)** Plain (left) and crossed polarised (right) light images of Main Röt Evaporite Member sampled at 1288.9 m, composed of anhydrite (95%) and silt/clay stringers of ductile rock fragments (mica and some carbonates). **D)** Crossed polarised light image of Röt Claystone Member core sample 1284.8 m, composed of anhydrite veins. The red-brown patches are haematitic, silty martial, partially with micritic carbonate.

4.1 Results - Petrography

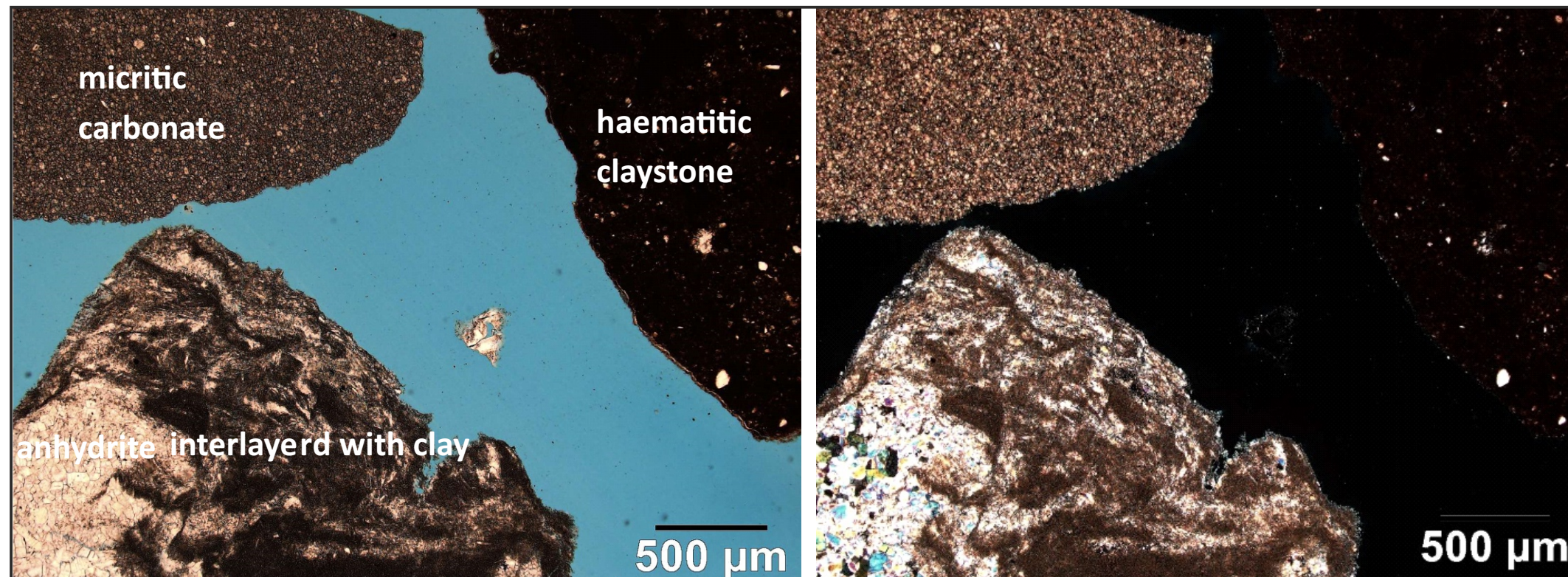


Figure 4.1.6: Thin section photography of Main Röt Evaporite Member cutting samples from well F18-09-02. Plain (left) and crossed polarised (right) light images from sample 4225.0 m. These cuttings pieces are composed mainly of haematitic claystone/siltstone, micritic carbonate and minor anhydrite interlayered with clay.

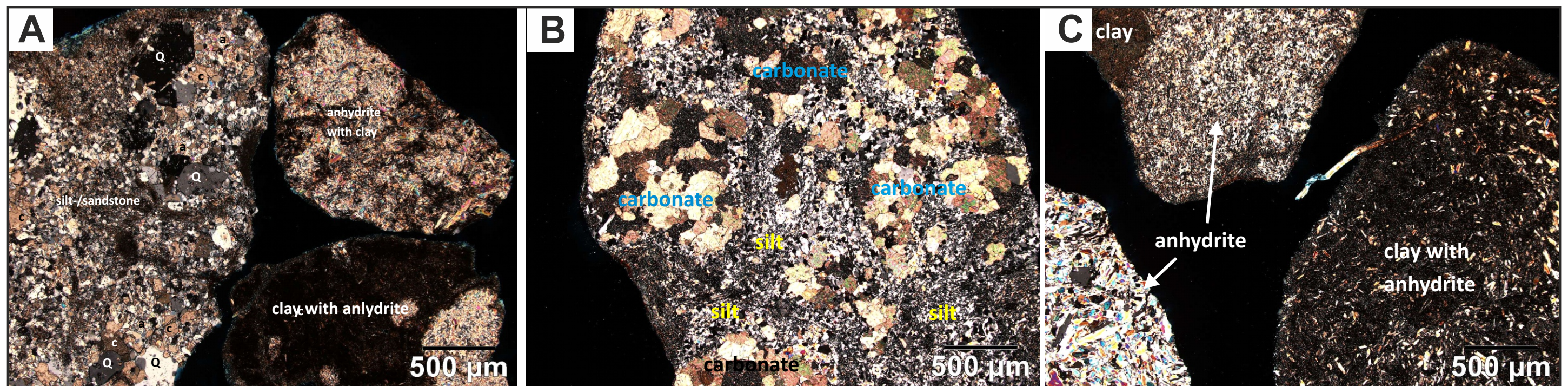


Figure 4.1.7: Thin section cross-polarized light photography of Main Röt Evaporite Member cutting samples from well F17-02. **A)** Cuttings sample from 2560 m. The silt/sandstone fragment is composed of quartz grains (Q) with quartz overgrowths and contains carbonate (c) and anhydrite (a) cement. The other fragments are mostly calcareous claystones with anhydrite patches. **B)** and **C)** Cuttings sample from 2610 m, composed of claystone and quartzite clasts containing dolomite cement and anhydrite.

4.1 Results - Geochemistry

Results of the isotope analyses can be found in Table 4.1. The $\delta^{34}\text{S}$ of reference core samples ranges from 24.5 to 27.0 ‰. Average $\delta^{34}\text{S}$ in core TWR-480 samples is 26.6 ‰ and core K13-02 25.3 ‰. Values of the two methods for S-isotope analyses were similar. S-isotope values from case study cuttings range from 15.2 to 26.1 ‰.

The S-isotope values from the reference sections are similar throughout the sequence that consists of Main Röt Evaporite and lower Röt Claystone Members (Fig. 4.1.8). There is also very little difference (~ 1 ‰) between $\delta^{34}\text{S}$ in wells TWR-480 and K13-02. The difference may be due to the fact that different S-containing phases (anhydrite, gypsum, halite) were analysed, related to the evaporative isotope fractionation (Raab & Spiro, 1991). Isotope data from well TWR-480 provides evidence that both S extraction and direct measurement on powdered samples are reliable. When compared to the global S-isotope curve the reference cores overlaps with the Röt Evaporite data from other European sections (Fig. 4.1.9). Regarding that there is a large shift in $\delta^{34}\text{S}$ between 240 and 250 Ma. it is likely that the running 50ka average does not capture the intermediate stages of the changing S-isotope values. The $\delta^{34}\text{S}$ values of the reference section still fit well into the global isotope trend and can be used as reference values for the Röt evaporites. The two lower sample from well F18-09-02 are classified by NAM in the composite well log as Main Röt Evaporite Member (Fig. 4.1.10). For the two samples we received $\delta^{34}\text{S}$ value of between 25 and 26 ‰, which is identical to the Main Röt Evaporite Member values in the two reference sections (Fig. 4.1.9). This is in agreement with the allocated stratigraphy by NAM and also supports the fidelity of the reference values. The 18.7 ‰ value for the Muschelkalk Evaporite Member is somewhat lower than expected when compared to the global S-isotope curve but still in the acceptable range for the age span.

One of the well L09-04 samples come from the level classified by Statoil as Main Röt Evaporite Member and has the $\delta^{34}\text{S}$ value of 25 ‰. This value falls into the range of the Main Röt

Evaporite Member values from the reference section and from well F18-09-02. This confirms that the sample belongs to the Main Röt Evaporite Member. The other two samples were considered to belong to the Röt Claystone Member. The moving average from the global S-isotope curve shows similarity with this sample around 440 Ma. However the values are very low compared to the Röt values from European and reference sections. Interestingly the values are, within error (analytical error bar for is less than 0.3 ‰, which is less than the size of the symbols in Figures 4.1.8 and 4.1.10), identical to the Muschelkalk Evaporite Member from well F18-09-02 (Fig. 4.1.10). It is thus more likely that the evaporites are of Muschelkalk Evaporite Member age (or younger?).

Only two samples were measured in well F17-02. According to the stratigraphic classification by NAM (taken from the composite log) the lower sample with the $\delta^{34}\text{S}$ of 15 ‰ belongs to the Lower Keuper Claystone and the upper sample with the value of 13 ‰ to the Main Keuper Evaporite (Fig. 4.1.10). Although the bottom sample with 15 ‰ does not comply with the moving average global isotope curve it falls within the lower limits of the European Keuper values and may therefore belong to the Keuper Formation. The upper sample has a very low value of 13 ‰ (Fig. 4.1.9) and falls entirely outside the global average and the European Keuper values (Fanlo & Ayora, 1998). Stratigraphically younger Jurassic rocks have values around 13 ‰. However, it is unrealistic for this interval to belong to the Jurassic as the Jurassic is well dated in the well. The other possibility is that the evaporite belongs to remobilised Zechstein deposits. The $\delta^{34}\text{S}$ value of the upper sample falls on the global S-isotope curve but is higher than what has been measured for the European Zechstein evaporites (Fig. 4.1.9). This leaves the age of the upper sample debatable. Further samples from this level should be analysed to confirm the low isotope values. The results also indicate that dating with S-isotopes is difficult due to the lack of a good $\delta^{34}\text{S}$ reference curve not only for Rot but also for other evaporite ages.

The outcome and discussion regarding these results are presented in Chapter 5.

Well	Depth	Method	$\delta^{34}\text{S}_{\text{V-CDT}}$
TWR-480	438.8	microdrilled	26.3
TWR-480	463.0	dissolved and re-precipitated	27.0
TWR-480	465.8	microdrilled	26.2
TWR-480	474.1	dissolved and re-precipitated	26.8
K13-02	1284.50	microdrilled	24.5
K13-02	1288.00	microdrilled	24.5
K13-02	1289.90	microdrilled	25.2
K13-02	1291.90	microdrilled	25.5
K13-02	1294.40	microdrilled	25.6
K13-02	1295.45	microdrilled	24.8
K13-02	1297.10	microdrilled	26.5
K13-02	1298.90	microdrilled	25.7
L09-04	3255	ground pieces	18.3
L09-04	3258	ground pieces	18.6
L09-04	3336	ground pieces	25.1
F18-09-02	3935	dissolved and re-precipitated	18.7
F18-09-02	4045	dissolved and re-precipitated	25.3
F18-09-02	4170	dissolved and re-precipitated	26.1
F17-02	2580	ground pieces	13.3
F17-02	2610	ground pieces	15.2

Table 4.1: Isotope analysis results

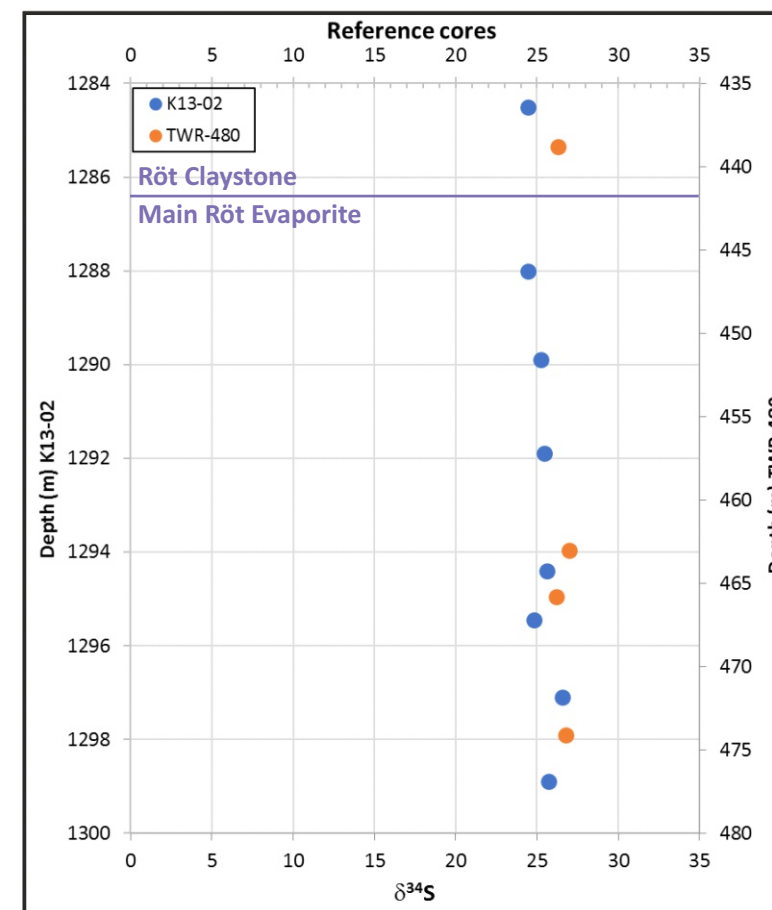


Figure 4.1.8: S-isotope values from reference core TWR-480 and K13-02. The scale and the reported stratigraphic unit is to the left for well K12-02 and to the right for well TWR-480.

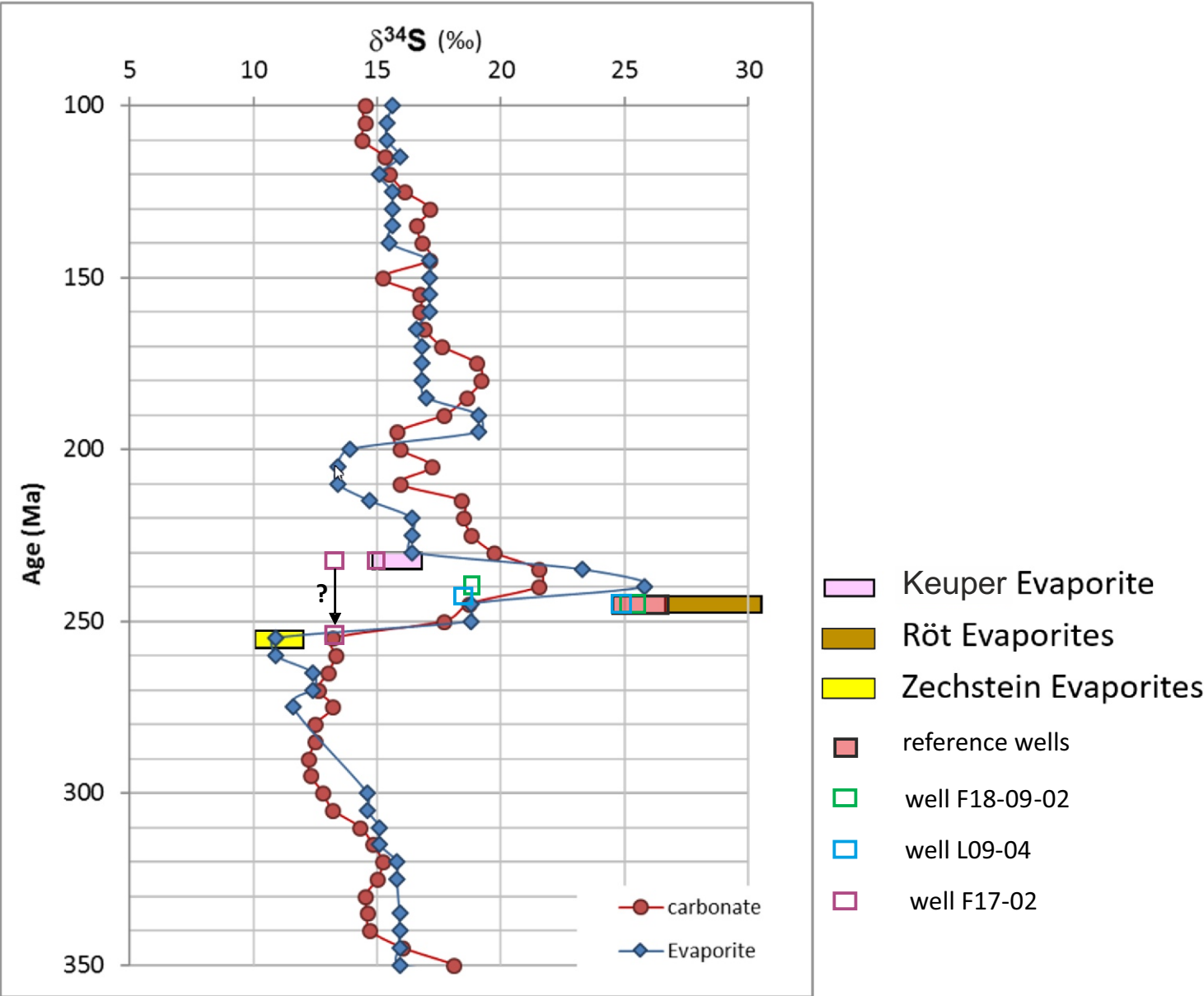


Figure 4.1.9: S-isotope results from this study plotted on the S-isotope curve from literature compilation. See Figure 3.3.2 for information regarding the background curves.

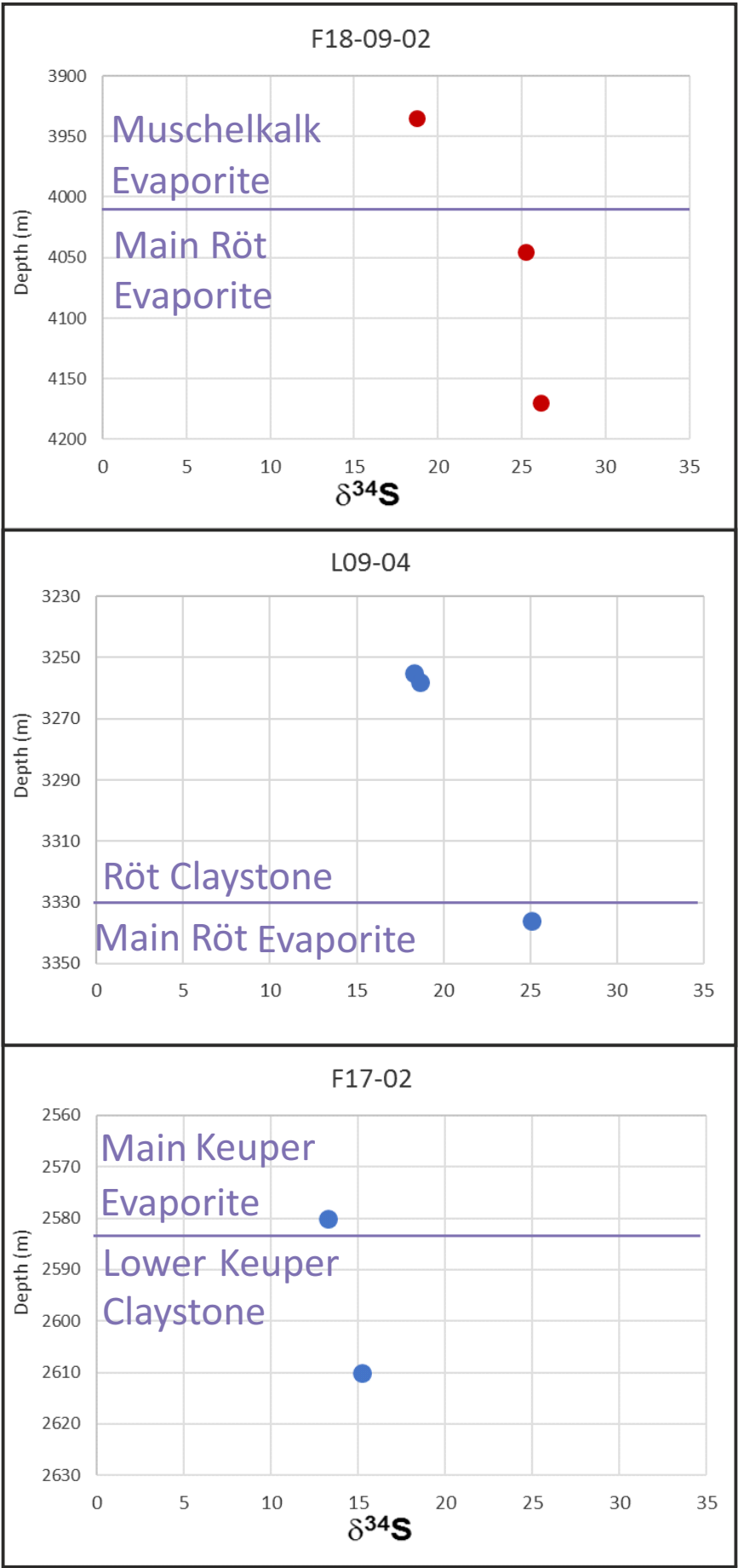


Figure 4.1.10: S-isotope values from case study wells F18-09-02, L09-04 and F17-02. Blue circles indicate S-analysed on powdered cuttings and red circles on BaSO_4 precipitates. Stratigraphic units are taken from the composite logs.

RESULTS
REGIONAL
STRUCTURAL
ANALYSIS

4.2

To better understand the early salt tectonics in the study area, three horizons were regionally interpreted, the Base Zechstein, the top Zechstein and the top Lower Germanic Trias Group as well as relevant syn-depositional faults and salt features. The time structure maps of each horizons are shown in Figures 4.2.1 to 4.2.3 and the time thickness maps shown in Figures 4.2.4 and 4.2.5. A total of 134 deep autochthonous salt bodies (salt pillow and rollers) as well as 50 shallow salt bodies (salt diapirs and salt walls) have been identified and are displayed in Figures 4.2.6 and 4.2.7.

A) Zechstein and Lower Germanic Trias Groups mapping

The Zechstein Group time thickness map (Fig. 4.2.4) shows a present day autochthonous salt thickness heterogeneous pattern. The mother salt is thin, welded out or eroded in most of the study area and is only relatively thick (more than 300 ms thick) in the Step Graben, the Cleaver Bank Platform, the Ameland Platform and the eastern part of the Schill Grund Platform. Note the sharp thickness change located between the black arrows in Figure 4.2.4. The Lower Germanic Trias Group (RB) time thickness map (Fig. 4.2.5) shows a depocenter located around the B and F blocks as well as smaller depo-thicks in the southern part of the Dutch Central Graben. Also note on this map that the lineament seen in the Zechstein time thickness map (Fig. 4.2.4) is also observed on this map, indicated that this feature was long lasting and controlled the original deposition of both the Zechstein Group and the Lower Germanic Trias Group (RB). RB is over all quite isopachous at the km-scale except in a few areas where growth stratigraphy is observed. RB growth minibasin configuration is observed in the A and E blocks (Fig. 4.2.8), with similar geometry as observed in the UK sector (Stewart and Clark, 1999 and Penge et al., 1999). However, these growth geometry are rare and RB in overall has a “rail-track” type seismic configuration in most of the study area.

The autochthonous salt bodies (Fig. 4.2.6) are observed in most of the study area with the exception of the northwestern part of the study area (western part of quadrant A) where the Zechstein Group is thin, absent due to non-deposition or even locally eroded, and in the northern part of the DCG (quadrant F) where identification of deep salt bodies are difficult due to the limited seismic resolution a greater depth. The deep autochthonous salt bodies vary in size and shape from small 1-2 km rounded pillows to elongated 30 km plus salt pillows. The shallow salt bodies (Fig. 4.2.7) are principally located in the DCG, the SG and the TB and around their bounding areas e.g. western part of the SCP). The salt bodies often have an elongated geometry and often form salt walls up to 60 km long. These salt wall and elongated salt diapirs are predominantly aligned over a N-S to NNE-SSW trend, mimicking the orientation of the bounding faults that controlled the DCG.

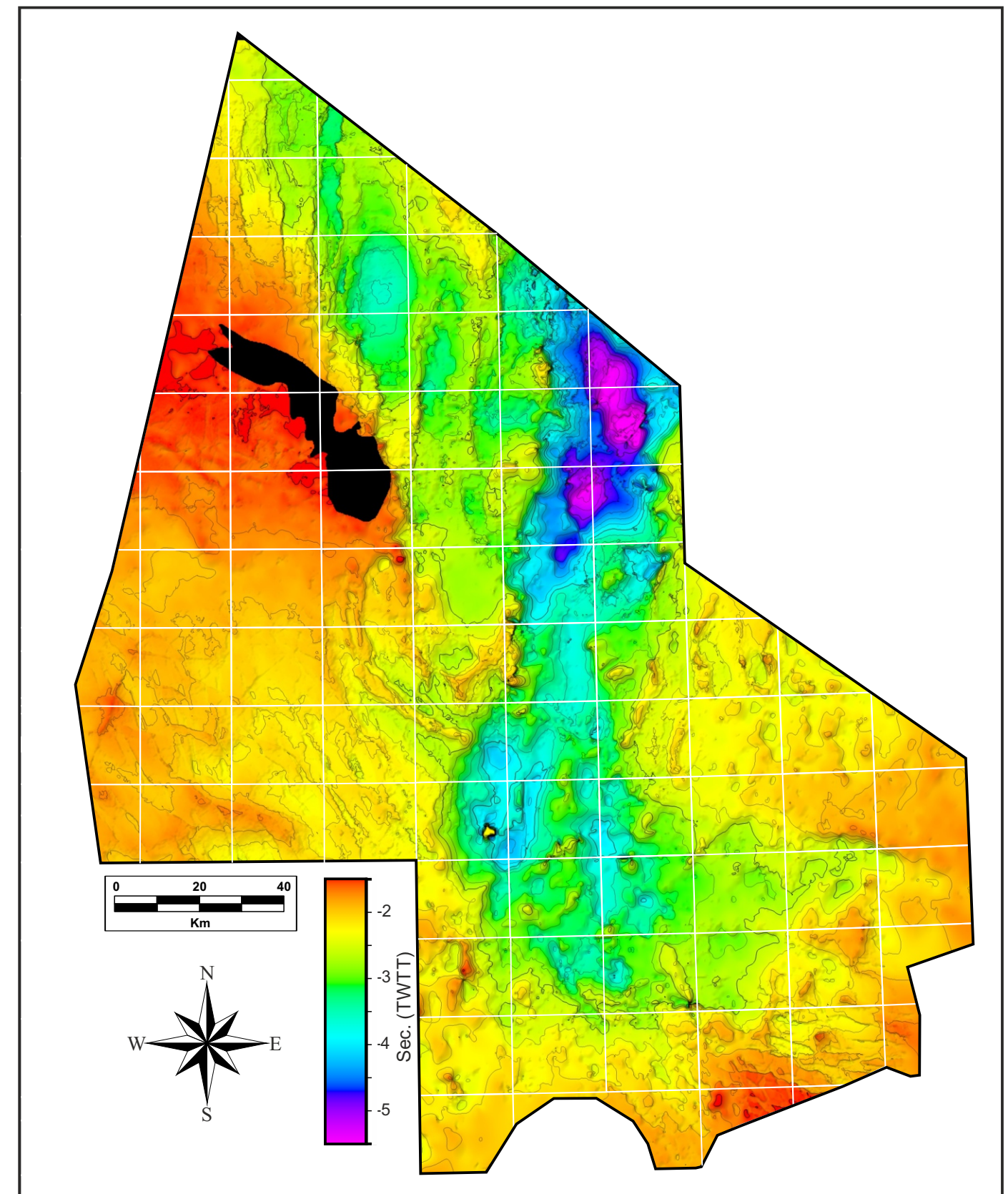


Figure 4.2.1: Base Zechstein time structure map.

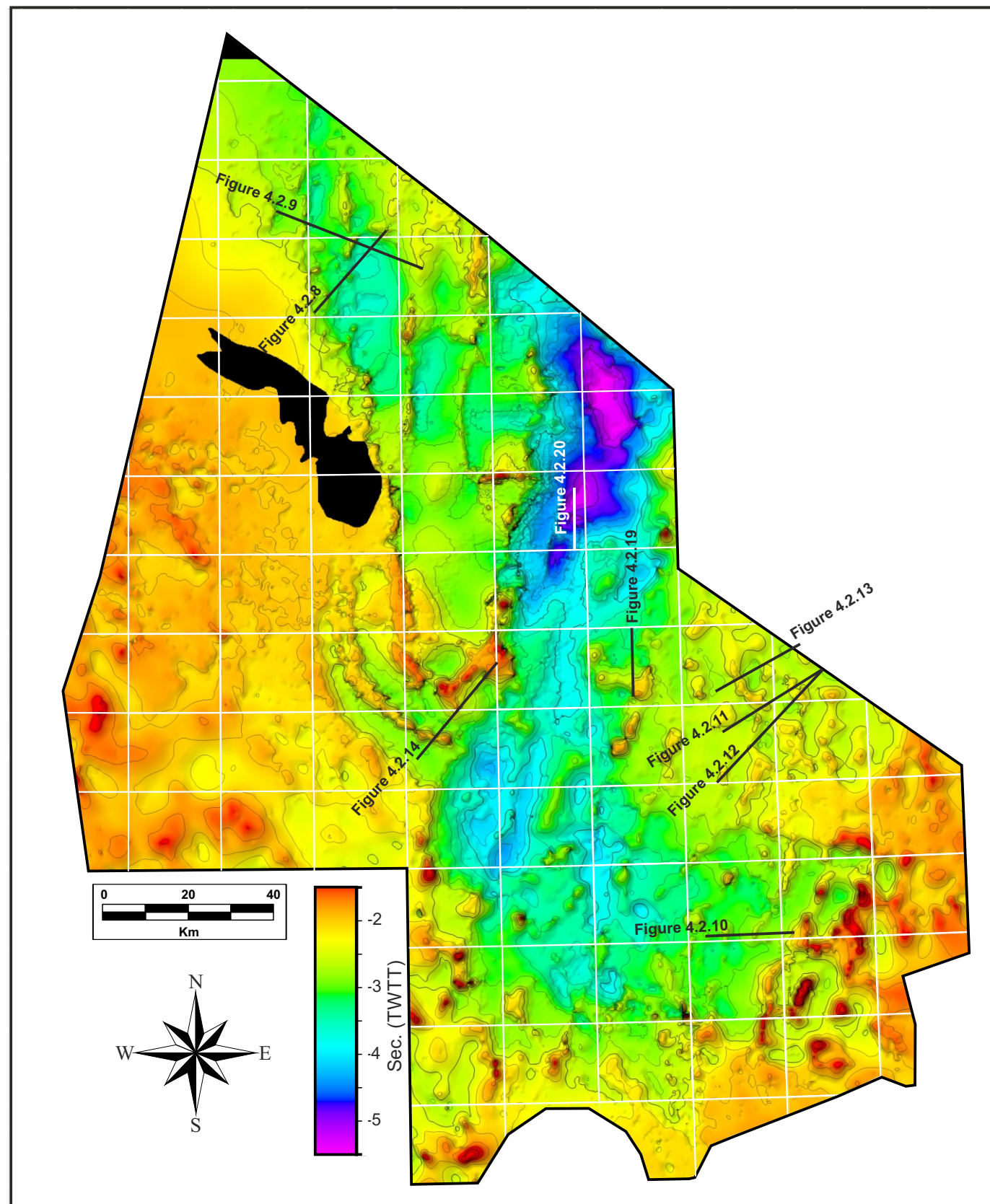


Figure 4.2.2: Top Zechstein time structure map.

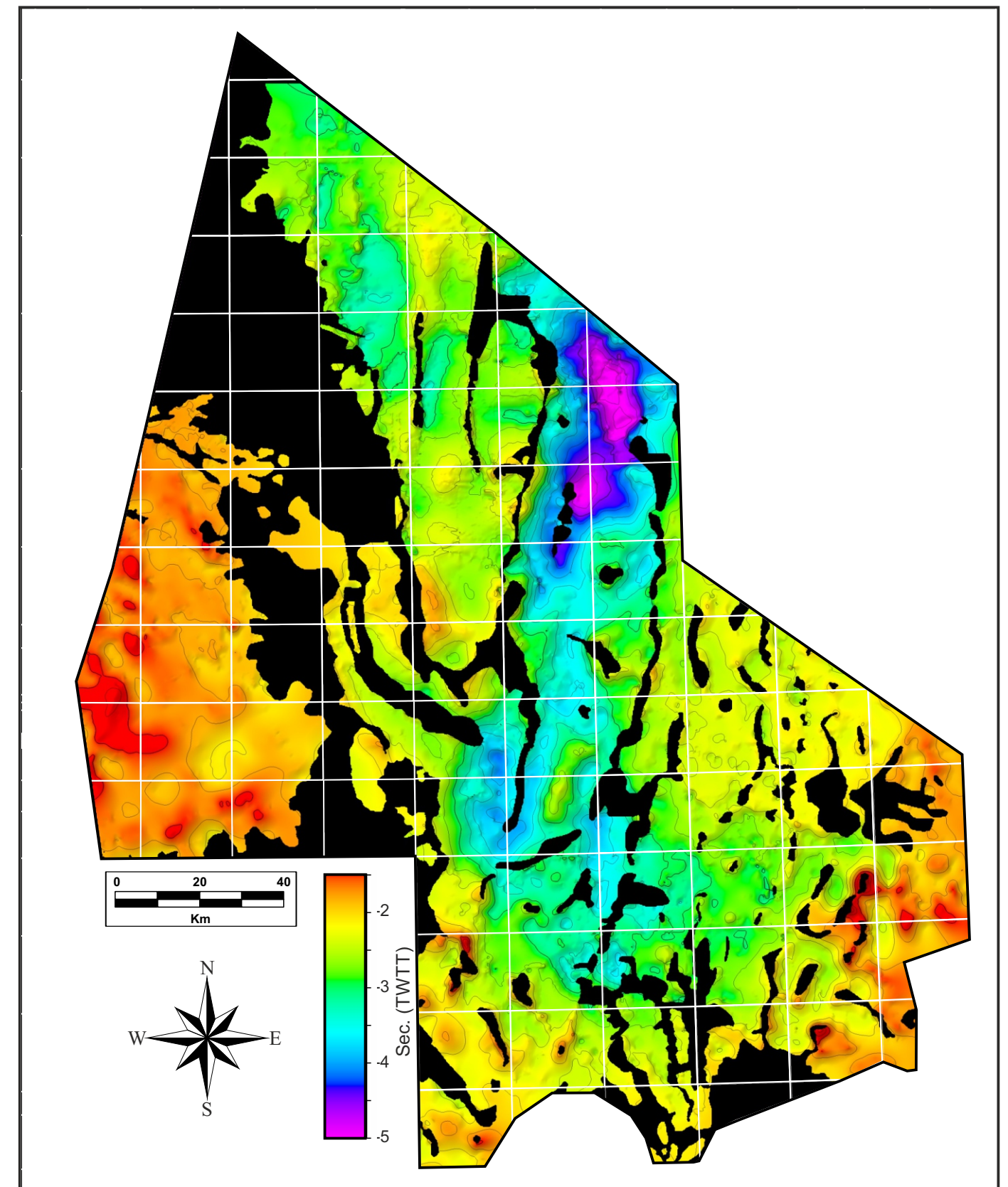


Figure 4.2.3: Top Lower Germanic Trias Group (RB) time structure map. Zones show in black have no Lower Triassic present.

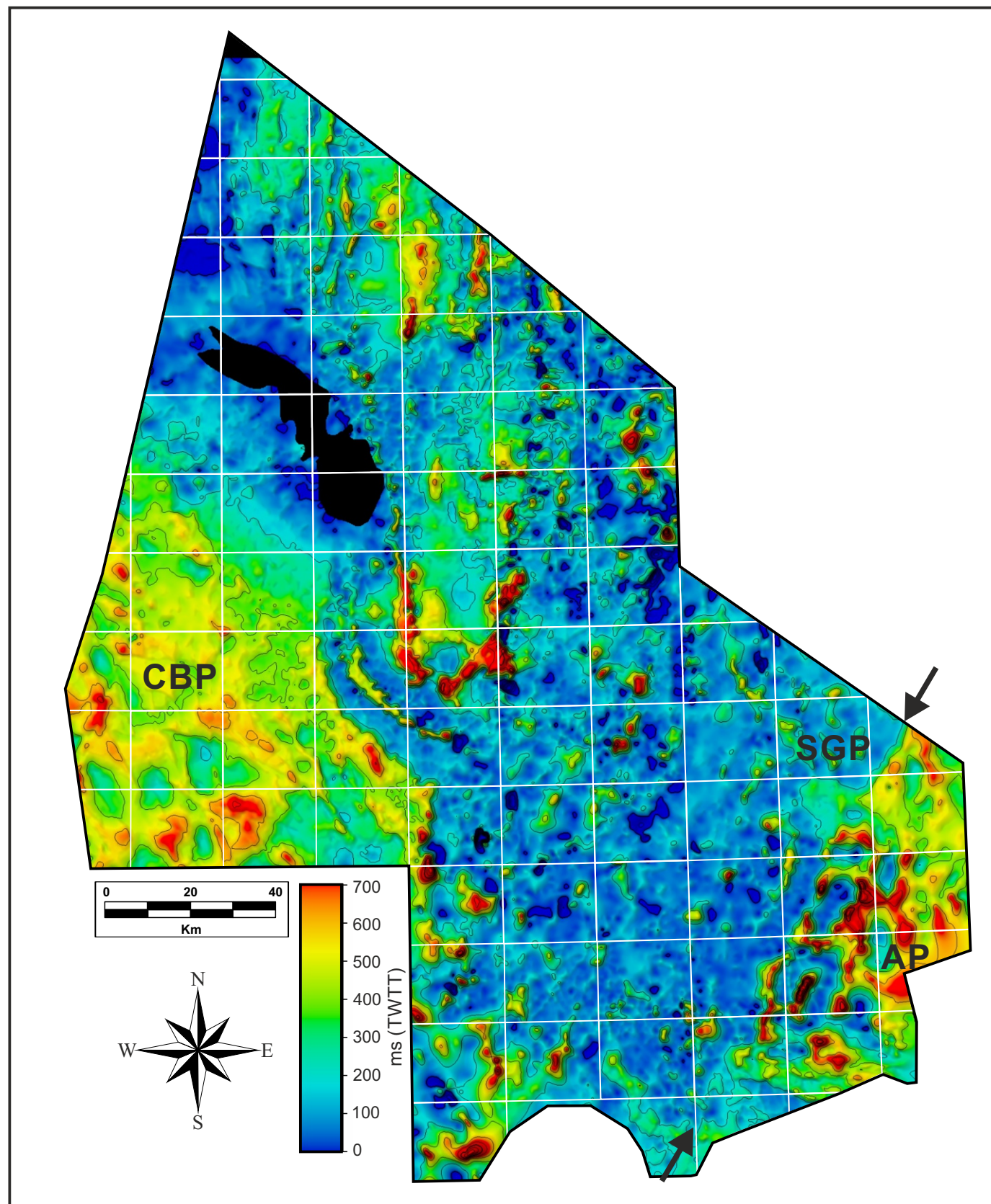


Figure 4.2.4: Zechstein Group time thickness map. Note that the present day mother salt is thickest on the Cleaver Bank Platform (CBP), the Ameland Platform (AP) and the eastern part of the Schill Grund Platform (SGP). Note the lineament between the arrows (see text for comments).

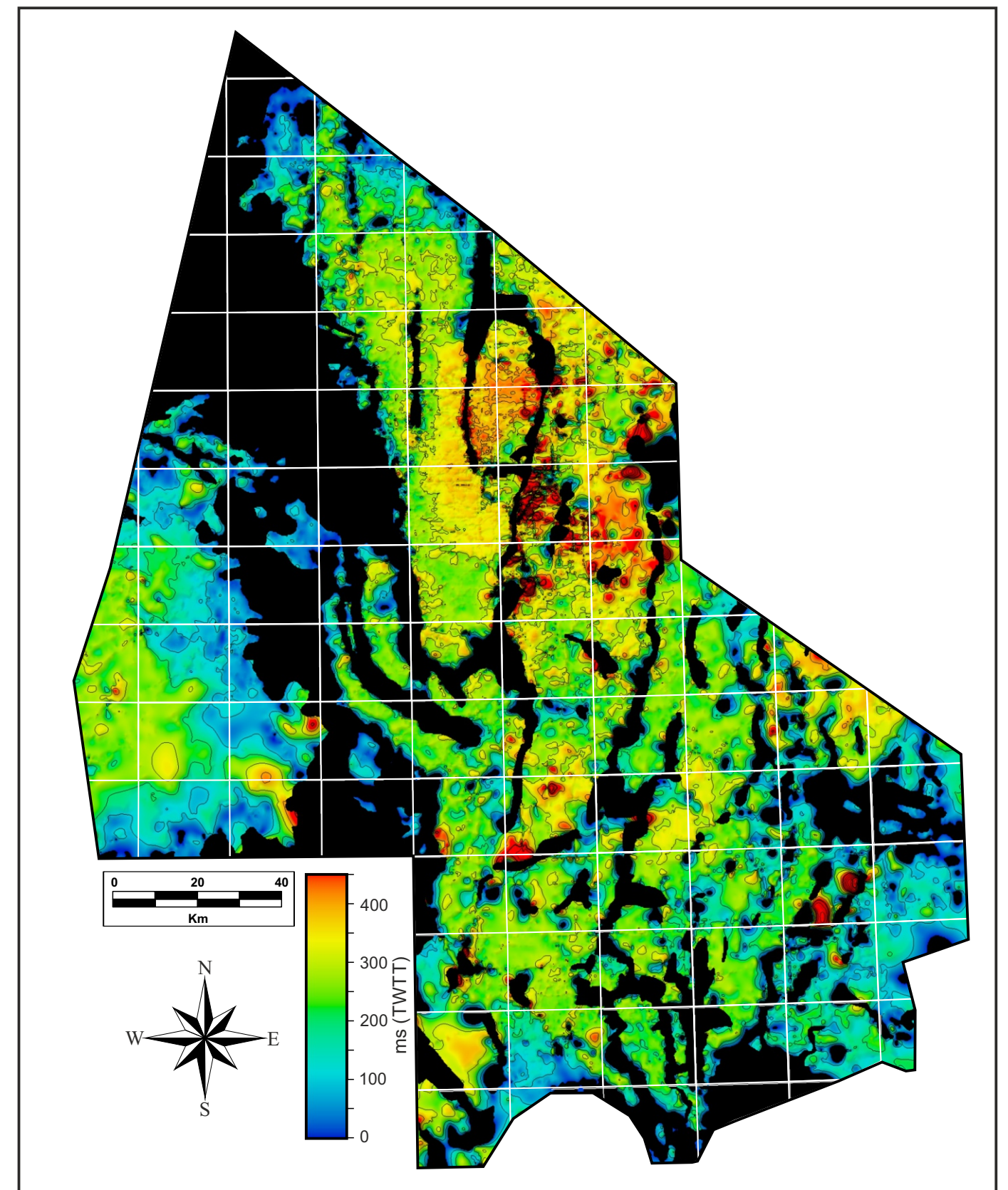


Figure 4.2.5: Lower Germanic Trias Group (RB) time thickness map. Zones show in black have no Lower Triassic present. See text for comments.

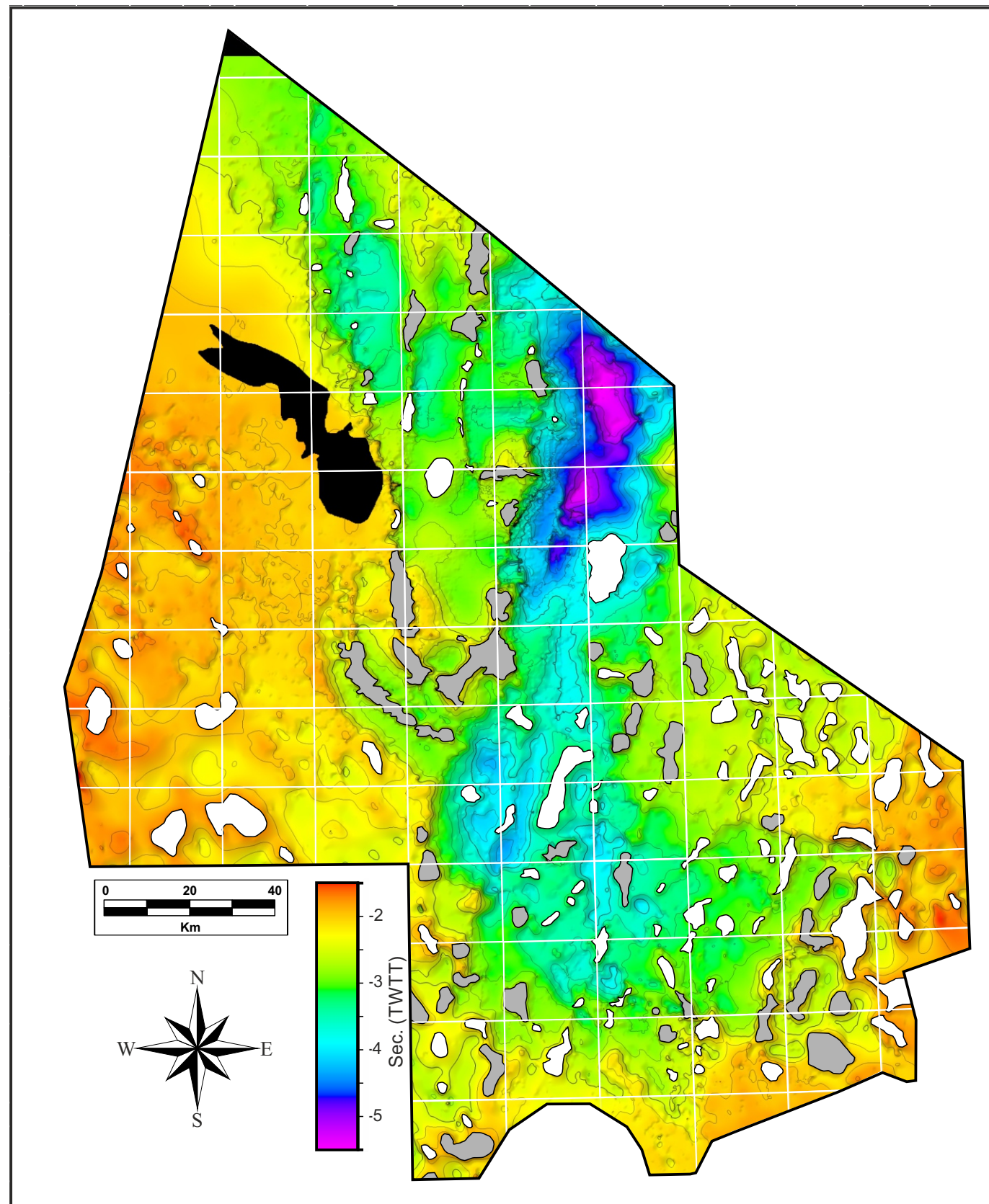


Figure 4.2.6: Deep autochthonous salt bodies map. The top Zechstein time structure map is show as background. White coloured salt bodies have less than 500 ms of relief, while grey-coloured salt bodies have more than 500 ms of relief.

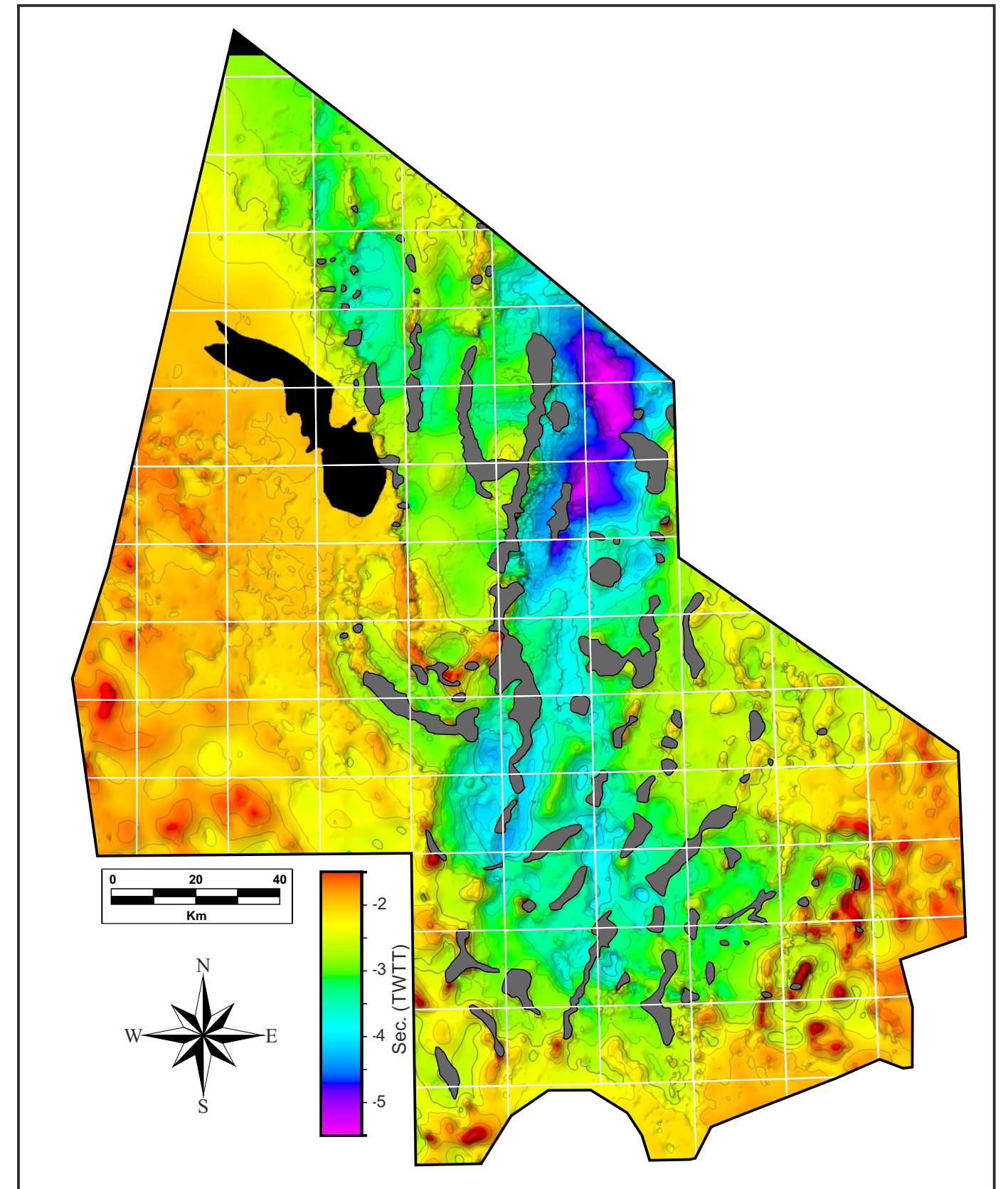


Figure 4.2.7: Shallow salt bodies map. The top Zechstein time structure map is show as background. This map was constructed using the multi-z seismic interpretation of the salt architecture.

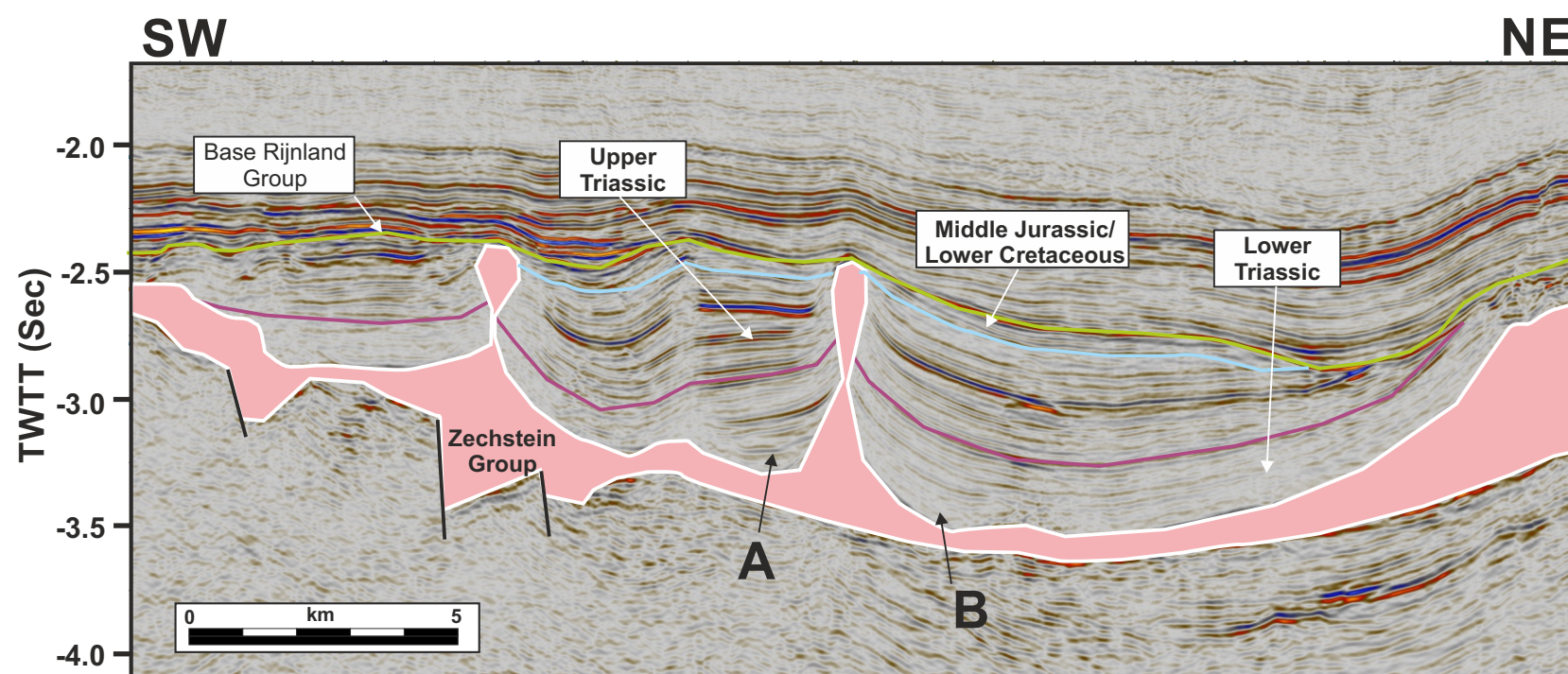


Figure 4.2.8: Interpreted 2D seismic line showing salt-related Lower Triassic minibasins (A and B). This line is located in the northern part of the study area (A15 and A13 blocks). See Fig. 4.2.2 for location.

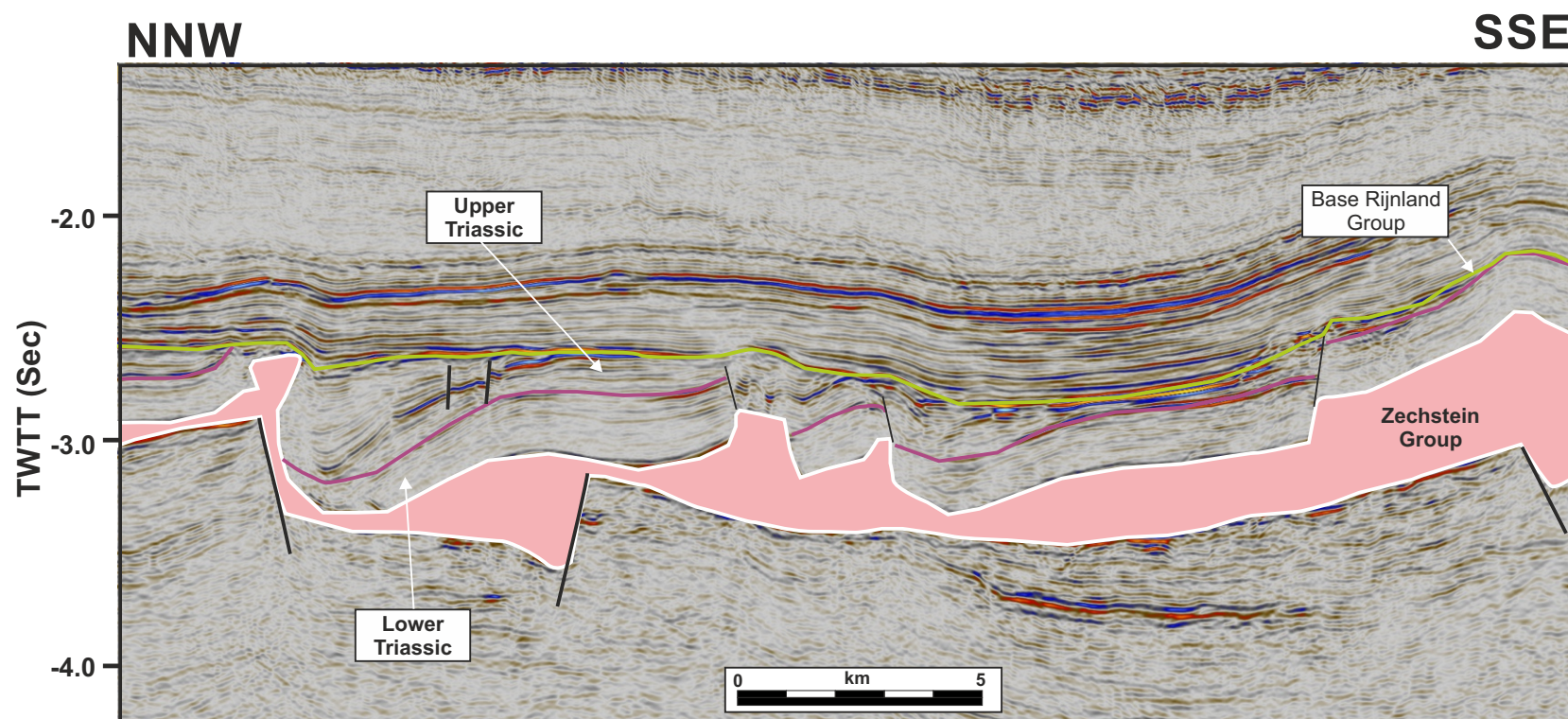


Figure 4.2.9: Interpreted 2D seismic line showing Lower Triassic fault blocks in the northwestern part of the study area. See Fig. 4.2.2 for location.

B) Growth fault/raft systems

Numerous growth faults were active during the Upper Triassic were identified and mapped during this regional phase of the research project. Examples of such faults can be seen in Figures 4.2.9 to 4.2.12. These fault systems have been mapped and are displayed in Figure 4.2.13. In some cases rafting of Lower Triassic structural block was involved, with up to 3-4 km of translation onto the Zechstein salt. In the case of the second structural restoration (Chapter 4.4), rafting with up to 18 km of translation was observed. The recognition of listric growth faults is often difficult in the Dutch offshore since the structures were often subsequently reactivated (e.g. Figs. 4.2.10 and 4.2.11) or partially eroded by later event (e.g. Kimmeridgian and or Base Cretaceous Unconformities). In some cases, the growth faults detached on shallower layers than the Zechstein, mainly the Triassic in situ salt layers or within the shale-rich Altena Group. In some cases, growth faults even sole into deeper ductile layers than the Zechstein, such as the thick halite layers in the Permian Silver Pit Formation (Fig. 4.2.12). Such original structural model can potentially explain the uneven geometry of the base autochthonous Zechstein salt in several other areas where steps are often observed at that level, but where no clear deeply rooted basement faults are observed underneath.

Mapping of the growth faults and growth fault/raft systems (Fig. 4.2.13) indicate that the direction of movement is not random but rather follows the configuration of the Triassic basin. The direction of displacement was mainly toward the central eastern part of the study area, with a few exception in the SGP where a few faults show displacement toward the east (toward Germany). The position of the faults also indicate that the gravitational gliding occurred along Triassic basin lineaments located along the western side of the SG and the eastern side of the SGP, TB and VP.

C) Collapse structures

Four type of collapse structures have been observed: Lateral salt body collapse, expulsion roll over, collapse graben and axial salt body collapse (minibasin).

In some cases the Lower Triassic is missing locally with no evidence of rafting or erosion. In Figure 4.2.14, areas located next to a salt bodies are devoided of Lower Triassic strata. These features are referred as collapse structures, where the salt locally deflated and migrated laterally. If growth wedges are present above the deflated salt (e.g. Upper Triassic wedge in Fig. 4.2.14A), an expulsion rollover model is suggested (Fig. 2.20). In several areas collapse grabens have been identified. Figures 4.2.15 and 4.2.16 show good examples of such elongated and narrow grabens that detached on Zechstein faults and form due to unidirectional salt withdrawal of a narrow salt pillow or wall, toward a shallower salt body. In the case of the E09 collapse structure (Figs. 4.2.17 and 4.2.18) the central part of a salt body collapse, creating a oblong-shaped minibasin with Upper Triassic fill.

4.2 Results - Structural analysis: Regional study

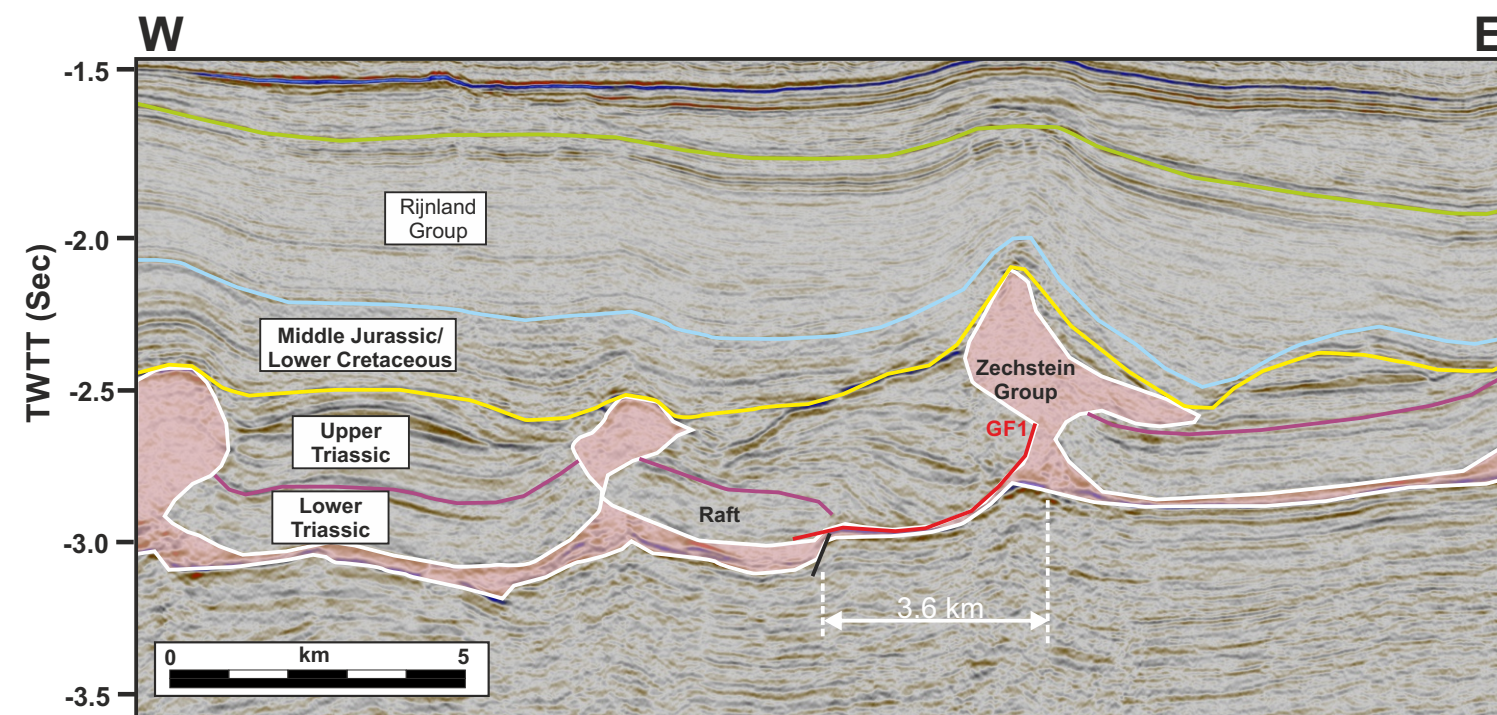


Figure 4.2.10: Interpreted seismic line from 3D seismic survey in the Terschelling Basin showing a growth fault/raft system. Note the large Upper Triassic rollover on the downthrown side of the fault GF1. The Lower Triassic raft translated westward on the mother salt by 3.6 km. See Fig. 4.2.2 for location.

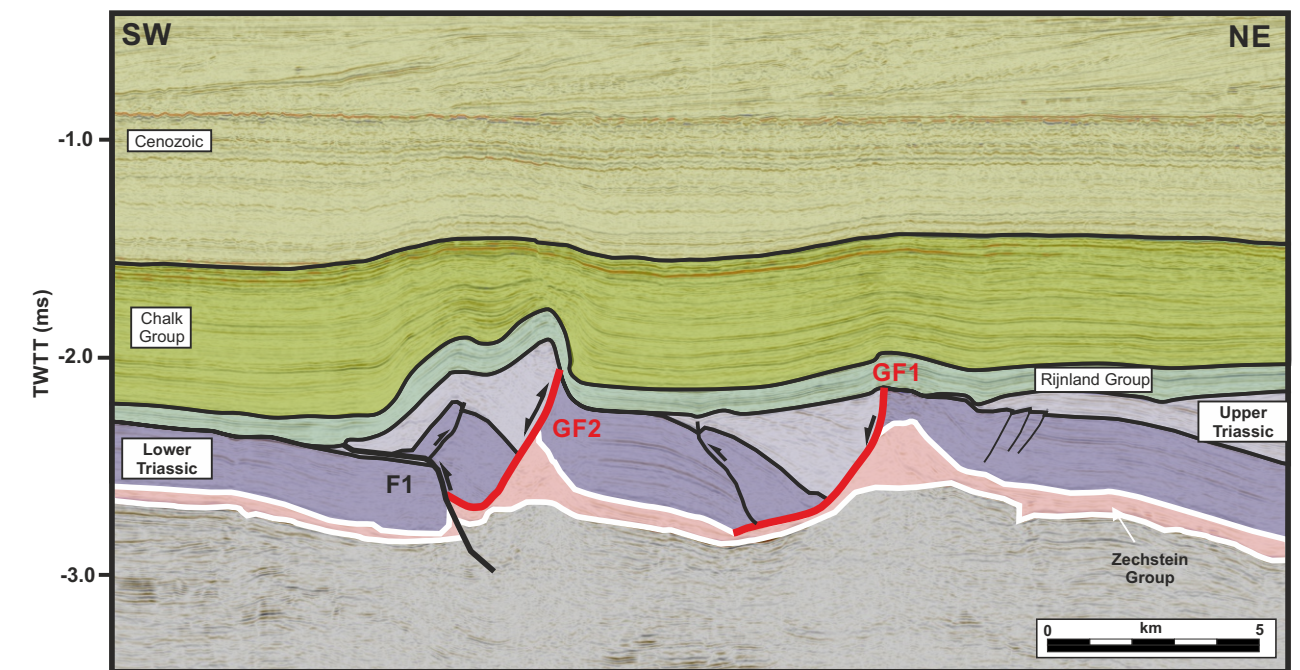


Figure 4.2.11: Interpreted seismic line from 3D seismic survey showing two growth faults (GF1 and GF2, red-coloured lines) that were active during the Upper Triassic period. Note that GF2 was later reactivated as a reverse fault during the Alpine orogen and forms a pop-up structures in conjunction with thrust fault F1. See Fig. 4.2.2 for location.

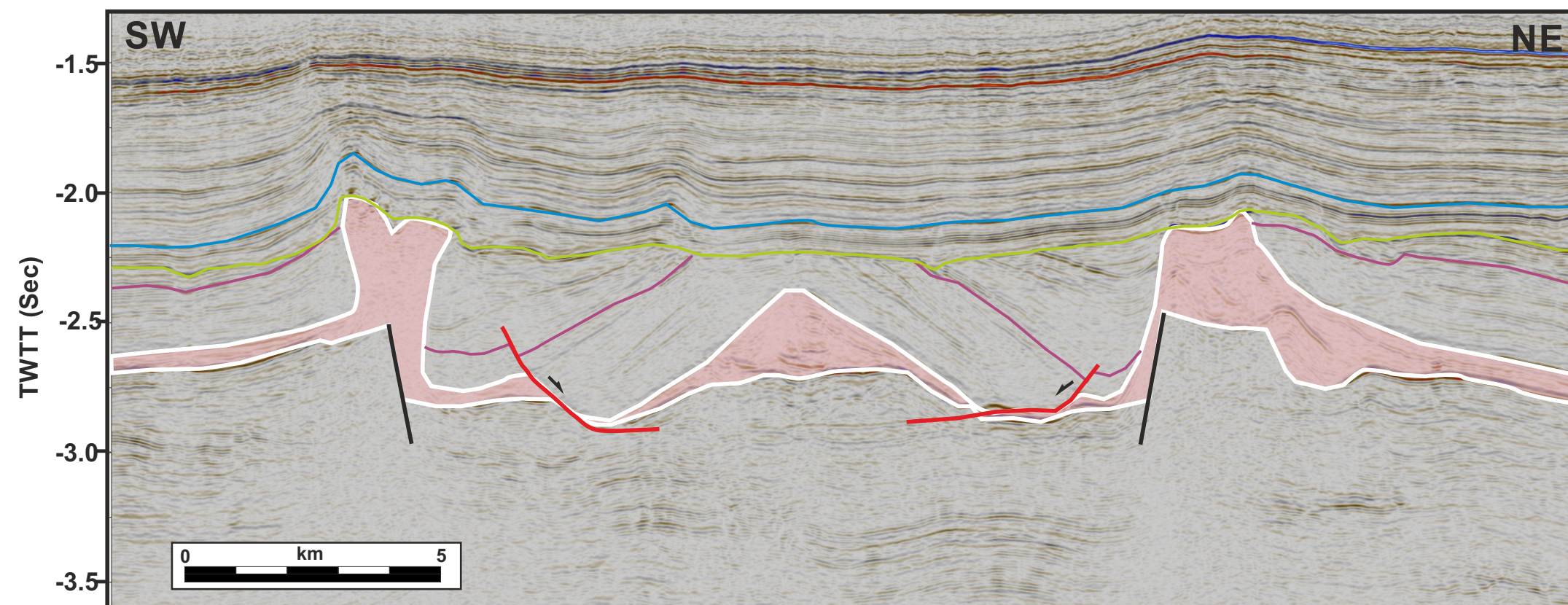


Figure 4.2.12: Interpreted seismic line from 3D seismic survey showing two Upper Triassic growth faults (red-coloured) that detached on a deeper stratigraphic level than the Zechstein, likely the thick halite layers of the Permian Silver Pit Formation. See Fig. 4.2.2 for location.

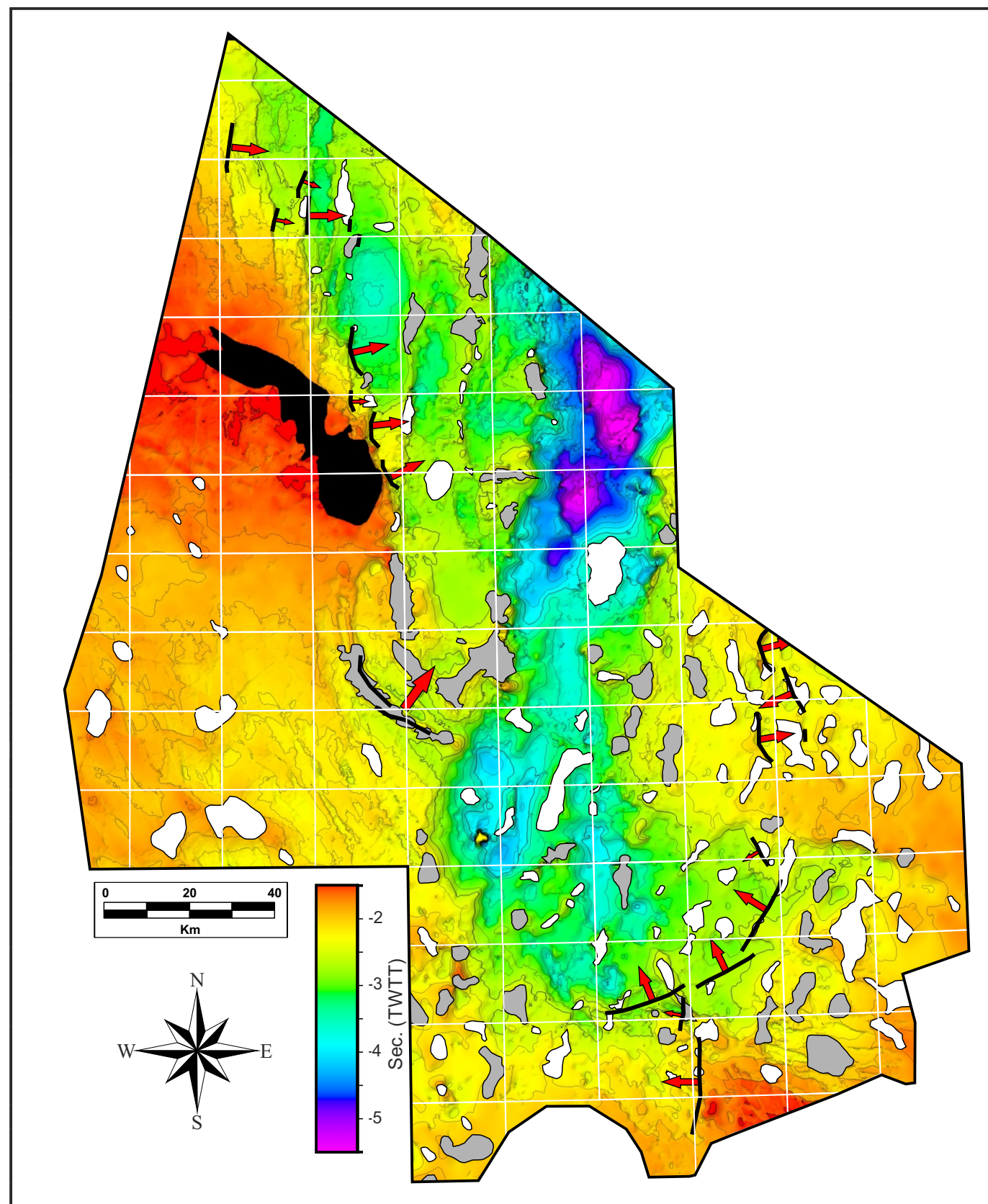


Figure 4.2.13: Upper Triassic growth fault/raft systems map. Base Zechstein salt shown as background. White coloured salt bodies have less than 500 ms of relief, while grey-coloured salt bodies have more than 500 ms of relief. The main growth faults are shown as black lines and the direction of rafting as red arrows.

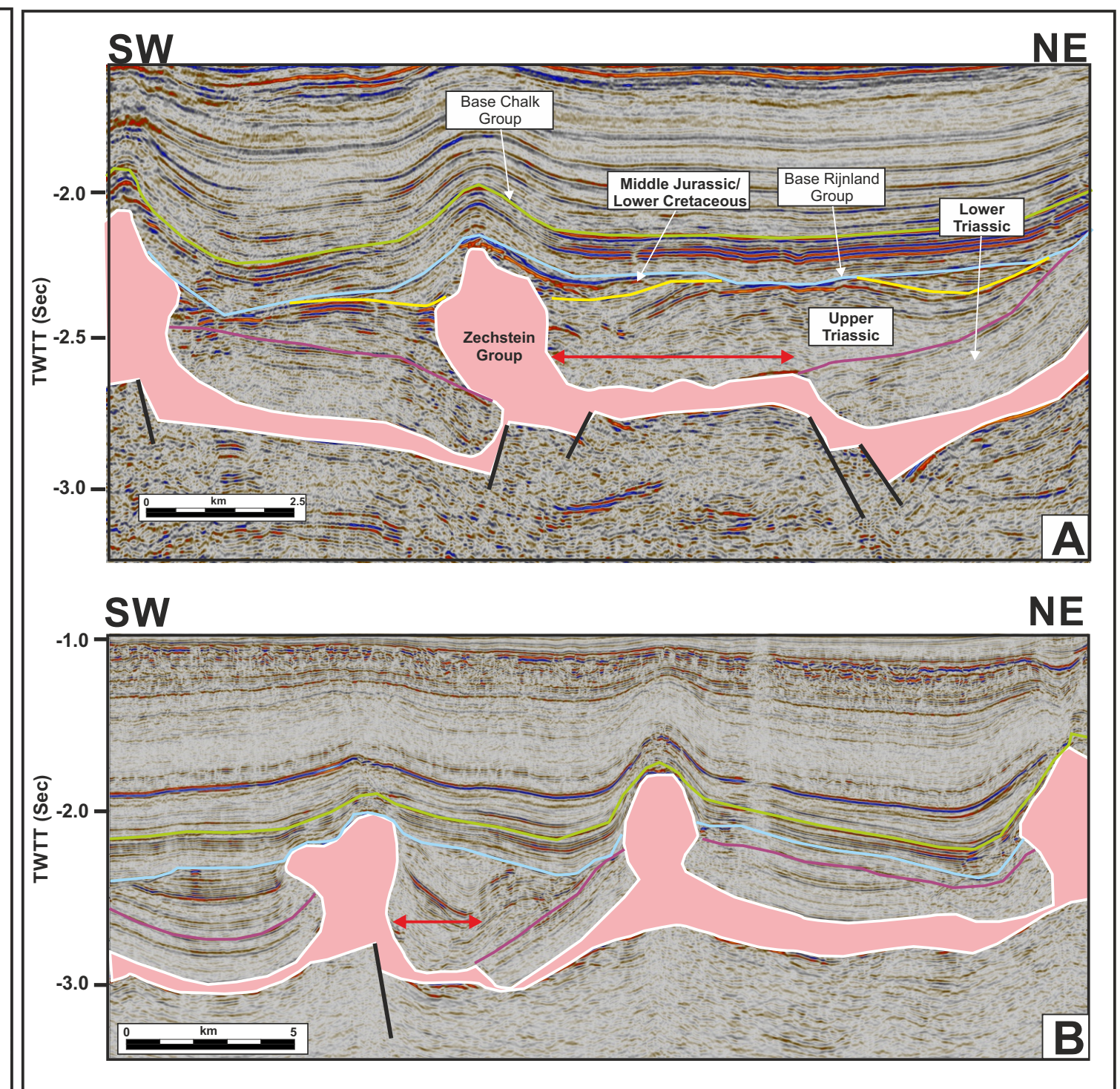


Figure 4.2.14: Interpreted seismic lines illustrating the absence of Lower Triassic strata locally. The red arrows show the locations where upper Triassic lies directly onto the mother salt. **A)** This line is located on the Schill Grund Platform, in the G10 and G11 blocks. Note the Upper Triassic wedge thickening toward the SW. This type of feature is referred to as an expulsion rollover. **B)** This line is located on the Cleaver Bank Platform. See Fig. 4.2.2 for location.

4.2 Results - Structural analysis: Regional study

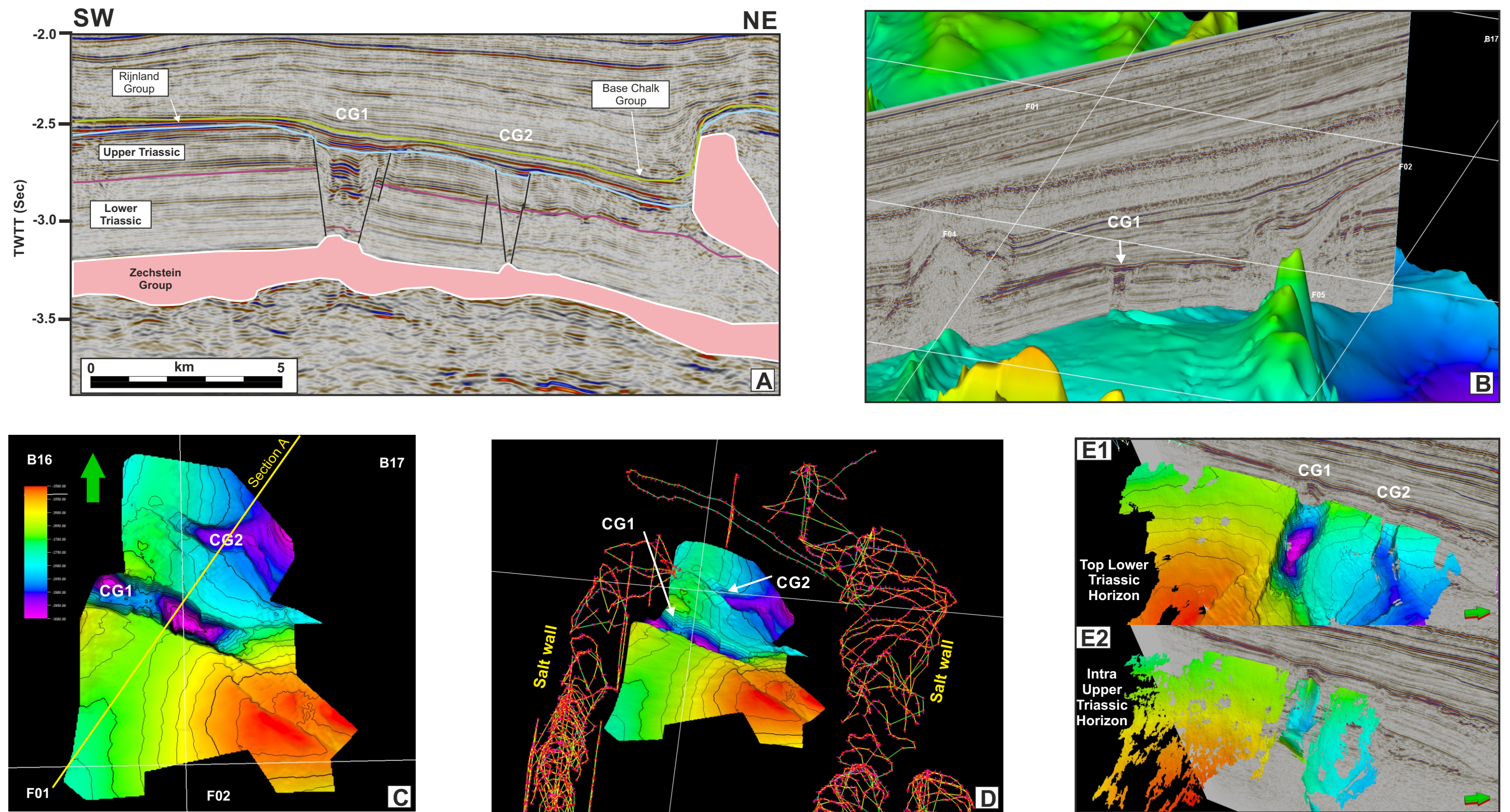


Figure 4.2.15: Collapse grabens in the B16/B17 blocks. Two collapse grabens (CG 1 and 2) oriented WNW-SSE are present. **A)** Interpreted seismic section showing the strike view across the two collapse grabens. See Figure 4.2.15C for location. **B)** Perspective view looking north-westward of seismic line A, with top Zechstein surface shown as a background. **C)** Map view of the top Lower Triassic Horizon. **D)** Perspective view looking northward of the top Lower Triassic horizon and the multi-Z top salt mesh. **E1)** Perspective view looking westward of the top Lower Triassic horizon. **E2)** Perspective view looking westward of the intra Upper Triassic horizon. Note the folded axial strata indicative of later contraction of the graben.

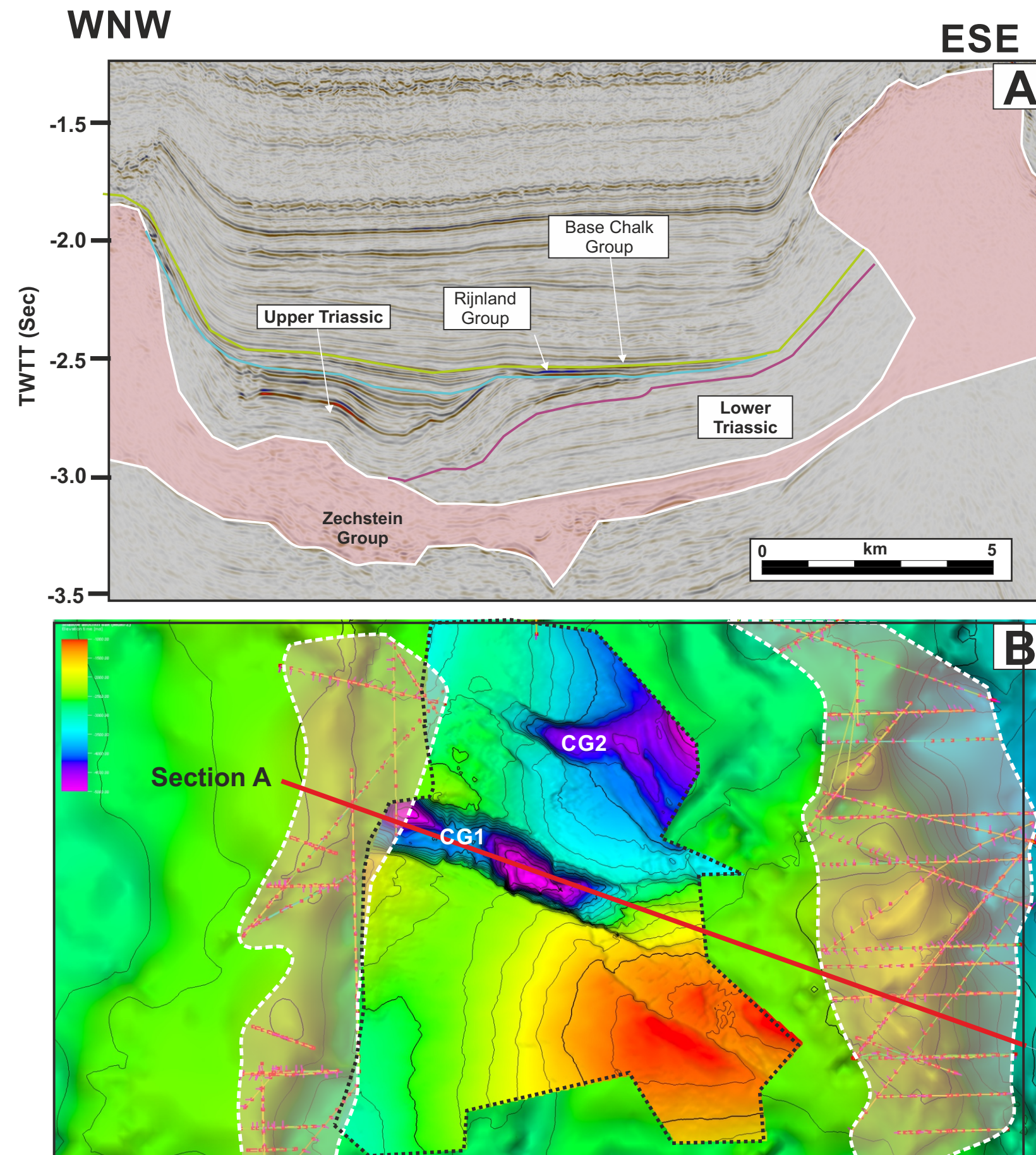


Figure 4.2.16: A) Dip seismic view along the axis of the collapse graben CG1. Note that the western part of the graben is filled with Upper Triassic strata. See (B) for location view. **B)** Map view off the collapse grabens and the surrounding shallow salt bodies (salt walls). The salt walls are shown in pink with white coloured dashed outlined and include the multi-z mesh. The background map is the top of the Zechstein Group. The shallower top Lower Triassic horizon is shown with a black dashed outline.

4.2 Results - Structural analysis: Regional study

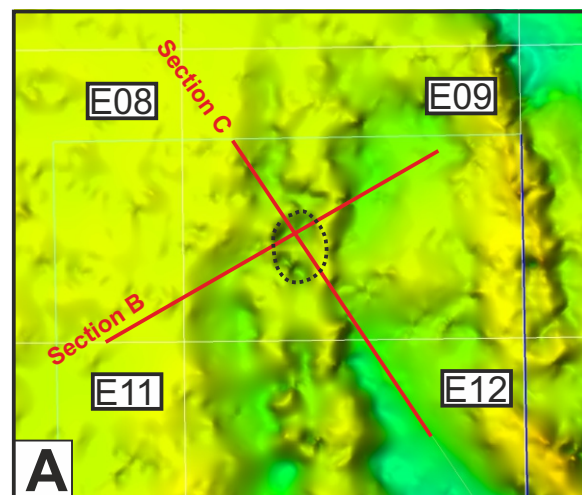
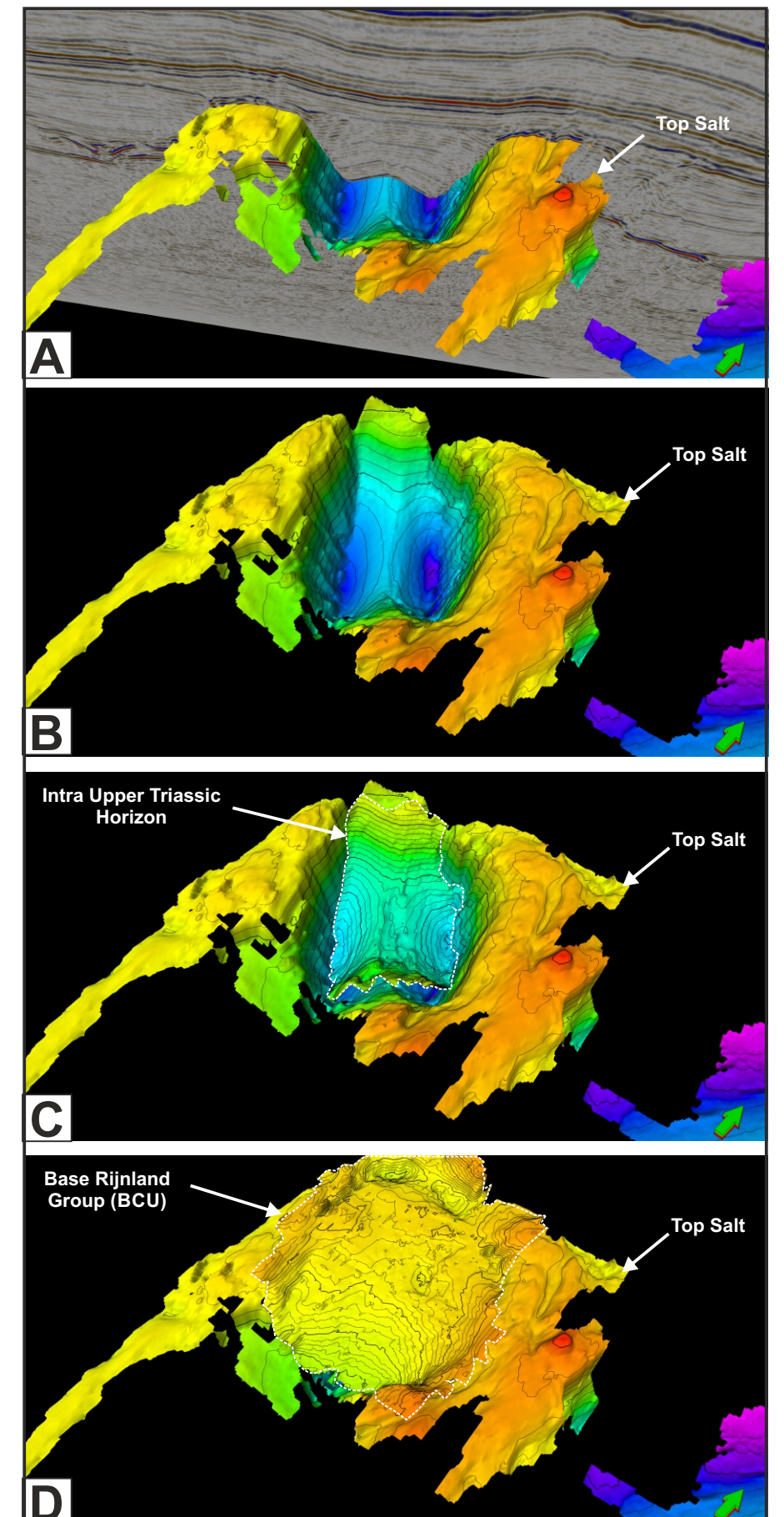
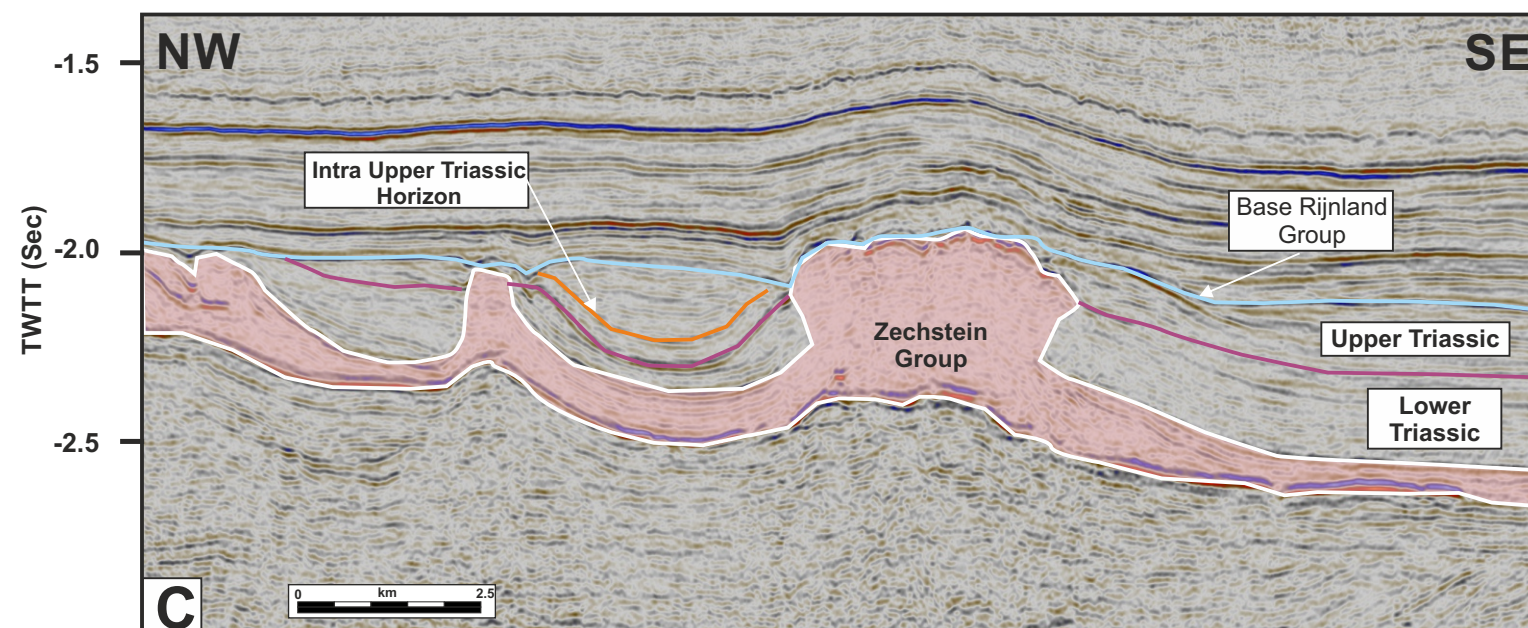
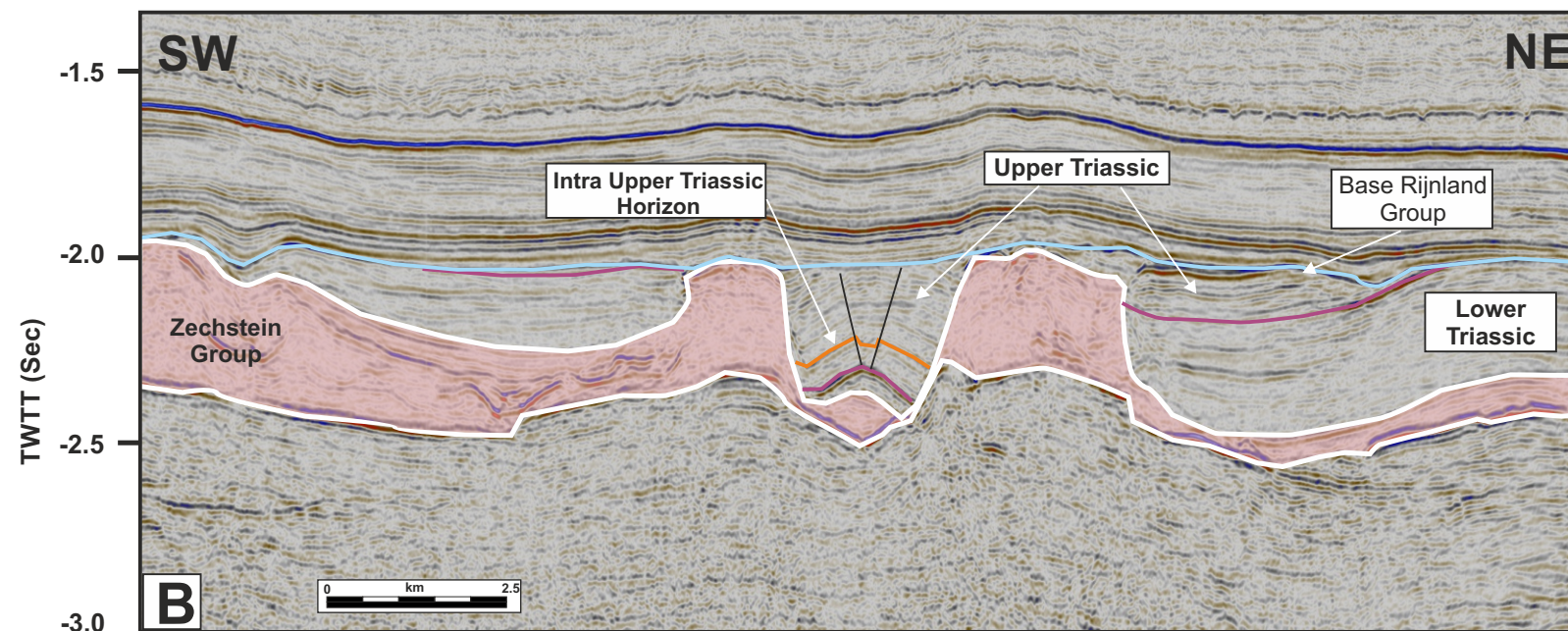


Figure 4.2.17: The E09 minibasin. **A)** Location map. The black dash line show the position of the minibasin. **B)** SW-NE seismic section showing the narrow minibasin configuration with Upper Triassic growth wedges along the margins. **C)** NW-SE seismic section showing the Upper Triassic basin fill with the depocenter in the central part of the minibasin.

Figure 4.2.18: Perspective views, looking toward the NW, of the E09 collapse minibasin. **A)** the top salt and a strike seismic line. **B)** the top salt horizon. **C)** The intra Upper Triassic horizon (orange coloured horizon of Fig. 4.2.18) overlaid on the top salt surface. **D)** The base Rijnland Group horizon overlaid on the top salt surface.



D) In situ Upper Triassic salt detachments

Many normal faults detached onto Upper Triassic in situ salt layers such as the Röt or Muschelkalk Evaporite Members. Locally these salt layers show thickness variations that are related to tectonic events rather than depositional patterns. Figure 4.2.19 shows a good example of structurally thickened Röt salt related to contractional features. In some cases, over-thickened

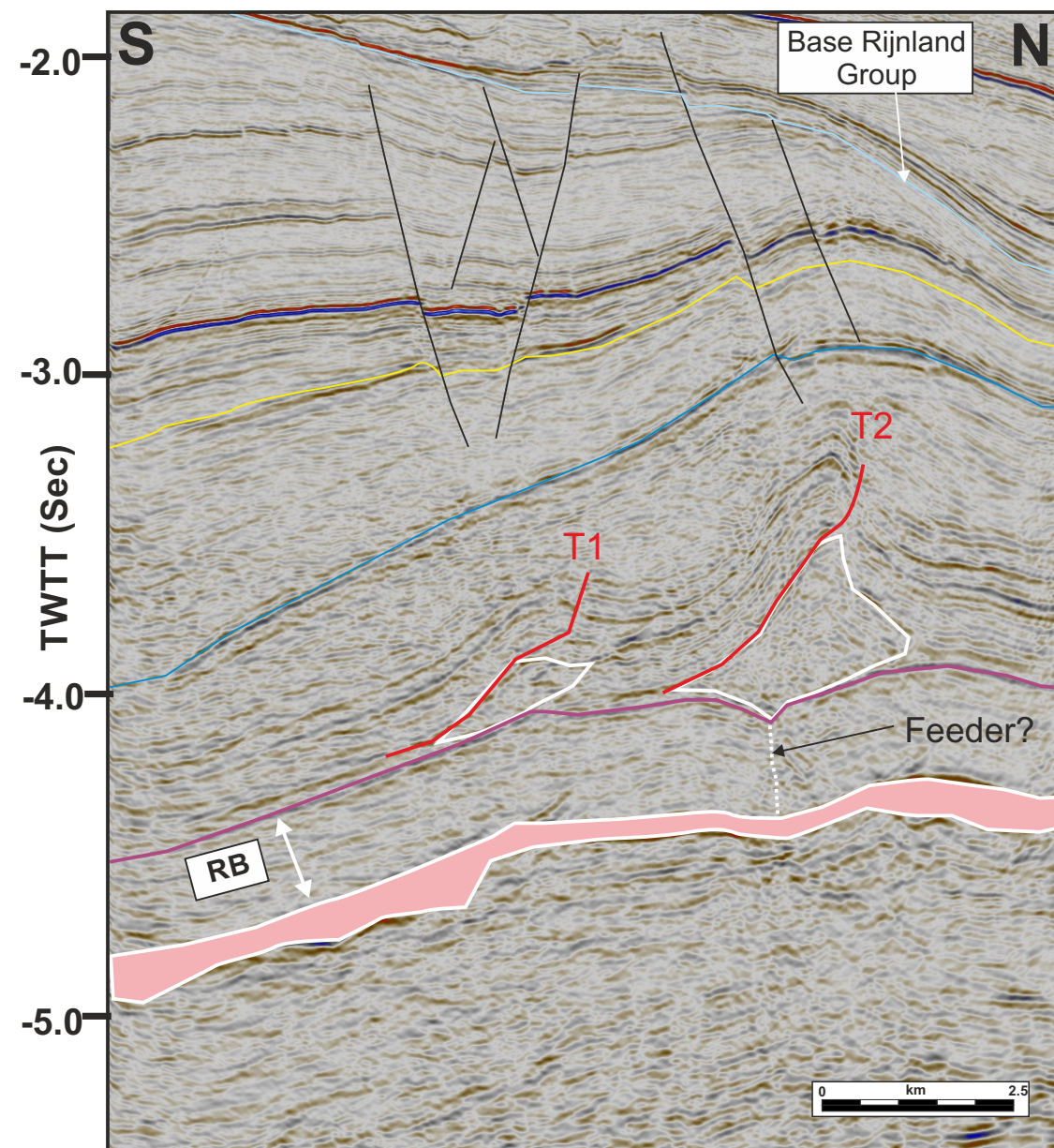


Figure 4.2.19: Upper Triassic contraction in the F2 Block. Two thrust faults (T1 and T2) are observed. These faults may be the downdip contractional part of the gravitational gliding systems observed updip along the Upper Triassic basin margins. These thrust faults are possibly salt-cored (white polygons), with the salt being either remobilized Zechstein salt (feeder) or structurally over-thickened Röt Evaporite Member. RB = Lower Germanic Trias Group. See Fig. 4.2.2 for location.

intra-Upper Triassic salt may be related to remobilized Zechstein salt emplaced within the Upper Triassic levels. Figure 4.2.20 shows two connected salt bodies at the base of the Upper Triassic that sit over two deeper normal faults that detached onto the Zechstein salt, forming a graben structure. It is possible that no Zechstein salt was remobilized upward in this case but further analysis and detailed 3D mapping would help coming up with a robust structural model to explain these features.

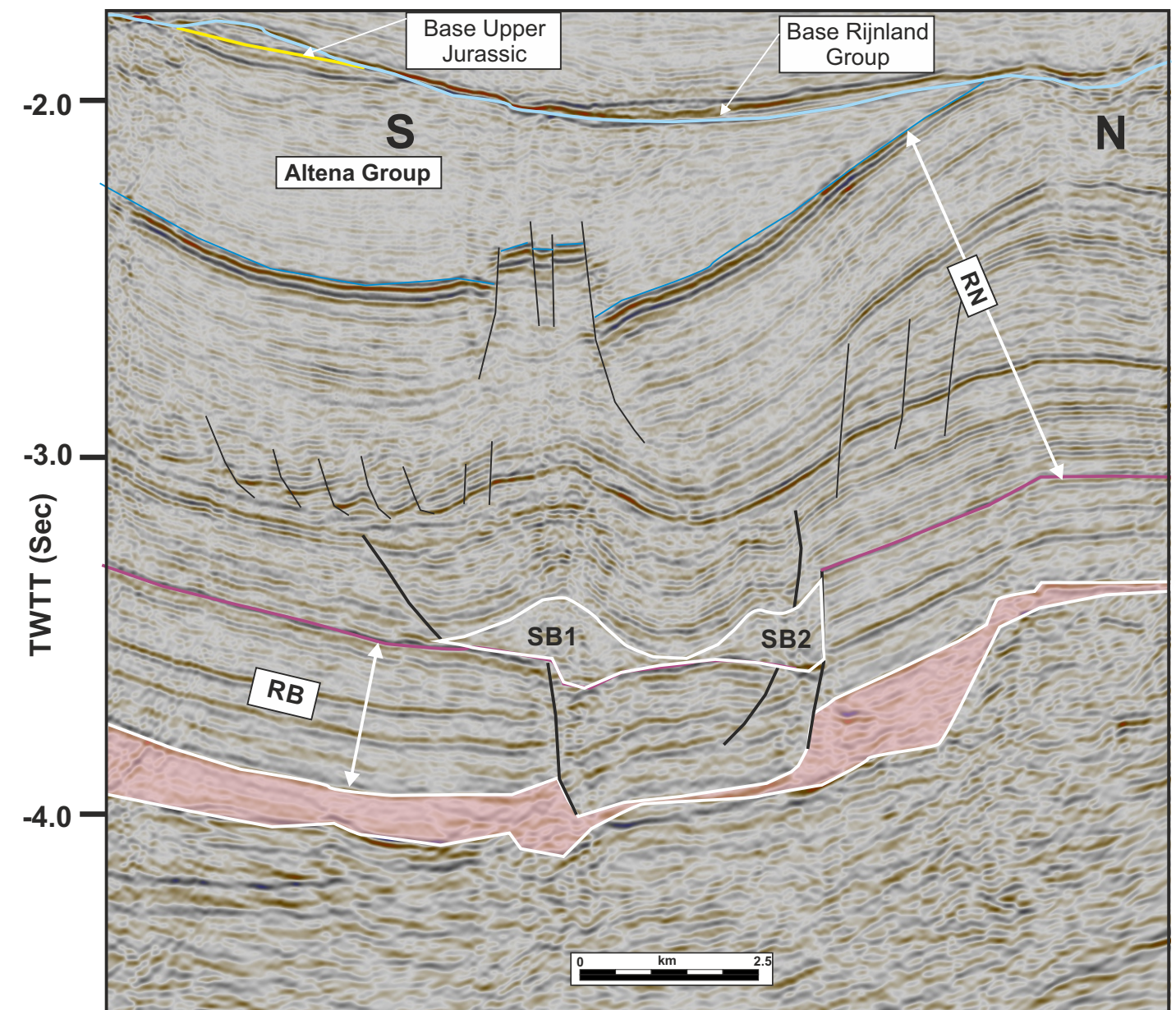


Figure 4.2.20: Intra Upper Triassic salt features in the F09 Block. This salt sheet has not been drilled and is composed of two salt bodies (white polygons, SB1-2) that are located stratigraphically above the top RB. The salt in those salt bodies can be interpreted either as over-thickened Main Röt Evaporite Member or remobilized Zechstein salt. Those salt bodies are sitting above a Lower Triassic graben. RB = Lower Germanic Trias Group; RN = Upper Germanic Trias Group. See Fig. 4.2.2 for location.

RESULTS
CASE STUDIES
STRUCTURAL
ANALYSIS

4.3

4.3 Results - Case studies structural analysis

Three case studies chosen jointly by TNO and the industry partners were carried out to investigate the salt tectonics during the Triassic in the Dutch Central Graben (CS1 and CS3), the Cleaver Bank Platform (CS3) as well as the Terschelling Basin and its southern platforms (CS2) (Fig. 4.3.1).

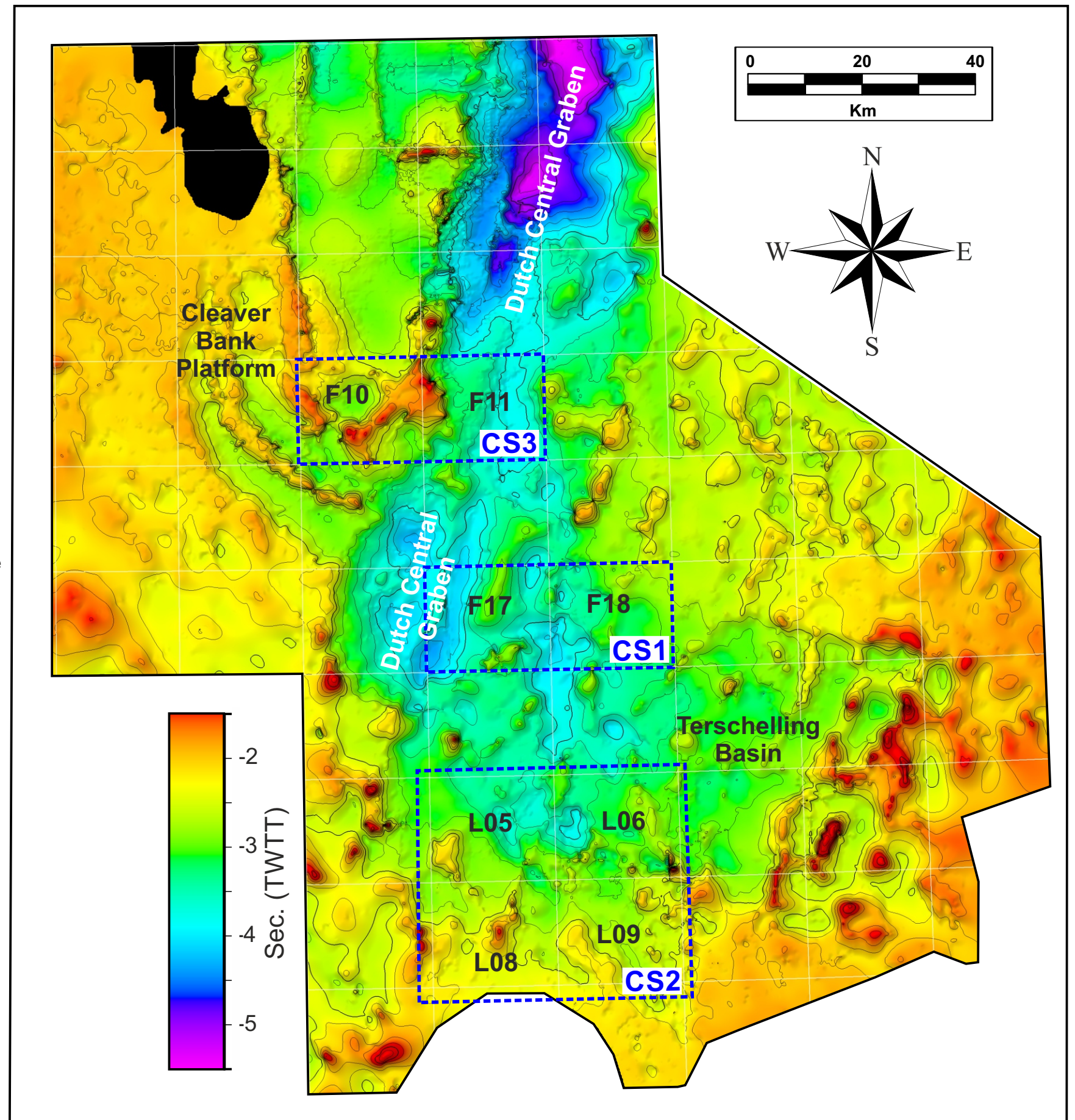
For each of these case studies, a detailed 3D seismic mapping of key horizons and structures was performed. In this chapter the key results are presented in the form of interpreted 2D depth seismic sections, structure maps of key horizons and thickness maps of key intervals. These results are used to investigate the tectono-stratigraphic evolution of the three study areas (F17-F18, L05-L06-L08-L9, and F10-F11).

A) Case study 1: F17-F18 blocks

This study area is located within the central part of the Dutch Central Graben where two large turtle structures (F17 and F18 turtles) are present (Figs. 4.3.4B and 4.3.10). Several deep and shallow salt features are present in the study area (Figs. 4.3.5, 4.3.7 and 4.3.8), including a salt pillow in the northern part of the F17 area as well as two salt bodies (salt bodies 1 and 2, Fig. 4.3.7). These two salt bodies are aligned along a SW-NE trend, which suggests that they may have been part of a salt wall that was later partially welded out. This interpretation is also based on the geometry of the area between those two salt bodies (Fig. 4.3.12). A NNE-SSW trending salt wall is present in the F18 block (Fig. 4.3.7). The two salt bodies and the salt wall have narrow stems as seen in Figures 4.3.8 and 4.3.10, 4.3.12. It is important to notice that all salt features present in the study area extends further into neighbouring blocks to the north and south of the study area, which means that some valuable observations regarding those features may be missing in this case study.

The base Zechstein ranges in depth from 6 to 4 km (Fig. 4.3.9). Note that the depth seismic data used was clipped below 6 km. In the western part of the F17 block and the southwest part of the F18 block the base Zechstein is lower than 6 km (but only slightly) (e.g. Figure 4.3.13A). The base Zechstein map shows an uneven surface with highs often located below the shallow salt bodies. This indicates that basement highs are present, especially below the salt bodies' stems, with clear basement faults seen on seismic (e.g. Faults F1 and F2, Fig. 4.3.10).

Figure 4.3.1: Location map of the three case studies (CS1-3). The top autochthonous salt time structure map is shown in the background.



4.3 Results - Case studies structural analysis: CS1

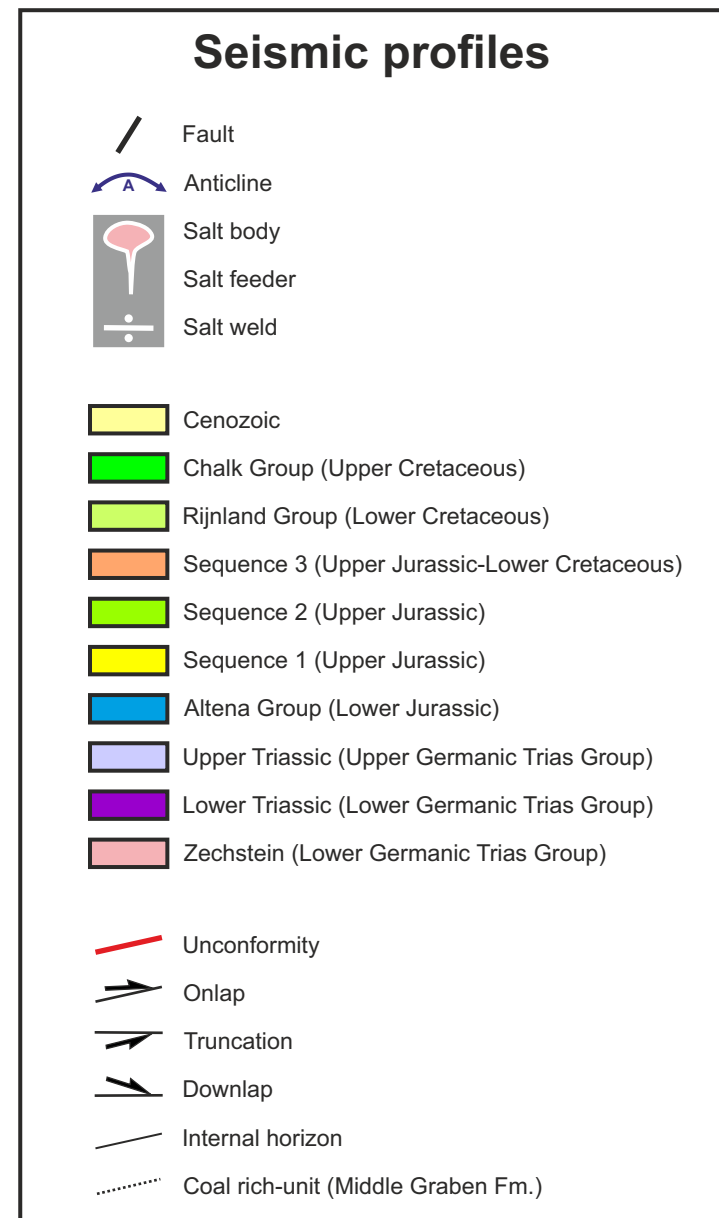


Figure 4.3.2: Legend for seismic section shown in Figures 4.3.4.

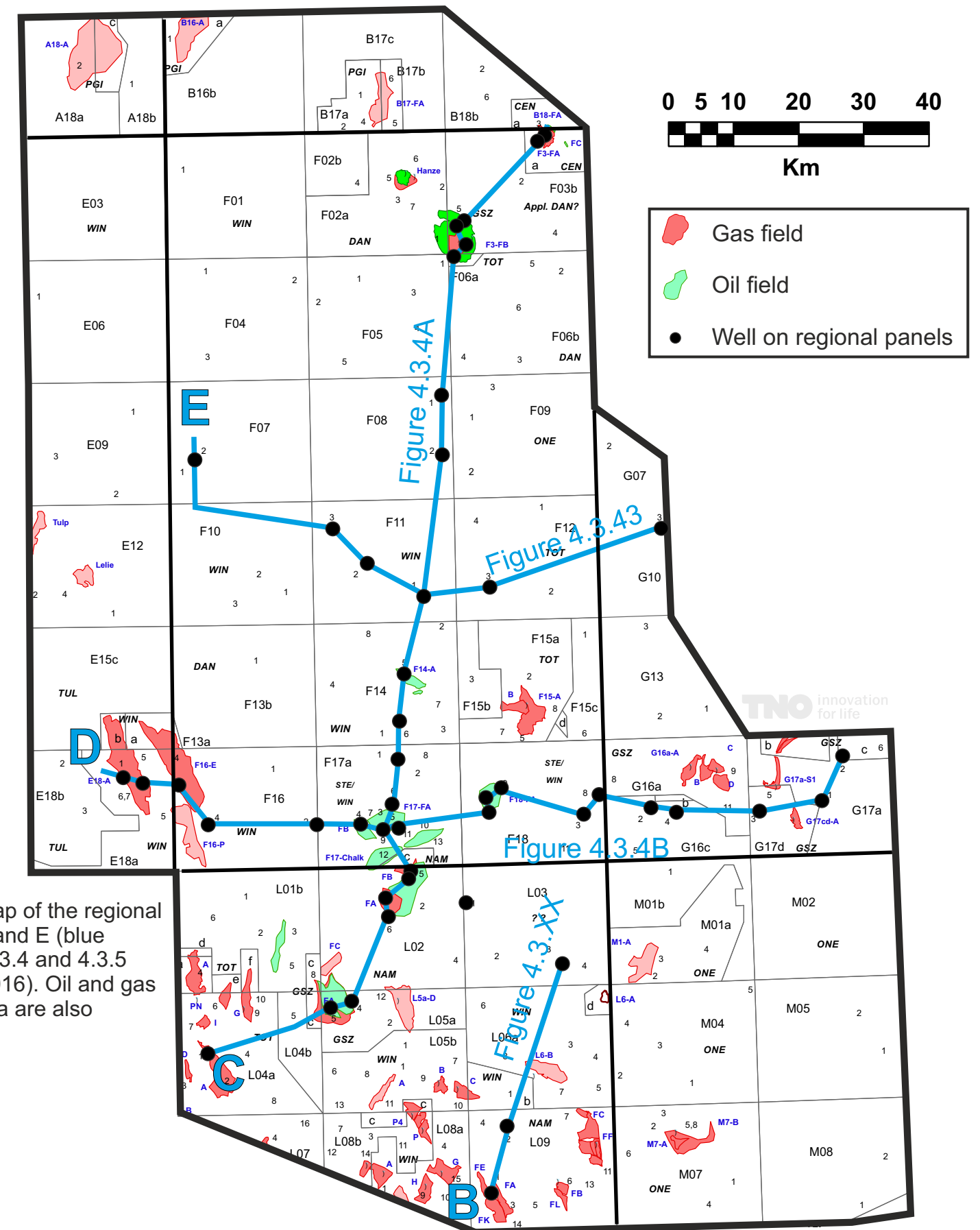


Figure 4.3.3: Location map of the regional seismic sections B, C, D and E (blue lines) shown in Figures 4.3.4 and 4.3.5 (from Bouroullec et al., 2016). Oil and gas fields within the study area are also shown.

4.3 Results - Case studies structural analysis: CS1

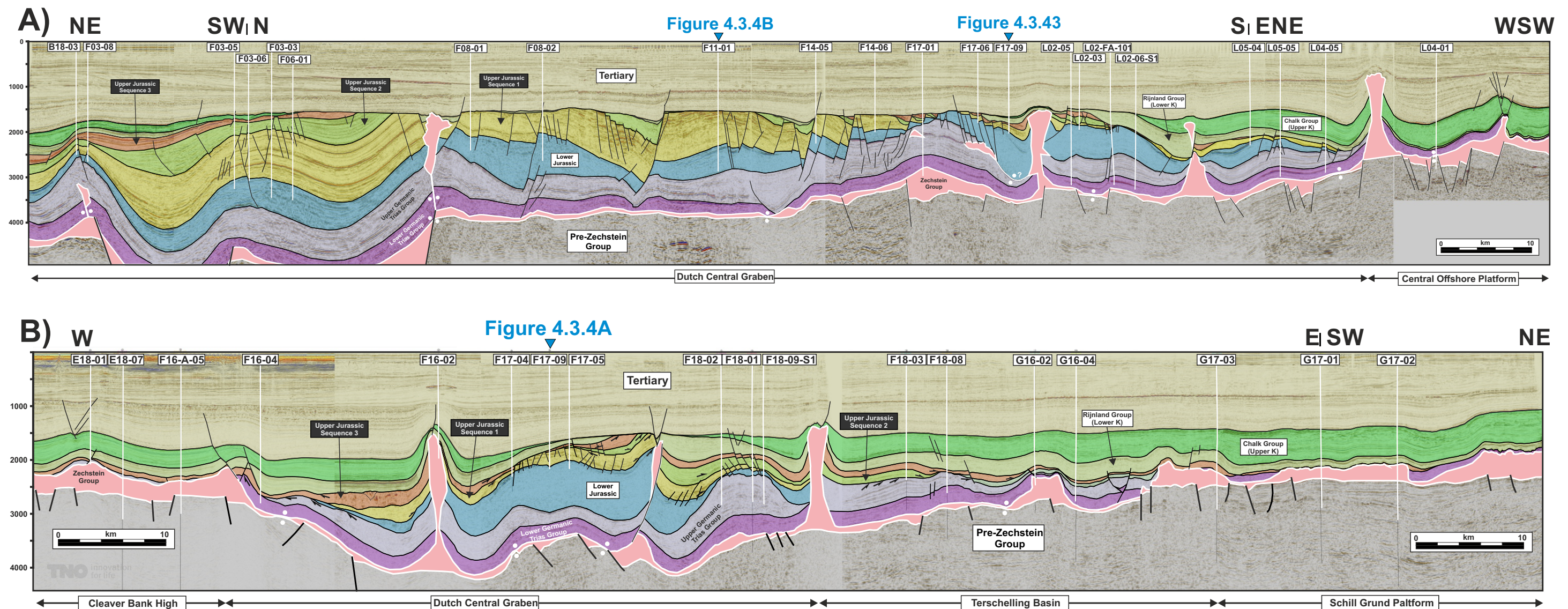


Figure 4.3.4: Regional seismic sections across the CS1 case study area (F17-F18) (from Bouroullec et al., 2016). **A)** Deep section along the axis Dutch Central Graben. This section is 170 km long, intercepts 21 wells and extends southward to the southern part of the Central Offshore Platform (COP). **B)** A strike section across the Dutch Central Graben and its lateral platforms. This section is located across four structural provinces, namely from east to west, the Cleaver Bank High, the Dutch Central Graben, the Terschelling Basin and the Schill Grund Platform. This section is 144,2 km long and intercept 9 wells. See Figure 4.3.2 for legend and Figure 4.3.3 for location.

The top Zechstein structural map, as well as the multi-z salt map, show a series of structural highs and lows that are related to salt withdrawal. Structural lows are present in the western part of both turtles structures (Fig. 4.3.7). Those lows are also observed in the successive Triassic structural maps (Figs. 4.3.11 and 4.3.14) and correspond to depo-thicks exclusively for the Upper Triassic interval (Muschelkalk/Keuper Formations thickness map, Fig. 4.3.15E) and the Lower Jurassic Altena Group thickness map (Fig. 4.3.15F). This indicates that either the autochthonous salt withdrawal increased during the later periods, or that the activity of rift bounding faults in the area occurred during these periods. It is widely believed that rifting was in a quiescence phase during the Lower Jurassic, which indicate than an increase in the intensity of salt migration triggered by differential loading is more likely.

Four Triassic and one Lower Jurassic thickness maps were constructed to evaluate the salt tectonic evolution of the area (Figs. 4.3.15B to F). These maps show lateral shifts of depo-thicks from map to map reflecting primarily the complex salt withdrawal dynamics.

The Lower Triassic thickness map (Fig. 4.3.15B) shows an interval ranging from 200 to 1200 m. Five zones can be seen: a relatively thin zone (200 to 500 m thick) in the central part of the F18 block (Zone 1), two zones of moderate thickness (400 to 800 m thick) in the block F17 (Zones 2 and 3), and two zones of greater thickness (800 to 1200 m) located in the eastern part of block F18 (Zone 4) and in the central part of Block F17 (Zone 5). It is important to notice that the over-thinned Zone 1 can be due to the presence of a horizontal salt weld below the F18 turtle, which may have resulted in structurally thinned Lower Triassic. The seismic quality of the deep section below the F18 turtle is relatively low due to a complex geological architecture and no clear final tectonostratigraphic model for this deep section was achieved.

4.3 Results - Case studies structural analysis: CS1

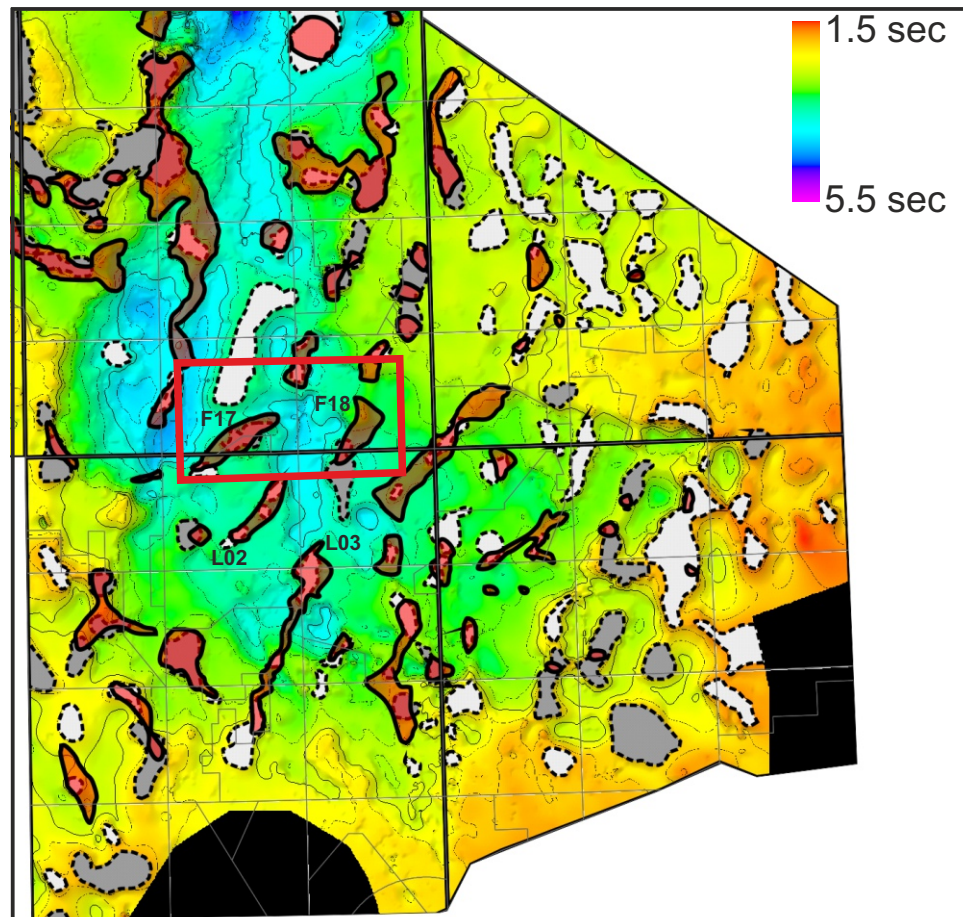


Figure 4.3.5: Location map of the study area for case study CS1. The PSDM cube used for this study extends covers a large part of the F17 and F18 blocks but also extends southward to the northern part of blocks L02 and L03. Deep autochthonous salt bodies are shown as dashed grey polygons, with light grey ones for salt bodies that have less than 500 ms of relief, and dark grey ones for salt bodies that have more than 500 ms of relief. Shallow salt bodies are shown as red polygons. Top Zechstein time structure map shown as background.

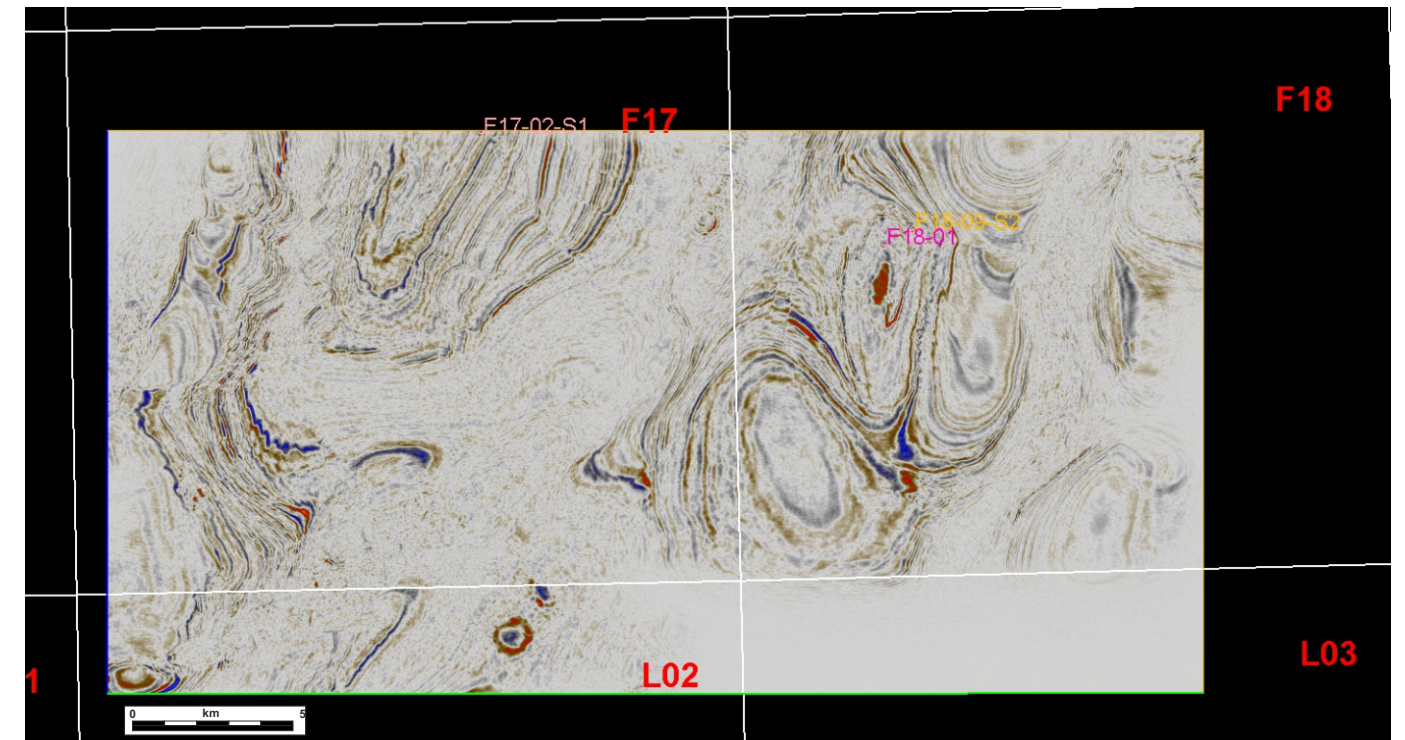


Figure 4.3.6: Location map showing the position of the 3D survey. Depth seismic slice (3 sec) shown as background. This 3D depth seismic data is of high quality. Note that the survey does not cover the entire blocks F17 and F18. Three wells (F17-02-S1, F18-01 and F18-09-S2) in the study area goes deeper than Jurassic.

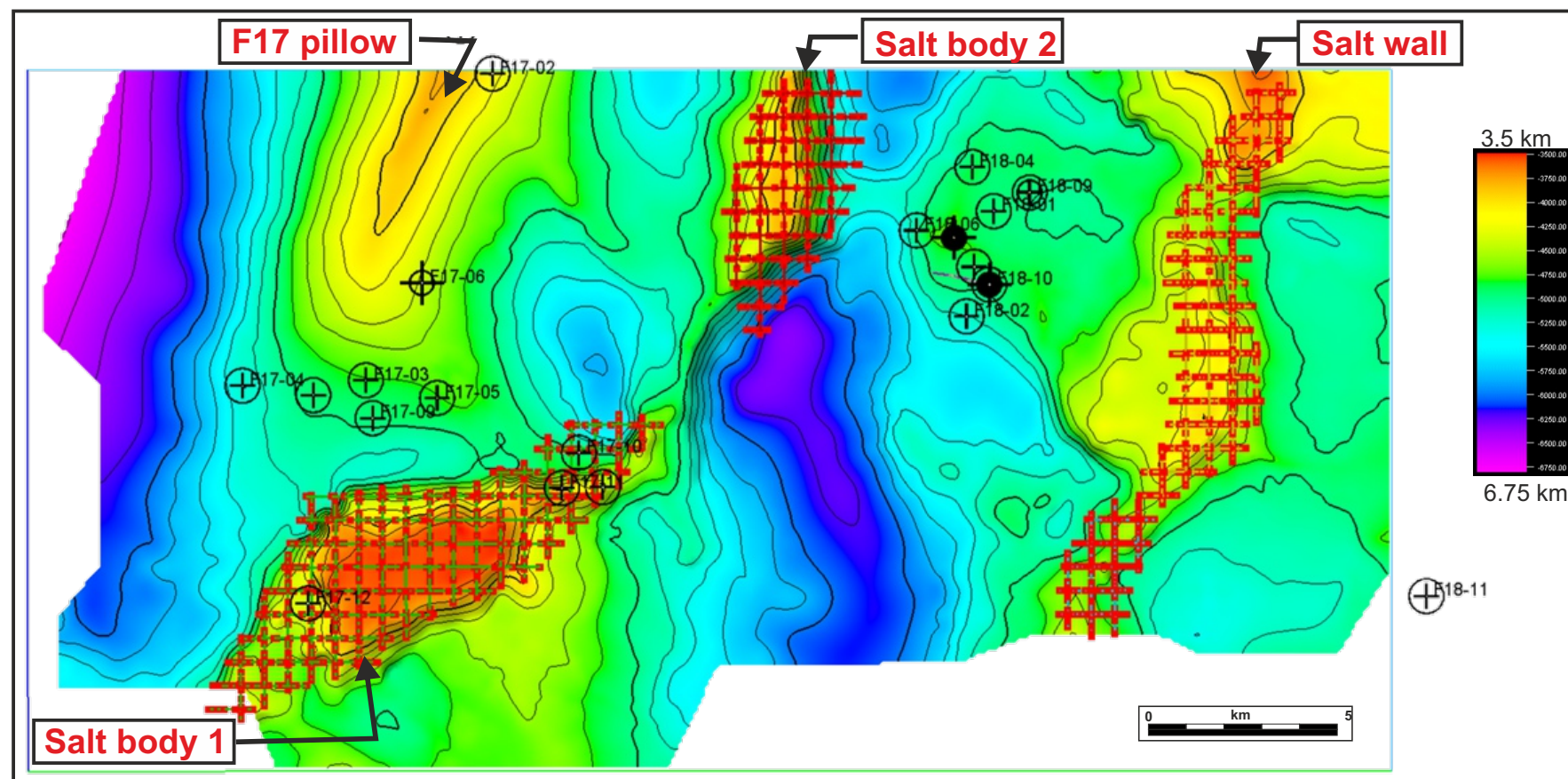


Figure 4.3.7: Top Zechstein structure map. The red mesh is the multi-z interpretation of the shallow salt features.

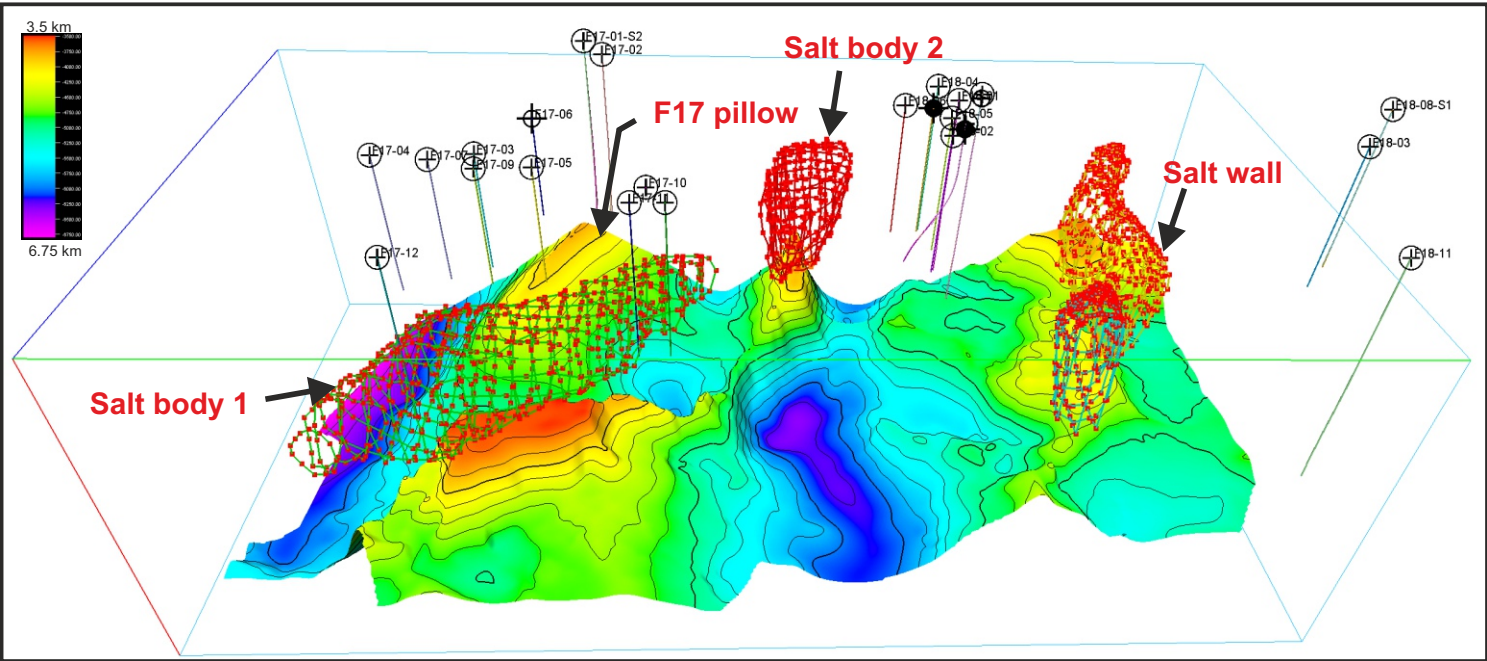


Figure 4.3.8: 3D perspective view looking toward the north of the top Zechstein surface and showing the multi-z (red mesh) interpretation of the top salt bodies.

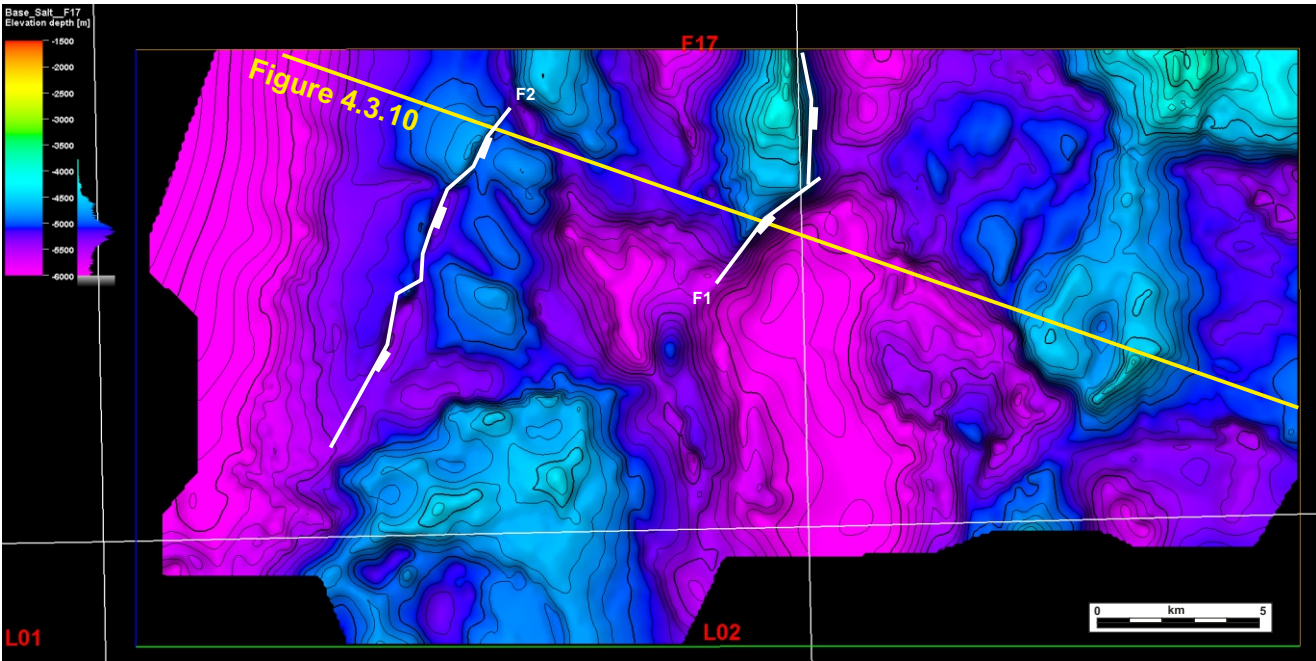


Figure 4.3.9: Base Zechstein surface. The base Zechstein is 4500 to 6000 meter deep in the study area.

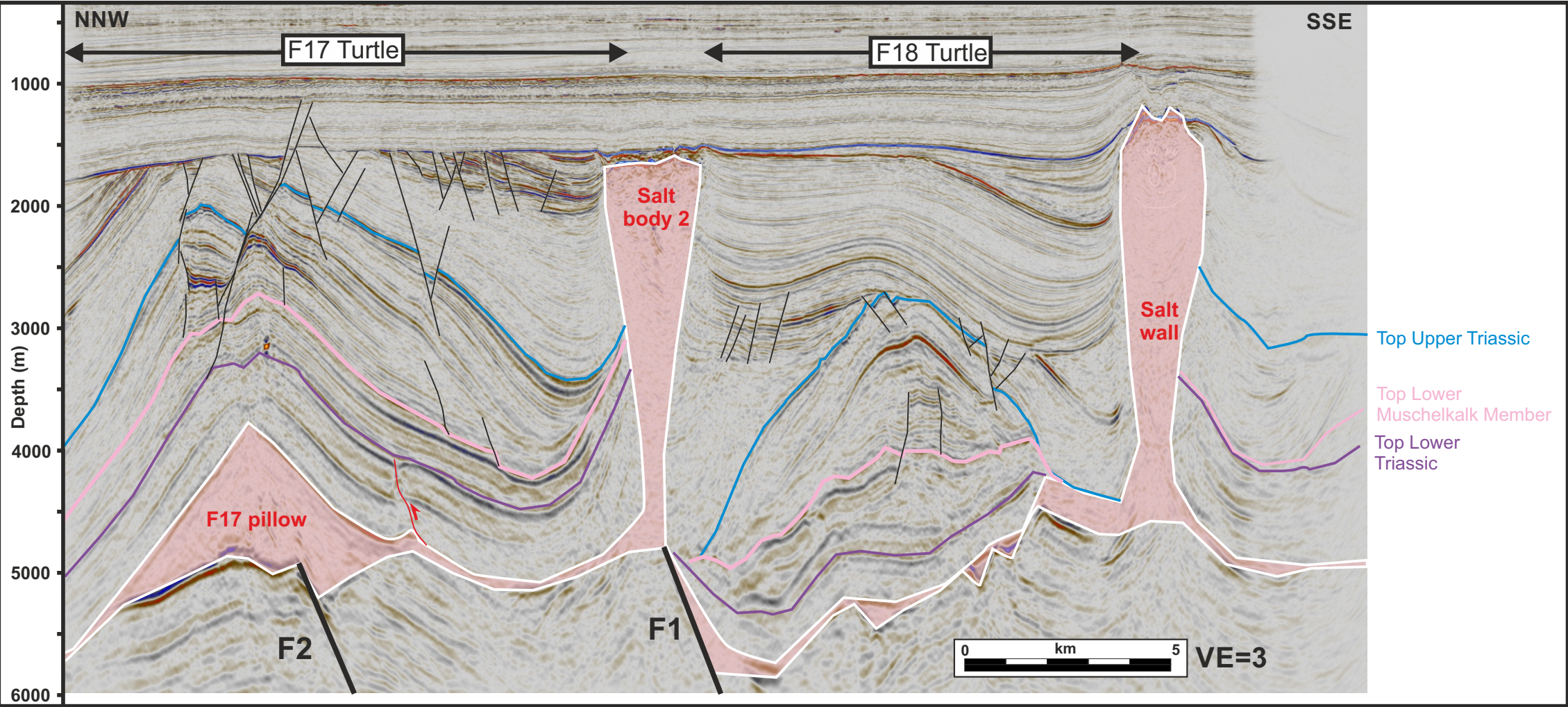


Figure 4.3.10: Interpreted seismic line illustrating the two turtle structures and associated salt bodies. See Figure 4.3.9 for location.

4.3 Results - Case studies structural analysis: CS1

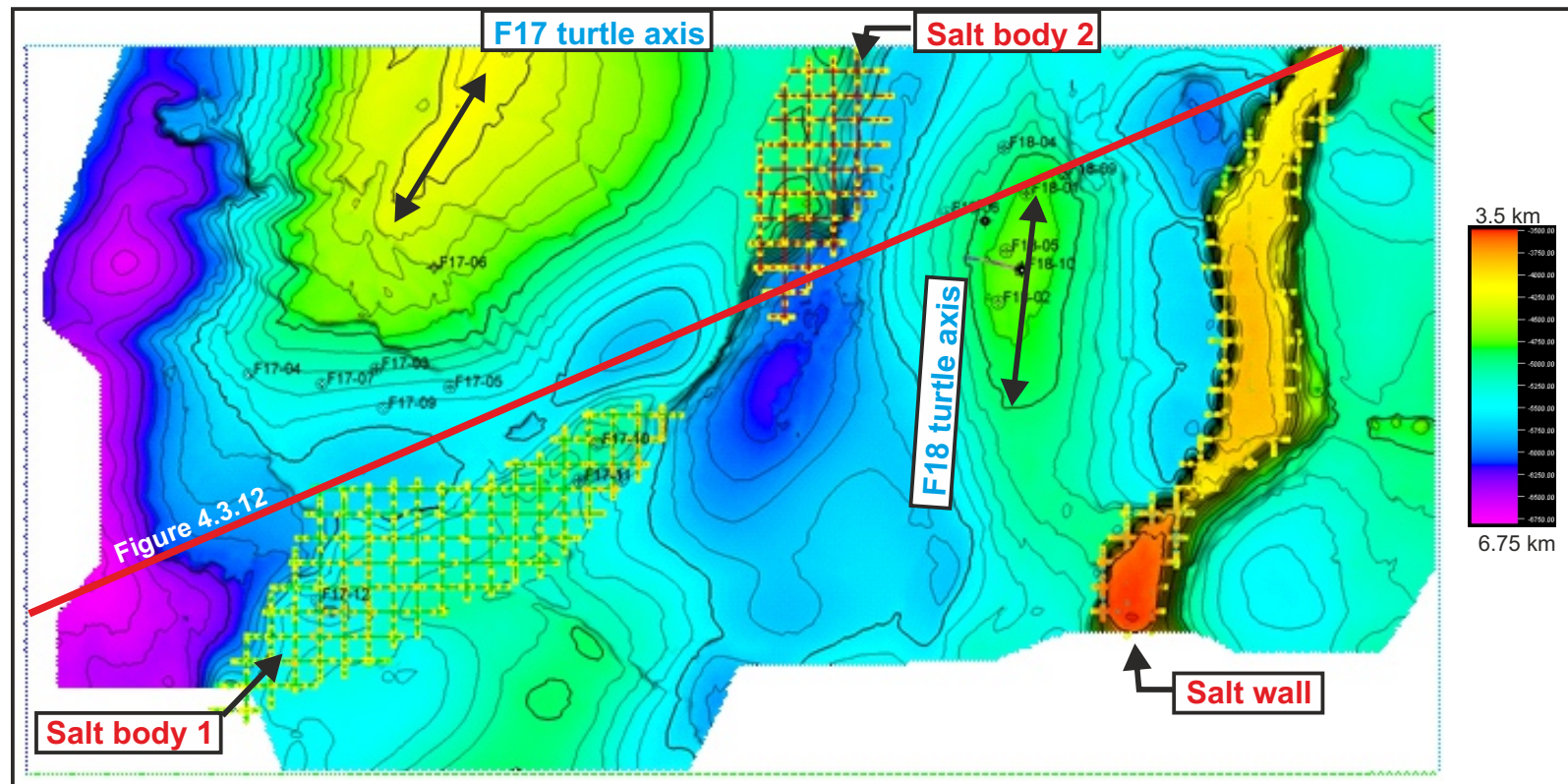


Figure 4.3.11: Top Triassic depth map and multi-z mesh interpretation of the top salt shallow features. Note at that level the crest of the two turtles are observed and highlighted by black arrows.

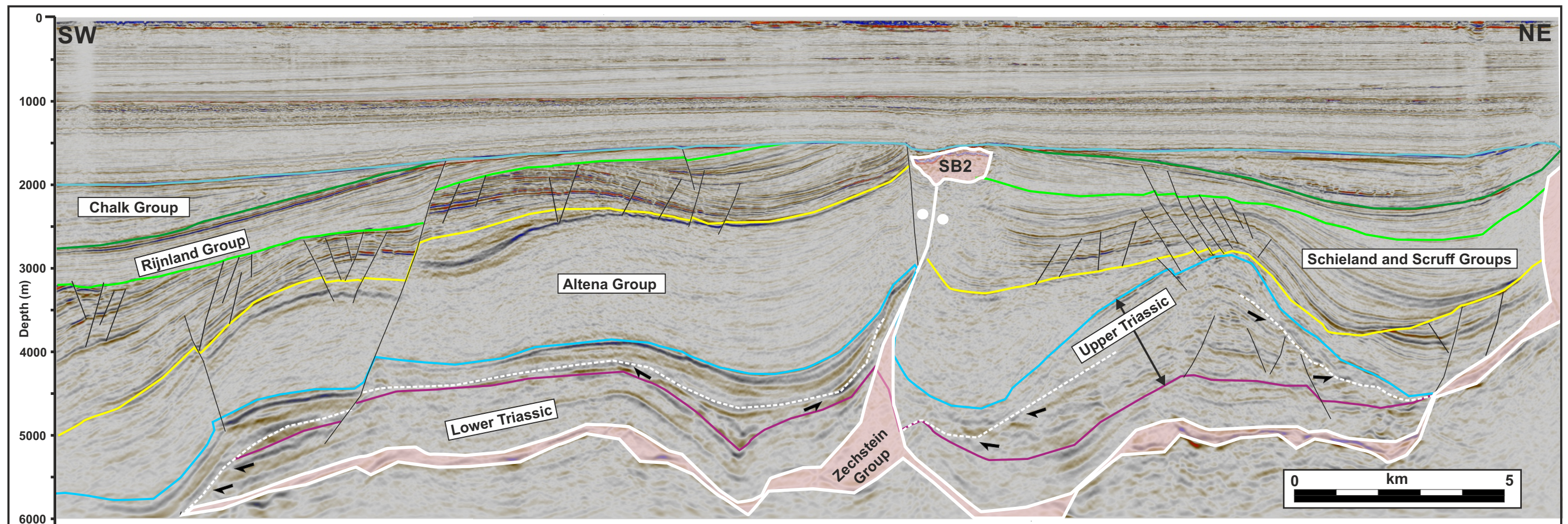


Figure 4.3.12: SSW-NNE interpreted seismic section across the F18 Turtle structure and the southern wedge of the F17 turtle structure. Possible salt welds are shown as dashed white lines.

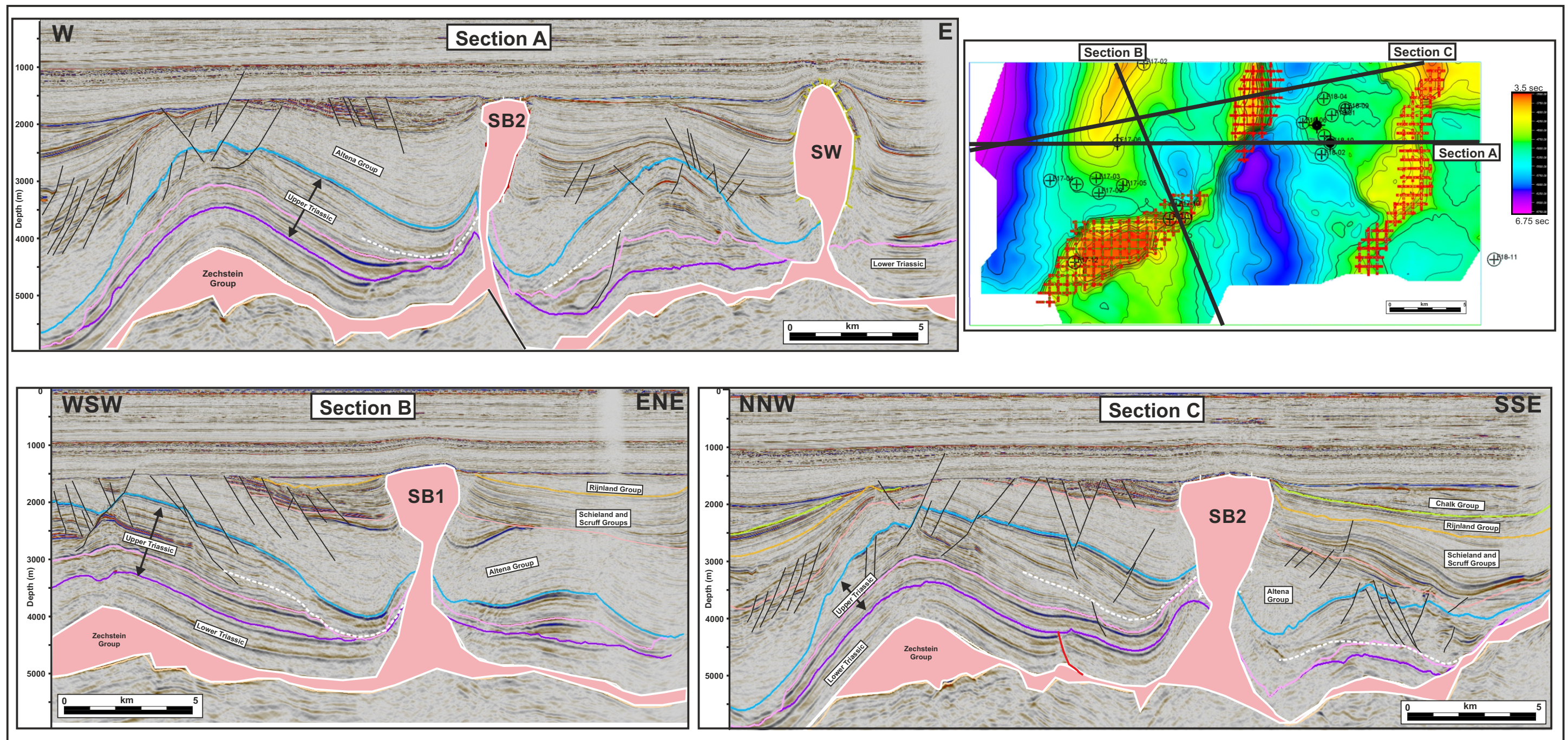
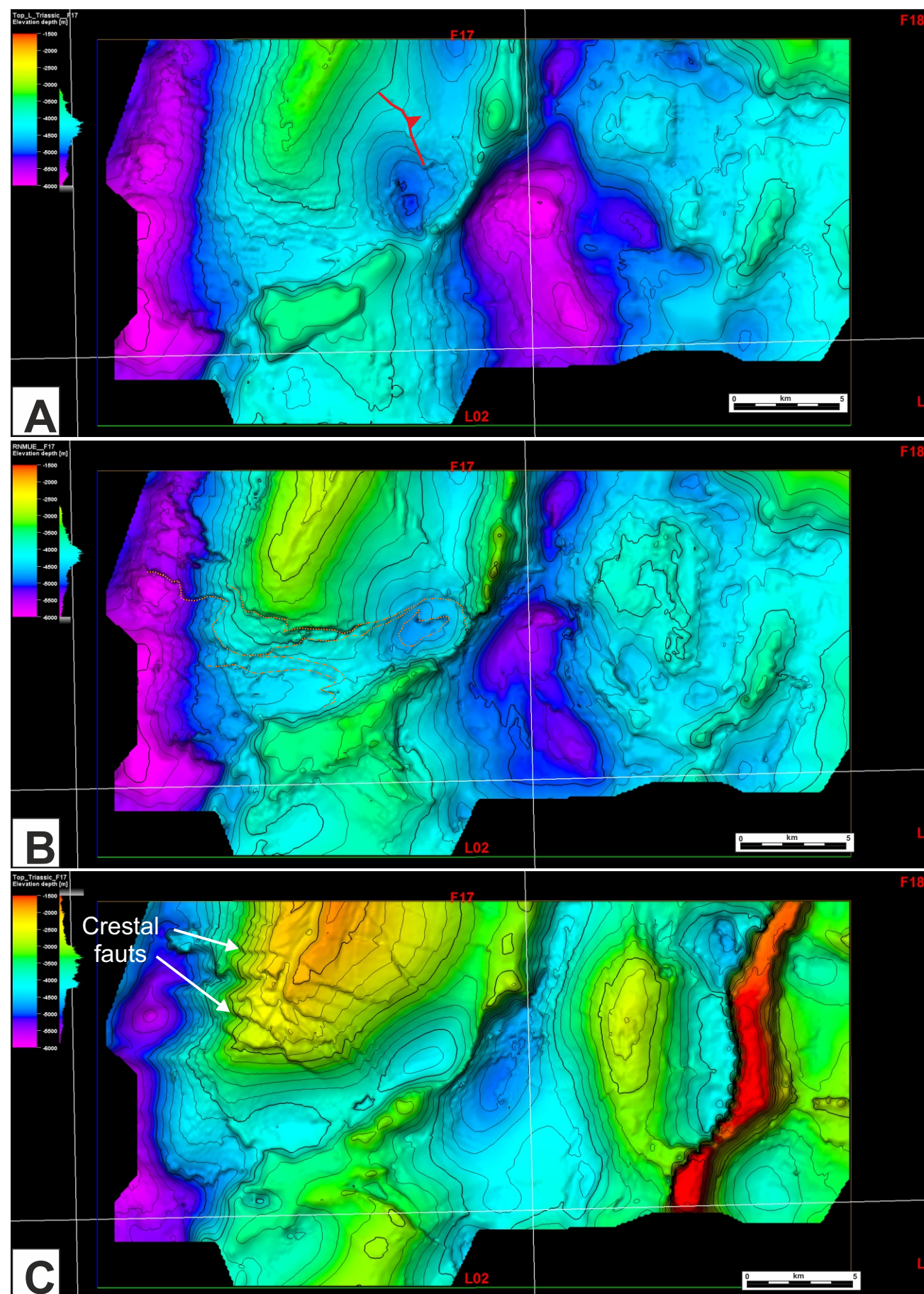


Figure 4.3.13: Three seismic examples of the salt geometry and associated fault systems present in the study area. See insert map for location of the sections. SB refers to salt bodies and SW to salt walls. Dashed white lines are possible salt welds.

4.3 Results - Case studies structural analysis: CS1



The Upper Triassic thickness map (Fig. 4.3.15C) shows a very different thickness distribution than the Lower Triassic (Fig. 4.3.15B). Two large depo-thicks are present below each turtle structure, reflecting axial subsidence typical of turtle structure growth model. However, the inversion of the turtle occurred at different time as seen in Figure 4.3.15D and E. The F18 turtle inverted during the Mulchekalk/Keuper Formations deposition time as seen by the lateral wedging (W1 and W2, Fig. 4.3.15E). This wedging continued during the Lower Jurassic (Fig. 4.3.15F, W3 and W4). In the case of the F17 turtle structure, the inversion occurred later, during the Lower Jurassic as seen by the wedging in Figure 4.3.15F (W5 and W6).

One of the main question arising from this study is the potential presence of a large salt weld. This potential salt weld can be seen in Figures 4.3.13, 4.3.16 and 4.3.17. This horizon was mapped and has a complex geometry that is often unconformal to older strata. Such a surface can either be interpreted as erosional surfaces related to a tilt of Triassic strata during salt movement followed by progressive erosion, or a salt weld related to the emplacement of an allochthonous salt sheet that was later deflated due to subsequent salt migration to shallower stratigraphic levels. This salt weld (or erosional surface) is located within the Upper Triassic (Fig. 4.3.13) with its stratigraphically shallower position roughly at the level of the Main Keuper Evaporite Member and as far low as the top of the Lower Triassic. Further discussion regarding the origin and evolution of this feature can be found in the discussion (Chapter 5). It is likely that the salt wall and the salt body 1 and 3 couple have been affected by strike slip movement.

Figure 4.3.14: Depth structure maps. **A)** Top Lower Triassic. The red fault in map A is the thrust fault observed in Figure 4.3.13C that offset the Lower Triassic. **B)** Top Muschelkalk Member. Note that the orange dashed lines represent the trend of the salt weld (or erosional surface) that drops stratigraphically down as observed in Figure 4.3.16. **C)** Top Triassic. Numerous NE-SE faults are observed in the F17 turtle structure. Most of those faults are crestal normal faults.

4.3 Results - Case studies structural analysis: CS1

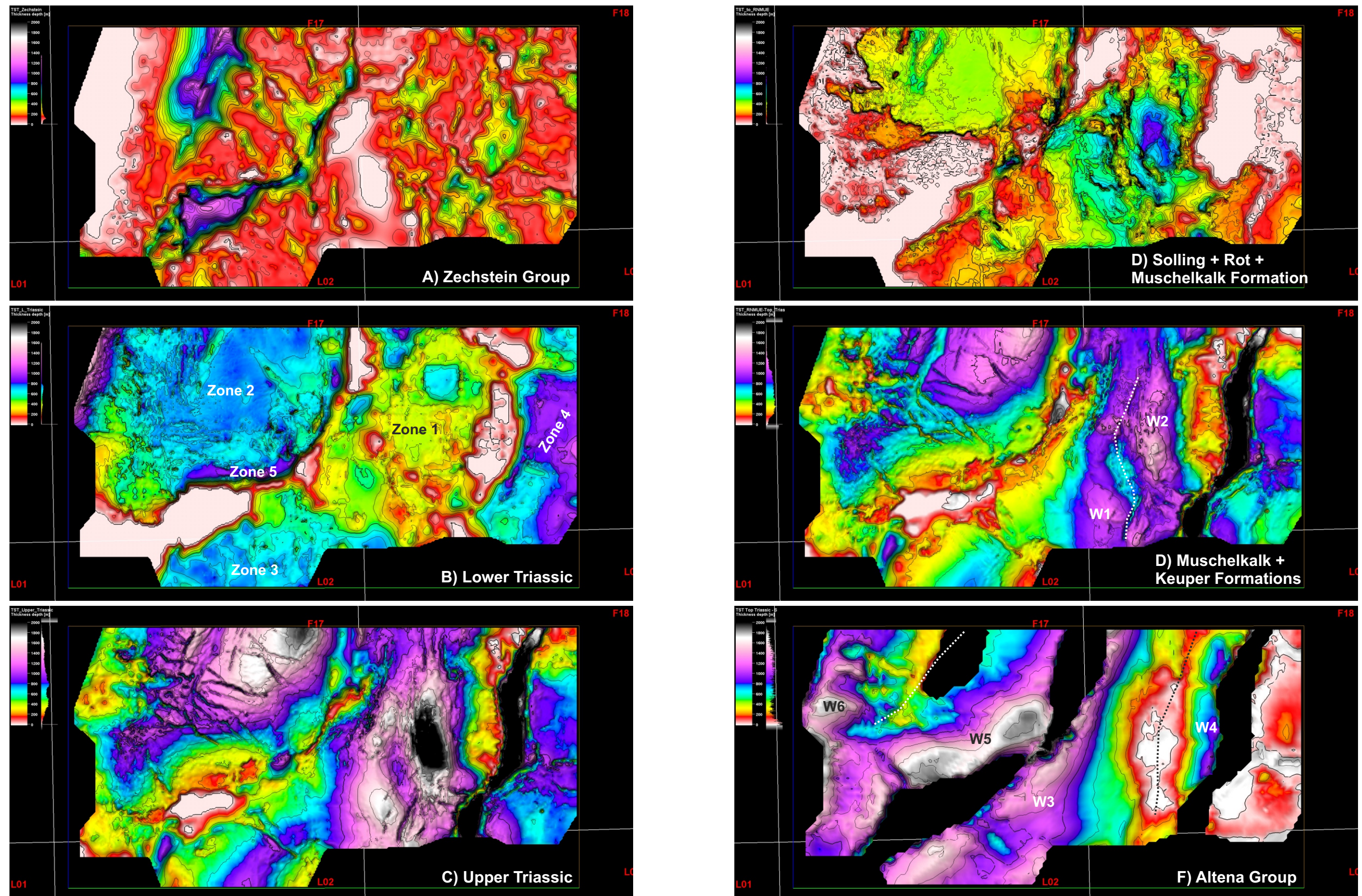


Figure 4.3.15: Thickness maps. W1-6 refers to stratigraphic wedges. Dashed lines show turtle structures axis. See text for additional comments.

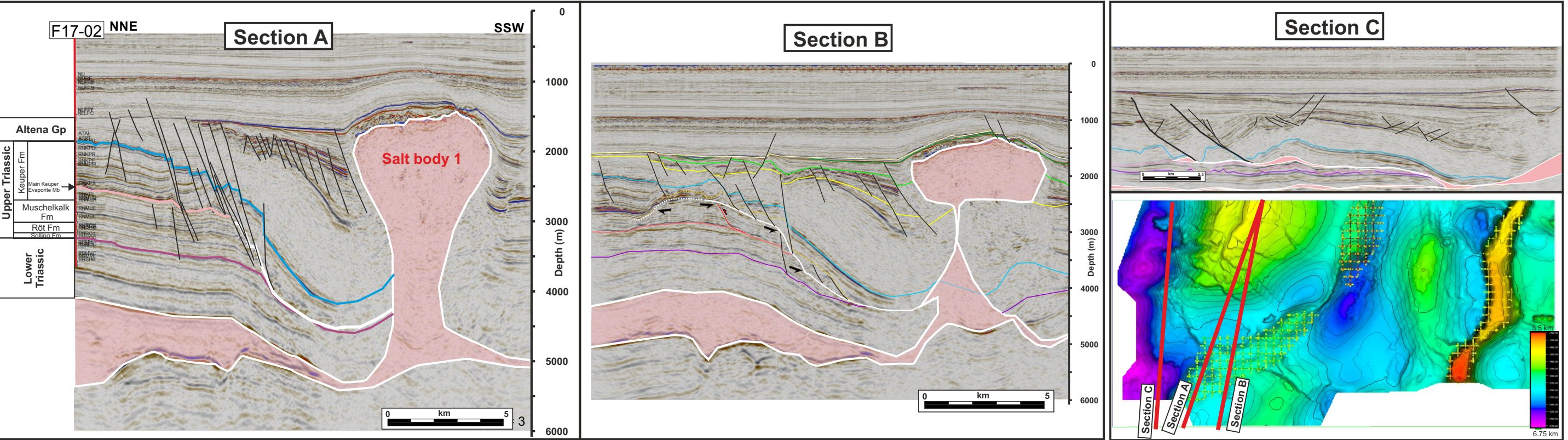
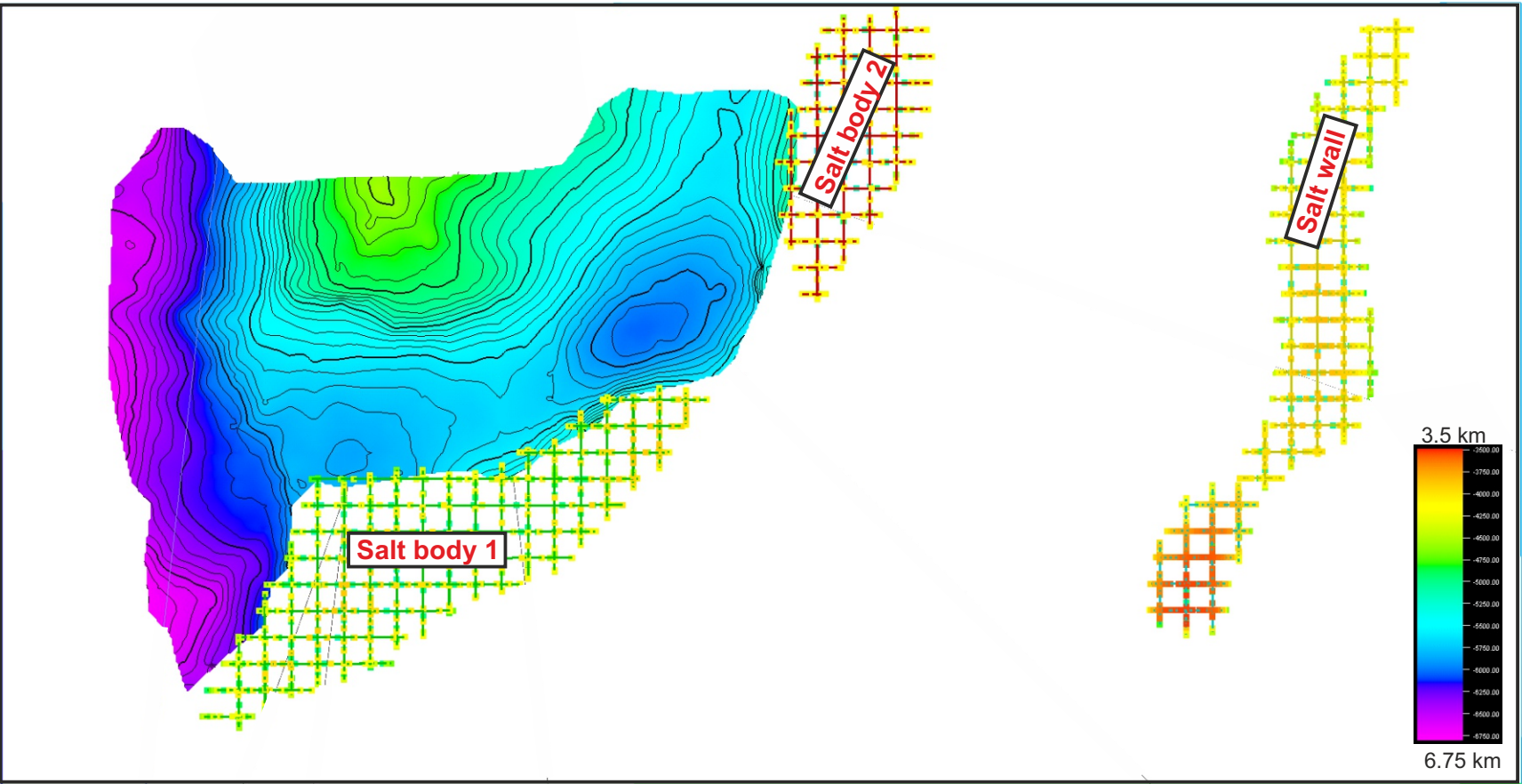


Figure 4.3.16: Interpreted seismic sections across the potential salt weld in the F17 block. The salt weld is shown as a white line. Note that section C is 1 to 1 in scale.



4.3.17: Structure map of the F17 salt weld/erosional surface and the surrounding shallow salt bodies.

B) Case study 2: L05-L06-L08-L09

The second case study is located in the southwestern part of the Terschelling Basin and extends southward onto the Friesland Platform (Fig. 4.3.18). The part of the Terschelling Basin is structurally complex with numerous large syn-depositional faults present (Fig. 4.3.19). The focus of this case study is on the distribution of salt bodies and the possible presence of horizontal salt welds in several zones. Figure 4.3.20 shows the distribution of shallow salt features (three salt bodies and two salt walls) and salt welds in the study area. The seismic section displayed in this chapter (Figs. 4.3.22 to 31) reveal a structurally very complex area, with rapid stratigraphic thickness changes for the Zechstein, Triassic and Jurassic strata and locally the absence of stratigraphic interval due to erosion and/or rafting/collapse dynamics (See Chapter 2 for description of those features).

The Lower Triassic is locally missing (e.g. Figs. 4.3.23 to 30). These absences are often related to the presence of:

- Large syn-depositional fault that lateral shifted the Lower Germanic Trias Group blocks (raft tectonics) such as in Figure 4.3.23 (Fault F1, raft R1) and Figure 4.3.24 (Fault F2, rafts R2 and R3).
- Possible salt extrusions, expulsion rollovers and/or salt body collapse in the case of Figure 4.3.23 (Salt Systems 1 and 2), Figure 4.3.24 (Salt System 4); Figure 4.3.27 (salt system 5); Figure 4.3.26 (salt system 6); Figure 4.3.27 (Salt Systems 7 and 8), Figure 4.3.28 (Salt System 9), Figure 4.3.29 (salt system 10) and Figure 4.3.30 (Salt System 11). These salt systems kinematics and conceptual models are presented in Chapter 5.

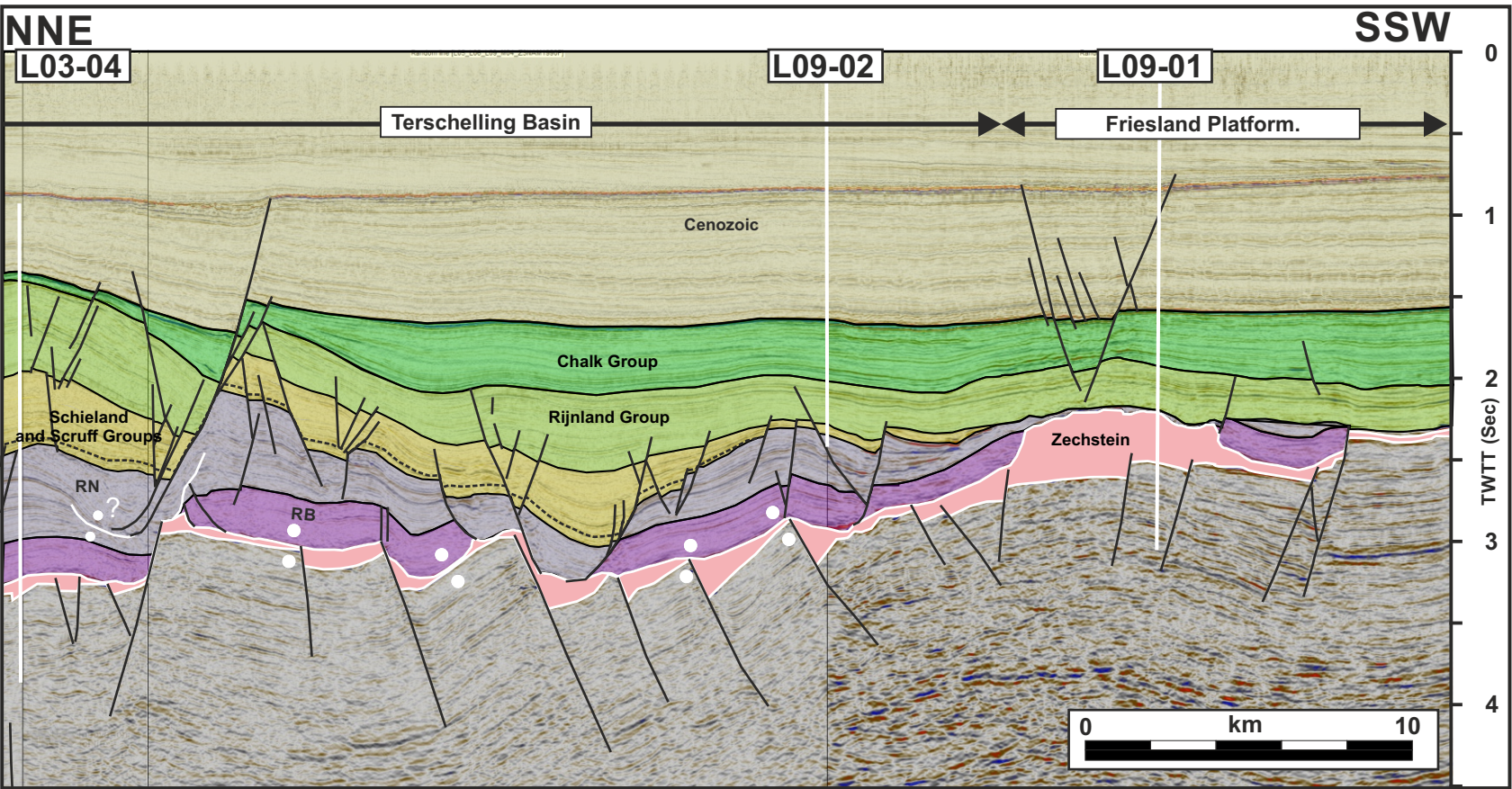
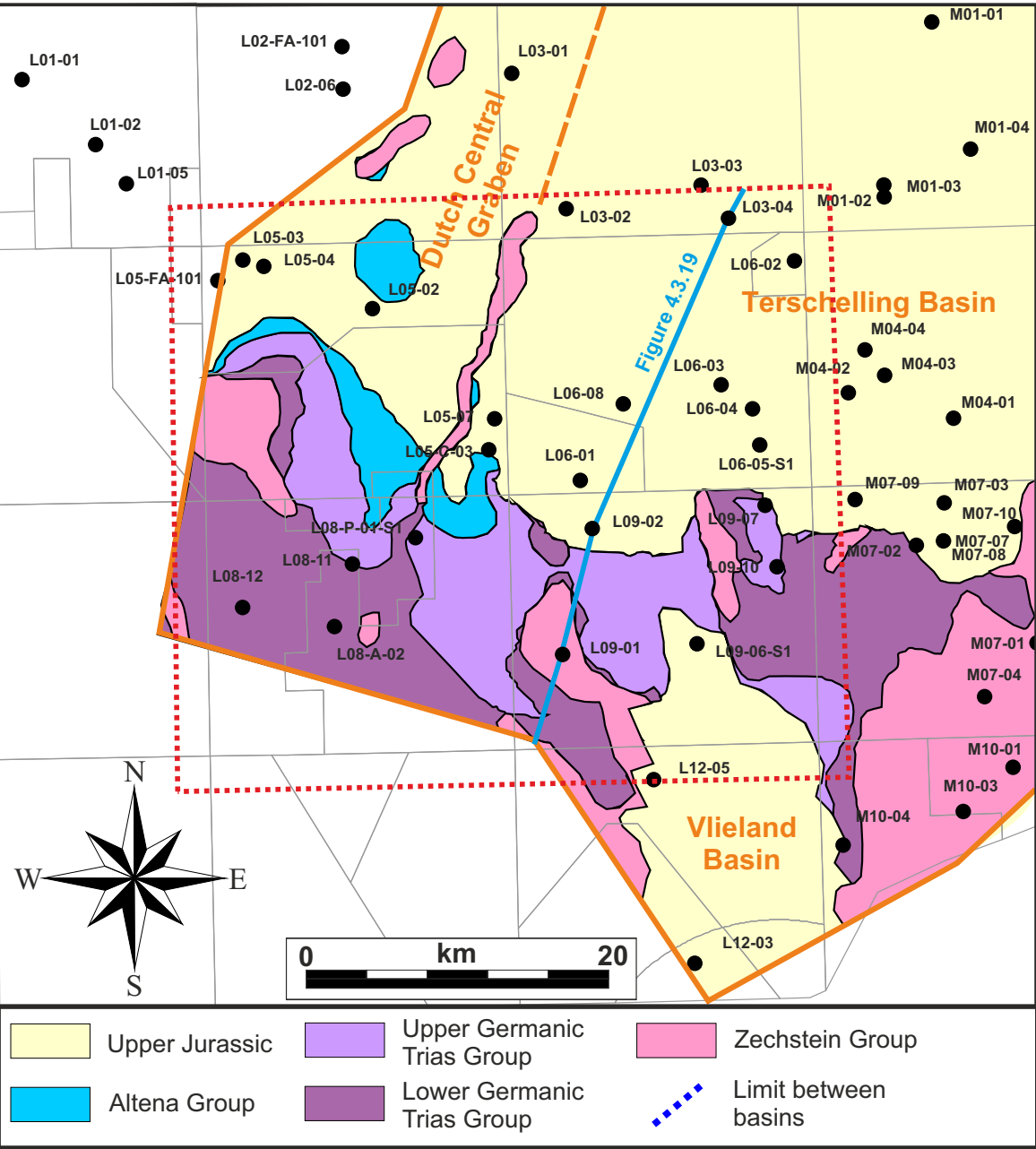


Figure 4.3.19: Seismic section across the study area of the case study 2 (from Bouroullec et al., 2016). RB = Lower Germanic Trias Group; RN = Upper Germanic Trias Group. See Figure 4.3.2 for legend and Figure 4.3.3 for location.

Figure 4.3.18: Location map of the study area that is shown as a dashed red box. The background image is the Rijnland Group subcrop map (Bouroullec et al., 2016).

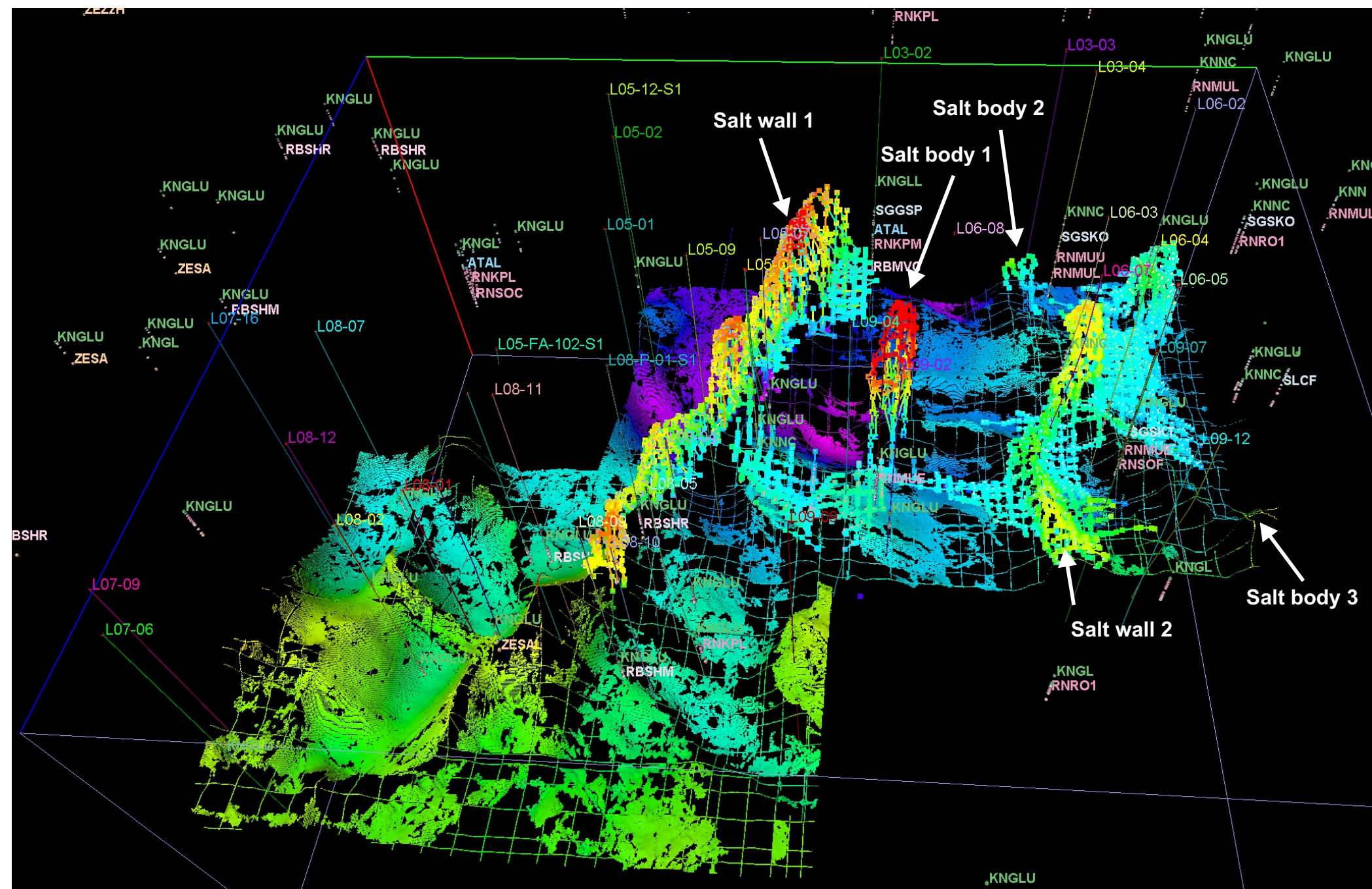
4.3 Results - Case studies structural analysis: CS2

A few Upper Triassic contractional features are observed in this area such as the thrust faults TF1 (Fig. 4.3.26), TF2/TF3 (Fig. 4.3.30) and TF4 (Fig. 4.3.31). These contractional structures are likely the downdip part of the extensional and translational growth fault/raft systems observed in the study area and beyond.

The base salt time structure map (Fig. 4.3.33) show a fault fabric with two predominant trends, NW-SE in both the TB and the FP and SW-NE mainly on the FP. The NW-SE trend is also observed on the top salt time structure map (Fig. 4.3.34) and Upper Triassic time structures maps (Figure 4.3.36), while the SW-NE trend is highlighted in the shallower intervals by the geometry of the salt bodies and salt walls that also trend the same way (Figs. 4.3.32 and 4.3.37).

The Zechstein group thickness map show a thinner unit in the north-western part of the study area (Block L05) (Figure 4.3.37). The Lower Triassic is up to 400 ms thick in three depothicks located in the eastern part of the study area (Zones 1-3, Fig. 4.3.38). The time thickness

maps shown in Figure 4.3.38 also show the areas (black zones 4-7) where the Lower Triassic is absent due to the reasons stated above. The Upper Triassic thickness map (Fig. 4.3.39) displays a complex thickness pattern, with a strong NW-SE pattern. The thickest zone (Zone 8) is in the north-western part of the study area, in the TB. When looking at a higher resolution for the upper part of the Upper Triassic (e.g. stratigraphic thickness for the top Middle Muschelkalk Marl Member to top Upper Triassic interval, Fig. 4.3.41), the SW-NE trends seen before becomes predominant, following the salt feature distribution pattern. The depo-thicks of this Upper Triassic interval is indicating that active salt withdrawal into shallower stratigraphy occurred during this period.



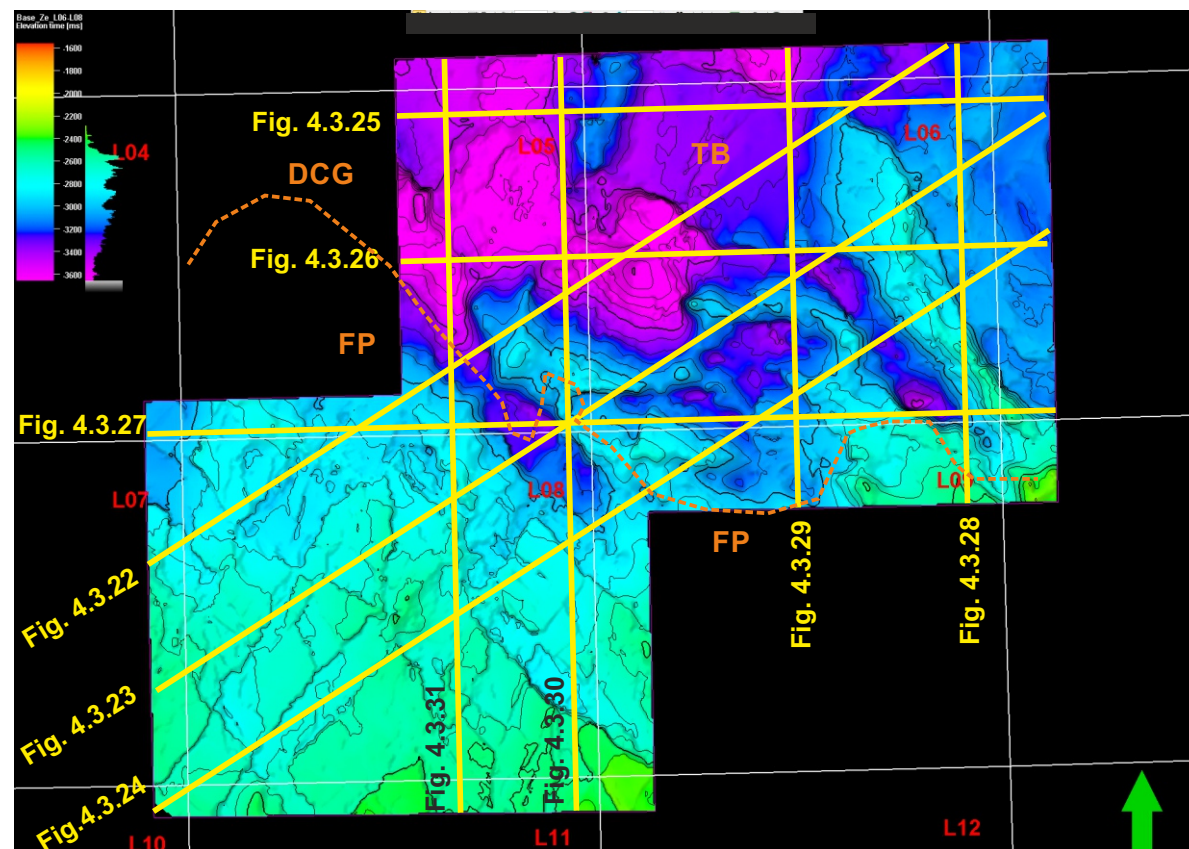


Figure 4.3.21: Location map for the seismic section shown in this report for this case study. The background map is the base Zechstein time structure map.

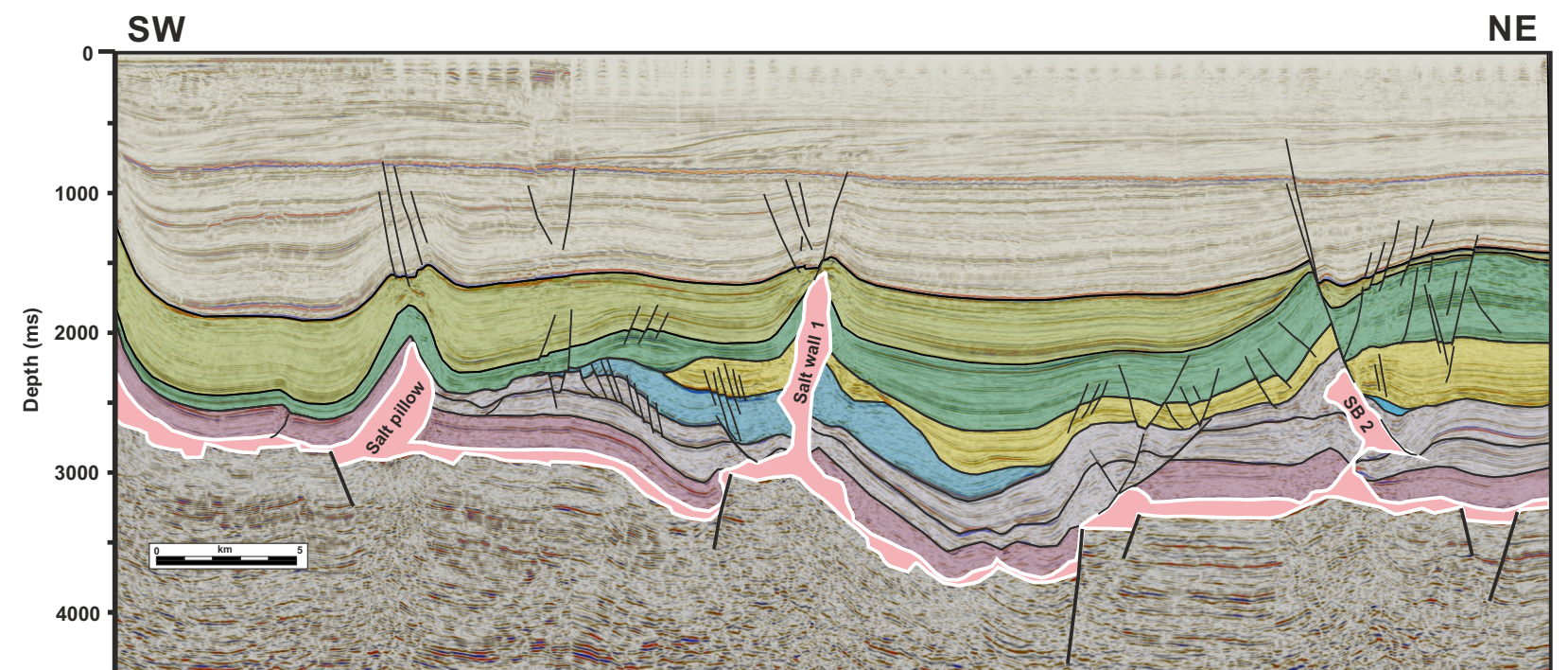


Figure 4.3.22: SW-NE seismic line across the study area. See Figure 4.3.21 for location.

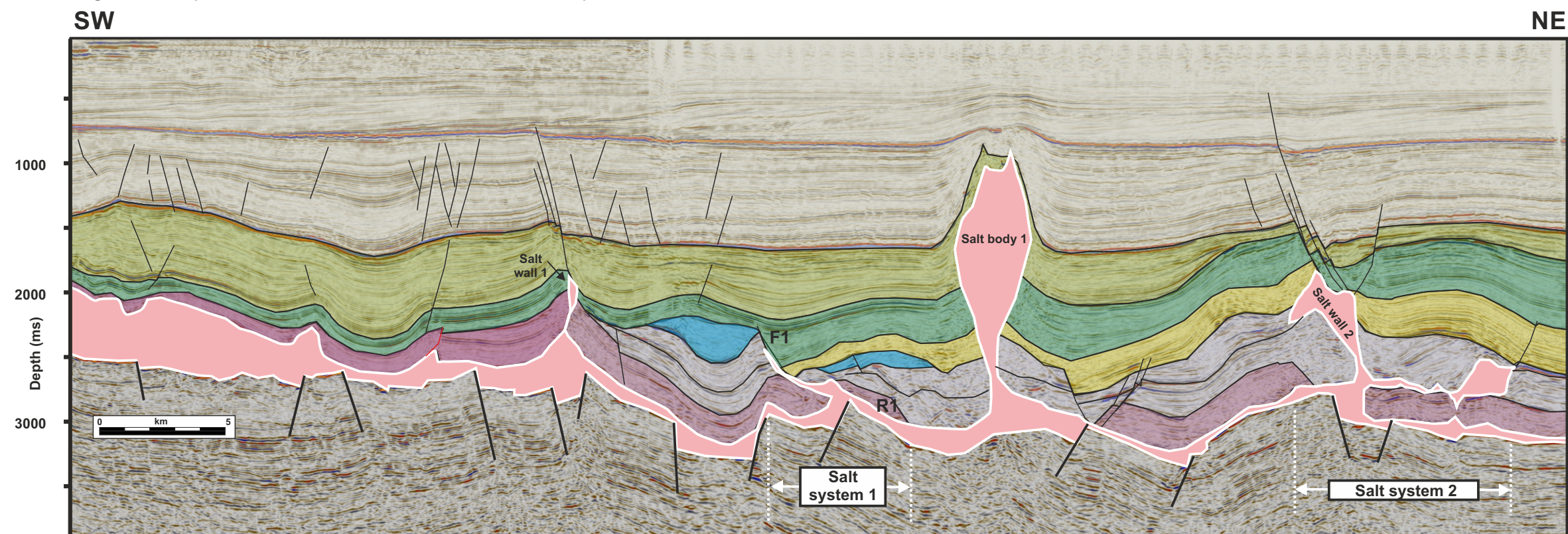


Figure 4.3.23: SW-NE seismic line across the study area. See text for comments. R1 is a raft related to growth of fault F1. See Figure 4.3.21 for location.

4.3 Results - Case studies structural analysis: CS2

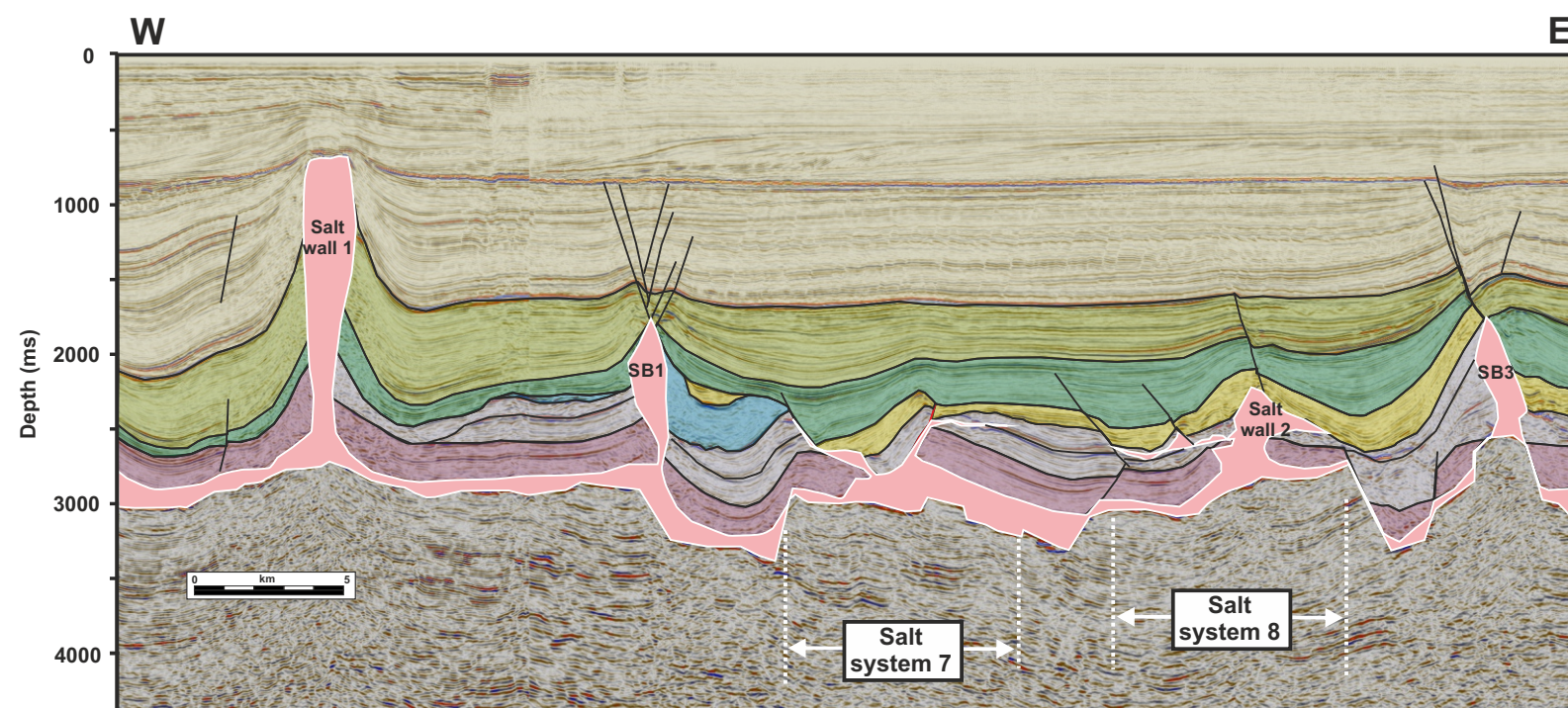


Figure 4.3.27: W-E seismic line across the study area. See text for comments. See Figure 4.3.21 for location.

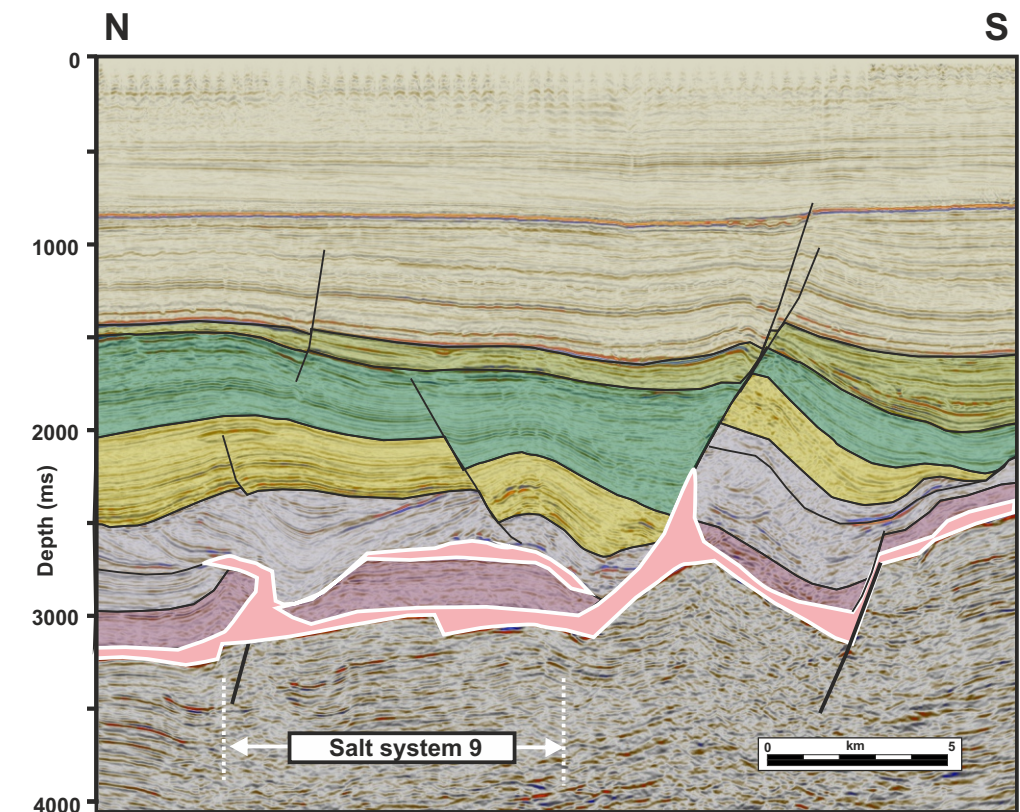


Figure 4.3.28: N-S seismic line across the study area. See text for comments. See Figure 4.3.21 for location.

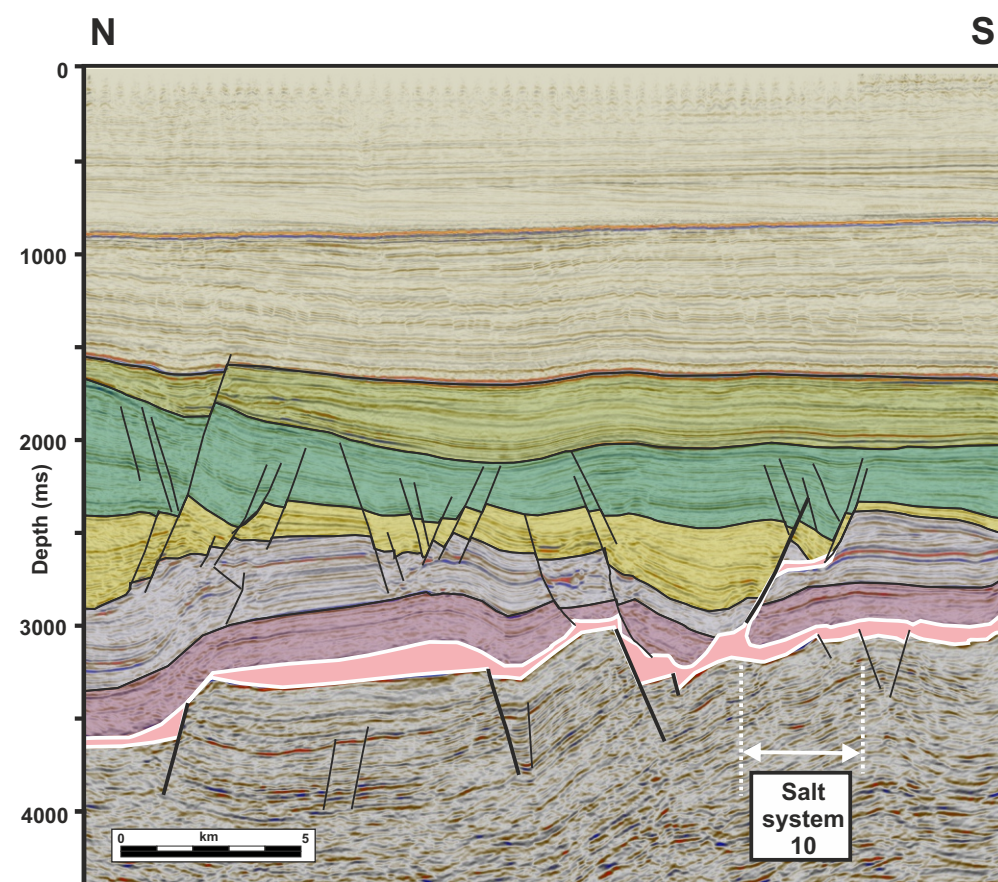


Figure 4.3.29: N-S seismic line across the study area. See text for comments. See Figure 4.3.21 for location.

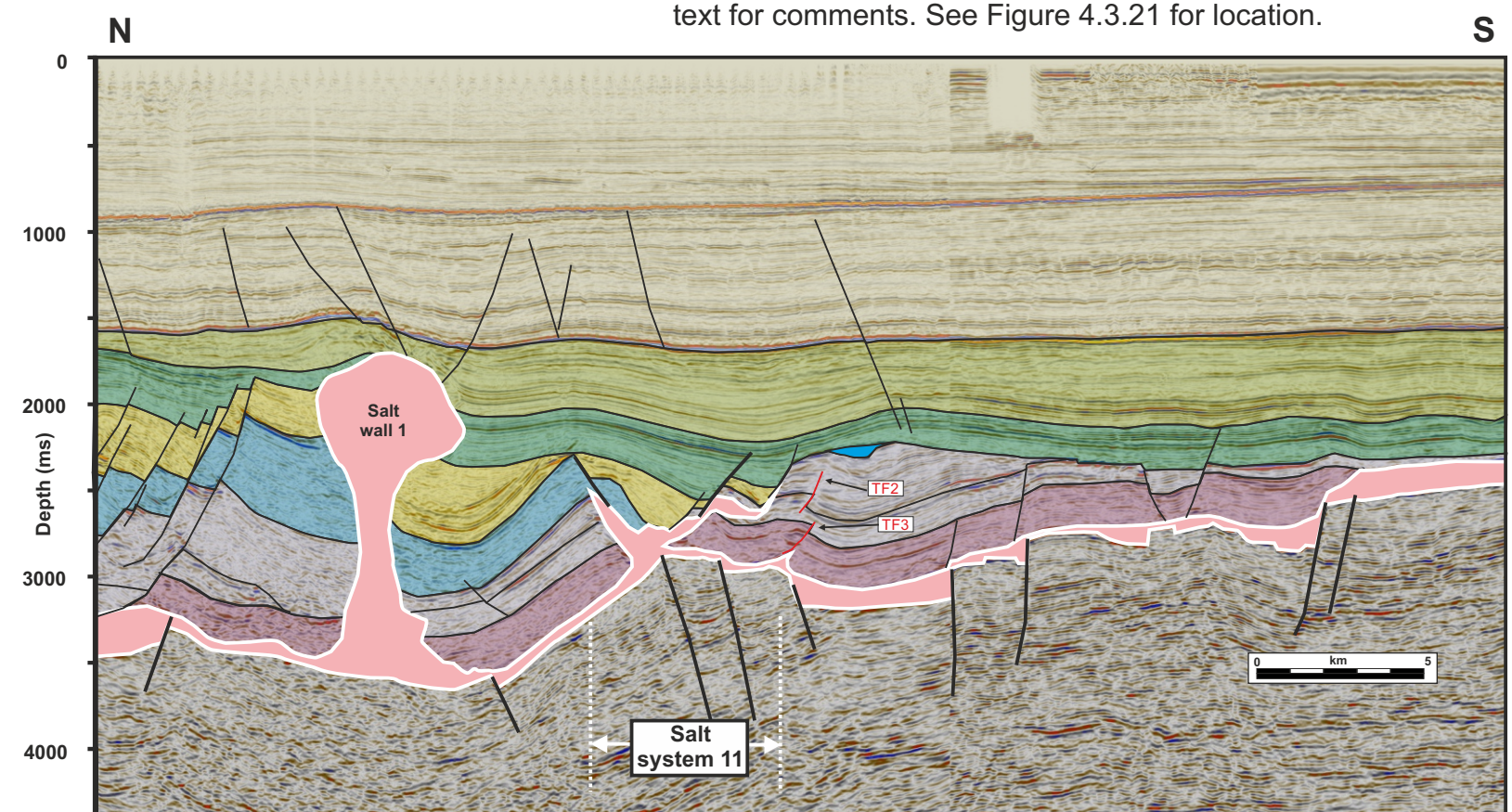


Figure 4.3.30: N-S seismic line across the study area. See text for comments. See Figure 4.3.21 for location.

4.3 Results - Case studies structural analysis: CS2

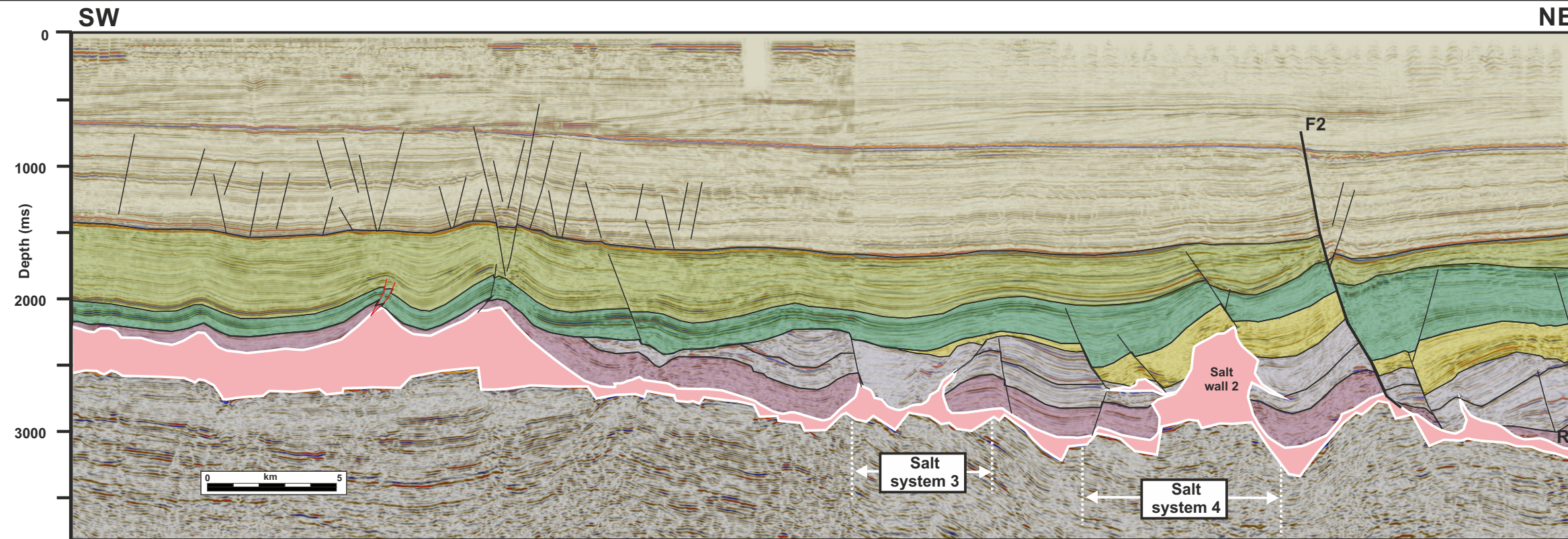


Figure 4.3.24: SW-NE seismic line across the study area. R2 is a raft related to growth of fault F2. See text for comments. See Figure 4.3.21 for location.

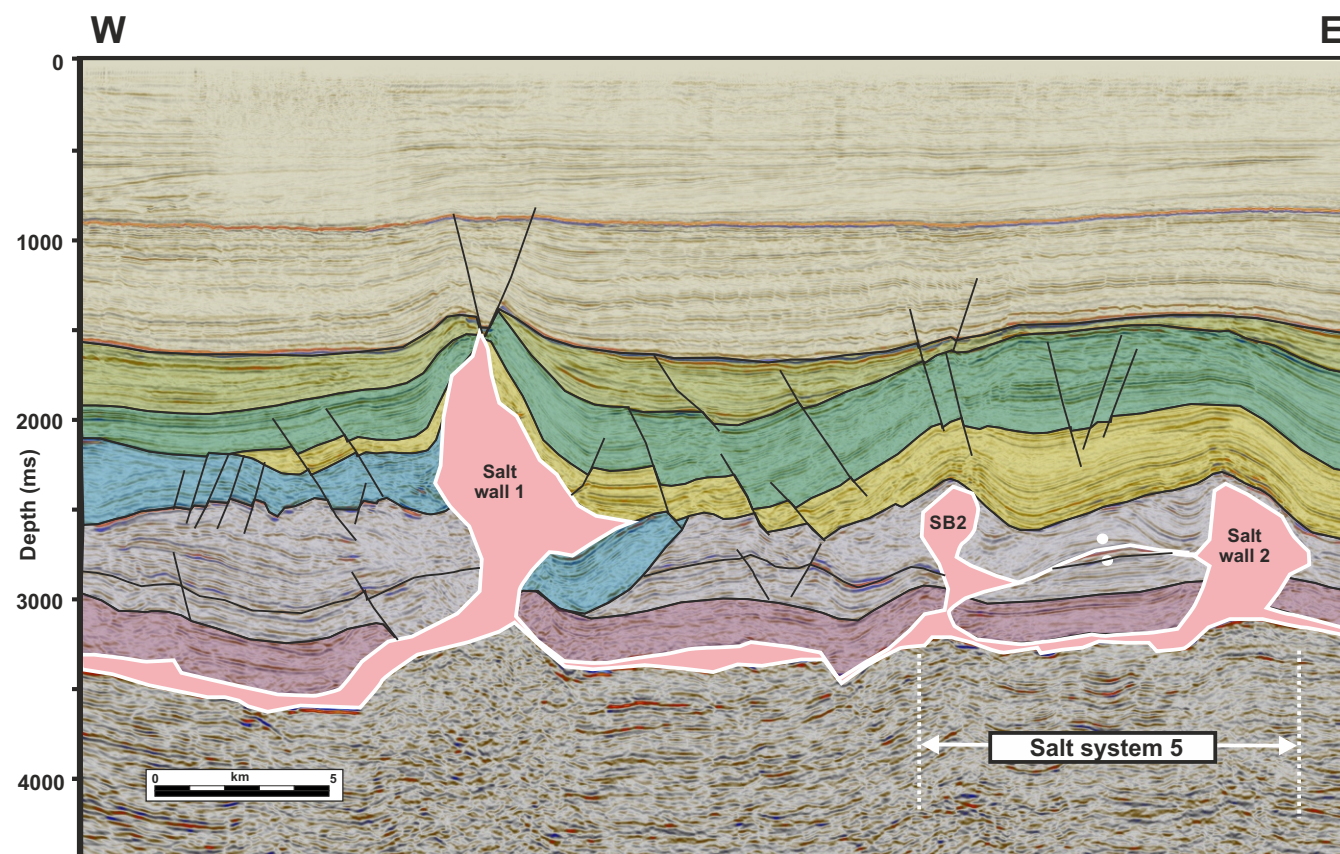


Figure 4.3.25: W-E seismic line across the study area. See text for comments. See Figure 4.3.21 for location.

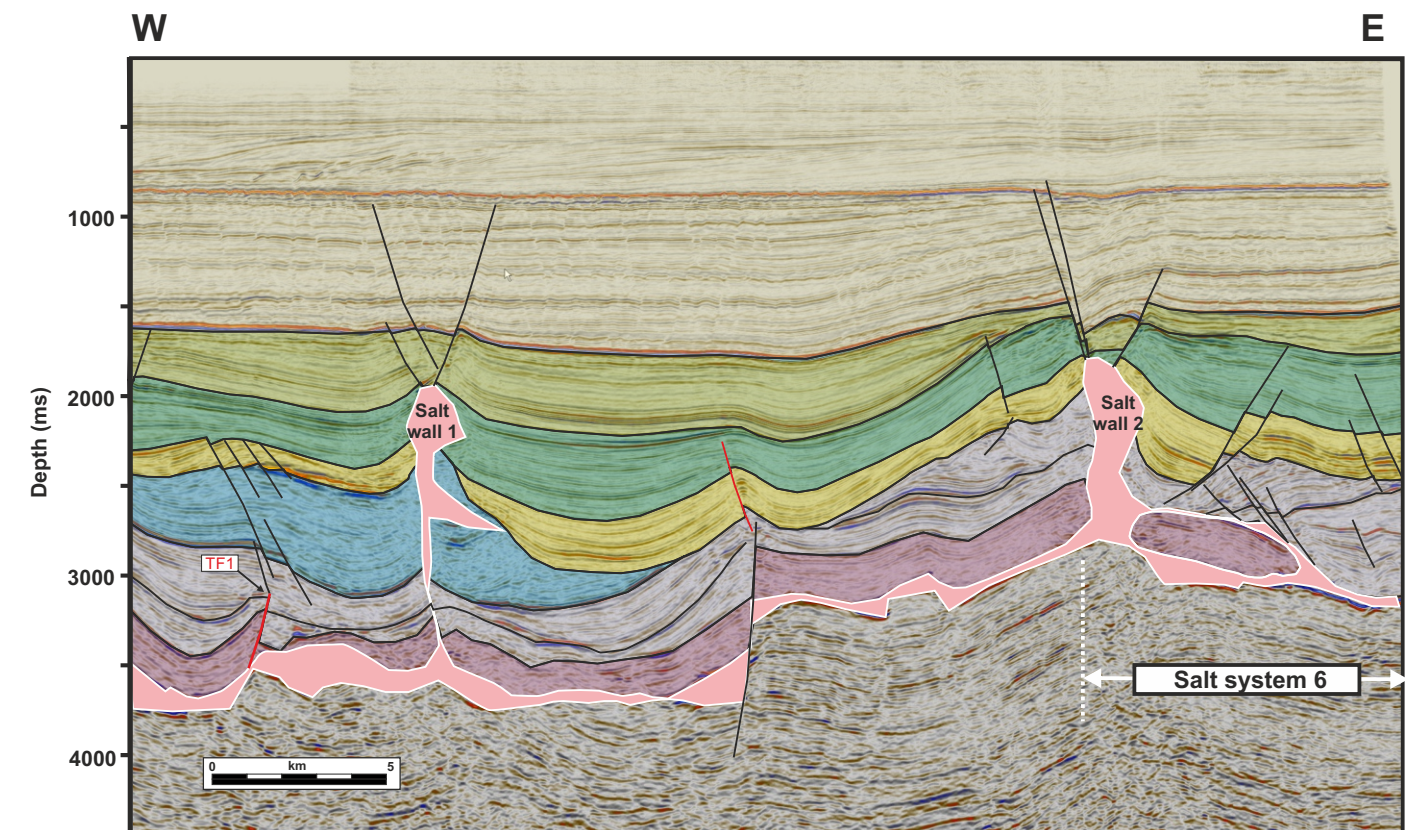


Figure 4.3.26: W-E seismic line across the study area. See text for comments. See Figure 4.3.21 for location.

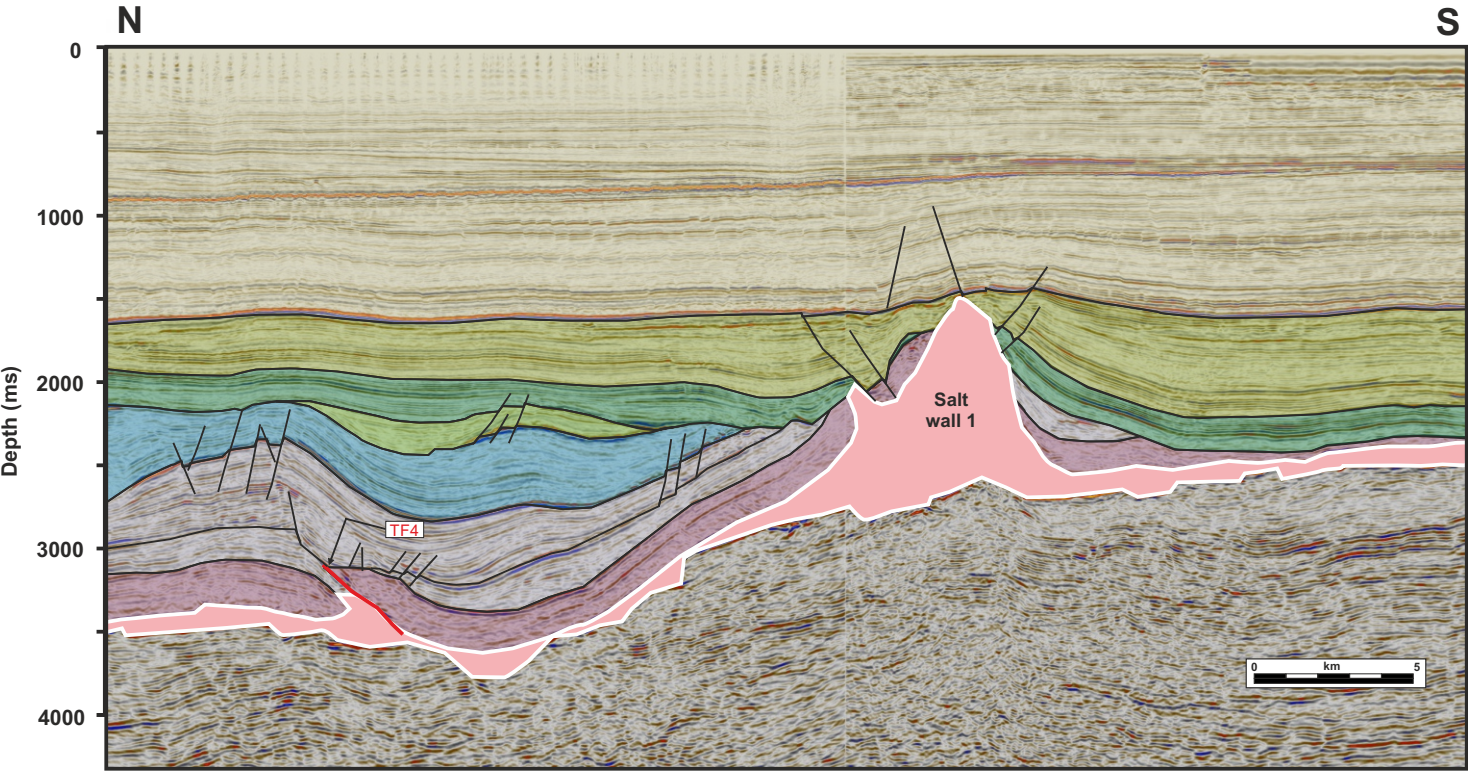


Figure 4.3.31: N-S seismic line across the study area. See text for comments. See Figure 4.3.21 for location.

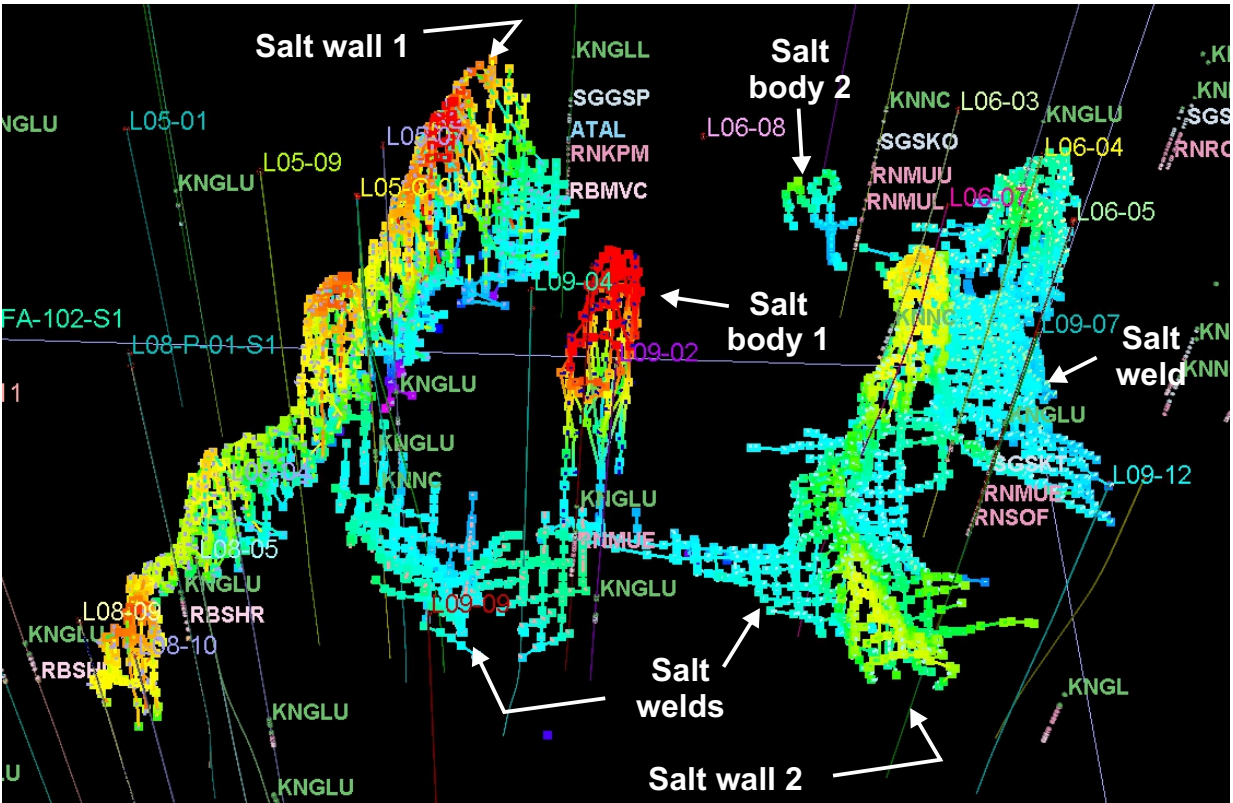


Figure 4.3.32: Perspective view of the shallow salt body mapped as a multi-z mesh.

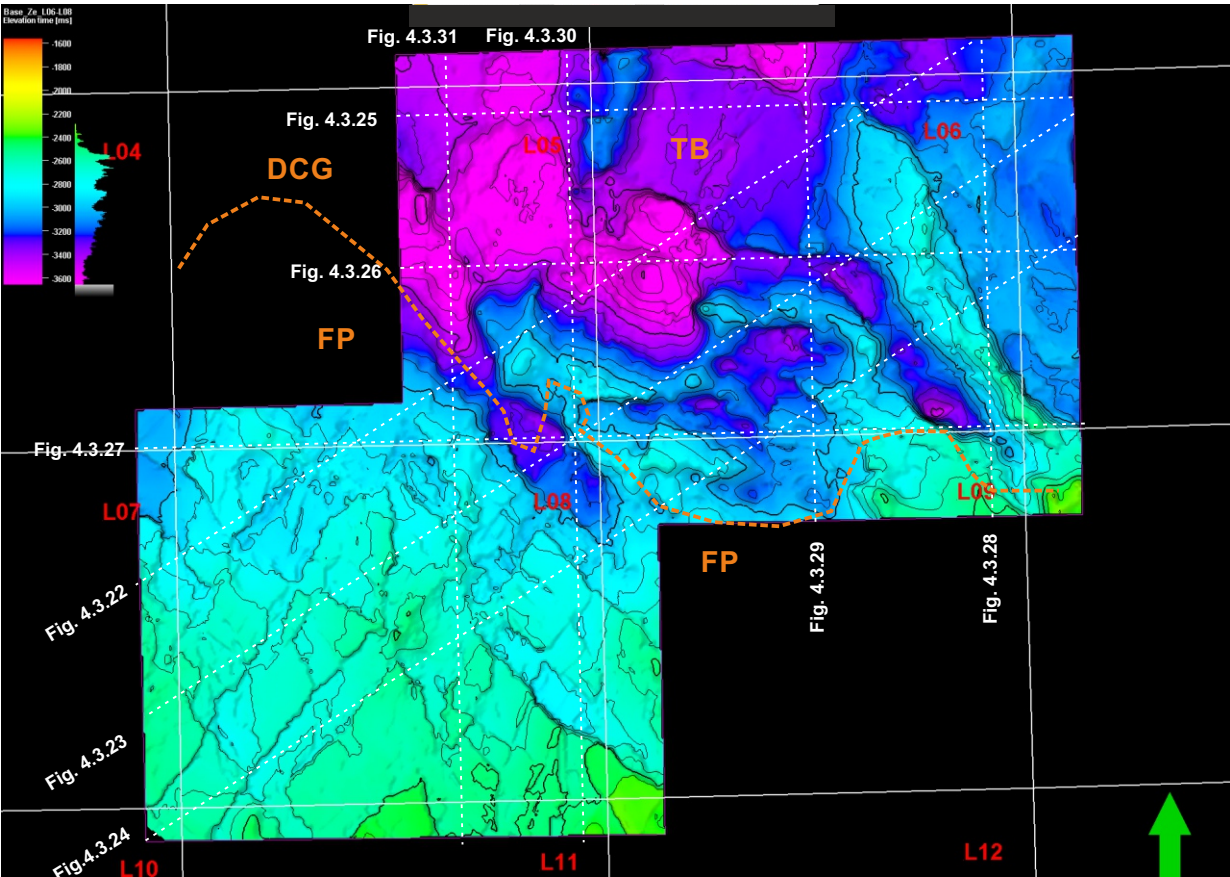


Figure 4.3.33: Base Zechstein time structure map.

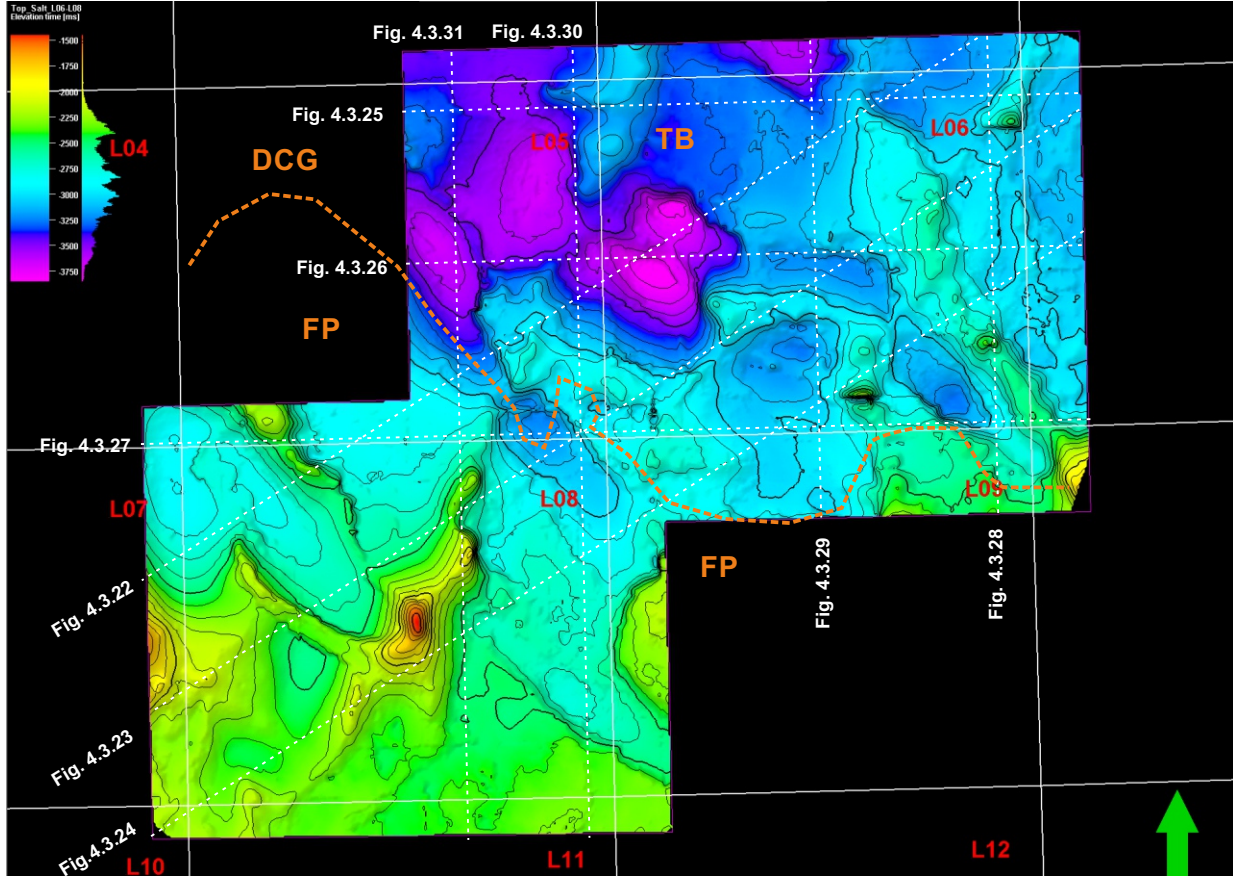


Figure 4.3.34: Top Zechstein time structure map.

4.3 Results - Case studies structural analysis: CS2

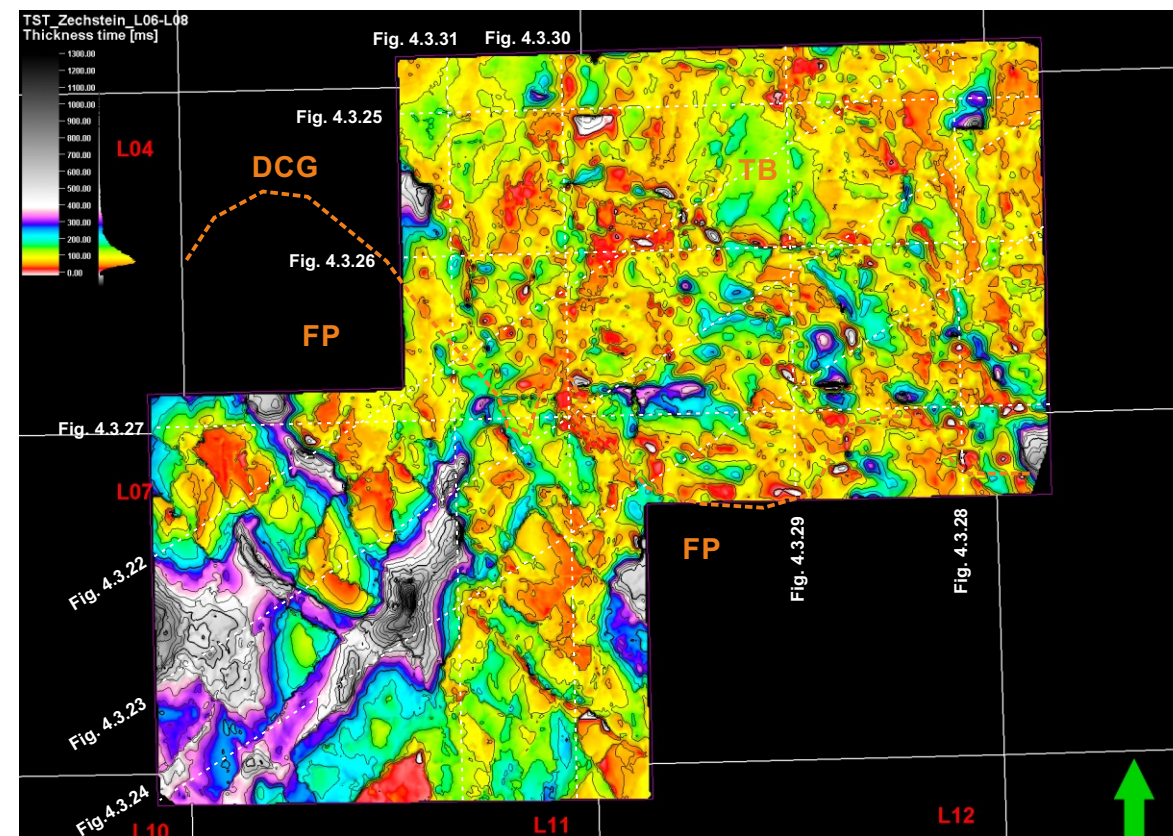


Figure 4.3.35: Top Lower Triassic time structure map.

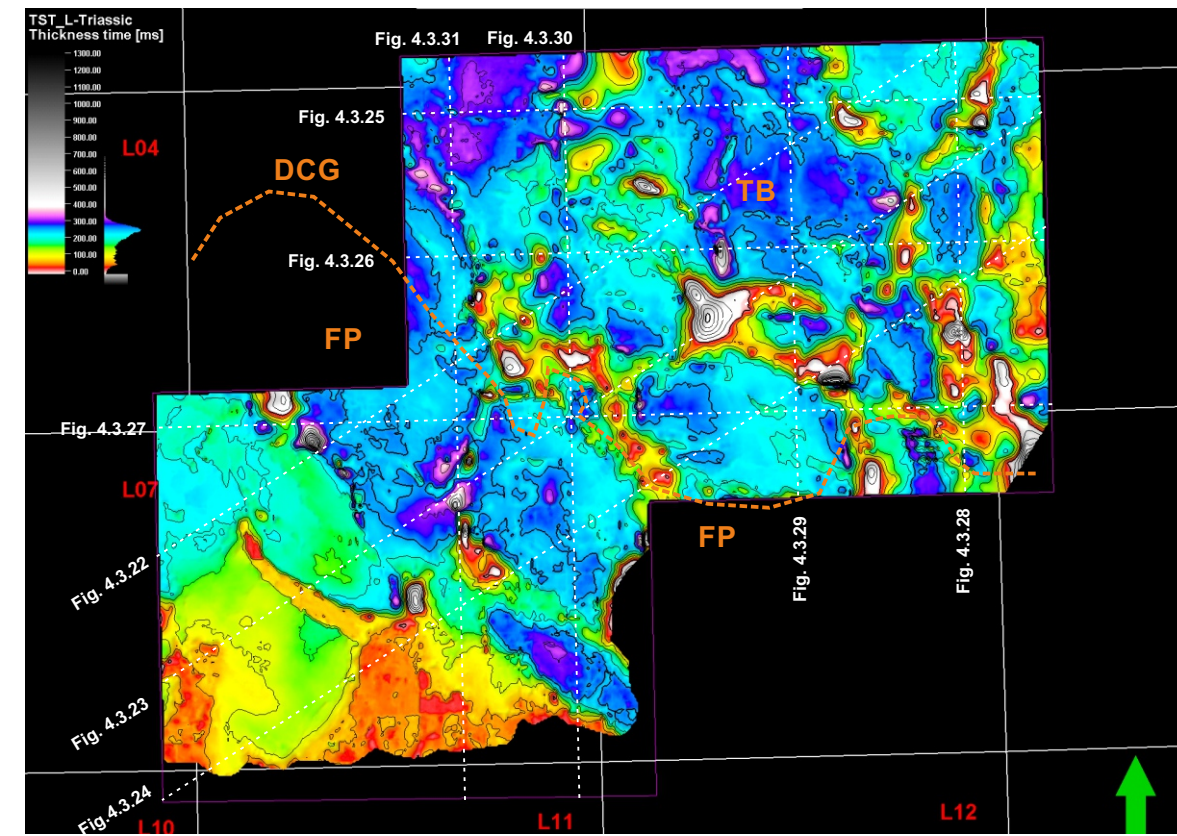


Figure 4.3.36: Top Middle Muschelkalk Marl Member (RBMUA) time structure map.

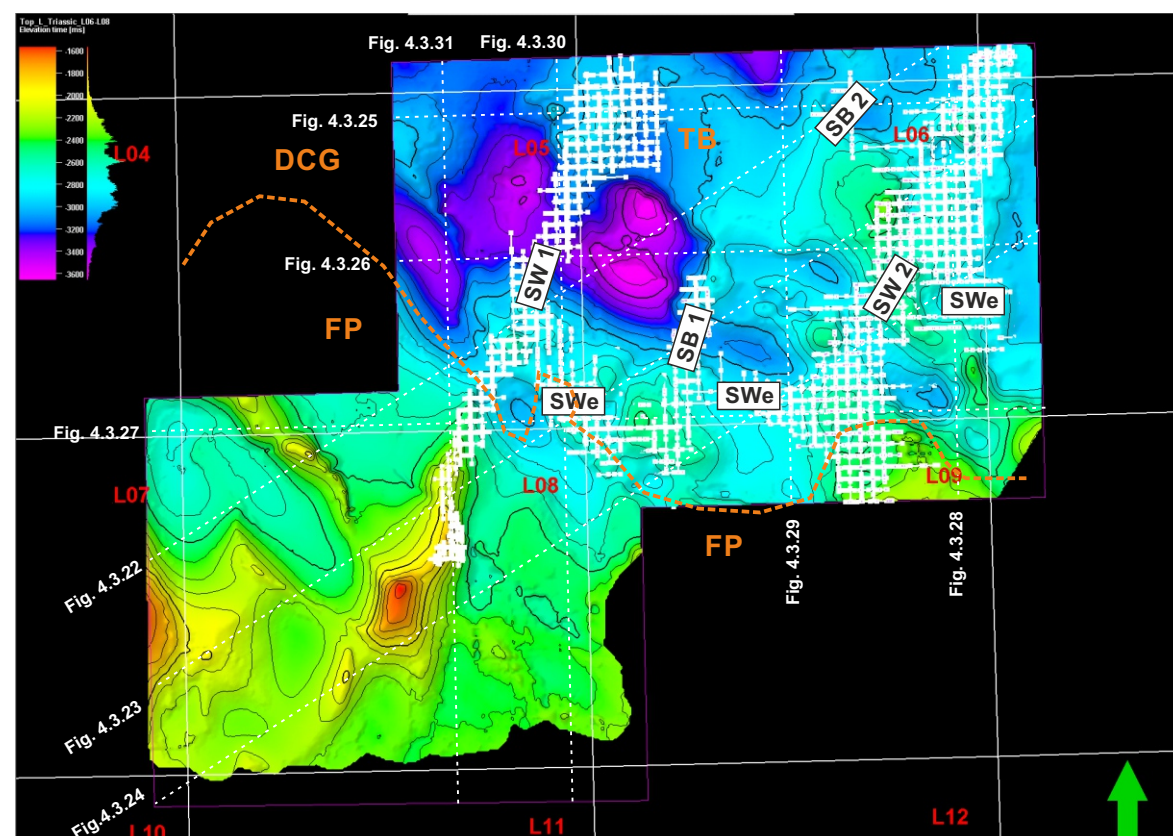


Figure 4.3.37: Zechstein Group time thickness map

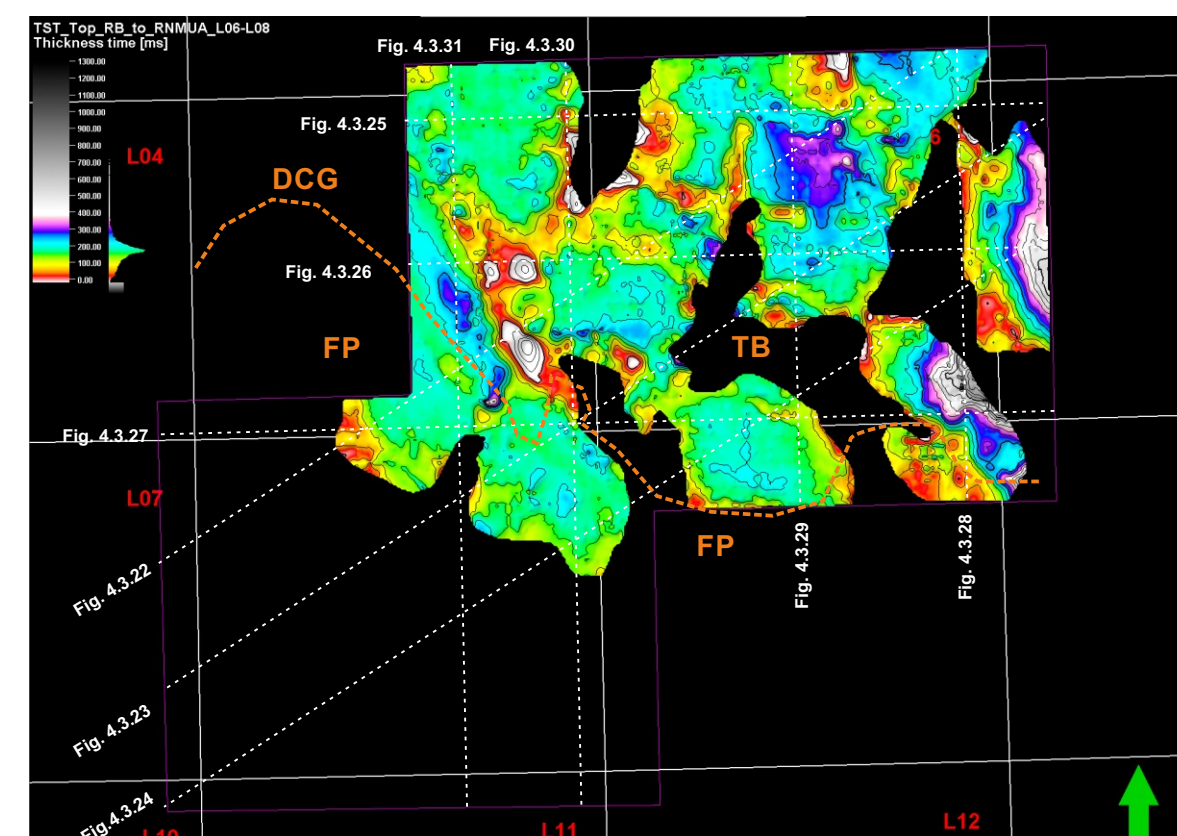


Figure 4.3.38: Lower Triassic Time thickness map

4.3 Results - Case studies structural analysis: CS2

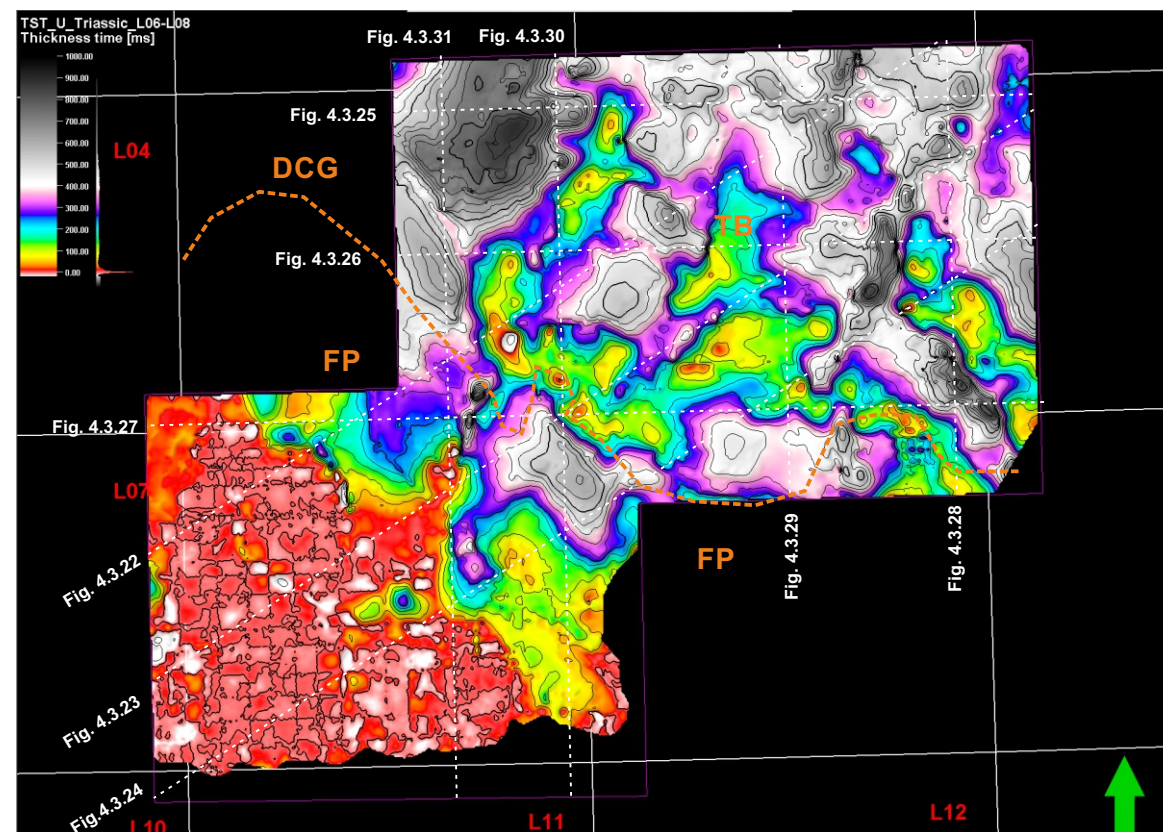


Figure 4.3.39: Upper Triassic time thickness map.

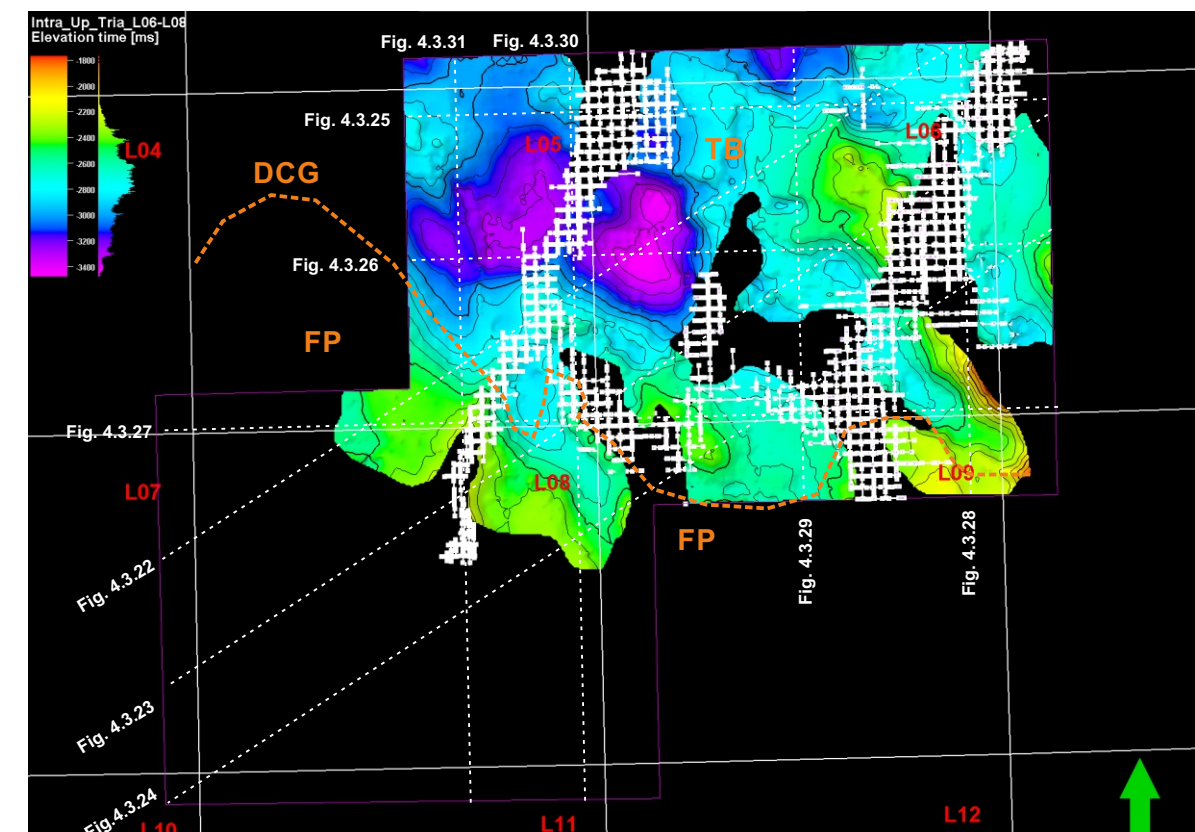


Figure 4.3.40: Top Lower Triassic to top Middle Muschelkalk Marl Member (RBMUA) interval thickness map.

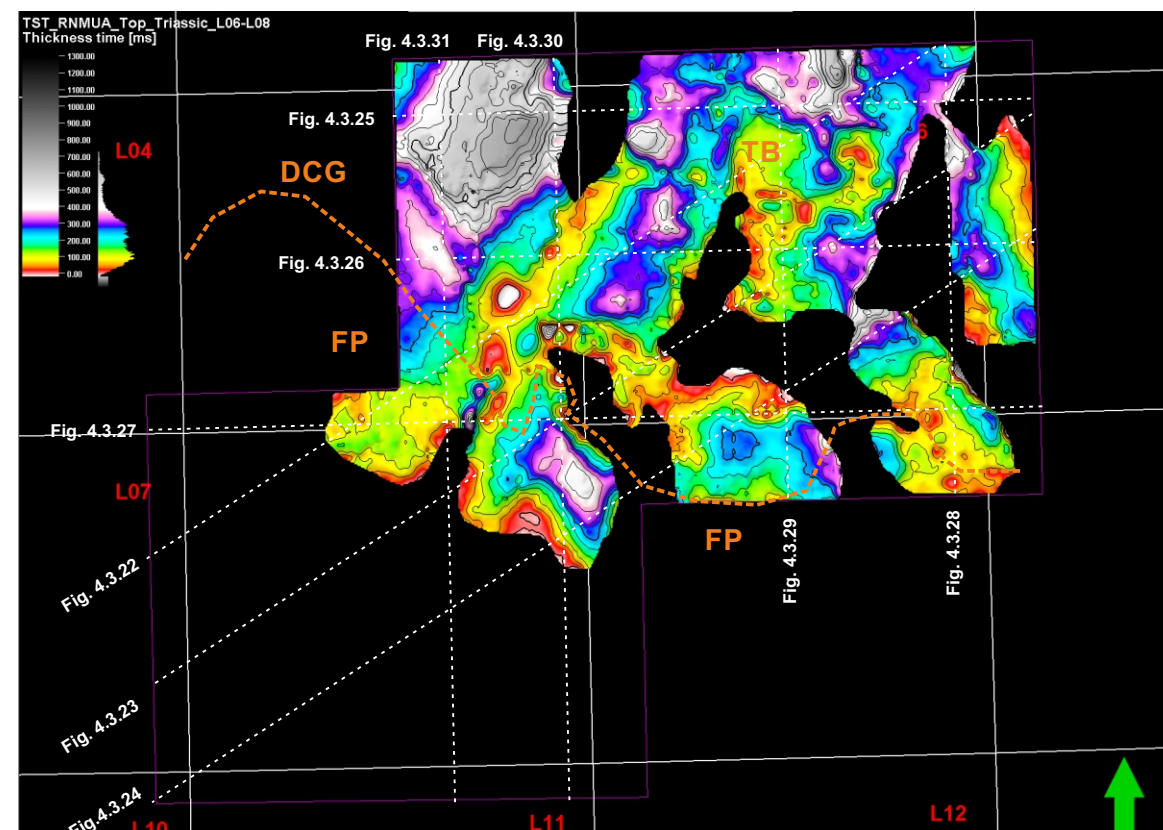


Figure 4.3.41: Top Middle Muschelkalk Marl Member (RBMUA) to top Triassic interval thickness map.

C) Case study 3: F10-F11 blocks

The third case study area is in the western central part of the DCG and on the southern part of the Step Graben (Fig. 4.3.42). In this area the central part of the Graben was uplifted and eroded during the Cretaceous as seen by the erosion of the Upper Jurassic in Figures 4.3.43 and 4.3.44. The geometry of the graben fill is also similar to a turtle structure with early deposition at the basin axis (Lower Jurassic and Upper Jurassic Sequence 1 in Fig. 4.3.43) to later deposition along the basin margins (Upper Jurassic to Lower Cretaceous Sequences 2 and 3. The salt withdrawal from the basin axis to its lateral margins created laterally shifting accommodation resulting to complex stratigraphic configuration with variable and geographically changing stratigraphic thickness, onlaps, truncation and syn-depositional faulting (Figs. 4.3.43 and 4.3.44).

One of the questions investigated in this case study is what is the origin and dynamics of the Upper Jurassic F11 minibasin located around the F11-03 well along the western margin of the DCG (Figs. 4.3.43 and 4.3.44)? Two models can be proposed: 1) This minibasin is part of a rim syncline due to the erosion of the Triassic strata during westward salt migration and rift fault motion, or 2) this minibasin formed onto an extruded allochthonous salt sheet that was later deflated and eroded. The presence of a 35 m thick salt layer at the base of the minibasin in Well F11-03 (Fig. 4.3.44) is intriguing. This salt can be either an in-situ Triassic salt layer such as the Rot Salt, or it represent the salt weld at the base of the minibasin. To investigate these different models, a detailed 3D tectono-stratigraphy interpretation of the reprocessed 3D seismic survey represented in this Section of the report, as well as two structural restorations presented in Section 4.4.

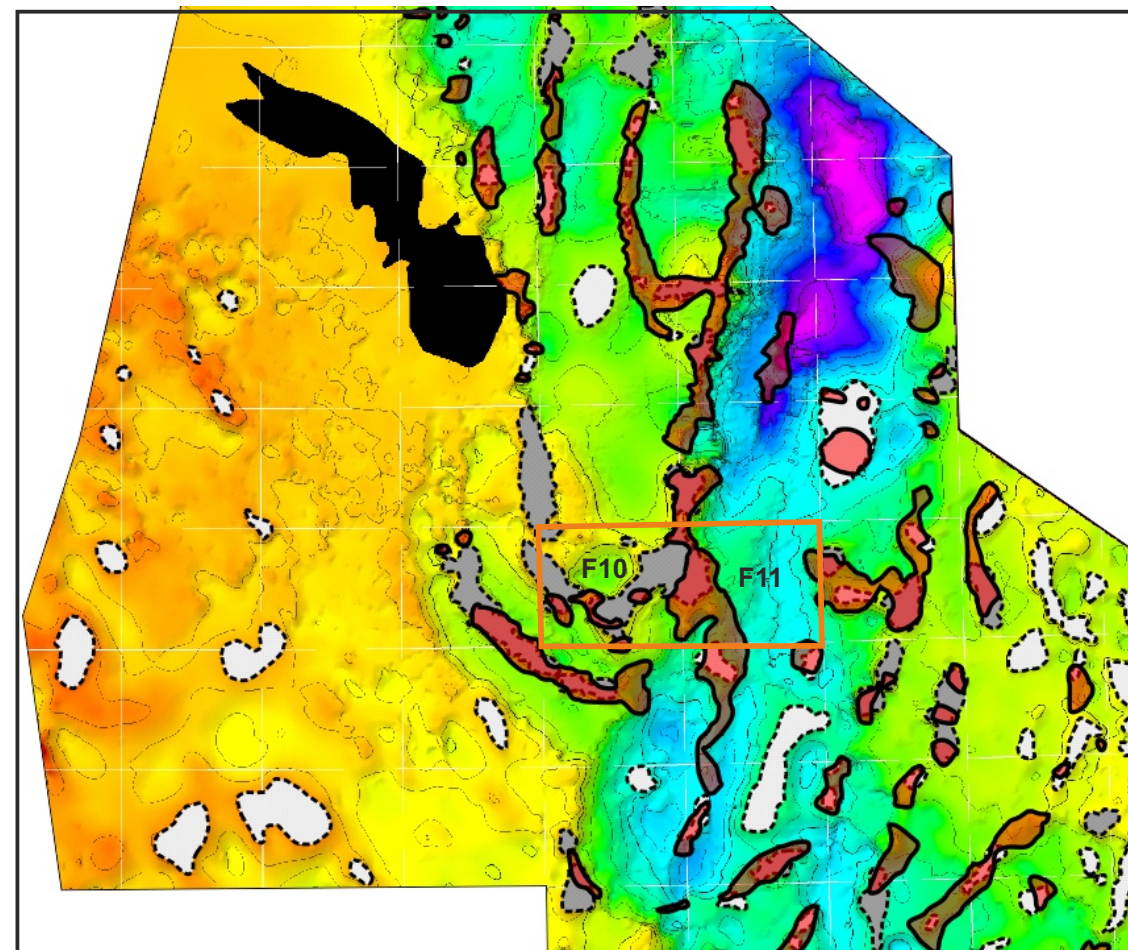


Figure 4.3.42: Top autochthonous salt time structure map of the area around the study case 3. Deep autochthonous salt bodies are shown as dashed grey polygons, light grey for salt bodies that have less than 500 ms of relief, and dark grey polygons for salt bodies that have more than 500 ms of relief. Shallow salt bodies as shown as red polygons. Top Zechstein time structure map shown as background.

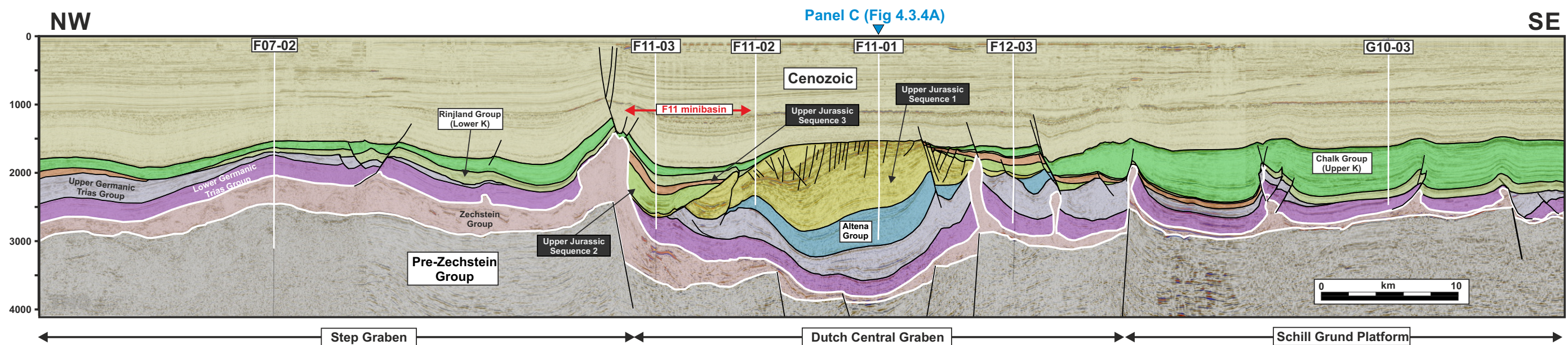


Figure 4.3.43: Regional seismic sections E that trends across the study area of the case study 1 (F10-F11) (from Bouroullec et al., 2016). This strike section across the DCG is 100 km long, intercepts 6 wells and extends eastward to the Schill Grund Platform and westward to the Step Graben. See Figure 4.3.2 for legend and Figure 4.3.3 for location.

4.3 Results - Case studies structural analysis: CS3

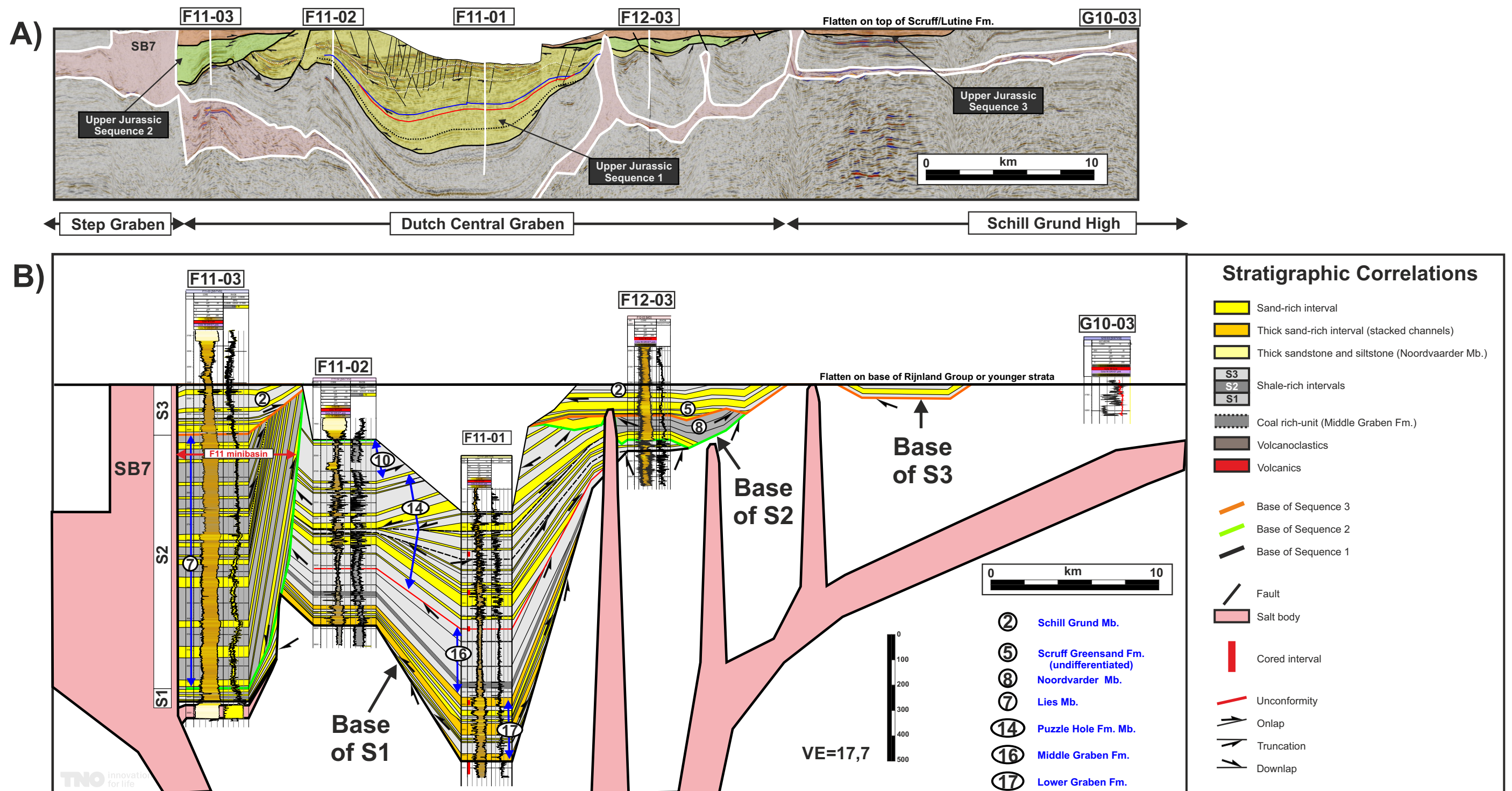


Figure 4.3.44: Flattened seismic (A) and stratigraphic correlation (B) of the Middle Jurassic to lowermost Lower Cretaceous along the central part of section E (Figure 4.3.43) (from Bouroullec et al., 2016). See Fig. 4.3.1 for location map and Fig. 4.3.2 for legend. See text for additional comments and description. **A)** Flattened seismic section showing the Upper Jurassic and Lower Cretaceous intervals. This section is flattened on top of Sequence 3, with Sequence 1 shown in yellow, Sequence 2 in green and Sequence 3 in orange. Note that the extended seismic flattening technique was used to compensate for the post-depositional erosion that occurred between wells F11-03 and F12-03. **B)** Stratigraphic well correlation of Sequences 1, 2 and 3. Sequence 1 is thick in the axis of the DCG (980 m) and was probably thicker (up to 1300 m) prior to later erosional events. Sequence 2 is deposited in two zones on the side of the DCG. In the east (well F12-03) S2 is deposited in a lens-shape geometry with evidence of erosion on the top surface. At this location S2 is relatively sandy and can be possibly referred as the Noordvaarder Mb., which is time equivalent to the Lies Member. On the western side of the DCG (well F11-03) S2 is very thick and accumulated within a minibasin on the side of salt body SB7. At this location S2 is higher N:G in its lower section and fine upward. Internal onlap surfaces are also observed on seismic within this marginal minibasin. Sequence 3 is also only present on the lateral basin margins (wells F11-03 and F12-03). A thin zone of S3 strata is observed to the east, west of well G10-03.

Five interpreted seismic sections illustrate the geometry of the salt systems and the key stratigraphic intervals (Figs. 4.3.46 to 4.3.50). The minibasin fill consists primarily of Upper Jurassic to Lower Cretaceous strata (Sequence 2 and 3) with a thin Sequence 1 interval at the base (See Fig. 4.3.64 to 4.6.70). Palynological evidence supports this model of a thin Sequence 1 above the salt layer (Fig. 4.3.44). The lithology of the Sequence 1 interval in Well F11-03 suggests that it is likely part of the Kimmeridge Clay Formation. However, in Figure 4.3.38, some high amplitude units above the proposed base of the minibasin can be observed, suggesting that Puzzle Hole Formation strata may have also been deposited in the minibasin. Locally, small salt bodies can be observed at the base of the minibasin (Figs. 4.3.47 and 4.3.50). This is not a “silver bullet” for either proposed models since over-thickened in situ Upper Triassic salt can be observed in other areas. It is however an important results and is one of the parameter discussed in Chapter 5.

A large salt massif, likely composed of multiple salt bodies that later merged, is located in the study area along the western flank of the DCG, on the Step Graben (Figs. 4.3.46, 4.3.53 and 4.3.54). Two other salt bodies are present in the western part of block F10 (Fig. 4.3.53) but have not been studies in detail in this project.

The seismic mapping of eleven horizons was performed to try to unravel the origin of the minibasin (Figs. 4.3.51 to 4.3.53; 4.3.57, 4.3.58 and 4.3.60). Out of this mapping exercise, time thickness maps were constructed (Figs. 4.3.55, 4.3.56, 4.3.59, 4.3.61, 4.3. 67 to 4.3.70).

The Lower Triassic time thickness map shows a slightly thicker area in the western part of block F11 (white dashed zone in Fig. 4.3.55). This is consistent with the results of the regional study (Chapter 4.2) where a thickening trend was observed toward the north for the Lower Triassic (Figure 4.2.7). For this case study this may also suggest that some salt movement may have occurred in the area already during the Lower Triassic, with some salt already moving westward toward the salt massif at an early stage.

The Upper Triassic time thickness map shows two depo-thicks in the northwestern and southeastern parts of the study area (Zones 1 and 2, Fig. 4.3.56) separated by NS to NNE-SSW trending depo-thin (Zone 3). The bend in the trend of Zone 3 could be related to dextral strike slip motion of fault F1 (Fig. 4.3.56). The fault F1 activity was long lasting since it also affected the thickness of the Schieland Group (Fig. 4.3.58). The Upper Triassic thickness map (Fig. 4.3.56) is interesting since the north-western (Zone 1) and south-eastern (Zone 2) part of the block F11 show active salt withdrawal that created accommodation at these locations. The depo-thin (Zone 3) later became a depo-thick (e.g. Kimmeridge Clay Formation, Fig. 4.3.61) and later again a depo-thin during the deposition of the Upper Jurassic Sequences 2 and 3, after the inversion of the turtle structure and the depositional shift toward the lateral basin margins (Fig. 4.3.43).

When focusing on the minibasin in the north-western part of the F11 block, the mapping of key horizons within this depocenter allows to distinguish several depositional trends and basin fills.

The salt weld/erosional surface structure map (Fig. 4.3.63) shows a structural low located north of the F11-03 well and a radial shallowing up geometry, especially to the east and southeast. Several linear features(lineaments) that trend NNW-SSE, can be seen on this surface. These features are either 1) steps at the base of the allochthonous salt sheet, commonly observed in the case of allochthonous salt sheets that was later welded out, or 2) paleotopographic features related to a progressive erosional event (rim syncline model) . The Upper Jurassic and Lower Cretaceous minibasin fill shows additional interesting parameters. The tectono-stratigraphic package 0, which corresponds to the lower unit (possibly Puzzle Hole Formation), is present in

two isolated elongated areas (Zone 1 and Zone 2, Figs. 4.3.64 and 4.3.67). The depositional package in Zone 1 is relatively thick (up to 400 ms thick) in the north-western part of the zone, which is counter-intuitive in the case of a rim syncline-type model, where the early shallow thickest deposition occurs farther away from the controlling marginal salt and progressively laps onto area closer to the salt body. The thickness map of the overall Upper Jurassic Sequence 1 within the minibasin (Fig. 4.3.68) shows that the maximum stratigraphic thicknesses occur within the same two zones (Zones 1 and 2,) and that a depo-thin (Zone 3) is present in the central part of the minibasin. The subsequent basin fill (Sequences 2 and 3, Figs. 4.3.69 and 4.3.70) shows stratigraphic wedges developing along the western bounding salt body, toward the SW. It is important to notice that most of the depo-thicks within the minibasin are wedges, except Zone 2 for Sequence 1 (Fig. 4.3.68), which is a trough-shape depo-thick. These stratigraphic wedges thicken toward the northwest (Figs. 4.3.68 and 4.3.70), the west (Fig. 4.3.68) and the SW (Figs. 4.3.69 and 4.3.70) and illustrate the main directions of salt movement contemporaneously to the deposition of those sequences.

4.3 Results - Case studies structural analysis: CS3

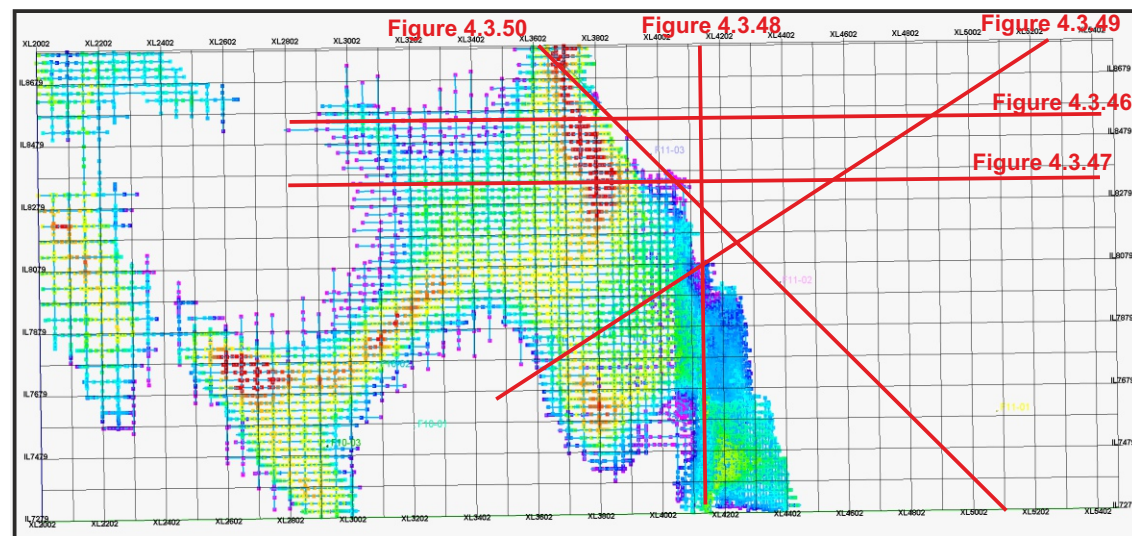


Figure 4.3.45: Location map for the seismic section shown in Figures 4.3.46 to 4.3.50. The background image shows the multi-z mesh of the shallow salt bodies.

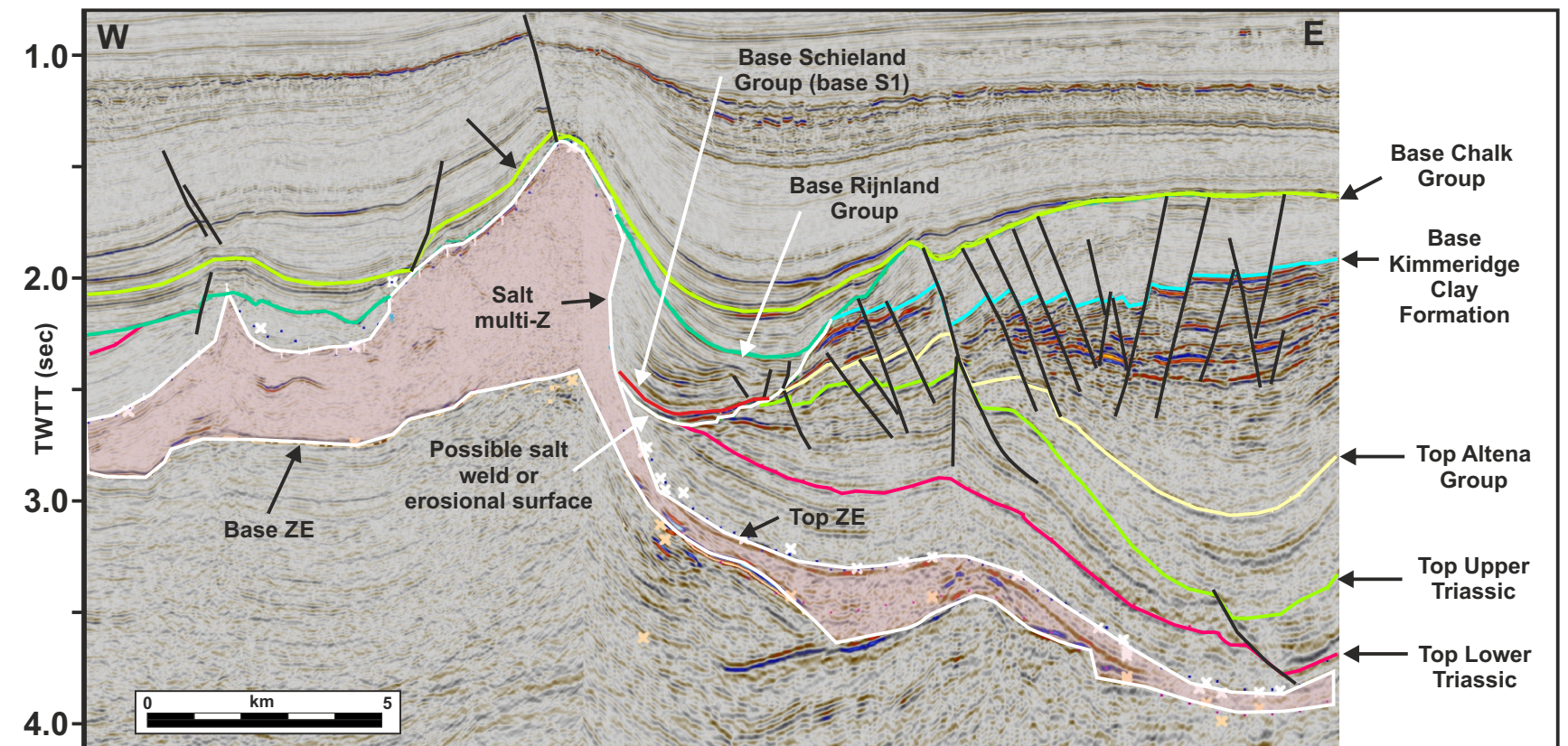


Figure 4.3.46: E-W interpreted seismic section.

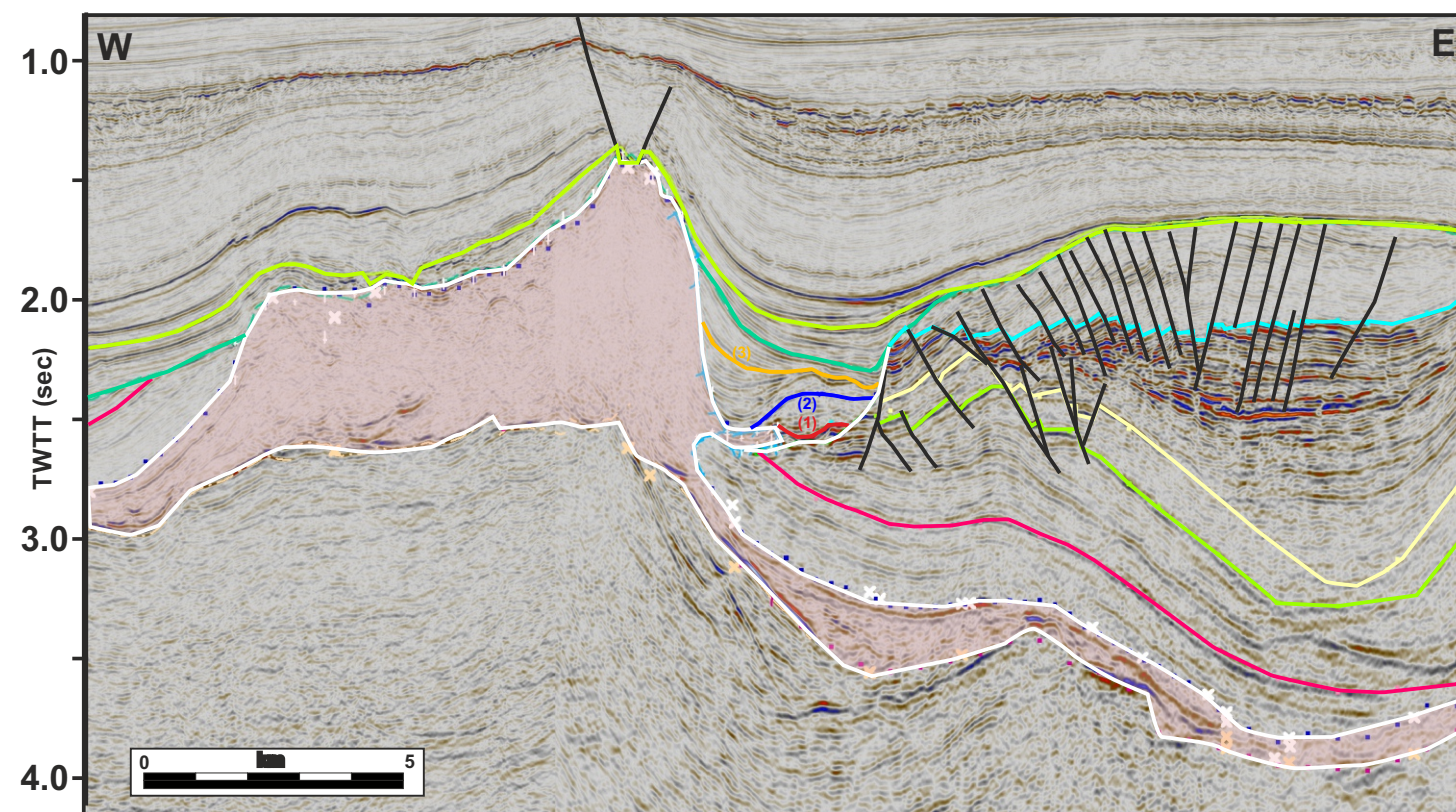


Figure 4.3.47: E-W interpreted seismic section. See Figure 4.3.46 for legend.

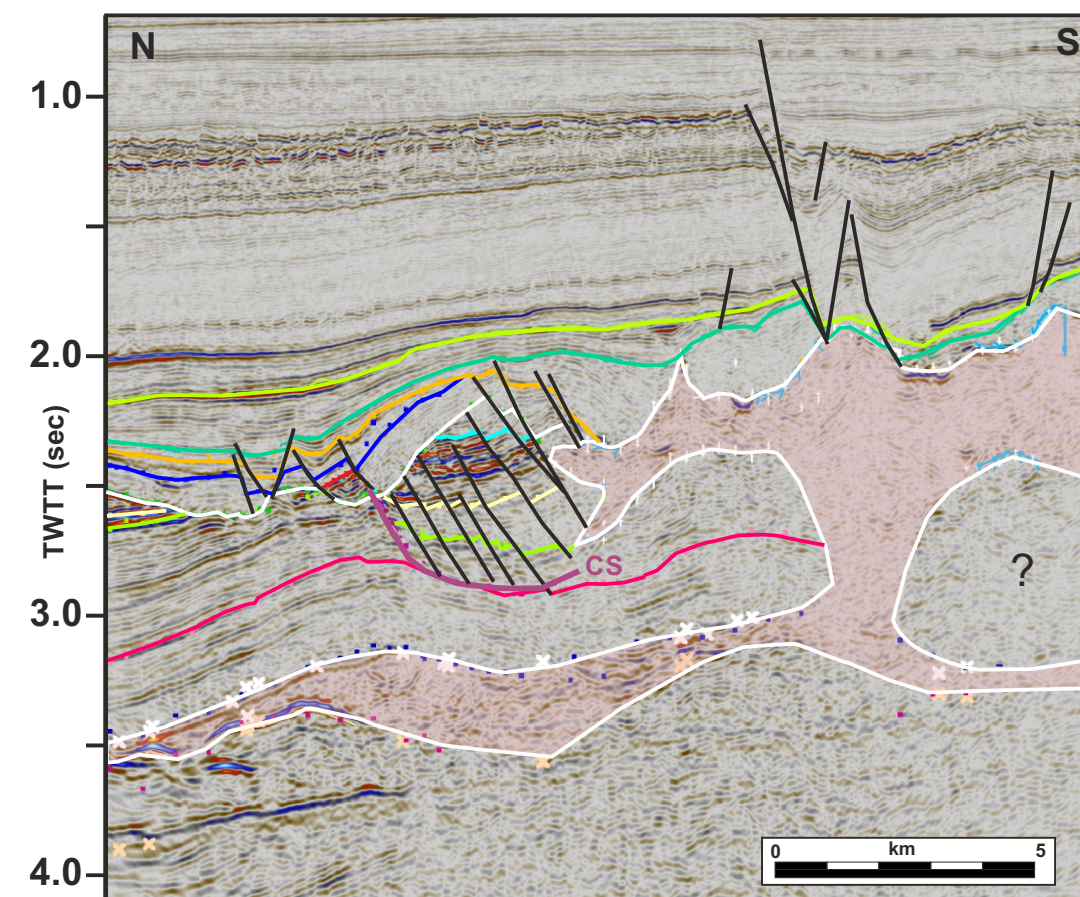


Figure 4.3.48: N-S interpreted seismic section. See Figure 4.3.46 for legend. The collapse structure (CS) is shown as a dark purple line.

4.3 Results - Case studies structural analysis: CS3

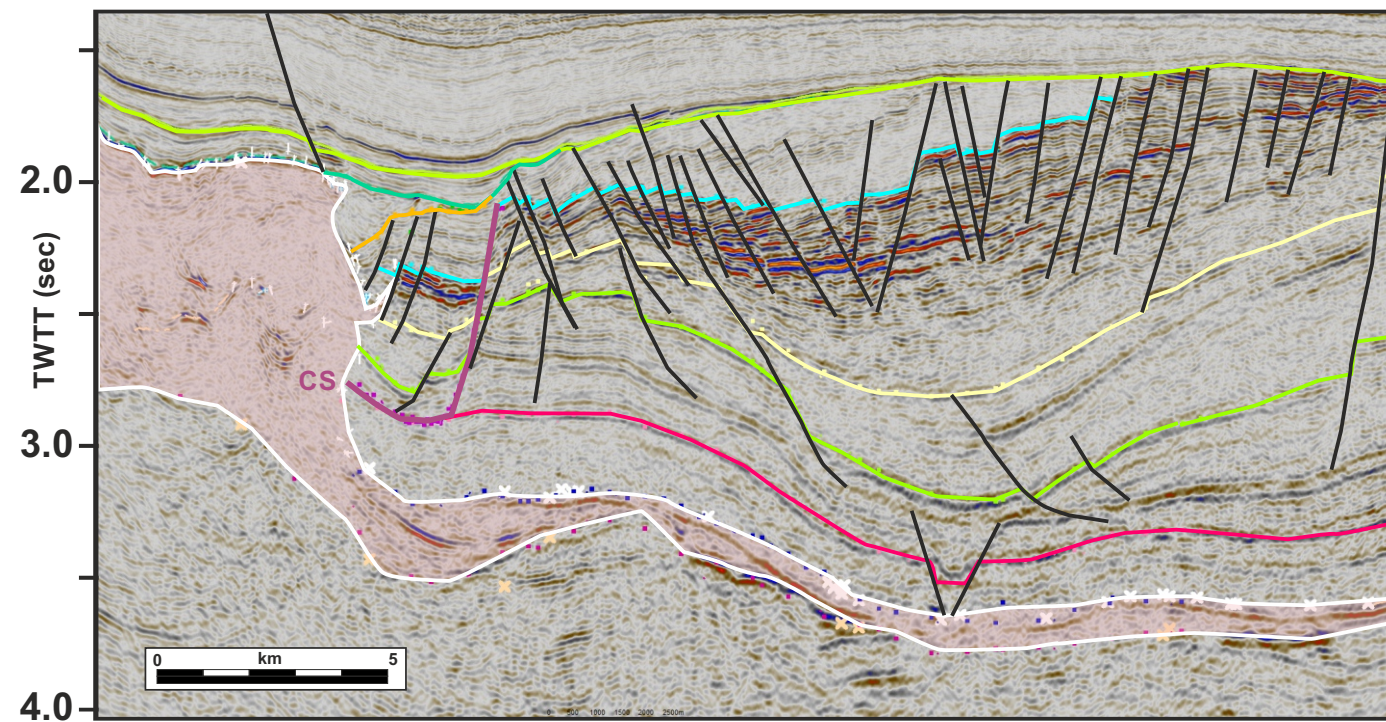


Figure 4.3.49: E-W interpreted seismic section. See Figure 4.3.46 for legend. The collapse structure (CS) is shown as a dark purple line.

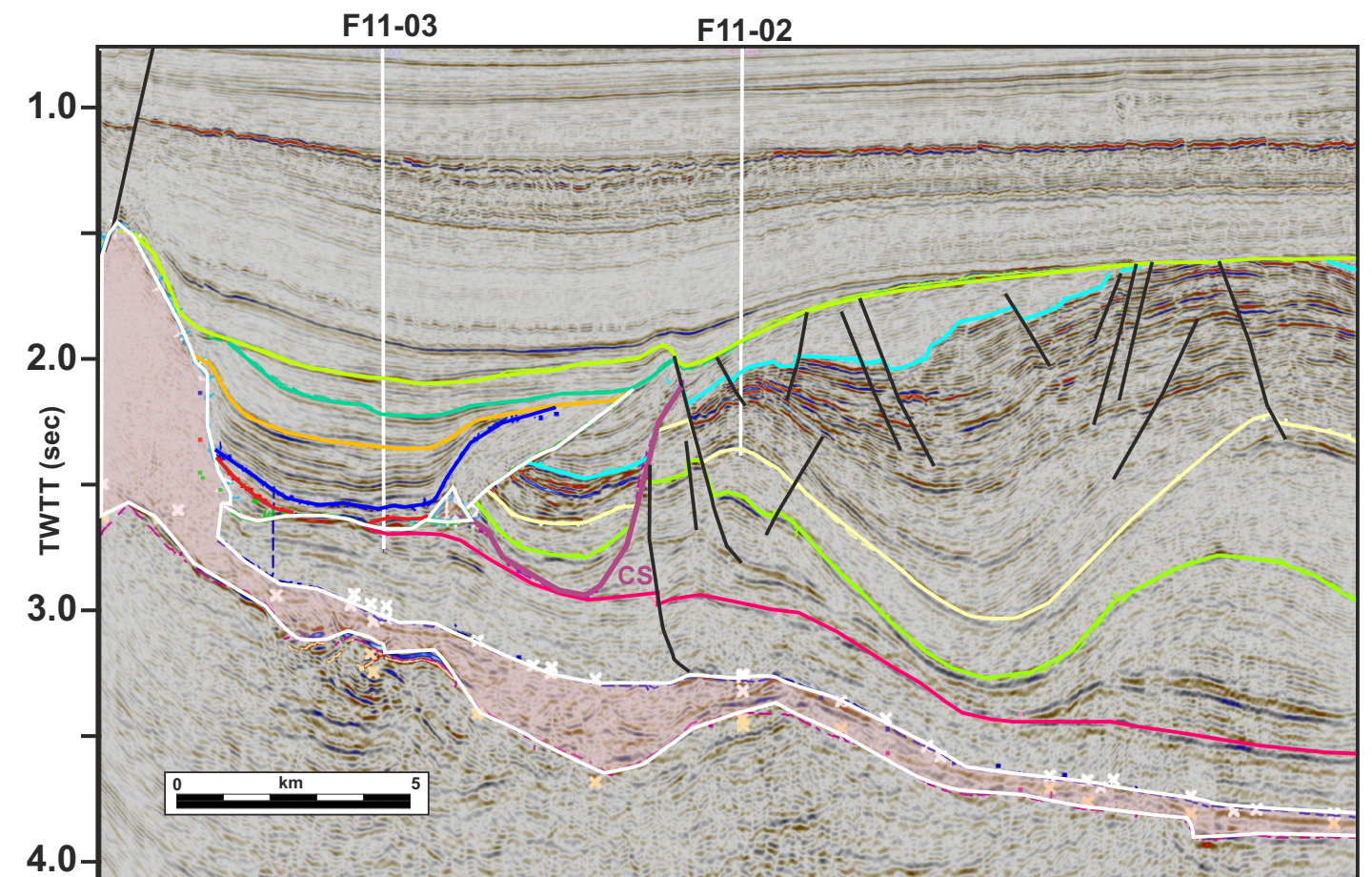


Figure 4.3.50: E-W interpreted seismic section. See Figure 4.3.46 for legend. The collapse structure (CS) is shown as a dark purple line.

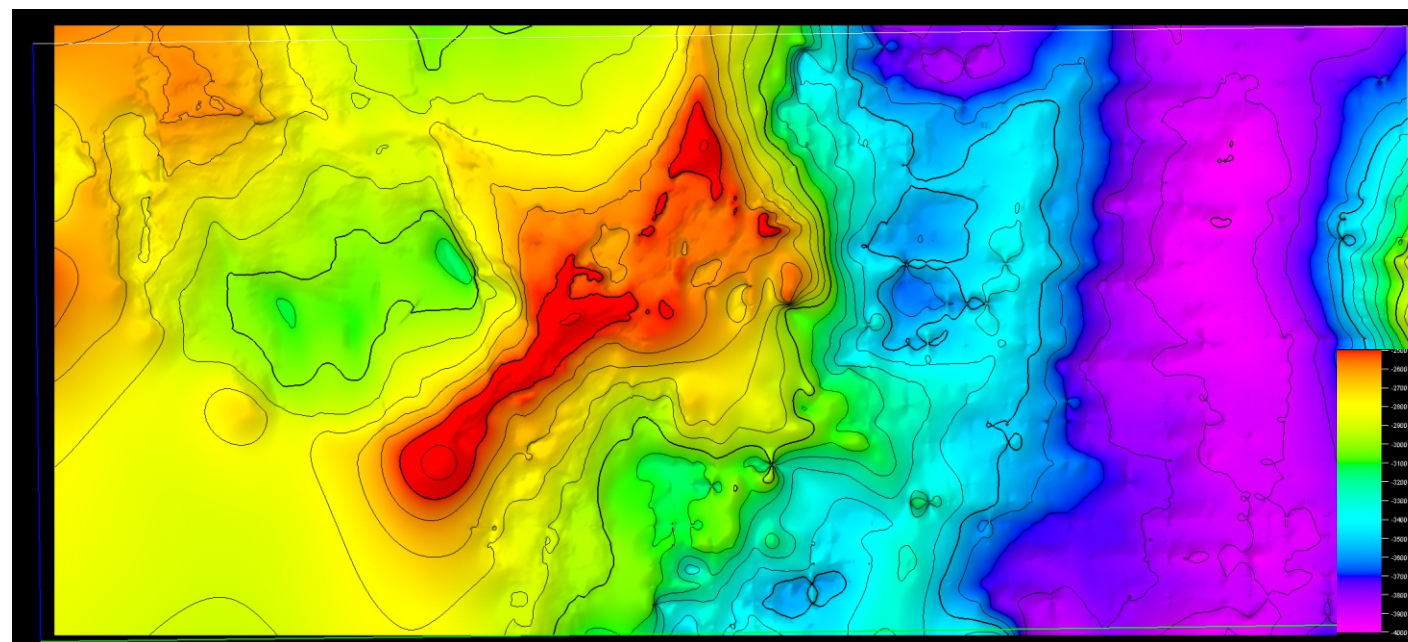


Figure 4.3.51: Base Zechstein time structure map.

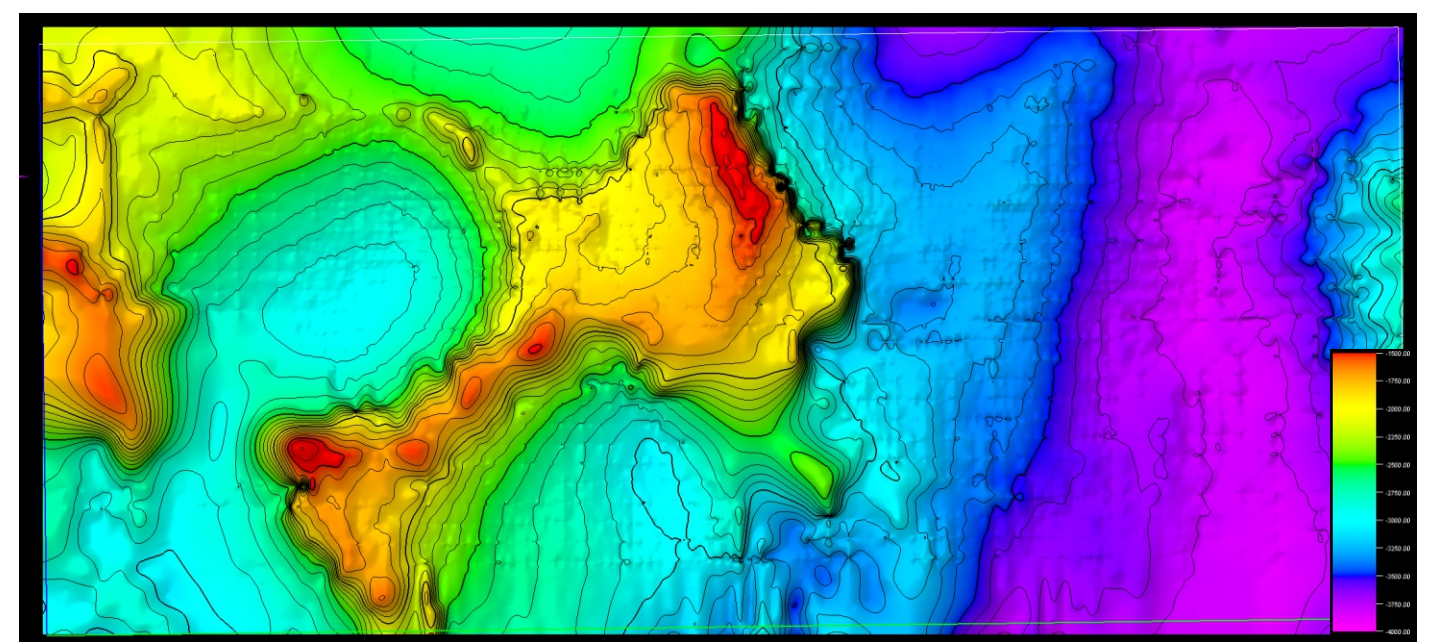


Figure 4.3.52: Top Zechstein time structure map.

4.3 Results - Case studies structural analysis: CS3

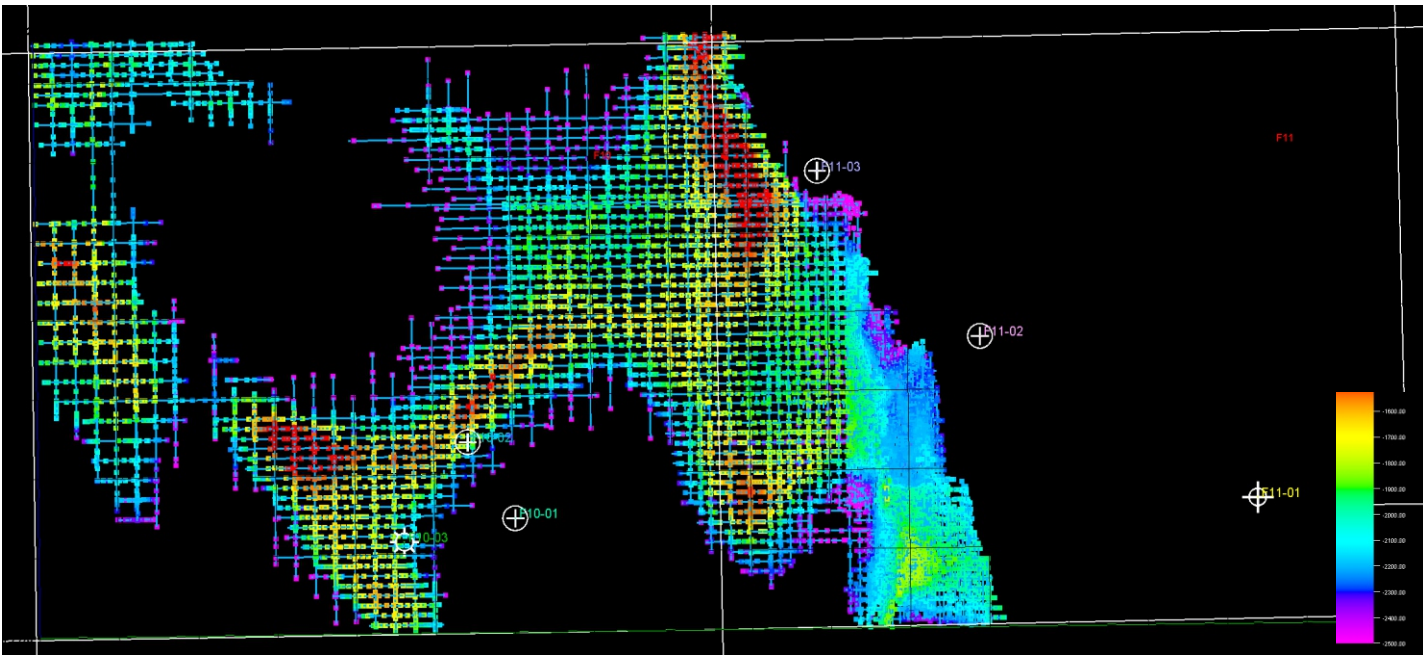


Figure 4.3.53: Top salt multi-z mesh map.

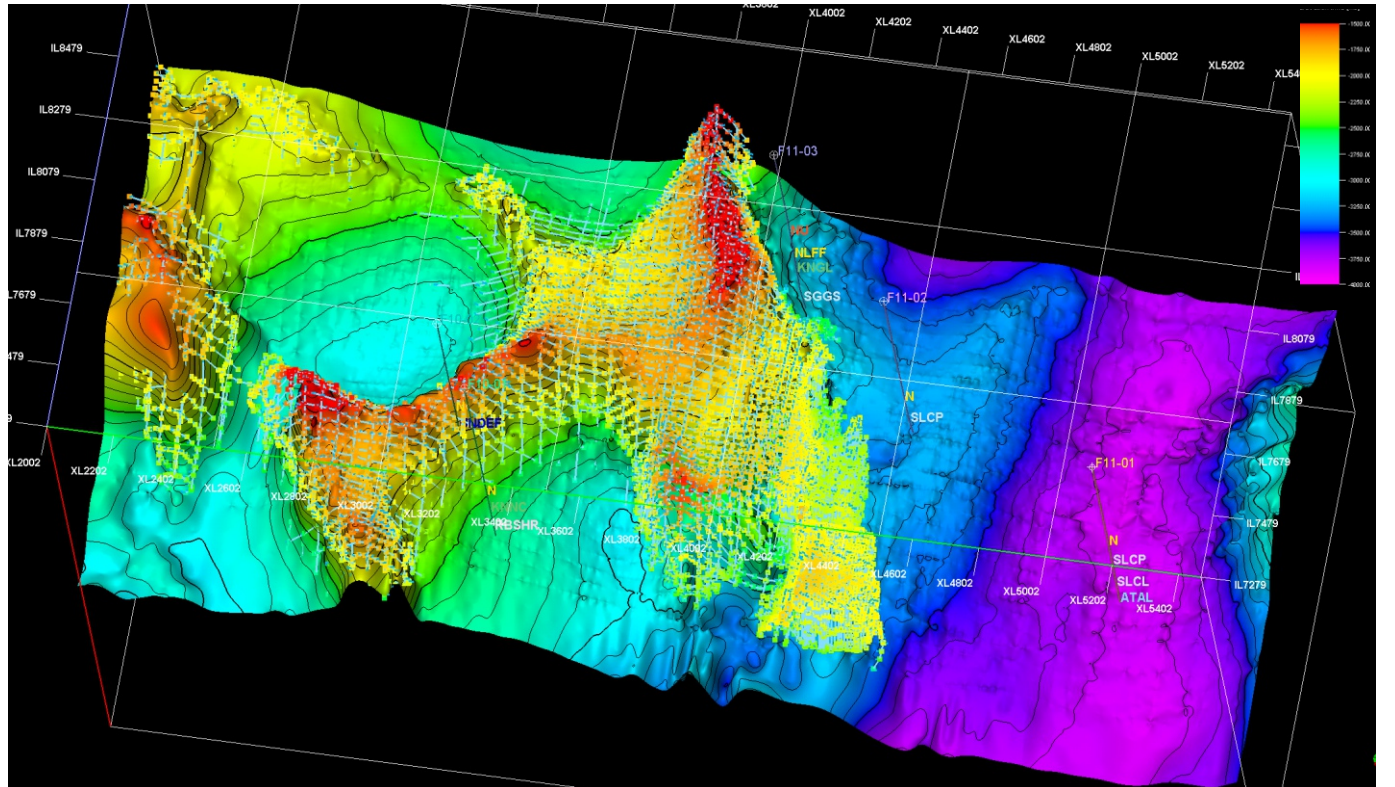


Figure 4.3.54: Perspective view toward the NNW of the top Zechstein horizon and the top salt and multi-z mesh overlay.

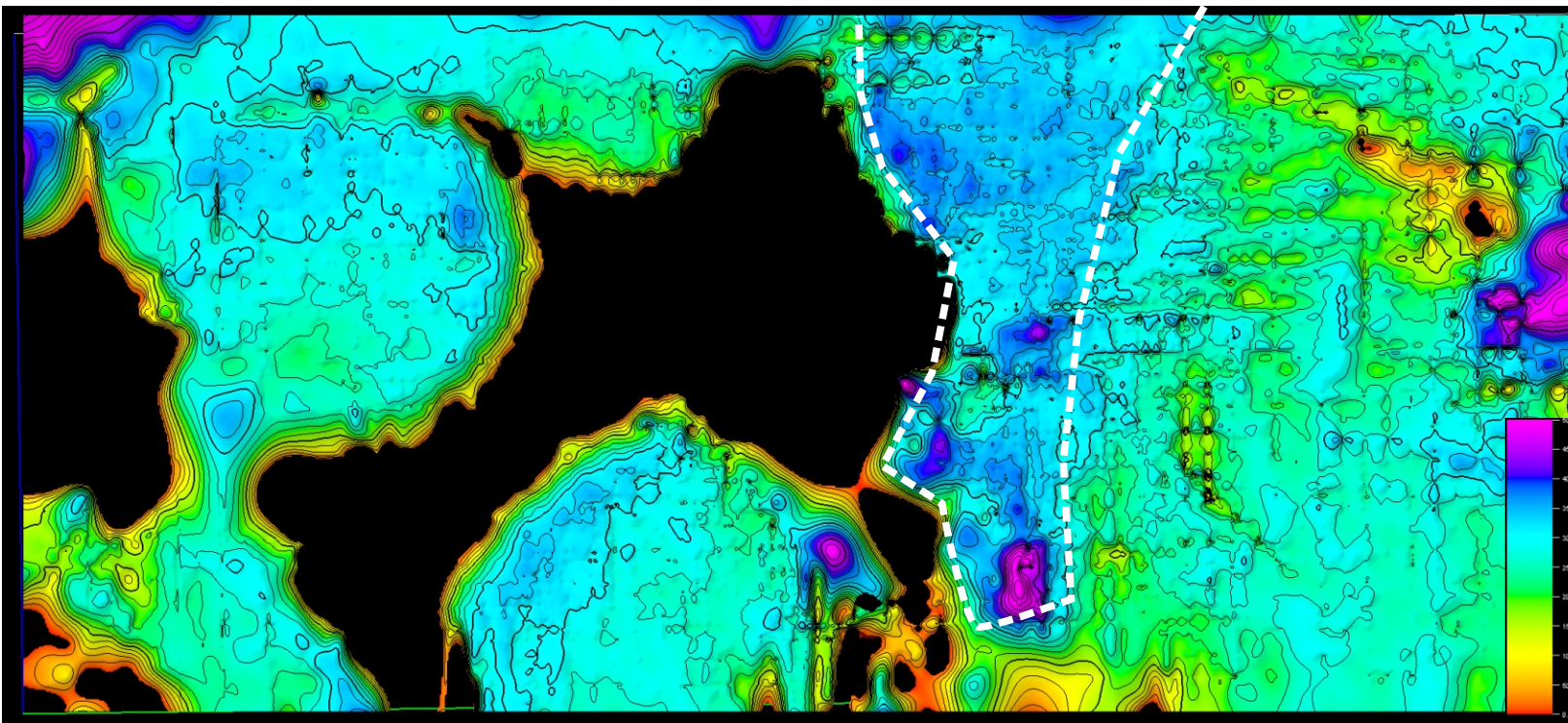


Figure 4.3.55: Lower Triassic time thickness map. Note the slightly thicker zone (dashed white polygon in the central part of the study area).

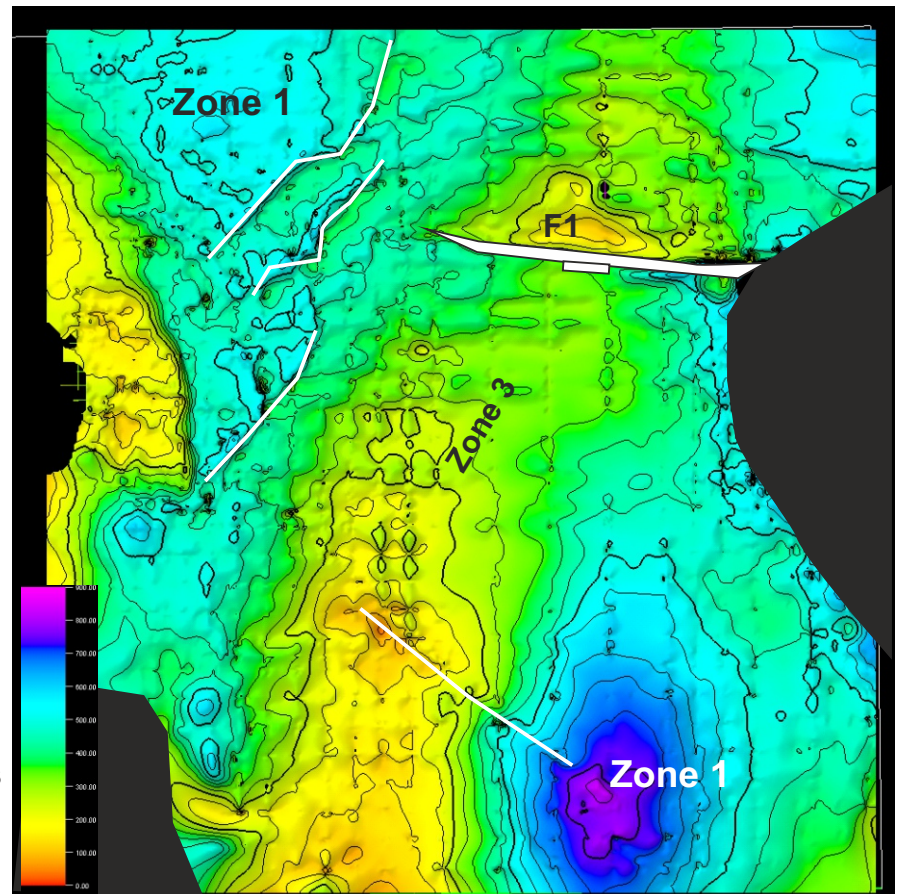


Figure 4.3.56: Upper Triassic time thickness map. This surface is only mappable in the F11 block since no Altona Group is present on the platform. A few faults are shown as white lines and polygons

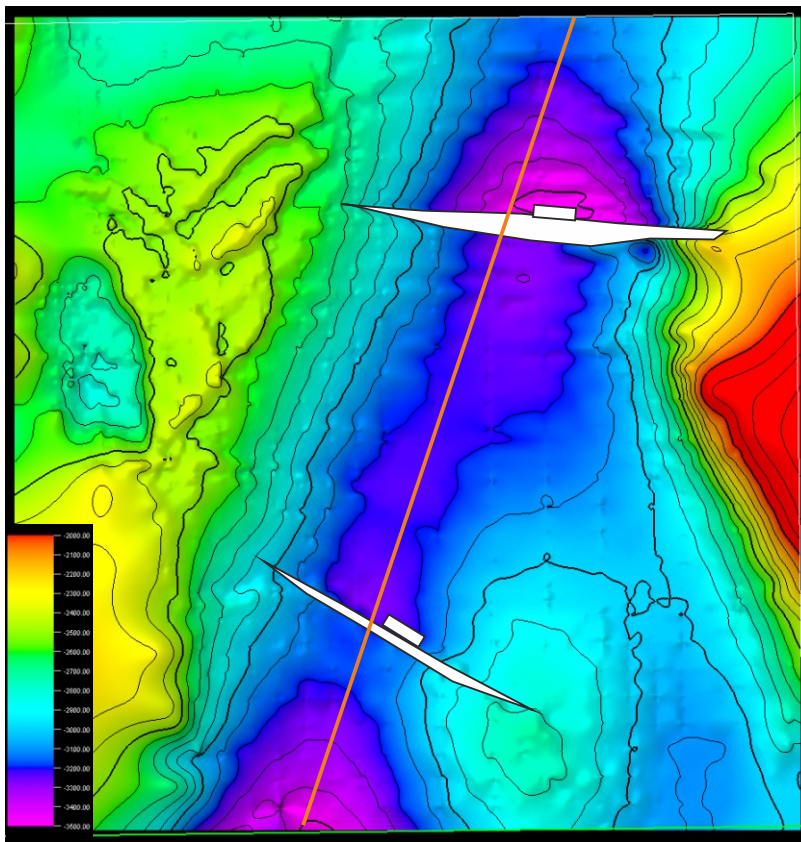


Figure 4.3.57: Base Altena Group time structure map. This surface is only mappable in the F11 block since no Altena Group is present on the platform. Two large north dipping normal fault offset the surface in the central part of the F11 block.

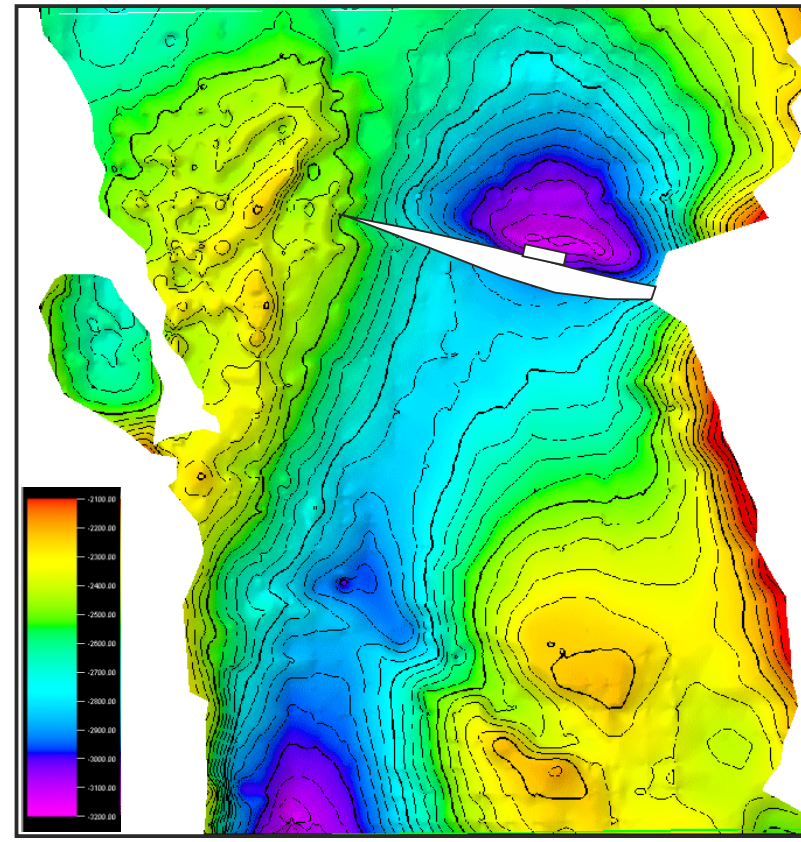


Figure 4.3.58: Base Schieland Group time structure map. This surface is only mappable in the F11 block.

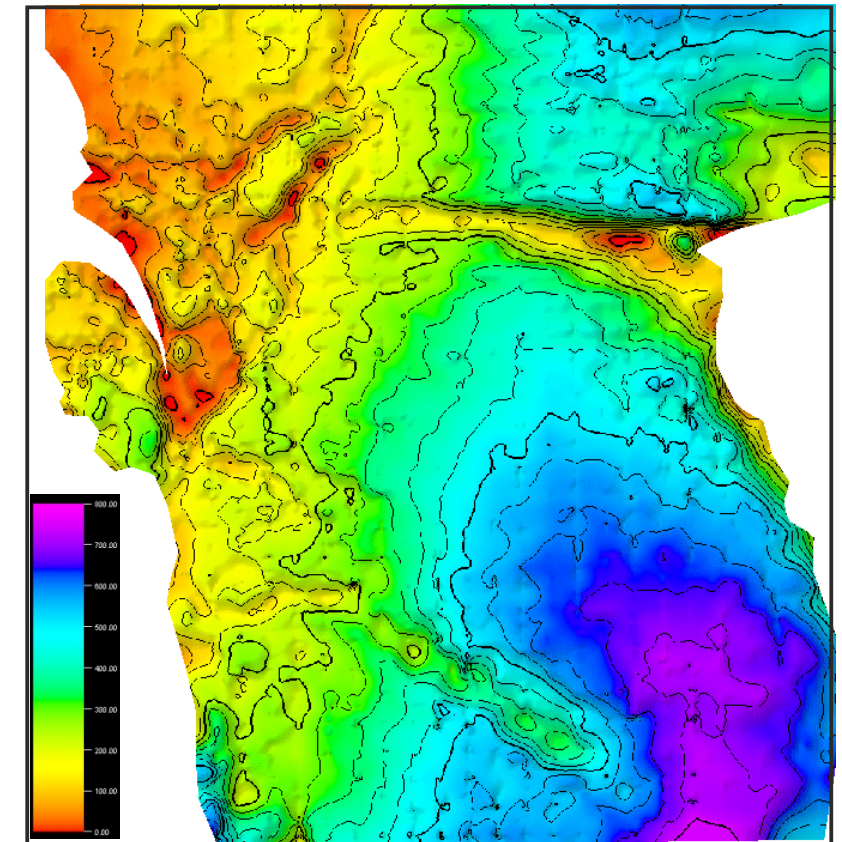


Figure 4.3.59: Altena Group time thickness map.

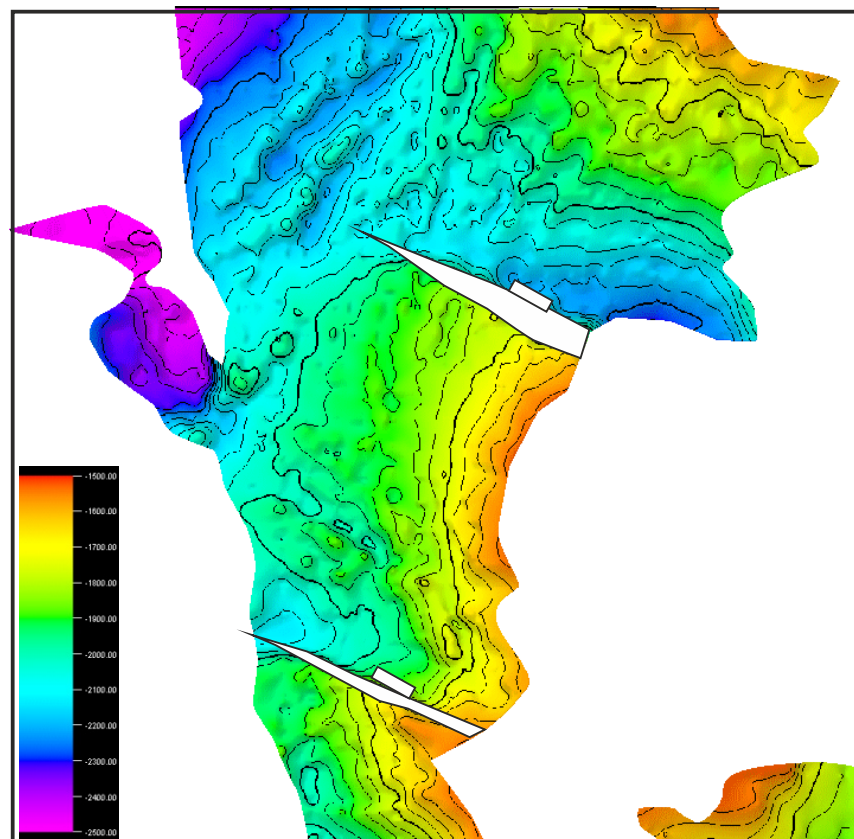
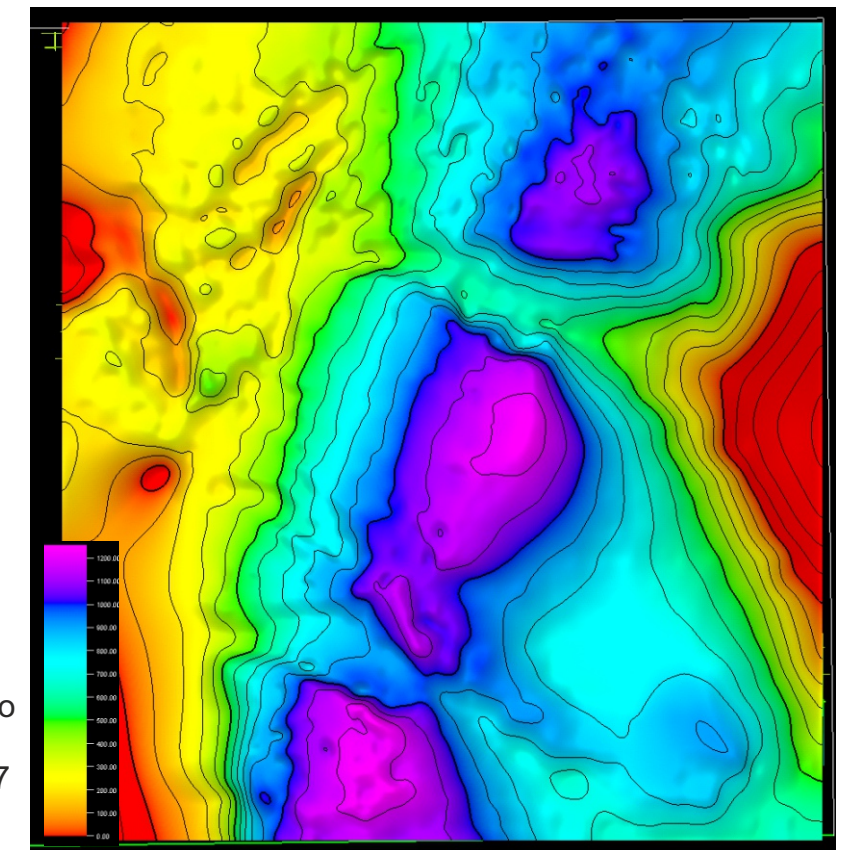


Figure 4.3.60: Base Kimmeridge Clay Formation time structure map. This surface is only mappable in the F11 block. The same large normal fault seen on Figure 4.3.57 are also offsetting the base of the Kimmeridge Clay Formation significantly.

Figure 4.3.61: Kimmeridge Clay Formation time thickness map. Note that the two NW-SE thins (A and B) are artifacts due to the two large normal faults seen in Figures 4.3.57 and 4.3.60.



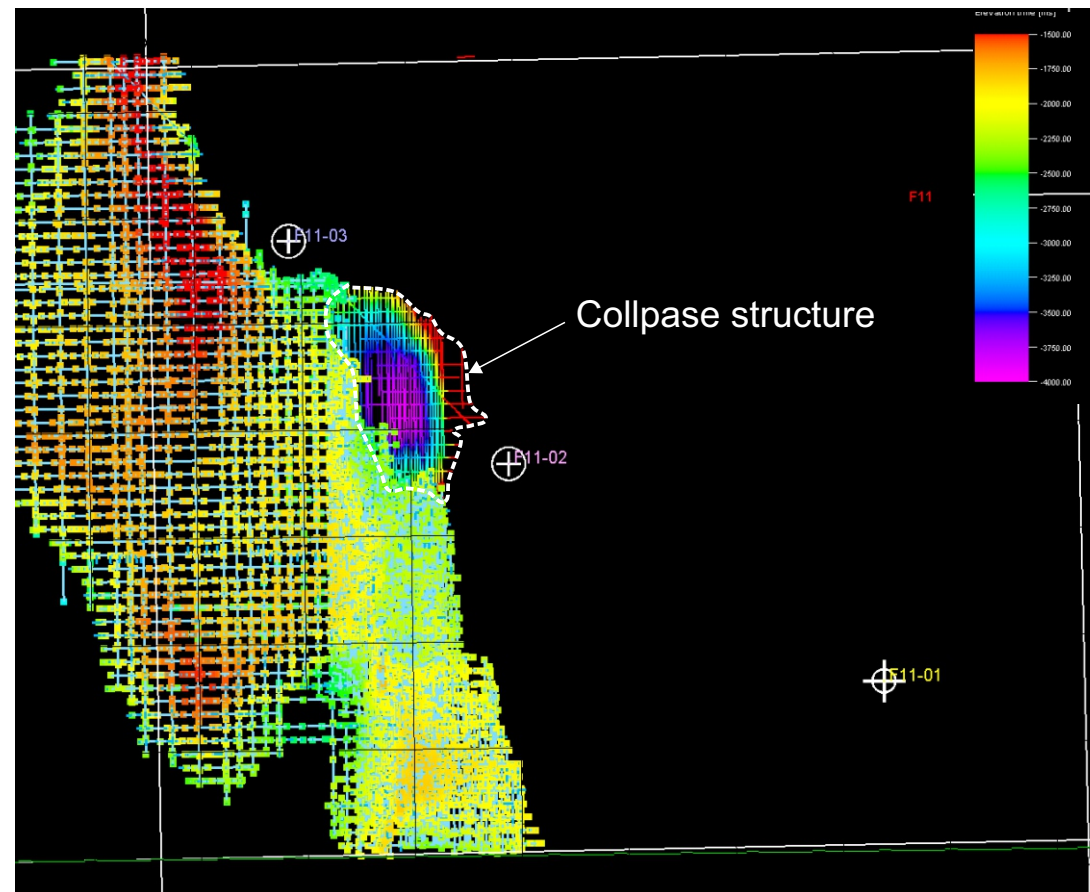


Figure 4.3.62: A collapse structure (CS) is present between wells F11-02 and F11-03 and has been mapped in 3D. On this figure the structure is highlighted with a dashed white polygon. This feature can be seen in Figures 4.3.48, 4.3.49 and 4.3.50.

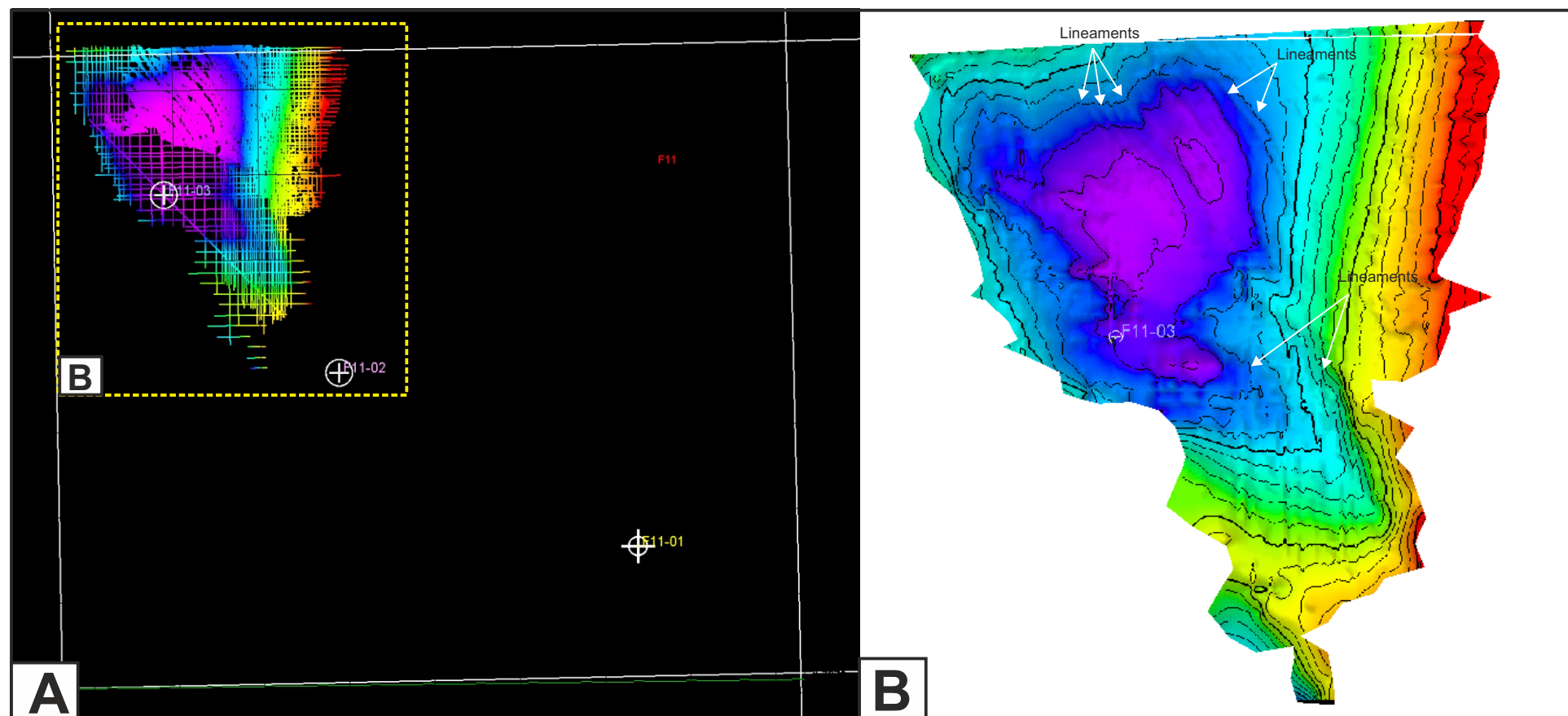


Figure 4.3.63: A possible salt weld was mapped in the northwest part of the F11 block. The salt weld model versus a rim syncline/erosional surface is discussed in the Chapter 5. A) Raw interpretation/time structure map of the salt weld. B) Close up view of the time structure map of the salt weld or erosional surface.

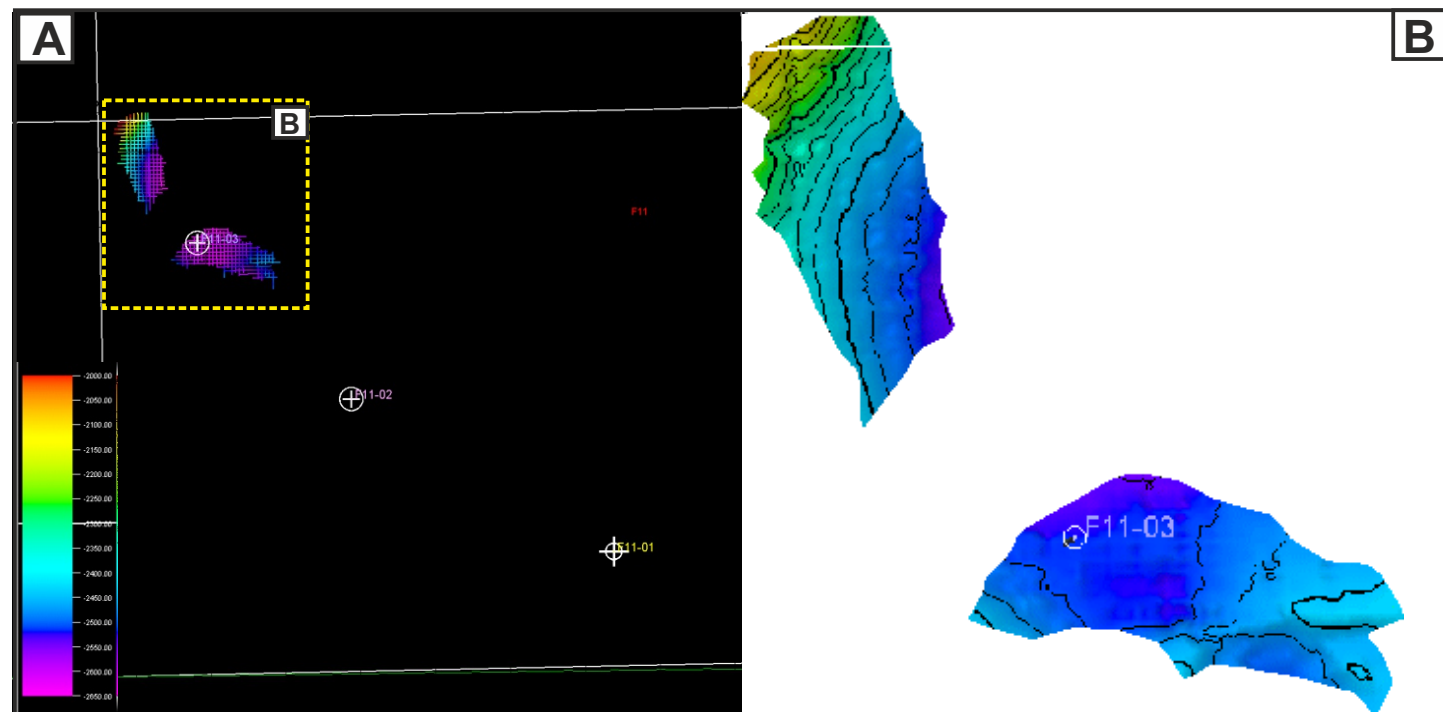


Figure 4.3.64: Time structure maps of the top of the tectono-stratigraphic package 0 that sits between the salt weld (or erosional surface) and the base of Sequence S1 (base of Schieland Group)

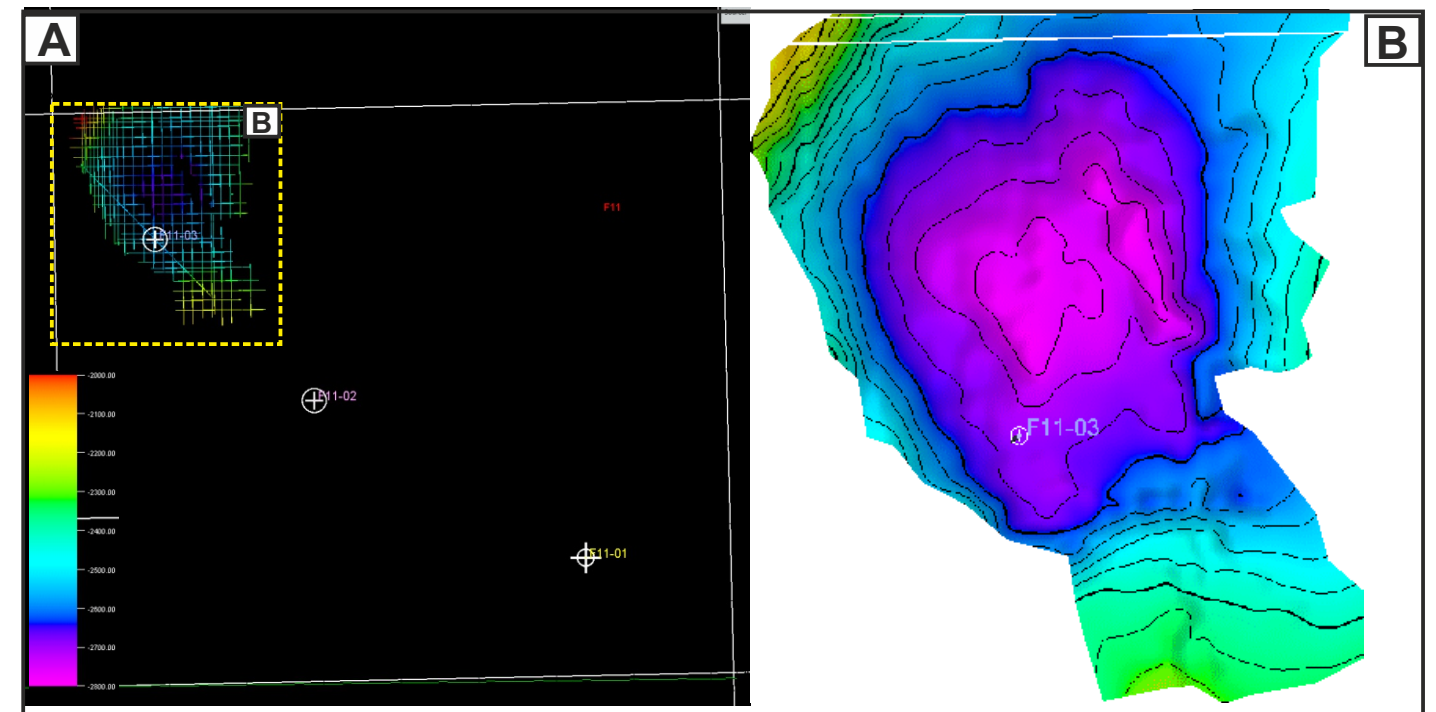


Figure 4.3.65: Time structure maps of the base of Sequence 2 (base of Scruff Group).

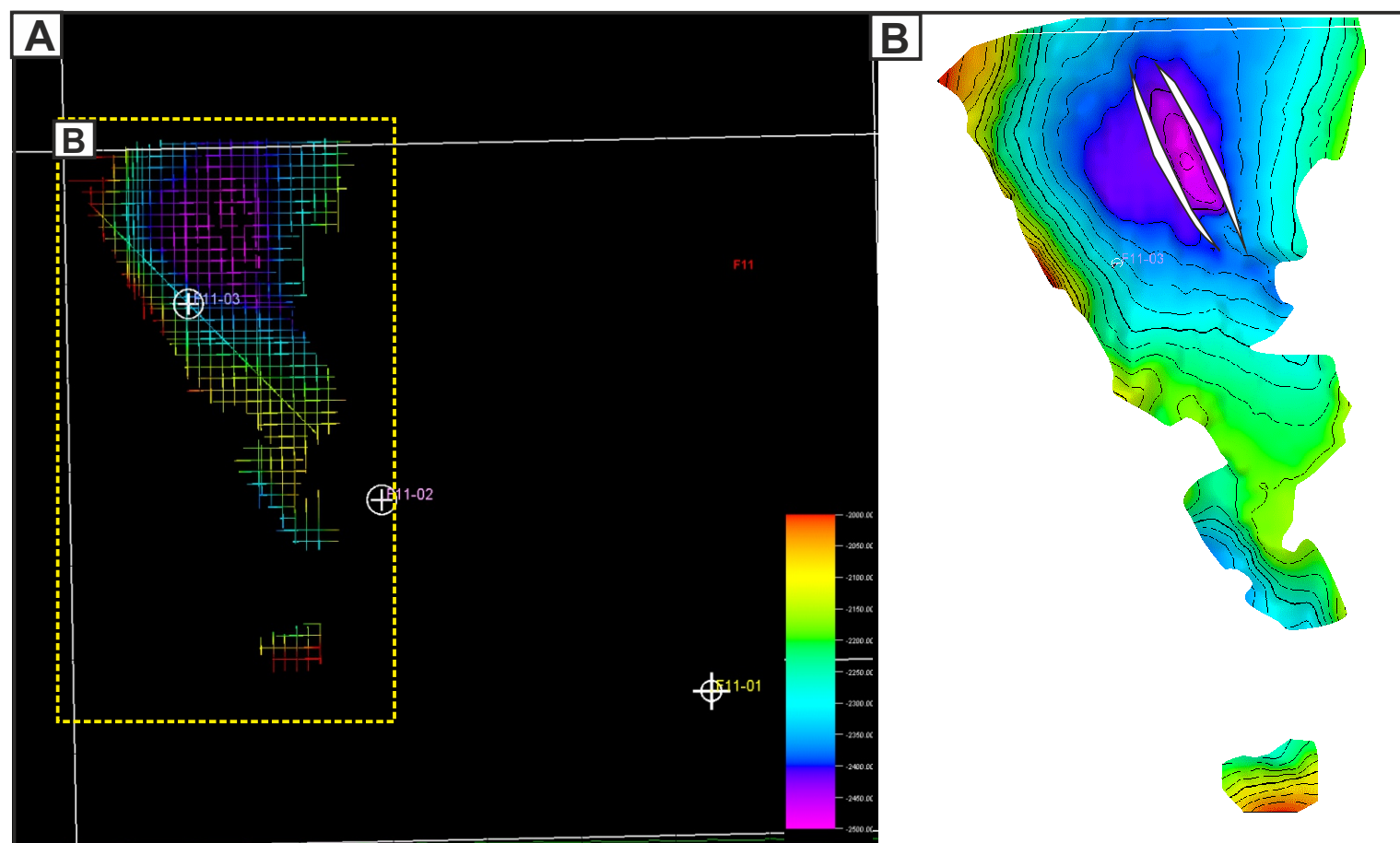


Figure 4.3.66: Time structure maps of the base of Sequence 3 (base of Scruff Formation). Two normal faults trending NNW-SSE are present in central part of the minibasin, forming a small graben that detached on the salt weld level.

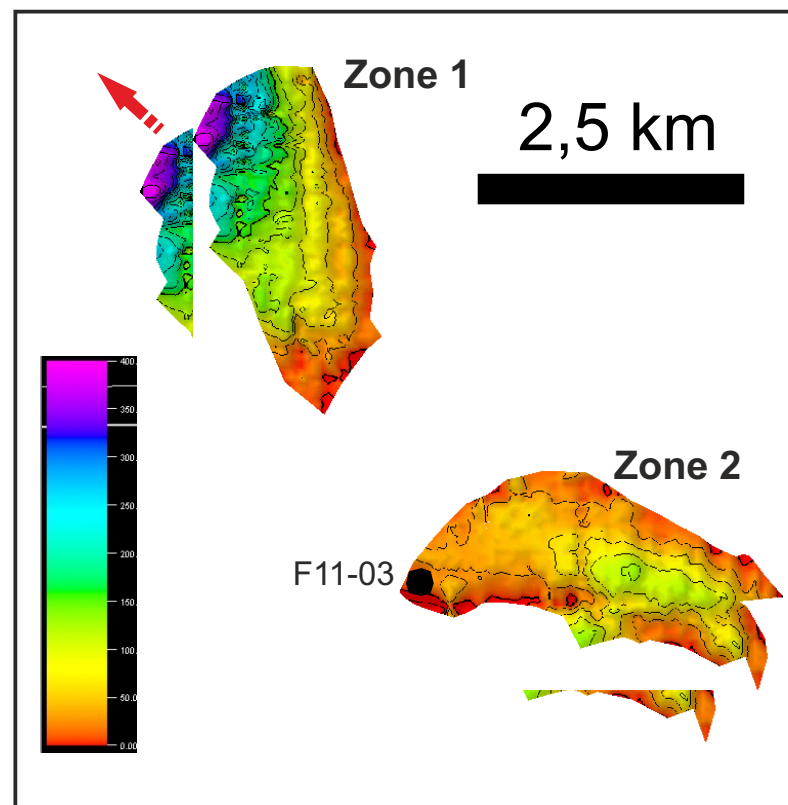


Figure 4.3.67: Time thickness map of the tectonostratigraphic package 0. Direction of wedging, representative of the salt movement direction, shown as red arrows. See Figure 4.3.64 for location.

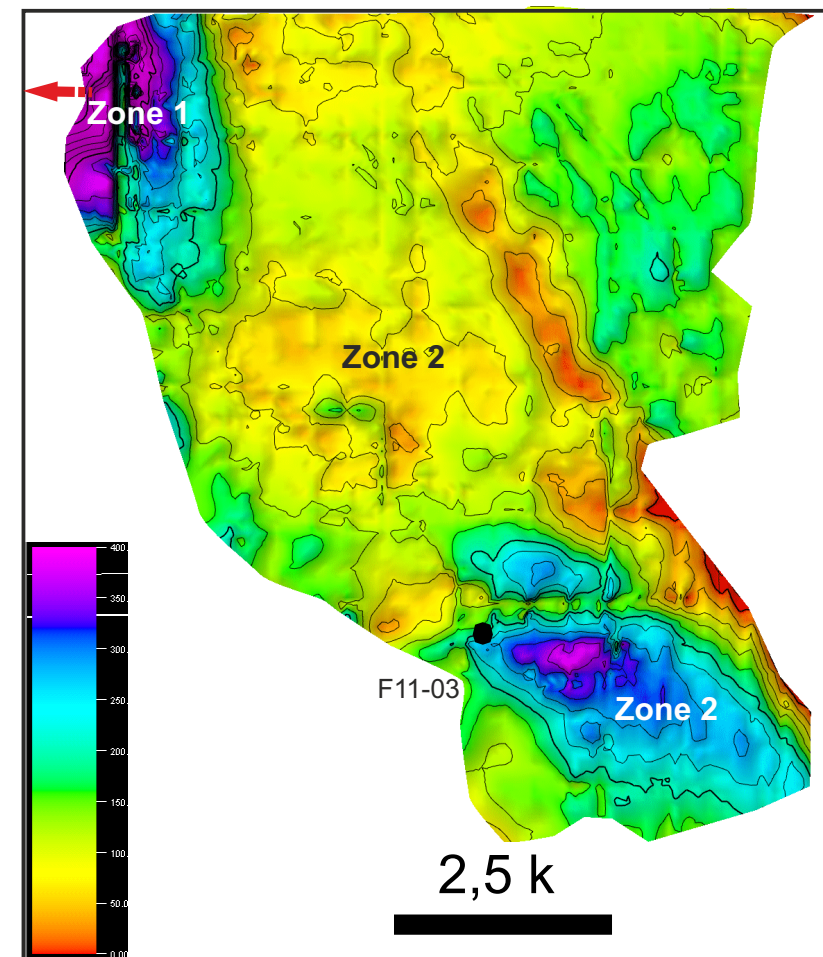


Figure 4.3.68: Time thickness map of the S1 in the minibasin area. Direction of wedging shown as red arrows. See Figure 4.3.65 for location.

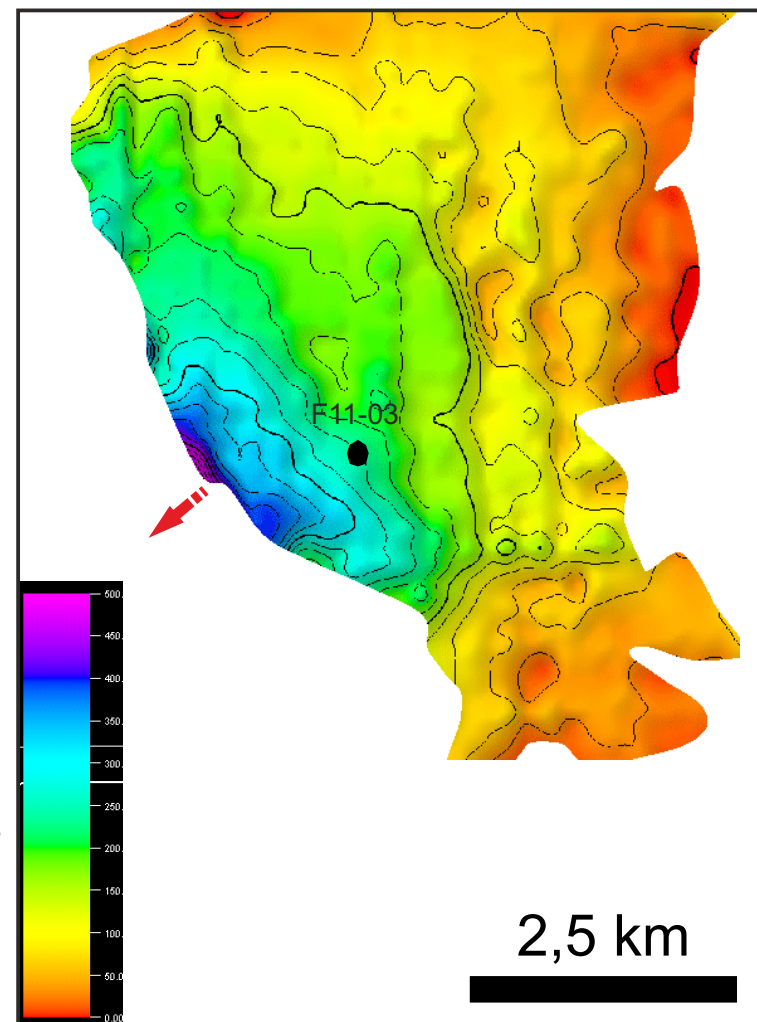


Figure 4.3.69: Time thickness map of S2 in the minibasin. Direction of wedging shown as red arrows. See Figure 4.3.65 for location.

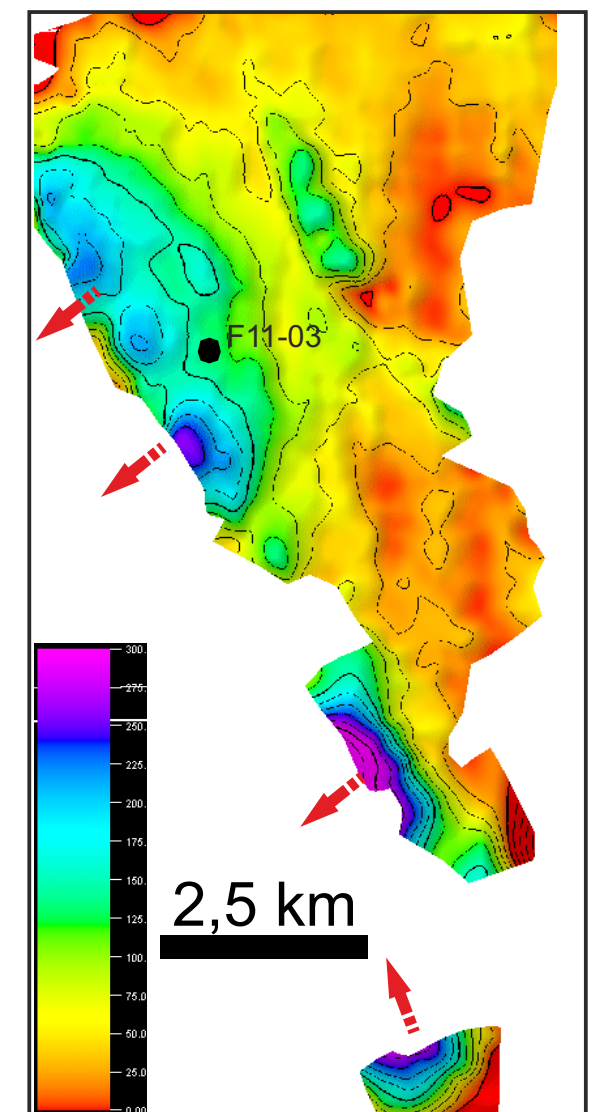


Figure 4.3.70: Time thickness map of S3. Direction of wedging shown as red arrows. See Figure 4.3.66 for location.

RESULTS STRUCTURAL RESTORATIONS

4.4

4.4 Results - Structural restorations

Three structural restorations, one per case study, were carried out to better understand the evolution of the basin and the interaction between salt, faults and the resulting basin- and block-scales stratigraphic architectures. The section restored are 80 to 95 km long and are E-W to NE-SW oriented (Fig. 4.3.1). Note that for convenience in the labeling of the restoration steps, the Lower and Upper Germanic Triassic Groups are referred as Lower and Upper Triassic, and the Schielland and Scruff Groups as Upper Jurassic, even if this interval extends from the Middle Jurassic (Callovian) to the lowermost Lower Cretaceous (Ryazanian). Also not that the term “basement” is used for sub-autochthonous salt stratigraphy.

To describe the results of structural restoration in written format is often difficult since such results are more practically explained in a poster session when the viewer can more easily distinguish changes of the modeled structure between successive steps and in relation to neighboring structures. The lessons learned from these structural restorations, as well as the summary tectono-stratigraphic charts are presented in Chapter 5 (Discussion) and the posters can be found in the Appendix 1. In the present chapter two to three individual restoration steps are shown per page to be able to observe in detail the geometry and change of geometry of key structures.

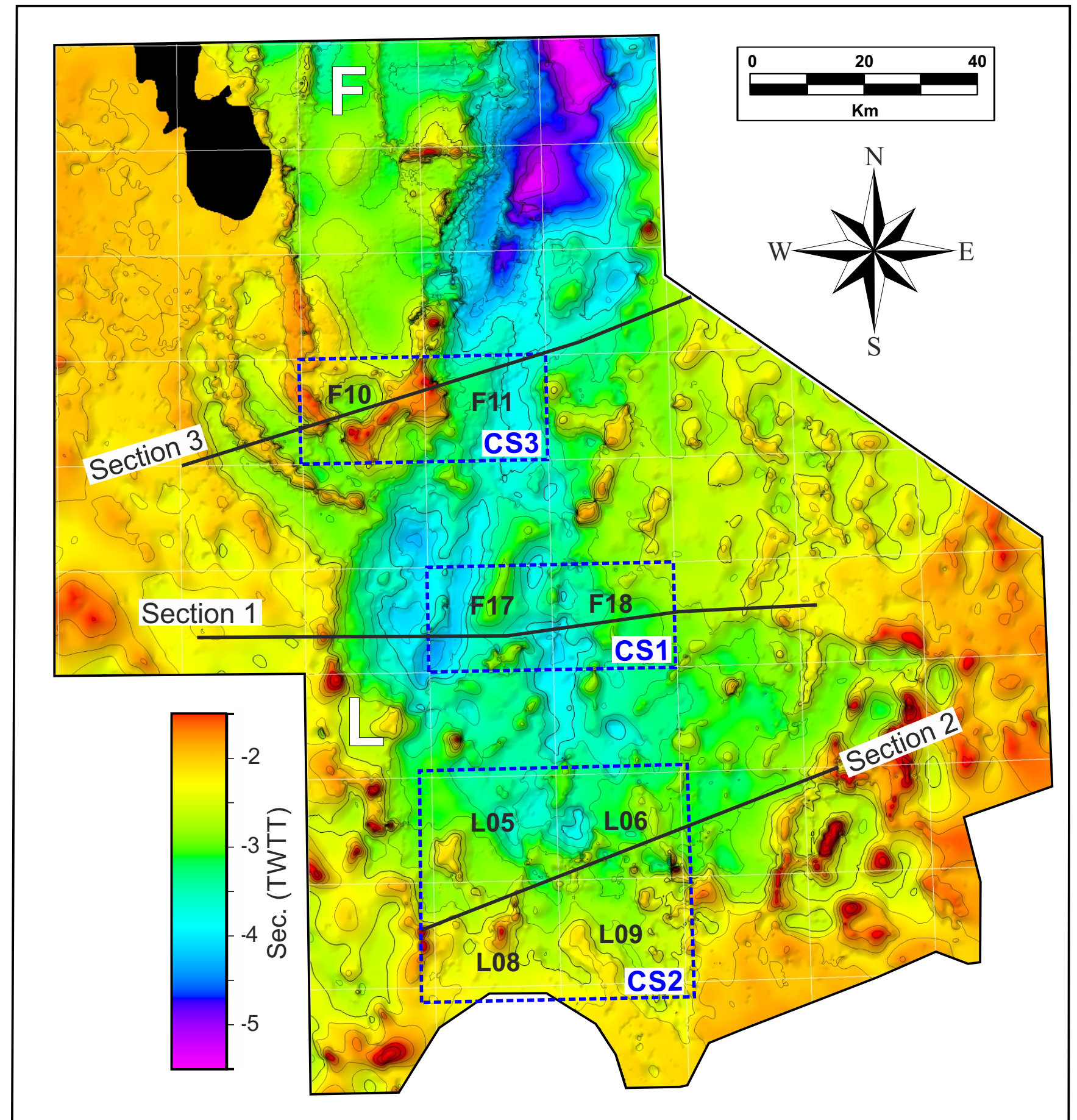


Figure 4.4.1: Location map of the three structurally restored sections (1-3) and their position in reference to the three case studies. Time structure map of the top Zechstein Group shown as background map.

A) Structural restoration 1 (F17-F18)

The first structural restoration was performed over the area covered by the case study 1 (CS1). The 2D section selected intercepts the blocks F17 and F18 but also extends farther west and east to the block E18 and G17 (Fig. 4.4.2). Part of the seismic data used for this section is a 2D extraction from the 3D depth seismic survey used in the case study 1, specifically over the blocks

F17 and F18. The rest of the seismic data used was time -depth converted to match the depth data in the F17/F18 area. Several wells (Fig. 4.4.2C) are present along this section, which allow for a robust geological interpretation of this section. The lessons learned from these structural restorations, as well as the summary tectono-stratigraphic charts are presented in Chapter 5 (Discussion).

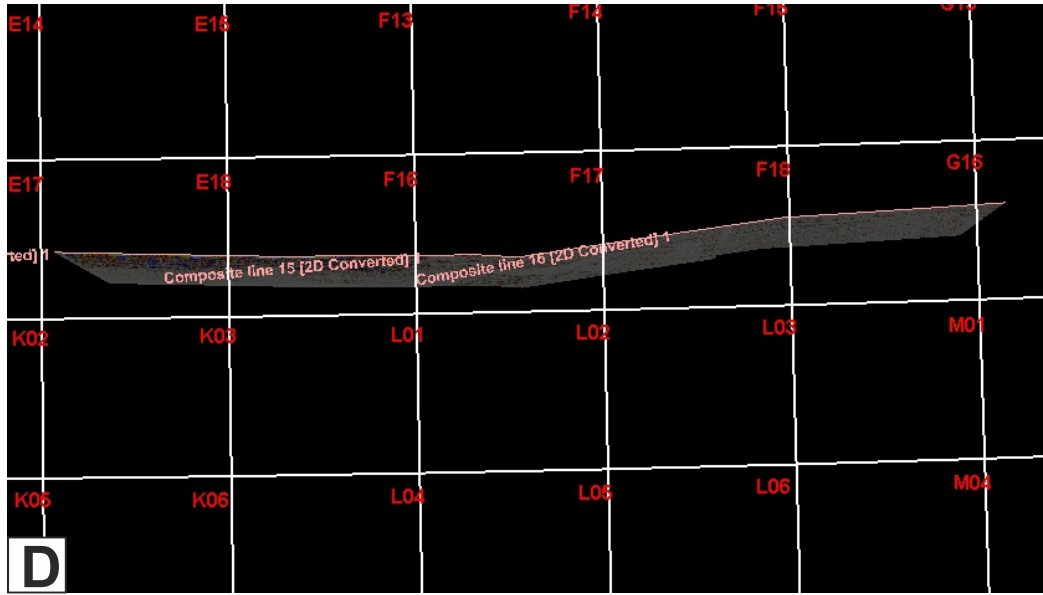
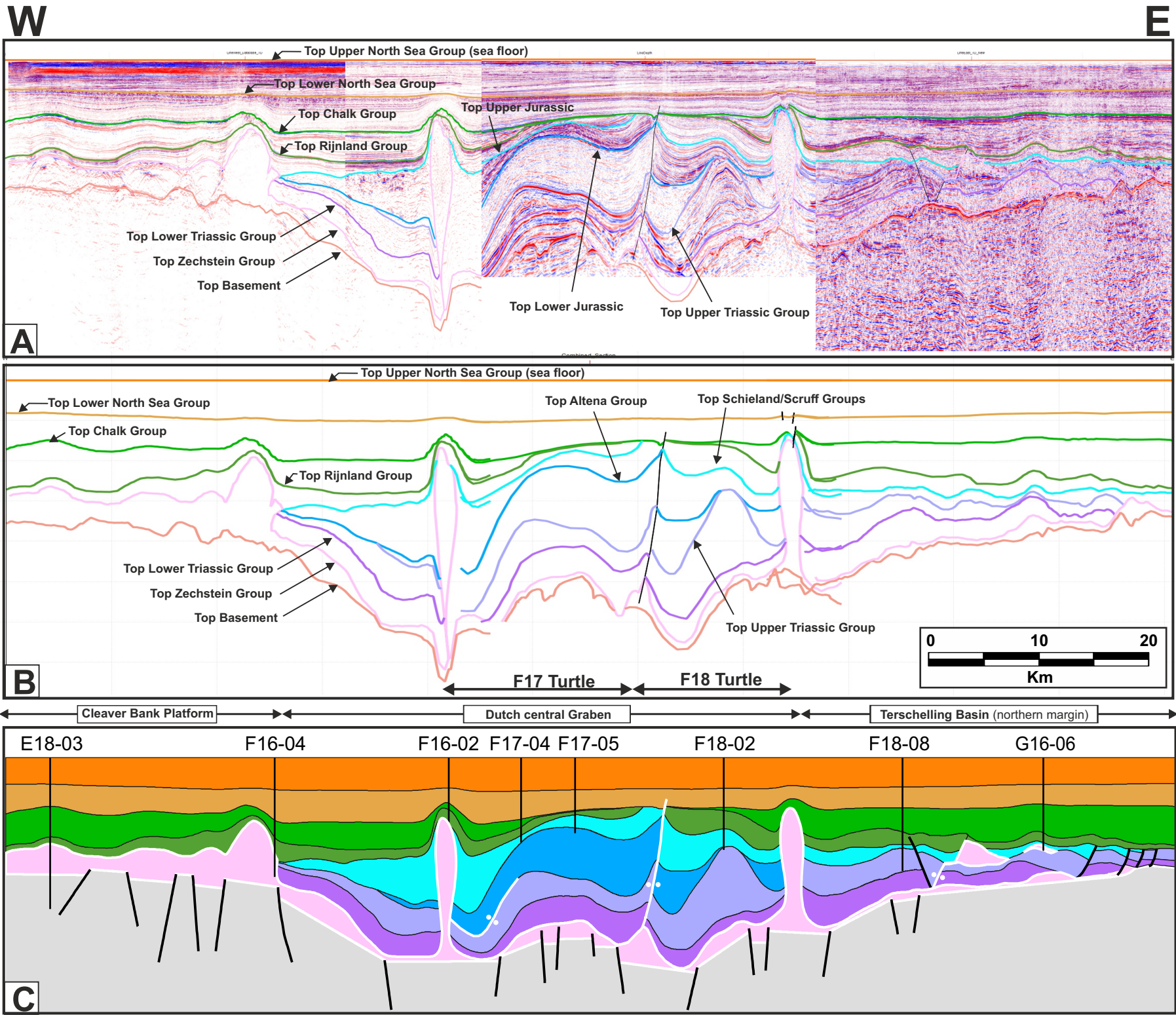
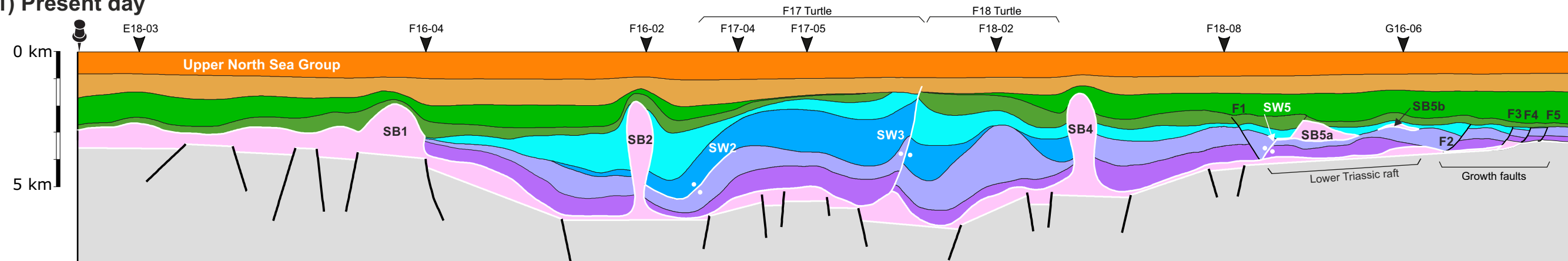


Figure 4.4.2: Structural restoration 1: **A)** Time-depth converted section. The central part of the section (F17/F18) was in depth while the rest of the section was in time, and was depth converted to match the depth data. **B)** Interpreted horizon were exported from Petrel to 2DMove. **C)** The 2D section is cleaned up including each stratigraphic unit, the basement geometry, the salt architecture and the fault patterns. Only large and significant faults are preserved in the model and are restored. **D)** Location map. Note that the section is not perfectly strait.

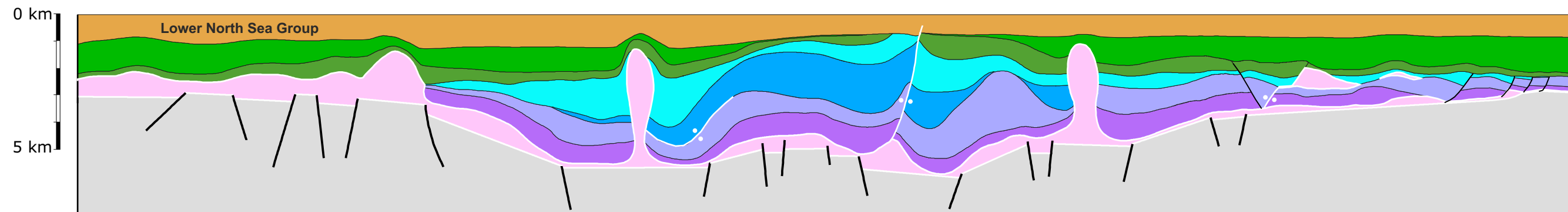
- | | |
|-------------------------|----------------------|
| Upper North Sea Group | Altena Group |
| Lower North Sea Group | Upper Triassic Group |
| Chalk Group | Lower Triassic Group |
| Rijnland Group | Zechstein Group |
| Schieland/Scruff Groups | Basement |
| Fault | Salt body and weld |

4.4 Results - Structural restorations: Section 1

1) Present day



2) Eocene - End of Priabonian (35 Ma)



3) Paleocene - End of Danian (62 Ma)

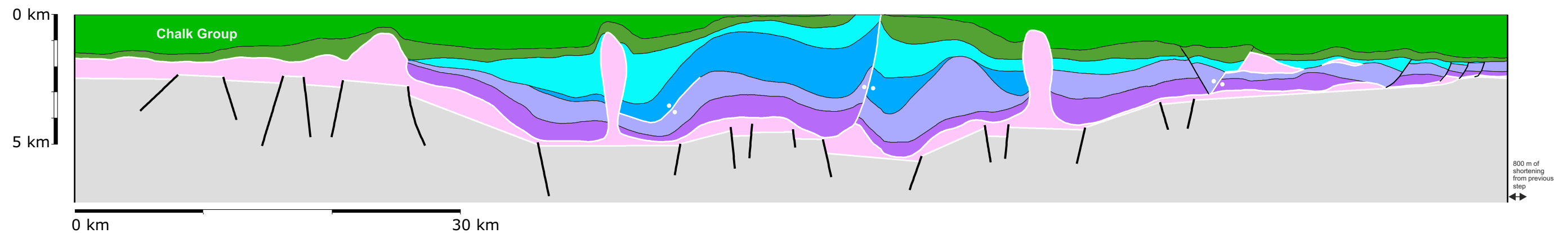
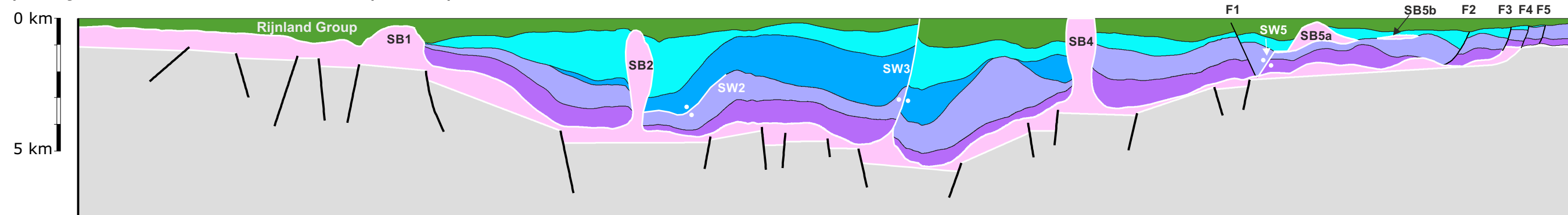


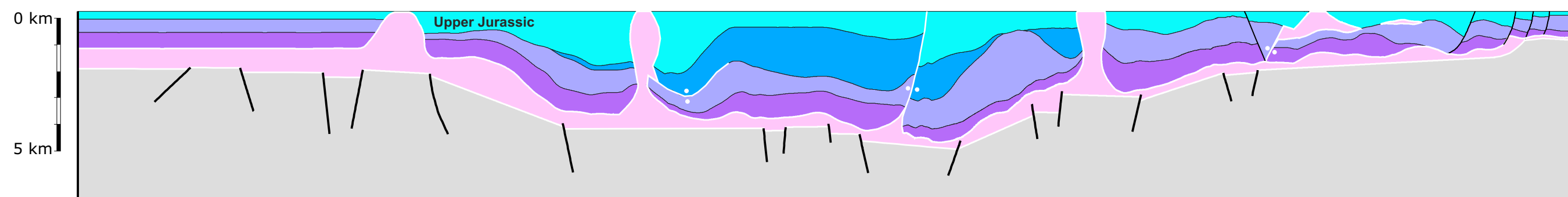
Figure 4.4.3 (part 1/4): Structural restoration 1. See text for comments, Figure 4.4.2 for legend and Figure 4.4.1 for location.

4.4 Results - Structural restorations: Section 1

4) Early Cretaceous - End of Albian (100 Ma)



5) Early Cretaceous - End of Ryazanian (141 Ma)



6) Middle Jurassic - End of Bathonian (166 Ma)

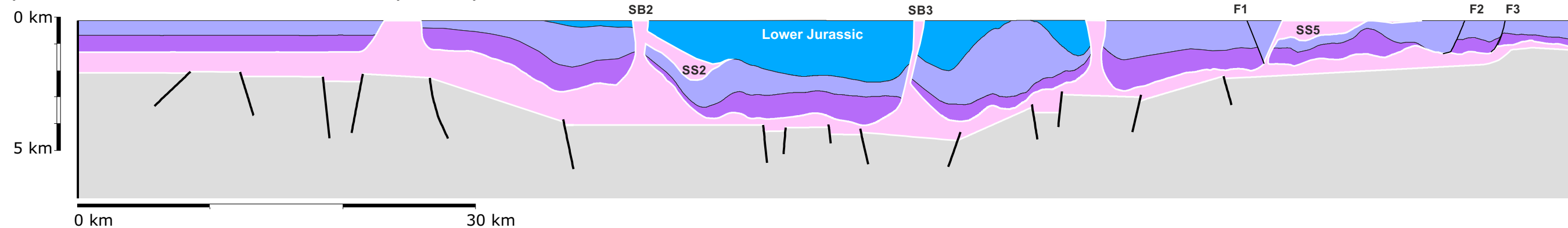
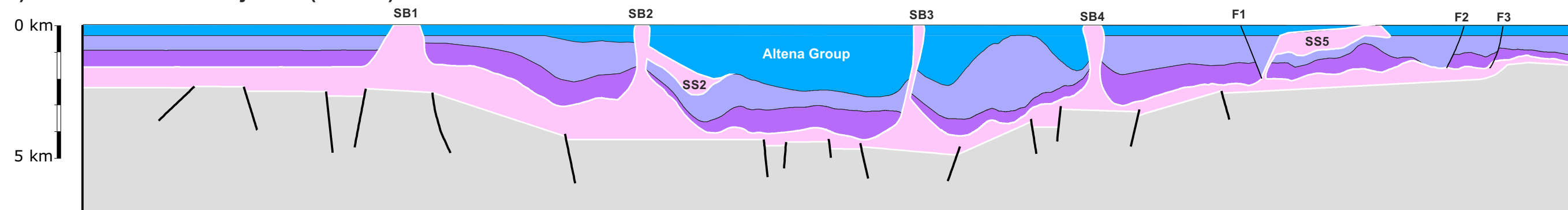


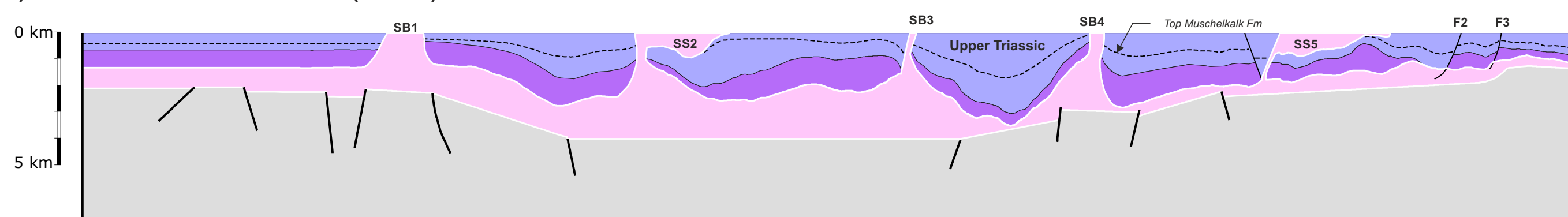
Figure 4.4.3 (part 2/4): Structural restoration 1. Specific salt structures can evolve through time and are either referred as salt bodies (SB), salt pillows (SP) or salt systems (SS). See text for comments, Figure 4.4.2 for legend and Figure 4.4.1 for location.

4.4 Results - Structural restorations: Section 1

7) Middle Jurassic - Bajocian (170 Ma)



8) Late Triassic - End of Rhaetian (199 Ma)



9) Middle Triassic - End of Anisian (241 Ma)

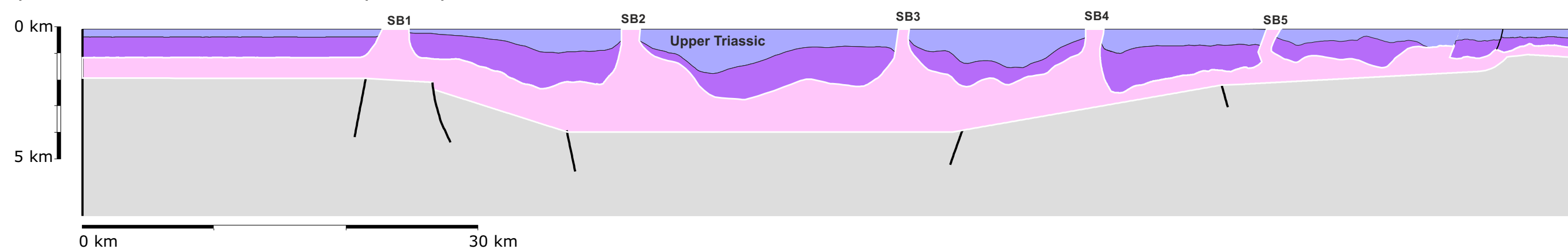
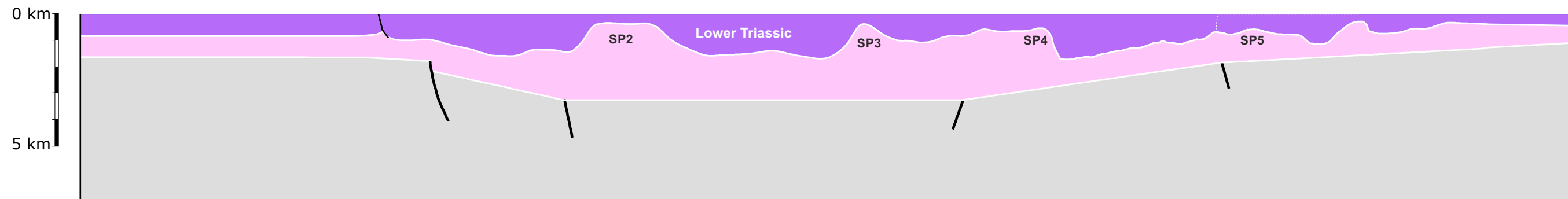


Figure 4.4.3 (part 3/4): Structural restoration 1. Specific salt structures can evolve through time and are either referred as salt bodies (SB), salt pillows (SP) or salt systems (SS). See text for comments, Figure 4.4.2 for legend and Figure 4.4.1 for location.

4.4 Results - Structural restorations: Section 1

10) Early Triassic - End of Olenekian (247 Ma)



11) Late Permian - End of Lopingian (252 Ma)

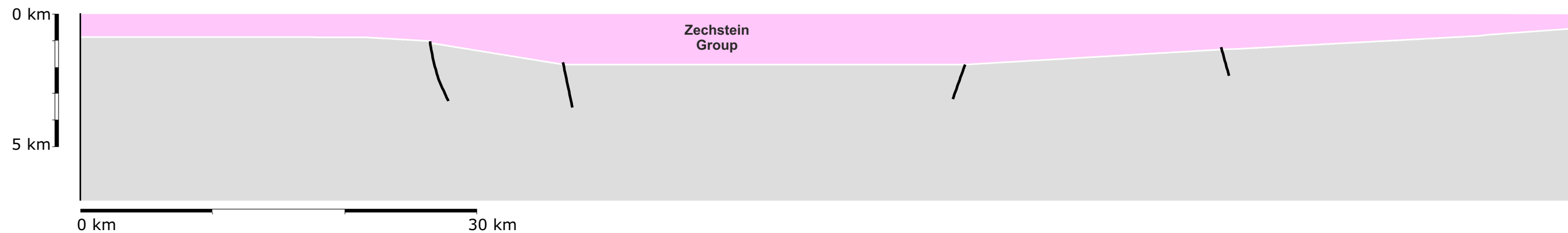


Figure 4.4.3 (part 4/4): Structural restoration 1. Specific salt structures can evolve through time and are either referred as salt bodies (SB), salt pillows (SP) or salt systems (SS). See text for comments, Figure 4.4.2 for legend and Figure 4.4.1 for location.

4.4 Results - Structural restorations: Section 2

B) Structural restoration 2 (L05-L06-L08-L09)

The second structural restoration was performed over the area covered by the case study 2 (CS2). The 2D section selected intercepts the blocks L08, L09, L06 and M04. The decision to extend the section farther to the NE to the M04 block, that comprise the eastern margin of the Terschelling Basin, was taken to capture the evolution of the area in a more regionally significant manner (Fig. 4.4.4). Several wells are located on the section or close by (Figs. 4.4.4 and 4.4.5).

The north-eastern two third of the section is located in the Terschelling Basin and the south-western third in the Friesland Platform.

Several salt bodies are present along this section (Fig. 4.4.5). Locally the Lower Triassic is not present due to rafting and salt body collapse as presented in Section 4.3. A large salt system that involves the extrusion of an allochthonous salt sheet (SB6, Fig. 4.4.5) is recognized and was modeled. The lessons learned from these structural restorations, as well as the summary tectono-stratigraphic charts are presented in Chapter 5 (Discussion).

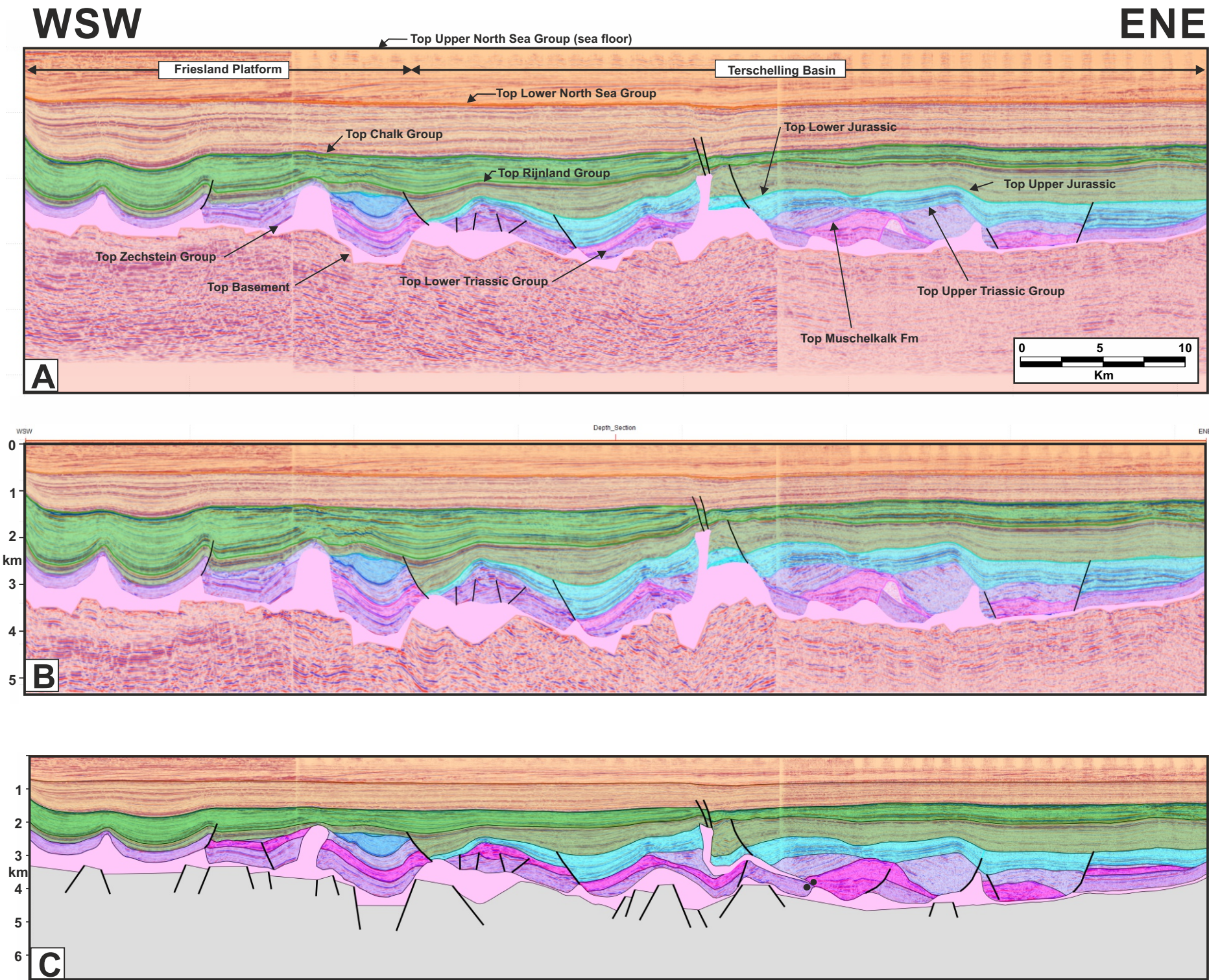
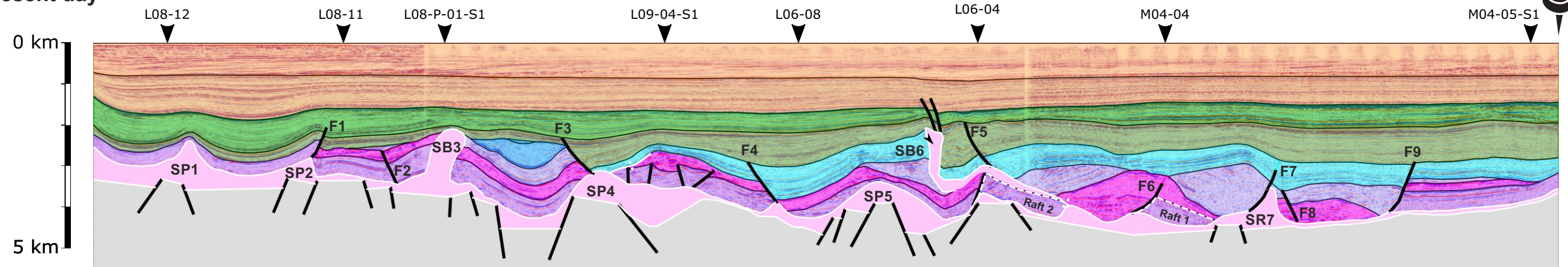


Figure 4.4.4: Structural restoration 2, blocks L05-L06-L08-L09: **A)** Interpreted time seismic section. **B)** Time-depth converted interpreted seismic section. Interpreted horizon were exported from Petrel to 2DMove. **C)** Cleaned up depth section, including each stratigraphic unit, the basement geometry, the salt architecture and the fault patterns. Only large and significant faults are preserved in the model and are restored. **D)** Location map. Several wells and additional seismic section were used to validate the interpretation and analyze the salt body architecture in areas located close to the restored section.

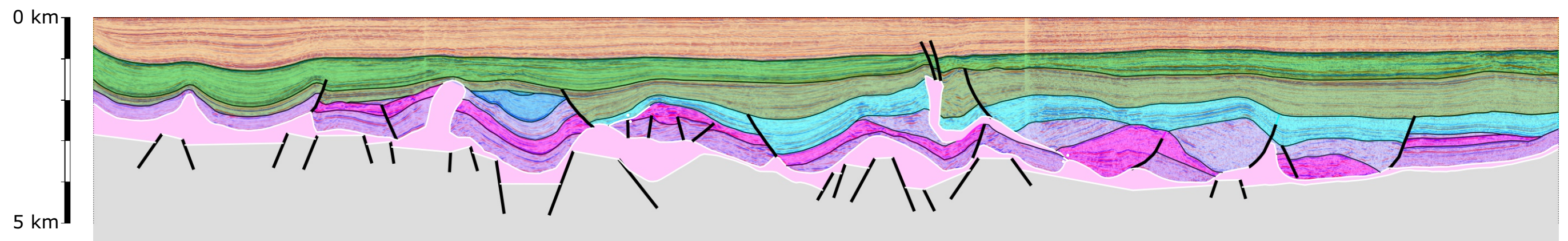


4.4 Results - Structural restorations: Section 2

1) Present day



2) Eocene - End of Priabonian (35 Ma)



3) Paleocene - End of Danian (62 Ma)

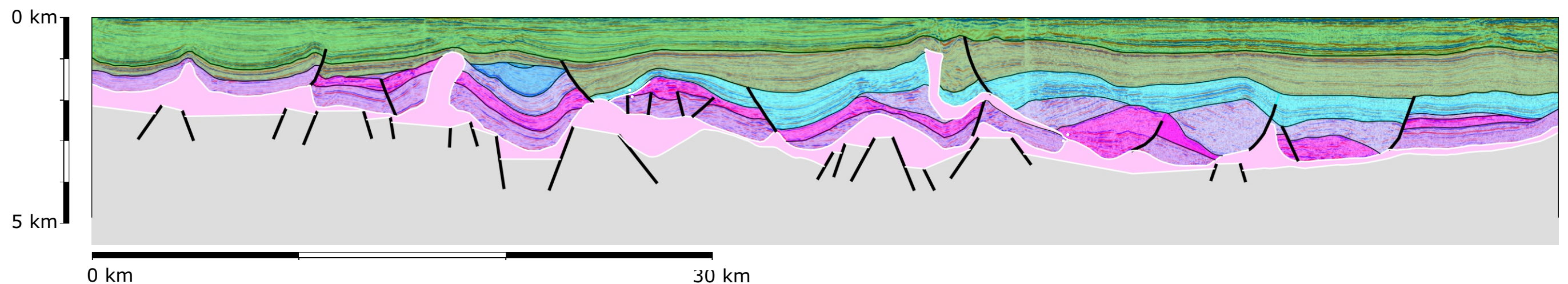
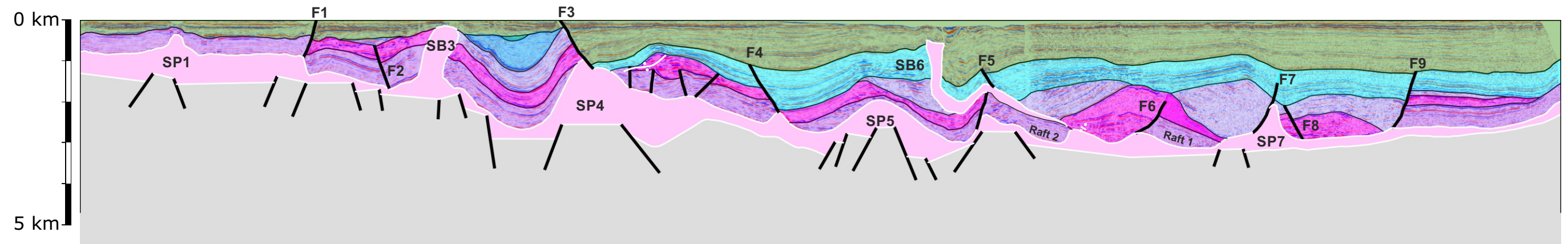


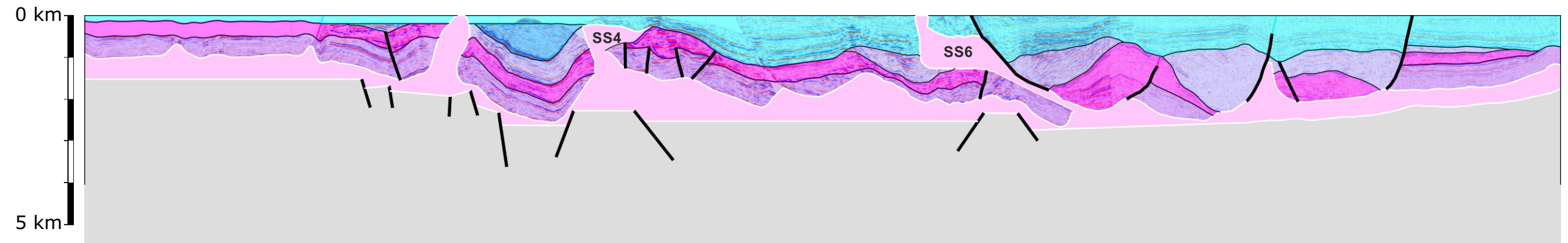
Figure 4.4.5 (part 1/3): Structural restoration 2. Specific salt structures can evolve through time and are either referred as salt bodies (SB), salt pillows (SP) or salt systems (SS). See text for comments, Figure 4.4.4 for legend and Figure 4.4.1 for location.

4.4 Results - Structural restorations: Section 2

4) Early Cretaceous - End of Albian (100 Ma)



5) Early Cretaceous - End of Ryazanian (141 Ma)



6) Middle Jurassic - End of Bathonian (166 Ma)

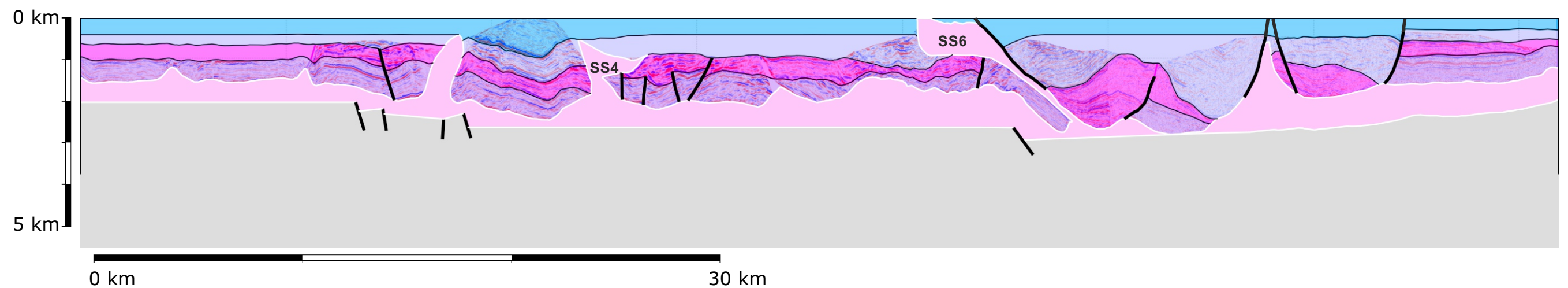
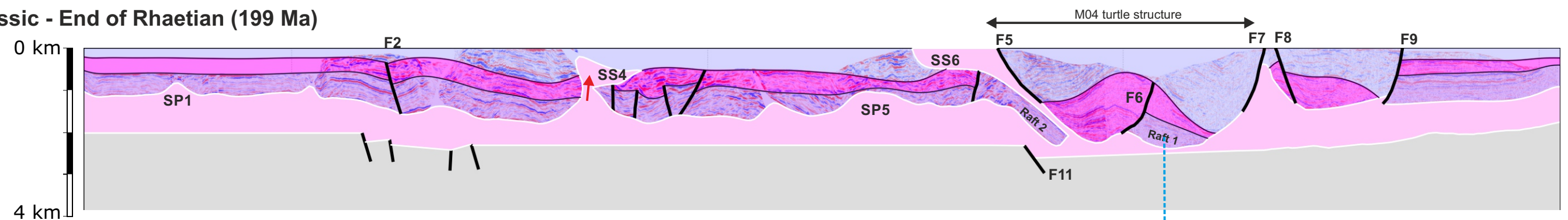


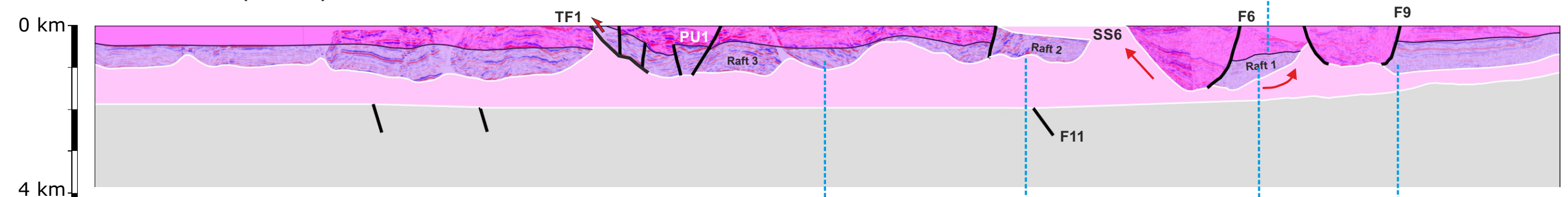
Figure 4.4.5 (part 2/3): Structural restoration 2. Specific salt structures can evolve through time and are either referred as salt bodies (SB), salt pillows (SP) or salt systems (SS). See text for comments, Figure 4.4.4 for legend and Figure 4.4.1 for location.

4.4 Results - Structural restorations: Section 2

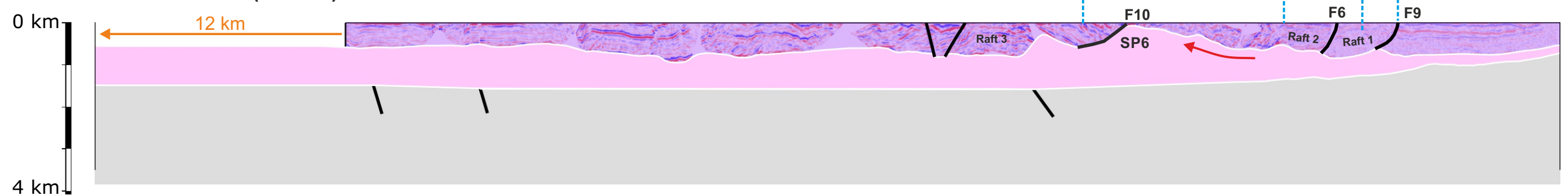
7) Late Triassic - End of Rhaetian (199 Ma)



8) Middle Triassic - End of Anisian (241 Ma)



9) Early Triassic - End of Olenekian (247 Ma)



10) Late Permian - End of Lopingian (252 Ma)

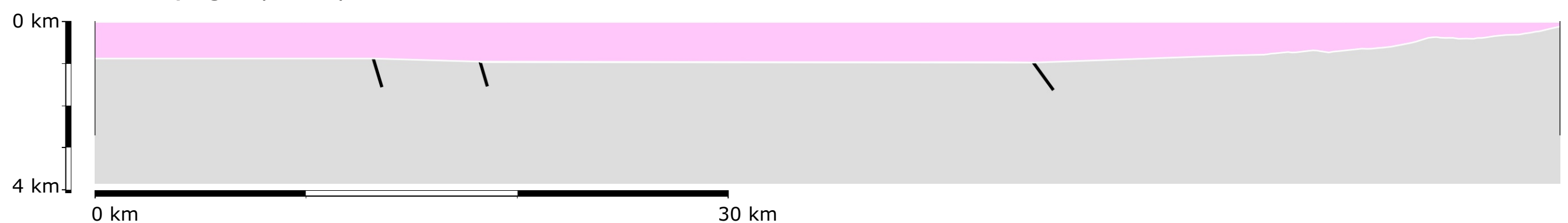


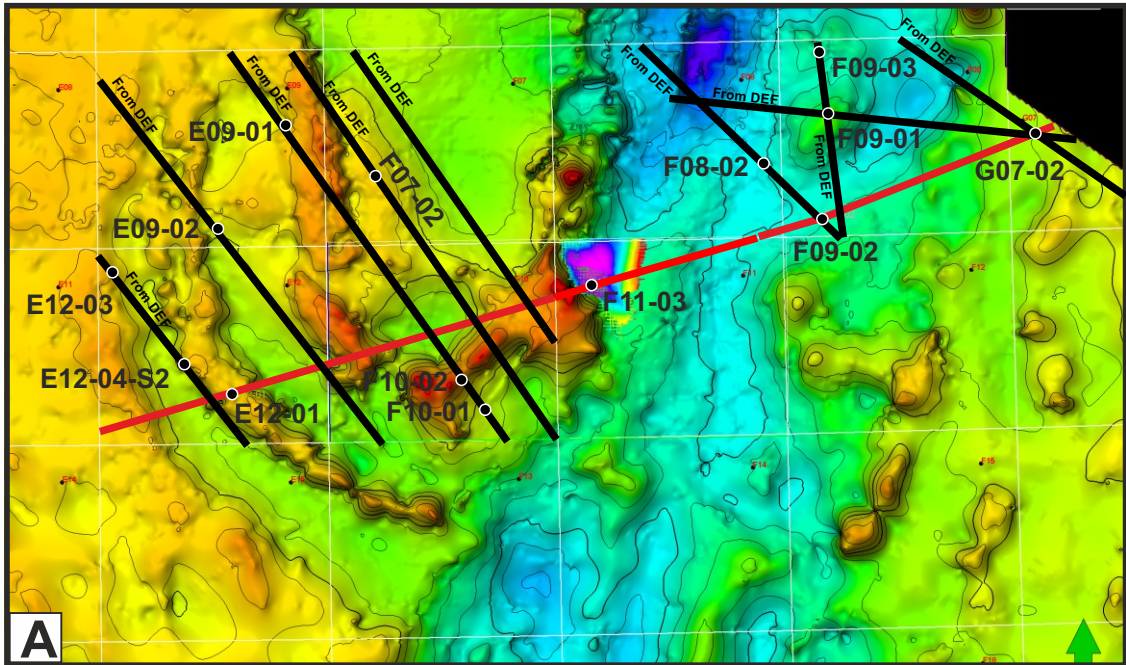
Figure 4.4.5 (part 3/3): Structural restoration 2. SP = Salt Pillow; SS = Salt System; PU = Pop Up structure; TF = Thrust Fault. Specific salt structures can evolve through time and are either referred as salt bodies (SB), salt pillows (SP) or salt systems (SS). See text for comments, Figure 4.4.4 for legend and Figure 4.4.1 for location.

4.4 Results - Structural restorations: Section 3

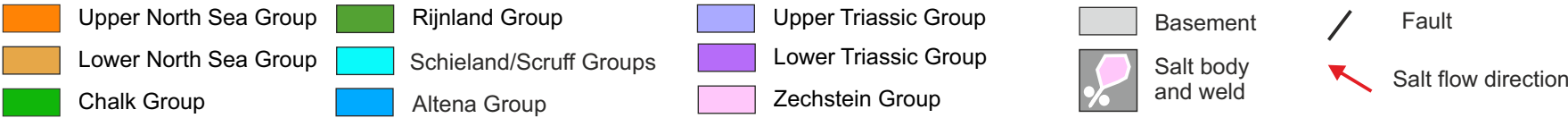
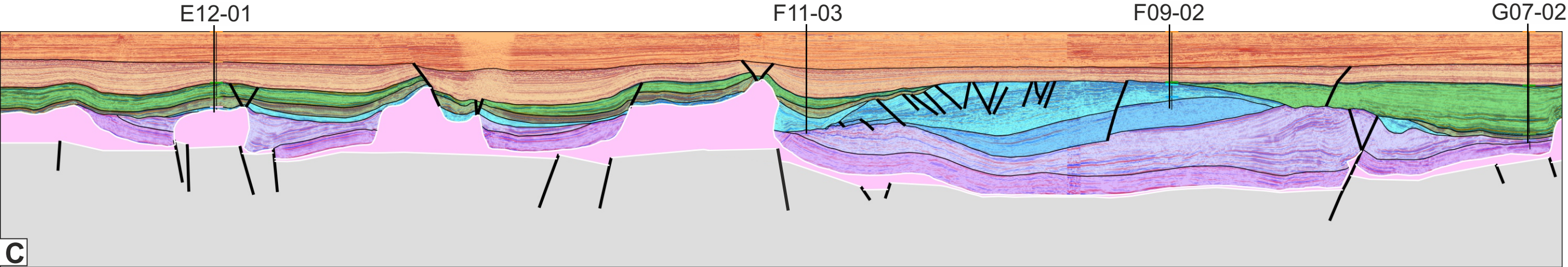
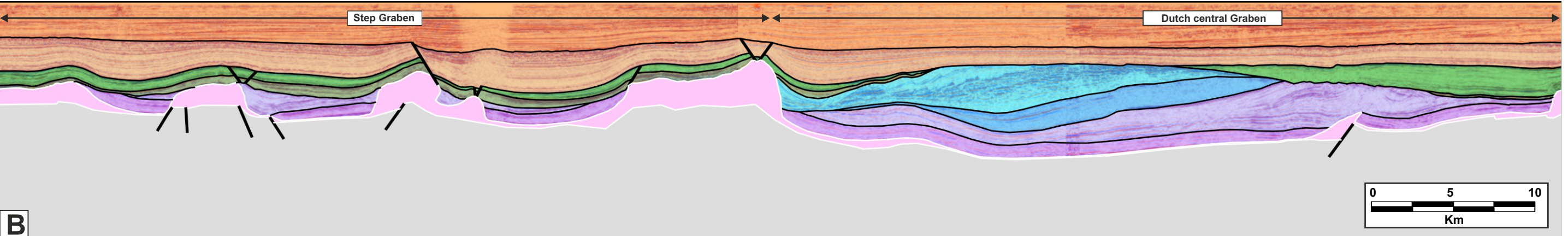
A) Structural restoration 3 (F10-F11)

The third and last section structurally restored is located in the same area than case study 3 (CS3: F10-F11 blocks). The section extends farther to the WSW (block E12) to the ENE (block G07) to also capture the structural evolution in the Step Graben and across the DCG. To be able to test two different models concerning the salt evolution around the F11-03 well, two different structural restoration chains (Figs. 4.4.7 and 4.4.8) were carried out from the Upper Jurassic to the Permian. For the prior restored steps (Cretaceous and Cenozoic) both restorations follow the same

Figure 4.4.6: The third restored section. **A)** Top autochthonous salt map showing the position of the 2D section (red line) and additional 2D lines used to tie to neighboring wells. The central part of the section (blocks F10 and F11) was extracted from the F10/F11 data set provided by EBN and partners and used during Phase 2.3 of the project. The seismic used for the rest of the section (blocks E12, F09 and G07) was extracted from the DEF survey and consisted of Spectrum in kind contribution to the project. **B)** Originally interpreted time seismic section. **C)** Interpreted time-depth converted seismic section. Note that several areas (e.g. Cleaver Ban Platform and eastern side of the Dutch Central Graben) have been reinterpreted using additional 2D and 3D seismic data. For example Upper Jurassic Sequence 3 has been added on part of the Cleaver Bank Platform.

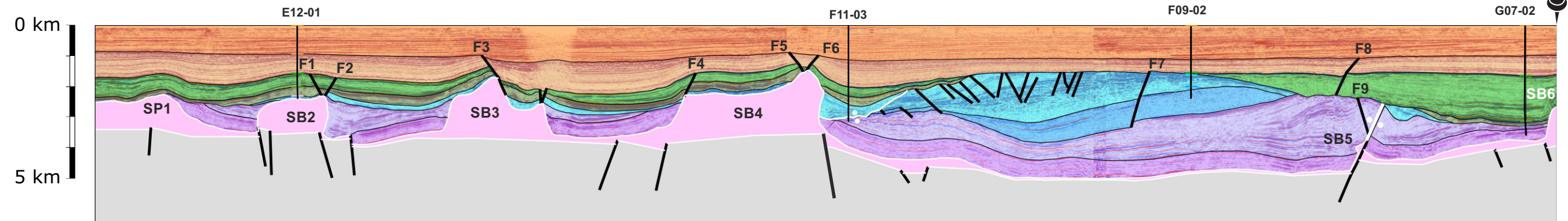


WSW ENE



4.4 Results - Structural restorations: Section 3

1A) Present day



2A) Eocene - End of Priabonian (35 Ma)

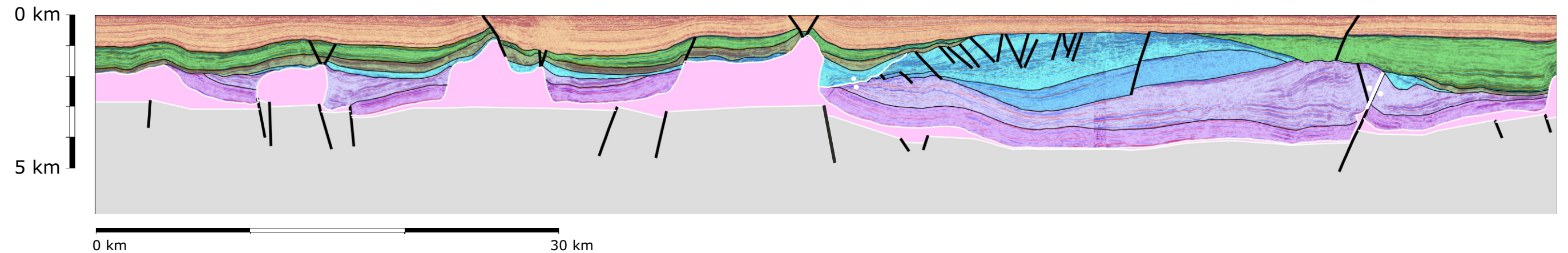
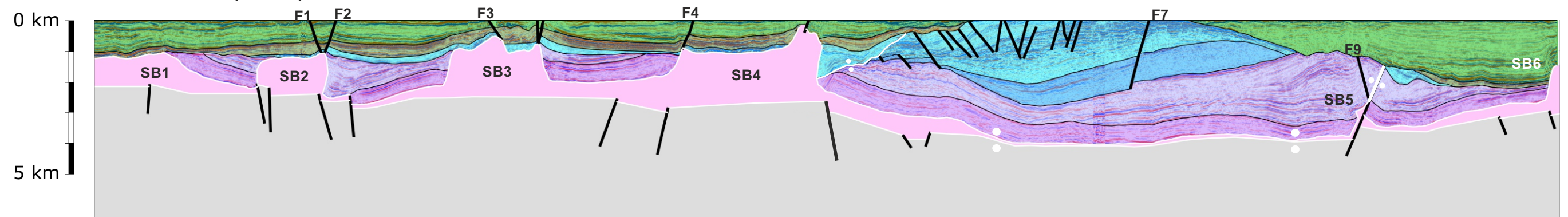


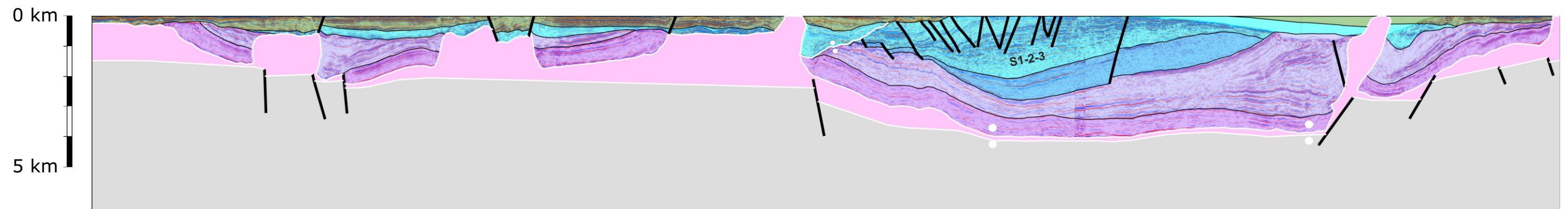
Figure 4.4.7 (part 1/4): Third structural restoration with salt weld model. Specific salt structures can evolve through time and are either referred as salt bodies (SB), salt pillows (SP) or salt systems (SS). See text for comments and Figure 4.4.6 for location and legend.

4.4 Results - Structural restorations: Section 3

3A) Paleocene - End of Danian (62 Ma)



4A) Early Cretaceous - End of Albian (100 Ma)



5A) Early Cretaceous - End of Ryazanian (141 Ma) - End of Scruff Group deposition

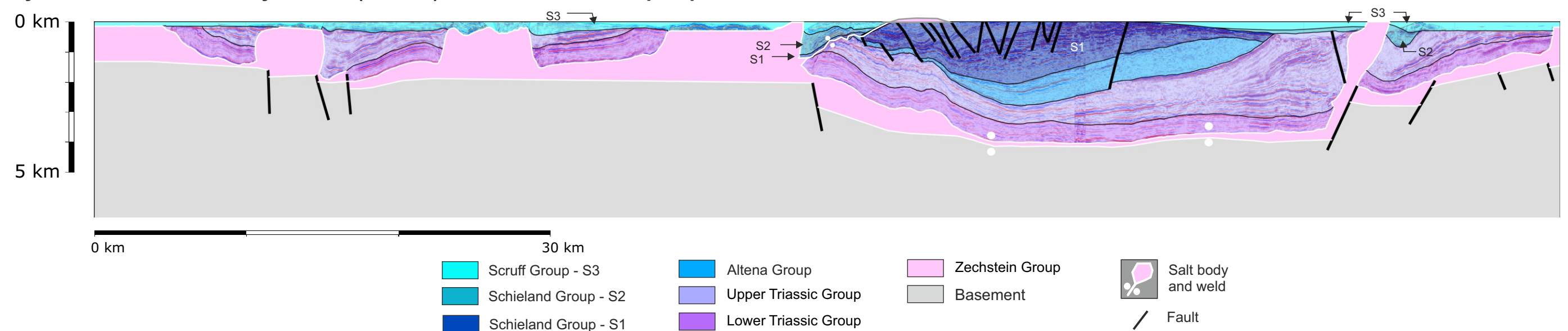
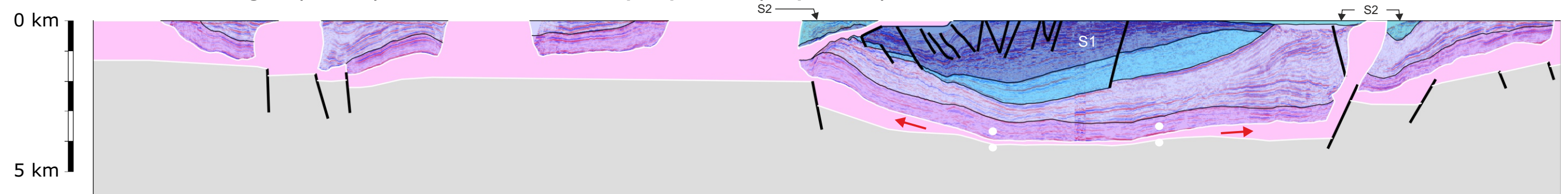


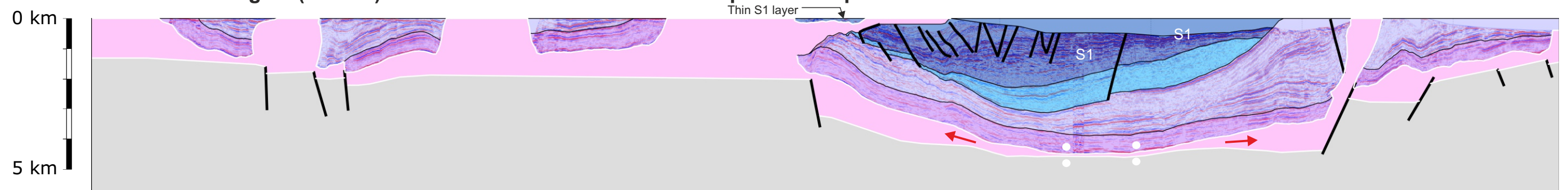
Figure 4.4.7 (part 2/4): Third structural restoration with salt weld model. Specific salt structures can evolve through time and are either referred as salt bodies (SB), salt pillows (SP) or salt systems (SS). See text for comments and figure 4.4.6 for legend. Note that the legend shown above for the Scruff Group and older strata relates to steps 5A to 7A for which the Schieland and Scruff Groups interval was divided into three stratigraphic intervals (S1, S2 and S3) the same sequences described by Munsterman et al. (2012) and Bouroullec et al. (2015).

4.4 Results - Structural restorations: Section 3

6A) Late Jurassic - Middle Volgian (146 Ma) - End of Schieland Group deposition (Sequence 2)



7A) Late Jurassic - Middle Volgian (156 Ma) - End of Middle - Late Jurassic Sequence 1 deposition



8A) Middle Jurassic - End of Bathonian (166 Ma)

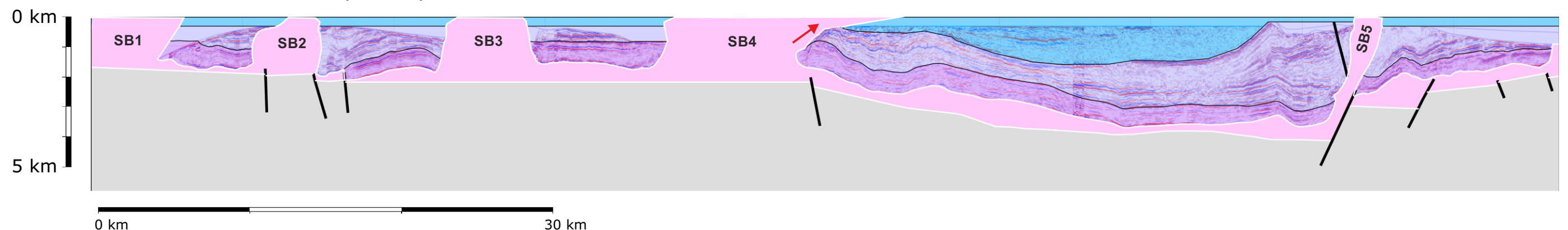
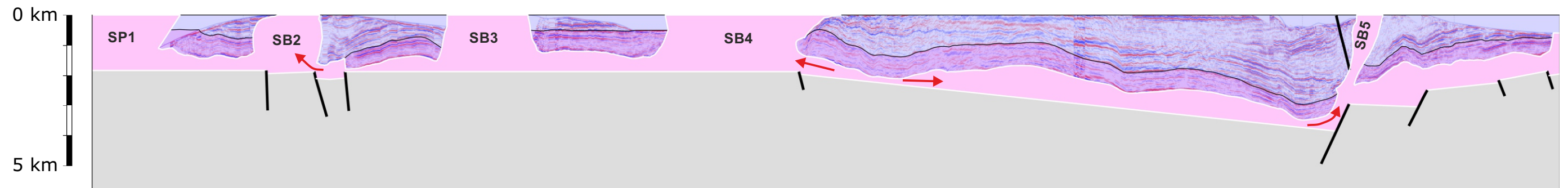


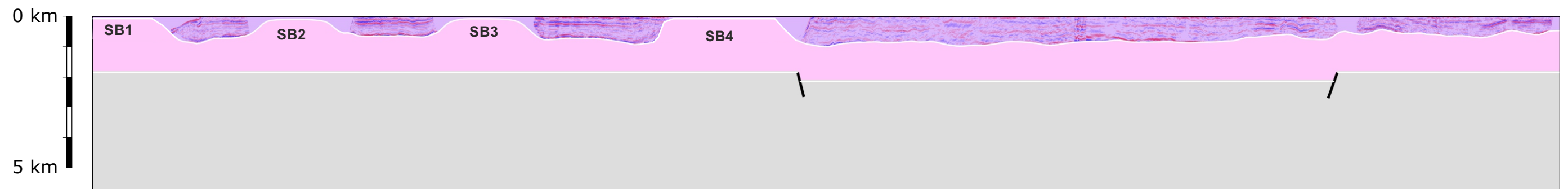
Figure 4.4.7 (part 3/4): Third structural restoration with salt weld model. Specific salt structures can evolve through time and are either referred as salt bodies (SB), salt pillows (SP) or salt systems (SS). See text for comments and Figures 4.4.6 for location and Figures 4.4.6 and 4.4.7(part 2) for legends.

4.4 Results - Structural restorations: Section 3

9A) Late Triassic - End of Rhaetian (199 Ma)



10A) Early Triassic - End of Olenekian (247 Ma)



11A) Late Permian - End of Lopingian (252 Ma)

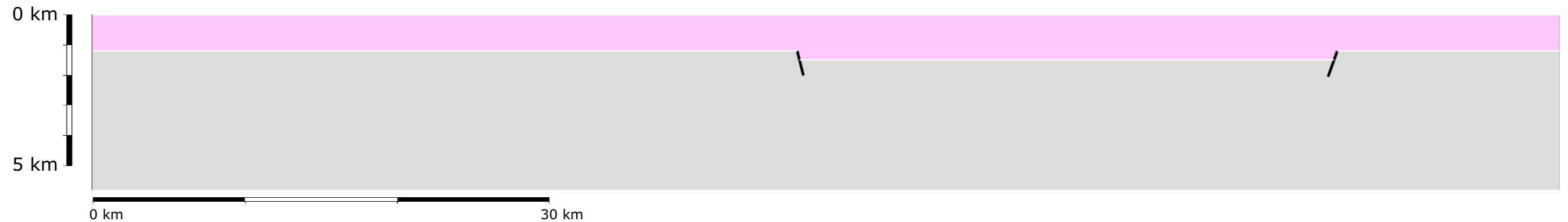
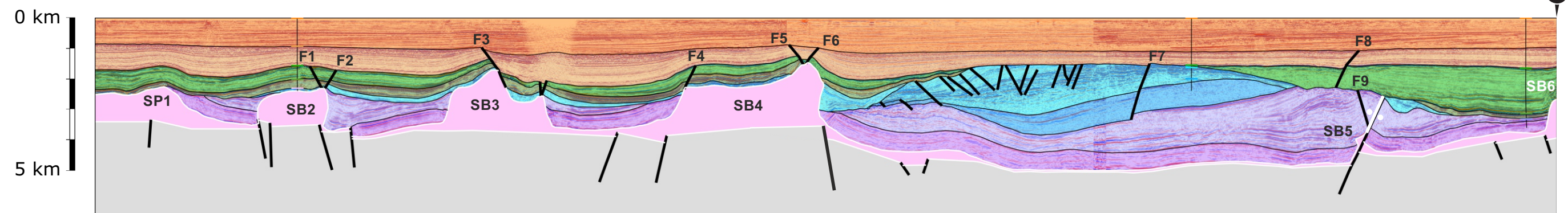


Figure 4.4.7 (part 4/4): Third structural restoration with salt weld model. Specific salt structures can evolve through time and are either referred as salt bodies (SB), salt pillows (SP) or salt systems (SS). See text for comments and Figure 4.4.6 for legend and location.

4.4 Results - Structural restorations: Section 3

1B) Present day



2B) Eocene - End of Priabonian (35 Ma)

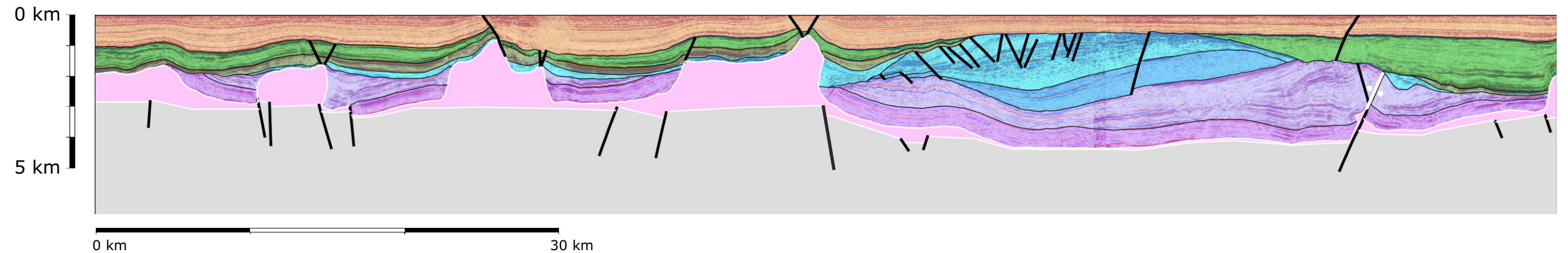
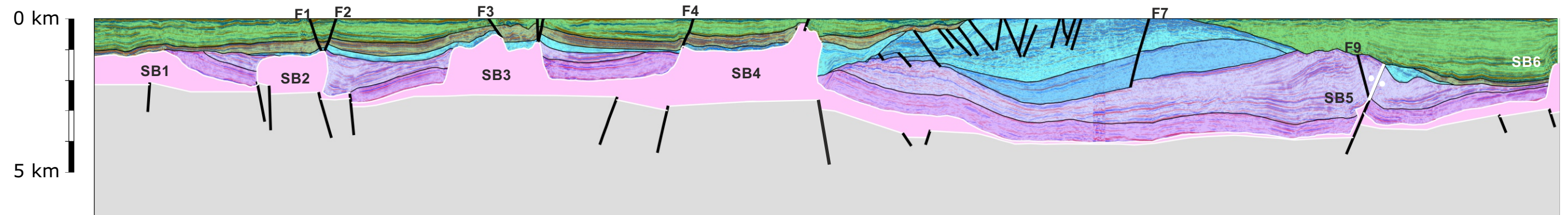


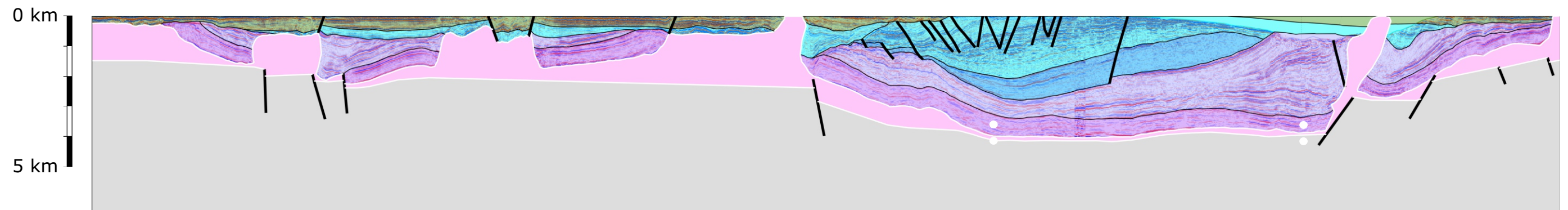
Figure 4.4.8 (part 1/4): Third structural restoration with rim syncline model. Specific salt structures can evolve through time and are either referred as salt bodies (SB), salt pillows (SP) or salt systems (SS). See text for comments and Figure 4.4.6 for legend and location.

4.4 Results - Structural restorations: Section 3

3B) Paleocene - End of Danian (62 Ma)



4B) Early Cretaceous - End of Albian (100 Ma)



5B) Early Cretaceous - End of Ryazanian (141 Ma) - End of Scruff Group deposition

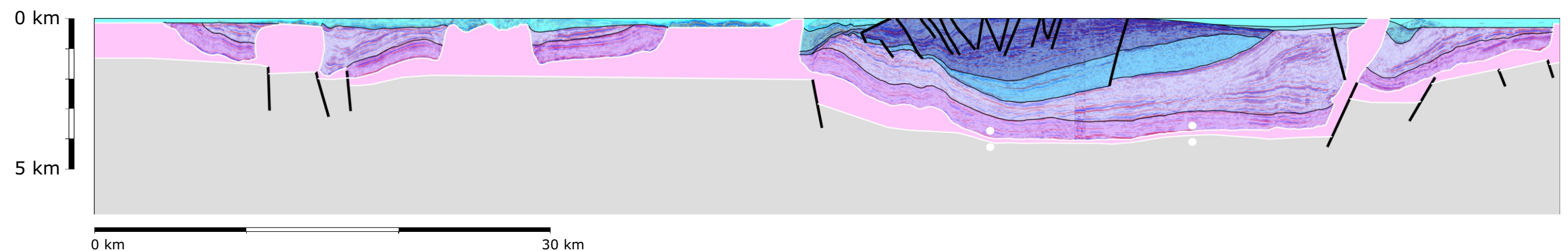
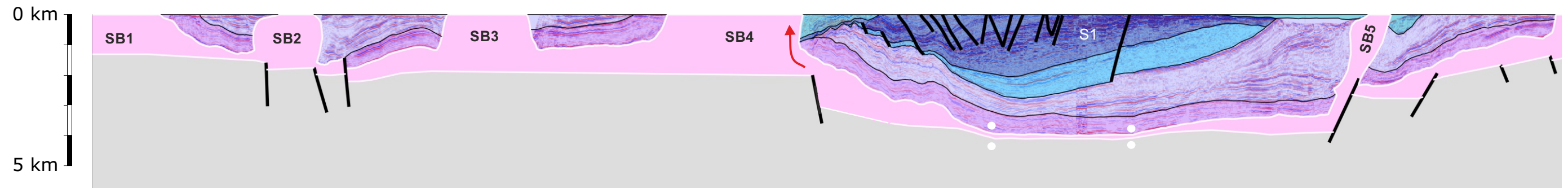


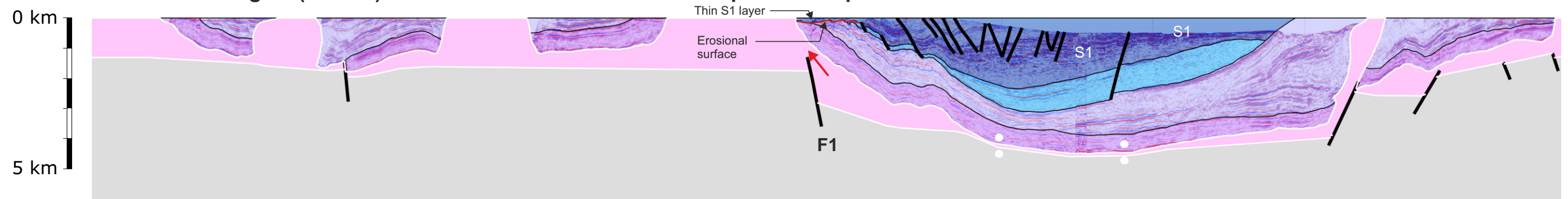
Figure 4.4.8 (part 2/4): Third structural restoration with rim syncline model. Specific salt structures can evolve through time and are either referred as salt bodies (SB), salt pillows (SP) or salt systems (SS). See text for comments and Figure 4.4.6 for legend and location.

4.4 Results - Structural restorations: Section 3

6B) Late Jurassic - Middle Volgian (146 Ma) - End of Schieland Group deposition (Sequence 2)



7B) Late Jurassic - Middle Volgian (156 Ma) - End of Middle - Late Jurassic Sequence 1 deposition



8B) Middle Jurassic - End of Bathonian (166 Ma)

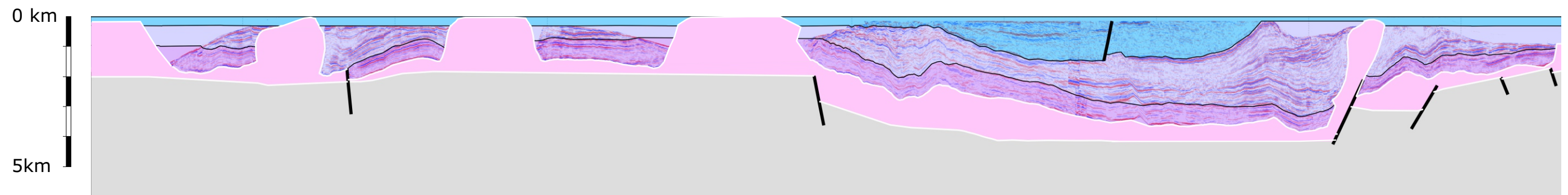
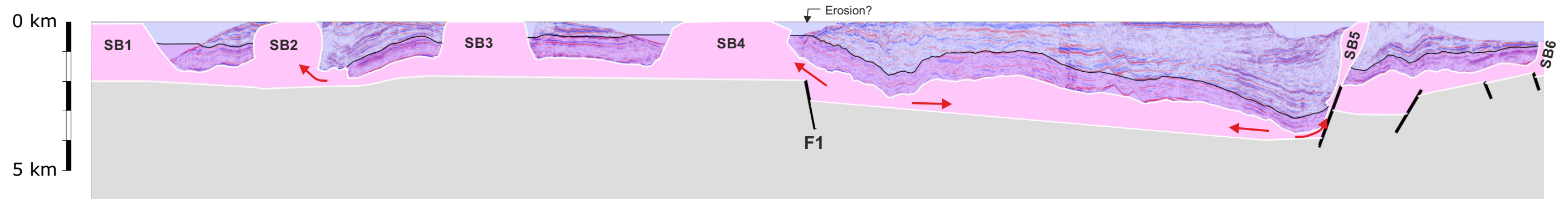


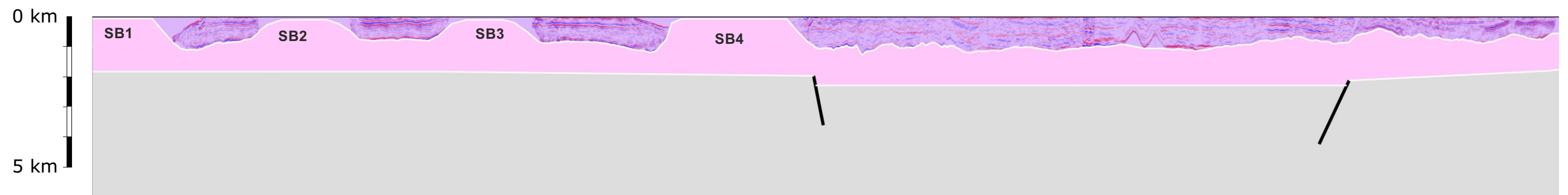
Figure 4.4.8 (part 3/4): Third structural restoration with rim syncline model. Specific salt structures can evolve through time and are either referred as salt bodies (SB), salt pillows (SP) or salt systems (SS). See text for comments and Figure 4.4.6 for legend and location.

4.4 Results - Structural restorations: Section 3

9B) Late Triassic - End of Rhaetian (199 Ma)



10B) Early Triassic - End of Olenekian (247 Ma)



11B) Late Permian - End of Lopingian (252 Ma)

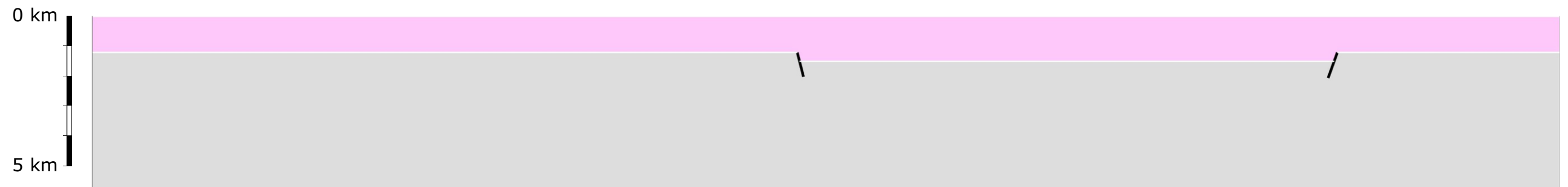


Figure 4.4.8 (part 4/4): Third structural restoration with rim syncline model. Specific salt structures can evolve through time and are either referred as salt bodies (SB), salt pillows (SP) or salt systems (SS). See text for comments and Figure 4.4.6 for legend and location.

DISCUSSION

5

Several topics are discussed in this chapter:

- 1) the main lessons learned from the structural restorations,
- 2) the kinematics of salt systems,
- 3) the allochthonous salt systems, and
- 4) basin-scale salt tectonics on petroleum systems.

5.1) Main lessons learned from the structural restorations

The three structural restorations shown in Chapter 4 (Fig. 4.4.3 to 4.4.8) show various salt kinematic behavior related to salt movement during the Upper Triassic and Jurassic.

In this section we discuss the specific results from each restoration and their implications in regards to the salt tectonics and the syn-tectonic stratigraphic response during the Triassic and Jurassic. This discussion is carried out in two ways: 1) In the text below in a chronological manner, discussing the succession of events and how the different structures evolved in relation to neighboring structural elements. 2) In form of three tectonic charts (Figs. 5.1 to 5.3) that present the evolution of individual structural elements such as salt features, turtle structures, growth faults, thrust faults and rafts, as well as the main periods of erosion, extension and contraction. Note that these 2D restorations do not preserve salt volume perfectly since salt move in 3D and only 2D salt motions are taken into account. The amount of salt eroded or dissolved is also difficult to estimate and a better control on these parameter should be considered for future restorations

After each section is discussed, a discussion on the overall structural restoration results is proposed (Section 5.1C).

A) Restored Section 1 - F17/F18 case study

This structural restoration suggests that the original Zechstein salt was up to 1.9 km thick in the position of the present day Dutch Central Graben and thinner to the west (900 m) and east (500 m) (Figure 4.4.3, Step 11). The Lower Triassic interval (Fig. 4.4.3, Step 10) is thicker in the central part of the section (up to 1.8 km decompacted thickness) than on the marginal zones (800 to 400 m thick).

The exact paleo-configuration of the salt bodies during the Early Triassic is not easily obtained using 2D restoration techniques. If the original seismic interpretation is correct for the deepest part of the seismic survey, the Lower Triassic shows thickness variations along this profile. This geometry shown in Figure 4.4.3 (Step 10) indicates that salt pillows created significant relief already at this stage, especially in the zone where the original Zechstein salt was thickest. These salt pillows were the precursors of the salt diapirs and walls that developed at later stages. The rapid collapse of the 16km wide SP3-4 salt pillow shown from Step 10 to 8 (Fig. 4.4.3) explains the difference of timing between turtle structures F17 and F18.

The turtle structures inversion (period at which salt welded out below the initial central depo-thick, and when lateral stratigraphic wedges start to form) occurred around the end of the Triassic (200 Ma) for Turtle F18 and around the end Middle Jurassic (165 Ma) for Turtle F17 (Figure 5.1). This difference in timing also likely affected the geometry of the asymmetric F17 Turtle due to the early salt migration from the F18 block toward the F17 Block (Step 8, Fig 4.4.3). This westward salt migration forced the eastern side of the F17 Turtle to subside relatively less compared to the western side (thinner Triassic). During the same period two salt sheets were emplaced at the free surface (SS1 and SS5, Figure 4.4.3, Step 8). These salt extrusions are related to the combination of 1) the excessive loading of the salt within the thick Triassic minibasins that pushed the salt laterally and upward, and 2) the squeezing of the salt bodies that balanced the lateral extension along the basin margin (growth fault/raft systems on the eastern side of the section during this period (F2-F3, Steps 9 and 8, Fig. 4.4.3). These extruded salt

sheets were buried during the Early Jurassic and partially (SS5) or totally (SS2) welded out during the Late Jurassic (Steps 6 to 5, Fig. 4.4.3). Also note that the salt body SB3 was squeezed during this period, forming a vertical salt weld. This process was possibly associated with strike slip movements that may have smeared laterally the pre-existing salt. This salt feature is linked to the two large neighboring salt bodies (SB1 and SB2, Fig. 4.3.7) and is likely the remain of a salt wall that extended previously from the position of SB1 to the position of SB2.

B) Restored Section 2 - L05/L06/L08/L09 case study

The restoration of this section that stretches from the L08 to the M05 blocks (through the L06 and M4 blocks) shows a very complex kinematic history of this part of the Dutch Offshore (Fig. 4.4.5).

The configuration of the original Zechstein is different from the first restored section with only 1.1 km of original restored salt thickness that thins to the ENE to a few hundred meters (Step 10, Fig. 4.4.5). The configuration of the base autochthonous salt is also different, being more regular than in the case of the first restoration (Fig. 4.4.3, Step 11). This more regular base salt affected the evolution of the area during the Triassic, favoring tectonic lateral translation illustrated by several large growth faults and rafts. As shown recently in the case of the West African margin and the Deep Gulf of Mexico (Weimer et al., 2004 and Bouroullec and Weimer, 2017), the initial base salt topography affects the subsequent salt evolution to a large extent, allowing or impeding lateral salt migration, and triggering either gravitational gliding structures, such as growth fault/raft systems and expulsion rollovers (Figs. 2.15, 2.16 and 2.19), or instead vertical salt migration (e.g. Fig. 2.18).

During the Early Triassic the suprasalt strata were moderately affected by salt movements as shown by limited stratigraphic thickness change along strike. However, a large stratigraphic wedge is present on the downthrown side of fault F10 (Figure 4.4.5 Step 9), which can be explained in two ways: 1) If this wedge is truly Lower Triassic in age, this indicates that minibasin-style deformation, as observed in the A block (Figure 4.2.8) and in the UK sector (Stewart and Clark, 1999; Penge et al. 1999), also occurred in the case study area. 2) If this stratigraphic wedge is not Lower Triassic but rather Middle or Upper Triassic in age, this would indicate that another growth fault/raft was present in the central part of the section. In this case the stratigraphic block located west of the wedge would be a raft (Raft 3, Fig. 4.4.5, Steps 9 to 8) and would have translated by up to 6 km westward. The latter scenario is more likely due to the geometry of that stratigraphic wedge and its position on the edge of salt pillow SP6 that was likely a salt roller during this period. In this case the amount of overall extension due to gravitational gliding along this section was up to 18 km instead of 12 km as shown in Figure 4.4.5 Step 9), similar to values seen in the Congo/Cabinda margin (16 km in Rouby et al. 2002 and 2003; Figs. 2.15 and 2.16).

During the Anisian (Solling, Röt and Muchelkalk Formations) the updip extension (eastern part of the section) is at its peak, with large roll overs developing on the downthrown side of the growth faults F9 and F6, and possibly F10 (see discussion above). Between 12 and 18 km of overall thin-skin extension occurred along this section during this period. This extension was only partially accommodated by downdip contraction observed within the study section (thrust fault TF1 and pop up structures PU1) and most of the contraction likely occurred outside of the section, farther to the west. During this period a large allochthonous salt sheet extruded at the free surface (SS6) due to salt migration forced by the large sediment wedges to the east. It is possible that basement fault F11 may have played a role in this event, creating a local impediment for westward salt migration and forcing the salt to extrude rather than flow along the autochthonous level. This is however conjectural due to the lack of evidence of having F11 present during this period.

During the deposition of the Keuper Formation (Step 7, Fig. 4.4.5) the updip extension persisted with fault F09 still active and a new growth fault (F7) appearing downdip. The allochthonous salt sheet (SS6) was loaded from the west side, with a stratigraphic wedge (SW1) developing on its western side. Such structures are frequently observed in the Gulf of Mexico and are referred to as a stepped counterregional salt system (Fig. 5.4, Bouroullec and Weimer, 2017). Overall, the geometry of the area located between fault F5 and F7 is reminiscent of a turtle structure (referred as “M04 turtle structure”) with inversion occurring at the end of the Anisian (241 Ma, Fig. 4.4.5, Step 8). During this period the Raft 1 translated further westward by up to 5 km. A small allochthonous salt sheet formed downdip (SS4) at the location where thrust fault TF1 formed.

During the Middle Jurassic and the Early Cretaceous (Steps 6 and 5, Fig. 4.4.5) growth fault F9 was still active but with little growth observed compared to previous periods. Fault F5 accommodated the continued withdrawal of the allochthonous salt sheet SS6, forming a significant stratigraphic wedge on its eastern side. The only remnant of Lower Jurassic strata along this section is observed on the western side of SS4 (Fig. 4.4.5, Step 5) as it was eroded everywhere else along this section. The preservation of the Lower Jurassic is due to the formation of a small and deep graben below this area that form due to rifting and allowing differential subsidence. During the Early Cretaceous (Step 4, Fig. 4.4.5) the allochthonous salt sheets SS6 and SS4 were further loaded, forming partial (SS6) and total (SS4) welding of the salt.

C) Restored Section 3: F10/F11 case study

Two different kinematic models were used to restore the geometry of the western side of the Dutch Central Graben at this location. In the first version of the restored section (Fig. 4.4.7), an extruded allochthonous salt sheet was modeled to explain the peculiar architecture of the basin fill. In the second model (Fig. 4.4.6), a rim syncline model was proposed. Each model is discussed separately below and a conclusion on the portability of each model to reflect the evolution of the area is discussed.

a) Extruded salt sheet model

In this model, the original salt (Fig. 4.4.7, Step 11a) was 1.1 to 1.2 km thick on the platforms and up to 1.4 km thick in the paleo-DCG. The Lower Triassic was overall quite isopachous. By the end of this period it is possible that a few salt pillows formed on the western side of the section (SB2 and SB3, Fig. 4.4.7, Step 10A). This architecture was selected due to the lack of evidence of growth faulting in this area that could have explained this geometry in the context of raft tectonics, as seen in the second restoration (Section 5.1.A).

By the end of the Triassic (Step 9A, Fig. 4.4.7) the rifting triggered an asymmetric structure in the form of an half-graben bounded by salt bodies (SB4 and SB5). Autochthonous salt was withdrawing actively in the Dutch Central (half-)Graben toward the basin margins. Salt body collapse took place on the western side of SB2, with salt moving westward and allowing a large Upper Triassic wedge to form.

During the deposition of the Altena Group (Fig. 4.4.7, Step 8A) the graben became more symmetric with a trough forming at the center of the present-day DCG. This is related to the salt withdrawal from the basin axis toward the basin margins. In this modeled scenario, the eastern side of the salt body SB4 was composed of an eastwardly extending allochthonous salt sheet that formed in response to the differential subsidence between the western side of the DCG and the edge of the Cleaver Bank Platform.

During the deposition of the Middle to Upper Jurassic Sequence 1 (Fig. 4.4.7, Step 7A), this salt sheet extended even farther toward the east, while accumulating a thin sediment layer on its western side. By the end of this period the autochthonous salt in the central part of the DCG

welded out as the accommodation shifted from the basin axis toward the margins where salt withdrawal still occurred. Note that the main erosional phase during the Callovian affected the Altena Group and some of the Triassic strata on the platforms and on the eastern part of the DCG, which was subsiding less than the western part during this period. The peculiar geometry of the eastern part of the DCG at this location is due to the change from a highly subsident zone during the Upper Triassic (Step from 9A, Fig. 4.4.7) to a zone of erosion during the Callovian and Oxfordian (Sequence 1).

During the Early Kimmeridgian, a significant erosion occurred (see Bouroullec et al, in press) that was followed by deposition of Sequence 2 (Kimmeridge Clay Formation) along the margins of the DCG. It is worth mentioning the possible deposition of the sandy Noordvaarder Member on the eastern side during this period (Bouroullec et al. in press). The loading of the allochthonous salt sheet to the west (Fig. 4.4.7, 6A) created additional accommodation, with up to 900 m of S2 strata deposited at the location of Well F11-03 (Fig. 4.4.6C). This salt sheet welded out during the deposition of Sequence 3 (Step 5A, Fig. 4.4.7) with a possible salt body exposed (positive relief?) in the western part of the DCG. During this period the platforms accumulated Sequence 3 sediments, which can be seen by some thin S3 deposits still present locally on the Cleaver Bank Platform, while it is mainly eroded on the Schill Grund Platform in this section.

b) Rim syncline model

The first three restored steps (Step 11B to 9B, Fig. 4.4.8) are very similar to the first restored scenario, with an asymmetric fill of the graben, but not as pronounced as in the first scenario (Fig. 4.4.7). This small, yet important difference explains the tilt of the Triassic along the western margin of the DCG due to salt moving upward toward SB4 above the deep fault F1. No clear evidence of local erosion around the DCG margins is observed at this time, however this cannot be totally discarded to explain the present day geometry (Fig 4.4.8, Step 9B).

During the deposition of the Altena Group (Step 8B, Fig. 4.4.8) the DCG axis was subsiding due to lateral salt migration, forming an axial depositional trough that persisted during the deposition of Sequence 1 (Step 7B, Fig. 4.4.8). The continued clockwise tilt of the Triassic in the western DCG margin continued prior to the main erosional event (Mid Kimmerian Unconformity). This increased tilt was the product of both continued salt migration from the basin axis toward SB4 as well as the activity of fault F1 (throw increased from 900 to 1200 m between Steps 8B and 7B). This erosion was followed by the deposition of a thin S1 unit along the western margin of the DCG. This area continued to subside during the deposition of S2 and S3 due to salt moving from underneath the depocenter (Steps 6B and 5B, Fig. 4.4.8).

c) Which model better explains the geometry observed?

Overall, the rim syncline model better explains the geometry of the basin fill on the western side of the DCG. This marginal Jurassic fill at the location of Well F11-03 has an original geometry due to successive erosional events (base of sequences S1, S2, S3 and base Rijnland Group) that eroded locally the Triassic, Jurassic and even the salt body SB4 that bounded the basin during this period. The configuration of the Middle Jurassic-Lower Cretaceous stratigraphic fill at this location (Figs. 4.3.62 to 4.3.70) can then be explained by uneven (in time and space) salt migration from the graben area toward the bounding salt body SB4 rather than the evacuation of an allochthonous salt sheet.

One caveat should however be mentioned while studying some of the results obtained during the site study of Stefan Peeters (Appendix 2). In Figure 5.5 the physical model presented shows salt extrusions occurring during rifting with geometry reminiscent of the extruded salt sheet scenario presented above (Fig. 4.4.7, Step 8A).

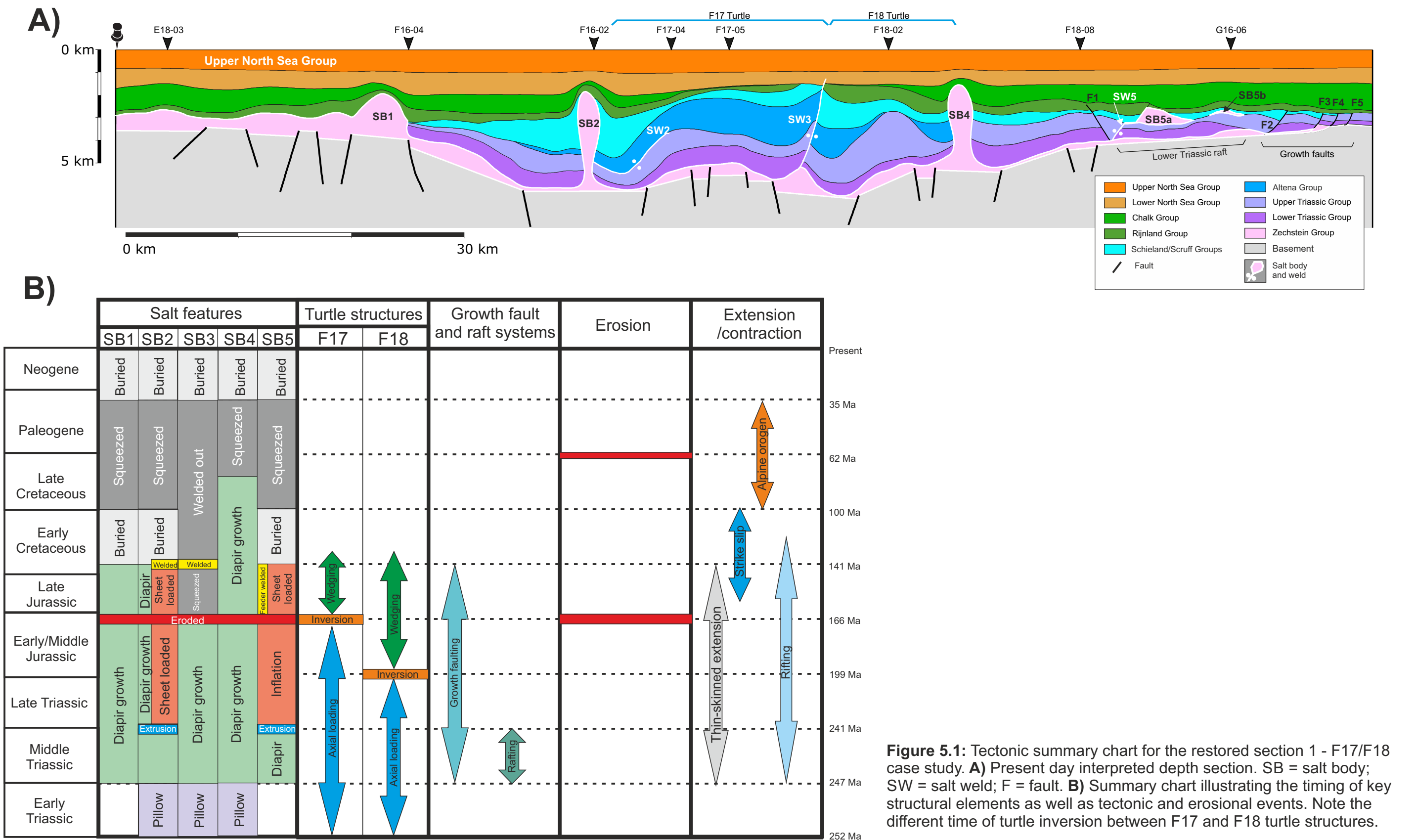
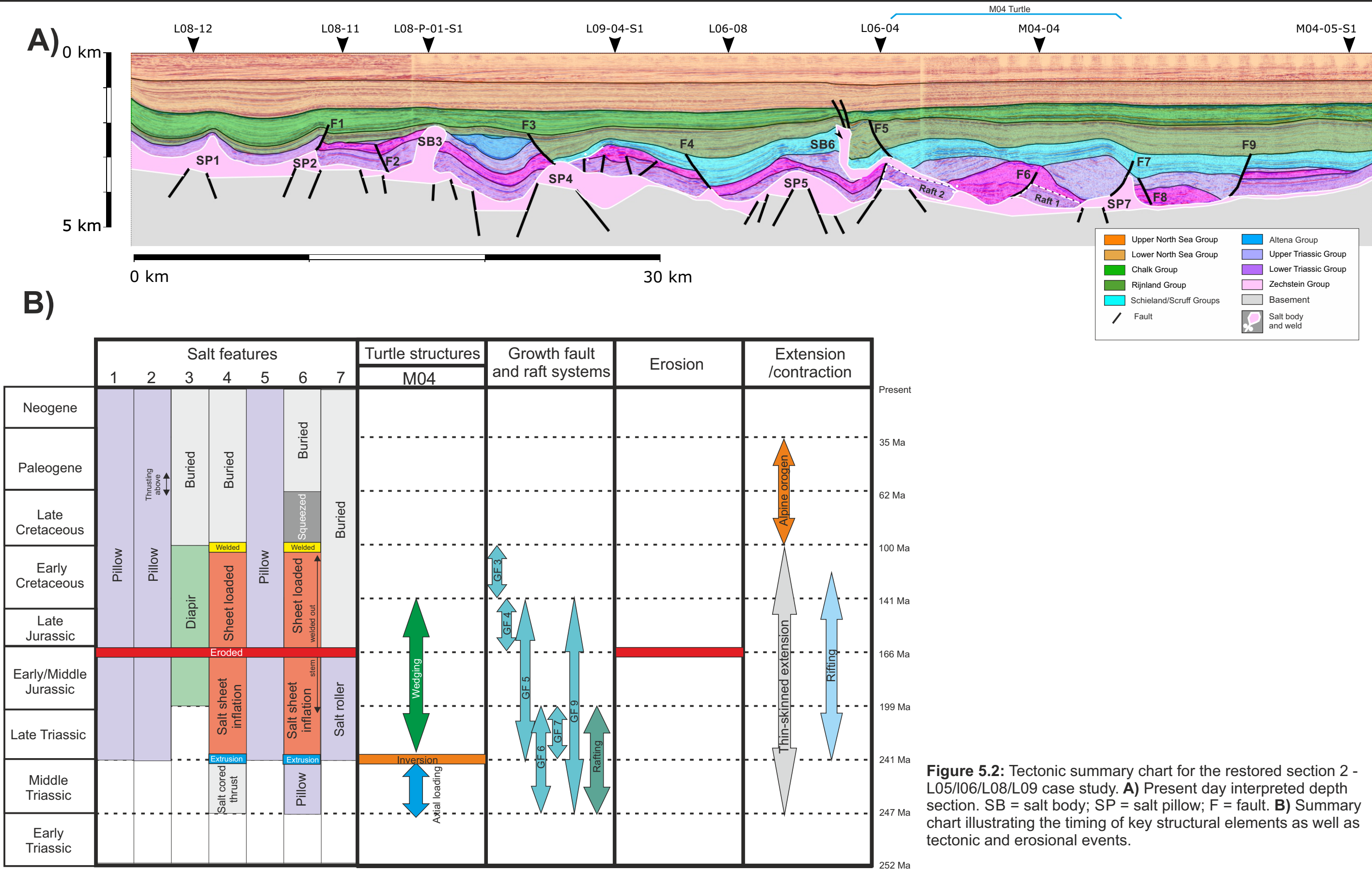


Figure 5.1: Tectonic summary chart for the restored section 1 - F17/F18 case study. **A)** Present day interpreted depth section. SB = salt body; SW = salt weld; F = fault. **B)** Summary chart illustrating the timing of key structural elements as well as tectonic and erosional events. Note the different time of turtle inversion between F17 and F18 turtle structures.



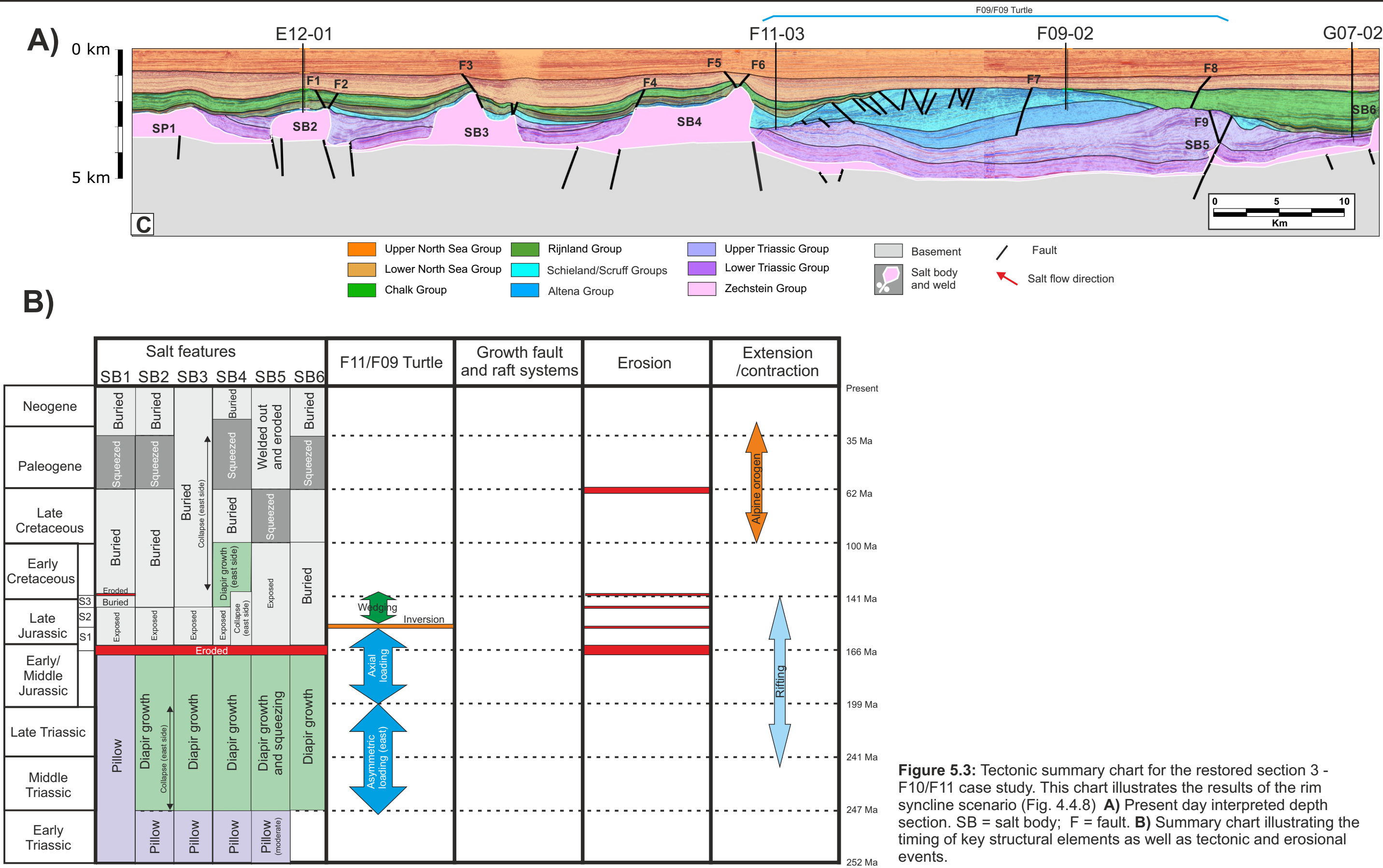


Figure 5.3: Tectonic summary chart for the restored section 3 - F10/F11 case study. This chart illustrates the results of the rim syncline scenario (Fig. 4.4.8) **A)** Present day interpreted depth section. SB = salt body; F = fault. **B)** Summary chart illustrating the timing of key structural elements as well as tectonic and erosional events.

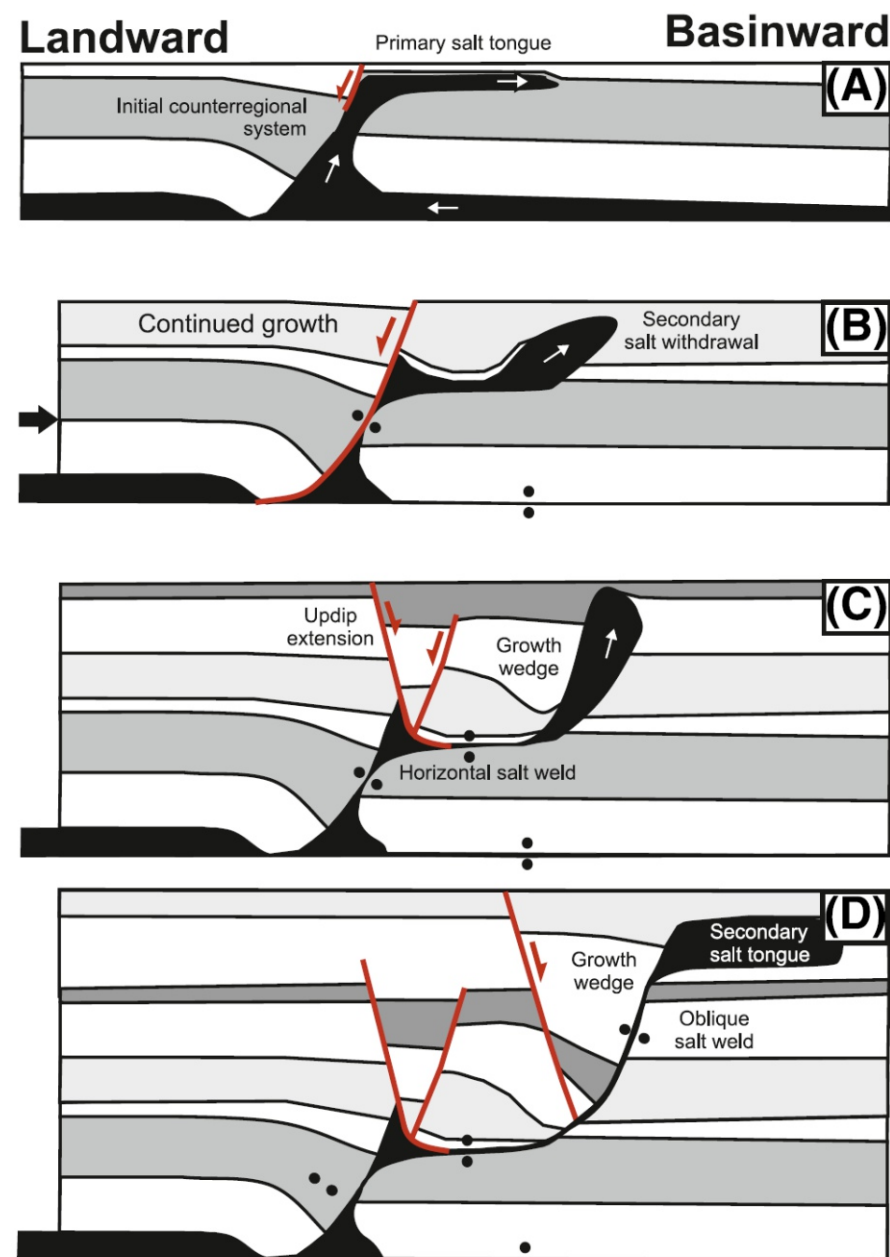


Figure 5.4: Schematic kinematic model showing the evolution of a stepped counterregional salt system. Salt is shown in black, other various layers in white or shades of gray, and faults in red. (A) Initial allochthonous salt tongue forms. (B) Salt feeder collapses and a landward-dipping normal fault forms along the oblique salt stem. (C) Allochthonous salt tongue is loaded and salt migrates upward through the section and basinward to form a secondary diapir. A basinward-dipping normal fault, or fault array, may form in the landward part of the system to accommodate local salt readjustments. (D) These normal faults accommodate late salt movement. The secondary salt diapir can expand at, or close to, the seafloor and form a secondary salt tongue. (From Bouroullec and Weimer, 2017)

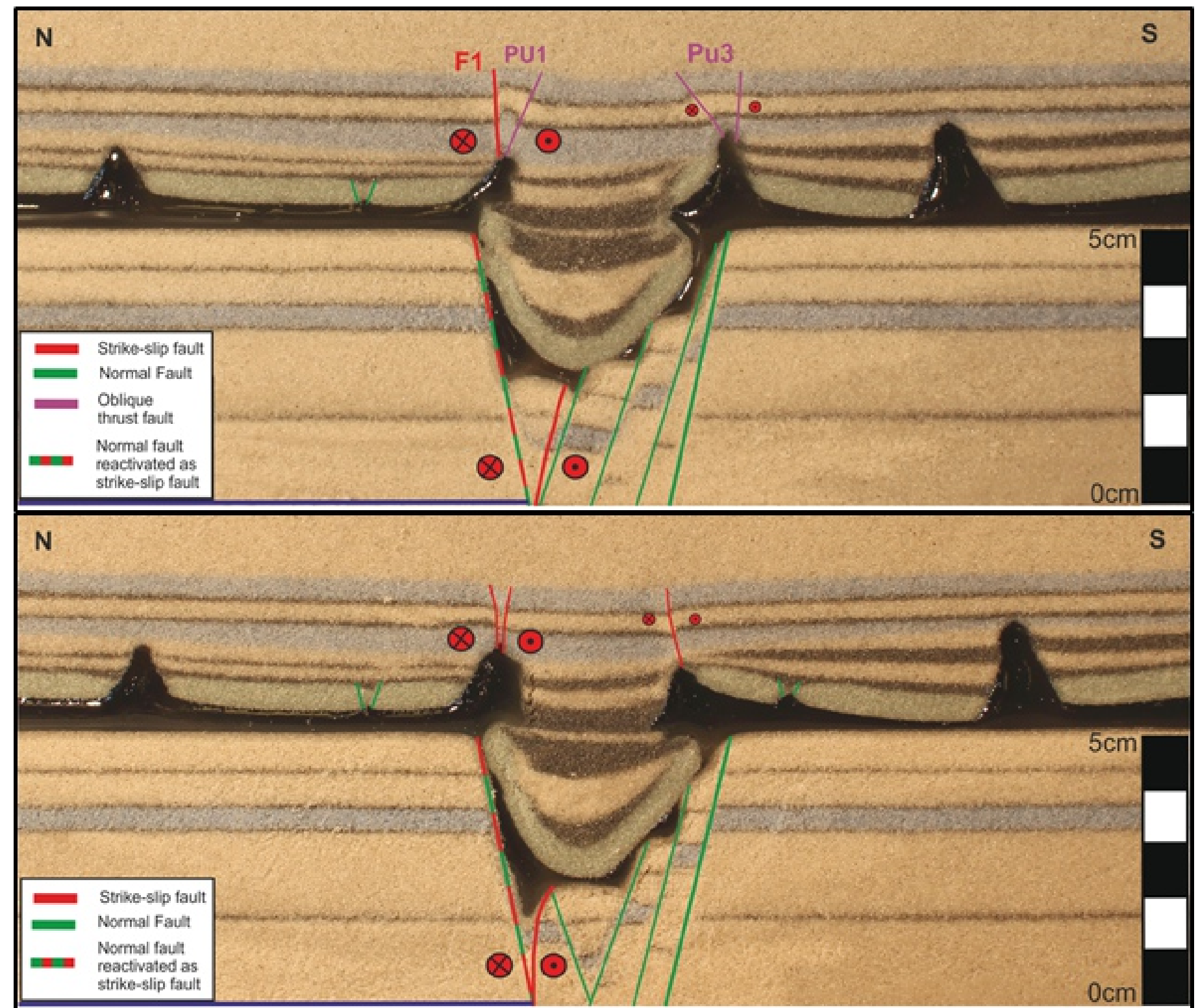


Figure 5.5: Cross sections of the physical model constructed by S. Peeters for his MSc research project that was carried out in parallel to the STEM Project. Note that the bounding modeled salt bodies (silicon) on the side of the graben have the tendency to migrate toward the axis of the graben, forming allochthonous salt bodies.

5.2) Salt systems kinematics

A few important topics and questions are discussed below regarding the timing and sequence of events related to specific types of Triassic salt systems encountered in the Dutch offshore.

A) Timing of salt tectonics in the Dutch offshore

The salt tectonics in the Dutch offshore starts as early as the Lower Triassic in the northern part of the area. Figure 4.2.8 shows growth stratigraphic geometry similar to the UK sector but yet more limited in amplitude and frequency. Growth faulting, rafting and salt body collapse structures developed during the Middle and Late Triassic (Figs. 4.2.10 - 4.2.12, 4.4.5 and 5.1 and 5.2). In the DCG and the TB most salt bodies continued to be active during the Jurassic and Early Cretaceous. They are often partially eroded on the platforms, which does not always allow for clear understanding of their complete kinematic evolution of these areas.

A few lessons can be learned from the structural summary charts shown in Figures 5.1 to 5.3. 18 salt bodies have been restored in these three restored sections. They generally evolved from a pillow-shape geometry to a diapir geometry (50% of them) but occasionally keep their pillow-shape geometry during the later stages of deformation. All of the salt body that evolved from a pillow to a diapir geometry did it during the Triassic, often at the beginning of the Middle Triassic (87.5% of the salt bodies). Diapiric growth occurred from the Triassic to the Late Cretaceous, followed by burial and shortening events from the Late Jurassic to present-day.

Four extrusive allochthonous salt systems are observed in the first two restored sections (Figs. 5.1 and 5.2). The timing of salt extrusion is the same for all four extruded salt systems, at the end of Middle Triassic/beginning of Upper Triassic, when gravitational gliding on the outer rims of the Triassic basin was occurring, forcing pre-existing salt bodies down dip to be shortened and salt to evacuate upward onto the free surface (salt glaciers). The emplaced allochthonous salt sheets were later loaded and welded out during Late Triassic to Early Cretaceous, period of high sediment deposition rate, especially in the rift basins (DCG and TB).

Four turtle structures (F17 Turtle, Fig. 5.1; F18 Turtle, Fig. 5.1; M4 Turtle, Fig. 5.2; and F09/F11 Turtle, Fig. 5.3) are observed in the restored sections. They all have an individual growth history with inversion occurring at various periods, such as the end of the Middle Triassic (M4 Turtle), the end of Triassic (F18 Turtle), the end of the Middle Jurassic (F17 Turtle) and the Early Kimmeridgian (F09/F11 Turtle). After the inversions, the stratigraphic growth (as lateral stratigraphic wedges) persisted consistently up to the Early Cretaceous, before the deposition of the Rijnland Group. This indicate that the kinematic history of these turtles are initially related to local parameters such as the amount of autochthonous salt available to be withdrawn for axial sediment loading and the local amount of thin-skin extension, while the final stage of turtles evolution (wedging and burial) was a basin-scale phenomena related to the main phase of rifting (Middle Jurassic-Early Cretaceous) and its cessation (Early Cretaceous).

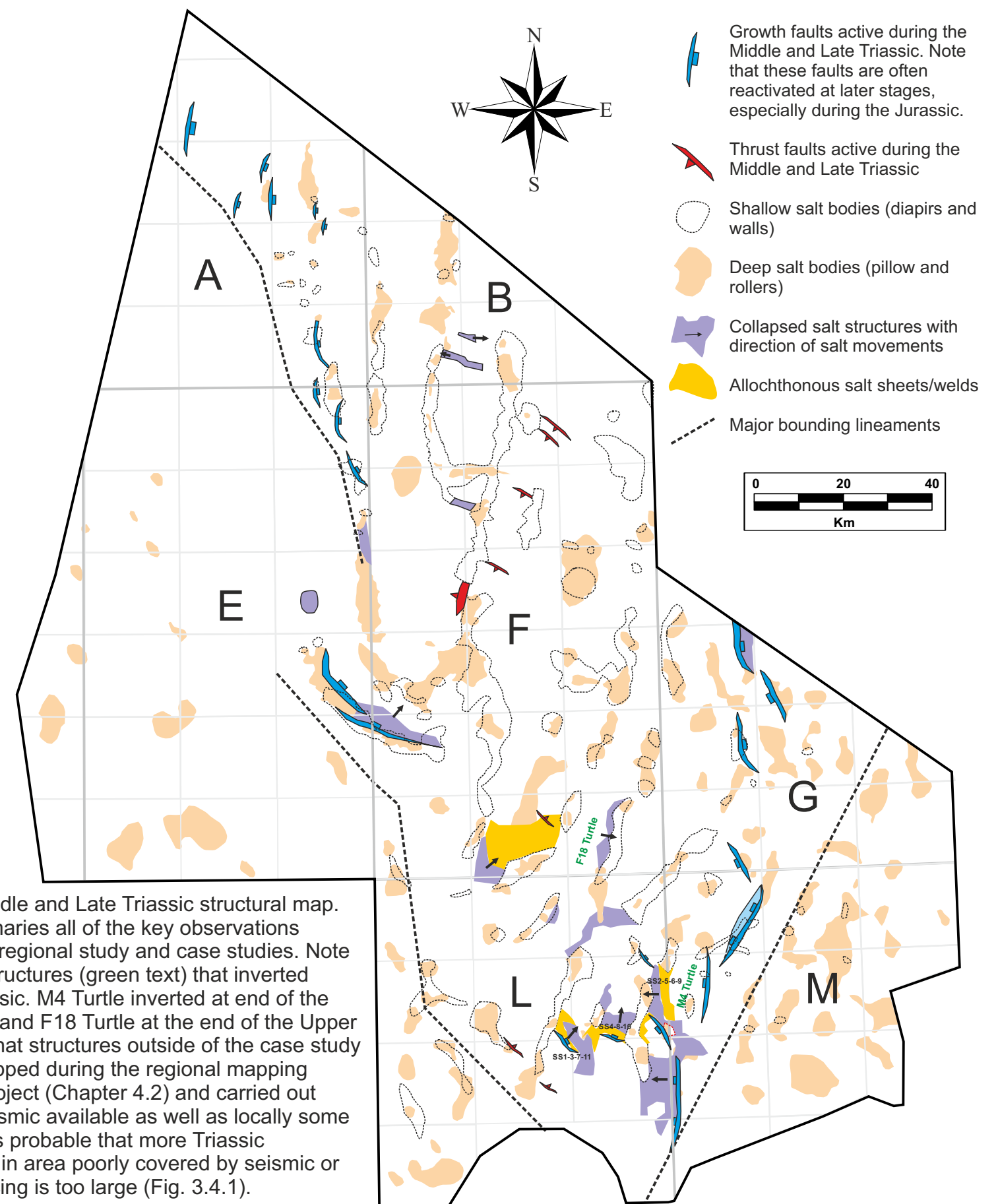


Figure 5.6: Middle and Late Triassic structural map. This map summarizes all of the key observations obtained in the regional study and case studies. Note the two turtle structures (green text) that inverted during the Triassic. M4 Turtle inverted at end of the Middle Triassic and F18 Turtle at the end of the Upper Triassic. Note that structures outside of the case study areas were mapped during the regional mapping phase of the project (Chapter 4.2) and carried out using all 2D seismic available as well as locally some 3D surveys. It is probable that more Triassic structures exist in area poorly covered by seismic or where line spacing is too large (Fig. 3.4.1).

B) Updip growth faulting/rafting versus downdip contraction

Numerous growth fault/raft systems have been identified and show a direction of movement toward the paleo-basin center that was located in the B and northern F blocks, for the northern gravitational gliding systems and in the L block for the southern system (Fig. 5.6). Figure 5.2 shows an interesting migration in time and space of the growth faulting. Older growth faults (e.g. GF9, 7 and 6) are active in the eastern part of the section while growth faults active in later stages (e.g. GF5, 4 and 3) are located farther to the west. This indicates that the amount of salt available as detachment for successive structures is remobilized toward the paleo-basin center.

A few contractional faults (Fig. 5.6) are observed down dip of the extensional systems in block F (Fig. 4.2.19, 4.3.10) and block L (Fig. 4.3.30, 4.3.31 and 4.4.5). The amount of contraction on those small thrusts and back-thrusts does not however balance the amount of updip extension (e.g. up to 12-18 km of rafting in Fig. 4.4.5) observed in the A, E, G, M and L blocks. This indicates that other processes may have been involved to balance this thin-skin extension such as pre-existing salt body shortening (e.g. salt body SS6 in the second restoration, Fig. 4.4.5, Step 8 to 7). Such shortening of pre-existing diapirs has been observed in the Kwanza Basin in Angola (Figure 5.7) and can accommodate great amount of updip extension. In the case of the Kwanza Basin (Fig. 5.7) the morphology of the base autochthonous salt played a role in the timing of successive diapirs shortening, which could possibly be tested in some Dutch offshore locations such as the M and L blocks by carrying out additional detailed mapping of the Triassic around specific salt bodies.

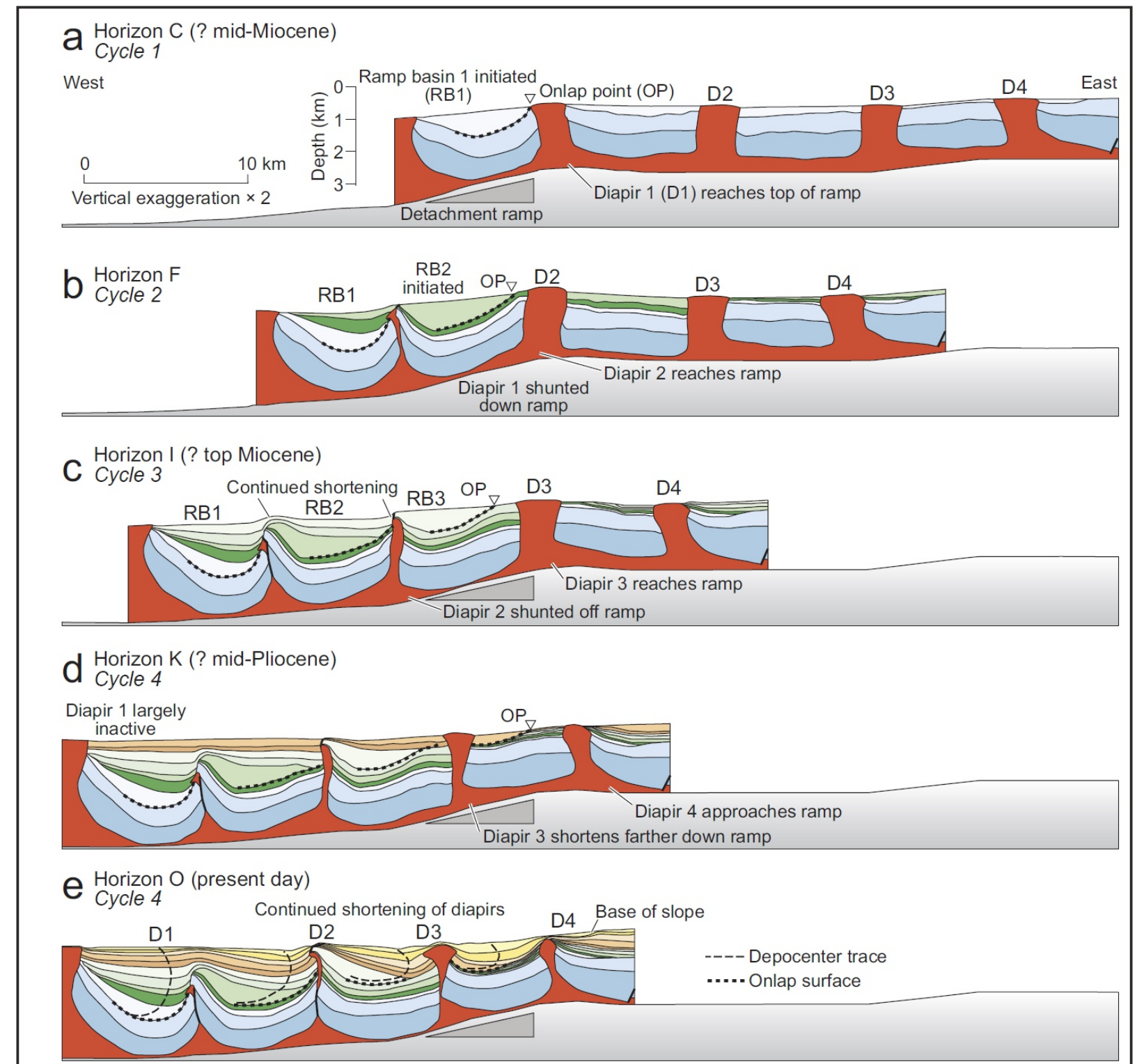


Figure 5.7: Four stick-slip cycles are recorded in Neogene translation down the Kwanza basin (Angola) continental slope. In each slip episode, a ramp syncline basin forms downslope from a topographic scarp. In each stick episode, a stationary diapir is laterally squeezed at the top of the ramp. After Jackson and Hudec (2005).

C) Collapse structures in the Dutch offshore

Several collapse structures (Fig. 4.2.14 - 4.2.18) were active during the Middle and Late Triassic and are observed in the B, E, F, L and M blocks (Fig. 5.6). These structures have various shapes:

- 1) Elongated graben-like structures (Figs. 4.2.15 and 4.2.16) indicative of unidirectional salt withdrawal of pre-existing elongated salt pillows. Such dynamic behaviour has been observed in the Gulf of Mexico (Fig. 5.8) where similar collapse graben structures were associated with local salt walls.
- 2) Bowl-shaped/minibasins developing above pre-existing salt bodies (Fig. 4.2.17 and 4.2.18) indicative of radial multidirectional salt migration. This model is similar to the model of diapiric fall developed by B. Vendeville (Fig. 5.8). In this model the diapiric fall/collapse is related to the overall extension of the system, which also occurred in the case of the Dutch offshore during the Middle and Late Triassic when rifting and rafting created space for the salt bodies to collapse.
- 3) Marginal salt body collapse (Fig. 4.2.14, 4.4.7 steps 10A to 9A) that form expulsion rollovers.

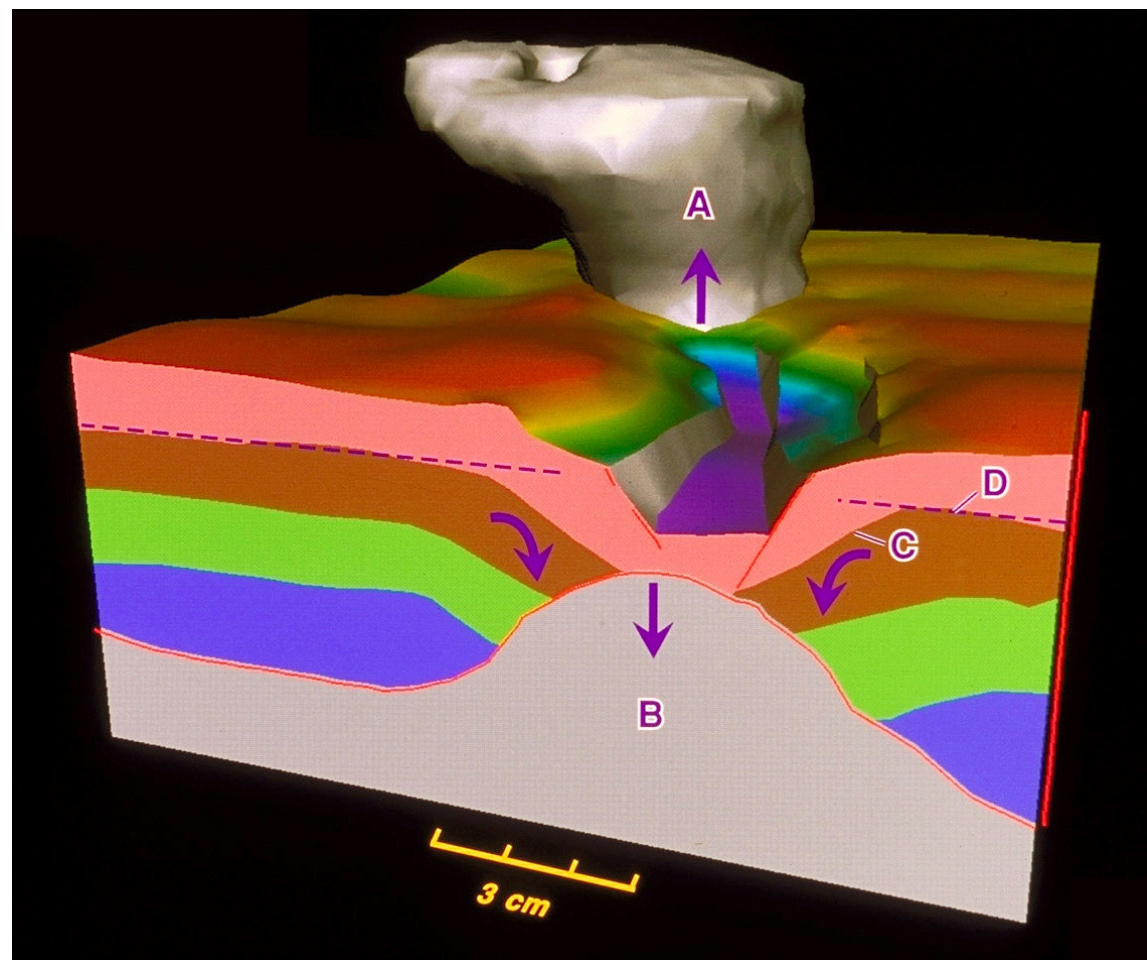


Figure 5.8: Graben-like collapse structure related to salt migration into salt bodies. Based on digitized physical modeling from the BEG, Austin (personal communication by B. Vendeville).

For salt bodies to withdraw in significant manners that allow abnormally thick Middle to Upper Triassic strata to accumulate in suprasalt locations, several parameters play a significant role. Regional thick-skin extension (rifting) and updip thin-skin extension (growth faulting/rafting) favor salt body collapse as seen in Figure 5.9 where the autochthonous salt welds out during extension, cutting off additional salt migration into salt bodies that become zones of sediment accumulations (depocenters). In the example shown in Figure 5.9 these depocenters further developed into mock-turtle structures while in the Dutch offshore these depocenters mainly developed into minibasins, collapse grabens or expulsion rollovers. The only location where a turtle structure developed in a similar way as shown in Figure 5.9 is the M4 turtle (Fig. 4.4.5). This is due to the extensive thin-skin gravitational gliding (12 to 18 km of extension) occurring down dip, southwest of the M4 turtle, specifically in the eastern and southern parts of the Terschelling Basin.

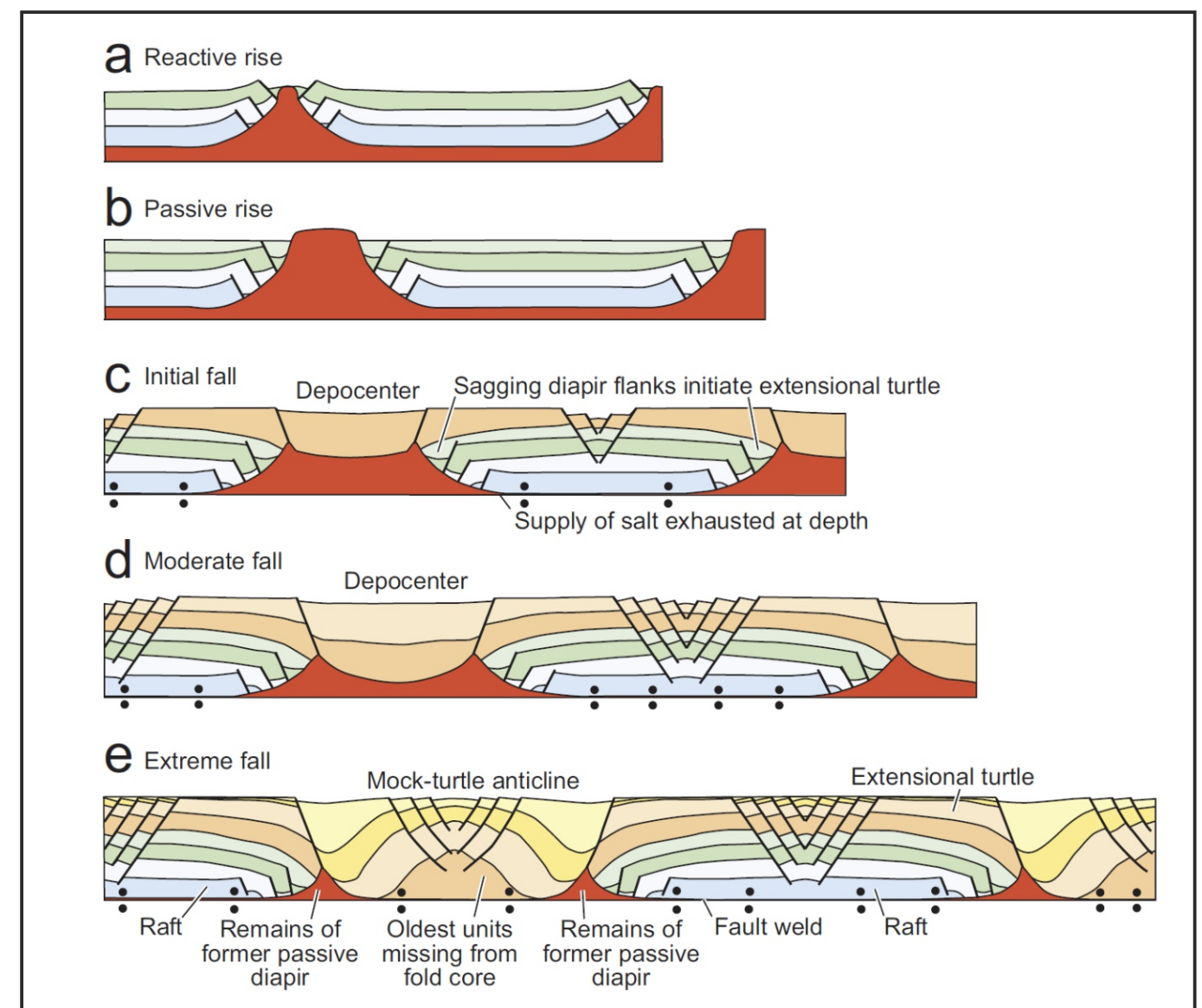


Figure 5.9: Extensional turtle-structure anticlines evolve between sagging diapirs, whereas extensional mock-turtle anticlines evolve above diapirs and can eventually divide them into two remnant diapirs. After Vendeville and Jackson (1992).

D) Growth fault/raft systems versus collapse structures

Why are growth fault/raft systems developing in some parts of the Dutch offshore while collapse structures developed in others? A simple explanation is proposed to explain this disparity, namely the presence or absence of pre-existing salt structures prior to the main extension during the Middle and Upper Triassic. Figure 5.10 shows two conceptual model showing the impact of pre-existing (precursors) salt bodies during thin-skin extension.

In the first example (Fig. 5.10a), no significant salt bodies were present prior to the main phase of extension, triggering growth faulting and rafting updip as well as reactive and passive diapirism downdip. Such geometry can be found in the northern part of the study area (Block A, NE of Block E, Block G and principally in Blocks L and M where growth faulting and rafting dominate the structural style (Fig. 5.6). In the second example (Fig. 5.10b), pre-existing salt diapirs were extended while the mother salt welded out, forcing the salt bodies to collapse and minibasins (or graben) to form above the salt bodies. This model can be found in the transitional area between the E and F Blocks (Fig. 5.6) as well as in the F and L blocks.

This indicate that one of the primary parameters controlling the geometry of the Middle and Upper Triassic growth stratigraphy during salt tectonic movements in the Dutch offshore was the presence of pre-existing salt features prior to the main extensional phase. Another parameter that should not be ignored is the paleo-morphology of the base autochthonous salt during salt movement as discussed in Section 5.1. A smooth and regular base salt favors lateral and horizontal salt migration associated with growth faulting/rafting, while an irregular base salt configuration favors vertical salt movements and diapirism.

5.3) Allochthonous salt systems

Based on the case studies carried out in the project, the amount and frequency of allochthonous salt system emplaced during the Triassic is not frequent but yet occurred.

In the case of the F17/F18 case study, the model of a welded out allochthonous salt system is favored compared to a rim syncline model, due to the geometry of the mapped salt weld/erosional surface (Fig. 4.3.12, 4.3.17) that merges with the autochthonous salt toward the west. The geochemical results from well F17-02 (Chapter 4.1; Figs. 4.1.9 and 4.1.10) indicate that one of the samples (B, Fig. 5.11) is clearly Keuper in age while the other can either be Keuper or Zechstein in age (A, Fig. 5.11). Additional sampling and analysis would be required to get a more conclusive answer on the age of these evaporite layers in well F17-02.

In the case of the F10/F11 case study, the structural restoration was performed using two conceptual models (rim syncline and salt sheet) and the most likely scenario was of a rim syncline along the western margin of the DCG at the location of the F11-03 well. The 3D mapping performed (Chapter 4.3, CS3) did not give any reason to discard the rim syncline model and only external methods such as palynology or geochemistry could make the case for a different interpretation.

Figure 5.10: For a given stretch, the effects of basement-detached extension depend on the original thickness of the salt layer and on whether precursor diapirs are present. Schematic forward models by Hudec and Jackson (2007).

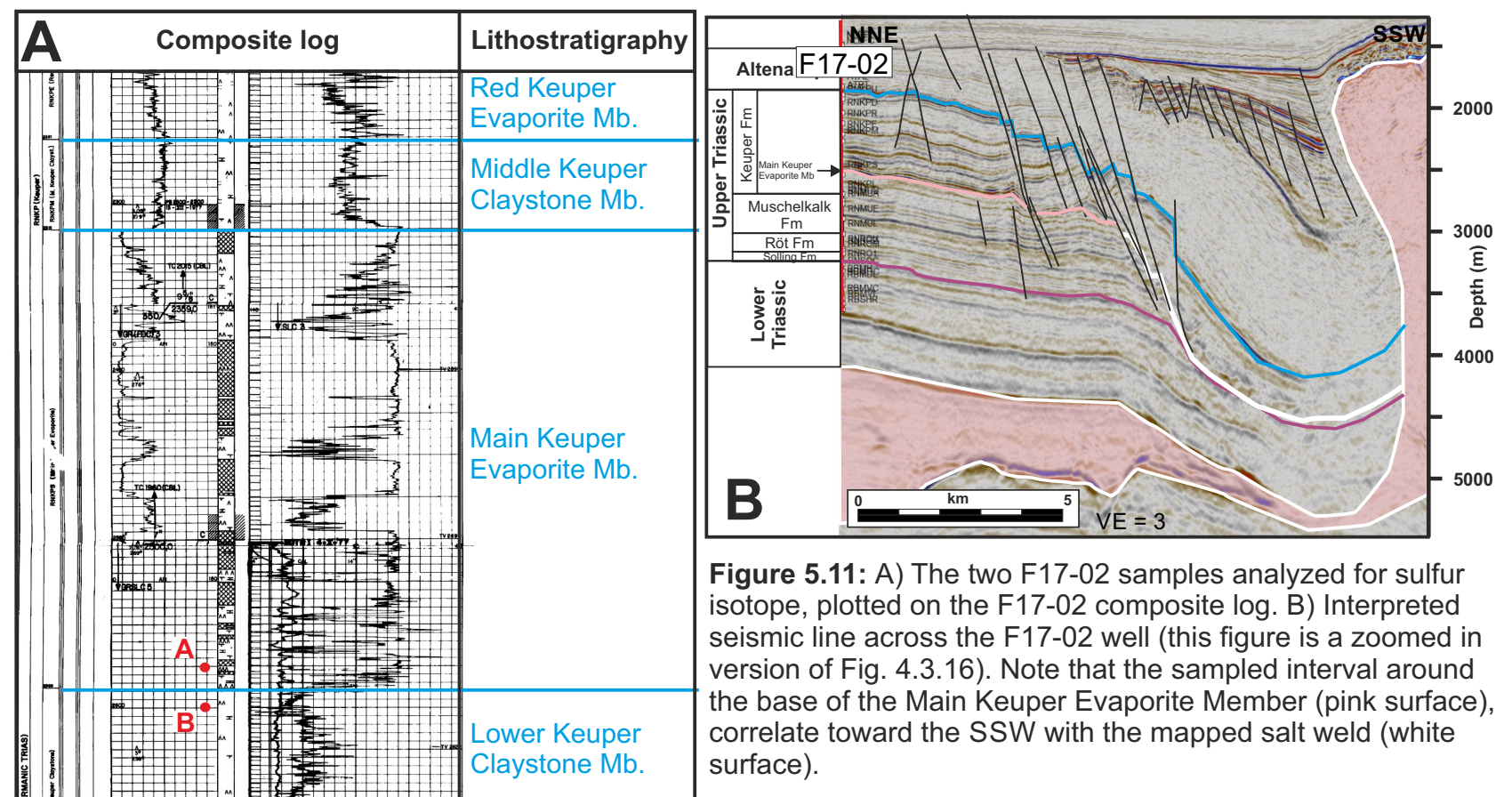
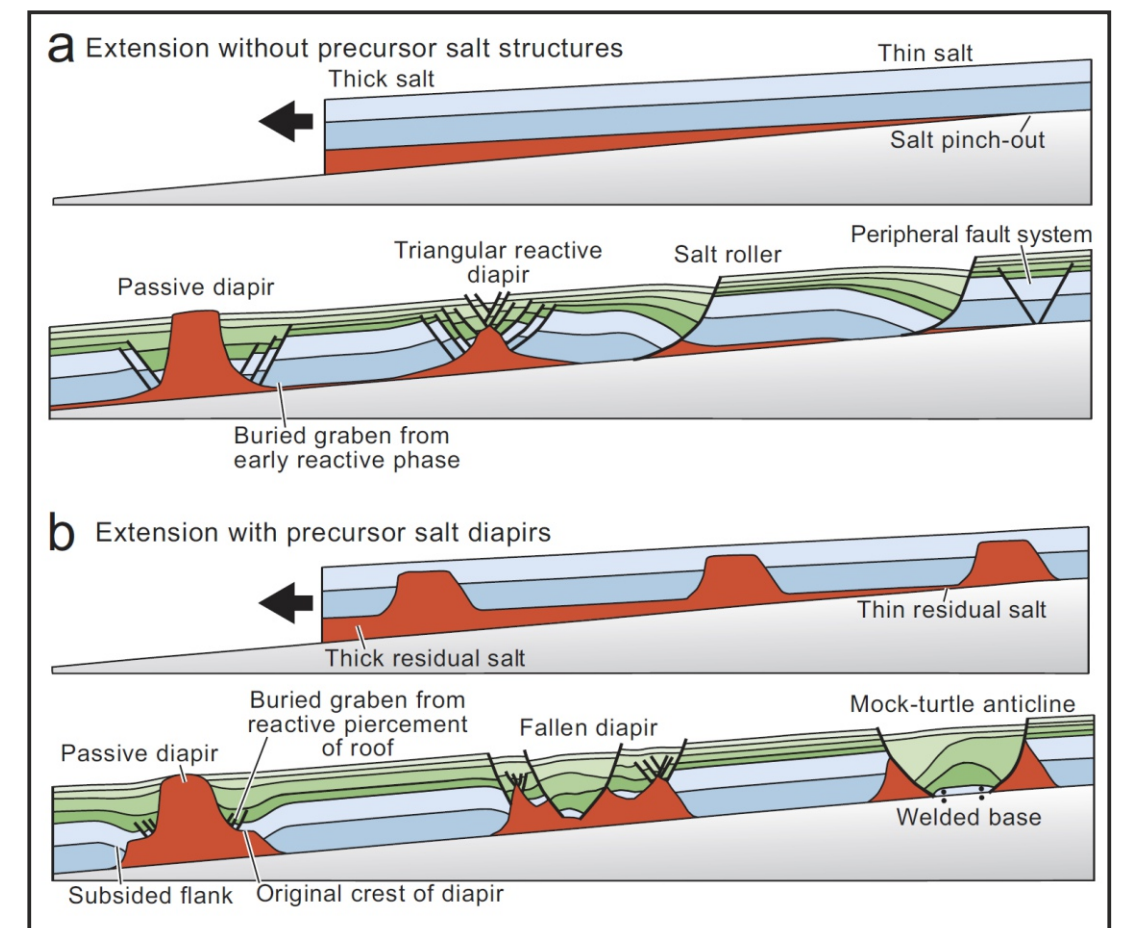


Figure 5.11: A) The two F17-02 samples analyzed for sulfur isotope, plotted on the F17-02 composite log. B) Interpreted seismic line across the F17-02 well (this figure is a zoomed in version of Fig. 4.3.16). Note that the sampled interval around the base of the Main Keuper Evaporite Member (pink surface), correlate toward the SSW with the mapped salt weld (white surface).

In the case study L05-L06-L08-L09, the evidence of allochthonous salt sheet emplacement toward the end of the Middle Triassic is significant (Fig 5.2). Two allochthonous salt sheets were deduced from the structural restoration (Fig. 4.4.6). The geometry of some of the Upper Triassic stratigraphic wedges observed (e.g. Fig. 4.3.23, salt system 2) are unlikely due to in-situ salt layer withdrawal in the form of an expulsion rollover but rather due to the evacuation of a pre-existing Zechstein salt body along the western flank of the M4 turtle structure as modeled and shown in Figure 4.4.5.

5.4) Basin-scale salt tectonic model for the Triassic

At a large scale, the structural evolution of the basin during the Triassic was dominated by the initiation of rifting during the Middle and Late Triassic that triggered complex salt tectonics in the form of growth faults, growth fault/raft systems, turtle structures, stepped counterregional salt systems, collapse structures, squeezed salt diapirs/wall and thrust faults. Most of the gravitational gliding systems formed on the outer rims of the Triassic basin (Fig. 4.2.5 and 4.2.13). The variability of paleo-basin margin structural styles (growth fault/raft systems vs collapse/expulsion rollover structures) is based on both the absence or presence of pre-existing salt bodies during the initiation of regional extension and likely the geometry of the base salt surface. The conceptual model presented in Figure 5.12 summarizes the different structural styles and their evolution during the Triassic.

A) During the deposition of the Lower and Main Buntsandstein Formations (Lower Triassic Germanic Group).

No rifting took place and only limited salt movement occurred in the northern part of the Dutch offshore (A block) as seen in the form of growth strata within suprasalt minibasins. These minibasins were similar to the Lower Triassic minibasin observed in the UK sector but are not as developed in the Dutch Sector.

At the transition between the Lower and Upper Triassic Germanic Group (around the depositional time of the Röt Formation) rifting started. This thick-skin extension created a stretching of the Lower Triassic suprasalt layer, allowing grabens and reactive salt bodies to form (Fig. 5.12B). This geometry may have been similar to the present day geometry observed in Canyonlands National Park in Utah (Fig. 5.13). Reactive diapirs formed during this phase (Fig. 5.9a) and were possibly followed by passive diapirism (Fig. 5.9b). The overall extension may have been limited, but allowed for Zechstein salt to flow into salt bodies, in a pattern possibly related to the base salt morphology, with salt diapirs often forming over basement faults.

B) During the deposition of the Röt and Muschelkalk Formations

The rifting continued and complex salt tectonics started to develop in the Dutch offshore. Collapse structures such as collapse grabens and expulsion rollovers formed at locations where several pre-existing salt diapirs were already present, such as on the Cleaver Bank Platform, the Northern part of the Schill Grund High and the Step Graben. Gravitational gliding systems developed in the form of (Figs. 5.12 and 5.14):

- 1) growth faults that were active in the northwestern part of the study area (A block),
- 2) growth fault/raft systems in the southeastern part of the study area (Friesland Platform, Terschelling Basin and Schill Grund Platform), and
- 3) collapse structures, in the form of collapse grabens and expulsion rollovers (B, F, G, L blocks).

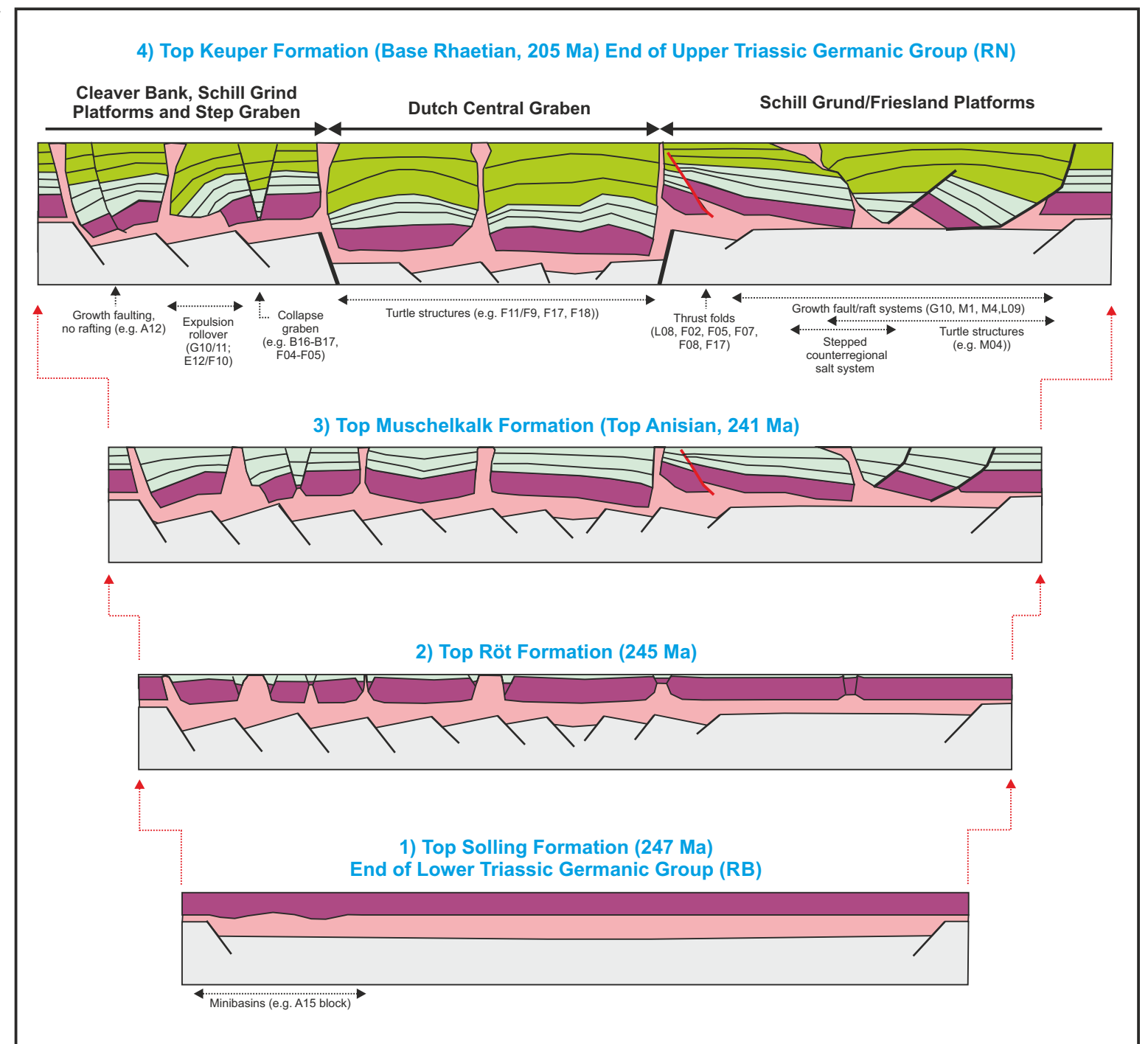


Figure 5.12: Conceptual kinematic model showing the structural configuration of the study area during the Triassic after the deposition of the Solling, Röt, Muschelkalk and Keuper Formations. This section does not represent the geometry of any particular section in the Dutch offshore but summarizes the different types of salt tectonic structures observed in the study area and at specific locations (see text above and below section 4). The approximate trend of this section is NW to SE. Note that these sections are not scaled.

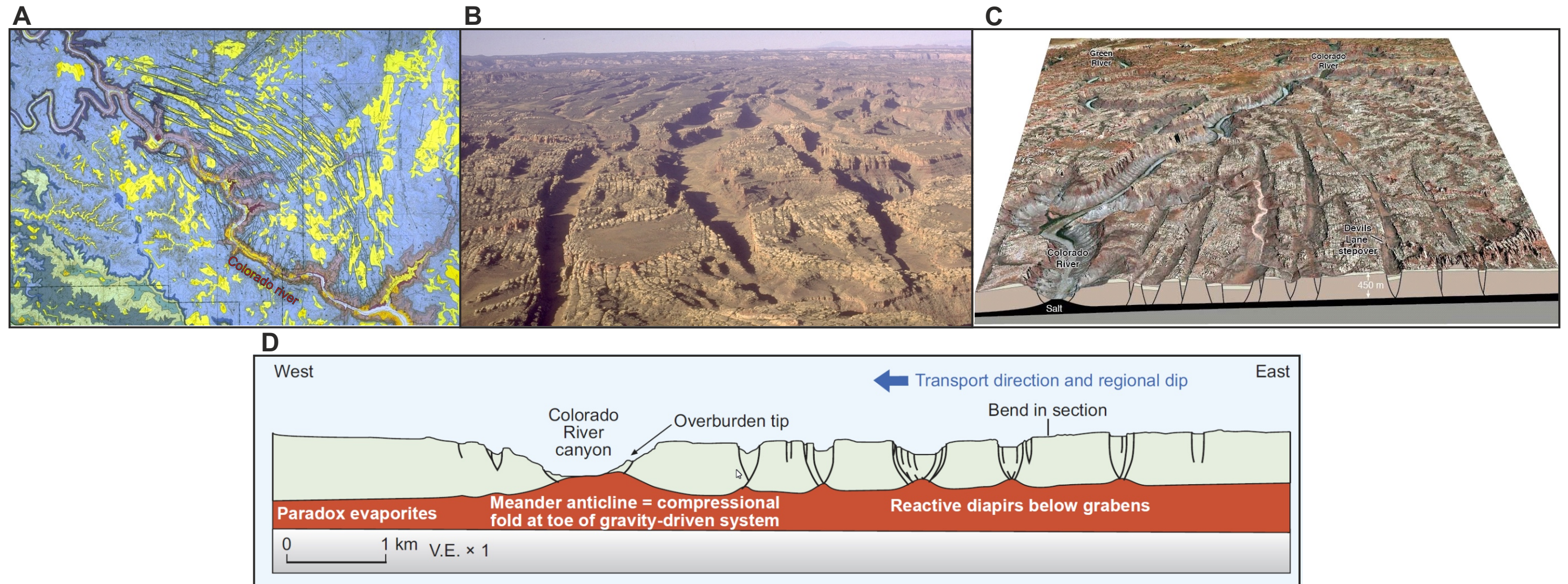


Figure 5.13: The Canyonlands horst and graben system detaching over the Paradox evaporites. This area is a good analogue to the geometry of the Dutch offshore at the onset of the deposition of the Upper Germanic Triassic Group, with reactive diapirs starting to form below the grabens due to the overall extension. **A)** Geological map of the Canyonlands area in Utah. Note the trend of the normal faults on the NE side of the Colorado River. **B)** Aerial photo of the Thousands Needles, located in the southern part of the Canyonlands National Park in Utah. Courtesy R. Bouroullec. **C)** Block diagram showing a rendered Digital Elevation Model of southern Canyonlands and a conceptual cross section linking the extensional system to the Paradox salt flow (black) toward the Colorado River incision. Courtesy of Bruce Trudgill, Colorado School of Mines. **D)** Gravity gliding of the Paradox salt overburden toward the Colorado River canyon began in the last 1.4 million years and continues today because of canyon erosion. After Schultz-Ela and Walsh (2002).

Contractional structures, in the form of thrusts and pop-up structures, developed downdip of these extensional systems during the Upper Triassic. They are observed in three areas located in the B, F and L blocks (Fig. 5.14). The zone with the largest number of thrusts is located in the F block and can be defined as a fold belt, the “F Block Fold Belt”. Interestingly, the orientation of most of the thrusts observed indicate a direction of thin-skin contraction toward the NE, which does not relate to the extensional systems to the west (block A) but rather to extensional systems located farther to the south around the E12/F10 area, where large expulsion rollovers are located. This indicates that a significant amount of thin-skin extension is taking place along these expulsion rollovers. This means that these extensional systems are most likely deformed growth fault/raft systems rather than typical expulsion rollovers (Fig. 5.15).

The number of contractional structures observed in the study area and the amount of shortening they represent is small relative to the amount of updip extension observed in the

extensional provinces (Fig. 5.14) where growth faults and growth fault/raft systems dominate. The only space available within the defined contraction areas (orange and yellow zones in Fig. 5.14) to balance the updip extension can be gained by shortening pre-existing salt bodies and squeezing salt upward, possibly forming allochthonous salt sheets locally (e.g. squeezed salt body in the B14-B17 blocks, Fig. 5.16).

The thrust faults observed in the L08 Block, in the southern part of the study area are at odd with the overall configuration of the other Triassic structures. However, Triassic thickness maps (Figs. 2.2) show that some Upper Triassic deposits were relatively thick farther south, especially the Muschelkalk Formation. We suggest that a thin-skin extensional salt system is located around block L10 or further south.

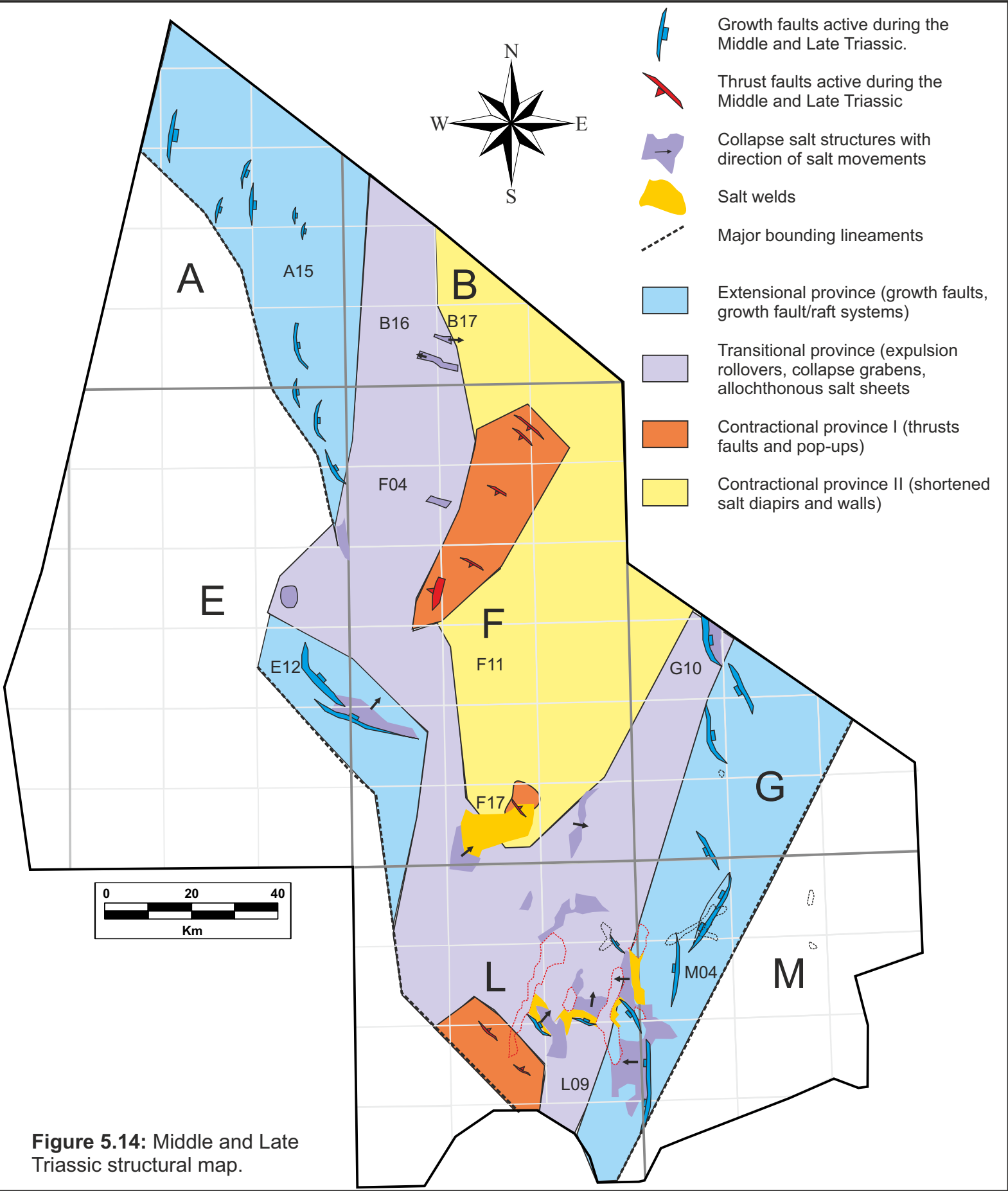


Figure 5.14: Middle and Late Triassic structural map.

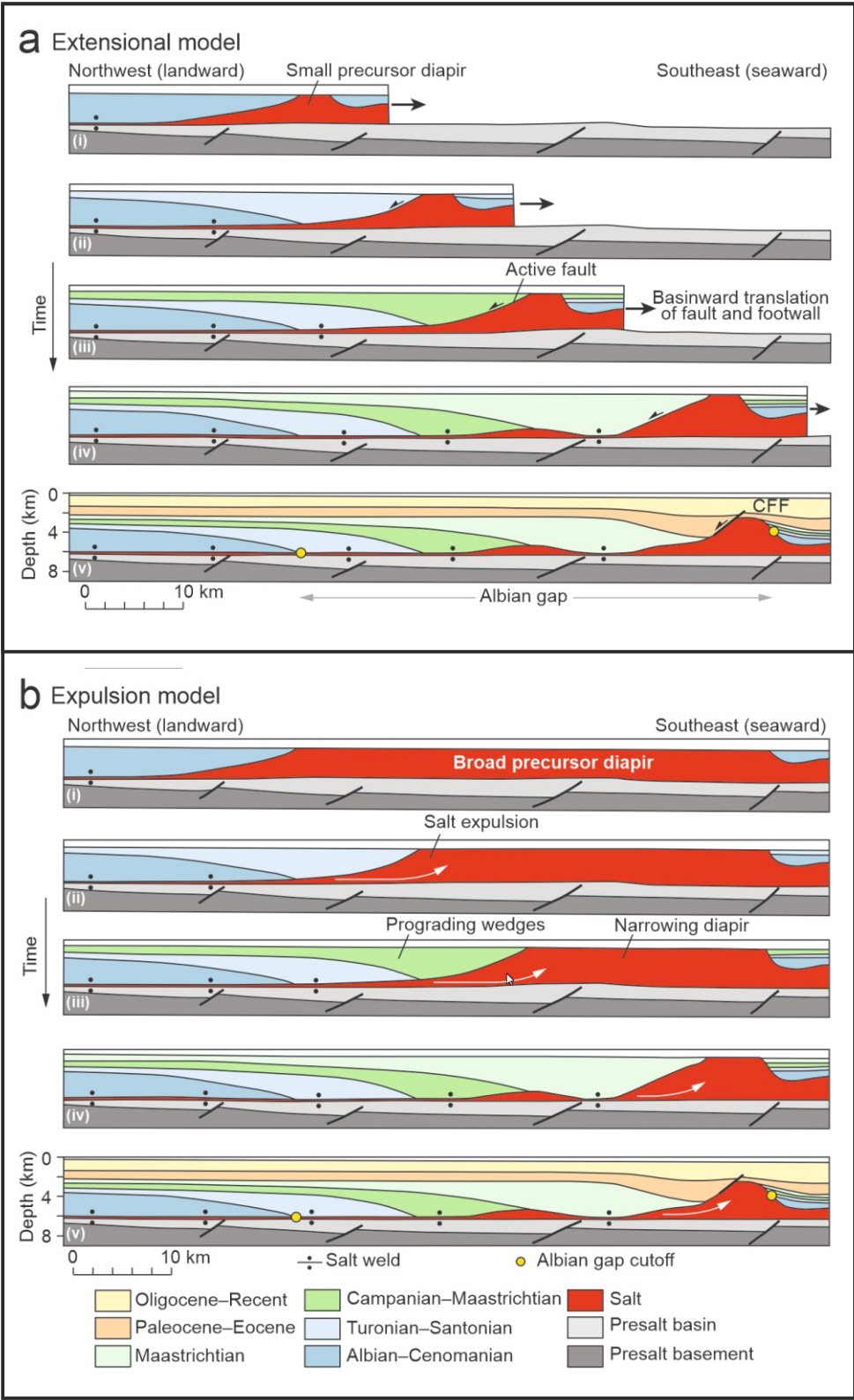


Figure 5.15: Extensional (a) versus expulsion (b) kinematic model for the Cabo Frio Fault system. Each model can result in the same identical end result. In the extensional model, a growth fault is active along the flank of the controlling salt body while in an expulsion model the salt is pushed horizontally to create space for successive stratigraphic wedges to form next to the moving salt body. Restoration after Rowan and Ratiff (2012), based on seismic example from Mohriak and Szatmari (2008)

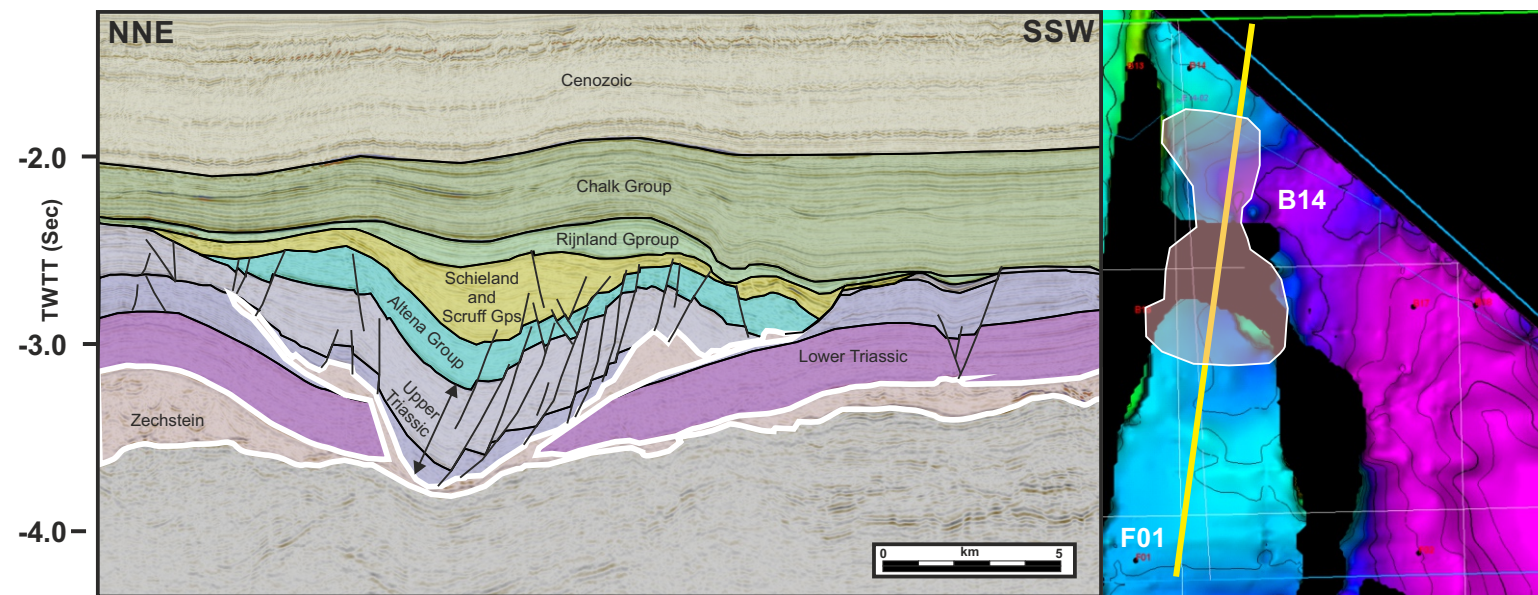
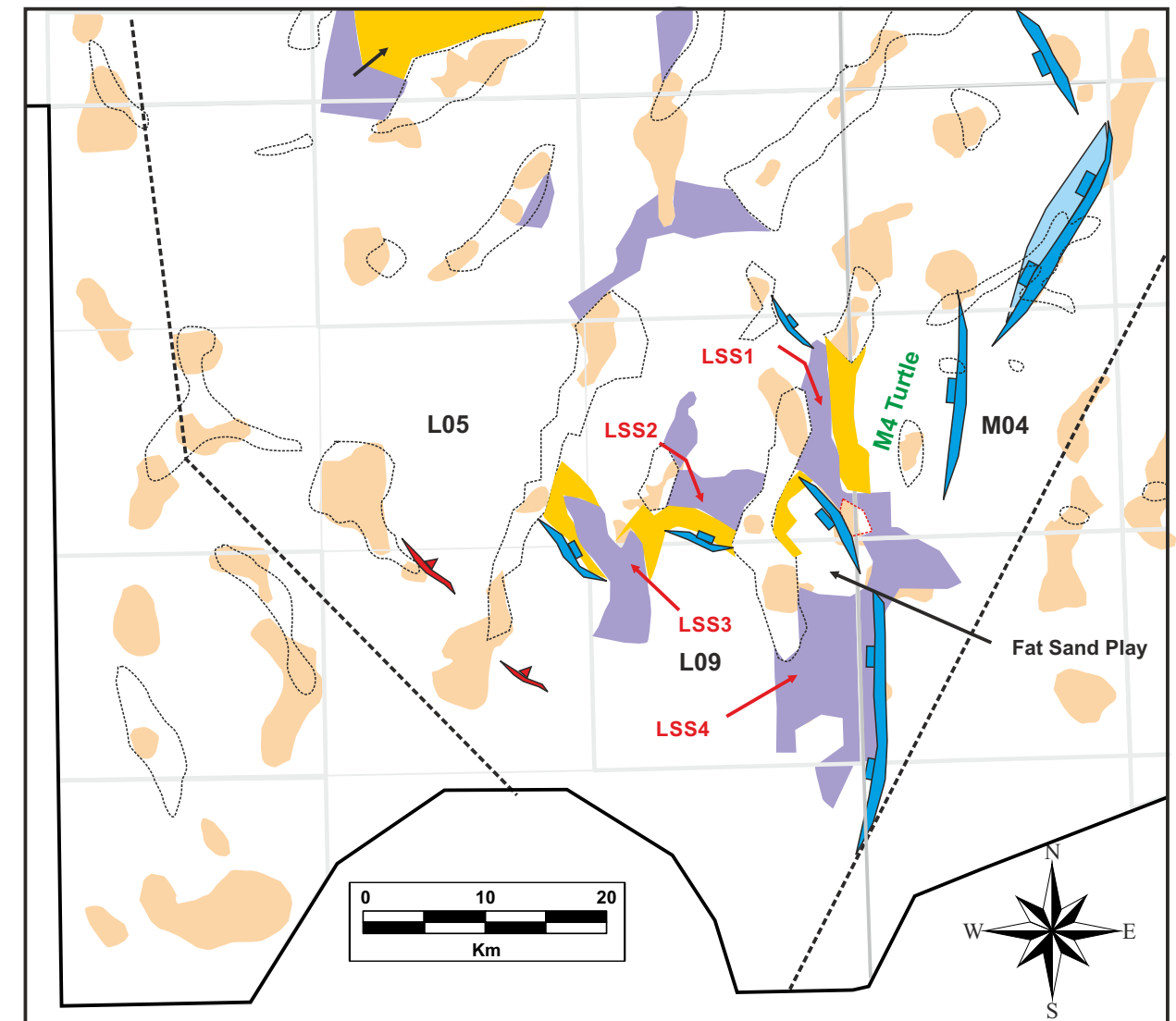


Figure 5.16: The B14-B17 squeezed salt body. A) NNE-SSW interpreted seismic line showing the morphology of a squeezed salt body. Part of the deformation is related to Cenozoic shortening but most of the salt deformation intra-Triassic is related to the shortening of a pre-existing salt body during the Middle Triassic that later loaded by Upper Triassic and Jurassic strata. B) Location map. The Pink polygon shows the extent of the salt body that stretches 20 km in N-S direction. From Bouroullec et al. (2016b)

Figure 5.17: The zoomed in version of Figure 5.6. See text below for comments. See Figure 5.6 for legend.



C) During the deposition of the Keuper Formation

Most of the structures active during the deposition of the Röt and Muschelkalk Formations are also still active during the deposition of the Keuper Formation, including the growth fault/raft systems, the collapse structures and the thrusts. A few specific salt tectonic elements developed exclusively during the deposition of the Keuper Formation, including the inversion of turtle structures such as the M04 turtle structure that inverted at the onset of deposition of the Keuper Formation (Fig. 5.2), and the F18 turtle structure that inverted toward the end of the deposition of the Keuper (Fig. 5.1). Another specific salt tectonic system that developed during this period is the stepped counterregional system observed in the eastern part of the L06 Block (Fig. 4.4.4, 4.4.5, 5.4, 5.6 and 5.12). This stepped counterregional salt system formed over an extruded allochthonous salt sheet that was initially a squeezed salt body down-dip of a growth fault/raft system located in M04 block. The salt movement was towards the west and a large stratigraphic growth wedge formed on the eastern side of the loaded salt body (seen in Fig. 4.3.23 as salt system 2 and Fig. 4.3.26 as salt system 6). The L06 stepped counterregional salt system (LSS1, see Fig. 5.17) can be seen on seismic in Figures 4.3.23, 4.2.25, 4.2.26 and 4.2.28 as the SS2, SS5, SS6 and SS9 salt systems.

Three other salt systems are observed in Figure 5.17:

- 1) The southern L06 salt system (LSS2), which is a squeezed salt body that formed an allochthonous salt sheet (shown as salt system 4 in Fig. 4.3.24; salt system 8 in Fig. 4.3.27 and salt system 10 in Fig. 4.3.29).
- 2) The LSS3 salt system is located at the junction between the blocks L05, L06, L08 and L09 and is a collapsed salt body with some minor amount of extruded salt associated (see Fig. 4.3.23, salt system 1; Fig. 4.3.24, salt system 3; Fig. 4.3.27 as salt system 7; and Fig. 4.3.30 as salt system 11). No clear direction of salt migration can be deduced for this salt system.
- 3) The last noticeable salt system observed in this area is the salt system LSS4 located in the M07/L09 area and is the southern continuation of the Fat Sand play system located farther north. The exact kinematic of this salt system is not clear since this area was not included in the 3D mapping, but the geometry observed on 2D sections seems to indicate that a growth fault/raft system model may be attributed.

5.5) Impact of Triassic salt tectonics on petroleum systems in the Dutch offshore

Salt tectonics impact petroleum systems in four main ways:

- the source rock maturity can be affected due to thermal effects,
- the reservoirs can have their configuration, presence and nature controlled by salt structures or associated faults and folds,
- the trapping of hydrocarbon can be directly related to salt systems geometry and evolution, and
- the migration can be controlled by salt body presence and evolution.

A) Source rock maturation

The high thermal conductivity of salt affects the thermal gradient in sediments located close or in contact with salt layers and salt bodies. In general terms, subsalt sediments will be cooled while suprasalt sediments will gain heat. In the case of source rocks located subsalt, the maturation can be retarded due to cooling. As an example, at 4 km depth, a 1km salt layer would cool subsalt shales by 40 °C (Mello et al., 1995).

In the case of the Dutch offshore, the Carboniferous source rocks are not likely to be affected by the temperature effect of the autochthonous Zechstein, since they are rarely in direct contact. In the case of the Posidonia Shale Formation, the deformation within the DCG and TB during the Upper Jurassic and Cretaceous, often brings the Posidonia shales in contact with salt bodies, especially around the basin margins where numerous salt bodies are located. The thermal effect will have to be modeled at these locations to have a more robust maturation history and a more accurate migration model that match the kinematic evolution of the salt systems studied.

B) Reservoir rock presence and configuration

Reservoir type, architecture and preservation in complex salt tectonics can vary greatly. In gravitational gliding systems, accommodation can be created and suppressed rapidly, allowing over-thickened reservoir sands to accumulate at the downthrown side of syn-depositional faults or along active salt bodies. De Jager (2012) (Fig. 5.18) showed that over-thickened Triassic sands are present in the Dutch Offshore due to growth faulting. This result, associated with the results of the STEM Project opens new avenues for studying in even greater detail the impact that gravitational gliding and contractional thin-skin tectonics had on the Triassic reservoirs in more details.

C) Trapping

Salt tectonics can produce a wide range of trap styles, especially when allochthonous salt emplacement is involved. Figures 5.19 and 5.20 show a few possible trap styles encountered in the Gulf of Mexico, some of which can be applicable to the Dutch offshore. A potential trap style that has been targeted in the West African marginal basins, are the rafts that can be in certain cases excellent targets due to their disconnection from updip stratigraphic equivalents, preventing updip leaking if the younger growth strata are good seals (see well 7 in Fig. 2.15). The allochthonous salt systems that are associated with shortened salt diapirs may also provide opportunities for subsalt traps if the remaining salt is sufficiently thick to prevent seal breach.

Figure 5.18: The Fat Sand play. From De Jager (2012).

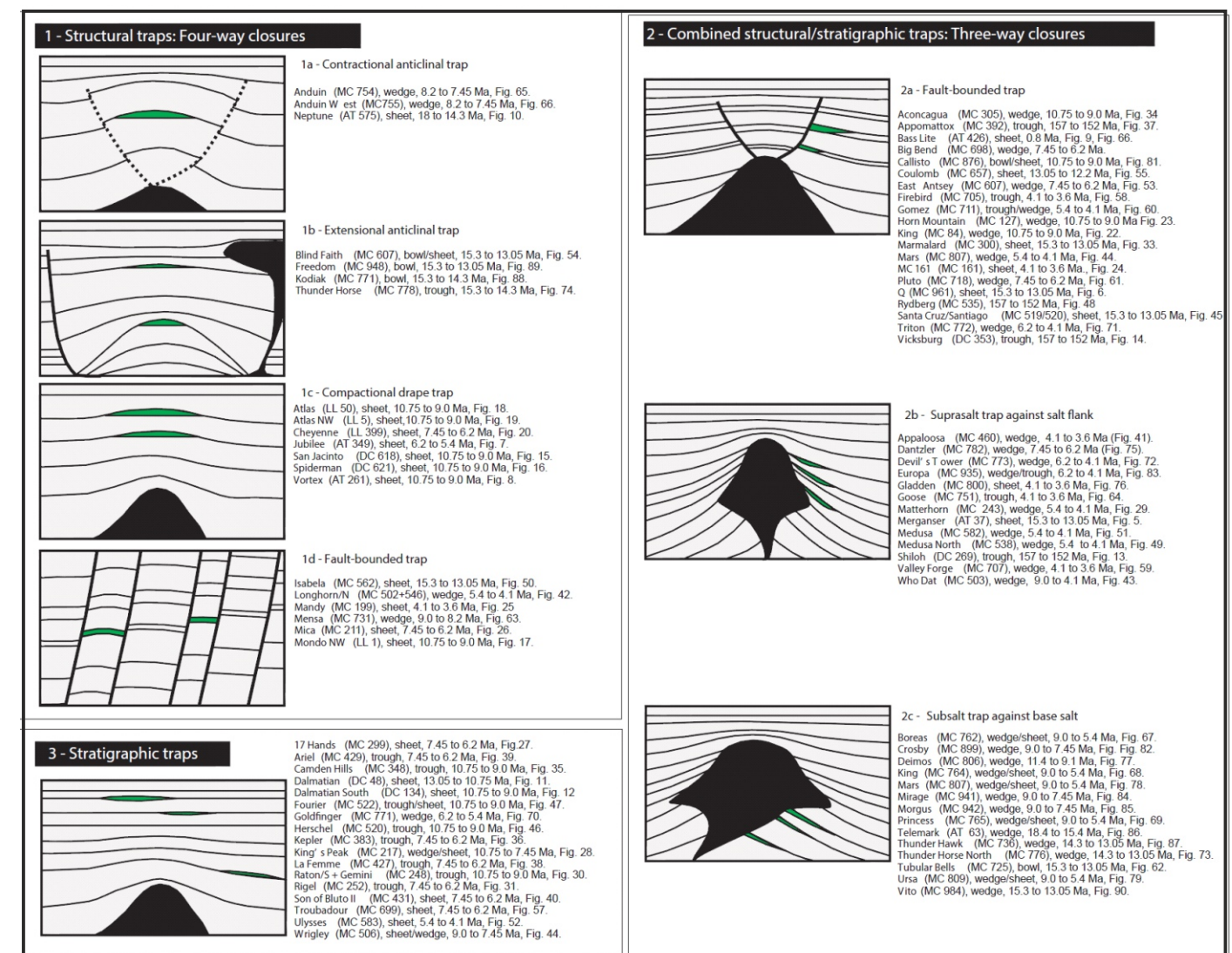
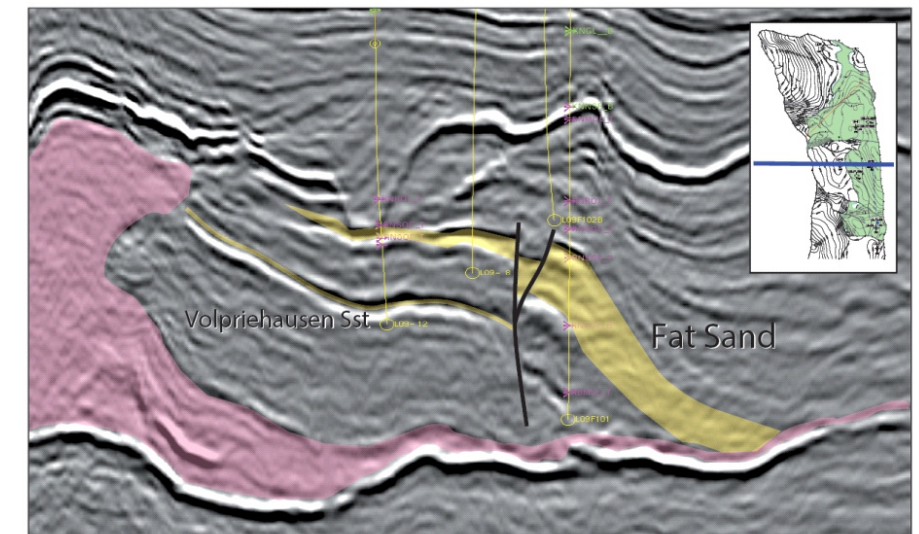


Figure 5.19: Schematic cross sections showing the three main trap styles related to salt systems in the eastern deep Gulf of Mexico: four-way closure, combined three-way closure, and stratigraphic traps. Listed are all the fields discovered in the region that have those types of trap style. The name and block numbers are given for each field. From Bouroullec et al. (2017).

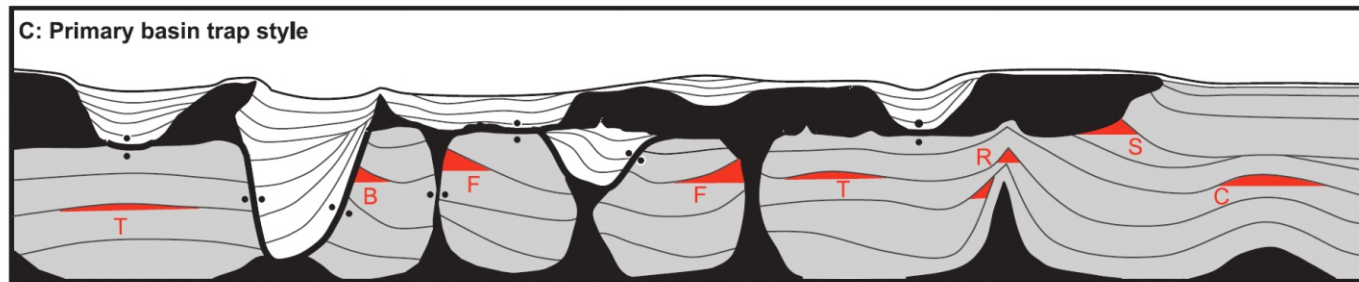


Figure 5.20: Trap style in primary basins and subsalt. From Pilcher et al., 2001

The possible trap configuration observed in the study area are either structural or combined traps (Fig. 5.19). They can be extensional anticlinal traps related to the turtle structures (e.g. F17 turtle; Figs. 4.3.10); contractional traps (e.g. Fig. 4.2.19) or subsalt trap (e.g. Fig. 5.18). The presence of horizontal allochthonous salt welds can also create local subsalt traps if the amount of salt left is sufficient and if the salt welds do not have significant fault offset. The subsalt trap configuration is difficult to estimate as a potential trap style in the Dutch offshore since it has not yet been attempted yet. New state-of-the art subsalt seismic acquisition techniques, as used in the deep Gulf of Mexico, may be required to efficiently evaluate seismically the potential of such traps.

D) Migration

Migration of hydrocarbons in complex salt tectonic settings can be a lengthy topic of discussion since the structural style of salt systems may vary greatly in space and time. For example structural geometry that favor vertical migration but later evolve to favor vertical migration (e.g. salt welds). Several parameters can affect migration as shown in Figure 5.21. One of the main foci of the STEM Project are the kinematics of salt bodies during the Triassic, with some evidence of downdip salt bodies being shortened due to updip extension, producing some salt extrusions and later salt welding (Fig. 5.22). The evolution of these salt systems has to be well understood to understand when these features are affecting vertical migration in a positive or negative way. The fault systems associated with these salt structures will also have to be included in the kinematic models to have a comprehensive model for migration pathways through time that incorporate brittle deformation. For example this can be observed in the salt system SS6 (Fig. 4.4.5).

It is highly recommended to have a high confidence regarding the presence of welded out allochthonous salt systems in the southern part of the study area where they are more prevalent. Not only their presence may have an impact on the migration pathways but knowing precisely the timing of welding of these allochthonous salt systems is also crucial when combined with maturity modeling of any given structure. Detailed 3D seismic mapping (potentially 3D structural restoration) associated with high-resolution seismic mapping of salt bodies, associated faults and growth stratigraphy, can provide significant information on the exact timing of salt motion and salt welding. Such information should be integrated in any petroleum system modeling of basin affected by complex salt tectonics to fully grasp the potential (and risks) of drilling in such geological context.

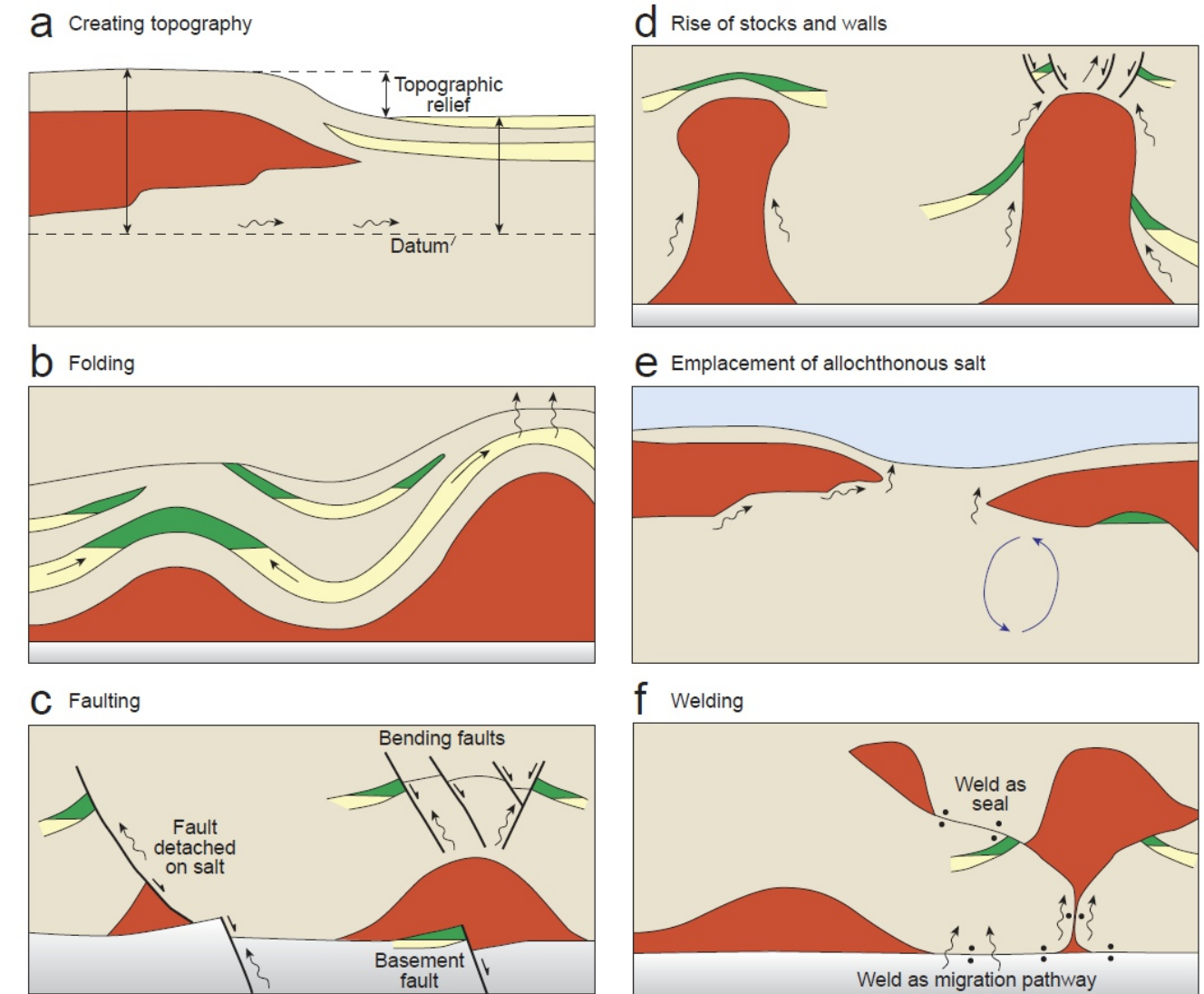


Figure 5.21: Salt structure effects on fluid migration. From Jackson and Hudec, 2017

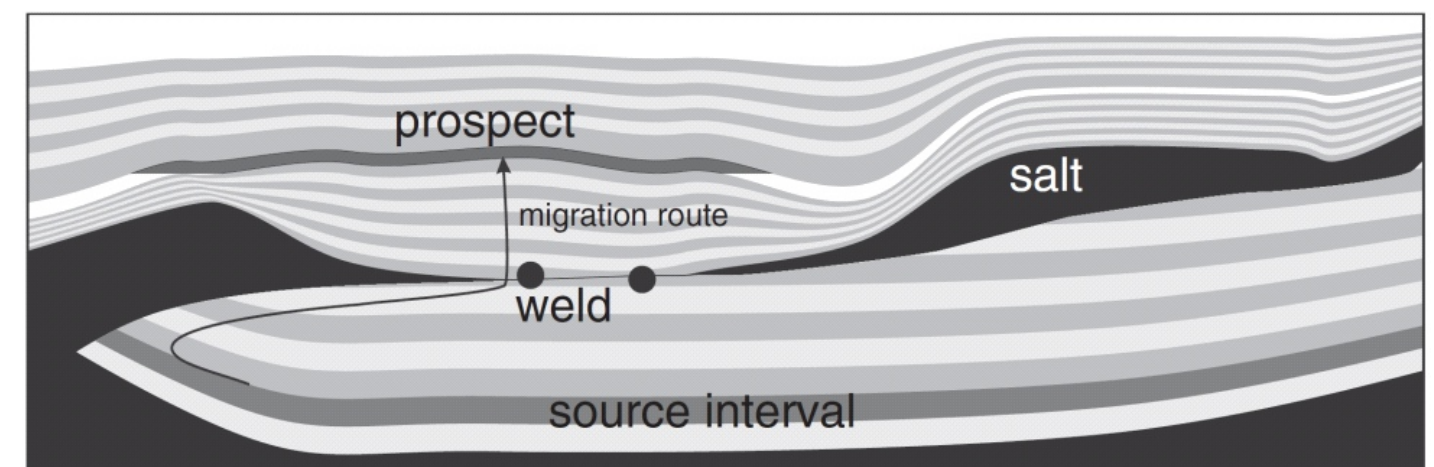


Figure 5.22: Understanding the geometry, timing and evolution of salt welds is crucial for robust migration models. From Peel, 2014.

CONCLUSIONS, FUTURE WORK & REFERENCES

The research on the early salt movement in the Dutch offshore carried out in the STEM project provides new insights on several previously understudied structural elements such as salt welds, allochthonous salt systems, growth fault/raft systems and collapse salt bodies. The multidisciplinary approach combining regional and local seismic mapping, 2D structural restoration, geochemistry and palynology allow to analyze several salt structures and gave an unique new perspective on the Triassic and Jurassic structural evolution of the Dutch offshore. Several results obtained in this study have significant implications for the structural history of the Dutch offshore.

Geochemistry

- Permian and Triassic salts can be dated with S-isotope stratigraphy.
- Salt sampled from case study wells F18-09-02 and L09-04 were confirmed by the S-isotope dating to be of Rot and possibly Muschelkalk ages.
- S-isotope dating of samples from case study well F17-02 may not belong to Keuper. Whether it is a remobilised salt from the Zechstein is still debatable. More samples would need to be analysed to depict the age with more accuracy.
- A continuous reference section with a good S-isotope curve is needed to strengthen the S-isotope dating.

Palynology

- It is not possible to distinguish the Permian and Triassic salt units by applying palynological analyses.
- Core samples from the Triassic Röt do yield age-indicative pollen and spores, but the palynological recovery of cuttings samples from Triassic salt layers is too low for reliable age datings.
- Core samples from the black stringers in the Zechstein do yield a variety of rich and well preserved Permian assemblages, but the palynological recovery of cuttings samples from Zechstein salt is too low for reliable age datings.
- The discovery of rich Permian assemblages in some of the black stringers in the Zechstein has relevance to petroleum geology: It explains the provenance of the well preserved Permian palynomorphs that sometimes found in great abundance in the Jurassic, and secondly, the excellent preservation and bright fluorescence of the palynomorphs, normally indicating low thermal maturity, possibly indicates the presence of oil in the stringers.

General salt tectonics and structural restoration

- Salt tectonics started during the Early Triassic but only as isolated structures in northern part of the Dutch sector (Block A). These structures show limited growth compared to similar structures in the UK sector.
- The first strong evidence of significant salt tectonic activity occurred during the Middle Triassic with salt pillowing, minibasin growth, growth faulting detaching on autochthonous salt, rafting and thin-skin thrusting.
- During the Late Triassic salt tectonics increased in activity with diapir growth becoming predominant as well as continued growth fault/rafting, salt body shortening (due to updip gravitational gliding) and allochthonous salt sheet emplacement, inflation and loading.
- Four turtle structures are identified and show different timing of inversion, from the Middle Triassic (M4 Turtle), the end of Triassic (F18 Turtle), the end of the Middle Jurassic (F17 Turtle) and the Early Kimmeridgian (F09/F11 Turtle).
- All turtle structures growth ceased before the deposition of the Rijnland Group. This indicates that the kinematic history of these turtles are initially related to local parameters while the final stage of turtles evolution was a basin-scale phenomenon related to the main

phase of rifting (Middle Jurassic-Early Cretaceous) and its cessation (Early Cretaceous).

- Growth fault/raft systems are clearly proven for the first time in the Dutch sector with up to 12-18 km of translation deduced from structural restoration. Nevertheless, most of the rafts experienced a more limited amount of translation, often less than 5 km, and have been reactivated in later stage of deformation, especially during the Cenozoic during the Alpine shortening.
- Extruded salt sheets developed in the rift basins but have not been observed on the platforms, which is likely due to the presence of squeezed pre-existing salt bodies in the central part of the basin. The salt body shortening is due to updip thin-skin extension as a triggering phenomenon for active upward salt migration and extrusion at the free surface.
- Three types of collapse structures have been recognized, 1) Elongated graben-like structures formed over salt walls, 2) bowl-shaped/minibasin formed over extended salt pillows, and 3) basin margin salt body collapse forming expulsion rollovers.
- The four 2D structural restorations carried out in this project give new constraints to evaluate the kinematic history of the study area and show that such techniques are very relevant to reach a critical level of understanding of these structurally complex areas.
- Two Middle to Late Triassic structural maps are constructed that display the growth fault/raft systems, the contractional structures associated with these gravitational gliding systems, the collapsed salt structures and the allochthonous salt sheets/welds. This Middle to Late Triassic structural summary map shows a basin that was composed of three zones, an outer zone predominately affected by extensional thin-skin tectonics, an inner zone affected by contractional tectonics and a middle zone, located between the previous two zones, that was predominantly a transitional province with collapsed salt structures and allochthonous salt sheets.
- A new conceptual regional kinematic model of the Triassic is proposed that involves 1) salt diapirism at the onset of the Middle Triassic, around the depositional time of the Röt Formation; 2) shortening of these salt diapirs due to concentric gravitational gliding around the Triassic basin margins (Blocks A, E, G, M and L); and 3) local extrusion of allochthonous salt sheets associated with this shortening of salt diapirs.

Case studies

Case study F17/F18:

- An allochthonous salt system was emplaced during the Late Triassic in the southern part of block F17. It came from the southwestern part of the Block 17/southeastern part of Block F16 and was later welded out during the Upper Jurassic.

Case study L05/L06/L08/L09:

- Three allochthonous salt systems and two growth fault/raft systems are located in the study area and in the neighboring block M04.
- The two growth fault/raft systems are located to the east in the M04/L06 and M07/L08 areas with direction of raft translation from east to west. The M07/L08 growth fault/raft system encompasses the fat sand play system.
- The three allochthonous salt systems are located westward and downdip of the growth fault/raft systems and are related to shortening of pre-existing diapirs, counterbalancing the updip thin-skin extension. One of these allochthonous salt systems is a stepped counterregional salt system, the first ever identified in the Dutch sector.

Case study F10/F11:

- The western part of the Dutch Central Graben in the F11 block is likely not a welded out allochthonous salt system, such as proposed at the beginning of the study, but rather an unusually shaped rim syncline related to complex salt withdrawal from the basin axis to the western basin margin.

The STEM Project creates a new platform, a foundation, for several new research focus, areas including geological characterization, mapping and modeling, as well as geochemical analysis to better characterize the salt layers and remobilized structures with more certainty. Several topics were identified that can be investigated in a follow up project (STEM2).

A) Effects of Jurassic/Cretaceous erosional events and Alpine shortening on salt structures in the Dutch offshore

One of the reason why deciphering the salt tectonic history of the Dutch subsurface is a difficult task is due to the successive major extensional, contractional and erosional events that affected the area in the Triassic, Jurassic and Cretaceous. On the platforms especially, the amount of Jurassic and Triassic remaining is limited and therefore many salt structures were either eroded or at least truncated significantly. It is very likely that more shallow salt features such as salt sheets or remobilized salt diapirs associated with collapse structures were present in more locations (e.g. Fig. 4.2.14) on the platforms, but are missing now due to successive erosions.

The salt features observed in the regional study and case studies of this project have often been deformed to a certain extent during the Alpine shortening (e.g. vertical salt weld in Fig. 4.3.12; salt system 7 in Fig. 4.3.27) and need to be better understood to better reconstruct the Mesozoic salt architecture.

Specific research regarding the effects of Cenozoic shortening on salt structures (including the ones that formed during the Triassic and Jurassic), would be of great value to have a more complete picture of the evolution of the basin and the evolution of the petroleum systems. This topic would involve mapping of Upper Jurassic, Cretaceous and a few Cenozoic units as well as salt structures, and detailed fault mapping around these structures.

B) Effects of Triassic shortening in the central part of the Dutch Offshore

Good evidence of thin-skin shortening during the Upper Triassic has been produced in the STEM Project. A focus on these structures and their relationship with the updip extensional system is required to fully understand their distribution and dynamics, as well as their effects on reservoir distribution and impact on successive phases of deformation.

Such research would require 3D mapping of shortened diapirs and thrust Triassic strata as well as additional 2D/3D structural restoration.

C) Geochemical analysis of salt layers

The geochemical techniques used in the STEM Project are promising and should be used to test new ideas regarding salt migration and identification in locations where sufficient core or cutting data are available. We recommend to measure $\delta^{34}\text{S}$ continuously from the Permian (Zechstein) to Triassic (Röt, Muschelkalk, Keuper) evaporites from European (preferentially Dutch) cores and outcrops and thus create a solid reference curve. This will create an exact dating methods using S-isotopes. Where carbonates were identified in cores and cuttings Sr-isotope analyses should be performed to confirm the S-isotope correlation. Alternatively Sr extraction can be performed on anhydrite, gypsum and halite on a limited number of samples.

D) 3D or map view restoration of growth fault/raft systems

To fully understand the gravitational gliding systems observed in the southeastern part of the study area, detail mapping and restoration of the Triassic would be required. This could be done in a similar way Rouby et al. (2002, Fig. 6.1) followed in the Congo/Cabinda Basin or in full 3D fashion.

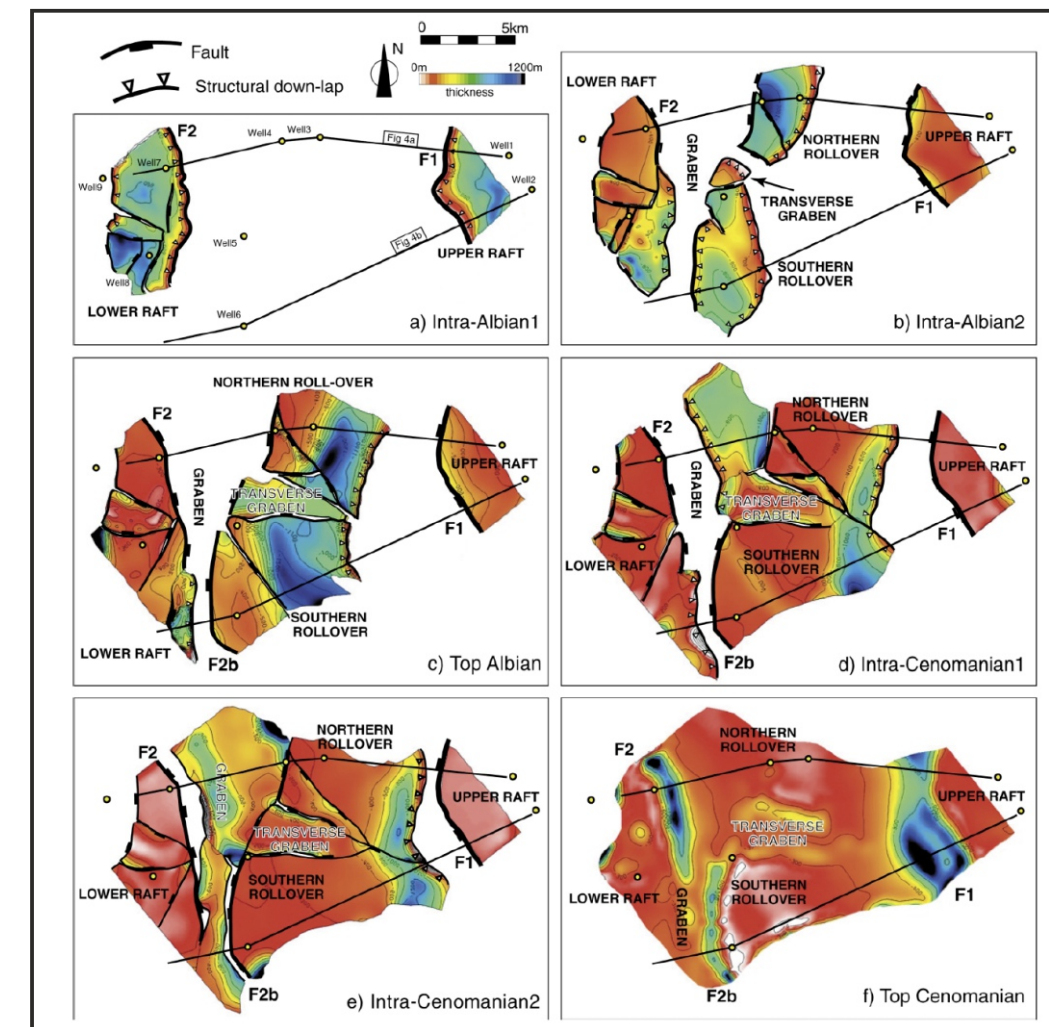


Figure 6.1: Restored successive isopach map of a growth fault/raft system in the Congo/Cabinda basin using 3D restoration. From Rouby et al. (2002).

E) Tectonostratigraphic analysis of Triassic growth strata

A similar approach to the upcoming TNO MAXIM Project, which focuses on the Middle Jurassic to Lower Cretaceous, can be proposed for the Triassic, to study the impact of salt tectonics on growth stratigraphy would be of great value to evaluate potential new plays in the Dutch offshore. This research could include amplitude mapping in conjunction with detailed 3D seismic mapping of reservoir units in the vicinity of salt systems that were active during the Upper Triassic.

Abdul Fattah, R., Verweij, J. M., Witmans, N. and Ten Veen, J. H., 2012, Reconstruction of burial history, temperature, source rock maturity and hydrocarbon generation in the northwestern Dutch offshore. In Netherlands Journal of Geosciences, Geologie en Mijnbouw, Exploring the deep subsurface of the Netherlands, Vol. 91, No. 4, p. 535-554.

Bachmann, G. H., Geluk, M. C., Warrington, G., Becker-Roman, A., Beutler, G., Hagdorn, H., Hounslow, M. W., Nitsch, E., Rohling, H.-G., Simon, T. and Szulc, A., 2010, Triassic. In: Doornenbal, J.C. and Stevenson, A.G. (editors): Petroleum Geological Atlas of the Southern Permian Basin Area. EAGE Publications b.v. (Houten), p. 149-173.

Bally, A. W., 1981, Thoughts on the tectonics of folded belts, in K. R. McClay and N. J. Price, eds., Thrust and nappe tectonics: London, Geological Society, Special Publication 9, p. 13–32.

Bouroullec, R., Verreussel, R. M. C. H, Geel, C. R, Munsterman, D., Bruin, G. de., Zijp, M. H. A. A, Janssen, M., Millan, I. and Boxerm, T., 2016, The FOCUS Project: Upper Jurassic sandstones: Detailed sedimentary facies analysis, correlation and stratigraphic architecture of hydrocarbon bearing shoreface complexes in the Dutch offshore. TNO Report, 228 pp.

Bouroullec, R. and Weimer, P., 2017, Geometry and kinematics of Neogene allochthonous salt systems of the Mississippi Canyon, northern Atwater Valley, western Lloyd Ridge, and western Desoto Canyon protraction areas, northern deep-water Gulf of Mexico: AAPG Bulletin, v. 101, p. 1003-1034.

Bouroullec, R., Weimer P. and Serrano, O., 2017, Regional structural setting and evolution of the Mississippi Canyon, Atwater Valley, western Lloyd Ridge, and western Desoto Canyon protraction areas, northern deep-water Gulf of Mexico: AAPG Bulletin, v. 101, p. 1035-1071.

Bouroullec, R., Verruessel, R. M. C. H., Geel, C.R., Bruin, G. de., Zijp, M., Munsterman, D., Janssen, N. and Kerstholt-Boegehold, S., in press, Tectonostratigraphy of rift basins affected by halokinetics: The syn-rift Middle Jurassic - Lower Cretaceous in the Dutch Central Graben, Terschelling Basin and neighbouring platforms, Dutch offshore. In Mesozoic Resource Potential in the Southern Permian Basin, GeoSoc.

Bruin, G. de., Bouroullec, R., Geel, C. R., Abdul Fattah, R., Hoof, T. B. van, Pluymaekers, M. P. D., Belt, F. van der, Vandeweyer, V. P. and Zijp, M. H. A. A, 2015, New Petroleum plays in the Dutch Northern Offshore, TNO report TNO 2015 R10920

Burollet, P., 1975, Tectonique en radeaux en Angola: Bulletin de la Société Géologique de France, 17, p. 503–504.

Canfield, D. E. and Farquhar, J., 2012, The Global Sulfur Cycle. Fundamentals of Geobiology, (Eds) Canfield, D. E. & Farquhar, J.. Blackwell Publishing Ltd, Ch. 5, p. 49-64.

Claypool, G. E., Holster, W. T., Kaplan, I. R., Sakai, H. and Zak, I., 1980, The age curve of Sulphur and oxygen isotopes in marine sulphate and their mutual interpretation. Chemical Geology 28, p. 190-260.

Cobbold, P. R. and Szatmari, P., 1991, Radial gravitational gliding on passive margins Tectonophysics, Vol. 188, 3–4, p. 249-289

Coward, M. P., Dewey, J., Hempton, M. and Holroyd, J., 2003, Tectonic evolution. In: Evans, D.J., Graham, C., Armour, A. and Bathurst, P. (Eds): The Millenium Atlas: Petroleum Geology of the Central and Northern North Sea. The Geological Society (London), p. 17-33.

Doornenbal, H. and Stevenson, A, 2010, Petroleum geological atlas of the Southern Permian Basin area. EAGE, 342 pp.

Dudas, F. O., Yuan, D.X., Shen, S-Z. and Bowing, S. A., 2017, A conodont-based revision of the ⁸⁷Sr/⁸⁶Sr seawater curve across the Permian-Triassic boundary. Palaeogeography, Palaeoclimatology, Palaeoecology 470, p. 40–53.

Duin E. J. T., Doornenbal, J. C., Rijkers, R. H. B. Verbeek, J. W. and Wong, T. E., 2006, Subsurface structure of the Netherlands - Results of recent onshore and offshore mapping, Netherlands Jopurnal of Geosciences - Geologie en Mijnbouw, 85, 4, p. 245-276.

Duval, B., Cramez, C. and Jackson, M. P. A., 1990, Raft tectonics in the Kwanza basin, Angola (abs.): Boulder, CO, Geological Society of America, Abstracts with Programs, 22, A48.

Fanlo, I. and Ayora, C., 1998, The evolution of the Lorraine evaporite basin: implications for the chemical and isotope composition of the Triassic ocean. Chemical Geology 146, p. 135–154.

Geluk, M. C., 2005, Stratigraphy and tectonics of Permo-Triassic basins in the Netherlands and surrounding areas, PhD Thesis, Utrecht University, 171 pp.

Geluk, M. C., 2007, Triassic. In: Wong, T.E., Batjes, D.A.J. and de Jager, J. (Eds): Geology of the Netherlands. Royal Netherlands Academy of Arts and Sciences (Amsterdam): p. 85-106.

George, G. T. and Berry, J. K., 1993, A new lithostratigraphy and depositional model for the Upper Rotliegend of the UK sector of the southern North Sea. In: North, C.P. and Prosser, D.J. (Eds): Characterization of Fluvial and Aeolian Reservoirs. Geological Society Special Publication (London) 73: p. 291-319.

George, G. T. and Berry, J. K., 1997, Permian (Upper Rotliegend) synsedimentary tectonics, basin development and palaeogeography of the southern North Sea. In: Ziegler, K., Turner, P. and Daines, S.R. (Eds): Petroleum Geology of the Southern North Sea: Future Potential. Geological Society Special Publication (London) 123: p. 31-61.

Glennie, K. W. (Ed), 1998, Petroleum Geology of the North Sea, Basic concepts and recent advances. Blackwell (Oxford): 636 pp.

Goldberg, T., Shields, G. A. and Newton, R. J., 2011, Analytical Constraints on the Measurement of the Sulfur Isotopic Composition and Concentration of Trace Sulfate in Phosphorites: Implications for Sulfur Isotope Studies of Carbonate and Phosphate Rocks. Geostandards and Geoanalytical Research, 35 (2), p.161-174.

Heybroek, P., 1975, On the structure of the Dutch part of the Central North Sea Graben. In: Woodland, A.W. (Ed.): Petroleum and the Continental Shelf of North-West Europe. Applied Science Publishers Ltd (London): p. 339-349.

Hudec, M. R. and Jackson, M. P. A., 2007, Terra infirma: Understanding salt tectonics: Earth-Science Reviews, 82, p. 1–28,

Hoffmann, N. and Stiewe, H., 1994, Neuerkenntnisse zur geologisch-geophysikalischen Modellierung der Pritzwalker Anomalie im Bereich des Ostelbischen Massivs. Zeitschrift geologischer Wissenschaften 22: p. 161-171.

Herngreen, G. F. W. and Wong, T. E., 1989, Revision of the Late Jurassic stratigraphy of the Dutch Central North Sea Graben. Geologie en Mijnbouw 68: p. 73-105.

Jackson, M. P. A. and Hudec, M. R., 2005, Stratigraphic record of translation down ramps in a passive-margin detachment: Journal of Structural Geology, 27, p. 889–911.

Jackson, M. P. A., Vendeville, B. C. and Schultz-Ela, D. D., 1994, Structural dynamics of salt systems: Annual Review of Earth and Planetary Sciences, 22, p. 93–117.

Jackson M. P. A. and Hudec, M. R., 2017, Salt tectonics : principles and practiceCambridge University Press, 494 pp.

Jager, J. de, 2007, Geological development. In: Wong, T.E., Batjes, D.A.J. and De Jager, J. (Eds): Geology of the Netherlands. Royal Netherlands Academy of Arts and Sciences (Amsterdam): p. 5-26.

Jager, J. de, 2012, The discovery of the Fat Sand Play (Solling Formation, Triassic), Northern Dutch offshore – a case of serendipity. Netherlands Journal of Geosciences, v. 91, Is. 04, p. 609-619.

Kampschulte, A. and Strauss, H., 2004. The sulfur isotopic evolution of Phanerozoic seawater based on the analysis of structurally substituted sulfate in carbonates. Chemical Geology, 204: p. 255-286.

Kley, J. and Voigt, T., 2008, Late Cretaceous intraplate thrusting in central Europe: Effect of Africa-Europe-Iberia convergence, not Alpine collision. Geology 36: p. 839-842.

Kombrink, H., Doornenbal, J. C., Duin, E. J. T., den Dulk, M., van Gessel, S. F., ten Veen, J. H. and Witmans, N., 2012, New insights into the geological structure of the Netherlands; results of the detailed mapping project. In Netherlands Journal of Geosciences, Geologie en Mijnbouw, Exploring the deep subsurface of the Netherlands, Vol. 91, No. 4, p. 447–464.

Kovalevych, V., Peryt, T. M., Beer, W., Geluk, M. and Halas, S., 2002, Geochemistry of Early Triassic seawater as indicated by study of the Rot halite in the Netherlands, Germany, and Poland. Chemical Geology 182, p. 549–563.

Krzywiec, P., 2004, Triassic evolution of the Kłodawa salt structure: basement-controlled salt tectonics within the Mid-Polish Trough (central Poland). Geological Quarterly 48 (2), p.123–134.

Lott, G. K., Wong, T. E., Duser, M., Andsbjerg, J., Mönnig, E., Feldman-Olszewska, A. and Verreussel, R. M. C. H., 2010. Jurassic. In: Doornenbal, J.C. and Stevenson, A.G. (editors): Petroleum Geological Atlas of the Southern Permian Basin Area. EAGE Publications b.v. (Houten): p. 175–193.

Marenco, P.J., Corsetti F.A., Kaufman A.J. and Bottjer, D.J., 2008, Environmental and diagenetic variations in carbonate associated sulfate: An investigation of CAS in the Lower Triassic of the western USA. Geochimica et Cosmochimica Acta 72, p. 1570–1582.

Martin E.E. and Macdougall, J.D., 1995, Sr and Nd isotopes at the Permian/Triassic boundary: A record of climate change. Chemical Geology 125, p.73–99.

Mello, U. T., Karner, G. D. and Anderson R.N., 1995, Role of salt in restraining the maturation of subsalt source rocks: Marine and Petroleum Geology, 12, p.697–716.

Mohriak, W. U., and P. Szatmari, 2008, Tectônica de sal, in W. U. Mohriak, P. Szatmari, and S. M. Couto Anjos (eds.), Sal geologia e tectônica: Exemplos nas bacias Brasileiras: São Paulo, Beca Edições, p.91–163.

Munsterman, D. K., Verreussel, R. M. C. H., Mijnlief, H. F., Witmans, N., Kerstholt-Boegehold, S. and Abbink, O. A., 2012, Revision and update of the Callovian-Ryazanian Stratigraphic Nomenclature in the northern Dutch Offshore, i.e. Central Graben Subgroup and Scruff Group. Netherlands Journal of Geosciences-Geologie en Mijnbouw, 91 (4): p. 555–590.

Newton R. J., Pevitt, E. L. Wignall, P. B. and Bottrell S.H., 2004, Large shifts in the isotopic composition of seawater sulphate across the Permo-Triassic boundary in northern Italy. Earth and Planetary Science Letters 218, p. 331–345.

Paytan, A., Kastner, M., Campbell, D. and Thiemens, M. H., 1998. Sulfur isotopic composition of Cenozoic seawater sulfate. Science 282, p. 1459–1462.

Penge J., Taylor, B., Huckerby, J. A. and Munns, J. W., 1993, Extension and salt tectonics in the East Central Graben. In: Parker, J. R. (ed.) Petroleum Geology of Northwest Europe: Proceedings of the 4th Conference. The Geological Society, London, p. 1197–1209.

Penge, J., Munns, J. W., Taylor, B. and Windle, T. M. F., 1999, Rift-raft tectonics: examples of gravitational tectonics from the Zechstein basins of northwest Europe. In: Fleet, A. J. & Boldy, S. A. R. (eds) Petroleum Geology of Northwest Europe: Proceedings of the 5th Conference, Geological Society, London, p. 201–213

Peryt T. M., Halas, S. and Hryniv, S. P., 2010, Sulphur and oxygen isotope signatures of late Permian Zechstein anhydrites, West Poland: seawater evolution and diagenetic constraints. Geological Quarterly, 54 (4), p. 387–400.

Petersen, K., Clausen, O. R. and Korstgard, J. A., 1992, Evolution of the salt-related listric growth fault near the D-a well, block 5605, Danish North Sea: displacement history and salt kinematics, Journal of Structural Geology, 14, p. 565–577.

Peeters, S., 2016, Mesozoic strike-slip faults in the Northern utch offshore; new insights from seismic and physical modeling data, Utrecht University, 107 pp.

Peel, F. J., 2014, The engines of gravity-driven movement on passive margins: Quantifying the relative contribution of spreading vs. gravity sliding mechanisms: Tectonophysics, 633, p. 126–142

Pharaoh, T. C., Duser, M., Geluk M., Kockel F., Krawczyk, C. M., Krzywiec P., Scheck-Wenderoth, M., Thybo H., Vejbaek O. and van Wees, J. D., 2010, Tectonic evolution . in Doornenbal, H. and Stevenson, A. G, eds. Petroleum geological atlas of the Southern Permian Basin area. Houten, the Netherlands, EAGE, p. 25–57.

Pilcher, R. S., Kilsdonk, B. and Trude, J., 2011, Primary basins and their boundaries in the deep-water northern Gulf of Mexico: Origin, trap types, and petroleum system implications: American Association of Petroleum Geologists Bulletin, 95, p. 219–240

Prokoph, A., Shields, G. A. and Veizer., J., 2008, Compilation and time-series analysis of a marine carbonate d18O, d13C, 87Sr/86Sr and d34S database through Earth history. Earth-Science Reviews 87, p. 113–133.

Raab, M. and Spiro, B., 1991, Sulfur isotopic variations during seawater evaporation with fractional crystallization. Chemical Geology 86, p. 232–333.

Remmelts, G., 1995, Fault-related salt tectonics in the southern North Sea, the Netherlands. In: Jackson, M.P.A., Roberts, D.G. and Snelson, S. (Eds): Salt tectonics: a global perspective. American Association of Petroleum Geologists Memoir 65: p. 261–272.

Roberts, A. M., Yielding, G., Kuznier, N. J., Walker, I. M. and Dorn-Lopez, D., 1995, Quantitative analysis of Triassic extension in the northern Viking Graben. Journal of the Geological Society 152: p. 15–27.

Rosendaal, E., Kaymakci, N., Wijker, D. and Schroot, B.M., 2014, Structural development of the Dutch Central Graben: new ideas from recent 3D seismic. Abstract, EAGE Meeting Amsterdam.

Rouby, D., Raillard, S., Guillocheau, F., Bouroullec, R., and Nalpas, T., 2002, Kinematics of a growth fault/raft system of the west African margin using 3-D restoration: Journal of Structural Geology, v. 24, p. 783–796.

Rouby, D., Guillocheau, F., Robin, C., Bouroullec, R., Raillard, S., Castellort, C., and Nalpas, T., 2003, Rates of deformation of an extensional growth fault/raft system (offshore Congo, West African Margin) from combined accommodation measurements and 3-D restoration: Basin Research, v. 15, p. 183–200.

Rowan, M. G. and R. A. Ratliff, 2012, Cross-section restoration of salt-related deformation: Best practices and potential pitfalls: Journal of Structural Geology, 41, p.24–37.

Schultz-Ela, D. D. and P. Walsh, 2002, Modeling of grabens extending above evaporites in Canyonlands National Park, Utah: Journal of Structural Geology, 24, 247–275.

Sclater, J.G. and Christie, P.A.F., 1980, Continental Stretching: An Explanation of the Post-Mid-Cretaceous Subsidence of the Central North Sea Basin. Journal of Geophysical Research, 85, 3711–3739.

Schroot, B. M., 1991, Structural development of the Dutch Central Graben. In: Michelsen, O. and Frandsen, F. (Eds): The Jurassic in the Southern Central Trough. Danmarks Geologiske Undersøgelse series B 16: p. 32–35.

Schuster, D. C., 1995, Deformation of allochthonous salt and evolution of related salt-structural systems, eastern Louisiana Gulf Coast, in M. P. A. Jackson, D. G. Roberts, and S. Snelson, eds., Salt tectonics: A global perspective: Tulsa, OK, American Association of Petroleum Geologists, Memoir 65, p. 177–198.

Sonderholm, M., 1987, Facies and geochemical aspects of the dolomite-anhydrite transition zone (Zechstein 1–2) in the Batum-13 well, northern Jutland, Denmark: A key to the evolution of the Norwegian-Danish Basin. In: The Zechstein Faies in Europe, Ed: T.M. Peryt, Vol. 10.

Stewart, S. A., 2007, Salt tectonics in the North Sea Basin: a structural style template for seismic interpreters. In Ries, A.C. Butler, R.W.H. and Graham, R.H. (eds). Deformation of the Continental Crust: The Legacy of Mike Coward. Geological Society, London, Special Publication, Vol. 272, p. 361–396.

Stewart, S. A. & Clark, J. A., 1999. Impact of salt on the structure of the Central North Sea hydrocarbon fairways. In: Fleet, A. J. & Boldy, S. A. R. (eds) Petroleum Geology of Northwest Europe: Proceedings of the 5th Conference, 179–200.

Surlyk, F. and Ineson, J. R., 2003, The Jurassic of Denmark and Greenland: key elements in the reconstruction of the North Atlantic Jurassic rift system. In: Ineson, J.R. and Surlyk, F. (Eds): The Jurassic of Denmark and Greenland. Geological Survey of Denmark and Greenland Bulletin 1, p. 9-20.

Talbot, C. J. and Jackson, M. P. A., 1987a, Internal kinematics of salt diapirs: American Association of Petroleum Geologists Bulletin, 71, 1068–1093.

Ten Veen, J. H., van Gessel, S. F. and den Dulk, M., 2012, Thin and thick-skinned salt tectonics in the Netherlands; a quantitative approach. In Netherlands Journal of Geosciences, Geologie en Mijnbouw, Exploring the deep subsurface of the Netherlands, Vol. 91, No. 4, p. 447-464.

Torsvik, T. H., Carlos, D., Mosar, J., Cocks, L. R. M. and Malme, T. N. M., 2002, Global reconstructions and North Atlantic paleogeography 440 Ma to recent. In: Eide, E.A. (Ed.): Batlas – Mid Norway plate reconstruction atlas with global and Atlantic perspectives. Geological Survey of Norway (Trondheim): p. 18-39.

Trusheim, F., 1960, Mechanism of salt migration in northern Germany: American Association of Petroleum Geologists Bulletin, 44, 1519–1540.

Underhill, J. R. and Partington, M. A., 1993, Jurassic thermal doming and deflation in the North Sea: implications of the sequence stratigraphic evidence. In: Parker, J.R. (Ed.): Petroleum Geology of Northwest Europe: Proceedings of the 4th Conference. The Geological Society (London): p. 37-345.

Van den Haute, P. and Vercoutere, C., 1990, Apatite fission track evidence for a Mesozoic uplift of the Brabant Massif – preliminary results. Annales Société Géologique de Belgique 112: p. 443-452.

Van Hoorn, B., 1987, Structural evolution, timing and tectonic style of the Sole Pit inversion. Tectonophysics 137: p. 239-284.

Van Adrichem Boogaert, H. A. & Kouwe, W. F. P., 1997, Stratigraphic nomenclature of the Netherlands, revision and update by RGD and NOGPA. Mededelingen Rijks Geologische Dienst, nieuwe serie, vol. 50, section a - j.

van Winden, M., de Jager, J., Jaarsma, B. and Bouroullec, R., in press, New insights in salt tectonics in the northern Dutch offshore: A framework for exploration Mesozoic Resource Potential in the Southern Permian Basin. In Mesozoic Resource Potential in the Southern Permian Basin, GeoSoc,

Veiweij J. M. and Witmans, N., 2009, Terschelling Basin and southern Dutch Central Graben mapping and modeling - Area 2A, TNO report, TNO-034-UT-2009-01569.

Veizer, J., Holser, W.T. and Wilgus, C. K., 1980, Correlation of 13C/12C and 34S/32S secular variations. Geochim. Cosmochim. Acta 44, 579–587.

Weimer, P., Bouroullec, R., and Tari, G., 2004, Chapter 9: Petroleum traps in deepwater settings, in Weimer, P., and Slatt, R. M., The petroleum systems of deepwater setting: in Society of Exploration Geophysicists, SEG Distinguished Instructor Short Course Book, p. 9-1 to 9-92.

Vendeville, B. C., and Jackson, M. P. A., 1992, The fall of diapirs during thin-skinned extension: Marine and Petroleum Geology, 9, p. 354–371.

Wong, T. E., 2007. Jurassic. In: Wong, T.E., Batjes, D.A.J. and de Jager, J. (Eds): Geology of the Netherlands. Royal Netherlands Academy of Arts and Sciences (Amsterdam): p. 107-126.

Wong, T. E., Batjes, D. A. J. and de Jager, J. (Eds), 2007, Geology of the Netherlands. Royal Netherlands Academy of Arts and Sciences (Amsterdam): 354 pp.

Ziegler, P. A., 1988, Evolution of the Arctic, North Atlantic and western Tethys. American Association of Petroleum Geologists: 198 pp.

Ziegler, P. A., 1990a, Geological Atlas of Western and Central Europe (2nd edition). Shell Internationale Petroleum Maatschappij B.V.; Geological Society Publishing House (Bath): 239 pp.

Ziegler, P. A., 1990b, Tectonic and palaeogeographic development of the North Sea rift system. In: Blundell, D.J. and Gibbs, A.D. (Eds): Tectonic evolution of the North Sea rifts. Oxford Science Publications (Oxford): p. 1-36.

Zhang, Y., Krause, M. and Mutti, M., 2013, The Formation and Structure Evolution of Zechstein (Upper Permian) Salt in Northeast German Basin: A Review. Open Journal of Geology, 2013, 3, p. 411-426.

APPENDICES

Mesozoic Strike-slip faults in the Northern Dutch offshore; *New insights from Seismic- and Physical Modeling Data*

A Msc. Thesis by
Stefan Peeters¹

Supervisors

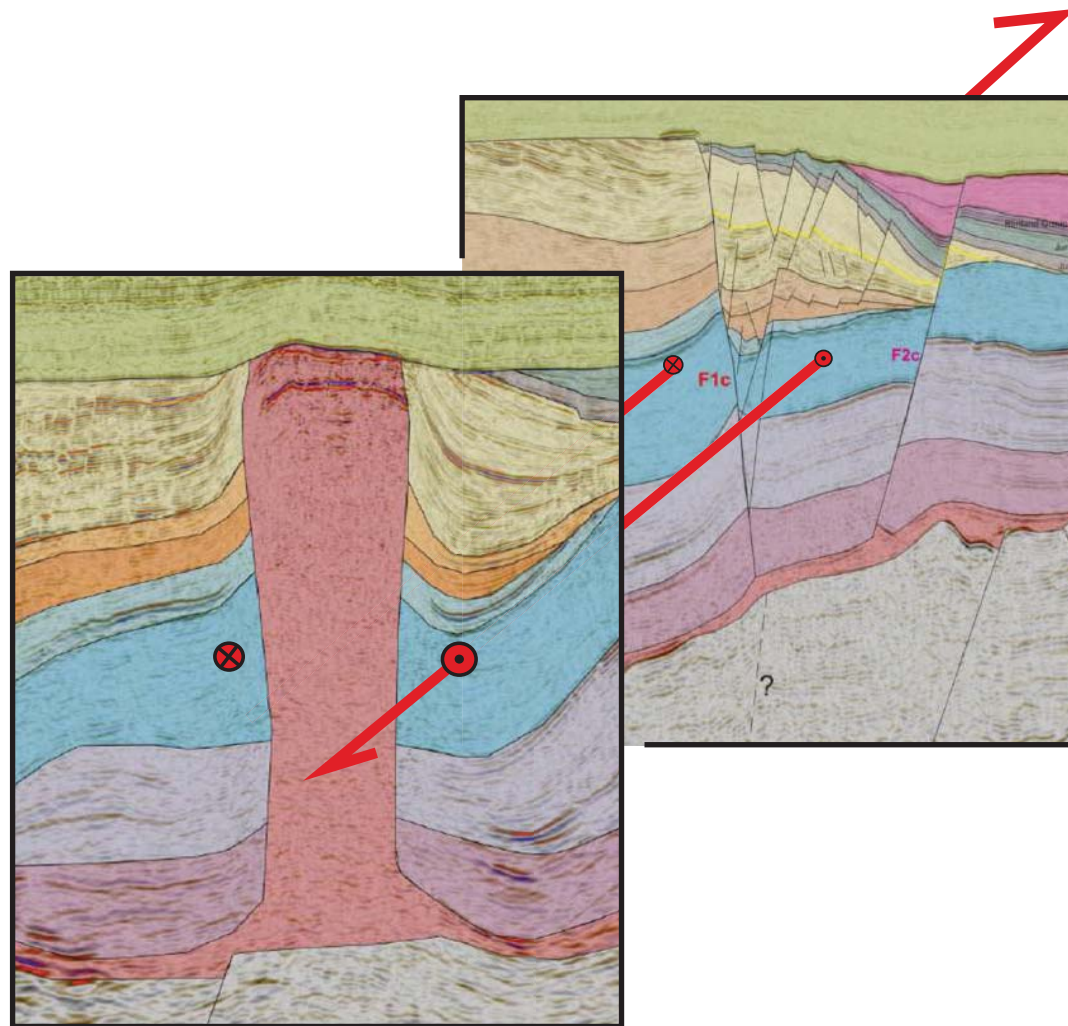
Dr. Renaud Bouroullec²

Dr. Jeroen Smit¹

Prof. dr. Dimitrios Sokoutis¹

Date

July 2016



Abstract

Mesozoic Strike-slip features in the northern Dutch offshore that occurred under regional extensional and compressional tectonics are often not recognised as such and even when they are, they often remain poorly understood. This study provides new insights into various strike-slip faults in the Northern Dutch Offshore in terms of location, timing, sense- and amount of displacement and fault salt interaction. These insights are gained by combining several detailed seismic analyses with an analogue modelling study.

On the Elbow Spit High and Elbow Spit Platform, a group of SW-NE to WSW-ENE strike-slip faults is present that have accommodated approximately 500m to 900m of dextral displacement on individual faults during the Upper Cretaceous and Early Paleogene. Because of the absence of Zechstein salt in this area, these faults display the clear characteristics of strike-slip faults; i.e. vertical fault planes, an upward widening of the fault pattern, local zones of transtension and transpression and (reactivated) Riedel faults.

Dextral movements along two identified strike-slip faults in the Dutch Central Graben, which are estimated to lie in the range of 900m to 2500m, occurred during the Upper Jurassic and possibly Early Cretaceous. In the Dutch Central Graben, the presence of Zechstein salt causes decoupling of the subsalt basement from the supra salt overburden, which changes the structural style of deformation. The identified supra salt strike-slip faults in the Dutch Central are characterised by a more curved strike. Additionally, the strike-slip faults link salt structures, which suggest that strike-slip motions were also accommodated by Zechstein salt structures. This is supported by analogue models, which show that strike-slip motions are preferentially accommodated by salt structures, as they are the mechanically weakest part of the rock column. The two observed strike-slip faults in the Dutch Central Graben are likely caused by differential motions on sub salt normal faults, enhanced by a component of gravitational gliding. No evidence is found for strike-slip movements along N-S trending basement faults that bound the Dutch Central Graben.

Dextral basement strike-slip movements did occur during the Middle to Late Triassic on the Variscan inherited NW-SE to WNW-ESE trending Rifgronden Fault Zone (RFZ) and Hantum Fault Zone (HFZ) that bound the Terschelling Basin. Evidence for these motions includes the right stepping of N-S to NNE-SSW trending Late Early Triassic to Late Triassic low angle detachment faults across the RFZ and HFZ, as well as the overall geometry of features in the Terschelling Basin with respect to features on the adjacent platforms. Displacements along the HFZ are estimated to be in the order of 5 à 6km. Displacements along the RFZ are estimated to be in the order of 2 à 3km. Additionally, thin skinned strike-slip motions occurred in the Terschelling basin due to differential motions between adjacent supra salt Triassic compartments. These Triassic compartments are largely enclosed by salt walls, which accommodated the strike-slip movements.

¹ Utrecht University; Heidelberglaan 8, 3584 CS Utrecht, the Netherlands

² TNO; Princetonlaan 6, 3584 CB Utrecht, The Netherlands

Table of Contents

- 1. Introduction 4**
- 2. Background..... 6**
 - 2.1. Geological history of the Northern Dutch Offshore..... 6
 - 2.1.1. Paleozoic..... 6
 - 2.1.2. Mesozoic and Cenozoic 7
 - 2.2. Stratigraphy 8
 - 2.3. Structural elements in the Northern Dutch Offshore 11
 - 2.4. Strike-slip tectonics in the Northern Dutch Offshore..... 13
 - 2.4.1. Late Paleozoic wrench tectonics 13
 - 2.4.2. Mesozoic strike-slip movements in an extensional regime ... 14
 - 2.4.2. Late Mesozoic/Early Paleogene strike-slip movements in a compressional regime..... 15
 - 2.5. Analogue modelling background 16
 - 2.5.1. Salt tectonics under extensional conditions 16
 - 2.5.1. Salt tectonics under strike-slip conditions 18
- 3. Methods..... 20**
 - 3.1. Seismic interpretation methods 20
 - 3.1.1. Identification of strike-slip faults 20
 - 3.1.2. Detailed analysis of specific strike-slip faults 21
 - 3.2. Analogue modelling methods 23
 - 3.2.1. Experimental set-up 23
 - 3.2.2. Material properties 23
 - 3.2.3. Scaling of the models..... 23
 - 3.2.4. Calculation of strength profiles 26
 - 3.2.5. Limitations of analogue modelling..... 27
 - 3.2.6. Experimental procedure; experiments 1 and 2 27
 - 3.2.7. Experimental procedure; experiments 3 and 4..... 28
- 4. Seismic interpretation results 30**
 - 4.1. Case study A..... 32
 - 4.2. Case study B..... 38
 - 4.3. Case study C..... 47
 - 4.4. Case study D 56
- 5. Analogue modelling results 62**
 - 5.1. Brittle Model 1; Strike-slip followed by extension 62
 - 5.2. Brittle Model 2; Extension followed by strike-slip 65
 - 5.3. Multilayer Model 3; Extension followed by strike-slip 67
 - 5.4. Multilayer Model 4; Extension followed by strike-slip 72

- 5.5. Discussion of the models 81
- 6. Integration and discussion 84**
 - 6.1. Strike-slip movements in the Northern Dutch offshore and analogue modelling 84
 - 6.2. The origin of the observed strike-slip movements in the Dutch Central Graben 87
 - 6.3. Strike-slip movements in the Terschelling Basin and at the Schill Grund High 89
 - 6.4. Natural analogies and comparison with other studies 92
- 7. Implications for hydrocarbon exploration 95**
- 8. Conclusions..... 96**
- 9. Recommendations for future work 98**
- 10. Acknowledgements 99**
- 11. References 100**
- 12. Appendices 103**

1. Introduction

The geology of the Dutch subsurface is characterized by a wide-array of different structures formed during various tectonic phases. By making use of a dense network of seismic lines and wells, a lot of these structures have been extensively studied, both on a regional and local scale. As a consequence, features corresponding to extensional- and compressional tectonics have been widely recognized in the Dutch subsurface (i.a. Ziegler, 1990a; Ziegler1990b; Baldschun et al., 1991; Nalpas et al., 1995; De Jager, 2003; Geluk, 2005). Also the influence of Zechstein salt on the structural style of deformation and on stratigraphic depositional patterns has been widely recognized and intensively studied (i.a. Nalpas et al., 1995; Geluk et al., 2007; Ten Veen et al., 2012; Harding and Muts, 2015; Msc. Thesis van Winden, 2015).

A relatively underexposed research area in the Dutch subsurface are strike-slip tectonics. A likely reason for this is that strike-slip features are not easily recognized on seismic images, as they are characterized by complex vertical and horizontal geometries that change rapidly along strike and with depth (Sylvester, 1988; Mann, 2007; Dooley and Schreurs, 2012). Often, strike-slip movements are recognized when observed geometries, both structural and stratigraphic, can't be solely explained with extensional and compressional tectonics. For instance, Late Permian dextral strike-slip movements were recognized in the southern North Sea area due to systematic lateral displacements of alluvial fan systems along NW-SE striking faults (George and Berry, 1997). These observations fit within a regional framework of wrench tectonics that is widely accepted for the Permian and Late Carboniferous interval (Ziegler, 1990a; Mattern, 1996; Lamarche et al., 2002; Ziegler, 2004). Strike-slip movements have also been recognized in the Dutch subsurface when older fault trends are systematically being offset, when profound flower structures are present or when local zones of transpression and transtension are present. The latter observations have led to a number of strike-slip features that are related to Late Cretaceous/Early Paleogene inversion.

However, during the majority of the Mesozoic period; i.e. Triassic, Jurassic and Early Cretaceous periods, strike-slip movements have been barely recognized. During this time, the southern North Sea region underwent several active rifting pulses in an overall extensional setting. Normal movements are indeed dominant during this time period in the southern North Sea area. However, the formation of dominant structural trends such as the WNW-ESE to NW-SE alignments and possibly also the N-S alignment preceded the Mesozoic rifting phases as they originate from the Paleozoic Variscan or even Caledonian orogenies. This means that these trends were reactivated during the Mesozoic; initially by roughly E-W oriented extension in the Triassic and later by roughly NE-SW extension during the Upper Jurassic and Early Cretaceous (Munsterman et al., 2012). Hence, some of the older fault systems were oriented almost parallel to the direction of extension, making it highly plausible that they have accommodated strike-slip movements, thereby linking the normal movements in the active rifting basins and functioning as transform faults (Kley et al., 2008b). Some direct evidence of strike-slip motions along these preformed basement faults is present in the Dutch offshore; for example, the en echelon pattern of the Rifgronden fault zone bounding the Terschelling basin which indicates that it has accommodated dextral strike-slip movements (De Jager, 2007). Usually though, direct evidence of Mesozoic strike-slip movements on preformed basement faults is absent, likely because of the complex reactivation history of the faults and because of the presence of a thick layer of remobilized Zechstein salt. Also the timing and amount of displacement on these preformed basement faults is poorly constraint. Additionally, supra salt Mesozoic strike-slip motions in the northern Dutch offshore are often neglected or poorly understood in terms of timing, sense and amount of displacement and fault salt interaction.

Hence, the main aim of this study is to gain better insight into several strike-slip features in the northern Dutch offshore during the Mesozoic (see fig. 4 for the outline of the wider study area). To achieve this, the following research questions are addressed in this study;

- Where are Mesozoic strike-slip faults located in the northern Dutch offshore?
- What is the timing, sense of displacement and amount of displacement of the identified strike-slip faults in the Northern Dutch offshore?
- How are strike-slip motions on subsalt preformed basement faults distributed into the supra salt interval in a salt-dominated basin?
- Are the identified strike-slip faults linked to deeper rooted basement faults?

To answer these research questions, this study consists of the following parts;

- 1) Regional identification of strike-slip faults at various Mesozoic stratigraphic levels in the northern Dutch offshore, based on literature and regional seismic interpretation.
- 2) Four in depth case studies of strike-slip faults in the Northern part of the Dutch offshore via detailed 3D seismic interpretation by making use of stratigraphic thickness maps and seismic attribute maps
- 3) Analogue Modelling performed at the Tectonics lab of Utrecht University on strike-slip faults and their interaction with salt. The aim of this part is to learn more about the distribution of strike-slip faults along preformed basement faults in a salt dominated basin.
- 4) The integration and interpretation of the results of part 1,2 and 3.

2. Background

In this section, some research background will be given regarding the geological history of the Northern Dutch offshore (section 2.1), the main stratigraphic groups (section 2.2), as well as the main structural elements encountered in the research area (section 2.3). Additionally, previous work on strike-slip tectonics in the Dutch subsurface will be discussed in section 2.4. Finally, some relevant findings from extensional and strike-slip analogue models including a weak layer to represent salt, will be discussed in section 2.5. These sections will allow the reader to better understand and appreciate the present research, which methods will be described in section 3.

2.1 Geological history of the Northern Dutch Offshore

In the following sections, a general geological history of the Northern Dutch offshore is given in the wider context of the southern North Sea area that developed as part of the Central European Basin (CEB) system. The main tectonics events that have affected the geological evolution of the Terschelling Basin are (Ziegler, 1990; Geluk, 2005):

- The Paleozoic Caledonian and Variscan orogenies
- An Early to Middle Permian phase of wrench tectonics
- Mesozoic rifting phases
- Alpine inversion phases

2.1.1 Paleozoic

Several compressional tectonic phases occurred in the present Southern North Sea Area during the Paleozoic. These compressional tectonic phases were caused by the convergence of a number of tectonic plates including; Baltica, Laurentia, Gondwana and the microcontinent of Avalonia.

At first, during Ordovician to Silurian times, Baltica and Laurentia collided, subsequently forming the continent of Laurussian. A few million years later, the Gondwana-derived Avalonia microcontinent, which included the stable London Brabant Massif, collided with the southern edge of Baltica. Due to this collision, Avalonia was incorporated into the Laurussian continent. Both events are generally known as the Caledonian orogeny (Ziegler, 1990b). A recent study suggests that the suture zone between Baltica and Avalonia is located in the subsurface of the Netherlands; trending NW-SE (Smit *et al.*, in press). This implies that the basement crust in the southern part of the Netherlands is derived from the Avalonia continent, while the basement rocks in the northern part of the Netherlands is derived from the Laurussian continent. After the formation of the Laurussian continent, which was now composed of Avalonia-, Laurentia- and Baltica derived continental fragments, the Iapetus Ocean between Gondwana and Laurussia gradually closed. During the Early Carboniferous, the Iapetus Ocean had fully closed due to ongoing subduction underneath the Laurussian continent. The subsequent full-scale collision resulted in the Himalaya type Variscan orogeny, towards the south of the current North Sea area (Geluk, 2005; De Jager, 2007). The most northern position of this Variscan fold and thrust belt runs approximately W-E through Belgium, and central Germany, just south of the Netherlands (De Jager, 2007). No evidence of Variscan compressional tectonics is found in the southern North Sea Area. Instead, the Southern North Sea area, including the Northern Dutch offshore, developed as a foreland basin during the Late Carboniferous. Thick Carboniferous sequences of the Limburg Group were deposited in this foreland basin, locally exceeding 5500m in the northern Dutch offshore area (Ziegler, 1990a). These deposits are often characterized by large amounts of organic material, as the Southern North Sea area was located just south of the equator during this time.

Towards the very end of the Carboniferous, the tectonic regime in the Carboniferous foreland basin changed, as the area was affected by post-orogenic collapse of the Variscan orogeny and associated wrench tectonics caused by ongoing crustal shortening in the Uralian and Appalachian domains (Ziegler, 1990a; Geluk, 2005; De Jager, 2007) These wrench tectonics led to transtensional faulting,

which was accompanied by intrusive and extrusive magmatic events and subsequent thermal uplift during the Early and Middle Permian. Faults that were active during this period, particularly show a NW-SE to WNW-ESE lineament in the Southern North Sea area (Ziegler 1990a; Schek-Wenderoth and Lamarche, 2004; Schroot and De Haan, 2003; Van Duin *et al.*, 2006). However, the NW-SE strike of the Avalonia-Baltica suture zone might indicate that this approximate NW-SE alignment was already established during the Caledonian orogeny. The thermal uplift caused by the Early to Middle Permian heating event caused widespread and deep erosion in the southern North Sea area, leading to significant hiatus of 60 to 70Ma. This hiatus is commonly known as the Saalian erosional phase in its broader sense (Ziegler, 1990a; Geluk, 2005; de Jager, 2007). Towards the end of the Permian, the lithosphere of the Southern North Sea area had cooled down again and consequently began to subside. This subsidence due to thermal sag led to the formation of a large E-W trending basin that stretched from current Great Britain to Poland, commonly known as the Southern Permian Basin (Fig. 1)(Bachman and Kozur, 2003 Geluk, 2005; van Wees *et al.*, 2000; de Jager; 2007). Towards the end of the Permian, the southern North Sea area had moved out of the equatorial zone and was now located around 20degrees north, where arid conditions prevailed (Geluk, 2005). Sediments of the Rotliegend Group were deposited in this arid environment. Because subsidence rates exceeded sedimentation rates, the area became landlocked (Ziegler, 1990a). During the Late Permian, seawaters invaded the landlocked basin episodically, leading to the cyclic deposition of the evaporites of the Zechstein Group (Geluk *et al.*,2007).

2.1.2 Mesozoic and Cenozoic

During the end of the Early Triassic, continental break-up of the Pangea super continent initiated in the North Atlantic (Ziegler, 1990b). A branch of this rift system extended southward into the current southern North Sea area and caused E-W rifting during the Middle and Late Triassic (Ziegler, 1990a; Ziegler, 1990b; Kockel, 1995; Geluk, 2005). Several rifting pulses occurred in the southern North Sea area during this time period. Each rifting phase was preceded by a thermal heating event and initial uplift, leading to several regional unconformities such as Hardegsen unconformity and the Early Kimmerian unconformity. After each rifting phase, a period of tectonic quiescence followed due to regional thermal subsidence. The biggest tectonic pulse though occurred during the Middle Jurassic (158-154Ma) (Ziegler, 1990a; van Duin *et al.*, 2006). During this time, thermal doming related to mantle plume activity caused widespread uplift and subsequent erosion in the southern North Sea area, leading to the formation of the Mid-Kimmerian unconformity. This heating event was followed by a period of NE-SW extension during the Upper Jurassic and Lower

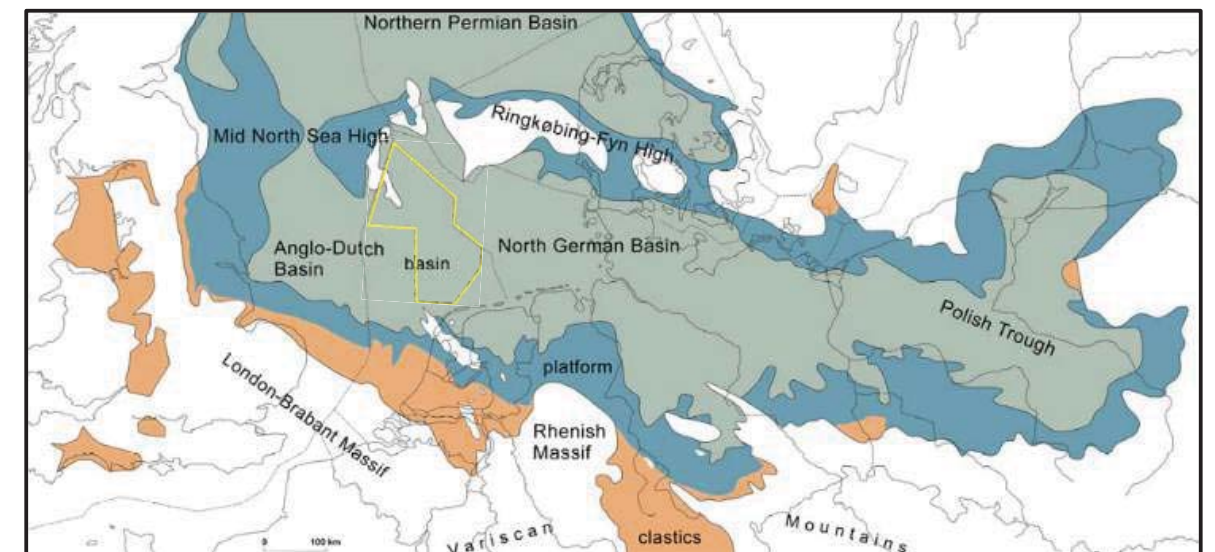


Fig.1. Map showing the Southern Permian Basin during the end of the Permian. White areas indicate crystalline Massifs, proximal areas are indicated in orange, green and blue indicate the outline of the distal part of the Southern Permian Basin. The research area of this study is indicated in yellow. Figure from Geluk, 2005.

Cretaceous in the southern North Sea area, forming new NW-SE faults but also reactivating older fault trends. Crustal extension was accommodated over a broad area, but most extension was created in the structural lows such as the Terschelling Basin and West Netherlands Basins, which subsided significantly due to their preformed basement structures that were favorable for reactivation by NE-SW extension. Additionally, significant subsidence occurred in the Dutch Central Graben during this time period. The basins were filled during the Upper Jurassic with detritic material that was derived from the rift shoulders. Towards the Middle Cretaceous, the North Atlantic had opened and active Mid-Oceanic spreading took place in this area. As a consequence, crustal extension focused in the North Atlantic and active rifting waned in the southern North Sea area (Ziegler 1988; 1990a; van Duin, 1996; De Jager, 2007). Because of thermal subsidence, though, the southern North Sea area continued to subside during the Middle and Late Cretaceous. As subsidence proceeded, depositional conditions gradually changed and over time the North Sea area evolved into a large open shallow marine basin (Ziegler, 1988; 1990a). During the early part of the Late Cretaceous, continental fragments of the African and Arabian lithosphere began to collide with Eurasia. This convergence led to the formation of the Alpine orogenic belt (de Jager, 2007). As convergence proceeded into the Late Cretaceous and Early Paleogene, compressional stresses from the Alpine convergence were increasingly transmitted into the Alpine foreland, including the Southern North Sea area, thereby reactivating older Variscan and Mesozoic faults and causing inversion tectonics (van Duin, 2006; De Jager, 2007). Inversion during this time is believed to have occurred during distinct pulses, of which the Laramide, Pyrenean and Savian inversion pulses were the most important (De Jager, 2007). Generally though, the Southern North Sea area continued to subside throughout the Cenozoic due to thermal subsidence. During the Neogene sedimentation rates increased, as large westward prograding deltaic systems deposited large amounts of sediments, derived from the Fennoscandian and Baltic shields, in the Southern North Sea area (Verweij, 2003; De Jager, 2007).

2.2 Stratigraphy

In this section, the most important stratigraphic groups in the northern Dutch offshore will be described. The stratigraphy in this section and in this report is based on the classification from Adrichem Booger and Kouwe (Fig. 2) (1993-1997). Where later revision has been applied on the stratigraphy, the concerning study is mentioned.

Limburg Group (DC)

The sediments of the Limburg Group comprise the Upper part of the Carboniferous. Sediments in the Limburg group are predominantly of siliciclastic and organic origin. The strata were deposited in the Variscan foreland basin (Kombrink, 2008). The Limburg Group is particularly known for its vast and good quality coal bearing formations, which also function as gas source rock in the northern onshore and offshore Netherlands.

Upper Rotliegend Group (RO)

Sediments of the Upper Rotliegend Group unconformably overlie sediments of the Limburg Group, separated by the Saalian Unconformity. Sediments in this stratigraphic group are mainly composed of siliclastic sediments. Towards the basin margins, thick sandstone sequences were deposited, while argillaceous material was deposited in the basin center.

Zechstein Group (ZE)

The Zechstein Group mainly comprises evaporitic deposits, of which halite is predominant. The evaporites precipitated in several cycles during the time that the Southern Permian Basin became landlocked. Estimates of its original depositional thickness vary from 650m (Verweij and Witmans, 2009) to 1500m (MSc. Thesis van Winden, 2015).

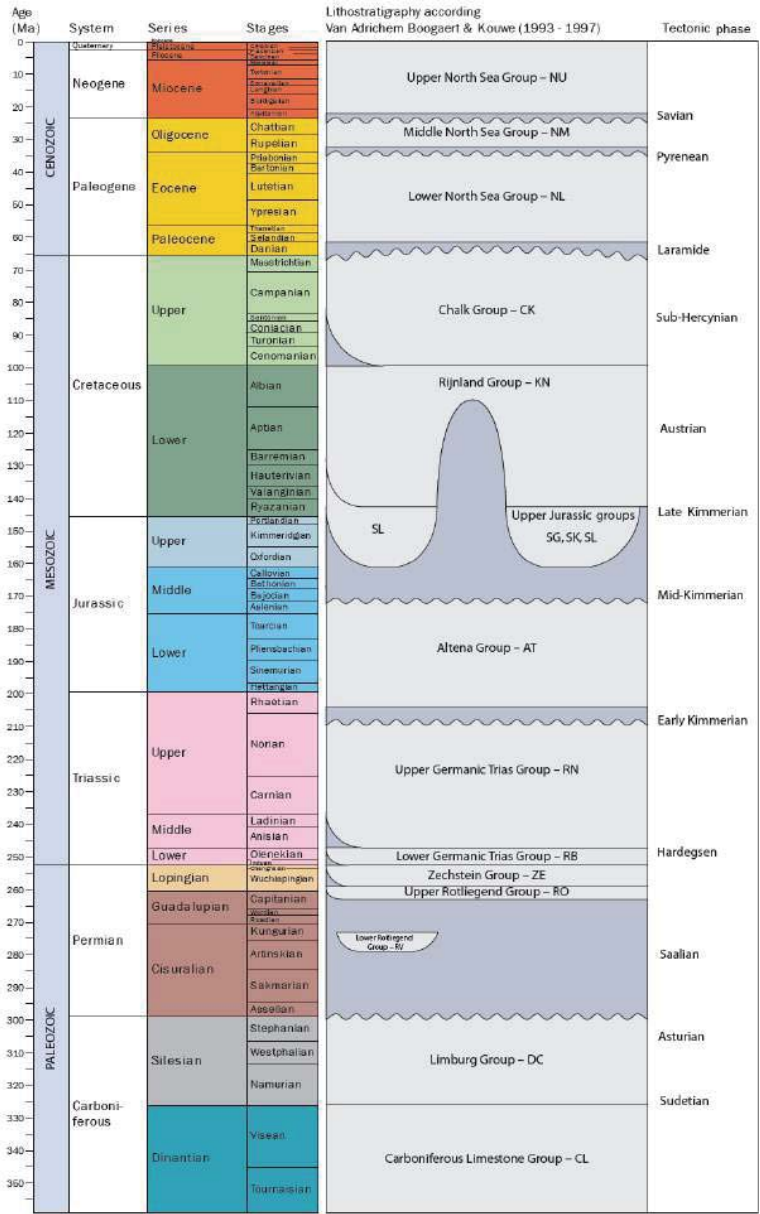


Fig.2. Schematic stratigraphic diagram of the Dutch subsurface, indicating the main stratigraphic groups according to van Adrichem Boogaart and Kouwe (1993-1997)

Lower Germanic Trias Group (RB)

The Lower Germanic Trias Group is comprised of sandstone and shale alternations. The sandstones of the Lower Germanic Trias Group are known for their good reservoir qualities and contain sufficient amounts of gas in the Dutch offshore, especially in the relatively thick and widespread Lower Volpriehausen sandstone formation. The sediments of the Lower Germanic Trias Group were deposited in a dry and hot environment that was characterized by endless flat plains where ephemeral braided streams and temporal lakes formed after occasional rains (Van der Zwan an Spaak, 1992)

Upper Germanic Trias Group (RN)

The Upper Germanic Trias Group comprises sediments of the Solling, Rot, Muschelkalk and Keuper formations. These formations are mainly comprised of evaporites and argillaceous sediments. In contrast to the sediments from the Lower Germanic Trias Group, these sediments were deposited in a marine environment that became landlocked several times.

Lower Jurassic Altena Group (AT)

The Altena Group comprises marine argillaceous sediments that were deposited during a period of Lower Jurassic quiescence during which the area of the northern Dutch offshore was gradually subsiding. During the latest part of the Lower Jurassic, closed and anoxic marine conditions due to Mid-Kimmerian uplift led to the deposition of the bituminous rich Posidonia shale formation in the Dutch Central Graben. This Mid-Kimmerian uplift and subsequent erosion are also the reason that the Altena Group has only been preserved in the Dutch Central Graben, the West-Netherlands basins and the Lower Saxony Basin.

Upper Jurassic Schielland (SL) and Scruff Group (SC)

The Upper Jurassic is characterized by a complex stratigraphic sequence comprising open marine, continental and various types of near shore deposits. The first characterization of Upper Jurassic sediments was made by Van Adrichem Boogaert and Kouwe (1997). The last few years, more data

has led to a better understanding of this complex stratigraphic interval. The Stratigraphic definitions adhered in this report are based on the new insights and definition as described by Abbink *et al.*, 2006 and Munsterman *et al.*, 2012 who classified the Upper Jurassic into 3 sequences (Fig. 3);

- Sequence 1 is the stratigraphic equivalent of the Schieland Group and is divided into 6 formations (fig. 4), which are generally characterized by Fluvio deltaic, near shore and marginal marine conditions. The following formations were recognized in case study B;
 - Lower Graben Formation, comprises fluvio-deltaic and coastal plain deposits
 - Middle Graben Formation, comprises lacustrine to marginal marine deposits
 - Upper Graben Formation, comprises marginal marine and barrier island deposits
 - Puzzle Hole Formation, comprises lower deltaic plain deposits as well as lagoonal, estuary and various types of near shore deposits. Due to this wide variety of deposits and continental signature with various channels providing the system with clastic input, the puzzle hole formation is characterized by a distinct slightly chaotic seismic response of high amplitude reflectors.
- Sequence 2 is the stratigraphic equivalent of the Scruff Group. In the northern part of the Dutch Central Graben, this sequence comprises the relatively deep marine sediments of the Kimmeridge Clay Formation. Further towards the south, coarser material was deposited in more lagoonal and near shore conditions, including the sands of the Terschelling Sandstone Member and the Noorvaarder Member.
- Sequence 3 mainly comprises marine deposits that are predominantly composed of shales. Although some sandstone intervals due occur.

Where possible, individual formations are indicated in this report(fig. 3), otherwise the Jurassic sequences 1, 2 and 3 are used for the interpretation of the seismic sections in this report.

Rijnland Group

Sediments of the Rijnland Group were deposited during the very end of the Late Jurassic (fig. 3) as well as during the Early Cretaceous. Sediments were deposited in open marine conditions. Sediment types include shales and marls. Especially at the base of the Rijnland Group, some sandstone intervals occur as well.

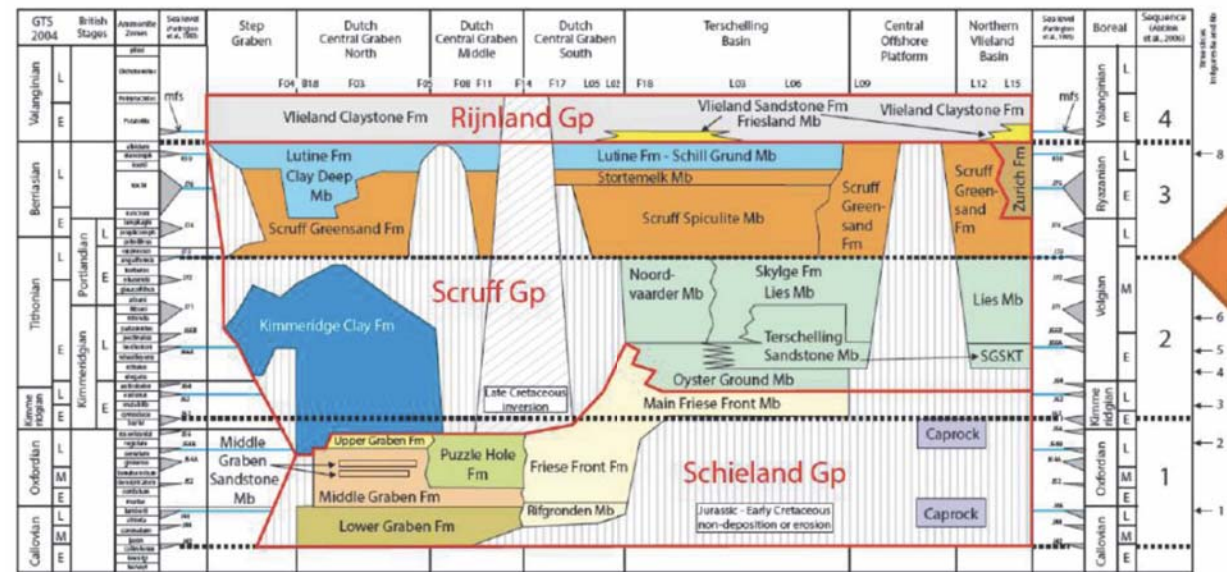


Fig.3. Stratigraphic diagram of the Upper Jurassic interval for the Northern Dutch offshore. Indicating the main stratigraphic groups, as well as the formations in which they are subdivided. Figure from Munsterman *et al.*, 2012.

Chalk Group

The Chalk Group comprises sediments of the Late Cretaceous and is mainly composed of carbonate successions that were deposited in a clear shallow marine environment. Deposition was of this stratigraphic group was often controlled by inversion tectonics.

Cenozoic sediments of the Lower-, Middle-, and Upper- North Sea Groups

Sediments in these groups were mostly deposited during shallow marine conditions and are characterized by prograding deltaic sequences that transported material from the Baltic and Fennoscandian shields towards the southern North Sea area. Sediment types include clays, silts and sands.

2.3 Structural elements in the Northern Dutch Offshore

The Dutch subsurface is divided in a number of regions based on stratigraphic similarities (fig. 4) (Heybroek, 1974; van Wijhe, 1987; van Duin *et al.*, 2006; Kombrink *et al.*, 2012). Three types of these structural elements exist; basins, platforms and highs. The term basin is applied for areas that are bounded by large normal/reverse faults and where at least Upper Jurassic strata have been deposited and preserved (van Duin *et al.*, 2006; Kombrink *et al.*, 2012). The term platform is used for areas where Late Kimmerian uplift and subsequent erosion has removed all of the Jurassic strata and parts of the Triassic strata. Permian strata have been preserved entirely on the platforms (van Duin *et al.*, 2006; Kombrink *et al.*, 2012). The term highs is used to describe areas where Late Jurassic uplift was strongest and where erosion has taken place down into Permian and Carboniferous strata (van Duin *et al.*, 2006; Kombrink *et al.*, 2012). Based on this classification scheme, which was first proposed by Heybroek (1974) and revised by Kombrink *et al.* (2012), the structural elements appear to be of Mesozoic origin. However, the major fault trends that are present in the subsurface of the Netherlands are of Variscan and possibly Caledonian origin. Hence, it is likely that the outline of the structural elements already formed before the Mesozoic. Nevertheless, the classification of the structural elements as redefined by Kombrink *et al.*, (2012) is adhered in this study because it immediately tells something about the deformation history of a region in terms of subsidence, faulting, uplift and erosion. In the following subsections, the main structural elements of the Northern Dutch offshore are briefly described.

Dutch Central Graben

The Dutch Central Graben is bounded in the east and in the west by roughly N-S trending faults. The base of the Zechstein Group increases gradually towards the north, where it lies deeper than anywhere else in the Dutch subsurface. The major opening of the Dutch Central Graben occurred in the Middle and Upper Triassic due to E-W extension. However, thickness maps of the Rotliegend interval indicate that it was already a low before this major E-W rifting phase, probably even in the Carboniferous (Ziegler, 1990a; Geluk, 2005). In the Dutch Central Graben, the entire Upper Triassic, as well as Lower Jurassic interval is present. However, Late Cretaceous inversion and subsequent erosion affected especially the southern part of the Dutch Central Graben. Due to this inversion, Cenozoic deposits directly overlie deposits of the Upper Jurassic sequence 1 in the center of the inverted Graben (Fig. 3).

Terschelling Basin

The Terschelling Basin is bounded in the north by the ENE-WSW trending Rifgronden Fault Zone and in the south by the ENE-WSW trending Hantum Fault Zone (Fig. 4). These fault zones are of Variscan and possibly Caledonian origin and have been repeatedly reactivated during Mesozoic times. The base of the Zechstein gradually increases towards the west, in the direction of the Dutch Central Graben. The area was affected by E-W extension, as is indicated by the presence of Upper Triassic low angle detachment and growth faults. However, the lack of major movements on N-S basement trends suggest that most of the E-W extension was accommodated in the Dutch Central Graben. During the Upper Jurassic, the Terschelling basin accommodated more extension as the HFZ

and RFZ were reactivated by the now NE-SW oriented stress regime. In the Terschelling Basin, Mid Kimmerian uplift and subsequent erosion has removed the Lower Jurassic strata as well as part of the Upper Triassic strata. Upper Jurassic strata of sequences 2 and 3 are deposited and preserved in the Terschelling Basin.

The Cleaverbank Platform, Elbow Spit platform and Elbow Spit High

This structurally high region is located west of the Dutch Central Graben and Step Graben and is part of the larger Mid North Sea High that stretches towards the northwest, into UK territorial waters (Fig. 4). On the Elbow Spit platform and Cleaverbank platform, Upper Cretaceous strata directly overlie Upper Triassic or Permian strata. On the Elbow Spit High, Upper Cretaceous strata directly overlie Carboniferous or locally even Devonian rocks. This area has likely been a high throughout the geological history, which has been attributed to the existence of a lower Devonian magmatic body, causing the crust to be relatively buoyant here (Donato *et al.*, 1983)

The Schill Grund platform and Central Offshore Platform

The Schill Grund Platform and Central Offshore platform bound the Terschelling Basin towards the north and the south (Fig. 4). On these platforms, Lower Cretaceous rocks overlie Lower Triassic rocks or locally Upper Triassic rocks. These areas have been affected by thin skinned extension during the Upper Triassic as is indicated by a zone of roughly N-S trending low angle detachment faults that developed above salt rollers and have accumulated thick sequences of Upper Triassic strata.

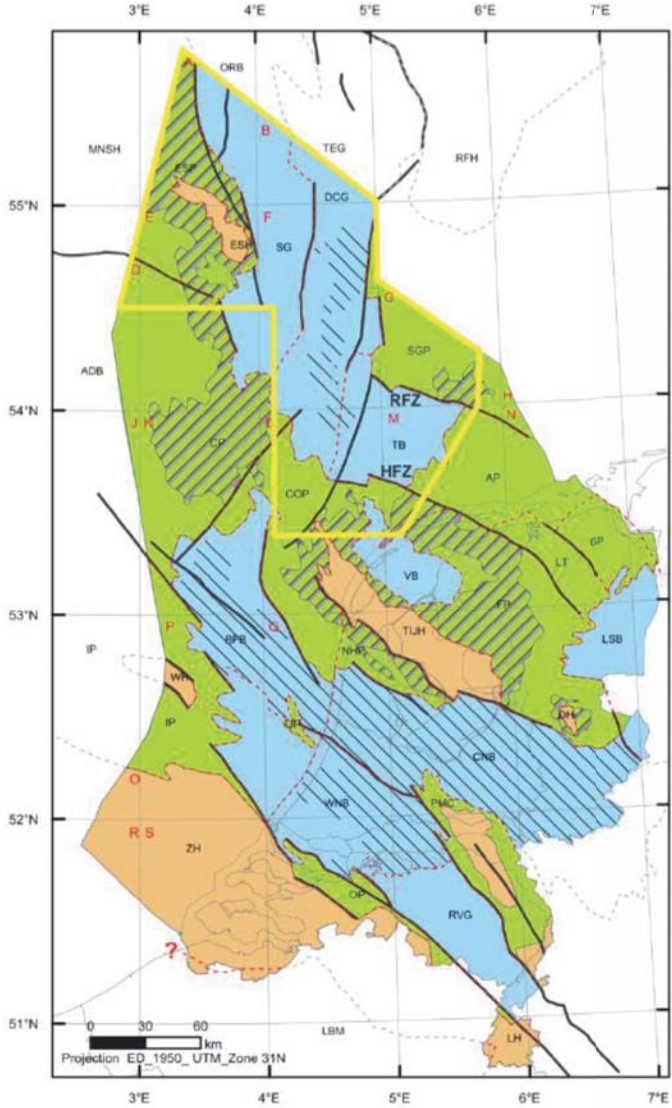


Fig. 4. Map indicating the structural elements of the Dutch subsurface. The outline of the research area is indicated in yellow RFZ = Rifgronden Fault zone; HFZ = Hantum Fault zone Figure from Kombrink *et al.*, 2012

2.4 Strike-slip tectonics in the Dutch offshore; *What is known?*

Although often overlooked or disregarded, some strike-slip motions have been recognized in the Dutch subsurface. This section summarizes some of the previous work that has been done on strike-slip tectonics in the Dutch subsurface.

2.4.1 Late Paleozoic wrench tectonics

The first episode of strike-slip faulting that is recognized in the Dutch subsurface are the Late Carboniferous to Early Permian wrench tectonics (Ziegler, 1990a; Geluk, 2005; Gast and Gundlach 2006). With the term wrench is meant that deformation occurred in a zone of overall strike-slip and extension (transtensional) movements. These wrench tectonics are believed to have been caused by ongoing crustal shortening in the Urals and the Appalachians, creating a dextral mega-shear system that accommodated these motions in the present Southern North Sea area (Arthaud and Matte, 1977; Ziegler, 1990a). This wrench model for the early Permian is supported by the presence of small pull-apart basins where early Permian sediments were deposited in the Elbe fault system as well as close to the Teisseyre-Tornquist zone (Kiersnowski and Buniak, 2006). Additionally, the en echelon pattern of sub-basins that developed in the Southern Permian Basin area during the Early and Permian favors this tectonic model. In the Dutch and in the UK sectors of the southern north sea, strike slip-motions as part of the regional wrench tectonic system are indicated by the presence of early Upper Rotliegend fans that display a systematic lateral displacement along synsedimentary faults (George and Berry, 1997). George and Berry (1997) concluded that the systematic rejuvenation trend of these fans indicates that dextral faults were active during deposition of these fans along NW-SE trends in the Southern North Sea area (Fig. 5). More recently, an internal TNO project has revealed a SE-NW trending fault in the northern Dutch offshore as well (de Bruin *et al.*, 2015). The vertical geometry of this fault, its upward widening fault pattern and the concave upward bending of strata on either side of the fault plane indicate that this fault accommodated strike-slip motions. The thickening of Upper Rotliegend strata in the downthrown side of the fault, has led to the conclusion that this fault was active during deposition of the Upper Rotliegend.

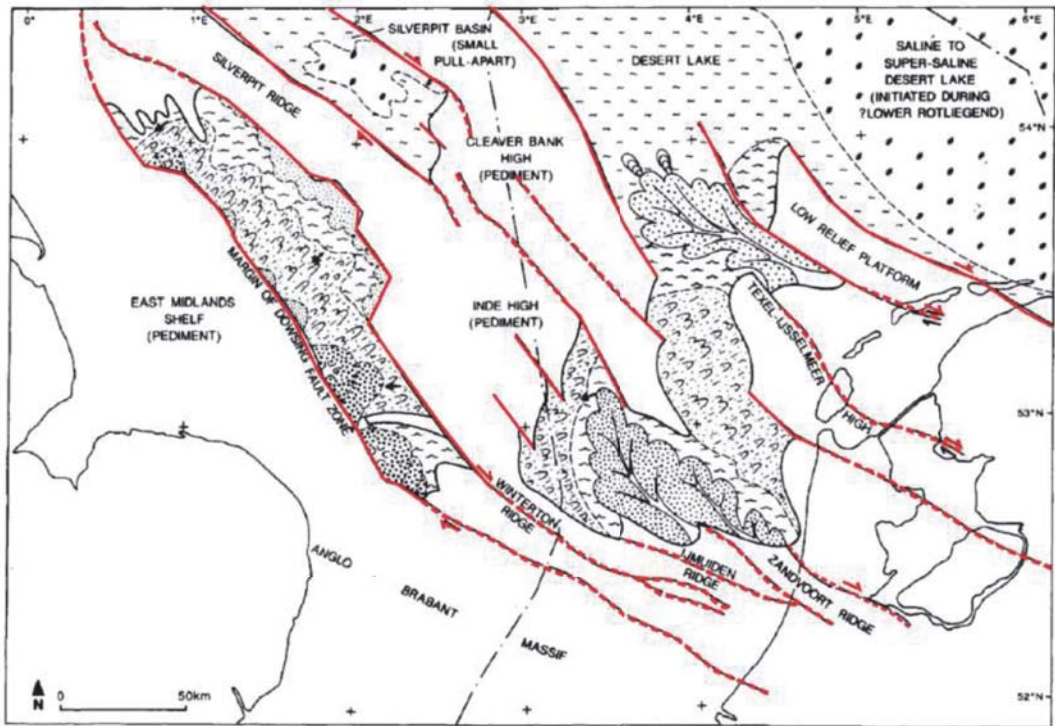


Fig. 5. Interpretation of the Upper Rotliegend depositional environment by George and Berry (1997) According tot his model deposition of alluvial and detaic fan deposits were influenced by dextral strike-slip faults during the Early part of the Upper Rotliegend. Figure from George and Berry (1997)

2.4.2 Mesozoic strike-slip movements in an extensional regime

While the transtensional tectonic model is widely accepted for the Upper Carboniferous and Rotliegend interval, strike-slip movements in the Mesozoic have not been recognized extensively in the Southern North Sea Area as it is commonly accepted that regional pulses of extension prevailed during this time period. However, according to the regional tectonic model for the Central European Basin system from Kley et al., 2008, strike-slip faults also occur in an overall extensional setting to accommodate differential motions on preformed basement faults. Kley et al., (2008) state that the opening of a set of parallel grabens (including the Central Graben, Horn Graben and Glückstadt Graben in Fig. 6) during the Triassic must have led to strike-slip faults at the northern and southern edges of these grabens to accommodate the motions that resulted from the active rifting of these grabens. This tectonic model is supported by the presence of an echelon faults towards the north of these four parallel grabens (indicated in red in Fig. 6). Additionally, strike-slip motions towards the south of these grabens could have been accommodated by Variscan inherited NW-SE trending faults (Kley et al., 2008), although direct evidence on these complex fault systems is not observed.

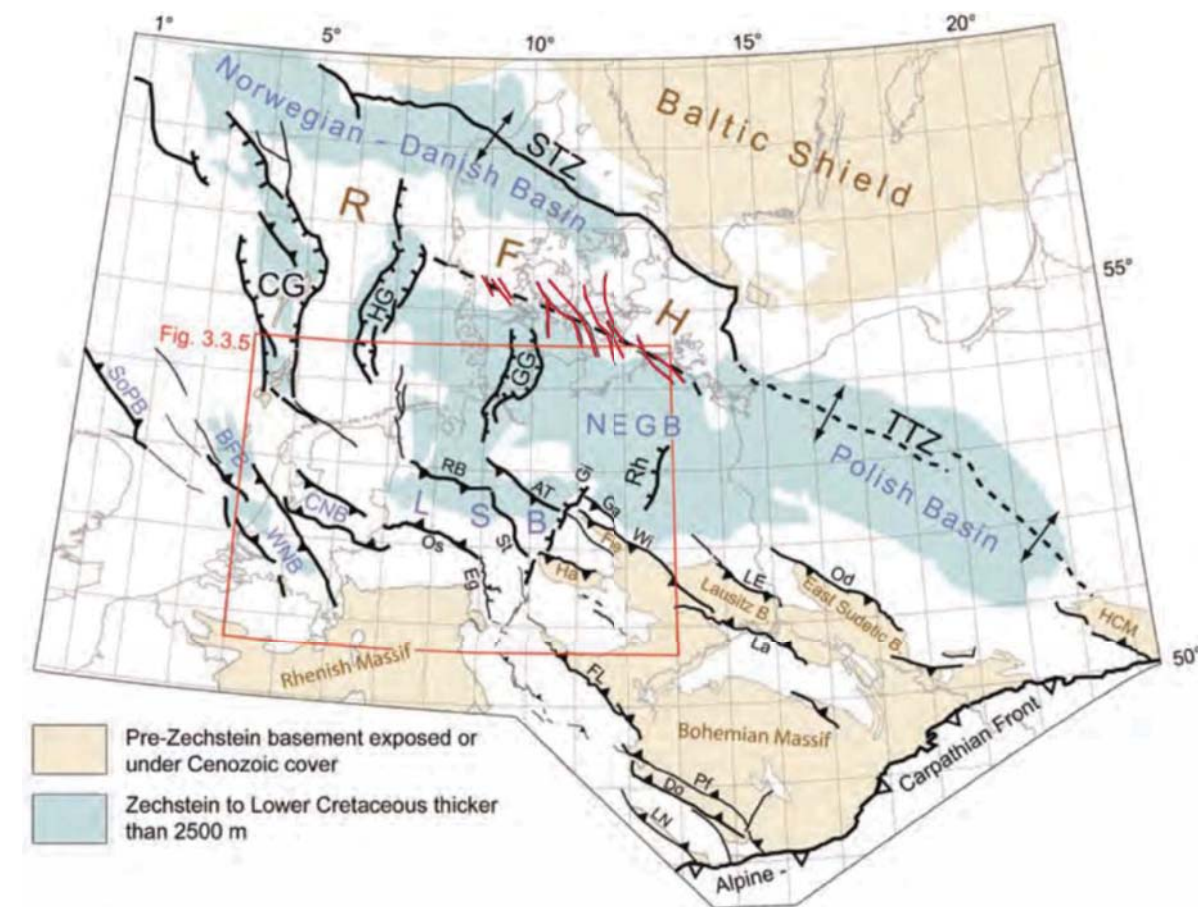


Fig. 6. Map showing the structural framework of the Central European Basin or Southern Permian Basin. Abbreviations are: Fault zones/structures (black): STZ Sorgenfrey-Tornquist Zone, TTZ Teisseyre-Tornquist Zone; CG, HG, GG Central, Horn and Glückstadt grabens, Rh Rheinsberg Trough; RB Rheder Moor-Blenhorst, AT Allertal, Gi Gifhorn, Ga Gardelegen, Wi Wittenberg, LE Lausitz Escarpment, La Lausitz Thrust, Od Odra, Os Osning, St Steinhuder Meer, Eg Egge, FL Franconian Line, LN Landshut-Neuötting, Do Donau, Pf Pfahl. Subbasins (blue): SoPB Sole Pit, BFB Broad Fourteens, WNB West Netherlands, CNB Central Netherlands, LSB Lower Saxony, NEGB Northeast German. Basement highs (brown): RFH Ringkøbing-Fyn High; Ha Harz, Fle Flechtingen High, B. "Block", HCM Holy Cross Mountains. Figure from Kley 2008b.

2.4.3 Late Mesozoic/Early Paleogene strike-slip movements in a compressional regime

During the Late Cretaceous and Early Paleogene Alpine inversion pulses, dextral reactivation along NW-SE fault trends in the Broad fourteens basin and in the West Netherlands Basin occurred due to N-S compression (Brun and Nalpas, 1996; Racero-Baene and Drake, 1996; De Jager, 2007). These strike-slip movements have been widely recognized, i.a. via flower structures that offset strata up to and including the Cretaceous interval. A well known example of a strike-slip formed hydrocarbon trap is the Pijnacker oil field (Racero-Baene and Drake, 1996). In the Lower Saxony Basin, also the Schoonebeek Graben was inverted with a dextral component during this time period (MSc. Thesis Smoor, 2016).

2.5 Analogue modeling background on extension and strike-slip in the presence of a weak layer

Basins that contain a thick sequence of ductile substrates (e.g. evaporates or shales), tend to deform in a different way than basins that lack the presence of such a sequence (Hudec and Jackson, 2007). This can be attributed to the mechanical properties of salt, which are inherently different from siliciclastic and carbonate rocks. For instance, salt is incompressible which causes it to be less dense than its overburden. Additionally, salt has the tendency to flow under geological conditions, as it deforms visco-elastically (Spiers *et al.*, 1990; Hudec and Jackson, 2007). This material behavior can be attributed to its mechanical weakness, which causes salt to decouple, or isolate the rock units above and below the salt in such a way that the deformation pattern of the two units differs (Vendeville and Jackson, 1992). The degree of similarity in the structural deformation style of the two units depends both on the thickness of the ductile layer, the rheology of the ductile layer and the rate of deformation (Vendeville and Jackson, 1992; van Keken *et al.*, 1993). Much of what we know today on the structural style of deformation in salt controlled basins comes from analogue modeling. Hence, some main findings from analogue models on the behavior of a weak layer in both an extensional and strike slip regime are described in this section.

2.5.1 Salt tectonics under extensional conditions

The ascent of salt and the subsequent formation of various kinds of salt structures had long been solely ascribed to density differences between the salt layer and the overburden that were assumed to be inherently unstable (i.a. Trusheim, 1960). According to this model, first described by Trusheim (1960), diapiric rise is a spontaneous process, triggered by Rayleigh-Taylor instabilities (similar to the ascent of a relatively dense fluid in a less dense fluid) and hence independent of regional tectonics. Supra salt extensional faulting was by these authors ascribed to be caused by the intrusion, withdrawal or dissolution of salt. In contrast to this, Vendeville and Jackson (1992) showed that salt diapirism is in general triggered by regional tectonics. Under extension, salt diapirism occurs in response to regional thin skinned extension of the brittle overburden rather than vice versa. This thin-skinned extension can either be caused by regional crustal scaled extension or by gravitational gliding. Based on analogue modelling, Vendeville and Jackson (1992) extensively describe three stages of salt ascent in an extensional setting;

- 1) The Reactive stage; During this stage, salt ascends in response to normal faulting and associated graben formation in the overburden (fig. 7). Salt is able to do so because faulting decreases the thickness of the overburden, thereby making it mechanically weaker. Additionally, the thinning of the overburden creates differences in supra salt loading. Since the pressure at the top of the salt layer, caused by the overlying rock column is lowest at the point where the roof is thinnest. Salt will preferentially ascent at this place.
- 2) The Active Stage; when the graben above the salt becomes deeper than a certain threshold and the roof is sufficiently thinned; the diapir pierces through the remaining part of the overburden, thereby shouldering aside the remaining material. During this stage, the diapir will emerge at the surface. And may start to extrude when sedimentation rates are too low in order to keep pace with the ascent of salt.
- 3) The Passive Stage; When the accumulation of sediments around the diapir balances the net ascent of salt, the diapir is able to grow vertically due to the down building of sediments around the diapir. If regional extension continues, the diapir will also widen.

Regional sedimentation has a profound influence on salt ascent and the evolution of diapirism (Vendeville and Jackson, 1992; Scheffer, 2016). High rates of sedimentation during extension tends to fill the grabens created during thin skinned extension, thereby maintaining the strength of the overburden. Consequently, high rates of sedimentation keep diapirs longer in the reactive stage because the thin-skinned graben is filled with sediments. Vendeville and Jackson (1992) found in their analogue models that the ascent of diapirs could be stopped if sedimentation is fast enough to counteract the thinning of the overburden caused by extension.

Sedimentation doesn't only influence the ascent of salt, locally it is also controlled by the ascent of salt itself. (Trusheim, 1960; Vendeville, 2002). According to a reinterpretation of Trusheim's model (1960) by Vendeville (2002), the initial thinning of strata towards a diapir, which is often observed in salt dominated basins, can be explained by a so called pillowing stage of the diapir. This pillowing stage (or reactive stage in the model from Vendeville and Jackson, 1992) leads to initial uplift of the area above the salt structure, causing the strata to thin towards the salt structure (Fig. 7.). When active piercing of the salt structure has occurred and the salt structure ascends passively, salt is withdrawn from the basal layer in the proximity of the salt structure, leading to subsidence around the ascending salt structure. This is a very effective way of increasing accommodation space around the salt structure and leads to the formation of a thick rim syncline around the salt structure (Vendeville, 2009; Harding, 2015). Overall, it can be concluded that the interplay between regional tectonics, rheological properties and sedimentation controls the exact structural style of deformation in salt dominated basins.

Salt Rollers

If one supra salt graben fault during the reactive stage, accommodates more subsidence than the other one, an asymmetric salt structure, generally known as a salt roller, is formed (Fig. 8) (Bally *et al.*, 1981; Brun and Mauduit, 2009). Such a structure is inherently asymmetric and when sufficient amounts of sediments are deposited, the salt will not reach the active diapir stage, but a listric growth fault will develop that detaches on the salt. When extension continues and sedimentation rates remain relatively high, a thick package of growth strata can develop in the hanging wall of the listric fault, thereby causing the pre-kinematic layer to drift away from its original position.

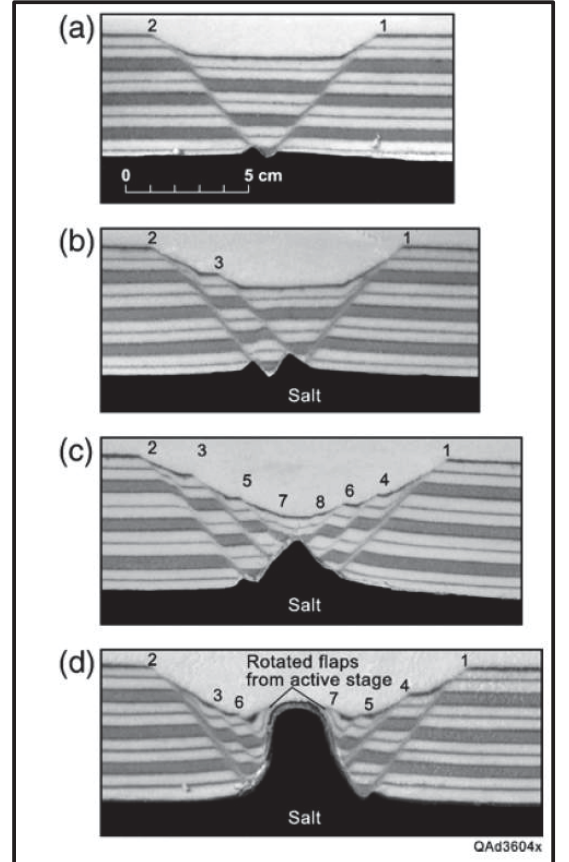
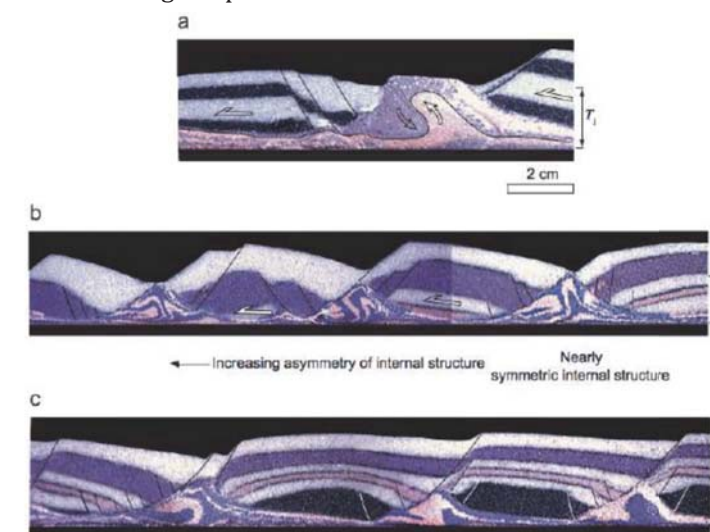


Fig. 7. Cross section through an analogue model indicating reactive- (A,B and C) and active (D) stage of salt ascent under regional extension. A) the first ascent of putty is triggered due to the thinning of its roof. This process continues in image B. C) The diapir is about to shoulder aside the overburden. D) the active stage of diapirism is reached. Figure from Hudec and Jackson, 2007.

Fig. 8. Three images from salt rollers in analogue models. A) active diapir, not enough sedimentation and overburden relatively thin. B) Almost piercing salt structures underneath symmetrical (right) and asymmetrical (left) faulting. C) Asymmetrical salt rollers with listric faults. Note the downlapping of strata in the hanging wall of the listric fault. Figure from Brun and Mauduit, 2009.

2.5.2 Salt tectonics under strike-slip conditions

Pure brittle strike-slip experiments

Strike-slip motions are characterised by complex 3D geometries, which rapidly change along strike, with depth and with continuous deformation. Due to their complex nature, and the difficulty of recognising strike-slip movements in seismic data, analogue modelling is a powerful tool that can help to better understand the structural evolution of strike-slip faults. The first strike-slip models

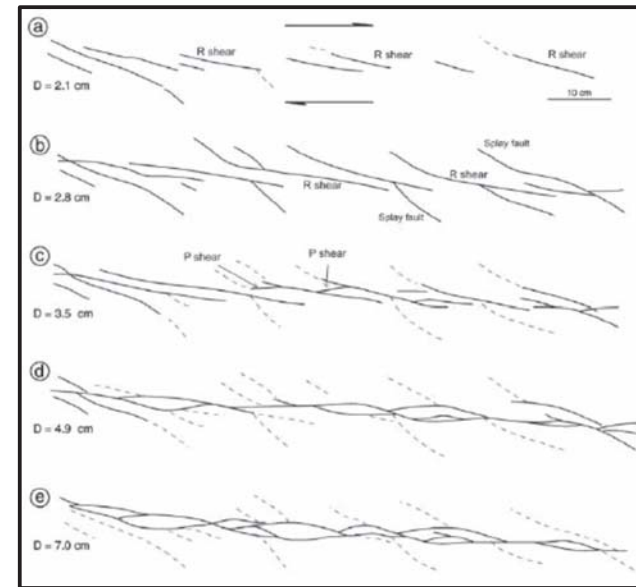


Fig. 9. Evolution of faults during a dry sand classic Riedel experiment. First R shears and splay faults form which are then subsequently linked by P shears to form anastomosing fault zone. Figure modified from Naylor *et al.*, 1986

investigated pure-strike-slip motions of a single brittle layer, underlain by a moving base plate. These experiments are generally known as the classic Riedel experiment (Riedel, 1929; Tchalenko, 1970; Richard *et al.*, 1995). These Riedel experiments describe the subsequent formation of R-shears, splay faults and P shears into an anastomosing main displacement fault zone that accommodates strike-slip motions after significant amounts of base plate displacement (Fig. 9, 10). Various amounts of classic riedel experiments have been published using different brittle materials such as (wet) clay, sand and glass beds (Tchalenko, 1970; Atmaoui *et al.*, 2006). The formation of local zones of transtension and transpression has also been studied, this is generally done by adding a step in the base plate (i.a. Dooley, 1994; Smit, 2008a; Smit, 2008b). All of these experiments have been particularly useful to better understand the geometries and evolution of large strike-slip zones that form in the absence of an upper crustal weak layer.

Multilayer strike-slip experiments

However, like in an extensional setting, the presence of an upper weak layer, such as an evaporite layer, has a profound influence on the style of deformation during strike-slip motions. Analogue models performed by Smit (2005) and by Dooley and Schreurs (2012) show that the presence of a weak body in the experiment causes either left or right stepping of the main displacement fault zone. Whether right or left stepping of the main displacement fault zone occurs, depends primarily on the initial geometry of the weak body with respect to the main displacement zone (Fig. 11). From Fig. 11 can also be inferred that the strike-slip faults deviate from their original strike as they approach the weak body, thereby showing a curved geometry towards the weak body. The right or left stepping of the main strike-slip fault at the weak body causes either transtension (right stepping on a dextral strike-slip fault or left stepping on a sinistral strike-slip fault) or transpression (left stepping on a dextral strike-slip fault or right stepping on a sinistral strike-slip fault) (Dooley and Schreurs, 2012). These zones of transpression or transtension, also trigger movements of the weak body. The strongest movements occur in zones of transtension, when the weak body is actively forced upwards. The weak body also ascends in zones of transtension, but here it ascends in a reactive way due to the thinning of its roof.

The weak layer used in the above described experiment from Dooley and Schreurs (2012) was placed in the experiment with a controlled and preformed outline and geometry. However, when a uniform weak layer is deformed by a pure strike-slip basement fault, no profound diapirs form. In this case, more subtle, appendix-like salt structures form in the weak layer (Appendix A; Smit,

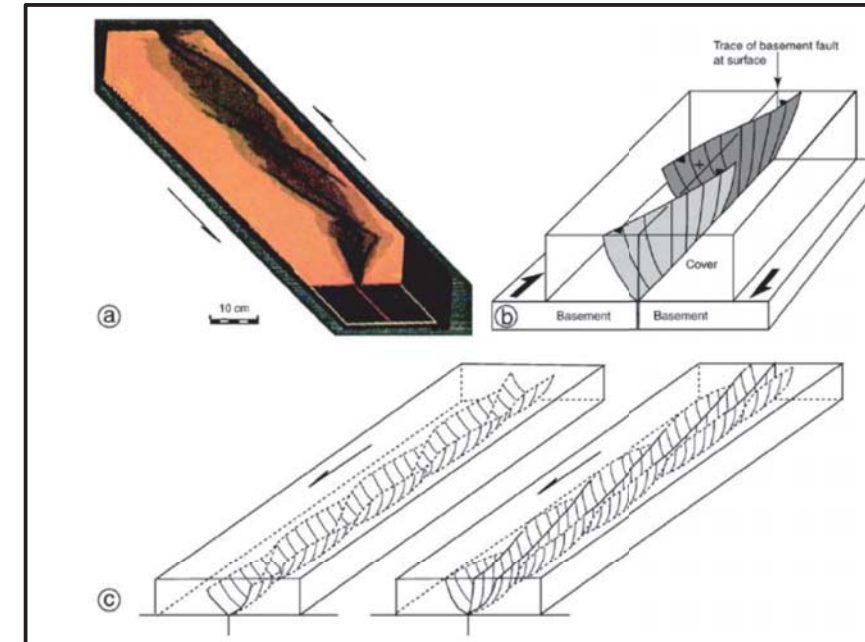


Fig. 10. Illustrating the curved concave upward geometry of R shears in a classic Riedel experiment. The R shears are en echelon arranged at the surface but with depth they root into the basement strike-slip fault. Figure from Dooley and Schreurs, 2012.

2016). The geometry of these structures is much narrower and more arcuate than salt walls and diapirs that form under extensional settings as described in section 2.5.1 (Smit, 2016). Salt ascent of an initial homogenous layer does occur in a pull-apart basin, but this is caused by local extension within the basin and the salt structures that evolve therefore show similarities with the salt structures formed under pure extension (Smit, 2008b).

Multilayer experiments with multiple deformation phases

To study the role of pre-existing normal faults above a basal ductile layer, Dooley and Schreurs (2012) applied two deformation phases. First a graben was created during extension. During the second phase, strike-slip deformation was applied via distributed strike-slip at the base of the ductile layer. They authors found that the strike-slip faults during the second phase of distributed strike-slip preferentially followed the outline of the preformed normal faults during the extension phase (Dooley and Schreurs, 2012). In their experiments, the ductile layer was positioned at the base of the experiment to simulate the presence of a ductile lower crust. Due to the relatively high viscosity of the weak layer, no significant uplift of this weak layer occurred during the extension phase. Hence, the base layer of silicon putty largely remained its original thickness during the extension phase. Because the strength of ductile and brittle materials depends on the thickness of the material, the model performed by Dooley and Schreurs (2012) was not characterised by large internal strength contrasts.

In the current study, analogue models are presented that were deformed by the same deformation as the models from Dooley and Schreurs (2012). However, the models in the current study, are composed of an initially uniform high layer of ductile material (silicon putty), underlain by a brittle basement to simulate the presence of an upper crustal evaporite layer.

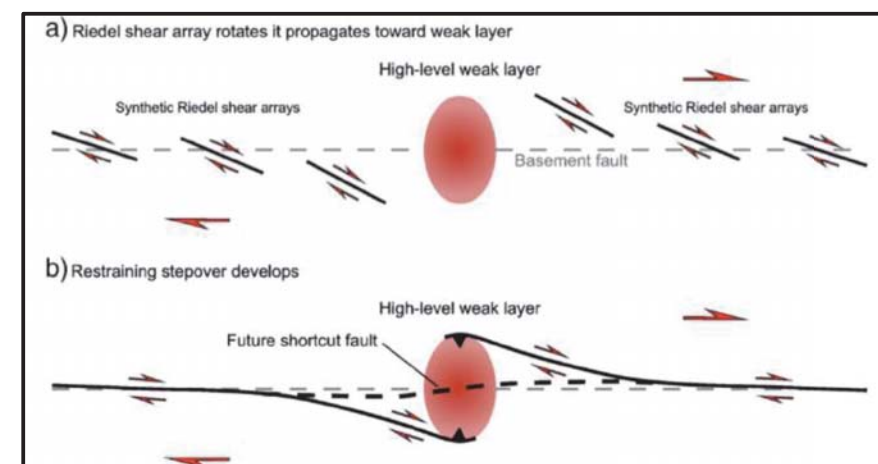


Fig. 11. Sketch illustrating the formation of a restraining step-over, over a high level weak layer. Note the rotation of the main strike-slip fault as it approaches the weak layer. Figure from Dooley and Schreurs, 2012.

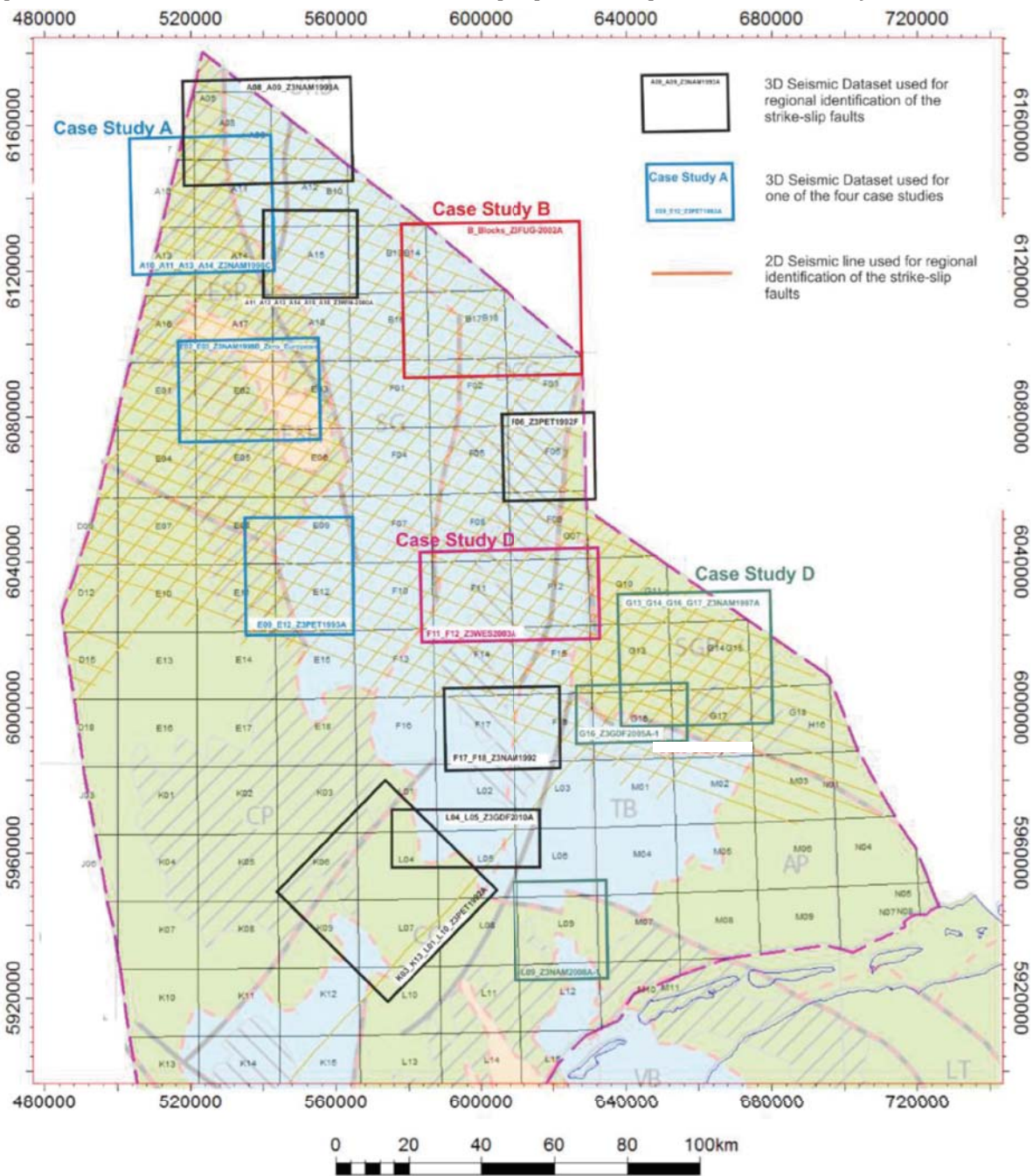
3.1 Seismic interpretation methods

The seismic interpretation part of the study consists of two sections;

- 1) Identification of strike-slip faults in the northern Dutch offshore with the purpose of locating strike-slip features in the northern Dutch offshore.
- 2) 4 in to depth case studies of strike-slip faults in the Northern Dutch offshore with the purpose of gaining a better understanding of specific structures in terms of timing, sense of displacement, amount of displacement and fault-salt interaction.

3.1.1 Identification of strike-slip faults in the northern Dutch Offshore

The first section of the seismic interpretation part of this study is the identification of strike-slip faults in the northern Dutch offshore. For this purpose, multiple 3D seismic surveys and 2D



applied either on a horizon, or on a seismic line, including a vertical time slice (Z-slice). A variety of seismic attributes exist and different software programs typically have developed their own seismic attributes. In this study, seismic attribute maps were constructed with OpendTect software. This software offers a wide variety of seismic attributes. The 3 attributes that were used the most are briefly explained below:

Similarity attribute;

A seismic dataset is composed of a 2D array of traces in the x and y direction. The traces are usually spaced in the order of 25m, depending on the resolution of the dataset. Each trace is composed of sample values in the Z direction (usually every 4mm), which contain information about the removal of the signal. The similarity attribute indicates how much a group of sample values on adjacent traces looks alike in terms of waveform and amplitude (OpendTect, manual) A similarity of 0 indicates that a group of samples on a specific trace is completely dissimilar to a group of samples on adjacent traces. The higher the similarity value, the more a group of samples on adjacent traces looks alike. A value of 1 indicates that they are completely similar. Hence, an area with a high degree of dissimilarity may indicate the presence of a fault or the presence of evaporites (which are usually characterized by a chaotic seismic signature). Stratigraphic features are slightly harder to detect with the similarity attribute (though not impossible), as stratigraphic features such as channels are often only defined in a seismic dataset by very subtle changes in amplitude.

Spectral Decomposition attribute;

The spectral decomposition attribute disentangles the seismic signal into the original frequencies of which it is composed. Therefore it applies basically a reverse Fourier Transform. This way, amplitude differences can be analyzed at a specific frequency, which might help to better detect subtle features that particularly stand out at a certain frequency. Spectral decomposition is particularly useful to detect and enhance very subtle stratigraphic features such as channels, turbidites and sedimentary fan deposits.

Case Study	Location of case study	Wells for which synthetic was created	3D surfaces created; base of stratigraphic intervals
A	Elbow High Spit High Elbow Spit Platform Step Graben	E02-01	Lower North Sea Group Zechstein Group
B	Northern part of Dutch Central Graben	B18-02, B18-03	Lower North Sea Group Chalk Group Base Rijnland Group Reflector in Kimmeridge Clay formation of the Scruff Group Scruff Group Schieland Group Altena Group
C	Central part of the dutch Central Graben	F11-02, F12-03	Puzzle Hole Formation Posidonia Shale Formation Altena Group Upper Triassic Muschelkalk formation
D	Terschelling Basin, northern part of the Central Offshore Platform and Schill Grund Platform	-	Rot evaporite Muschelkalk evaporite

Table 1. Table shows the formations that were mapped for the case studies and the wells for which synthetics were made.

3.2 Analogue modelling methods

3.2.1 Experimental set-up

The experimental set-up of the analogue models consisted of a plastic sheet (600x17x0.1cm), which lied upon a table (table2 in Fig. 14 and 15). Half of the model was built on top of the plastic sheet, the other half was build directly on top of table 2. Wooden bars (indicated in yellow in Fig. 14 and 15) were attached at the plastic sheet. One wooden bar on the long side and one wooden bar on the short side of the plastic sheet. These wooden bars were used to transfer the movement from the engine (positioned on table 1 and indicated in red in (Fig. 14 and 15) on to the plastic sheet. For the extension phase, the plastic sheet was pulled by the engine via the wooden bar on the long side of the plastic sheet (Fig. 14). For the strike-slip phase, the plastic sheet was pulled by the engine via the wooden bar on the short side of the plastic sheet (Fig. 15). To switch from extension to strike-slip or vice-versa, the engine was decoupled from the plastic sheet and the table on which the model was built, was rotated 90 degrees.

To record deformation during the course of the experiment, photographs were taken at regular time intervals (generally every 2 minutes), with a camera that was positioned above the model. When the experiment was finished, the experiment was covered with sand and subsequently poured with water to preserve the structures that had formed during deformation. To analyse the structures at the end of deformation, vertical cross-sections were cut with a knife at regular intervals.

In total, four analogue models are described and discussed in this report. In section 3.2.6 the experimental procedure of the four models, as well as their stratigraphic sequence is described. The following sections first describe the properties of the materials that were used to build the models and explain why these materials where used.

3.2.2 Material properties

Quartz sand was used to simulate the brittle behaviour of natural rocks in the upper crust. The quartz sand that was used had a density (ρ) of 1500kgm³, a grainsize between 100µm-300µm, a negligible cohesion (C) and a coefficient of internal (ϕ) of 0.58. Silicon putti was used to represent the ductile behaviour of salt under geological conditions. The silicon putti that was used in the experiments had a density of 970kg/m3 and a dynamic viscosity of 2.4*10⁴Pa.s.

In the following sections will be explained why these model materials were chosen and why the analogue models are a valid first order approximation of reality.

3.2.3 Scaling of the models

An analogue model that simulates a natural occurring process, can only be a good approximation of reality if it is geometrically, dynamically, kinematically and rheologically similar to the natural process. (Hubbert, 1937, Ramberg, 1981, Davy and Cobbold, 1991). If this is the case, the model will resemble a similar evolution as the process occurring in reality, even though the dimension (i.e. length width and height) scale is much smaller and the time-scale is much faster.

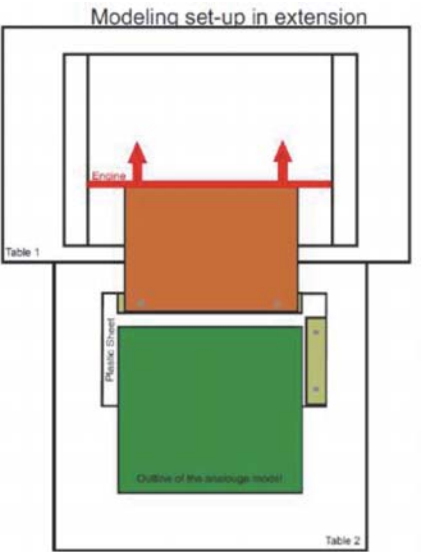


Fig.14. Schematic illustration of the experimental set-up during the extension phase

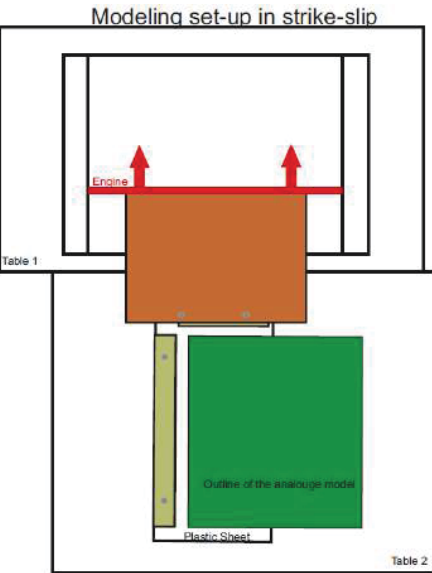


Fig. 15. Schematic illustration of the experimental set-up during the strike-slip phase

Scaling of dimensions

The scaling conditions that must be satisfied in order for analogue models to represent a natural process can be derived from the equation of dynamics (as performed i.a. by Davy and Cobbold, 1991; Brun, 2002; Smit, 2005) and are as follows;

$$\sigma^* = \rho^* g^* L^* \quad (1)$$

$$\varepsilon^* = g^* (t^*)^2 \quad (2)$$

Where σ is the vertical stress in Nm⁻², ρ is the material density in kgm³, g is the gravitational acceleration in ms⁻², L is the dimension of the model in m. The designation * refers to the ratio between the model and the natural prototype (e.g. $\sigma^* = \frac{\sigma_{model}}{\sigma_{natural prototype}}$).

Where $\rho^* = 1$ because the density of upper crustal rocks in nature (ranging from 2300kgm⁻³ to 3000kgm⁻³) and the density of quartz sand used in the laboratory (1500kgm⁻³) are in the same order of magnitude. Also $g^* = 1$, as gravity is approximately equal everywhere on earth. Therefore equation 1 can be written as:

$$\sigma^* \sim L^* \quad (3)$$

This means that the stress ratio has to be approximately equal to the ratio of dimensions for the model to be a realistic representation of the natural prototype. The dimension scale ratio (L^*) between the model and prototype is $L^* = 10^{-5}$, which means that 1cm in the experiment is approximately equal to 1km in nature.

Scaling of material properties.

Brittle materials

The brittle deformation of rocks is described by the Mohr coulomb criterion (Byerlee, 1978);

$$\tau = \mu \sigma_n = C \quad (4)$$

Where τ is the shear stress on the fault plane, σ is the normal stress on the fault plane, C is the cohesion of the material and μ is internal coefficient of friction. When dividing equation 4 by σ , substituting ρgh for σ and taking into account that the models should be dynamically scaled to nature according to equations 1 and 3, The following expression is obtained according to Bonini et al., 2000;

$$\mu_{model} = \frac{C_{model}}{\rho_{model} g L_{model}} = \mu_{nature} = \frac{C_{nature}}{\rho_{nature} g L_{nature}} \quad (5)$$

Besides the density and gravity values, also the values of μ_{model} and μ_{nature} are of a similar order of magnitude. Hence equation 5 can be written as follows;

$$\frac{L_{model}}{L_{nature}} \sim \frac{C_{model}}{C_{nature}} \sim L^* \sim C^* \quad (6)$$

Rocks in nature typically have a Cohesion around 50MPa. Since the length scale ratio (L^*) of the experiments is 10⁻⁵, it means that the brittle materials used in the models should have a negligible cohesion compared to natural rocks. Hence because of its negligible cohesion, its density, which is in the same order of magnitude as natural rocks, and its coefficient of friction, which is in the same order of magnitude as natural rocks, quartz sand is suitable to represent brittle deforming natural rocks.

Ductile Materials

The deformation of salt under geological conditions is described by multiple mechanisms, such as dislocation creep and diffusion creep. The dominant mechanism depends on the temperature conditions, grain sizes, strain rate and whether or not fluids are involved (Spiers et al., 1990; van

Keken et al., 1993). Ductile deformation can by approximation be described via a Dorn creep power law equation of the following form, (Goetze and Evans, 1979; Weijermans and Schmeling, 1986);

$$\dot{\varepsilon} = A \exp\left(\frac{-Q}{RT}\right) (\sigma_1 = \sigma_3)^n \quad (7)$$

Where $\dot{\varepsilon}$ is the strain rate in s⁻¹, Q is the activation energy in J, R is the gas constant in JK⁻¹mol⁻¹, T is the Temperature in Kelvin, $\sigma_1 = \sigma_3$ is the maximum differential stress Nm². A is a material constant and n is the stress exponent. Experiments have shown that it is a valid assumption to assume that salt behaves as a Newtonian fluid under geological conditions, which means that its resistance to flow is linearly dependent on the strain rate. (Spiers et al., 1990; van Keken et al., 1993). Hence, the silicon putti used in the experiments is a Newtonian viscous fluid, which yields that the stress exponent (n) in equation 7 is 1. Because Newtonian fluids deform (by approximation) by simple shear (Brun, 2002), the shear strain rate is used as an approximation for the strain rate; $\dot{\varepsilon} \sim \dot{\gamma}$. The shear strain rate of a Newtonian viscous fluid is described by the following equation (Spiers et al., 1990);

$$\dot{\gamma} = \frac{1}{\eta} \tau \quad (8)$$

Where η is the viscosity in Pa.s and where τ is the shear stress, which is related to the differential stress ($\sigma_1 = \sigma_3$) as follows:

$$2 \tau = \sigma_1 = \sigma_3 \quad (9)$$

By substituting equation 9 into equation 8 and by assuming that the shear strain rate can be used as an approximation to describe deformation of a Newtonian viscous fluid, equation 8 can also be written as follows (according to Brun 2002; Smit, 2005):

$$\dot{\gamma} = \frac{\sigma_1 - \sigma_3}{2\eta} \text{ or } \dot{\varepsilon} = \frac{\sigma_1 - \sigma_3}{2\eta} \quad (10)$$

Like the brittle part of the model, also the use of the silicon putti has to be scaled down to values according to equation 3. This means that the following equation has to be satisfied;

$$\dot{\varepsilon} = \frac{\sigma^*}{\eta^*} \quad (11)$$

Where η is the viscosity in Pa.s and the designation * refers again to the ratio between the model and the natural prototype. Experiments have shown that for relatively high-temperature conditions and a small grain size, the viscosity of salt in nature is around 10¹⁷Pa.s (van Keken et al., 1993). The viscosity of the silicon putti used in the models, described in this report, is 2.4*10⁴Pa.s, indicating that: $\eta^* \sim 10^{-13}$. In accordance with the adopted scaling of the dimensions; $\sigma^* \sim 10^{-5}$. Additionally, orogenic strain rates ($\dot{\varepsilon}_{nature}$) are in the range from 10⁻¹³ to 10⁻¹⁵ (Pfiffner and Ramsay, 1982). When a natural strain rate of 10¹³ is assumed, equation.. indicates that the model should be deformed with a strain rate that is the order of $\dot{\varepsilon}_{model} \sim 10^{-5}$. This indicates that the velocity of the base plate should be in the order of centimeters per hour. Because both the viscosity of salt in nature, as well as the natural strain rates are not exactly known, the strain rate was varied in the testing phase of the models to look for the strain rate that produced the best structures. It turned out that during the extension phase, a deformation velocity of 0.5cm resulted in the formation of well-developed silicon putti walls. During the strike-slip phase, a faster velocity of 1.5cm/hour was applied.

$$\sigma_1 = \sigma_3 = 2\eta\dot{\gamma} \text{ or } \sigma_1 = \sigma_3 = 2\eta\dot{\varepsilon} \quad (12)$$

3.2.4 Calculation of the strength profiles

The deformation pattern resulting from multilayer analogue models is largely dependent on the strength of the different materials and in particular on their strength contrast, which is tested here under different tectonic stress regimes. (Hubbert, 1937; Brun and Nalpas, 1995; Brun, 2002; Smit, 2008a; Smit, 2008b). The following section explains how the strength, which is defined as the maximum differential stress ($\sigma_1 = \sigma_3$), can be calculated for the brittle part of the models.

Calculating the Brittle strength

The vertical stress in a brittle layer is determined by the weight of the overlying rock column;

$$\sigma_v = \rho g T_b \quad (12)$$

In an extensional setting, the maximum principle stress (σ_1) is equal to the vertical stress;

$$\sigma_v = \sigma_1 \quad (13)$$

To determine the maximum differential stress (i.e. the strength) of the sand, an expression for the minimum principle stress (σ_3) is also required. This relation follows from the Mohr Coulomb criterion and is as follows (Jaeger and Cook, 1979):

$$\sigma_3 = -\frac{\sin\Phi}{\sin\Phi + 1} \sigma_1 \quad (14)$$

Where Φ is the materials angle of internal friction, which is related to the friction coefficient (ϕ) by the following relation

$$\phi = \tan\Phi \quad (15)$$

the coefficient of internal friction (ϕ) of quartz sand is 0.58 and the minimum principle stress can be expressed as a part of the maximum principle stress by filling in the equations 13 and 14. This leads to the following expression:

$$\sigma_3 = \frac{1}{3} \sigma_1 \quad (16)$$

From this relation and from the fact that in an extensional setting, the maximum principle stress is equal to the vertical stress, it follows that the strength of a brittle layer in extension is;

$$\sigma_1 = \sigma_3 = \frac{2}{3} \rho g T_b \quad (17)$$

In a strike-slip setting, the intermediate principle stress (σ_2) is equal to the vertical stress;

$$\sigma_v = \sigma_2 \quad (18)$$

The Mohr Coulomb failure criterion for three dimensions can be used to express σ_2 in terms of σ_1 or σ_3 :

$$\frac{\sigma_1 - \sigma_2}{2} = \left[\frac{\sigma_1 - \sigma_2}{2} \right] \sin\phi + c \cos\phi \quad (19)$$

Where c is the cohesion, which is negligible in the case of quartz sand. By using relation 18 and the 3D Mohr Coulomb equation, it follows that the strength of quartz sand during strike-slip deformation can be calculated as follows;

$$\sigma_1 = \sigma_3 = \rho g T_b \quad (21)$$

Calculating the Ductile Strength.

The strength of the ductile part of the model can be obtained from equation 12. However, from this equation, the average strength of a layer of silicon putti is obtained. The true strength of a ductile layer however, also depends on its thickness (Spiers et al., 1990; van Keken et al., 1993). Hence the strength of the silicon putti layer was calculated by using the following formula (Smit, 2005):

$$\sigma_1 = \sigma_3 = \frac{2\eta V}{T_d} \quad (22)$$

Where V is the deformation velocity in cm/hour and Td is the thickness of the silicon putti layer in m.

3.2.5 Limitations of analogue modelling

It has to be emphasized that the analogue models described in this study are just a first order approximation of reality, as the complexity of nature can't be exactly reproduced in a lab. Hence, simplifications are made in the models regarding the rheology of the materials, but also regarding the geometrical variations. First of all it has to be noted that the models presented in this study are solely composed of a brittle basement. In nature, a ductile lower crust is present, which distributes deformation at the base of the upper crust. Hence, the results of the models described here can only be considered as an analogy for the upper brittle crust. For these brittle rocks applies that they are seldom homogenous in composition. Instead their heterogeneity or anisotropy often influences the deformation pattern. Additionally, as mentioned in section 3.2.3, the exact viscosity of salt varies under different geological conditions, as it depends on grain size, temperature and the presence of fluids. All these parameters are poorly constrained for distinct areas and time intervals and are impossible to incorporate in the model. Additionally, it is not possible to include processes like isostasy or flexural behaviour and also erosional processes were not included in the model. However, it is not the intention of analogue modelling to exactly reproduce natural structures. Analogue modelling is about studying the structural evolution of features in the lab that can be regarded as analogues to natural examples. For this purpose it provides a useful tool, as analogue models allow observing the evolution of structures. While in nature, only the present state of structures can be observed.

3.2.6 Experimental procedure; Experiments 1 and 2 (table 2)

Models 1 and 2 are purely brittle models, solely composed of different colored layers of quartz sand to represent brittle behavior. The total thickness of the layers before deformation commences is 5.5cm (see Fig. 16 and 17). Both model 1 and 2 were subjected to two deformation phases, however the sequence of these deformation phases was different. Model 1 was first subjected strike-slip, after which it was subjected to extension. Model 2 was first subjected to extension, after which it was subjected strike-slip. During the extension phase, sedimentation was applied in the graben 3 times at regular time intervals (every 20 minutes). The purpose of these two models was to test, to what extent deformation during the second deformation phase would reactivate faults that were formed during the first deformation phase.

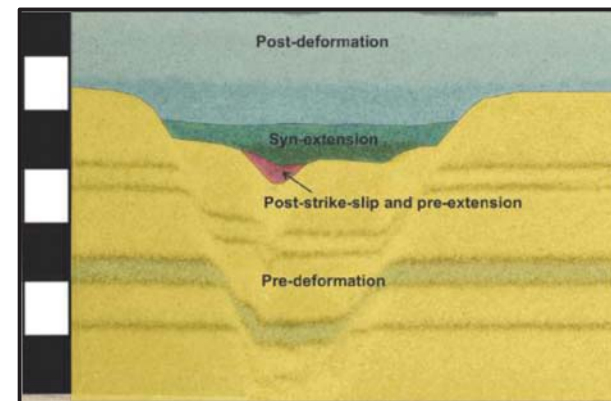


Fig. 16. Section 1.1 of model1, showing the deformation phases during or after which the sediments were deposited as well as the thicknesses of the sediments

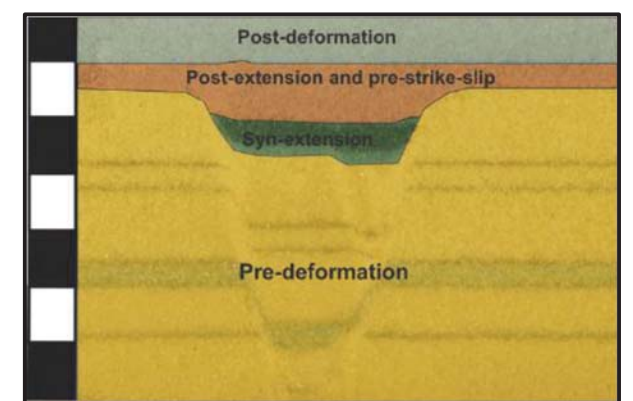


Fig. 17. Section 2.1 of model 2, showing the deformation phases during or after which the sediments were deposited as well as the thicknesses of the sediments

3.2.7. Experimental procedure; experiment 3 and 4 (table 2)

Models 3 and 4 are multilayer models, composed of both brittle and ductile materials. The two models are composed of a 5cm thick brittle basement, underlying a layer of silicon putti with an initial thickness of 1cm. On top of the silicon putti layer, a green layer of quartz sand was deposited with a thickness of 0.5cm (Fig. 18 and 19).

These pre-kinematic layers were in both models subsequently subjected to 2 deformation phases and one resting phase in the following order:

- Extension Phase; 4 hours at a deformation rate of 0.5cm/hour
- Resting Phase; 8 hours
- Strike-Slip Phase; 2 hours at a deformation rate of 1.5cm/hour

With ongoing extension and subsidence of the graben during the extension phase, sedimentation was applied at regular time intervals (every hour) to simulate syntectonic sedimentation. After the extension phase, no deformation was applied for 8 hours during the resting phase, allowing the silicon putti walls to grow passively. During this resting phase, sedimentation was applied again at regular time intervals (every two hours). The difference between experiment 3 and 4 is the following; In Experiment 3, sedimentation was applied homogeneously across the entire experiment thereby keeping the graben normally filled with respect to the platforms (i.e. no topography between the graben and platform after sedimentation). In Experiment 4, part of the graben was kept underfilled (part C in Figure 73), allowing the silicon putti to extrude laterally into the graben. The other half of the graben (Part D in Figure 73) was normally filled. During the first two hours of the resting phase, part A of the basin was kept underfilled with 6mm of difference between the graben and the platforms (indicated as extremely underfilled in Fig. 19). During the subsequent 2 hours, the basin was also kept underfilled with a 3 to 4mm difference between the graben and the platforms (indicated as underfilled in Fig. 19). During the last four hours of the resting phase, part A of the basin was kept underfilled with a difference of 1 to 2mm between the graben and the platform, thereby reducing the topography (indicated as normally filled in Fig. 19). Subsequently, the strike-slip phase of the experiment was applied parallel to the pre-formed graben, in order to test the influence of different salt geometries on the strike-slip deformation pattern.

Experiment number	First deformation phase	Sedimentation during first deformation phase	Resting Phase	Sedimentation during resting phase	Second deformation phase
Model 1	Strike-Slip; 1 hour with 3cm/hour	NA	NA	Every 20Minutes	Extension; 1 hours with 1cm/hour
Model 2	Extension; 1 hour with 1cm/hour	Every 20 minutes	NA	NA	Strike-Slip; 1 hour with 3cm/hour
Model 3	Extension; 4 hours with 0.5cm/hour	Every Hour	8hours	Every two hours. Entire graben was kept normally filled	Strike-Slip; 2 hours with 0.5cm/hour
Model 4	Extension; 4 hours with 0.5cm/hour	Every hour	8 hours	Every 2 hours. Half of the graben was kept underfilled during the first 4 hours of resting	Strike-Slip; 2 hours with 0.5cm/hour

Table 2. Table showing a schematic overview of experimental procedure for the 4 models.

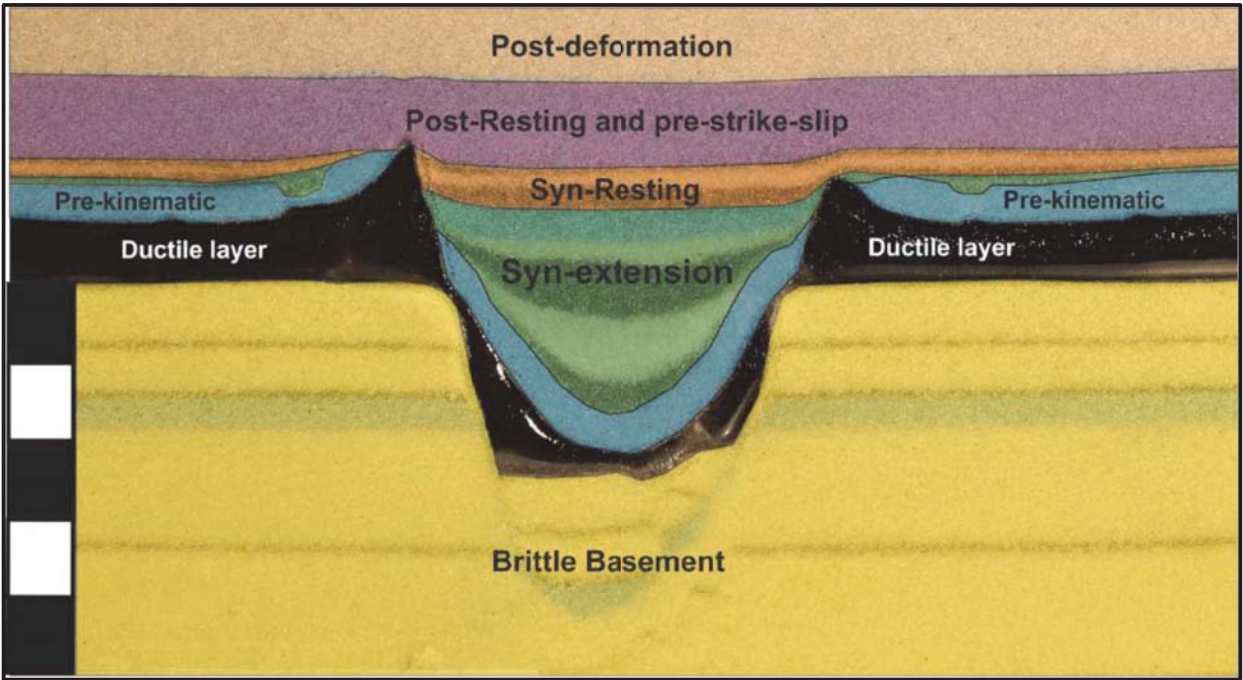


Fig. 18. Section 3.1 of model 3, showing the deformation phases during or after which the sediments were deposited as well as the thicknesses of the sediments. This figure represents model 3 as well as the normally filled part of the basin of model 4.

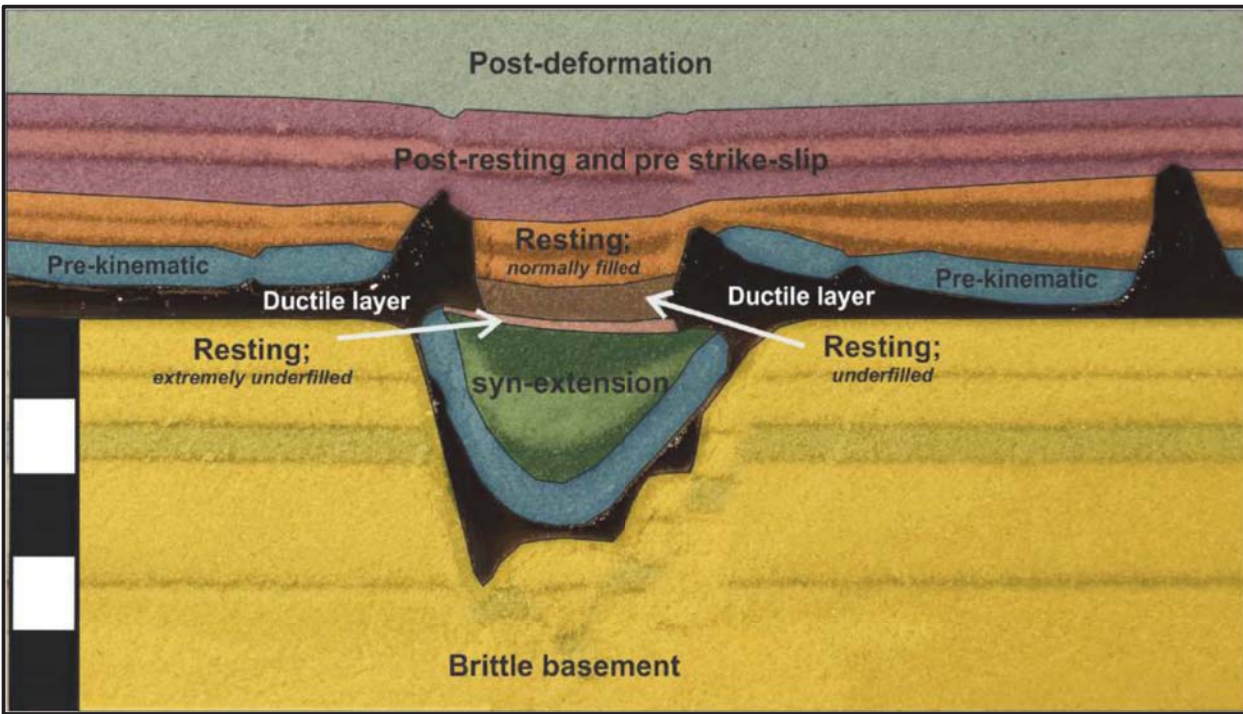


Fig. 19. Section 4.2 of model 4, showing the deformation phases during or after which the sediments were deposited as well as the thicknesses of the sediments. This figure represents the underfilled part of the basin of model 4.

4. Results obtained from seismic data

The strike-slip faults that are identified in this study are indicated in Fig. 20. The main characteristics of the identified strike-slip faults are indicated in table 3, which shows i.a. the orientation, sense- and amount of displacement and timing of the identified strike slip faults. In the next sections (4.1-4.4) will be elaborated on the fault characteristics of the four case studies (indicated by the black squares in Fig. 20), which are briefly introduced below.

From Figure 20 can be inferred that a group of roughly WSW-ENE trending strike-slip faults was identified on the Elbow Spit Platform, Elbow Spit High and Cleaverbank Platform, west of the Step Graben. These faults can only be recognised on the platform areas. As soon as they approach the Step Graben, they can't be identified anymore. This group of faults is further described in Section 4.1, as case study A. Several strike-slip faults were also identified in the Dutch Central Graben. Because of the Dutch Central Grabens complex history of multiple deformation phases, it was sometimes not exactly clear if a fault had accommodated strike-slip movements or not. Hence, a quality code is used for strike-slip motions in the Dutch Central Graben ranging from low probability strike-slip feature to a high probability strike-slip feature. Some of these strike-slip faults are indicated with a star in Figure 20. This is either because there was no available 3D seismic data to unravel the strike (as is the case for feature I, briefly described in appendix B) or because the strike of the concerning feature could not be derived (as is the case for feature II, a low probability strike-slip feature, which is described in appendix C). From the strike-slip movements that were identified in the Dutch Central Graben, two strike-slip faults are discussed in detail in case studies B

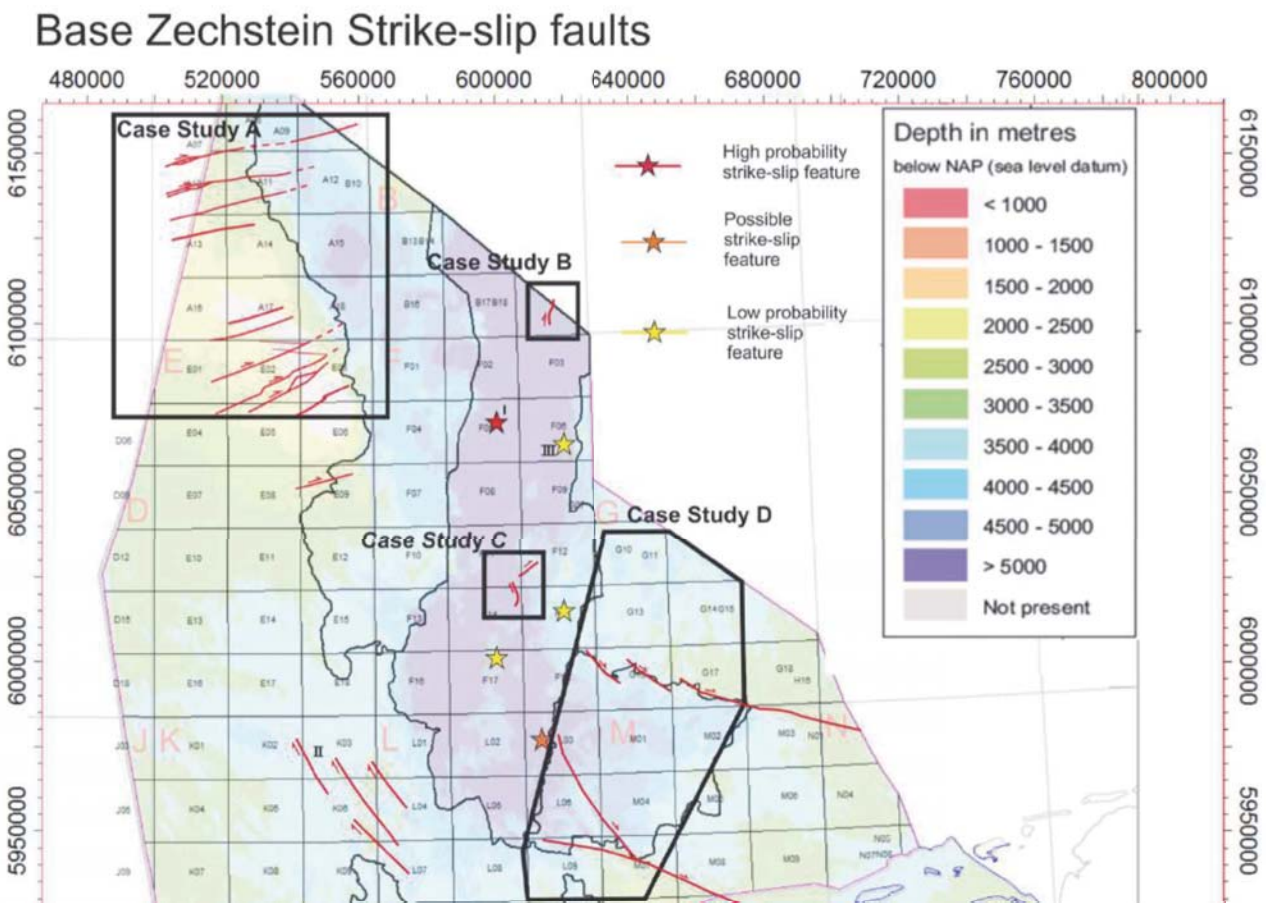


Fig. 20. Map of the base Zechstein showing the strike-slip faults that were identified in this project, as well as the outline of the case studies that are presented in the section 4.1-4.4. The fault Group that is identified in the K and L blocks was identified by Ping Chen (Ping Chen, Msc. Thesis, 2016)

(Section 4.2) and C (Section 4.3). Case study B describes a strike-slip fault in the northern part of the Dutch Central Graben. Case study C describes a strike-slip fault in the central part of the Dutch Central Graben, which has accommodated strike-slip movements in between two salt structures. Finally, case study D (Section 4.4) describes two types of strike-slip faults in the northern part of the Central Offshore Platform, Terschelling Basin and Schill Grund Platform. The first type of strike-slip faults are subtle supra salt, thin-skinned strike-slip faults. The second type are major strike-slip faults on the two faults that bound the Terschelling Basin towards the north and the south; the Rifgronden Fault Zone and the Hantum Fault Zone.

Case Study/ Reference number	Location	Fault orientation	Sense and estimation of the amount of displacement	Reactivation of older structures?	Timing	Relation with salt
Case Study A	Elbow Spit Platform and Elbow Spit High (Northern A-blocks)	N075 to N085	Dextral; 700m to 900m on single fault	Partly reactivation of older structures	Upper Cretaceous, Early Paleogene. Possibly earlier activity	No salt present; thickskinned
Case Study A	Elbow Spit Platform and Cleaverbank Platform (Northern E-blocks)	N060 to N070	Dextral; 500m to 800m on single fault	Partly reactivation of older structures	Upper Cretaceous; Possibly earlier activity	No salt present; thickskinned
Case Study B	Northern Dutch Central Graben (B18-block)	N170 to N030	Approximately 700m	No; but possibly induced by reactivation of sub-salt basement faults	Late Jurassic (post Jurassic sequence 1) to Early Cretaceous.	Supra salt strike-slip fault
Case Study C	Central Dutch Central Graben (At the gathering of the F11, F12, F14, F15-blocks)	Rapidly curving strike; varying between NE and NW	Approximately 800m-2500m	No; But possibly induced by reactivation of sub-salt basement faults	Late Jurassic (likely post Upper Jurassic sequence 1) and pre Paleogene.	Supra salt strike-slip fault. Linking strike-slip motions that are primarily accommodated by salt structures.
Case Study D; thin skinned	Terschelling Basin, Schill Grund Platform, Central Offshore Platform	N090 to N110	Up to 3000m in Terschelling Basin; up to 1500m at Schill Grund Platform	No	Late Early Triassic to Late Triassic	Thin skinned; Strike-slip features arise to accommodate for lateral differences between different raft blocks. Movements are accommodated by the salt
Case Study D; Hantum Fault Zone	Terschelling Basin	N110-N120; Curving into N-S towards DCG	2500m	Yes	Middle to Late Triassic	Strike-slip movements on pre-formed basement fault. Activity likely transmitted into overlying salt but no evidence found.
Case Study D; Rifgronden fault zone	Terschelling Basin	N290-310	5000m à 6000m	Yes	Middle to Late Triassic	Strike-slip movements on pre-formed basement fault. Activity likely transmitted into overlying salt but no evidence found.
I; Appendix A	Northern Dutch Central Graben (F5-/block)	Exact unknown; approximately N-S	?	Uncertain but not likely	?	Strike-slip movements seem to be partly accommodated by salt structures.
II; Appendix B (Msc. Thesis Ping Chen)	Southern Cleaver Bank Platform	N320-330 or N160-170 (depending on fault dip)	Around 1000m	Yes	Late Cretaceous/Early Paleogene	?

Table 3, table summarizing the main characteristics of the identified strike-slip faults. The location of the strike-slip faults is indicated in Figure 20.

4.1 Case Study A; Strike-Slip faulting on the Elbow Spit High

Structural observations

This case study emphasizes on a family of faults that is present in the region west of the Dutch Central Graben and the Step Graben. Due to the absence of Zechstein evaporites in this area, and the relatively shallow position of Paleozoic rocks, fault patterns can be recognized in the Upper Carboniferous. This is shown in Fig. 21, which shows a similarity map of the Northern E-blocks at 2100ms TWT, roughly corresponding to the Upper Carboniferous interval of the Hanze Subgroup (DCHP) in most of this area. And in Fig.23, which shows a similarity map of the base of the Zechstein Group in the Northern A blocks.

Four fault families (FF) were recognized from Figures 21 and 23. The characteristics of these four fault families are indicated in Table 3, where the colors of the fault families correspond to the faults in the maps of Figure 21 and 23. From Fig. 21 and 23 can be inferred that FF 1 cross-cuts all the other fault families, as these other fault families display a right stepping geometry across the faults of FF1. Additionally small zones of uplift and subsidence are related to movements along faults of FF1. These small zones of uplift and subsidence can be recognized both in the A and in the E blocks. However in the E blocks they are generally larger. Fig. 22 shows a cross section through such a small zone of uplift. From this figure can be inferred that the vertical faults related to this small zone of uplift display an upward widening of the fault pattern and offset rocks up to an including the Chalk Group and locally also rocks of the Lower North Sea Group (southern part of the northern E-blocks). Additionally, rocks of the Chalk Group and Lower part of the Lower North Sea Group are thinning over this small zone of uplift. Displacements along the faults of FF1 can be measured on several points by measuring the offsets between older fault families. Displacements are in the order of 500-900m per individual fault. Noteworthy is that the faults of Family 1 can't be observed in the Step Graben, also not at deeper intervals. This is the case both in the E blocks as in the A blocks.

Fault families 2 and 3 display always offsets in the Carboniferous and Devonian interval and sometimes also in the strata up to and including the Chalk Group. Pre-Zechstein strata show signs of thickening in the hanging wall of these faults. This thickening can also be observed sometimes in the Zechstein and in the Chalk Groups. Their mutual cross-cutting relationship is a bit ambiguous, as at some places Family 2 cross-cuts Family 3 (indicated with I in Fig. 21), while at other places, Family 3 seems to cross-cut Family 2 (indicated with II in Fig.21). Additionally, some ENE-WSW trending faults can be recognized that are characterized by approximately the same orientation as FF2 but instead show a nearly vertical fault plane. These faults are oriented en echelon across faults of FF1.

Faults of fault Family 4 form the boundary between the Elbow Spit Platform and the Step Graben. In the hanging wall of these faults, a thicker sequence of Mesozoic rocks is present including Zechstein evaporates, Lower and Upper Triassic and Lower and Upper Cretaceous rocks. The Upper Cretaceous rocks of the Chalk Group are thicker in the hanging wall of these faults. They are more abundant in the A-blocks than in the E-blocks and also there orientation varies between these two blocks as they are more NNE-SSW oriented in the A-blocks and more NW-SE oriented in the Eblocks.

Fault Group	Fault orientations	Fault dip	Sense of displacement	Amount of displacement	Timing
1	060 to 070 in the Eblocks 080-085 in the Ablocks	Nearly vertical	Strike-slip; dextral	500 to 1000m	Late Cretaceous/Early Paleogene . Possibly earlier but no sedimentary record in this area.
2	90-110	Inclined	Normal faults	>800m	Carboniferous/Devonian with some later reactivation during Mesozoic times.
3	020-040	Inclined	Normal faults	?	Carboniferous/Devonian with minor reactivation during Mesozoic times
4	130 in the Eblocks 170 in the northern A blocks	inclined	Normal Faults	> 1000m	Mesozoic

Table 4; fault characteristics of the main fault families on the Elbow Spit High and Elbow Spit Platform

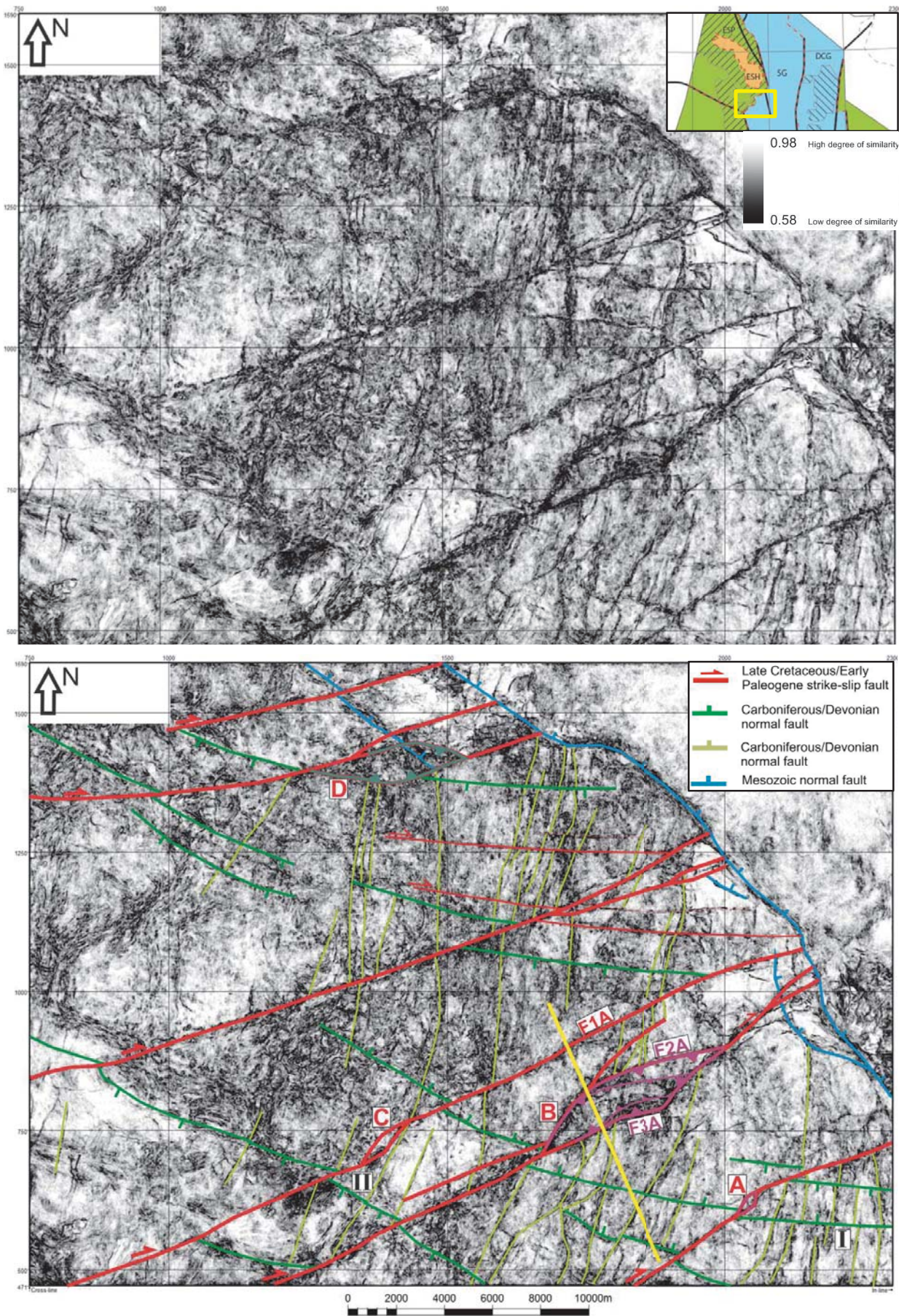


Fig.21. Similarity map at 2100ms TWT in the northern E blocks. The yellow line indicates the location of the seismic line in Fig. 22. For the classification of the different fault families see table 4.

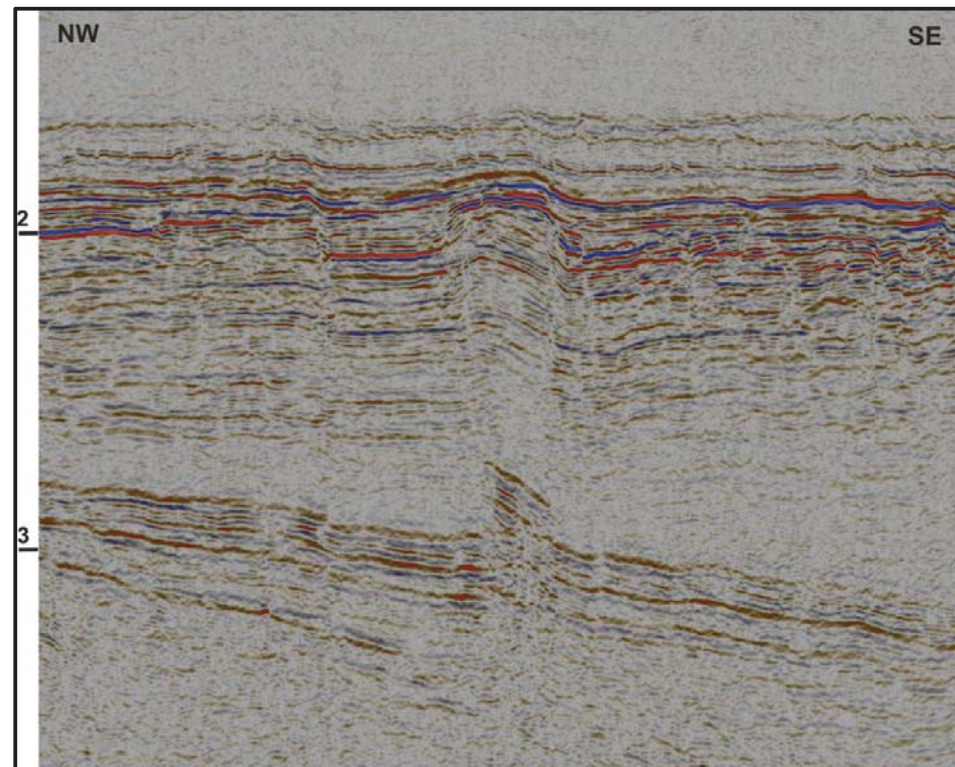


Fig. 22. Interpreted (bottom) and uninterpreted (top) seismic cross section through the southeastern E-block, showing three faults of fault family 1, including a pop-up structure, as well as two Carboniferous faults. The Carboniferous interval is composed here of the Step Graben Formation (DCHP), Yoredale Formation (CFYD), Elleboog Formation (CFEB) and Cementstone Formation (CFCS).

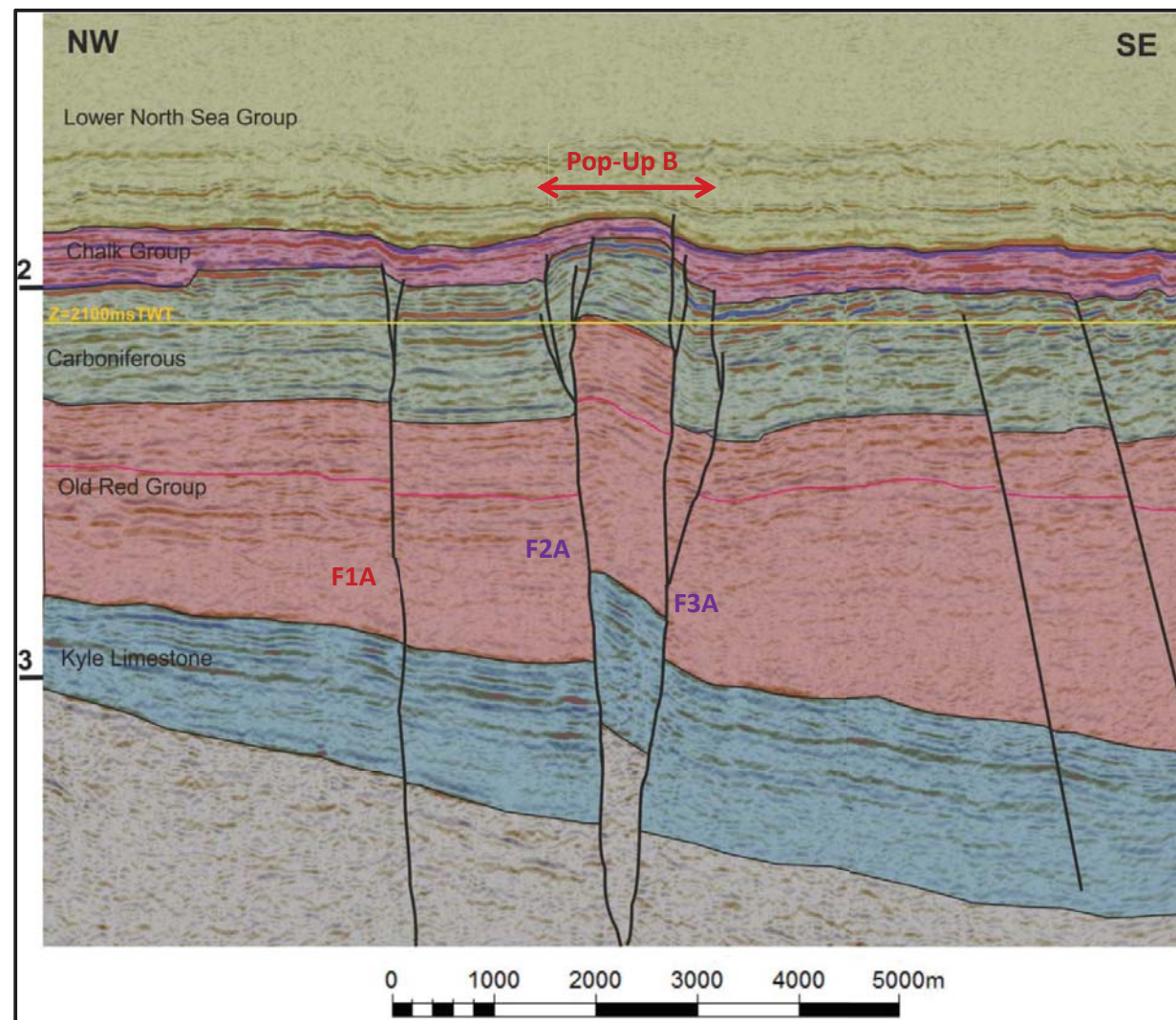
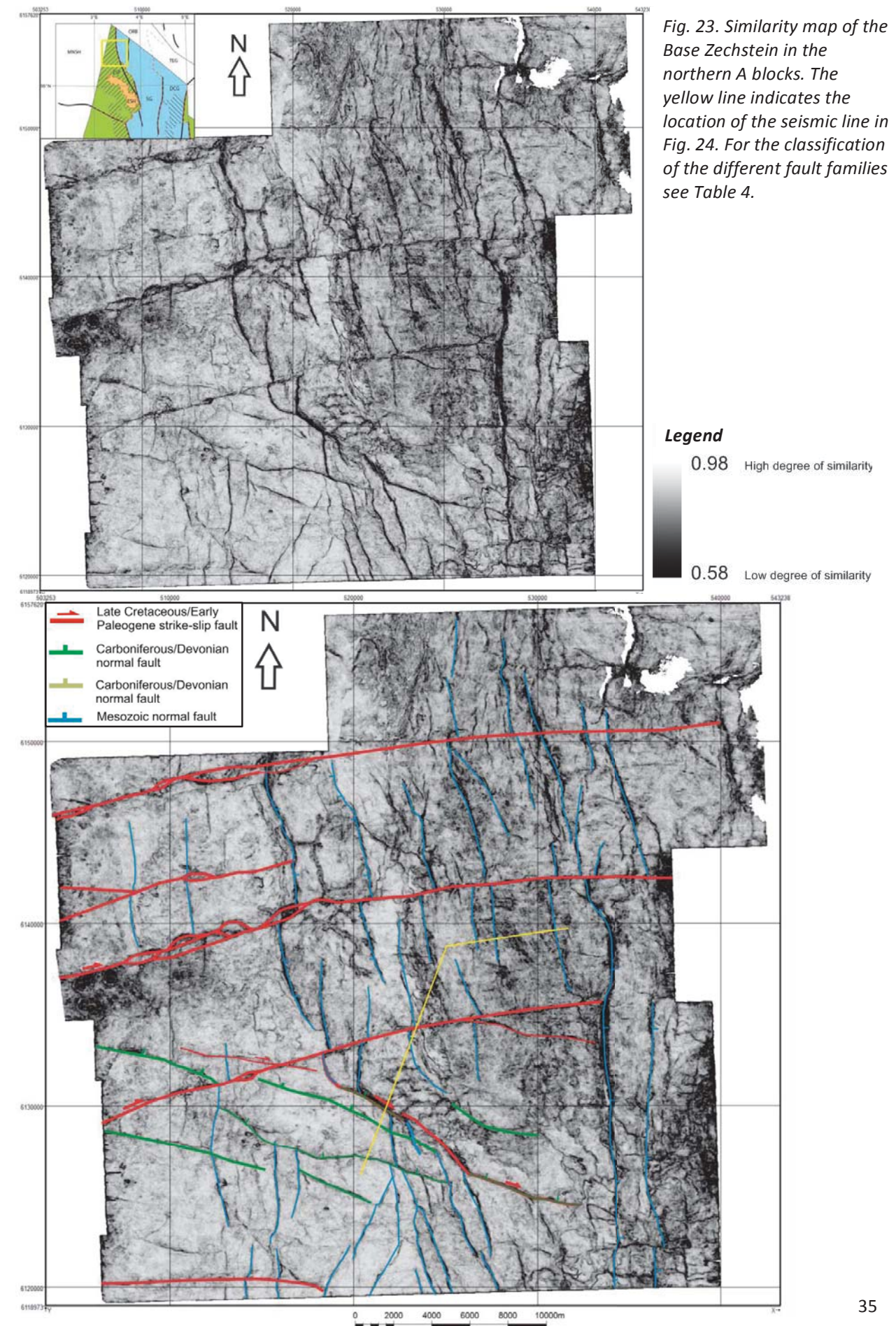


Fig. 23. Similarity map of the Base Zechstein in the northern A blocks. The yellow line indicates the location of the seismic line in Fig. 24. For the classification of the different fault families see Table 4.



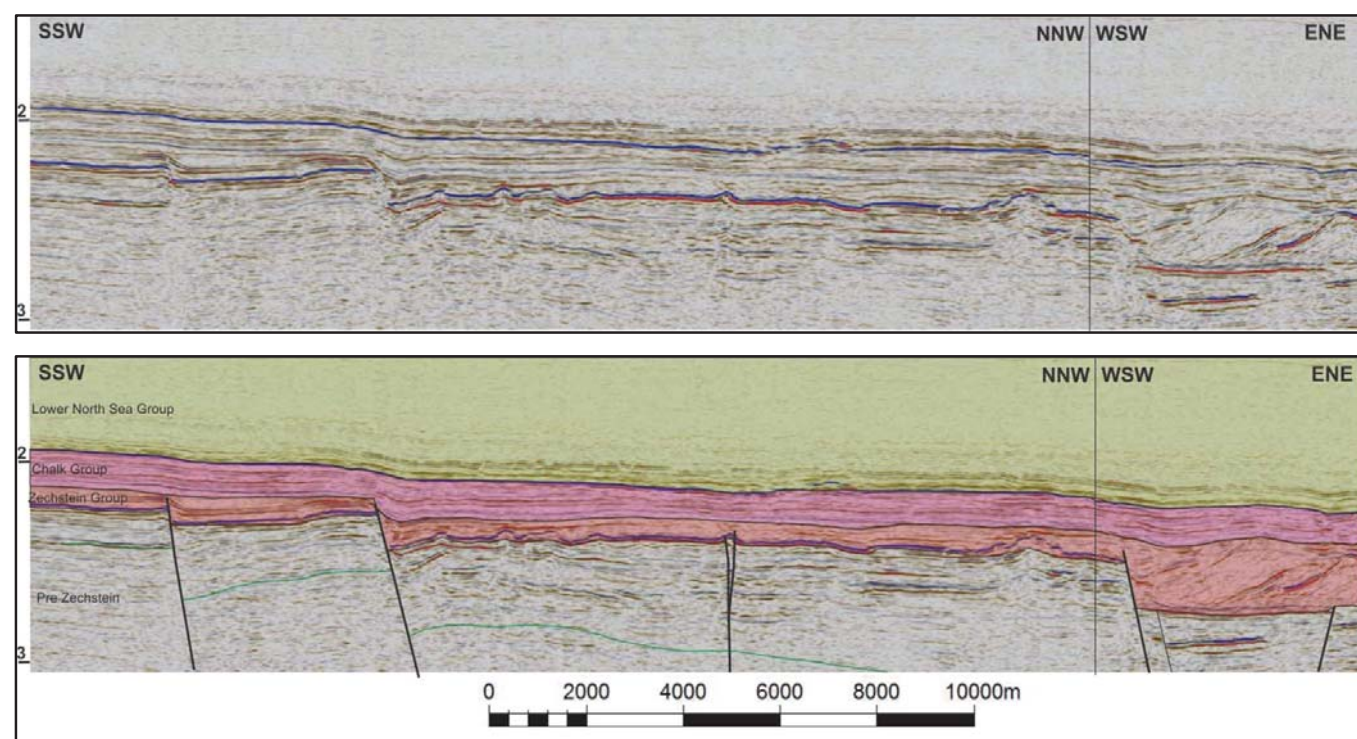


Fig. 24. Interpreted (bottom) and uninterpreted (top) seismic cross section in the northern A blocks. Showing reactivated Paleozoic faults, as well as a strike slip fault (middle fault). The Green line indicates an Upper Carboniferous reflector, showing the thickening of Upper Jurassic strata in the hanging wall of the Paleozoic faults.

Interpretations

The nearly vertical fault plane of the faults in FF, the upward widening pattern of the faults, the local zones of transpression and transtension, the en echelon pattern of (occasional) R Riedel faults and the right stepping of older faults across the fault plane of FF, indicate that these faults are strike-slip faults. The right stepping indicates that these faults are dextral faults with a displacement in the order of 500-900m on individual faults. The local zones of uplift (pop-ups) and subsidence (pull-aparts) are probably caused by interference with older fault patterns, especially in the E-blocks. In the E-blocks, it appears that interaction with faults of family 2 (orientation of around 020-040) locally causes left stepping of the dextral faults (at pop-ups A,B and C, Fig.21 and Fig. 22), leading to zones of transpression. Additionally, interaction with faults of family 2 seem to cause right stepping of the dextral faults, leading to zones of transtension (at pull-apart D in Fig.21). The pop-ups indicate that the dextral faults in the E-blocks were active during deposition of the Chalk Group, with minor and eventually waning activity during the lower Paleogene. In the A-blocks the dextral faults were active during deposition of the Chalk Group but activity had ceased before the Early Paleogene. It might very well be possible that activity initiated earlier on the dextral faults than the Upper Cretaceous. However, due to the missing stratigraphic record, this can't be ascertained.

Faults of FF2 and FF3 are formed during the Carboniferous as is indicated by a thicker Upper Carboniferous interval in the hanging wall of these faults (Fig. 24). Some of the faults of FF2 also penetrate the Zechstein and Cretaceous rocks and also show a thickening of strata in these intervals (Fig. 24). This lead to the interpretation that they were reactivated during the Mesozoic. Additionally, some parts of FF2 faults seem also to have accommodated strike-slip motions that cut structures of FF4, which were interpreted as Mesozoic faults. This might be explained by their

approximate Riedel geometry which might have been favorable for reactivation during the Upper Mesozoic strike-slip faulting in this area.

Origin of the dextral strike-slip faults

The dextral sense of displacement, combined with a NE-SW to WNW-ESE orientation of the fault plane would require a main principal stress orientation between 090 and 115 degrees (Fig. 25). The Upper Cretaceous to early Paleogene timing of dextral fault activity would correspond to the Sub-Hercynian or Laramide inversion phases related to the Alpine orogeny (Nalpas et al., 1995; van Wees and Cloetingh, 1996; De Jager, 2007)). However, the main principal stress related to these deformation phases is generally estimated to be roughly N-S to NNW-SSE (Nalpas et al., 1995; De Jager, 2007), making it unlikely that these faults have been formed by Alpine inversion. Another regional force that could be responsible for the formation of these dextral faults is the ridge push force related to the opening of the Atlantic Ocean. Sea Floor spreading initiated in the Middle Jurassic (de Jager, 2007) and the resulting gravitational positional energy, caused by the difference in topography would have been directed approximately E-W. This potential energy would increase after a few tens of Ma, when the firstly formed oceanic lithosphere had cooled down, thereby increasing the topography and hence the ridge push force.

The idea that ridge-push could be responsible for deformation has been proposed by several authors (Vagnes, et al., 1998; Clausen et al., 1999; Wessel and Müller, 2007)) and attributed at least partly to the formation of gentle anticlines and associated faulting along the western Norwegian shelf (Clausen et al., 1999). The idea that ridge-push could localize deformation at certain areas in the lithosphere is supported by numerical modelling performed by Mahatsente and Coblentz, 2015 who find that the magnitude of the ridge push force is significantly less than the strength of the oceanic lithosphere, therefore they concluded that the ridge push forces may be transmitted into the continental margin areas where deformation might occur if the ambient force exceeds the strength of the lithosphere (Mahatsente, 2015).

In any case, the orientation of the ridge push force resulting from the opening of the Central Atlantic would better correspond to the observed dextral strike-slip faults than the orientation of forces related to the Alpine inversion. However, it might very well be possible that interaction of these stresses, perhaps combined with the buoyant nature of the Mid North Sea high, have led to the formation of these strike-slip faults during the Upper Cretaceous.

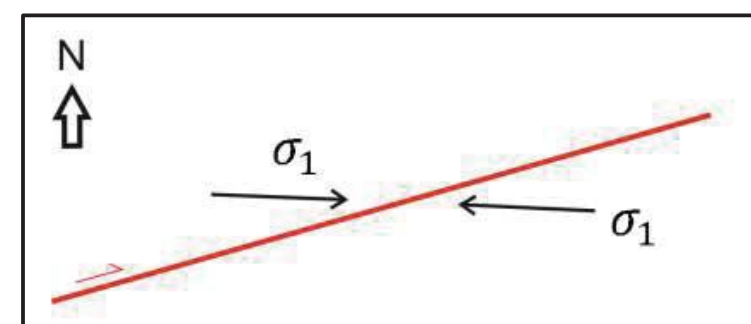


Fig. 25. Figure indicating the approximate direction of the main principal stress (σ_1) direction that must have triggered activity along the faults of FF1.

4.2 Case Study B; Strike-slip fault in the northern part of the Dutch Central Graben

Observations regarding Fault F1b and related faults

Structural observations

Fault F1b is located in the B18 block, which encompasses the northern part of the Dutch Central Graben (Fig. 20). The fault is indicated as Fault F1b on the similarity map of the base Rijnland Group in Figure 26. From this Figure can be inferred that Fault F1b is characterized by a curved strike. At the faults origin in the south of the B18 block, the fault strikes almost N-S (355 degrees). Further northwards, the fault gently curves into a NNE-SSW strike. Fault F1b continues with this strike for a length of around 4km. Further towards the north, across the EEZ border with Germany, the fault bends back to its approximate N-S strike (355 degrees). Fig. 27 shows a WNW-ESE seismic cross-section through Fault F1b. From this cross-section can be inferred that Fault F1b is composed of a set of smaller faults. These smaller faults are positioned around one main sub-vertical fault (highlighted in red in Fig. 27). The faults towards the west of these two sub vertical faults dip roughly towards the east. The faults towards the east of the sub vertical faults dip roughly towards the west. Overall, these faults display an upward widening of the fault pattern in the strata of the Lower and Upper Jurassic and in the lower most part of the Rijnland Group. Strata on either side of the two main sub vertical faults are characterized by an upward concave bending, thereby forming a so called tipi-shape. This tipi shape of strata can clearly be observed in the Lower Germanic Trias Group, the Upper Germanic Trias Group, the Lower Jurassic Altona Group and the Upper Jurassic Sequences 1, 2 and 3.

Observations regarding stratigraphic thickness distribution

Noteworthy when regarding Fault F1b are the major thickness differences of the Upper Jurassic Sequence 2 on either side of Fault F1b. Although the strata of Jurassic sequence thin stratigraphically towards the ESE, as can be inferred from the western part of the fault (Fig. 27), an abrupt decrease in thickness occurs across Fault F1b. Fig. 28 shows that this thickness difference of Jurassic sequence 2 is accommodated across several reflector intervals. To a lesser extent, also the strata of Jurassic Sequence 1 and the strata of the Lower Jurassic Altona Group display this thickness difference as all these stratigraphic groups are thicker towards the west of Fault F1b than towards the east of Fault F1b. This is remarkable as Fault F1b is dipping slightly towards the east. The stratigraphic difference in thickness is visualized in Figure 29, which shows a thickness map of the Jurassic interval of the area (interval between the base of the Rijnland Group and the base of the Altona Group). From this map can be inferred that the general depocenter in this area during the Jurassic was located towards the west-southwest. It can also be inferred that Fault F1b runs parallel to the contour lines in the southern part of the fault. However, as Fault F1b gradually bends towards a more NNE-SSW orientation, Fault F1b cuts through the contour lines. The thickness pattern of the Upper Jurassic interval displayed in figure 30 seems to be affected by Fault F1b as it shows an abrupt increase in thickness towards the west of Fault F1b. On the other hand, when the thickness distribution Rijnland Group is considered (fig.31) it can be observed that the thickness pattern of this stratigraphic group doesn't change across Fault F1b.

Depositional features

Depositional features were recognized in this area by applying seismic attributes on the base of the Rijnland Group surface. These attribute maps visualized the depositional features by enhancing their slight variations in frequency and amplitude. The Channels that were recognized are indicated in yellow in fig. 26. Channels running approximately N-S can be found in the northwestern part of the area. Especially noteworthy is the channel that displays a left stepping geometry and thereby cuts the crestal faults. Additionally, by making use of a spectral decomposition attribute, two features were recognized that display a widening pattern in the direction of the main depocenter

(fig. 33). These features were interpreted as submarine depositional fans. Noteworthy is that both features don't cross Fault F1b. Instead, the eastern feature seems to follow the outline of Fault F1b.

Observations regarding Fault F2b and Fault F3b.

Fault F2b follows the same strike as Fault F1b. However, its fault plane is less steep than Fault F1b and the strata on either side of the fault don't show any sign of a concave upward dipping pattern. The fault is offsetting strata of the Upper Jurassic sequences 2 and 3, strata of the Rijnland Group, strata of the Chalk Group and strata of the Lower Paleogene North Sea Group. The strata of the Chalk Group and the Lower Paleogene North Sea Group are thicker in the hanging wall of Fault F2b than in the footwall of Fault F2b, as can be inferred from figures 27 and 32. The Upper Jurassic and Lower Cretaceous strata of the Rijnland Group don't show any differences in thickness on either side of Fault F2b. Fault F3b is dipping towards the west, into the opposite direction of Fault F2b. The fault is offsetting strata of the Upper Jurassic and Cretaceous. Strata of the Chalk Group are slightly thicker in the hanging wall of Fault F3b than in the footwall.

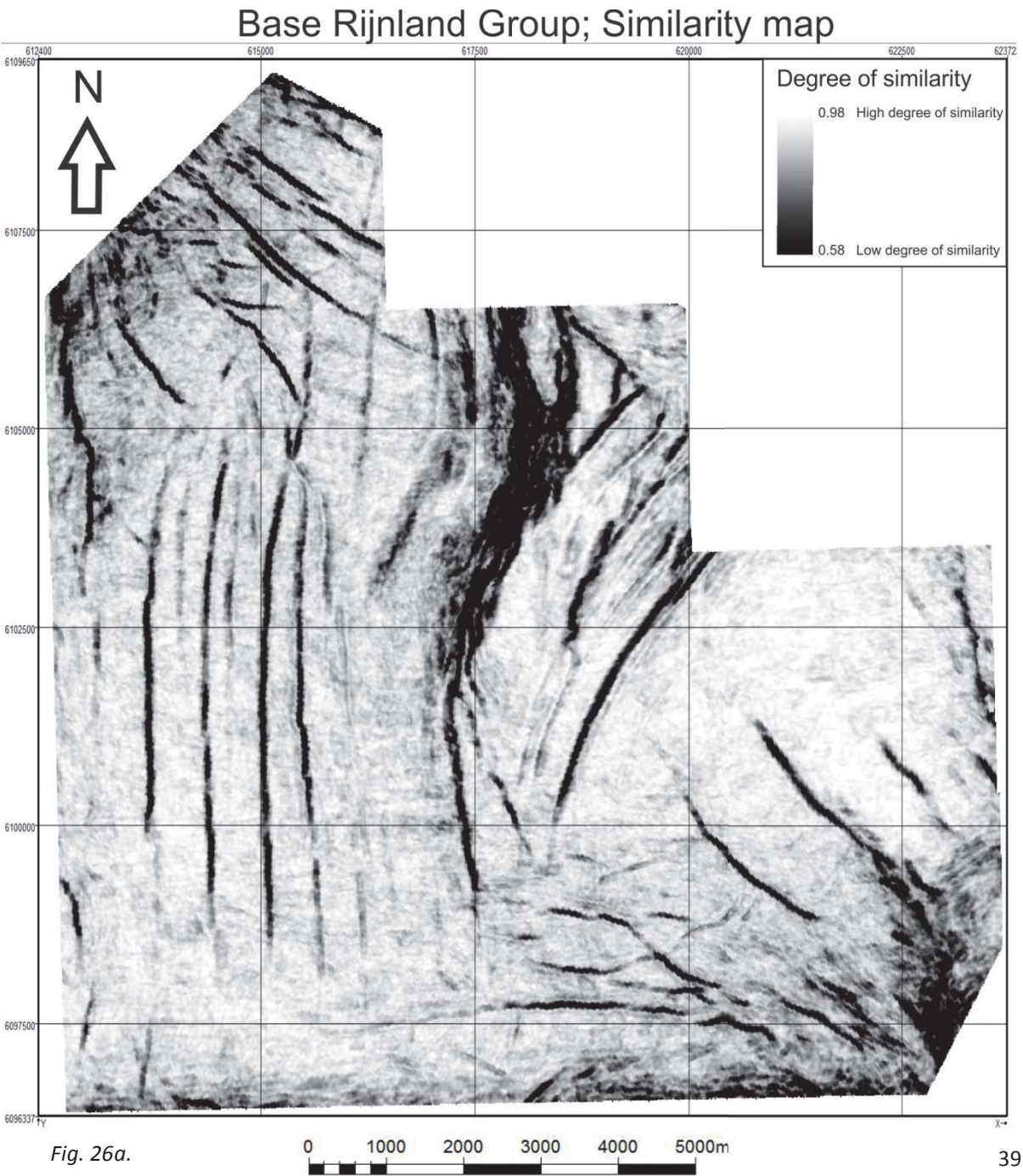


Fig. 26a.

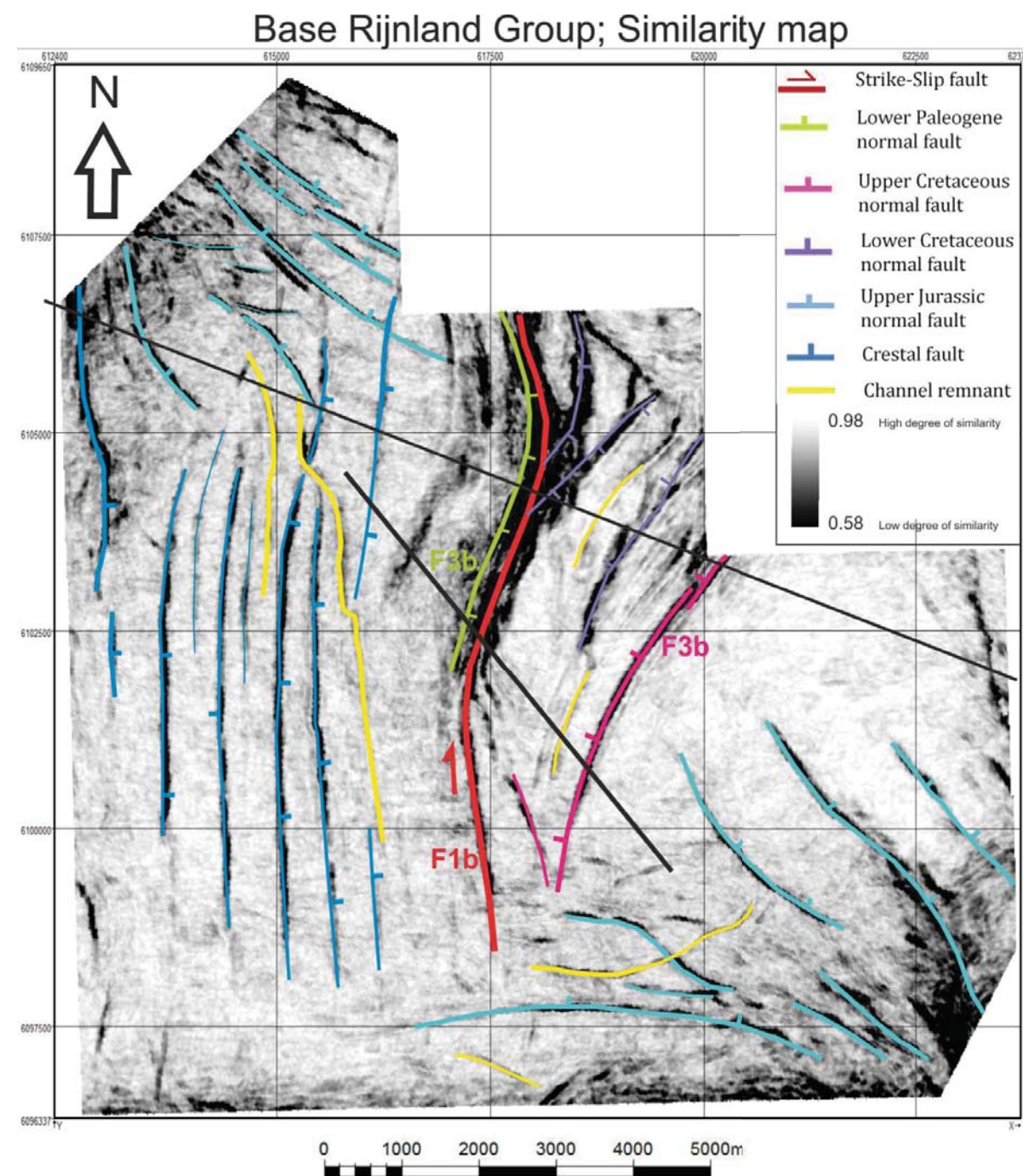


Fig. 26b. Similarity attribute map of the base of the Rijnland Group in block F11. The black areas indicate a high degree of dissimilarity, the white colors indicate a high degree of similarity (see methods). The bright green straight lines indicate the location of Figures 29, and 30. The uninterpreted Similarity map can be found in Figure 28a.

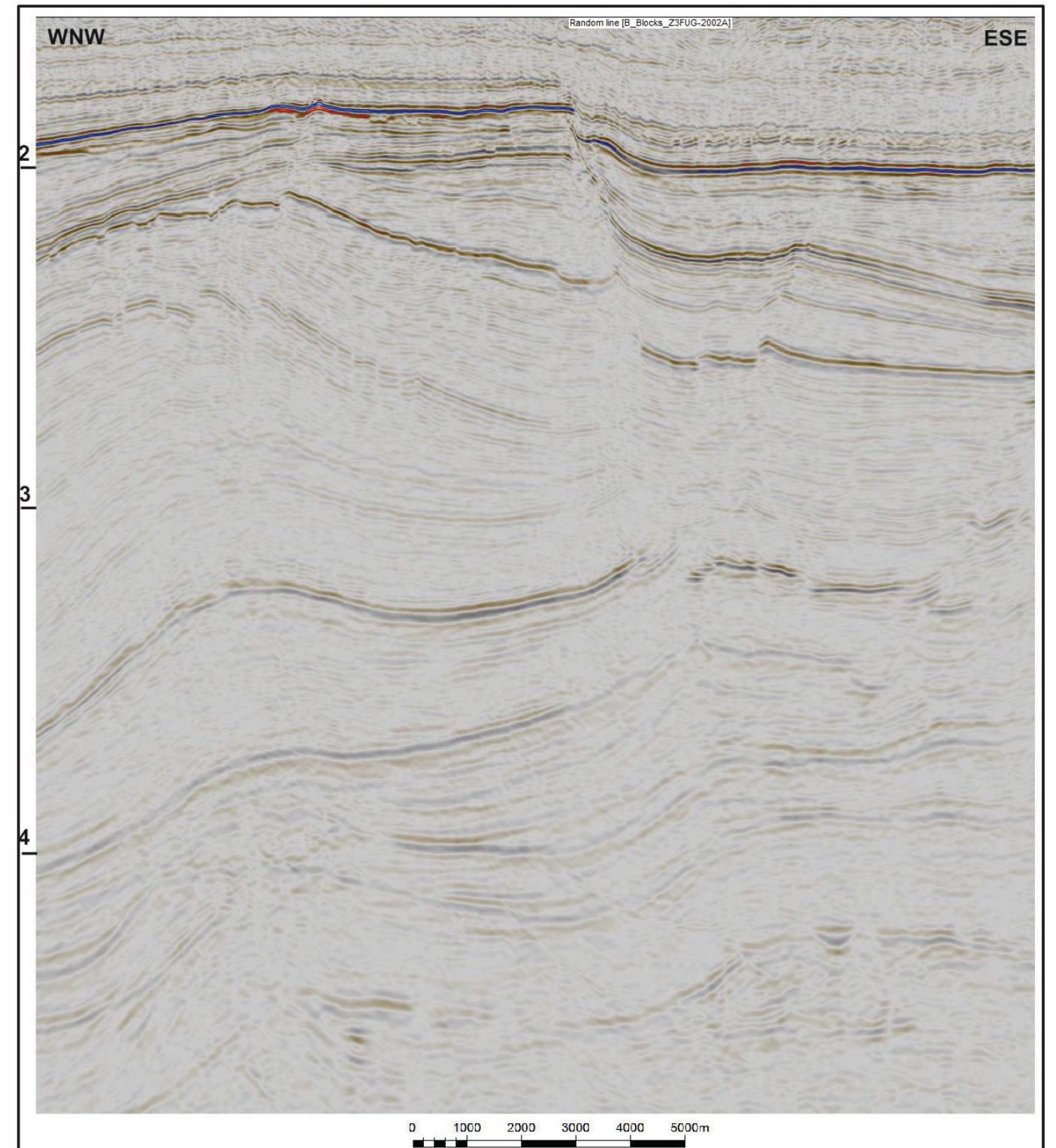


Fig. 27a. WNW-ESE seismic cross section showing the fault F1b, F2b and F3b. The location of the seismic cross-sections indicated by the straight black line in figure 26b. The Uninterpreted section can be found in figure 27a, the interpreted section can be found in figure 27b.

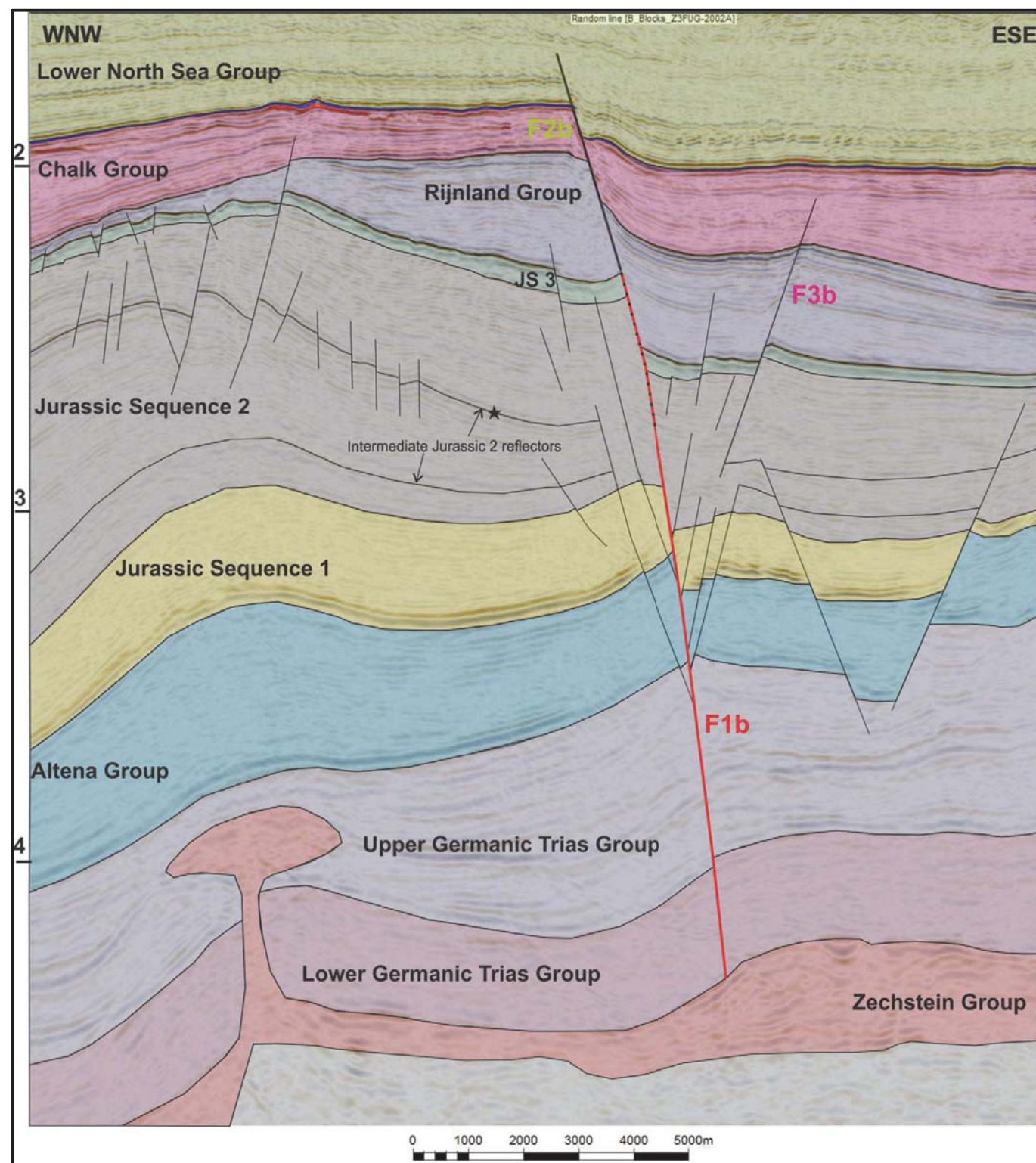


Fig. 27b

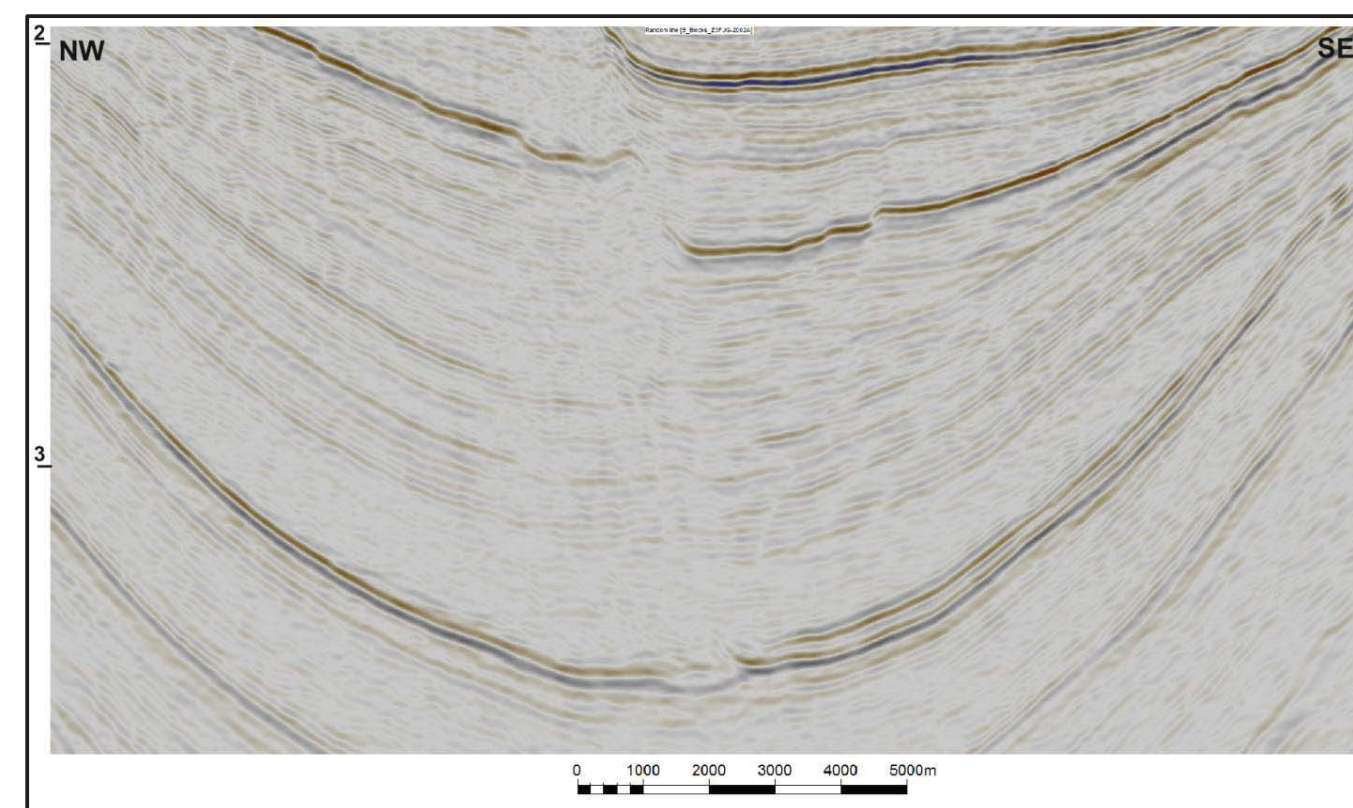


Fig. 28. NW seismic cross section showing displaying the upper Jurassic interval in more detail. Several onlaps, downlaps and toplaps can be observed, indicating a complex system of prograding and retrograding sequences with internal unconformities. Another important observation is that every interpreted interval in the Jurassic Sequence 2 is thinner towards the east of the fault system. Together this adds up to a significant thickness difference on either side of the fault.

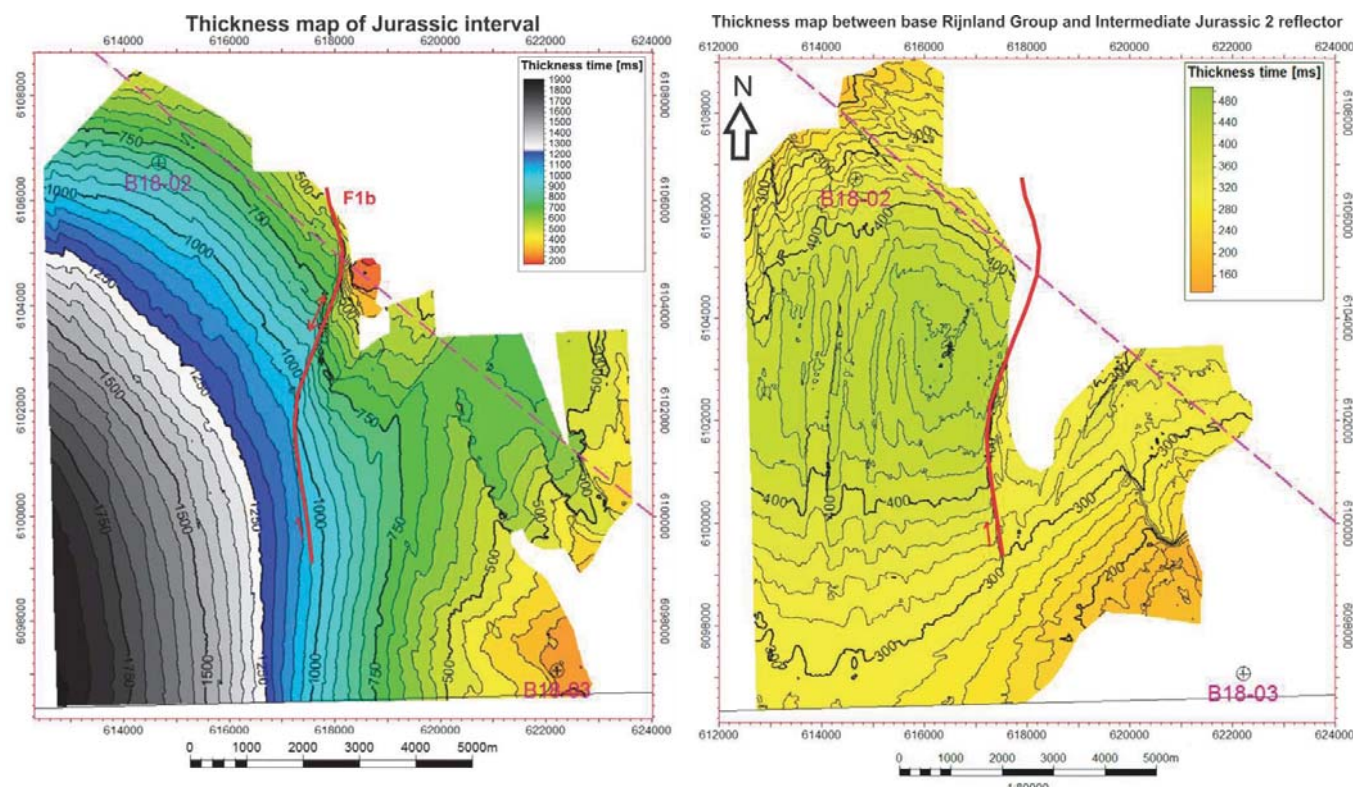


Fig. 29. Thickness map of the Jurassic, the outline of Fault F1b is indicated in red. The line along which the lateral displacement was estimated is indicated by the red arrow.

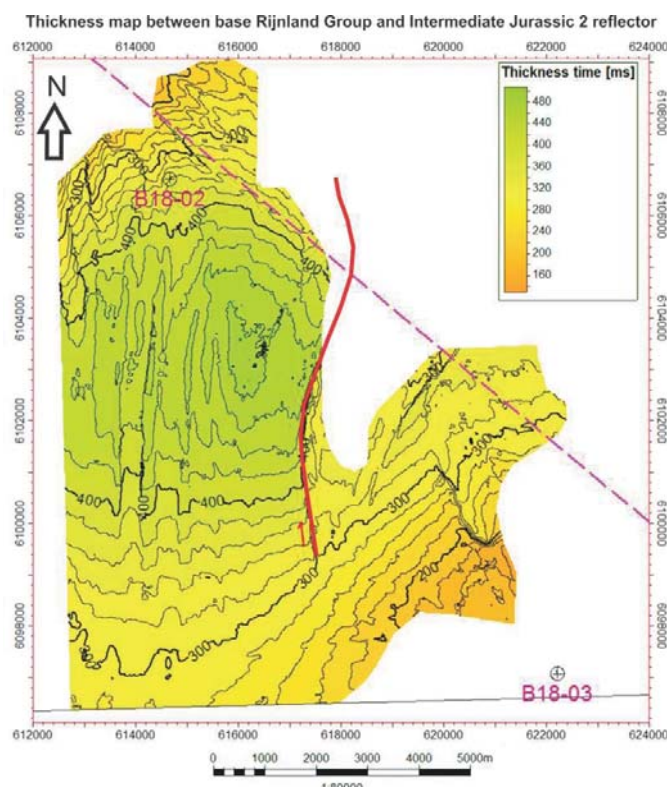


Fig. 30. Thickness map of an Upper Jurassic interval between the base of the Rijnland group and the upper black line in Jurassic Sequence 2 in Figure 27.

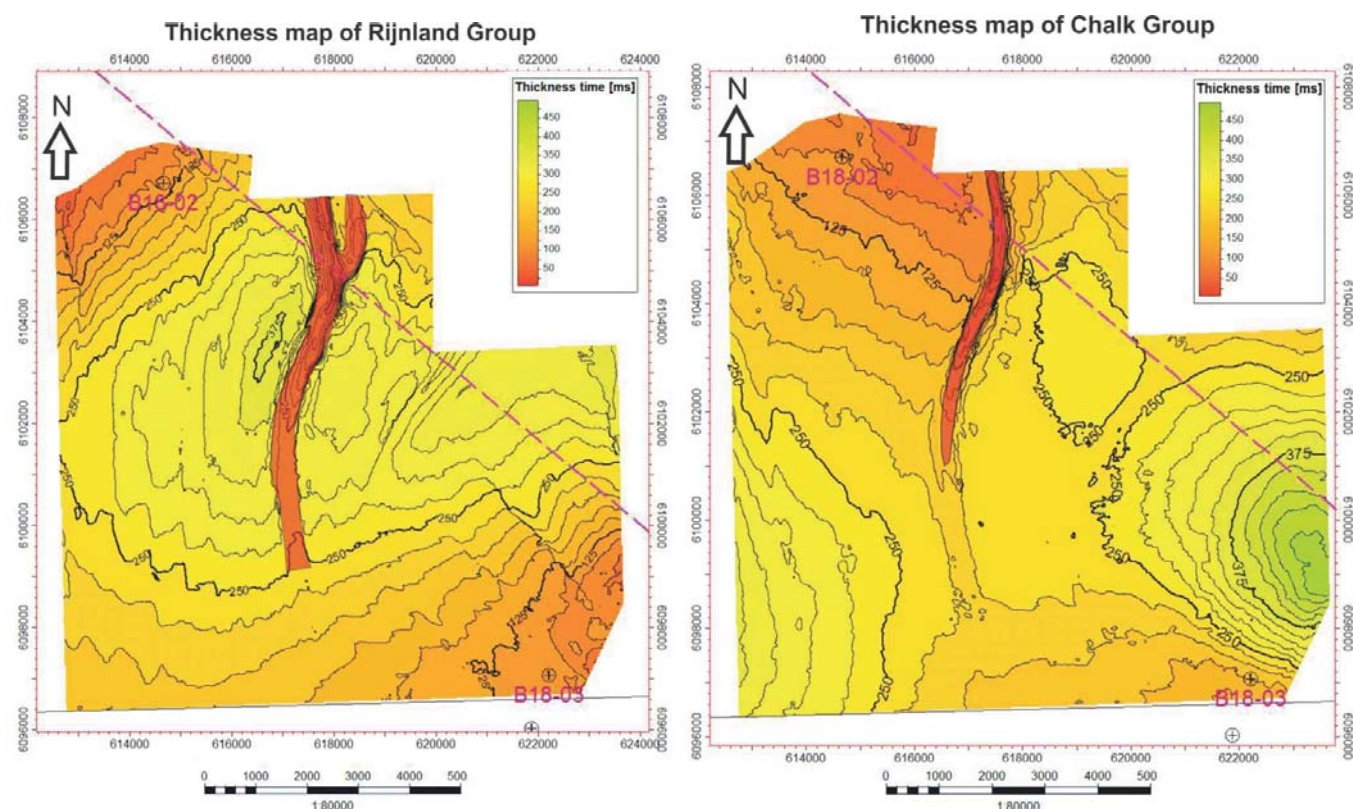


Fig. 31. Thickness map of the Rijnland Group. The fault gap of Fault F3b is indicated in red.

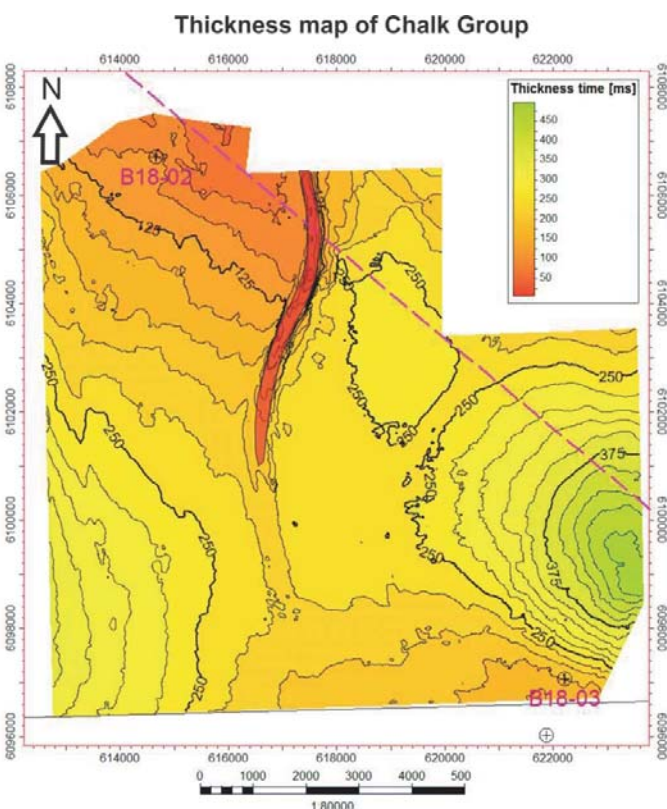


Fig. 32. Thickness map of the Chalk Group. The fault gap of Fault F3b is indicated in red.

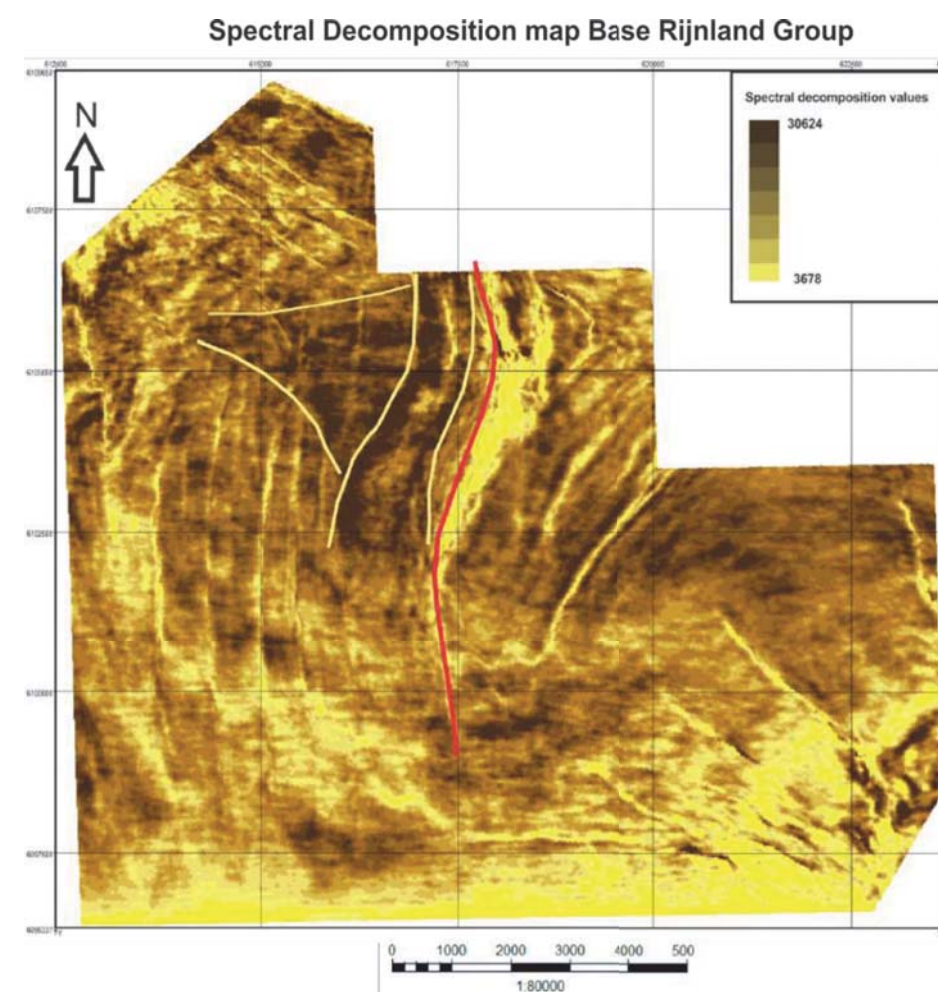


Fig. 33. Spectral decomposition of the base of the Rijnland Group. The outline of the interpreted depositional fans is indicated by the bright yellow lines. The outline of fault F1b is indicated in red.

Interpretations

Why is Fault F1b a strike-slip fault

Because of the upward widening of the fault pattern in the Jurassic interval, the unresolved stratigraphic thickness differences on either side of the fault, the nearly vertical fault plane of Fault F1b and the upward concave bending of the fault, Fault F1b has been interpreted as a strike-slip fault. This strike-slip component is hard to recognize in the southern part of the fault as Fault F1b runs parallel here to the Jurassic contour lines (Fig. 29). Along the part where Fault F1b runs more NNE-SSW though, it can be inferred that the strike-slip motion brought a deeper part of the basin where more sediments had accumulated during the Jurassic next to a more proximal part of the basin, where the Jurassic stratigraphic interval is thinner (Fig. 29). This thickness difference can't be explained by a normal fault because the fault plane of Fault F1b is too steep and is even dipping slightly towards the east, which would have caused sediments to be thicker toward the east of the fault if caused by normal faulting. And although the Jurassic strata generally thin towards the east-northeast in this area (Figs. 27, 28 and 29) it is unlikely that the abrupt thickness difference of 200ms_TWT is of pure stratigraphic origin.

What is the sense of motion of Fault F1b and how much lateral displacement did occur along the fault plane of F1b?

The thickness of the Jurassic interval on either side of the fault, as well as the general depositional pattern during the Jurassic can be used to obtain the sense of shear of strike-slip fault F1b, as well as to make a rough estimate about the amount of displacement that occurred along fault F1b. For this purpose, the thickness map of the Jurassic in Figure 29 was used. From this map it can be inferred that the general depocenter of the basin during the Jurassic was towards the west-southwest. Because movement on fault F1b positioned a deeper part of the basin on the western side against a

shallower part of the basin on the eastern side, motion along Fault F1b had to be dextral. When regarding the 750ms contour line on either side of the fault, a right stepping of this contour line can be observed across fault F1b. This step has a length of around 900 meters (measured along the arrow in Fig. 29). Consequently the amount of displacement that was accommodated by fault F1b lies in the order of 900 meters.

When was fault F1b active?

The fact that fault F1b offsets strata of the entire Upper Jurassic indicates that it was active during or after the (Upper) Jurassic. From Fig. 31 can be inferred that the distribution of the Rijnland group was controlled by a larger antiform that extends across fault F1b. Hence, fault F1b already formed before the Rijnland Group was deposited. A narrower constraint on the time can be obtained from Figure 30, which shows the thickness of a Upper Jurassic sequence 2 interval. Although it was not possible to extract a detailed and complete thickness map of this stratigraphic interval on both sides of Fault F1b because of resolution difficulties, it seems that the isopach lines curve into Fault F1b on its western side, thereby suggesting that the depositional pattern was controlled by Fault F1b. This would mean that Fault F1b was active during the Later part of the Upper Jurassic. Additionally a time constraint of Fault F1b can be obtained from Figure 33, which shows a spectral decomposition map of the base of the Rijnland Group. Two depositional fan sedimentary structures can be seen in this map, as indicated by the darker, high frequency areas. The eastern structure seems to be bounded by Fault F1b as it follows the outline of the fault. This would suggest that the deposition of this fan was bounded by Fault F1b. Possibly because Fault F1b had created some topography which inhibited the fan of crossing the fault. Overall, it is concluded that Fault F1b was active during the latest part of the Upper Jurassic and perhaps during the very earliest part of the Cretaceous.

What is the relation between Fault F1b and the Faults F2b and F3b?

Fault F2b and Fault F3b are both normal faults that were active during the Upper Cretaceous and lower Paleogene (F2b). It is remarkable that both Fault F2b and Fault F3b have the same strike as Fault F1b, thereby creating a small graben above Fault F1b in the Upper Cretaceous and Lower Paleogene. This could be explained by the fact that strike-slip Fault F1b had created a weak zone, which was more easily deformed during the Late Cretaceous and Lower Paleogene in a regional setting of thermal sag, following the Jurassic rifting. An additional factor that might have played a role could be that normal faulting occurred here due to different amounts of material compaction on either side of the fault, as different parts of the basin were placed against each other

4.3 Case Study C ; Strike-slip fault with fault-salt interaction.

Observations regarding Fault F1c

Fault F1C is located in the F11 block, which encompasses the central part of the Dutch Central Graben (Fig. 20). The fault is indicated as Fault F1C on the similarity map of the base of the Altena Group in Figure 34. From Fig. 34 can be inferred that Fault F1C is characterised by a curved strike and that it connects two diapirs; Diapirs A and B. The southern part of Fault F1C strikes NNE-SSW (020) . Further towards the north, the strike of the fault slightly curves towards N-S (000) and subsequently towards NW-SE (330) upon approaching salt Diapir B. Before merging with this salt diapir at its northwestern tip, Fault 1C runs parallel to the salt Diapir B. Fig. 35 shows a ENE-WSW cross-section through Fault F1c, from this can be inferred that Fault F1c is characterised by a nearly vertical dip angle of the fault plane, which is slightly dipping towards the east. The fault also displays an upward widening of the fault pattern, as well as concave upward dipping strata on either side of the fault; a so called tipi shape of the strata. The fault is offsetting strata of the Upper Jurassic Puzzle hole formation, Middle Graben formation and Lower Graben Formation, as well as strata from the Lower Jurassic Altena Group (including the Posidonia shale formation) and strata of the Upper Germanic Trias Group. Strata of the Lower Germanic Trias Group appear also to be displaced by Fault F1c, although this can't be determined with certainty. Whether Fault F1C penetrates the salt of the Zechstein group and offsets also sub-Zechstein strata is unclear due to the reduced resolution of the seismic data at this depth. Striking, when regarding Fault F1c, are the major differences in stratigraphic thickness of the Jurassic formations on either side of the fault. Both the Lower Jurassic as well as the Upper Jurassic formations are thicker on the western side of the fault than on the eastern side of the fault. This is visualised in Fig. 36 , which shows a thickness map of the Lower Jurassic Altena Group.

Observations regarding Fault F2c

Fault F2c two forms the same curved fault pattern as Fault F1c; striking NNE-SSW (020) in the southern part and subsequently turning towards N-S (000) and NW-SE (330) towards the northern part of the fault (Fig.34). The fault terminates at salt Diapir B. The fault is dipping towards the west and the fault plane is less steep than Fault F1c (Fig. 35). Fault F2c shows clear vertical offsets of around 150ms TWT in the strata up to and including the chalk group. The strata of the Lower North Sea Group display a small vertical offset of around 20ms TWTT. Both the Triassic and the Jurassic formation don't display any thickness differences that are related to activity along Fault F2c. Strata of the Chalk Group do show a thickness increase towards Fault F2c in the form of a syn-kinematic wedge.

Observations regarding Fault F3c

Fault F3c is striking E-W to ENE-WSW. It is located between Diapir B and a salt wall towards the west (not shown in Fig. 34). Fig. 37 shows a SSW-NNE cross section of Fault F3c. From this cross section can be inferred that the dip angle of Fault F3c increases with increasing depth. It can also be inferred from Fig. 37 that Fault F3c has accommodated an offset of around 150msTWT of the Lower North Sea Group. Fault F3c has also affected the entire Jurassic interval where it has accommodated an offset of around 350ms TWT. The fault seems to detach on an Upper Triassic evaporite; either the Röt evaporite or the Muschelkalk evaporite. No signs of syn-kinematic growth strata can be observed in the hanging wall of Fault F3c

Observations regarding Fault F4c, F5c and F6c

From Fig. 34 can be inferred that the Base of the Posidonia shale northeast of salt Diapir B is affected by several faults that strike approximately NE-SW. When this fault zone is seen in cross-section (Fig. 38), it turns out that the majority of these faults detach in the evaporates of the Upper Germanic Trias Group, likely the Keuper evaporite. These faults are indicated as F5c in Fig. 38. Faults F5c are characterised by inclined fault planes and affect the strata that are present above the Triassic Keuper formation up to and including the strata of the Chalk Group. Generally, the Chalk Group is thicker in the hanging wall of these faults. Fault F6c also detaches intra Upper Triassic and affects the Lower North Sea Group, the Chalk Group, Rijnland Group, the Upper Jurassic and the

Altena Group and has accommodated a minor normal offset of around 30ms in these formations. Fault F4C on the other hand also accommodates offset in the Lower part of the Upper Germanic Trias Group, the Lower Germanic Trias Group as well as in the Altena Group. Whether or not Fault F4c offsets strata in the Upper Jurassic Group and the Rijnland Group is unclear due to the limited thickness of these Groups. The strata on either side of Fault F4c show a slight upward dip towards the fault plane. This tipi shape is profound in the Upper Germanic Trias Group and the Altena Group but is for sure absent in the Chalk Group and the Lower North Sea Group . Additionally, Fault F4c displays an upward widening of the fault pattern up to and including the strata in the Altena group.

Because of Mid-Kimmerian and/or Alpine erosion, which has affected the Jurassic strata up to and including the Altena Group west of the fault, it is hard to say something about the stratigraphic thicknesses of the Jurassic strata on either side of Fault F4c. The Upper Germanic Trias Group has been entirely preserved on either side of the fault. The Lower part of the Upper Germanic Trias Group (probably the Röt and the Muschelkalk formations) are thinning towards salt Diapir C. Strata of the upper Germanic Trias Group (likely the Keuper formation) strongly increase in thickness towards salt Diapir C. However, despite this increase in thickness towards salt Diapir C, the strata of the Upper Germanic Trias Group appear to make a sudden increase in thickness across Fault F4c.

Observations regarding the salt structures

Salt Diapir A is only partly located within the seismic dataset of case study C but it appears to have a circular geometry (confirmed with other seismic data). Strata of the Upper Germanic Trias Group display thinning towards the salt dome. Strata of the Lower Jurassic Altena Group as well as strata of the Upper Jurassic become thicker towards the salt Diapir A.

Salt Diapir B has an elongated geometry. The salt structure is at its widest in the NW-SE direction (around 7km) and at its shortest in the NE-SW direction (around 2km). Salt Diapir B furthermore also extends towards the east, outside of the seismic dataset. Strata of the Uppermost part of the upper Germanic Trias Group, as well as strata of the Lower Jurassic Altena group become thinner towards the salt dome. Strata of the upper Jurassic become thicker towards salt Diapir B.

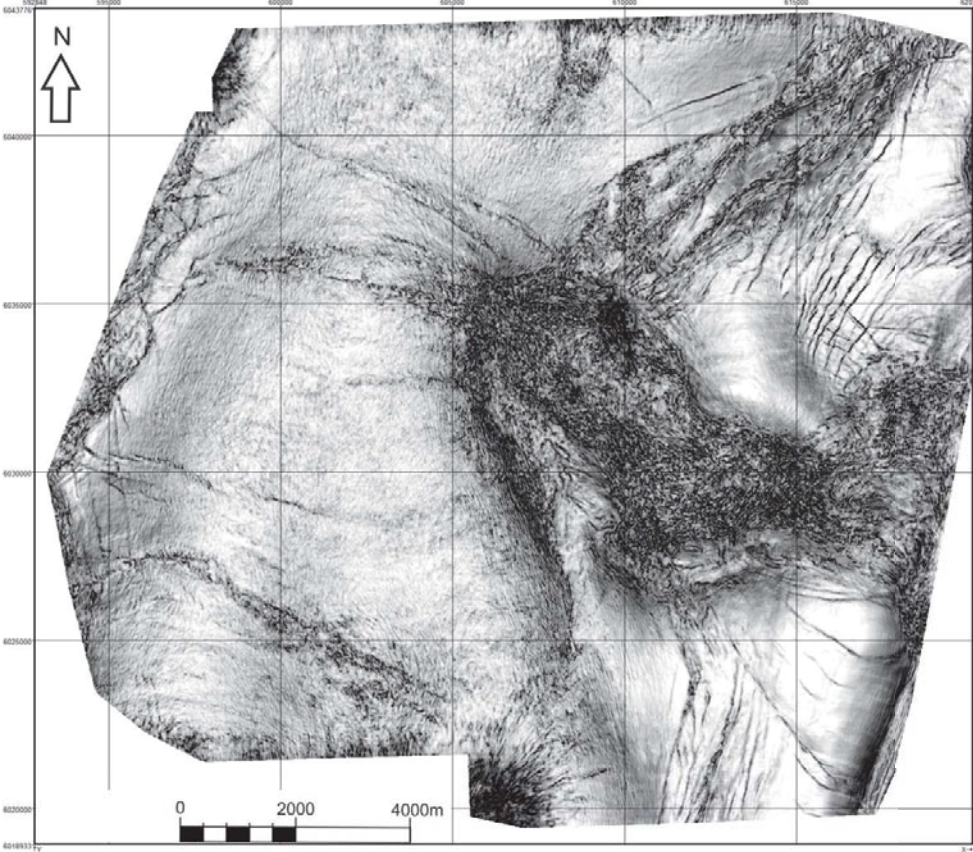


Fig. 34a.
Uninterpreted
similarity
attribute map of the

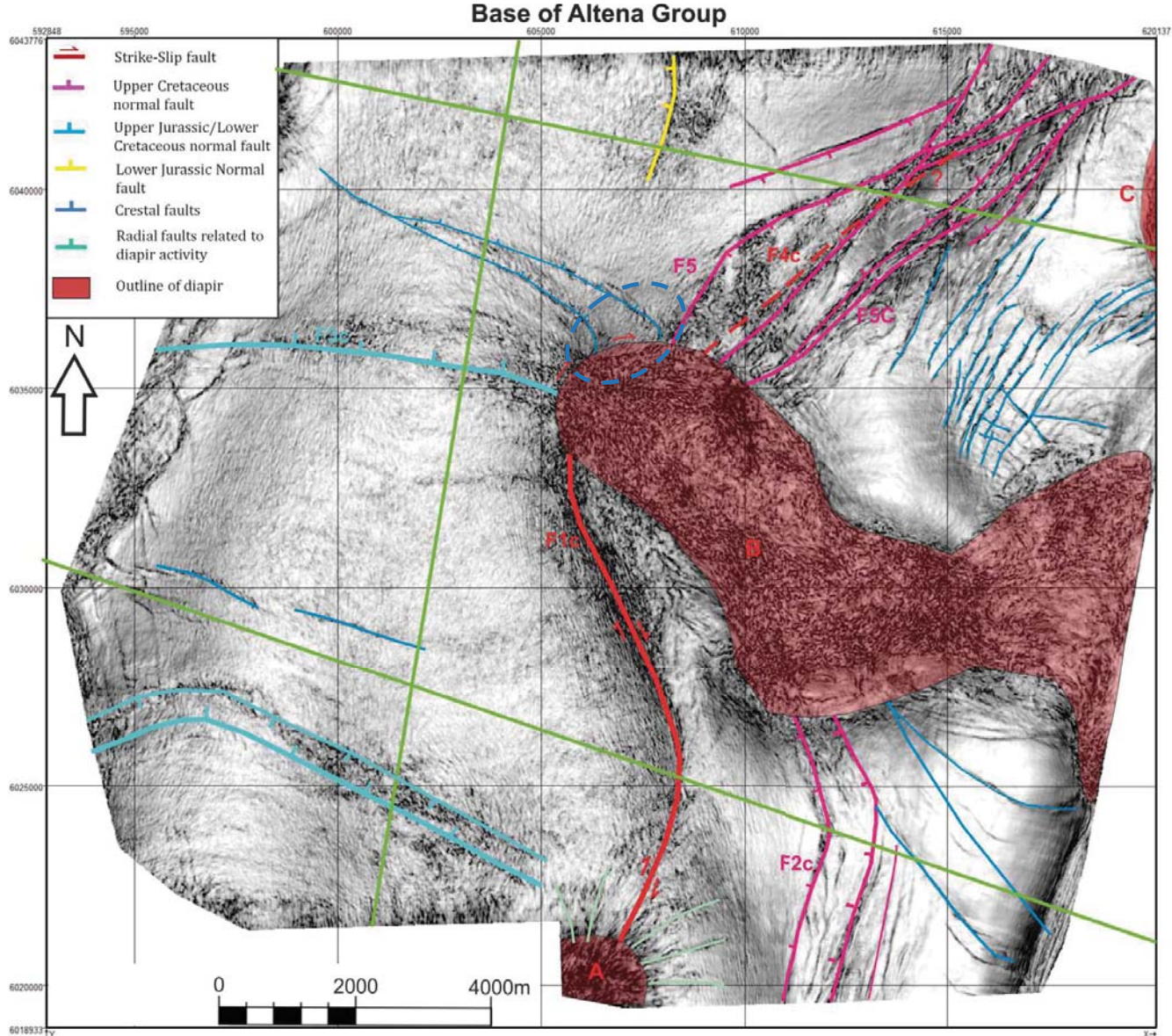


Fig. 36b. Similarity attribute map of the base of the Altena Group in block F11. The black areas indicate a high degree of dissimilarity, the white colours indicate a high degree of similarity (see methods). Fig 36a shows the interpreted similarity map of the base Altena Group. The bright green straight lines indicate the location of the seismic lines in the Figures 37, 39 and 40.

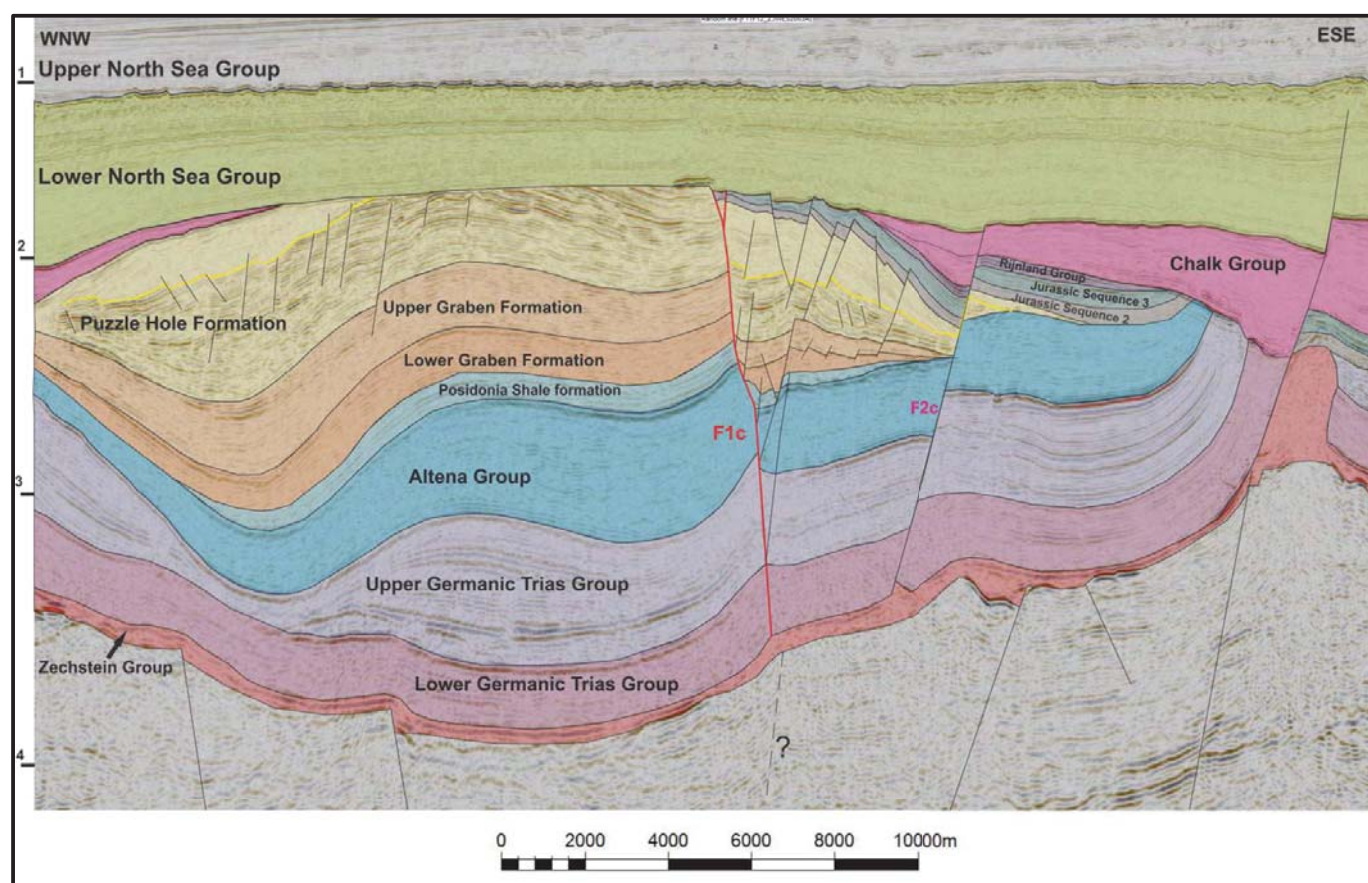
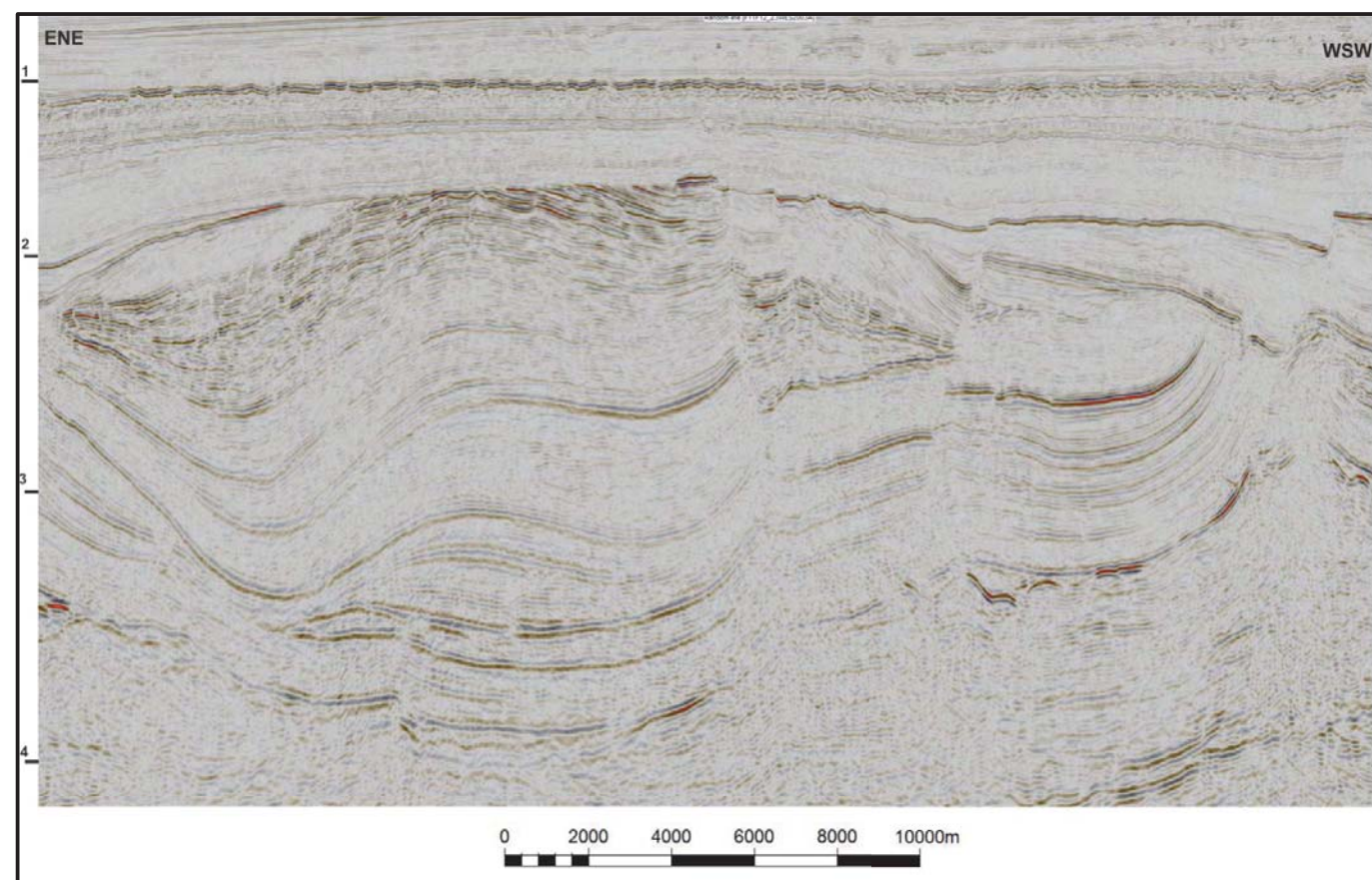


Fig. 35. ENE-WSW cross-section showing fault F1c and fault F2c. The top figure shows the uninterpreted seismic line, the bottom figure shows the interpreted seismic line. The location of the seismic line is indicated by the straight bright green line in Figure 36b.

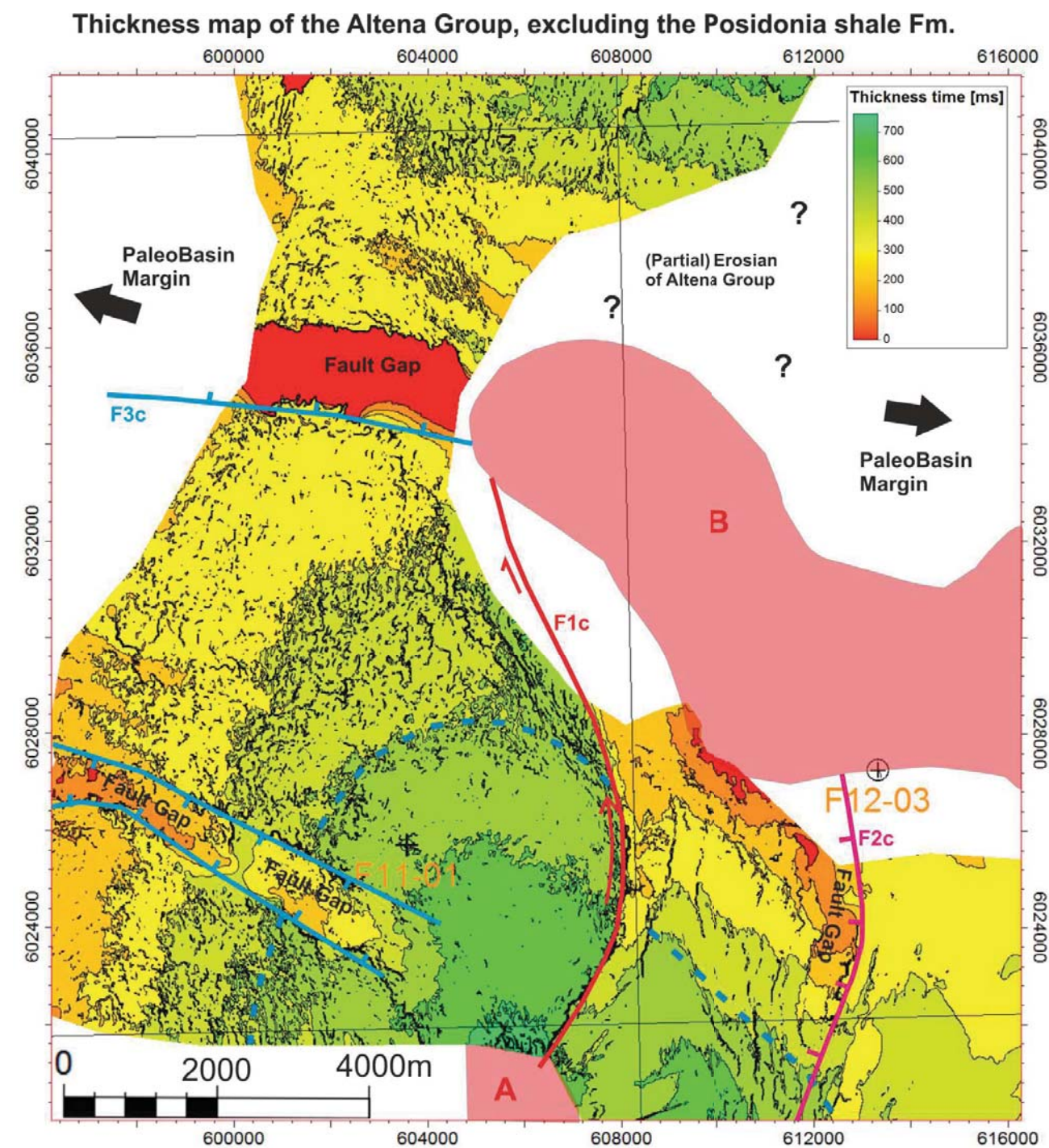


Fig. 36. Isopach (TVT) map of the Altena Group in the F11 block. The Dashed Blue line indicates the approximate position of the 500ms contour line from which an estimate of the amount of displacement along Fault F1c is made. A reliable thickness map of the area could not be made towards the north of salt Diapir B as the Altena Group is not complete there because of Mid-Kimmerian erosion.

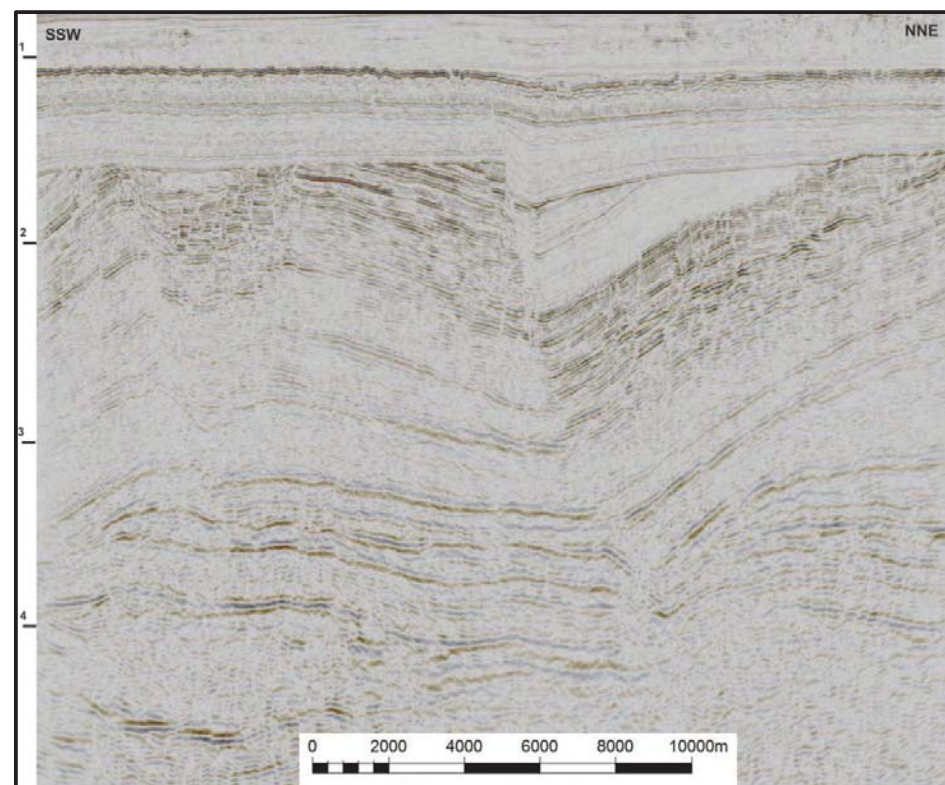


Fig. 37. NNE-SSW seismic cross-section showing fault F3c. The location of the seismic line is indicated by the straight bright green line in Figure 34b.

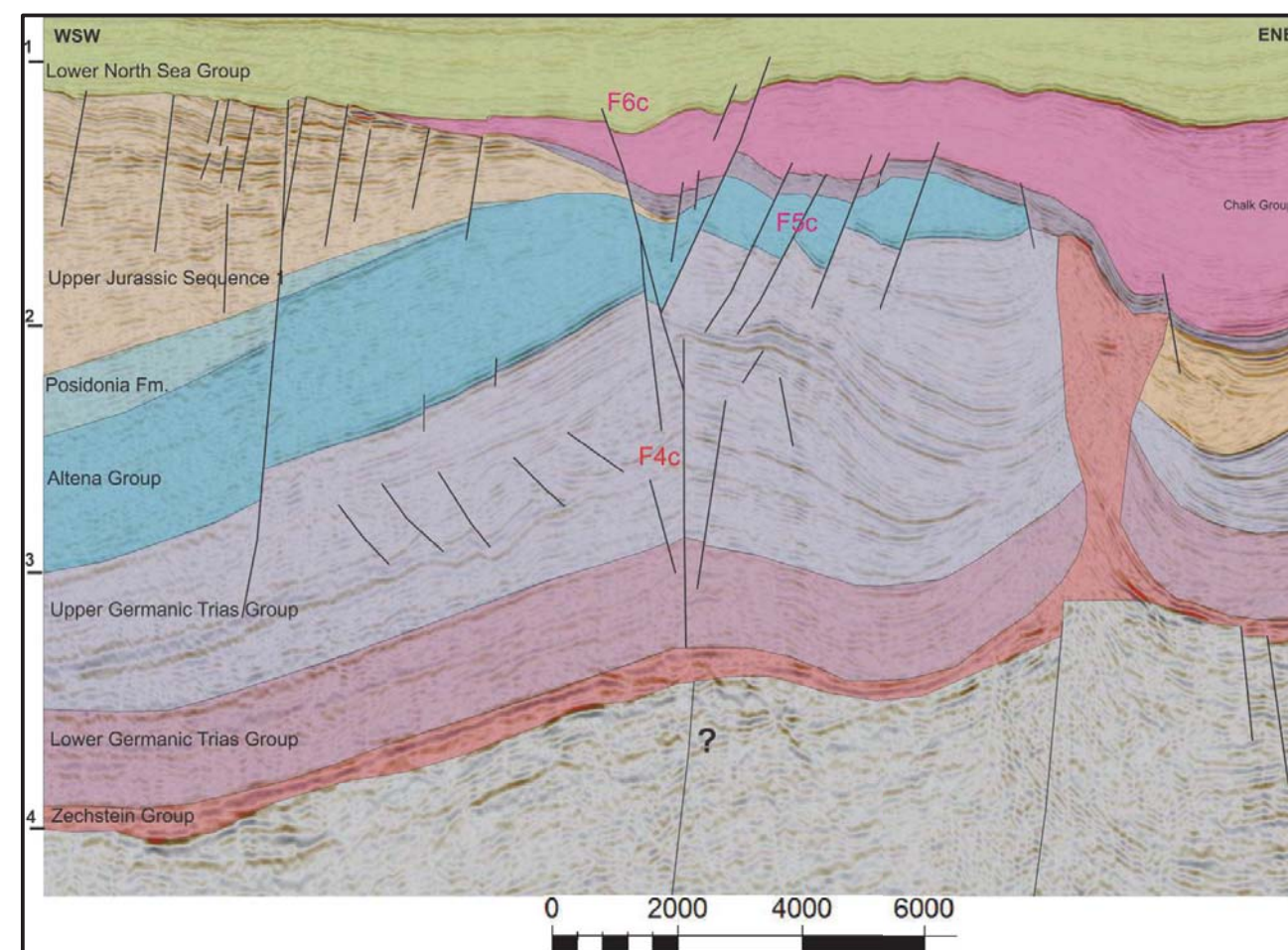
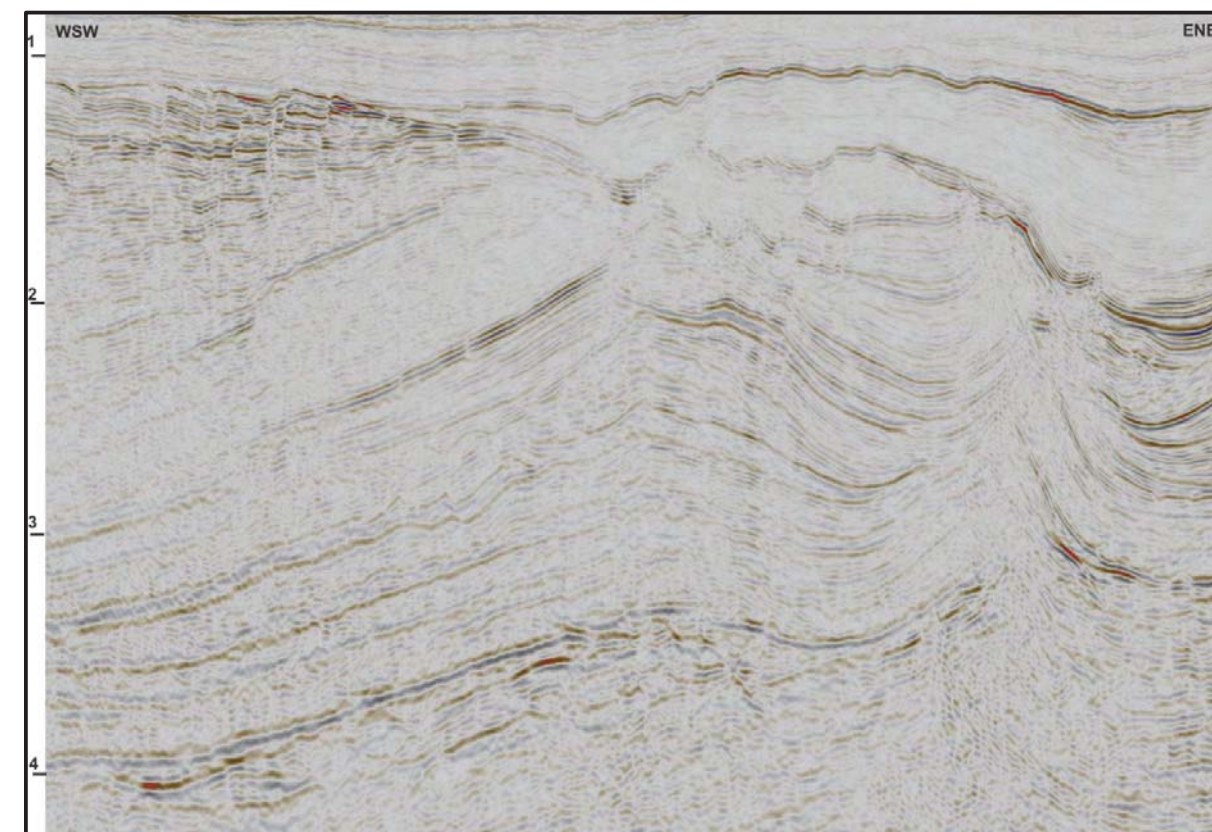


Fig. 38. ENE-WSW seismic cross-section showing the faults F4c, F5c and F6c. The location of the seismic line is indicated by the straight bright green line in Figure 36b.

Interpretations

Why is Fault F1c a strike-slip fault?

The nearly vertical fault plane of Fault F1c, as well as the concave upward bending of strata on either side of the fault, the upward widening of the fault pattern and the unresolved stratigraphic thickness differences on either side of the fault, leads to the interpretation that Fault F1c has accommodated strike-slip motions. This strike-slip motion would have brought a deeper part of the basin where more sediments had accumulated during the Lower Jurassic next to a more proximal part of the basin, where the Lower Jurassic formations are thinner. The option that a normal fault (with growth strata in the hanging wall) would be responsible for the observed stratigraphic thickness differences is ruled out because such a fault would have had a westward dipping fault plane. Additionally, the thinning of Jurassic strata towards the basin margin in the east can't explain the sharp contrast in stratigraphic thickness that is observed across the fault plain.

What is the sense of motion of Fault F1c and how much lateral displacement did occur along the fault plane of F1c?

The thickness differences in the Jurassic on either side of the fault can be used to obtain the shear sense of the strike-slip fault. They can also be used to make a rough estimate about the amount of displacement that was accommodated by Fault F1. This was done by making use of the thickness map of the Altena Group in Fig.36. From this map can be inferred that the regional depositional pattern is characterised by a general thickening of Lower Jurassic strata towards the south. The fact that the Lower Jurassic interval towards the west of Fault F1c is thicker than the Lower Jurassic interval towards the east of Fault F1c indicates that the block towards the west of the fault has moved in northern direction with respect to the eastern block, thereby opposing a relatively thick lower Jurassic interval at the west of the fault against a relatively thin Lower Jurassic interval at the eastern side of the fault. When regarding the 500ms contour line of the Lower Jurassic Thickness map (indicated by the dashed blue line in Fig. 36), an estimate about the amount of displacement on Fault F1c can be made by assuming that it was displaced as described above and that it originally correlates with the 500ms contour line on the other side of the fault. When this is done, the amount of displacement turns out to be in the order of 2km. It is imported to notice that the dashed blue line in Fig. 36 along which the distance was measured doesn't follow the outline of the light green area because this area contains some mapping uncertainty as it is close to Diapir B. Hence it was chosen to follow the normal distance between the 500 and 600ms contour line as is indicated by the regional depositional pattern, which leads to a curved dashed line.

Additionally a rough estimate on the amount of displacement that occurred along Fault F1c can be obtained by the drag that can be seen in Lower Jurassic crestal faults (encircled by the dashed blue line in Figure. 34b) the fact that these crestal faults curve into the salt diapir confirms the dextral sense of motion that was obtained from the interpretation of the thickness map of the Altena Group. When the distances between the tip of the crestal fault right next to the diapir, and the assumed normal location of the crestal fault is measured. A minimum of 700m of horizontal motion should have occurred along this part of the fault-diapir system.

When was Fault F1c active?

The fact that the fault is offsetting the Jurassic strata up to and including the Puzzle Hole formation indicates that the fault was active either during deposition of the Puzzle Hole formation but most likely after deposition of the Puzzle Hole formation. In the F11 block, the Lower North Sea Group is overlying the Puzzle Hole formation in the centre of the Dutch Central Graben. This means that there is a hiatus present where the Jurassic Sequences 2 and 3, as well as the entire Cretaceous is missing. It is likely that Fault F1 was active somewhere during this time interval. The minor offset which is present in the Lower North Sea Group is likely to be caused by a later episode of normal faulting along or above Fault F1c.

What is the relation between Fault F1c and the salt Diapirs A and B?

The fact that the strata of the Lower Jurassic Altena Group and the strata of the Upper Jurassic Sequence 1 thicken into salt Diapir A indicates that salt Diapir A was in the active piercing stage during this time period, thereby creating a rim syncline directly around the diapir which caused the strata of the Altena Group and the Jurassic Sequence 1 to thicken into the diapir. Salt B reached the piercing stage slightly later, as no thickening in the Altena Group can be observed towards the diapir. However, during the deposition of the Upper Jurassic Sequence 1, salt Diapir B must have been in the active piercing stage as well.

As mentioned, the exact timing of strike slip Fault F1c remains a bit elusive. However, activity on Fault F1c for sure postdates the puzzle hole formation and hence Jurassic Sequence 1. This means that the Diapirs A and B likely predate Fault F1c. Because the salt diapirs are mechanically weak, they have probably accommodated strike-slip motions in this area as well, which is supported by the drag that is observed at the crestal faults (Fig. 34b). It is suggested that because of the absence of salt in the area around F1c, strike-slip motion had to be accommodated in a brittle way by creating Fault F1c. Fault F1c hence links Diapirs A and B that likely have both accommodated strike-slip motions as well.

It is likely that strike-slip motion did not cease at Diapir B, but that it continued along Fault F4c. Surely Fault F4c shows characteristics of a strike-slip fault including a nearly vertical fault plane, upward widening of the fault pattern and a tip-shape of strata on either side of the fault. Therefore it is suggested that the strike-slip motion accommodated by Fault F1c continued via Diapir B into Fault F4c. The different strike of Fault F4c compared to Fault F1c could be explained by the presence of Diapir B, which could have refracted the strike-slip motion to some extent. However, this interpretation regarding strike-slip motions on Fault F4c needs to be hedged as the Upper Jurassic around F4c is missing due to erosion.

Case Study D; Strike-Slip faulting in the Terschelling Basin and on the Schill Grund High

Structural Observations

NW-SE to WNW-ESE striking faults.

Terschelling Basin

The Terschelling Basin is bounded in the North and South from the Schill Grund Platform and Central Offshore Platform by the Rifgronden fault zone (RFZ) and the Hantum Fault Zone (HFZ) respectively (Fig.39). The HFZ is characterised by a generally straight ESE-WNW strike and dips towards the NE. When the HFZ approaches the Dutch Central Graben, it splits into multiple branches of which the most northern branch shows a curved geometry and eventually merges with the N-S trend of the Dutch Central Graben. The RFZ is composed of more shorter fault segments than the generally straight and continues HFZ. These fault segments display an overall en echelon type of geometry. The majority of the faults that form the RFZ dip towards the Southwest, but some antithetic faults are also present, forming a pop-up geometry on faults of the RFZ. Strata of the Upper Jurassic and the Lower Cretaceous Rijnland Group thicken into the hanging wall of both the HFZ and the RFZ (Peeters, 2015). Strata of the Chalk Group and the Lower Paleogene North Sea Group are sometimes thicker in the footwall than in the hanging wall of the faults that form the HFZ and the RFZ. Besides the large RFZ and HFZ, also smaller NW-SE to WNW-ESE striking faults occur in the Terschelling Basin (Fig. 39). These faults generally detach on the Zechstein salt and also display thicker Upper Jurassic and Lower Cretaceous strata in their hanging wall (Fig. 39).

Schill Grund Platform.

On the Schill Grund Platform, the NW-SE, WNW-ESE fault trend is generally not well developed (Fig.40 and Fig. 41). However, there are some areas where thin-skinned extension occurred along WNW-ESE trending supra salt grabens (Figs. 41 and 43). These grabens show an increase in thickness of the Upper Cretaceous Rijnland Group. Some grabens additionally display a slightly thinner Upper Cretaceous Chalk Group above their core. The Grabens detached on a thin layer of Zechstein salt. This thin layer of Zechstein salt has been pushed-up by another evaporite layer that has its origin in the Upper Rotliegend interval. This Upper Rotliegend evaporite seems to be present only in the southern part of the Schill Grund Platform. In the Terschelling Basin, no evidence of these Upper Rotliegend evaporites has been found.

N-S to NNE-SSW striking low Angle Detachment faults.

The Lower and Upper Triassic interval in the Terschelling Basin, and the adjacent Schill Grund Platform and southern part of the Central Offshore Platform, has been affected by a zone of low angle detachment faults. In the Terschelling Basin and on the Central Offshore Platform, there is one dominant low angle detachment fault (indicated as DF1 in Fig. 39). The low angle detachment faults strike roughly N-S on the Schill Grund High and on the Central Offshore platform (Figs. 39, 40 and 41). In the Terschelling Basin, the main low angle detachment fault trends more NNE-SSW. Additionally, also the salt walls in the Terschelling Basin, as well as the outline of the Lower Triassic Röt compartments that are bounded by the salt walls display this NNE-SSW trend.

The low angle detachment faults are not characterised by true fault planes. In fact, movements are accommodated by the salt as extension continues. These kind of structures have been described by Hudec and Jackson (2007) as salt rollers. The Lower and Upper Triassic interval both downlap on the Zechstein salt that acts as a decollement for the salt rollers (Fig. 42). This downlapping is accompanied with a dramatic increase in thickness of the Upper Triassic interval (Fig. 42).

Thickness maps of the Upper Triassic formations (Peeters, 2015) indicate that some low angle detachment fault segments caused a dramatic increase in the thickness of the Röt Formation,

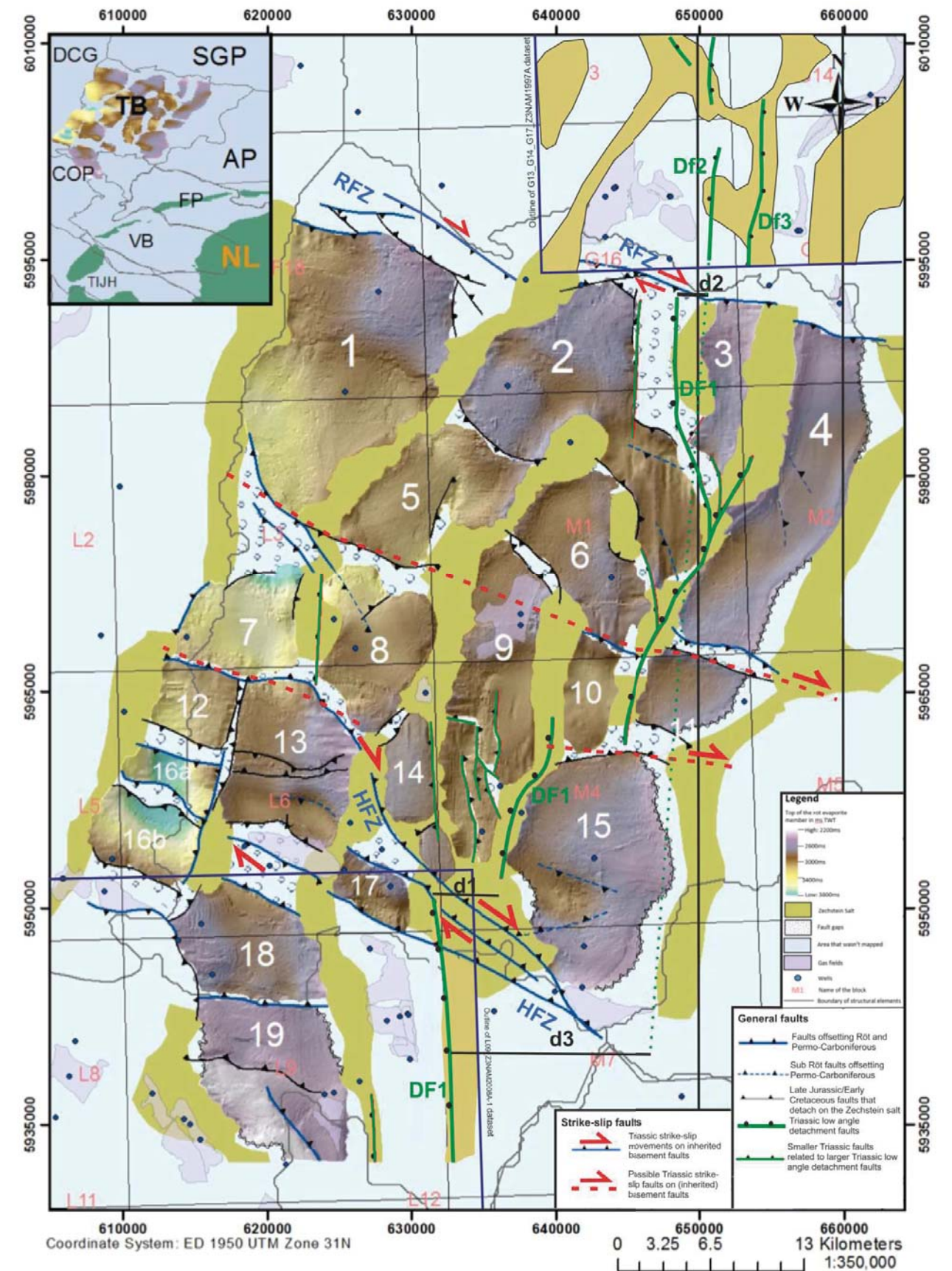


Fig. 39. Map showing the base of the Upper Triassic Röt evaporate in ms TWT. As well as the regional fault trends. Abbreviations; HFZ=Hantum Fault Zone, RFZ=Rifgronden Fault Zone, DCG= Dutch Central Graben, SGP=Schill Grund Platform, TB= Terschelling Basin, AP=Ameland Platform, COP= Central Offshore platform, VB= Vlieland Basin, FP=Friesland Platform, TIJH=Texel IJsselmeer High. Picture modified from an EBN Project (Peeters, 2015)

while others show thickening of the Muschelkalk Formation and/or the Keuper Formation. Locally also the the Latest Upper Triassic interval dramatically thickens due to movements along the detachment faults as is the case in the northern part of the Central offshore platform and in compartment 17 in the Terschelling Basin (Fig. 39)(De Jager, 2012; Peeters 2015). In these areas, Late Lower Triassic movements caused the deposition of a thick sandstone interval known as the Solling Fat Sandstone Member, which holds significant amounts of gas in the G14 fields (Fig. 39) (De Jager, 2012).

In the Terschelling Basin, the low angle detachment faults dip solely towards the WNW. In the Adjacent northern part of the Central Offshore Platform, the main low angle detachment fault dips towards the West. On the Schill Grund High, the low angle detachment faults form shorter segments and dip both towards the west, as well as towards the east. Thereby forming opposing pods of thickened Upper Triassic Strata (Fig. 40). On the Schill Grund Platform, some fault segments show a left stepping pattern (indicated with the letter A in Figure 40). This left stepping pattern can also be found in the basement faults underlying the Zechstein salt in this area (Fig. 41). Noteworthy is also that the sub Zechstein basement faults display an overall NNW-SSE trend, which slightly contradicts with the N-S trending low angle Triassic detachment faults. The stepping geometry of the low angle detachment faults can also be observed in the Terschelling basin. Both left and right stepping of the main low angle detachment fault can be observed here, although the right stepping pattern seems dominant (Fig. 39). Noteworthy is also the right stepping of fault DF1 across the Hantum fault zone and across the Rifgrunden Fault Zone. The right stepping of DF1 across the HFZ and RFZ, as well as within the Terschelling Basin causes that, although DF1 on the Central Offshore Platform has the same strike as the low angle detachment faults on the Schill Grund High (named DF2 and DF3 in Fig 36), their present location is not inline with each other. Instead a distance d3 is present with respect to their imaginary continuation (Fig. 39).

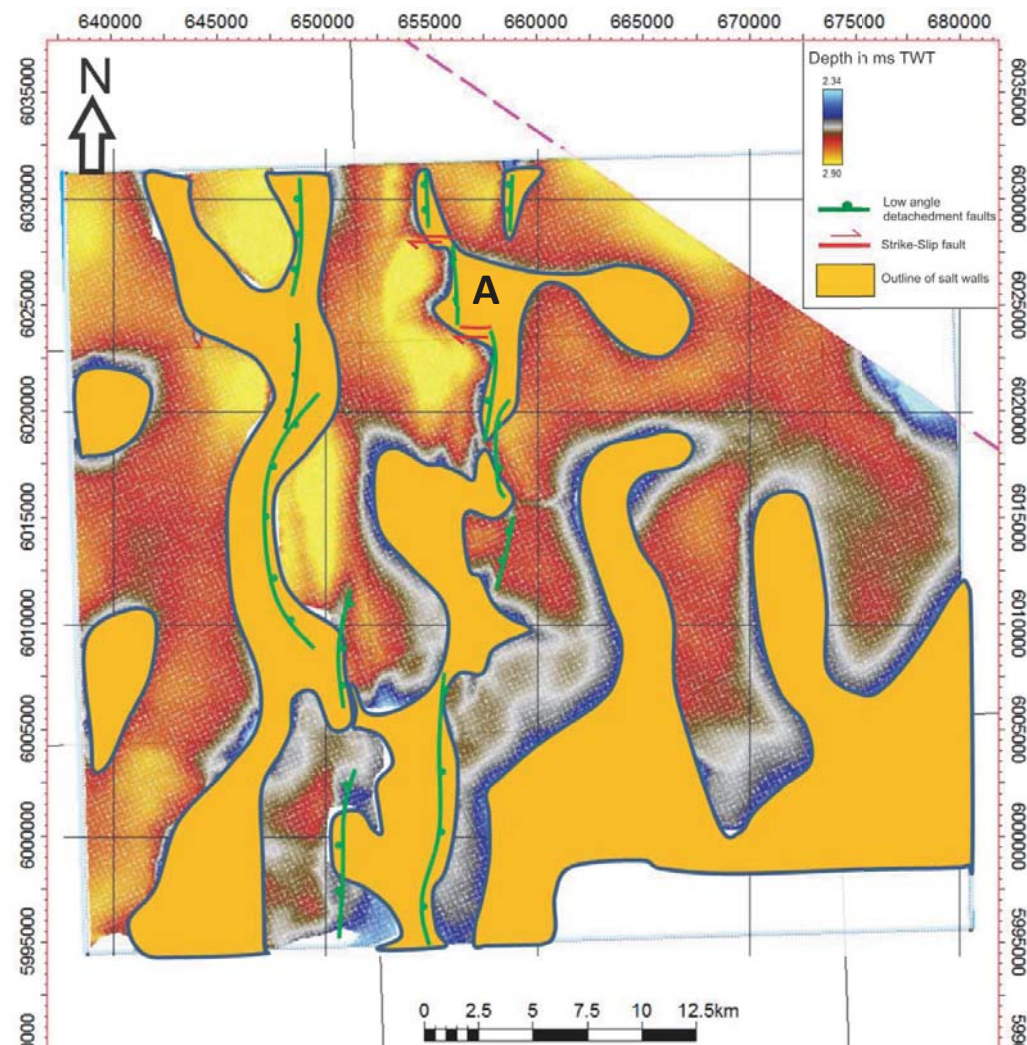


Fig.40. Map showing the base of the Zechstein Group at the Schill Grund High. The southeastern part of this map corresponds to the northeastern part indicated by the blue square in figure 39.

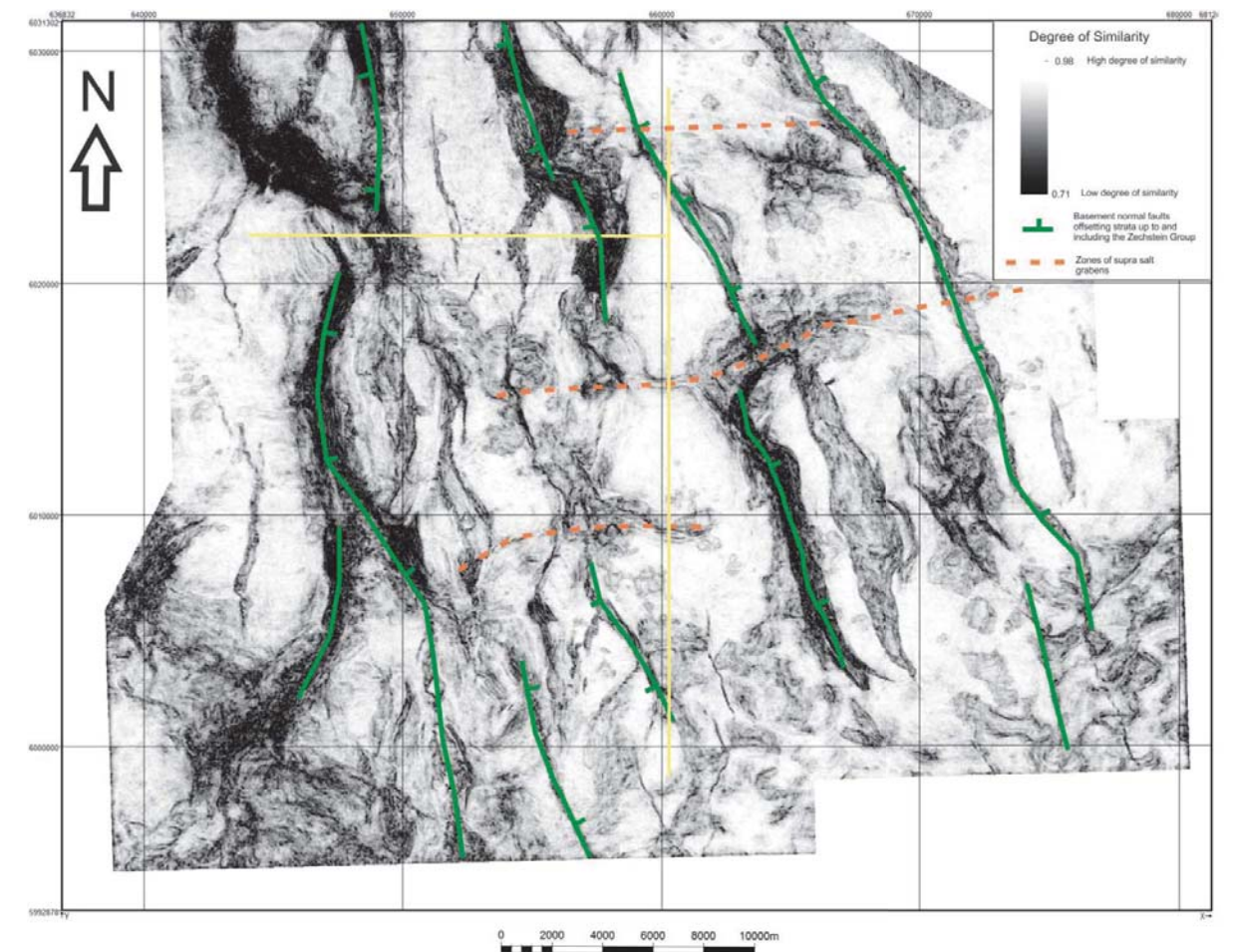


Fig.41. Map showing a similarity attribute of the base of the Zechstein Group at the Schill Grund high. The location of the cross-sections in fig. 39 and fig. 40 is indicated by the yellow lines.

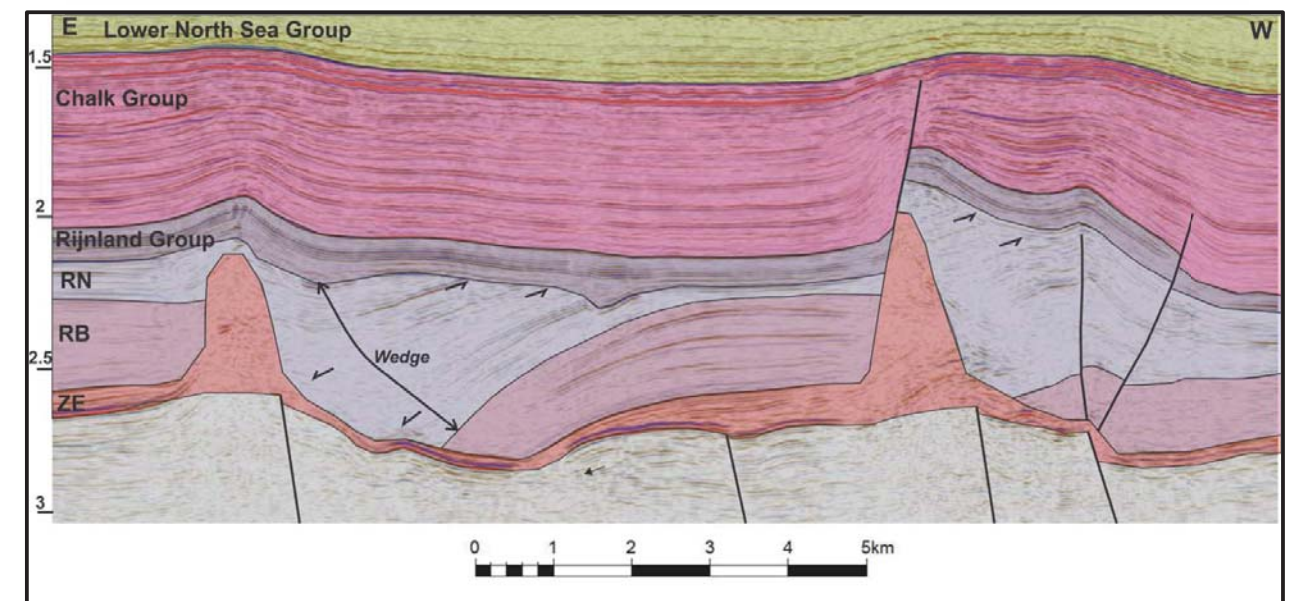


Fig.42. E-W cross-section through the northern part of the Schill Grund High, showing two westward dipping Upper Triassic low angle detachment faults. The most western low angle detachment fault has been inverted during the Upper Cretaceous.

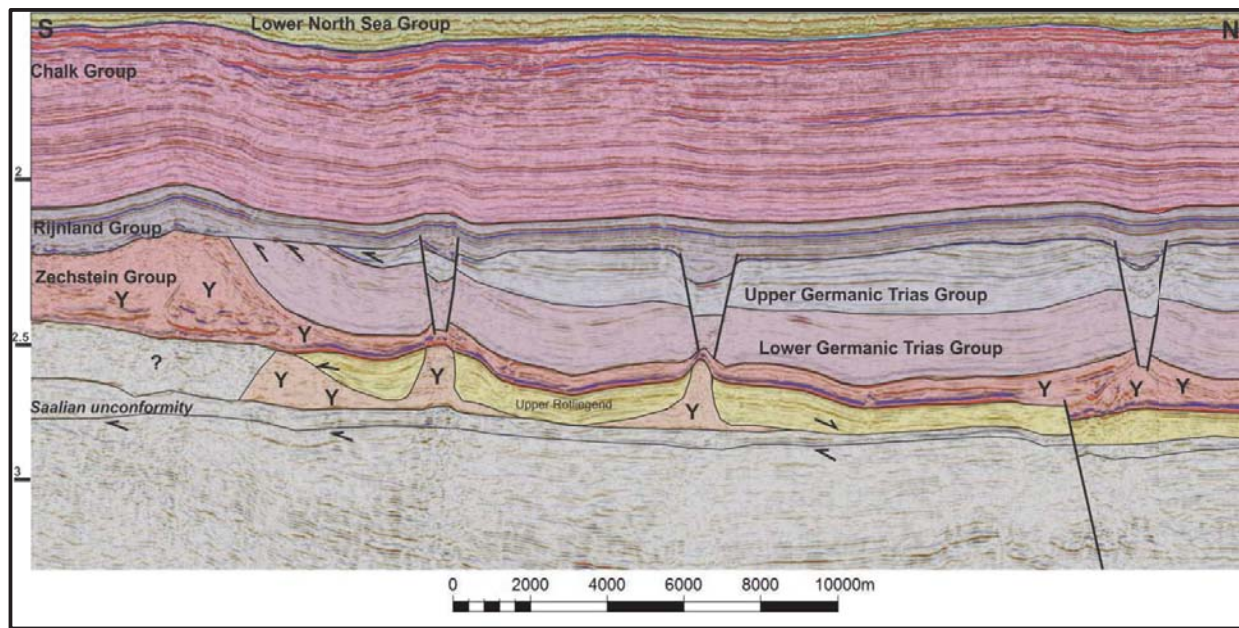


Fig.43. N-S cross-section through the Schill Grund High showing ESE-WNW trending supra salt grabens that formed during the Early Cretaceous as a result of thin-skinned extension. The southern graben was later inverted. Note also that the grabens caused the ascent of Upper Rotliegend Salt, which pushed the remaining Zechstein salt upwards. The location of the seismic line is indicated in figure 41.

Interpretations

Although direct evidence for strike-slip movements in the Terschelling Basin and the adjacent platform areas is not straightforward, regional observations on fault and salt trends described above suggest that strike-slip movements occurred in the Terschelling Basin and to some extent on the adjacent platforms.

Thin skinned strike-slip-motions

The irregular thickness distribution of the Solling, Röt, Muschelkalk and Keuper formations indicates that activity along the low angle Upper Triassic detachment faults did not occur simultaneously. Additionally, the amount of extension on fault segments varies throughout the area. It is likely that these differences in timing and amount of extension led to strike-slip movements during the Middle and Upper Triassic and possibly the Lower Jurassic (although no strata have been preserved of this interval in this area). Surely, differential motions over such a short area have to be compensated. This is indicated for example by the left stepping of the N-S trending low angle detachment fault in the northern part of the Schill Grund Platform (indicated by the letter A in Fig. 40) and the subsequent shift in depocenter towards the northwest (indicated by the arrow in Fig. 40). To form such a structure, the individual fault segments have to be linked by a transform fault that compensates for these differential motions. The strike-slip motions are likely accommodated by the Zechstein salt salt walls that developed in the area in response to regional extension. The motions along these faults is generally small and no evidence has been found that the displacements of these motions exceeds the width of the step between two individual low angle detachment faults. Hence, these displacements are generally in the order of 1 to 2km on the Schill Grund Platform. The displacement are likely larger in the Terschelling Basin, where the steps of the low angle detachment faults are larger than on the Schill Grund High.

These extensional and strike-slip motions are thin skinned as the low angle detachment faults used the Zechstein evaporite as a decollement. The N-S orientation of these low angle detachment faults on the Schill Grund and Central Offshore Platform indicates that the regional stress regime, causing these motions, was E-W extension. This corresponds with the (further) opening of the N-S oriented Dutch Central Graben in the Middle and Upper Triassic. However, these thin skinned motions had to be caused by motions along basement faults, as is indicated by analogue modelling (Vendeville and

Jackson, 1992). Indeed small offsets of the Zechstein Group are observed on the Schill Grund High (Fig. 42). The NNW-SSE trend that was recognised on the Schill Grund platform from the basement faults that offset the Zechstein Group might indicate that the NNW-SSE trend was already established and that the faults following this trend were (obliquely) reactivated during Middle-Upper Triassic E-W extension. In contrast to the Terschelling Basin, the Base of the Zechstein doesn't display a significant deepening towards the west on the Schill Grund Platform (Fig.42). This deepening of the Base of the Zechstein Group in the Terschelling Basin indicates that it is likely that gravitational gliding towards the west (in the direction of the Dutch Central Graben) enhanced thin skinned extension. This would explain why the low angle detachment faults in the Terschelling Basin solely dip towards the west, while on the Schill Grund Platform, they also dip towards the east.

Thick Skinned (basement) Strike-Slip motions in the Terschelling Basin.

The only direct evidence for strike-slip faults on basement faults are the en echelon geometry of the fault segments of the Rifgrunden Fault Zone (RFZ), which suggests that dextral motions occurred along this fault zone. Additionally, also the pop-up geometry of the RFZ may indicate that the fault has accommodated strike-slip motions, although this pop-up geometry might also have been caused by Late Cretaceous inversion. No direct evidence was found for strike-slip motions on the Hantum Fault Zone. However, the fact that the main low angle detachment fault shows a significant rightstepping across the fault zone indicates that dextral strike-slip motions occurred on the Hantum Fault Zone (line d1 in Fig. 39). When the distance of the step across the HFZ is measured along the line d1, a dextral displacement of 5km to 6km is obtained. This displacement estimate might not be very reliable though, as both Late Jurassic/Early Cretaceous extension, as well as Late Cretaceous/Early Paleogene inversion may have modified the original displacement caused by the HFZ. Additionally, it can't be stated with certainty that the fault segments of Fault DF1 were originally attached in the first place. However, the fact that this stepping occurs exactly at the HFZ makes it very likely that the HFZ caused the majority of this displacement as indicated at place d1 in Fig.39. Hence, a dextral motion of 5 to 6km might be a fairly good first order approximation of the strike-slip motion that occurred after the establishment of the low angle detachment fault. Surely, because the HFZ offsets the low angle detachment fault DF1, dextral motions on the HFZ must have postdated the latest Early Triassic, as this is the time that activity along this fault segment initiated. However, it does not mean that dextral motions along the Hantum Fault zone must have postdated the Upper Triassic, when the low angle detachment faults became inactive. Surely, the low angle detachment faults and the dextral activity along the HFZ could have occurred simultaneously.

The main low angle detachment Fault DF1 also appears to be offset by the RFZ in the north of the Terschelling Basin in a similar way as by the HFZ. On the Schill Grund Platform though, multiple low angle detachment faults formed, hence it is a bit unambiguous if DF1 relates to DF2 or DF3 (Fig. 39). However, because DF1 dips towards the west, it is likely related to DF2, which would indicate a dextral displacement of around 2.5km on the RFZ (indicated by line d2 in Fig. 39).

Overall, the NNE-SSW strike of the low angle detachment faults in the Terschelling Basin deviates from the low angle detachment faults on the Schill Grund Platform and the Central Offshore Platform. Additionally also the distribution of the salt walls and the intra-salt Triassic compartments shows this deviating NNE-SSW strike. It is suggested that this deviating trend can be explained by an overall dextral shearing of the Terschelling Basin along its northern (RFZ) and southern (HFZ) boundary faults. Additionally, strike-slip motions inside the graben might have occurred to accommodate for the differential motions between RFZ and HFZ (indicated by the dashed red lines in Fig. 39). To estimate the total amount of dextral displacement that occurred across the Terschelling Basin, an imaginary line from DF2 is drawn south following its strike. Subsequently, the distance between DF1 and this imaginary line is measured. This distance (d3 in Fig. 39) is approximately 13km. Again this distance only provides a rough first order approximation of the total amount of dextral displacement across the Terschelling Basin, as later reactivation of faults might have changed the post-Triassic configuration.

5. Analogue Modelling Results

5.1 Experiment 1; Dextral Strike-Slip followed by Extension. Purely brittle experiment

Strike-Slip Phase

The strike-slip phase of this purely brittle model developed similar to classic Riedel experiments described i.a. by Tchalenko (1970) and Richard et al. (1995). Initially, Y shears and R shears developed during the strike-slip phase of model 1. The first Y and R shears developed after 7% of bulk strike-slip (i.e. after 7% of the total amount of strike-slip movement, which was 3cm in this experiment). The R shears display an en echelon geometry and generally have an angle between 18° and 24° with the trace of the basement fault (i.e. the vertical in figures 44-46). The Y shears develop more or less parallel to the trace of the basement fault. After 25% of bulk strike-slip, the first P shears develop that link the R and Y shears (fig. 44). These P shears develop at a small angle of max 10° to the trace of the basement fault. As the R, Y and P shears become more and more connected, an anastomosing fault pattern develops, here referred to as main displacement zone; or F1. After 40% of bulk strike-slip, the displacement is almost solely accommodated by F1. The interference of P faults with R faults leads to a left stepping of fault F1 in the center of the experiment, where a pop-up is formed and to right stepping of the fault F1 at the lower and upper end of the experiment, where pull-aparts are formed (figures 45). The formation of these pull-aparts is enhanced due to the fact this area is close to the end of the experiment. Consequently, the F1 fault moves out of the experiment with a curve and enhances the subsidence in the pull-aparts. After 55 percent of bulk strike-slip, the main displacement fault zone F1 cuts the anastomosing fault pattern and the pop-up in the center is no longer active. From this moment displacement is solely accommodated by the main displacement fault zone F1 (fig. 46).

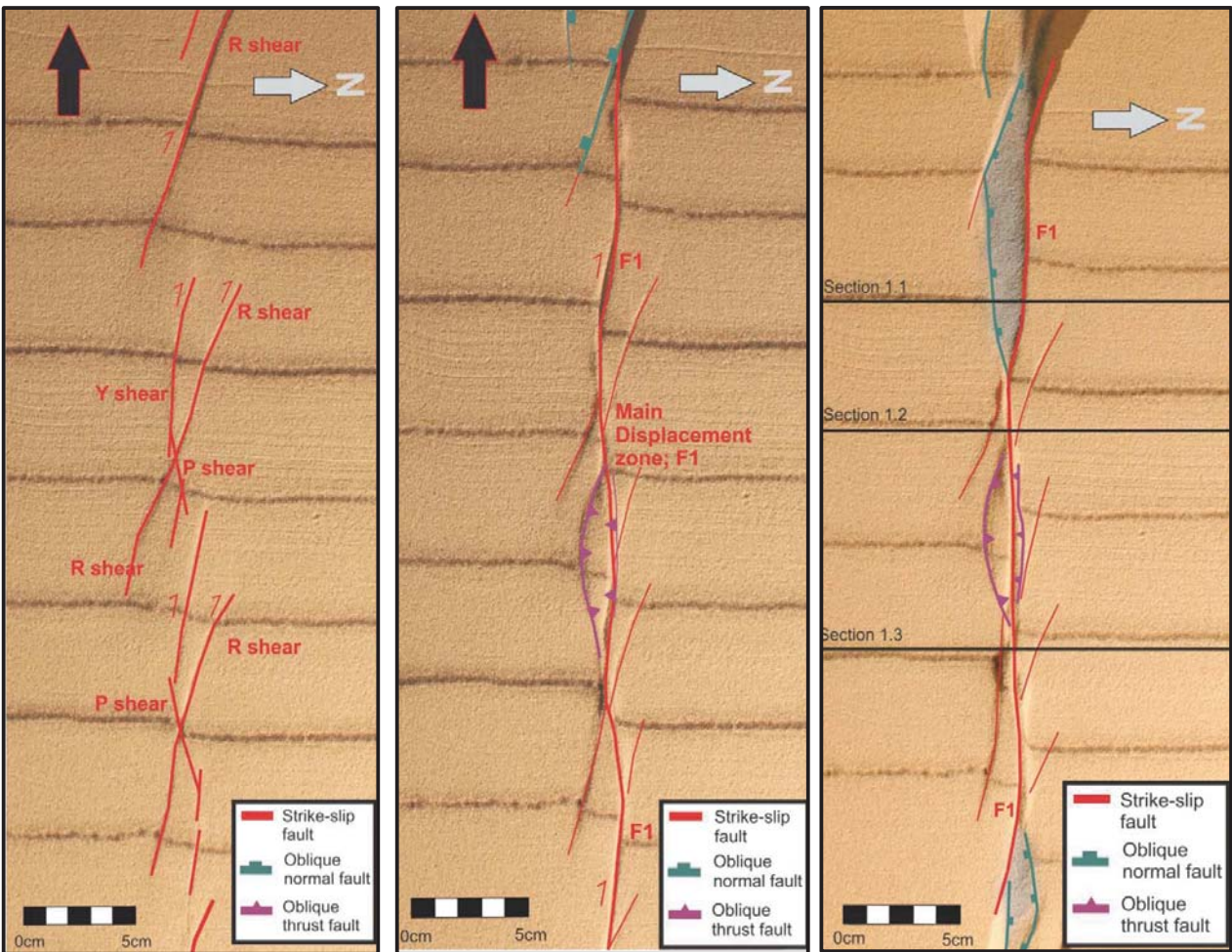


Fig. 44. Top view of model 1 after 28% of bulk strike-slip. The black arrow indicates the side of the experiment where the underlying moving plastic sheet is located. The grey arrow indicates the artificial north

Fig. 45. Top view of model one after 40% of bulk strike-slip. Pop-ups and pull-aparts have formed due to interference between the linked P shears and Riedel shears. Nearly all displacement occurs along F1

Fig. 46. Top view of model one at the end of the strike-slip phase. The locations of the cross-sections are indicated by the black lines.

Extension Phase

Initially, extension is accommodated along inherited R Riedel faults (fig.47 and figures 51-53). Subsidence on these faults is generally not very large and new normal faults develop after 20% of bulk extension(fig.49). The new normal faults first develop towards the artificial north of the strike-slip zone. Initially, these normal faults are relatively short and display a curved geometry. After 27% of bulk extension, these faults get interconnected and a long normal fault develops. This long normal fault first develops on the northern side of the graben. After 35% of bulk extension, a long normal fault has also developed on the southern side of the graben (fig.48). The new deformed normal faults accommodate less subsidence during this stage of the experiment at the western part of the experiment, in the area of the preformed pull-apart basin. After 50% of bulk extension, the long normal faults are fully developed over the entire length of the experiment and displacement solely takes place on these long normal faults (fig.49). The graben gradually subsides during the remaining time of the experiment and the basin floor stays pretty much horizontally. By the end of the extension phase, the former strike-slip zone is located in the center of the graben (cross sections 1.1, 1.2 and 1.3 in figures 51-53). Because it is buried by sediments, it can't be recognized anymore. The graben is at its widest in the western and in the eastern part of the experiment, where the pull-aparts structures had developed during the strike-slip phase.

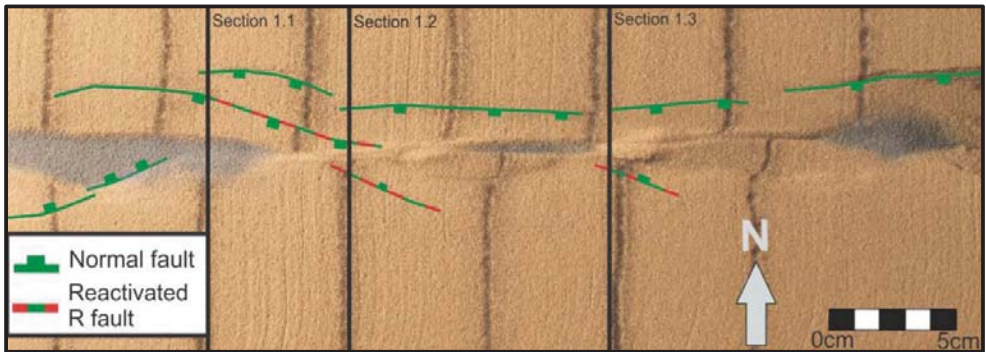


Fig. 47. Top View after 25% of bulk extension. Displacements are still partly accommodated by Riedel faults that developed during the strike-slip phase. Towards the north of the extinct strike-slip zone, a series of connected normal faults develop. The cross-section can be found in figures 51-53.

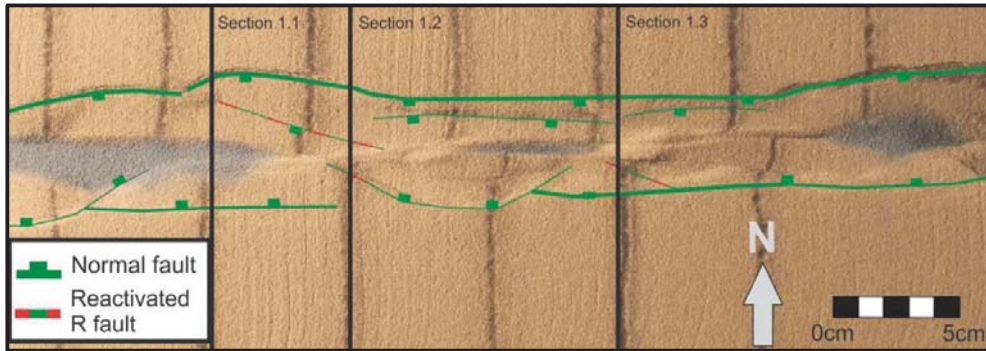


Fig. 48. Top View after 50% of bulk extension. The normal fault zone north of the extinct strike-slip zone is completely interconnected. Also in the south, a large normal fault is being formed. The large normal faults are not well developed yet in the area of the preformed pull-apart basin.

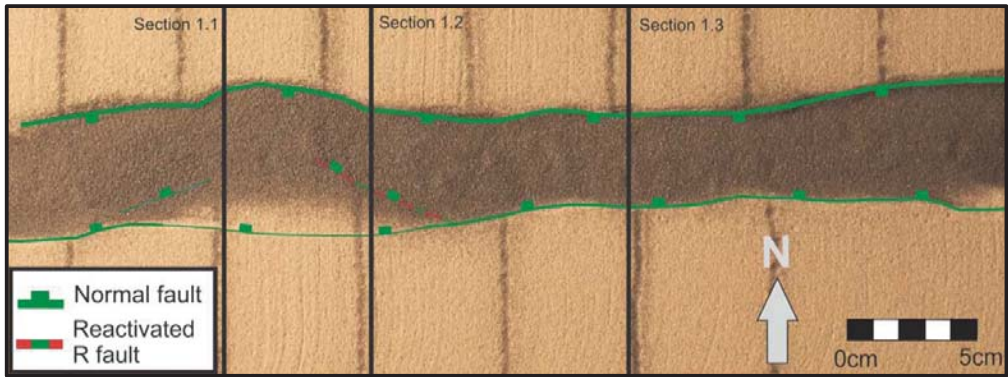


Fig. 49. Top View after 75% of bulk extension. During this stage of the experiment, the large normal faults that bound the graben accommodate all of the displacement.

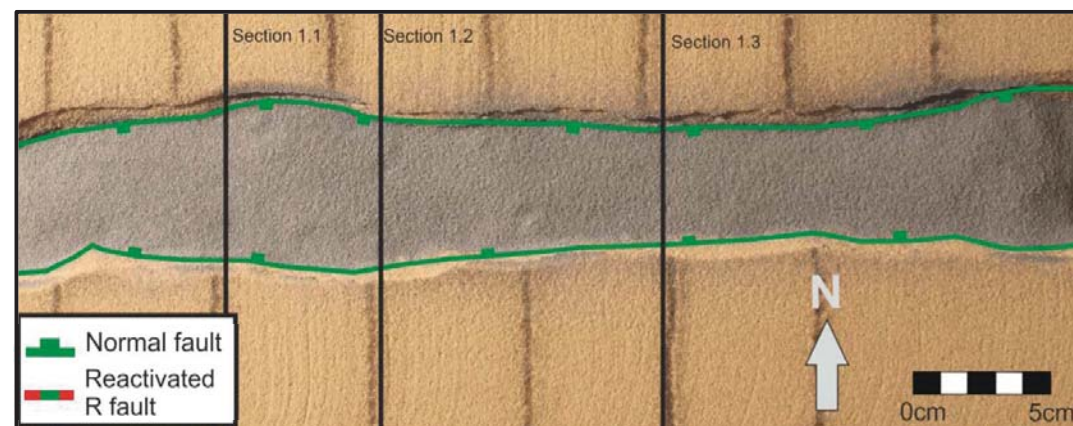


Fig. 50. Top View after the final stage of extension. The graben is at its widest where the pull aparts formed during the strike-slip stage. The strike-slip zone is located in the center of the graben but because it is covered by sediments, can't be recognized in plan view.

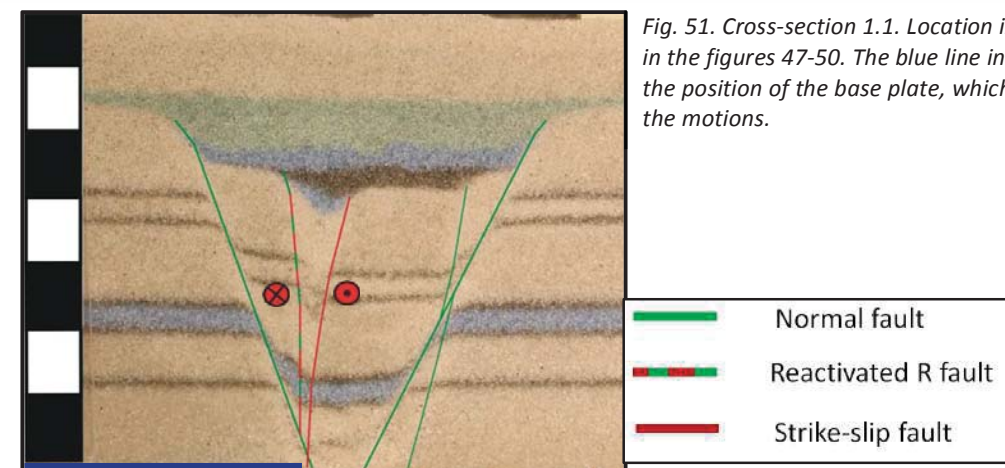


Fig. 51. Cross-section 1.1. Location indicated in the figures 47-50. The blue line indicates the position of the base plate, which induced the motions.

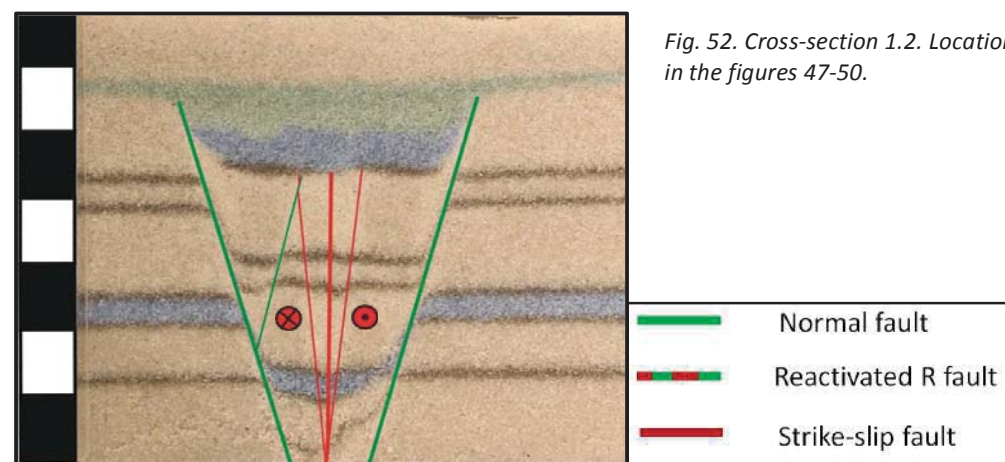


Fig. 52. Cross-section 1.2. Location indicated in the figures 47-50.

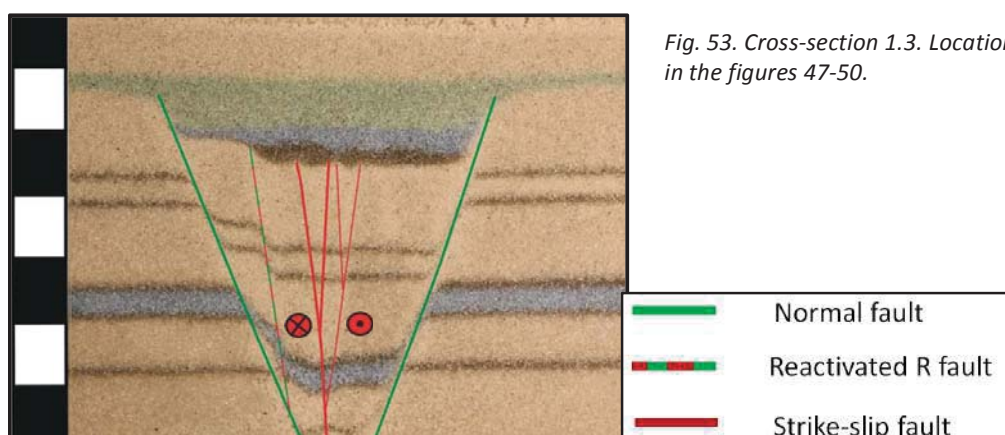


Fig. 53. Cross-section 1.3. Location indicated in the figures 47-50.

5.2 Experiment 2; Extension followed by Dextral Strike-Slip. Purely brittle experiment

Extension phase

After 15% of bulk extension, a series of normal faults with opposing fault dips formed. These faults initially had a slightly curved strike with a conchoidal fault plane. After 20% of bulk extension, these faults got interconnected and a graben formed in between the opposing faults; NF1 and NF2. When extension continued, subsidence in the graben was accommodated along these two faults. Both faults appeared to have accommodated similar amounts of displacement. After 55% of bulk extension, smaller normal faults started to form inside the graben as well. Two antithetic faults that terminated on fault FN2 formed in the western part of the experiment (FN4 and FN5). FN5 was the latest to form and formed after 80% of bulk extension. In the eastern part of the experiment, a fairly large northward dipping fault formed (FN3) (fig.54).

Strike-Slip phase

During the first 20% of bulk strike-slip, strike slip movements were accommodated by Riedel R shears and eventually also Riedel P shears. The Riedel R shears were less well developed than during the strike-slip phase of model 1 and were also shorter. Only limited amounts of displacement, generally not more than 2mm developed along the R shears. The Riedel R shears as well as the P shears developed over the preformed FN1. However, a very minor amount of displacement was also accommodated by the preformed fault NF2 during the first 10% of bulk strike-slip (fig. 55). After this, no more movements occurred along NF2. After 20% of bulk strike-slip, strike-slip motion was solely accommodated on the main displacement Fault Zone F1, which formed due to reactivation of the pre-established fault NF1 (fig. 55 and fig. 56). After 25% of bulk strike-slip, a right stepping of fault F1 formed in the eastern part of the experiment (fig. 55). This right stepping continued to develop and after 27% of bulk strike-slip another oblique normal fault formed due to left stepping of fault F1 (fig. 55). This right stepping occurred due to the fact that base of fault FN3 is located close to the baseplate along which the motion takes place (fig. 54 and fig. 60). Hence in the eastern part, strike-slip motions are also accommodated by reactivation of fault FN3, which causes the right stepping of fault FN1 and the subsequent formation of a pull apart in the eastern part of the experiment. It is likely that this right stepping is enhanced by the fact that the experiment ends soon towards the east of the pull-apart basin. Hence the formation of this pull-apart is influenced by boundary effects. In the western part of the experiment, FN3 is absent and consequently nearly all of the displacement was accommodated by fault zone F1 that formed by reactivation of NF1.

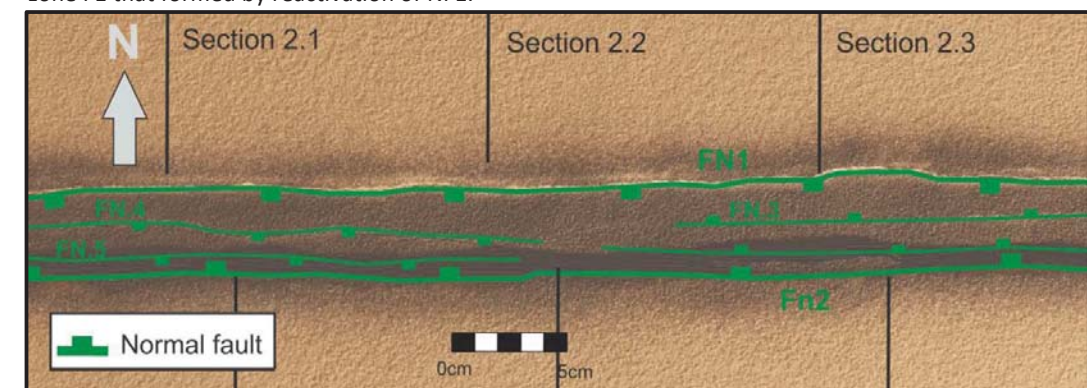


Fig. 54. Top View after the end of the extension phase of model 2. Most of the subsidence is accommodated by FN1 and FN2. However minor amounts of subsidence is also accommodated by faults FN2-FN5.

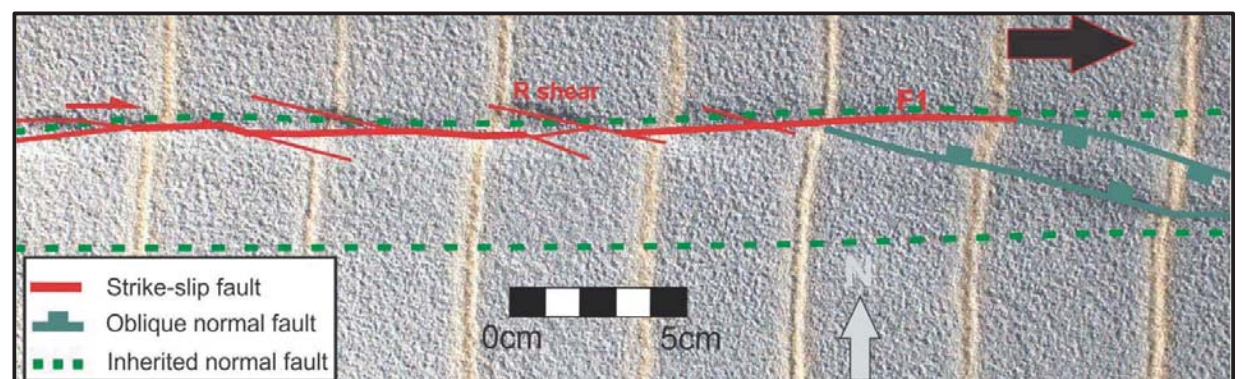


Fig. 55. Top View after 30% of bulk strike-slip. In the western part, motion is solely accommodated by fault F1. In the eastern part, the presence of FN3 causes right stepping of fault F1, enhanced by boundary effects due to the proximity of the edge of the model

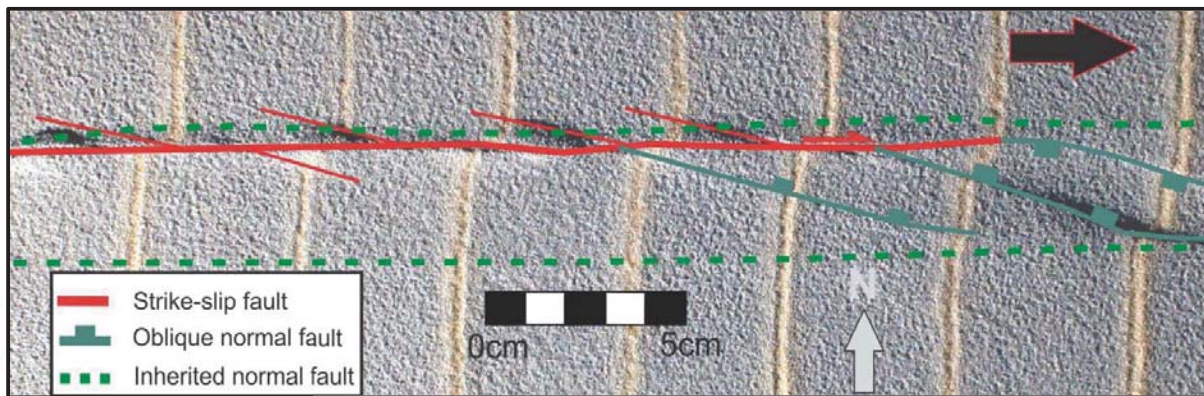


Fig. 56. Top View after 40% of bulk strike-slip. In the western part, motion is solely accommodated by fault F1. In the eastern part another oblique normal fault forms due to right stepping of fault F1

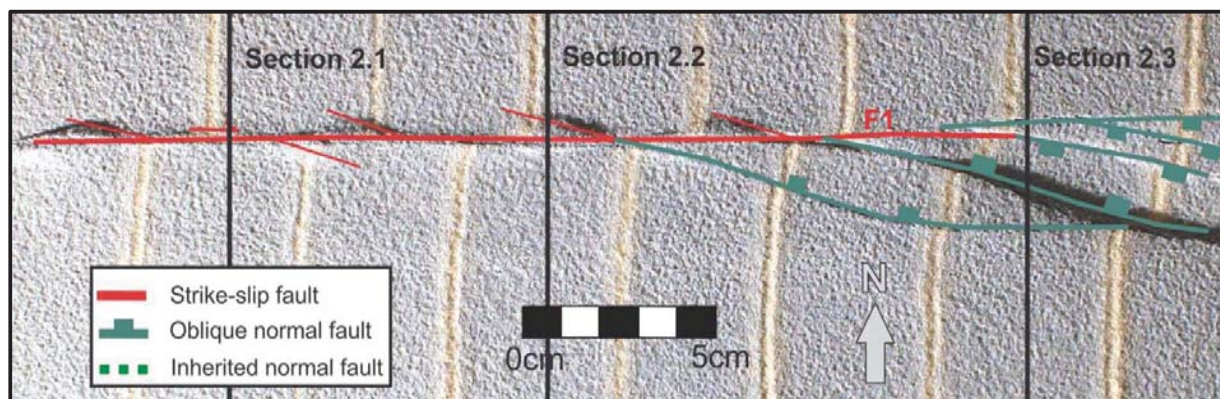


Fig. 57. Top view of model 2 after the end of the strike-slip phase. The locations of the cross-sections are indicated by the black lines.

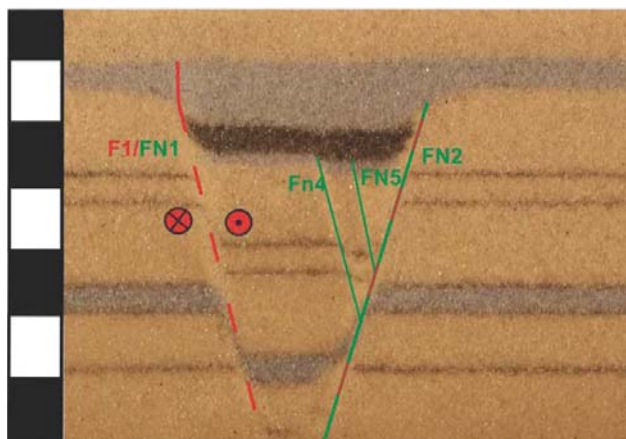


Fig. 58. Cross-section 2.1. Location indicated in figures 54 and 57

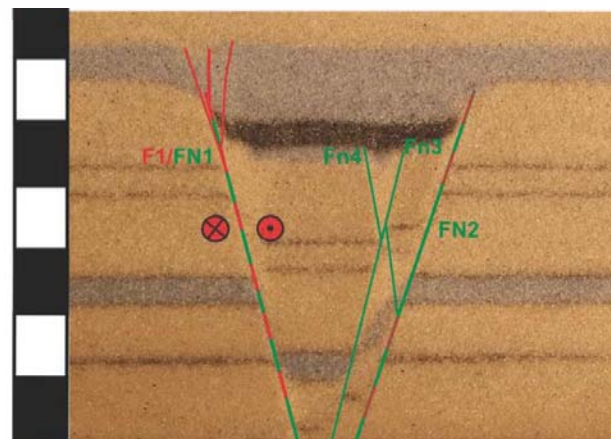


Fig. 59. Cross-section 2.2. Location indicated in figures 54 and 57

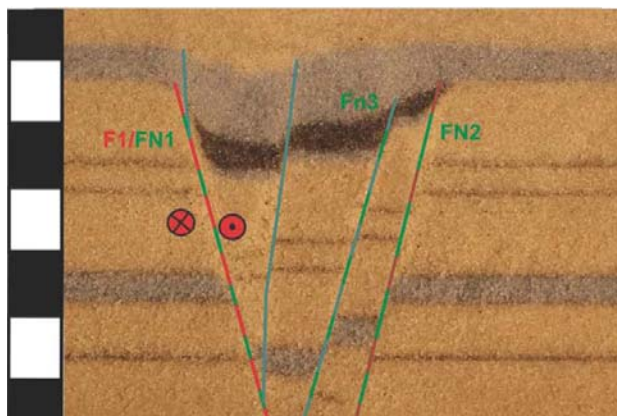


Fig. 60. Cross-section 2.2. Location indicated in figures 54 and 57

5.3 Experiment 3; Extension followed by dextral strike-slip; with vertical salt walls

Extension phase

During the extension phase, a symmetrical graben formed in the experiment. In contrast to experiment 2, no major boundary faults on either side of the graben can be observed at the surface of experiment 3 during the extension phase (Fig. 62). Instead, the graben subsides with a gradually curved geometry, showing the strongest subsidence in the center of the graben and the lowest towards the platforms (Fig. 61). With ongoing deformation, extension was also transmitted onto the platforms via the putti. This led to thin skinned extension on the platforms; both

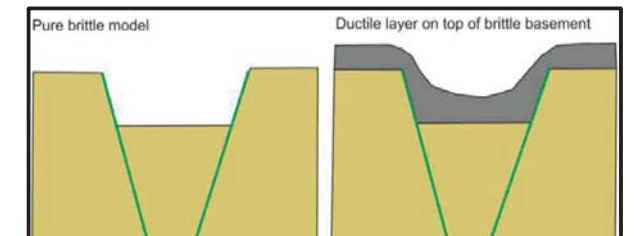


Fig. 61 Sketch indicating the difference in graben formation during pure extension for a purely brittle model (left) and a multilayer model (right).

close to the graben, as well as further away from the graben. This thin skinned extension on the platforms lead to the formation of small Grabens in the brittle overburden above the putti (Fig. 62). Where extension localized and the supra salt grabens became deep enough, the putti was able to pierce through the overburden once the piercing threshold was overcome (as described by Vendeville and Jackson, 1992). This piercing stage is described by Vendeville and Jackson (1992) as the active stage of diapirism. Piercement of the silicon putti walls only occurred in this experiment on the graben shoulders bounding the basin and took place for the first time after 72 percent of bulk extension (Fig. 62). The piercing threshold was not overcome further on the platforms, as some sedimentation was also applied on the platforms, thereby balancing the loss in overburden in areas of localized thin skinned extension and prohibiting active piercement of the silicon putti walls further on the platforms. Consequently the largest silicon putti walls in this model are located on top of the footwall of the basement boundary faults. From Fig. 62 can be inferred that the northern salt wall runs approximately parallel to the graben. The southern salt wall makes a gently turn towards the south, as the salt wall towards the southeast of the graben is located further away from the basin. This can also be inferred when the cross-sections 3.1-3.3 are compared (fig. 65-67).

Resting Phase

The salt walls that reached the active piercement stage during the extension phase, continued to grow passively and vertically upward during the resting phase, as sedimentation was applied every two hours. The silicon putti walls in the eastern and especially the southeastern part of the experiment didn't grow as high as the silicon putti walls in the western part of the experiment (fig. 62).



Fig. 62. Top View of model 3 after 75% of the extension phase. The transparent red areas indicate where the silicon putti walls reached the active piercing stage during this stage of the experiment. Both areas will expand slightly further towards the east during the rest of the experiment. Towards the east, the putti walls will not reach the active piercing stage.

Strike-Slip phase

Strain Distribution

R Riedel shears are the first faults that form after 15% of bulk strike-slip. They first form above a zone which coincides with the northern silicon putti wall. Displacement along these faults is small; generally less than 1mm. After 20% percent of bulk strike-slip, the majority of the displacement in the overburden takes places at two faults which follow the outline of the silicon putti walls that have formed during the extension and resting phase (fig.63). Initially, some local pop-up structures and a pull-apart structure form due to interference of the main displacement zone F1 with the Riedel R-shears. After 25% of bulk strike-slip, the main displacement zone F1 cuts through these small zones of transpression and transtension. Although the majority of the strike-slip displacement is accommodated by F1 and F2, a significant amount of displacement is also accommodated by a network of small faults of which the far majority is located inside the graben (fig. 63). The amount of displacement on these individual faults is small, but all together they accommodate a significant amount of displacement which is higher than the displacement accommodated by fault F2 (fig. 68). The amount of displacement that is accommodated by F1 and F2, seems to be related to the height of the salt wall that is located at the base of these faults, as is indicated in figure 69 (see figure for more explanation). Another parameter that seems to control the amount of displacement along F1 and F2 is the horizontal between these faults and the trace of the basement fault, which is indicated in fig. 70.

Shape of the silicon putti walls

From the cross sections in figures 65-67 can be inferred that the shape of the northern silicon putti wall, along which the majority of the displacement occurs, deviates from the shape of the southern silicon putti wall. This difference becomes also clear when the shape of the northern putti wall is compared with the shape of a diapir that has developed after a similar amount of extension and resting were applied to an experiment (Scheffer, 2016 Appendix D). The difference lies in the shape of the northern putti wall, which is more triangular when compared to the silicon putti walls that have accommodated no or less strike-slip. Furthermore, the northern salt wall also appears to be thinner towards the top. Another difference is the small appendix that has formed during strike-slip on the top of the northern silicon putti wall at some places (Fig. 66). This appendix is absent at the silicon putti walls that accommodated no or less strike-slip.

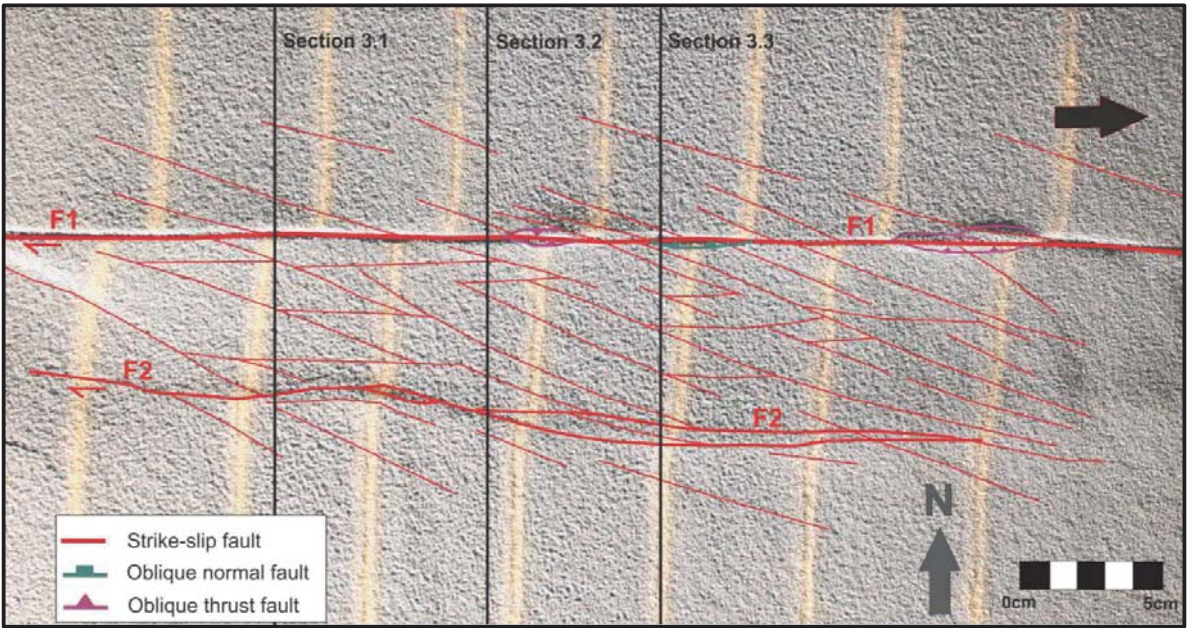


Fig. 63. Top view of the final stage of strike-slip deformation of model 3. It can be seen that most of the displacement on individual faults is accomodated by the faults F1 and F2. However, a fairly large amount of displacement is also accomodated by smaller faults of which the majority is located inside the graben.

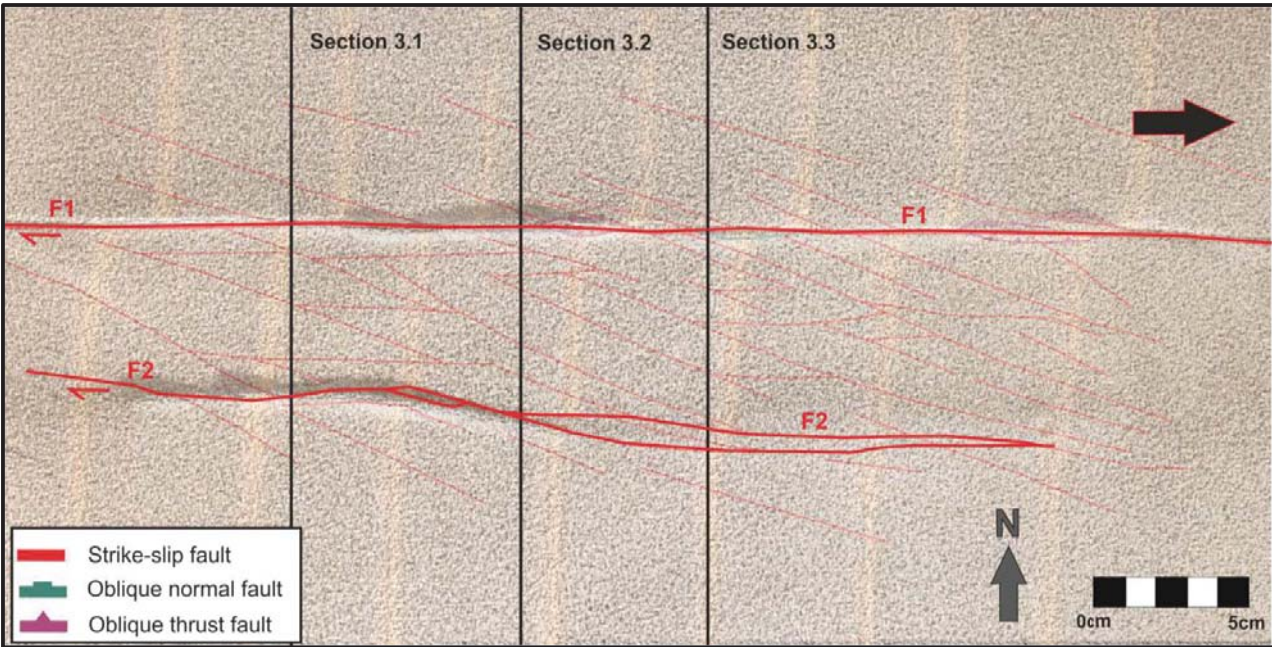


Fig. 64. Top View of the model after the end of the strike-slip phase. A transparant view of fig. ... is laid over the end of the strike-slip phase. Showing that the main strike-slip faults are located above the silicon putii walls.

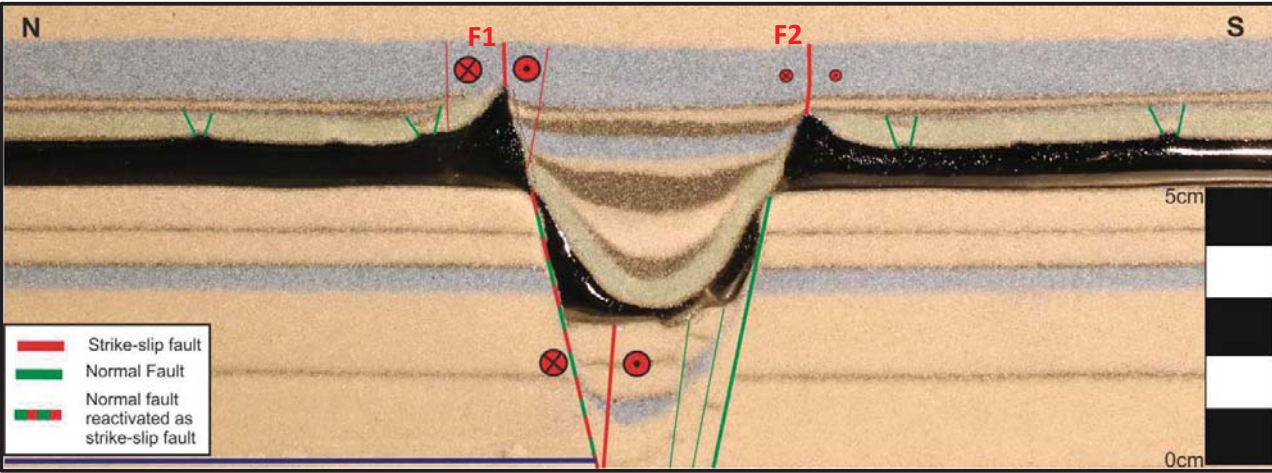


Fig. 65. Cross section 3.1. of model 3. The location of the cross-section is indicated in the figures 24 and 25. Clear in this cross-section is the small appendix that has formed on top of the northern (here left) silicon putti wall.

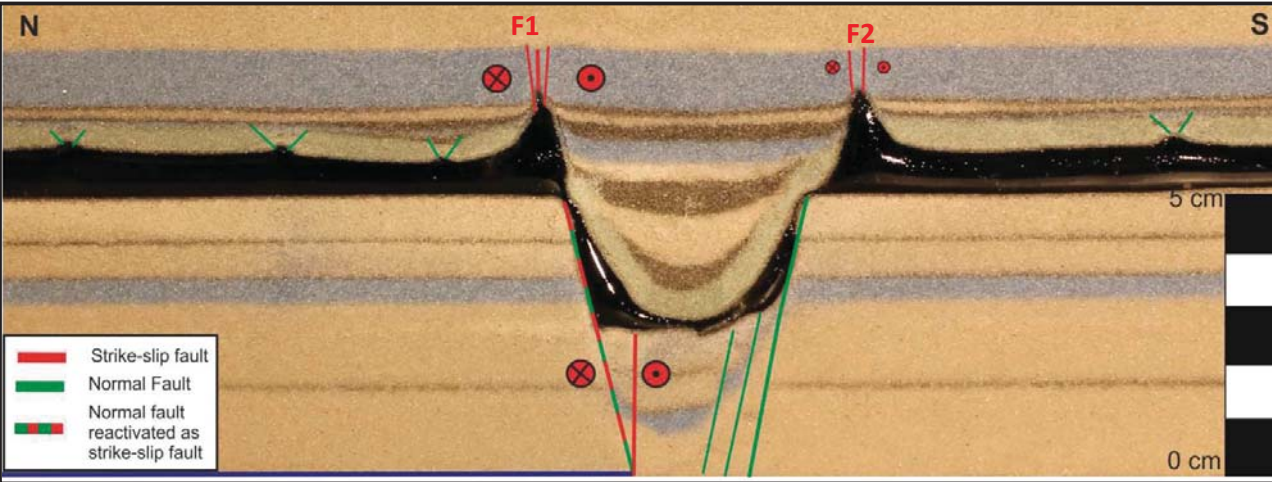


Fig. 66. Cross-section 3.2 of model 3. The location of the cross-section is indicated in the figures 24 and 25. Clear in this cross-section is the ore trianauar and narrow shape of the northern (here left) silicon putti wall.

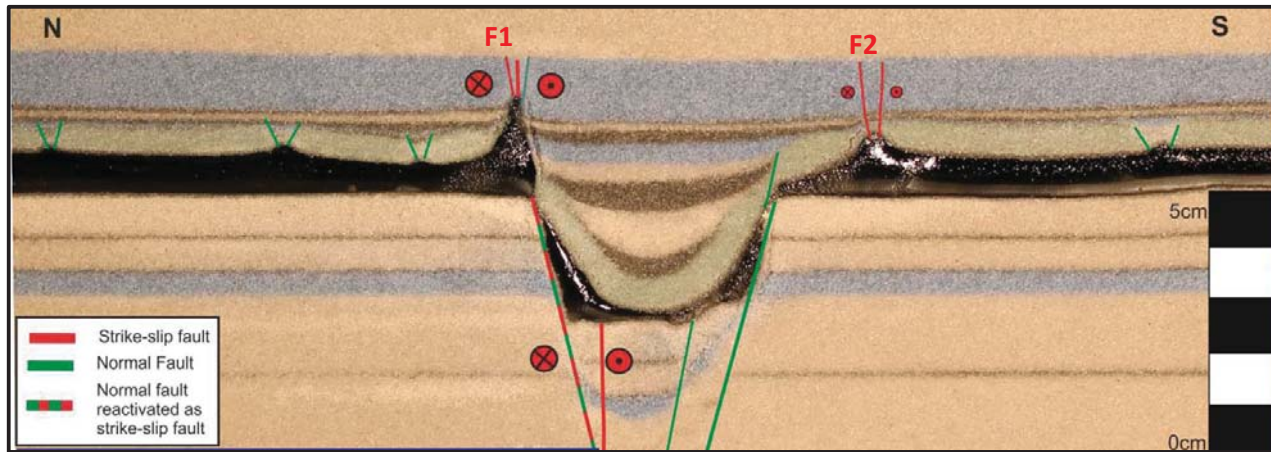


Fig. 67. Cross-section 3.3 of model 3. The location of the cross-section is indicated in the figures 24 and 25. Note the increased distance of the southern (here right) salt wall from the graben

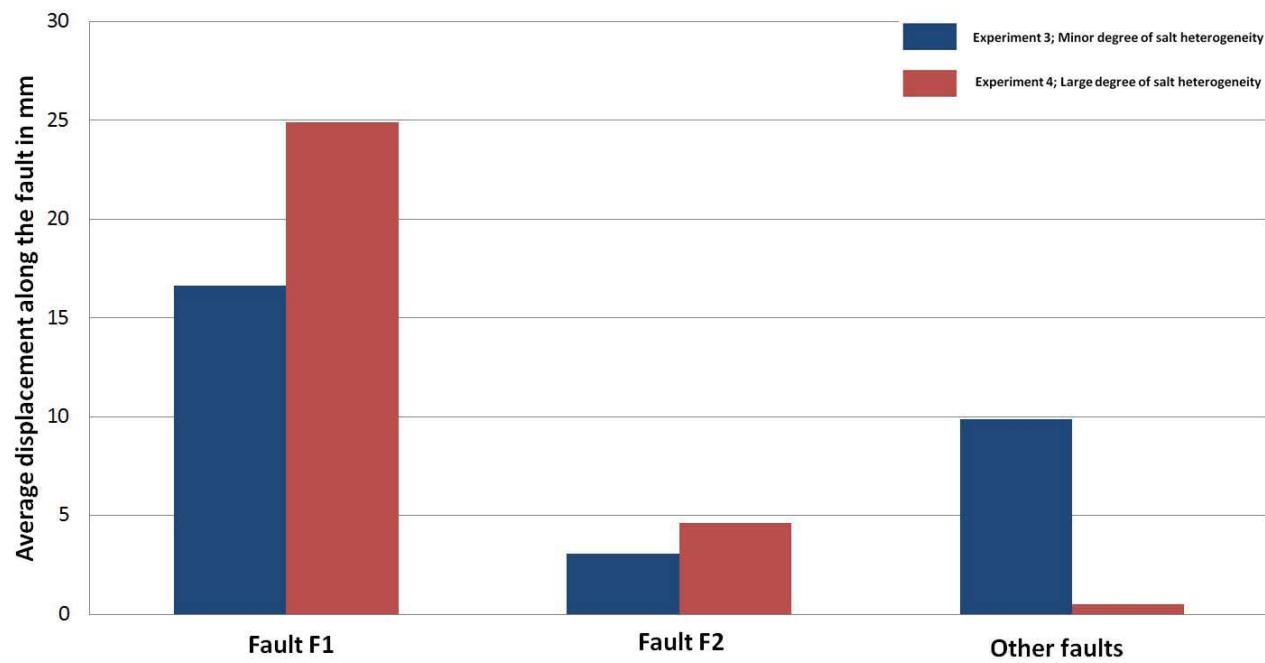


Fig. 68. Diagram indicating the average displacement along the faults F1, F2 and other faults for experiment 3 and 4. Noteworthy is the relatively large amount of displacement that is accommodated by other faults in experiment 3 with respect to experiment 4. The majority of these faults is located inside the graben, bounded by the two salt walls. The average was obtained by 7 measurements in each experiment; all measurements were taken along the white lines of figure 61

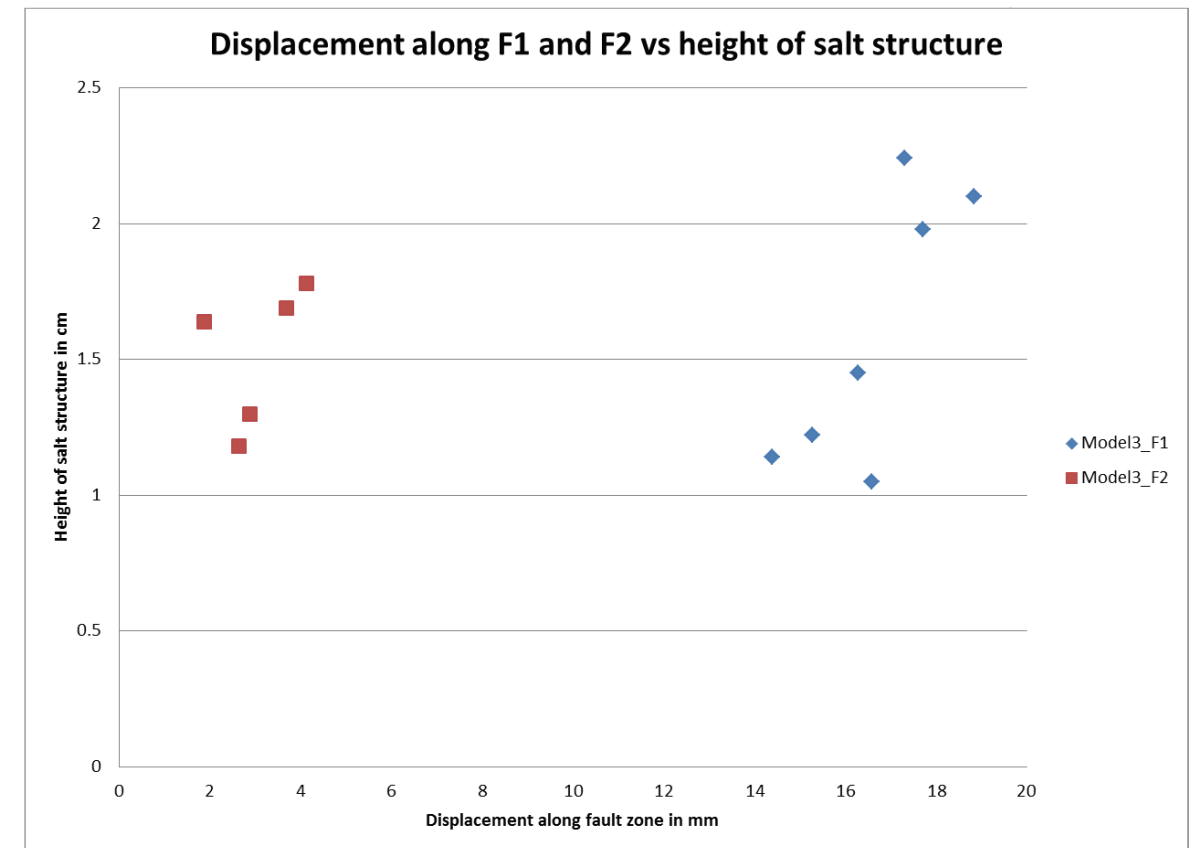


Fig. 69. Graph where the height of the salt structure is plotted against the amount of displacement that is accommodated by the faults F1 and F2 above it. The displacements were measured along 7 fault segments of fault F1 and 5 fault segments of fault F2, along the white lines in figure 24. The distance along F2 in the eastern part of the fault were too small to measure properly. Striking is that the higher the salt wall, the more displacement is accommodated by the fault above it and hence likely also by the salt wall itself.

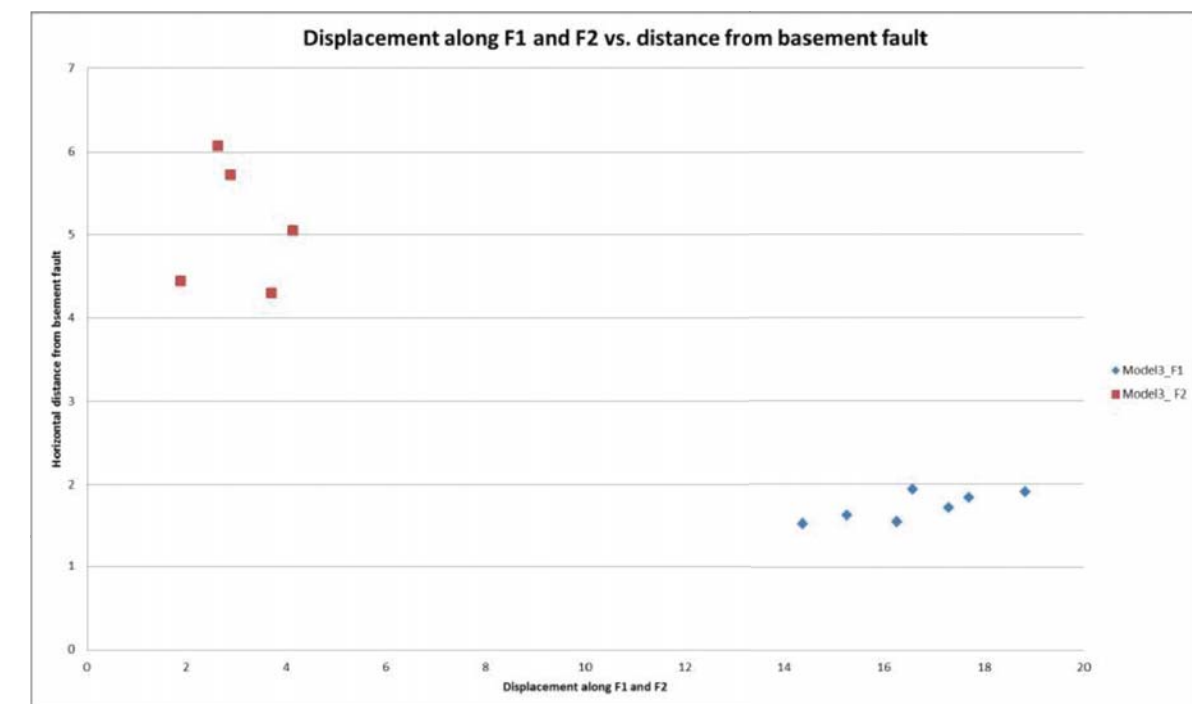


Fig. 70. Graph where the displacement along the faults F1 and F2 is plotted against the distance from the basement fault. Because it is not exactly sure where the faults in the basement are located, the distance between F1 (or F2) and the trace of the basement fault as defined by the location of the base plate was measured. The measurements along fault F1 suggest that there is a strong correlation between the distance of the basement fault and the displacement along F1.

5.4 Experiment 4. Extension followed by dextral strike-slip; large differences in salt wall orientation

Extension phase

During the extension phase, a graben formed in the experiment above the place where the base plate was pulled away. In contrast to experiment 2, no major faults can be observed at the surface of experiment 4. Instead, the graben subsides with a gradually curved geometry, showing the strongest subsidence in the center of the graben and the lowest towards the graben margin. With ongoing deformation, extension was also transmitted onto the overburden via the silicon putty, leading to thin skinned extension on the platforms; both close to the graben, as further away on the platforms. This thin skinned extension on the platforms resulted in the formation of small Grabens in the brittle overburden above the putty. Where extension localized and the supra salt grabens became deep enough, the putty was able to pierce through the overburden once the piercement threshold was overcome. This stage of diapirism was described by Vendeville and Jackson (1992) as the active stage of diapirism. The first places where piercing of the silicon putty occurred were the graben shoulders, located directly outside of the graben. The first piercing of the silicon putty occurred therefore on top of the footwall formed by the basement normal faults bounding the graben. Piercing of the silicon putty occurred in these places at 70 percent of bulk extension. After the initial piercement of the silicon putty, the silicon putty walls grew vertically upward, as can be inferred from fig. 71 and 72, which shows the end of the extension phase of model4. By the end of the extension phase, the silicon putty walls located on the platform shoulders, closest to the graben, had reached the active diapir stage on the full length of the model (fig. 71, 72). Two salt walls further away from the graben had also pierced the overburden in the southern part of the experiment. Anomalies to this general pattern of pierced salt walls occur in the areas A and B in figure 71. In these areas, the salt walls that pierced the overburden are not located directly on top of the hanging wall, but are located slightly further towards the platform.

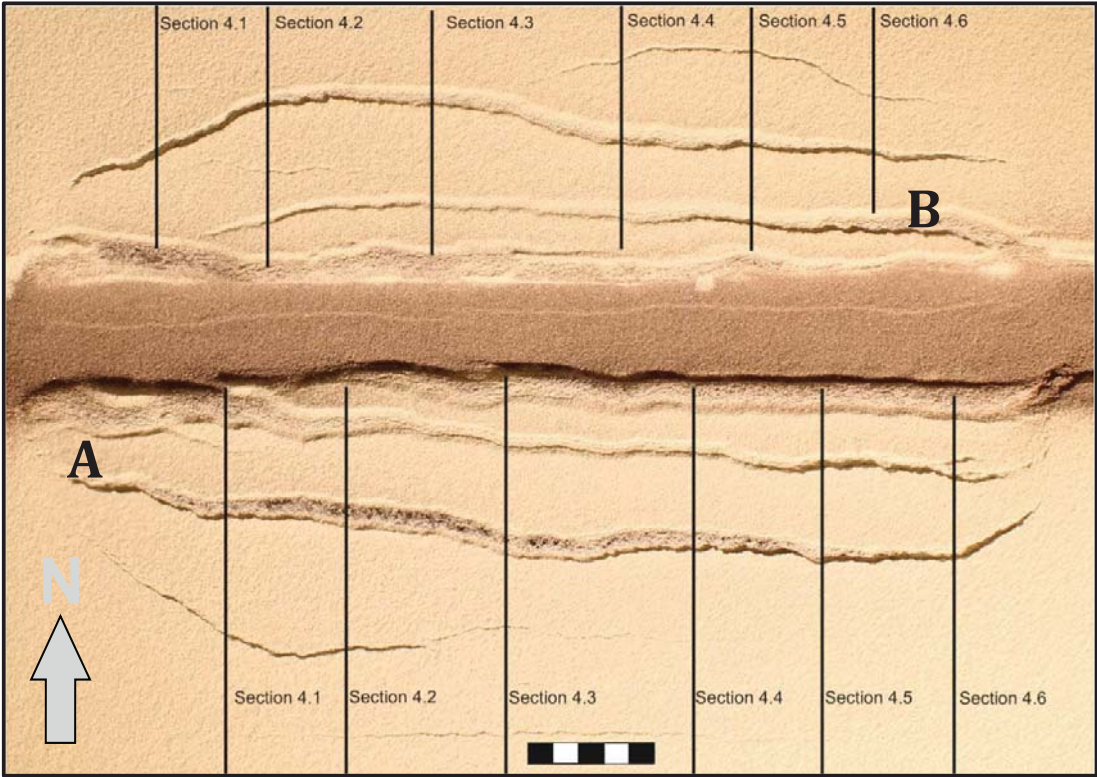


Fig. 71. Top view of model 4 at the end of the extension phase. This figure shows that the salt walls have reached the active stage over the full length of the experiment and grow vertically upward. Salt walls are located on the footwall close near the graben. Except for the locations A and D where the salt walls are located slightly further on top of the platforms.

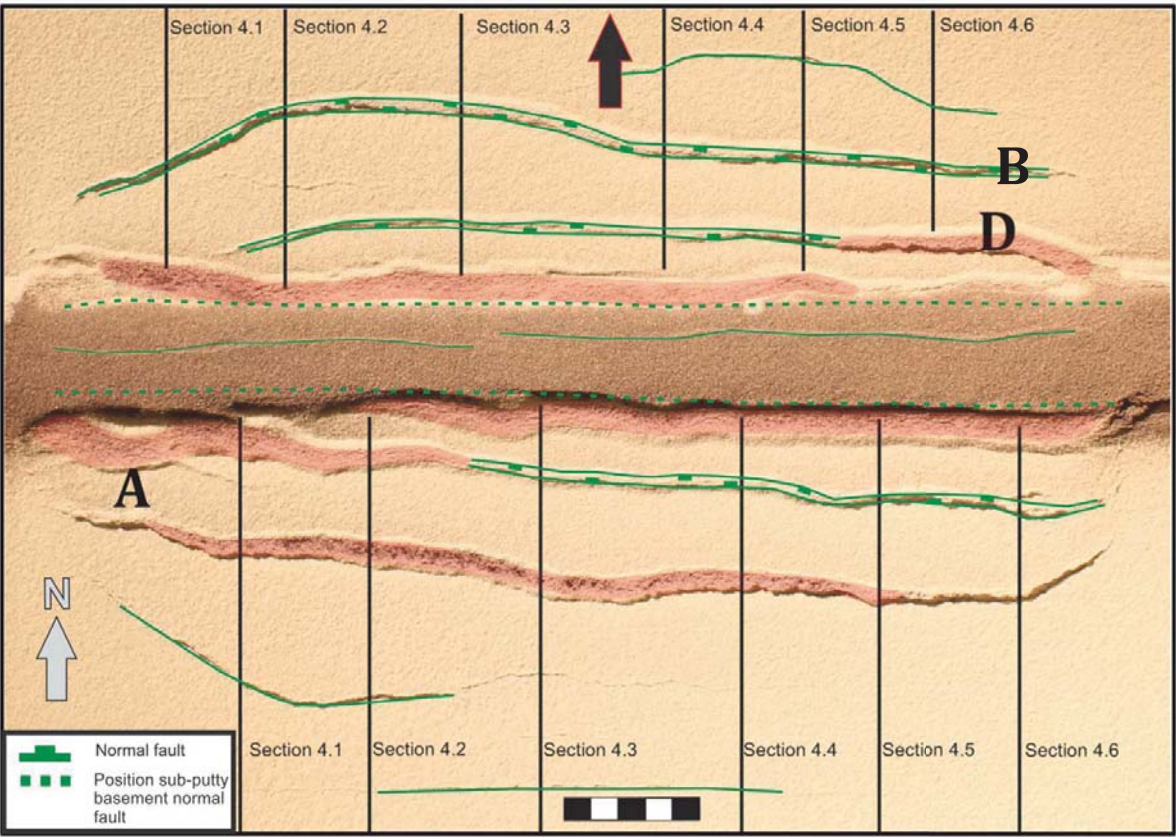


Fig. 72. Interpreted top view of model 4 at the end of the extension phase. The salt walls that have reached active piercing stage are indicated by the transparent red areas. For the uninterpreted top view see fig. 73.

Resting Phase

During the first two hours of the resting phase, the salt walls in the normally filled part of the basin grew vertically upward by passive diapirism, as sedimentation kept on track with the vertical rise of the diapirs. This can be seen in fig. 73, where the blue part of the graben represents the normally filled part of the basin (part C) and the white part represents the underfilled part of the basin (part D) after the first two hours of the resting phase. In the underfilled part of the basin, gravity caused the salt walls to grow towards the graben and subsequently to spread onto the graben infill. This can be seen when the final stage of extension (fig. 71, 72) is compared with the first two stages of the resting phase (figures 73 and 74). This gravitational spreading of putty is visualized in fig. 74, where the distance D between two opposing salt structures is plotted against the resting time. This distance D was measured at 6 places of the experiment, indicated by the dashed yellow lines in fig. 73. From the graph in fig. 83 becomes clear that the distance between two opposing salt walls on either side of the graben remains largely the same in the normally filled part of the basin. In the underfilled part of the basin, which is represented by measurements along the lines of sections 4.1-4.4, it becomes clear that the salt structures have grown towards each other during the first four hours of the resting phase, which represents the time that the basin was extremely underfilled. This can also be inferred from the corresponding sections of the underfilled part of the basin (figures 77, 78, 79), where it can be seen that the silicon putty has spread on top of the thin white layer (figures 77 and 79) or on top of the black layer in a slightly later stage of the resting phase (fig. 78). During the last four hours of the resting phase, when the basin was less underfilled, the diapirs grew again almost vertically upward. Indicated by the waist shape figure of the diapirs (especially observed in the northern putty wall of figure 78, but also in the putty walls of the figures 77, 79), which indicates new active piercing after putty extrusion. Hence, after four hours of resting, the distance between the two opposing diapirs on either side of the graben doesn't decrease anymore (fig. 83).

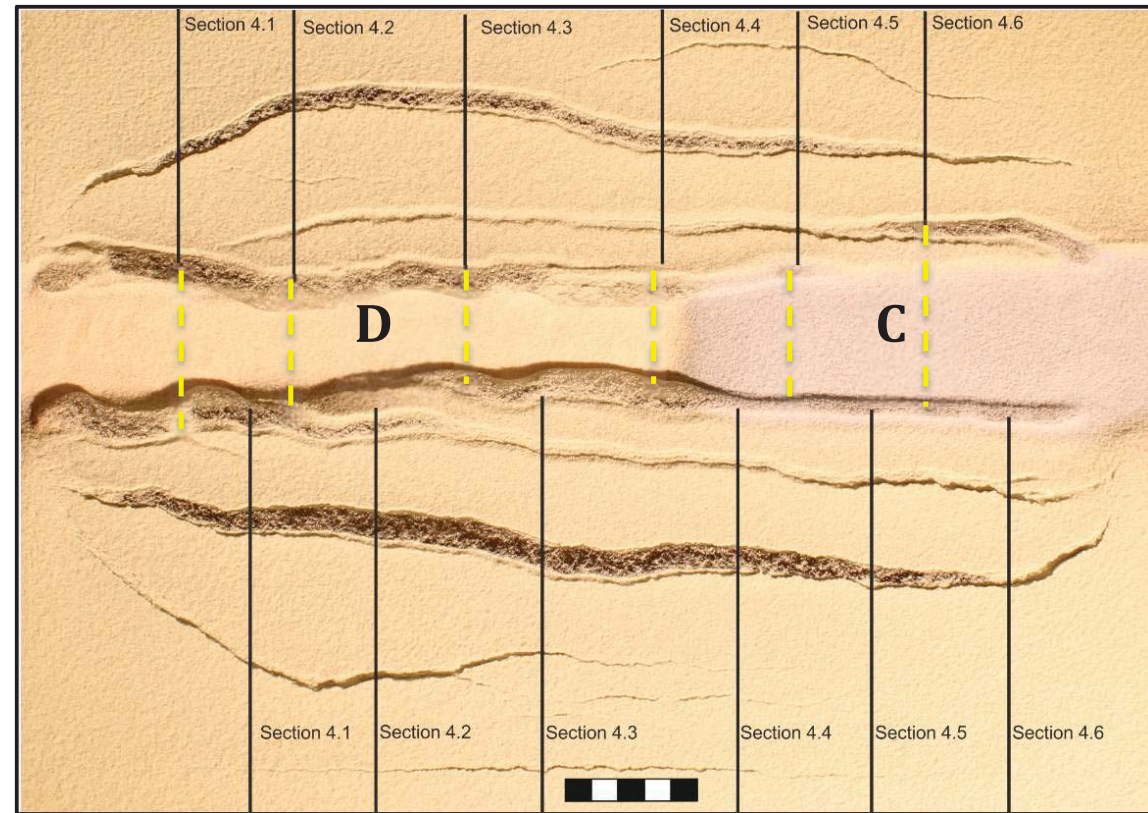


Fig. 73. Top view of model 4 after two hours of resting. The Blue part of the basin (part C) is normally filled, the white part of the basin (Part D) is underfilled with a topography difference of 5mm between the basin floor and the surrounding platforms. During this phase of the experiment, the silicon putty in the underfilled part of the basin slowly spreads towards the center of the basin by gravitational spreading.

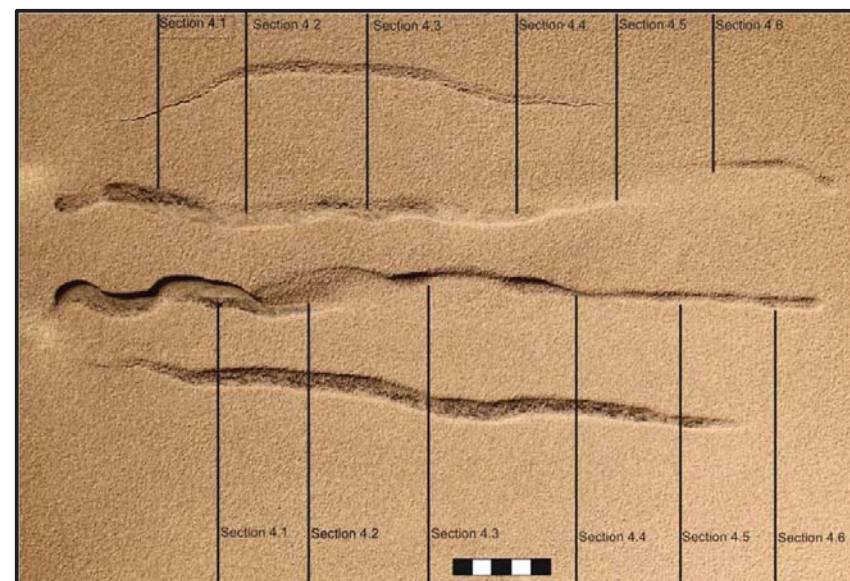


Fig. 76. Top View of the model after four hours of resting. During this part of the model, the left part of the basin was still underfilled, though slightly less than during the first two hours of the resting phase.

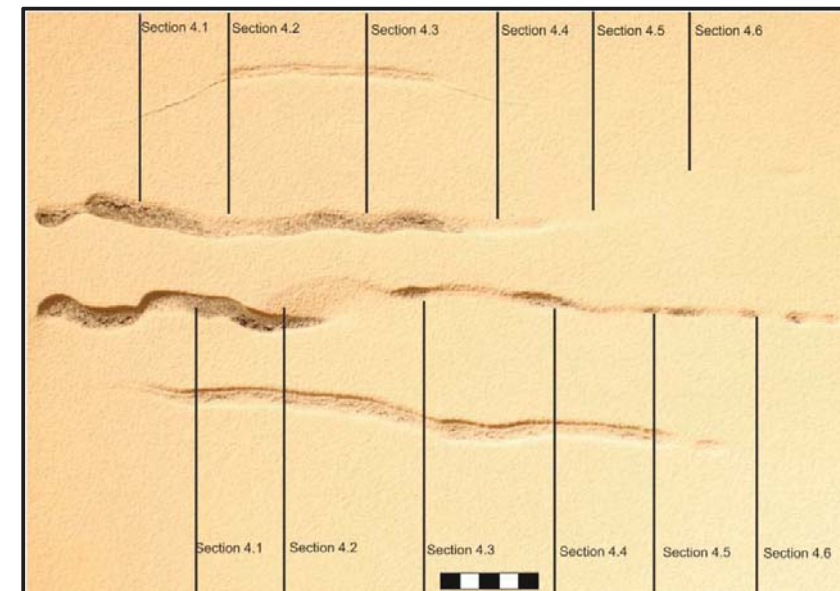


Fig. 75. Top View of the model after six hours of resting. During this part of the model, the left part of the basin was only slightly underfilled.

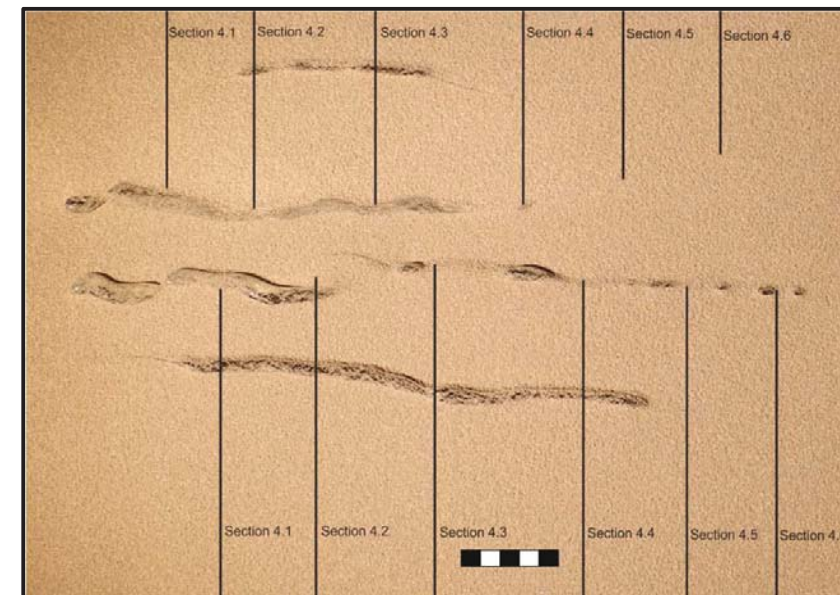


Fig. 76. Top View of the model after eight hours of resting. During this part of the model, the entire part of the basin was normally filled as is indicated by the absence of shadows north of the diapirs.

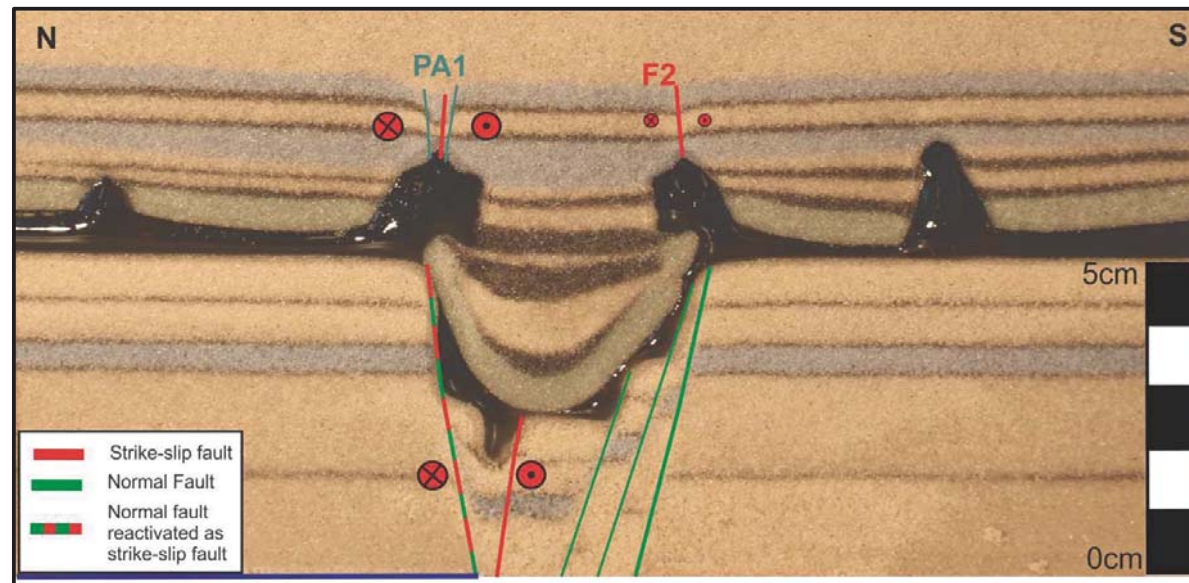


Fig. 77. Cross section 4.1. the location of the cross-section is indicated at the top views of the experiment.

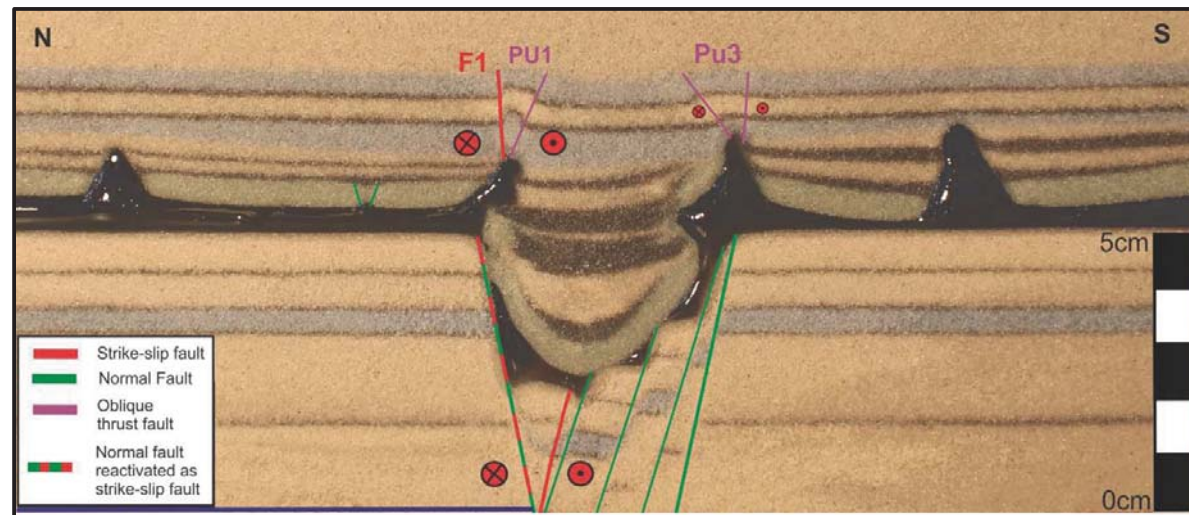


Fig. 78. Cross section 4.2. The location of the cross-section is indicated at the top views of the experiment.

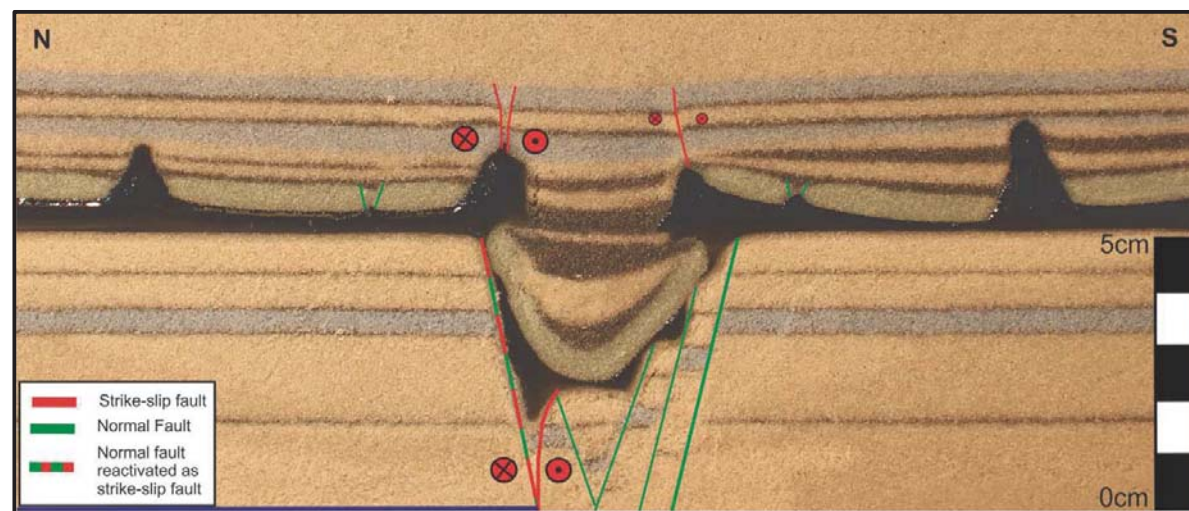


Fig. 79. Cross section 4.3. The location of the cross-section is indicated at the top views of the experiment.

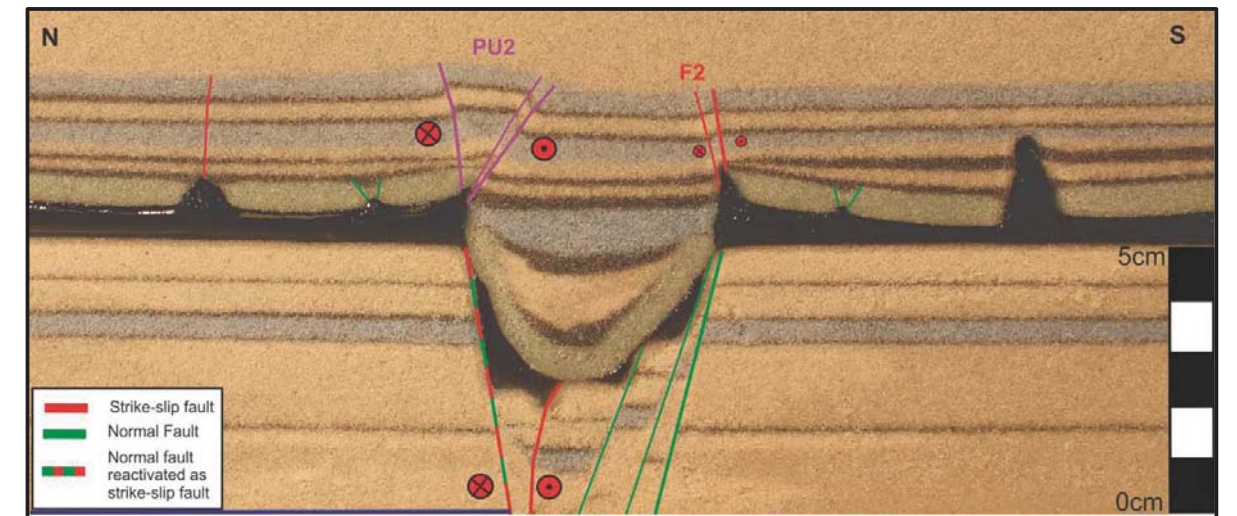


Fig. 80. Cross section 4.4. The location of the cross-section is indicated at the top views of the experiment.

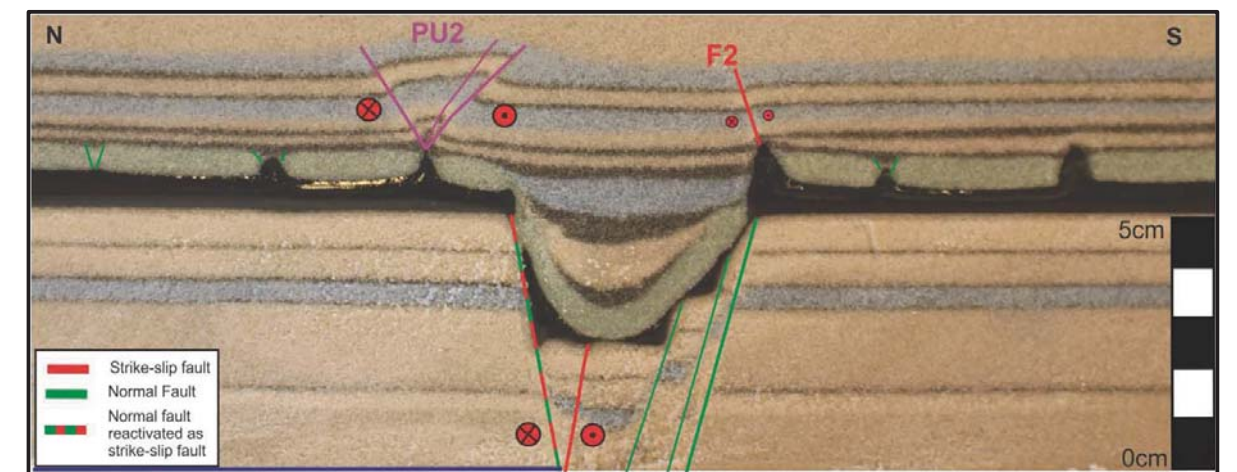


Fig. 81. Cross section 4.5. The location of the cross-section is indicated at the top views of the experiment.

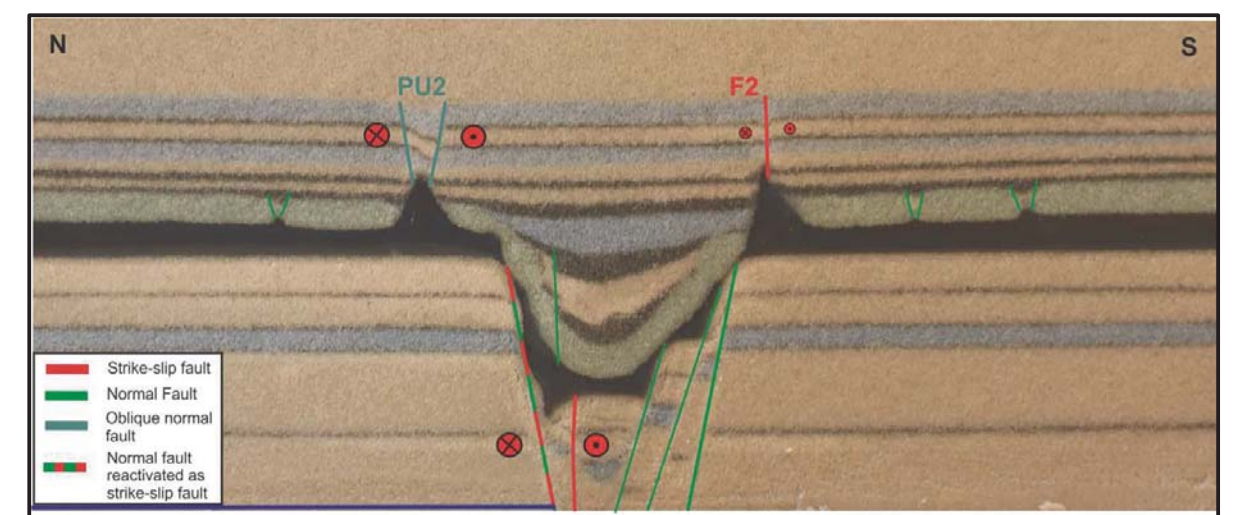


Fig. 82. Cross section 4.6. the location of the cross-section is indicated at the top views of the experiment.

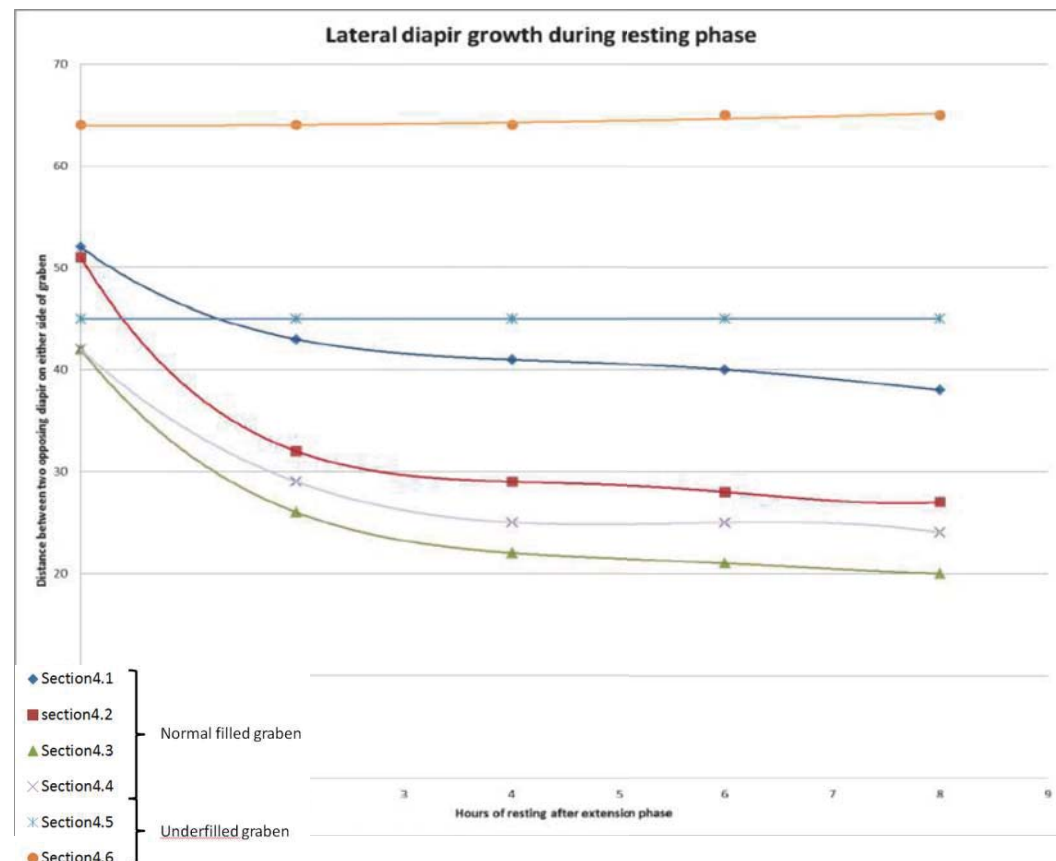


Fig. 83. Graph showing the distance between two opposing salt structures varying through time during the resting phase, indicating the differences in lateral salt movement when the underfilled part of the basin is compared to the normally filled part of the basin.

Strike-Slip phase

Strain distribution

The first structures that form during the strike-slip phase are R Riedel faults. These faults form after 5 percent of bulk strike-slip. Generally less than 1mm of displacement occurs on these faults and with a distance of around 5cm to 7cm in between two Riedel faults, they are quite widely spaced. After 15 percent of bulk strike-slip, these Riedel faults become inactive and most of the displacement takes place on two faults which are shown in figures 84, 85 and 86 as F1 and F2. Minor displacements (less than 1mm) occur at faults within the graben, which generally have display a R Riedel orientation (fig. 84-86). Additionally some minor displacements take place on slightly curved faults located on the platforms. In accordance with model 3, the major fault F1 and F2, as well as the slightly curved faults on the platforms, follow the outline of the salt walls (fig. 87). At the end of the experiment (fig. 86), most of the displacement has occurred on fault F1 as is indicated in figure 64.

Zones of transpression and transtension

During this experiment, several zones of transpression and transtension developed due to either left or right stepping on the strike-slip faults. After 20% of bulk strike-slip, the contours of a small pull apart (PA1) structure, as well as a small pop-up structure become visible in the western part of the experiment (PU1) (fig. 84). However, this pop-up quickly becomes inactive when F1 cuts through the pop-up structure (fig. 85). A larger pop-up structure (PU2) forms in the eastern part of the experiment due to left stepping of fault F1 (fig. 84-86). This pop-up structure remains active for the entire duration of the experiment and displays significant topography of up to 5mm with respect to the surrounding area. Towards the far east of the experiment, F1 steps to the right and a large pull-apart structure formed, showing up to 5mm of subsidence. A third pop-up

structure (PU3) forms due to left stepping of fault F2 (fig. 85 and 86). This pop-up structure remains also active for the entire duration of the experiment but topography is lower than at PU2.

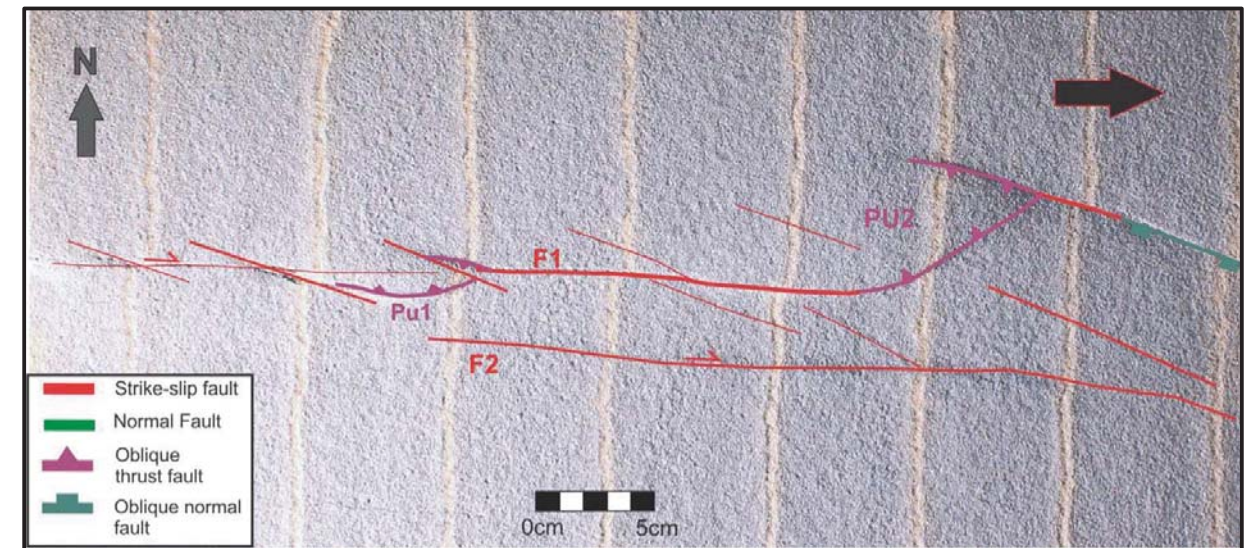


Fig. 84. Top View of the model after 33% of bulk Strike-slip. By this time, deformation already takes place along the main fault zones, which are located above the diapirs. Riedel faults have become largely inactive, except for the Riedel faults located insight the graben.

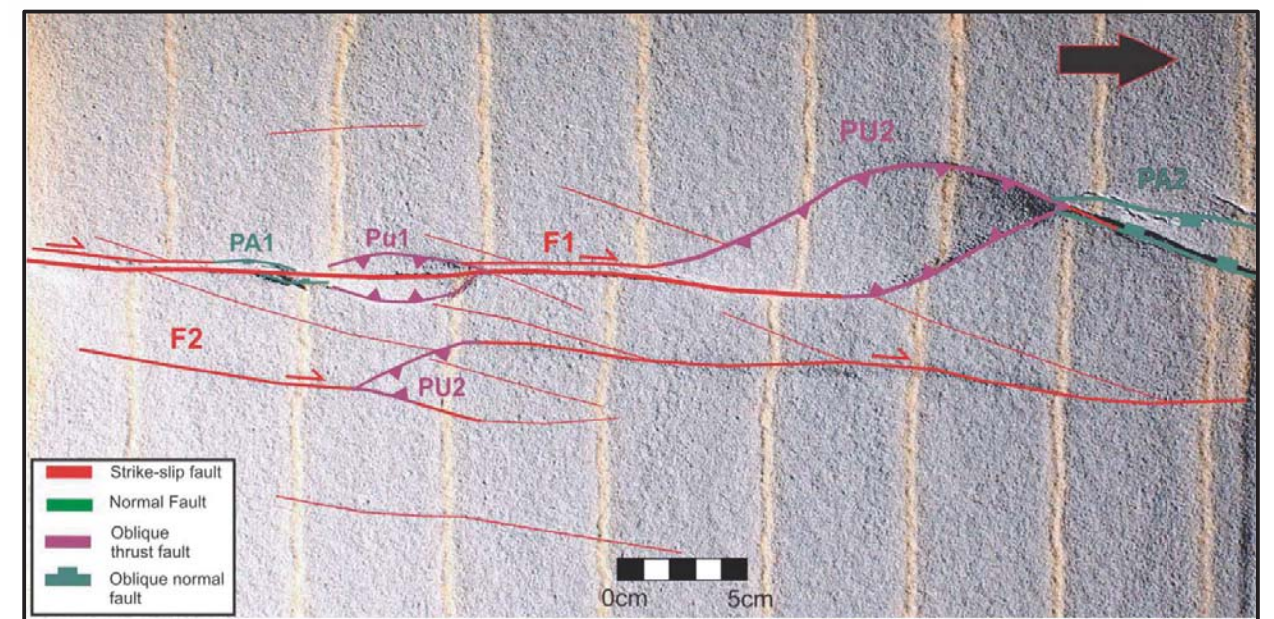


Fig. 85. Top View of the model after 66% of bulk Strike-slip. By this time, Pop up 1 has become inactive but pop-up 2, pull-apart 2 and pop-up 3 will remain active for the entire duration of the experiment.

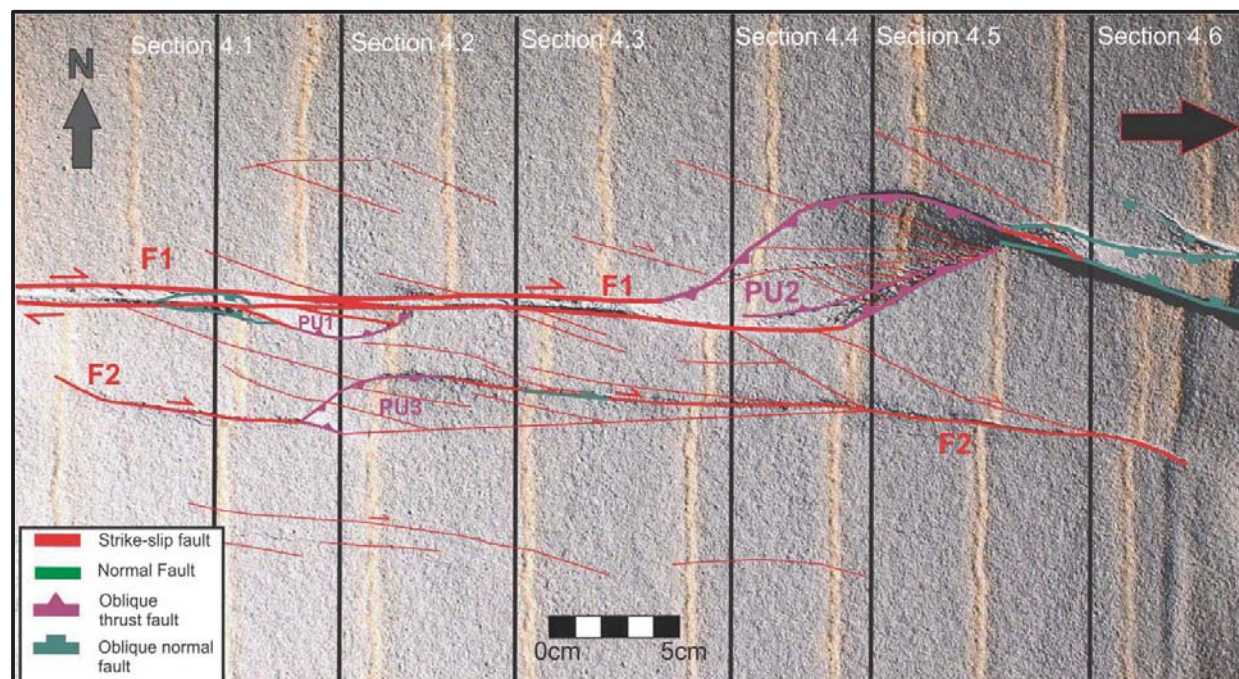


Fig. 86. Top View of the model end the end of the strike-slip phase.



Fig. 87. Top View of the model after the end of the strike-slip phase. A transparent view of fig. 5 is laid over the end of the strike-slip phase. Showing that the main strike-slip faults are located above the silicon putty walls and that the pop-up and pull-apart structures are formed due to lateral variations in the distribution of the silicon putty walls.

5.5 Discussion of the models 2,3 and 4.

The models demonstrate that the presence of a weak layer in a preformed basin has a profound effect on the deformation pattern when the preformed basin is subjected to strike-slip deformation. In the western part of the purely brittle model 2, the strike-slip deformation is almost solely accommodated along the preformed normal fault, bounding the basin. Hence it is assumed that, in accordance with model 2, most of the deformation in the basement of models 3 and 4 is accommodated along the preformed, sub-salt basement fault as well as on some vertical strike-slip basement faults that can be recognized in cross section and terminate on the base of the silicon. The presence of the weak layer of silicon putty redistributes the strike-slip deformation and causes decoupling from the strike-slip deformation below the weak layer, with respect to strike-slip deformation above the weak layer. This decoupling results in different deformation patterns below and above the weak layer. The main strike-slip faults in the overburden follow the outline of the silicon putty walls, as can be inferred from figures 64 and 87. This can be explained from the mechanical strength of the supra-salt interval; which is lowest above the diapirs. The reason for this is twofold and can best be explained by fig. 88, which shows how the strength ($\sigma_1 - \sigma_3$) of a brittle and a ductile material depends on the thickness of the layer. From this figure can be inferred that the strength of the silicon putty decreases with increasing layer thickness. In contrary, the strength of the sand increases with decreasing layer thickness. Because of this material behavior, the models 3 and 4 are characterised by lateral strength contrasts, as the basins are significantly stronger than the platform directly outside of the basins where the salt walls are located (fig. 89). The strength of the models also varies along strike, as diapirs don't reach the same height over the full length of the model. In model 3 for example, the southern diapir is significantly lower on the eastern side of the model than on the western side of the model. A higher diapir is mechanically weaker and fig. 69 indicates that the higher the diapir, the more displacement is accommodated along that diapir. This can be seen in the southeastern part of model 3 where the diapir is lower. Above this diapir, strike-slip fault F2 is not well developed. Instead displacements are distributed over a larger area.

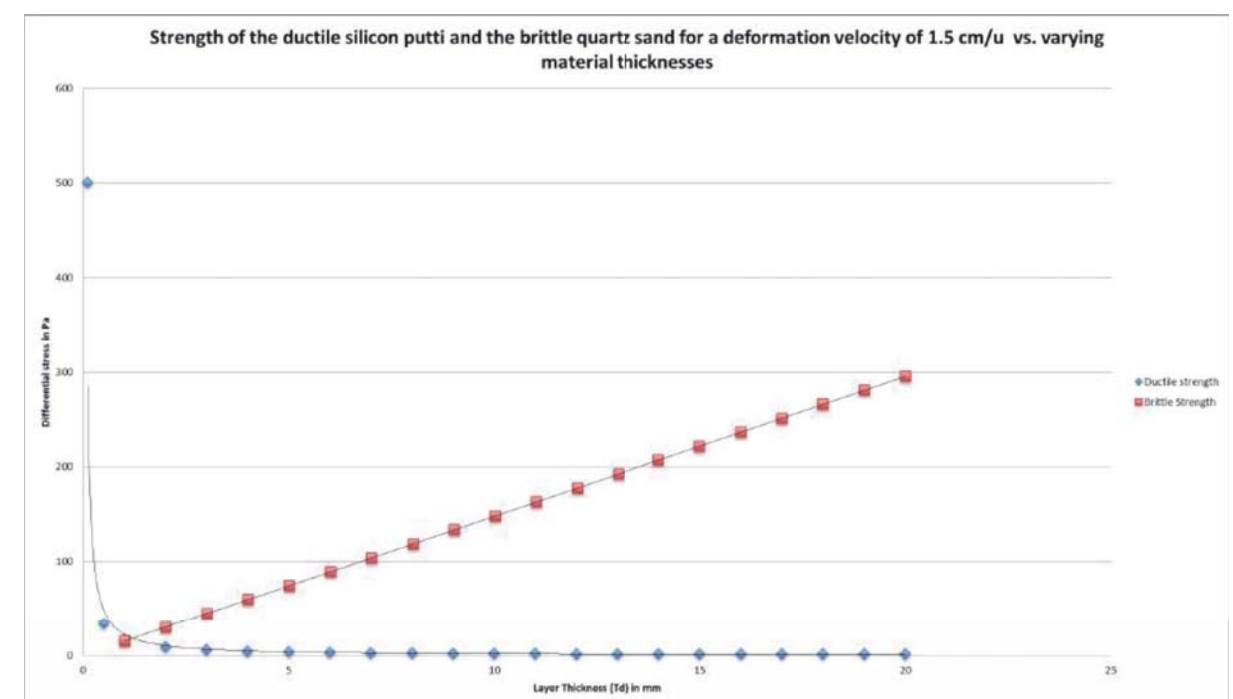


Fig. 88. Graph showing the variations of the mechanical strength of the silicon putty layer and the brittle quartz layers. It can be inferred from this figure that the silicon putty quickly becomes weaker for increasing thickness. The brittle quartz layers on the other hand linearly increase in strength with increasing thickness. The brittle strength was calculated by making use of equation 21. The ductile strength was calculated by making use of equation 22 (Smit, 2005).

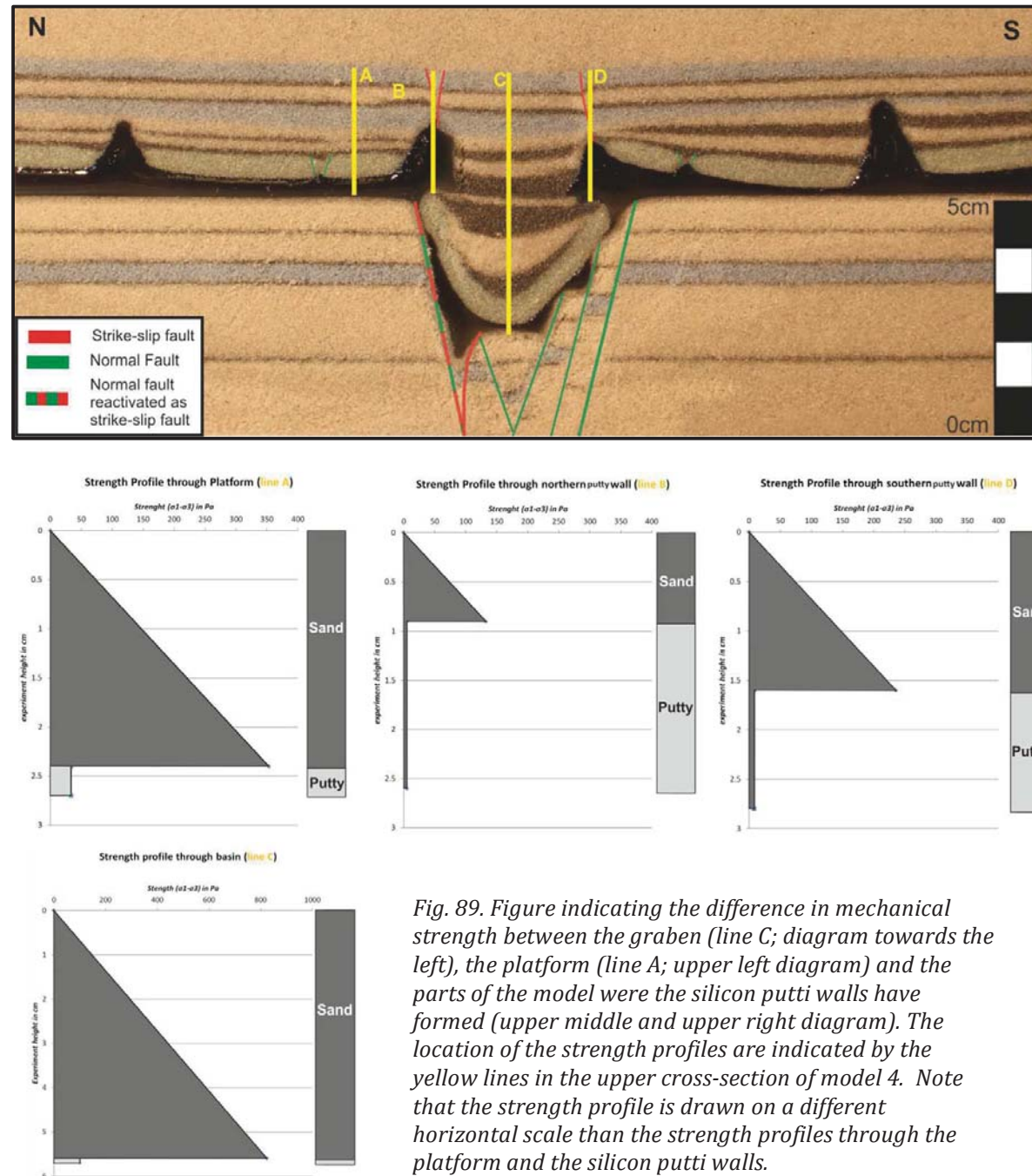


Fig. 89. Figure indicating the difference in mechanical strength between the graben (line C; diagram towards the left), the platform (line A; upper left diagram) and the parts of the model where the silicon putty walls have formed (upper middle and upper right diagram). The location of the strength profiles are indicated by the yellow lines in the upper cross-section of model 4. Note that the strength profile is drawn on a different horizontal scale than the strength profiles through the platform and the silicon putty walls.

When the models 3 and 4 are compared, it can be concluded that the models don't have the same lateral strength profile, as is indicated by Fig. 90. Surely, the silicon putty walls in model 3 are more evenly distributed than in model 4, as the silicon putty walls in model 3 run approximately parallel on either side of the graben (Fig. 90). Model 4 on the contrary shows a higher degree of variation in the distribution of putty, as silicon putty in this model extruded in the underfilled part of the basin. Because the main strike slip faults follow the outline of the silicon putty walls, sharp bends in the distribution of silicon putty walls causes right and left stepping of the main strike-slip faults in experiment 4 and the subsequent formation of profound pop-ups and pull-aparts. Because these sharp bends in silicon putty walls are absent in model 3, this model shows neither profound pop-up structures nor pull-apart structures.

Another difference between model 3 and 4 is the strain distribution inside the graben. Based on strength contrasts, one wouldn't expect to find much strike-slip displacement inside the graben, as

the brittle overburden here is relatively thick and the silicon putty relatively thin, making the center of the graben mechanically strong. However, as can be inferred from figure 68, a significant amount of the strike-slip displacement in model 3 is accommodated by small strike-slip faults in the graben. Although the amount of displacement on individual faults is very low (generally less than 1mm), together they accommodate a significant amount of displacement. The amount of strike-slip displacements in the graben is likely related to the distance between the two main strike-slip faults in the overburden. This distance is less in model 4 than in model 3, because the silicon putty walls in model 4 had extruded and hence had grown towards each other, thereby reducing the distance D (fig. 83). Because the main strike-slip-faults follow the outline of the silicon putty walls, also the main strike-slip faults are closer spaced with respect to each other in model 4 than in model 3. The majority of the displacement takes place on these two faults, which is also the case in model 3. However, most of the displacement occurs on the faults F1 and less on the faults F2. This means that the area between these faults has to partly accommodate this difference in displacement. The difference is thus accommodated by the graben in the form of small faults that together function as a zone of approximate simple shear. Because the distance between the two main strike-slip faults is smaller in model 4, the area of simple shear between the faults is less than in model 3. Hence less faults form and less displacement has to be accommodated on these faults. Additionally, the amount of displacement along a strike slip fault in the overburden depends on its distance with respect to the basement fault, as was inferred from fig. 70. Although this was only measured for strike-slip faults on top of the silicon putty walls, it is reasonable to assume that this is also valid for small strike-slip faults within the graben to some extent. Because the graben in model 4 is smaller, less difference in motion is present between the north and the south side of the graben. Hence less faults needed to develop in model 4.

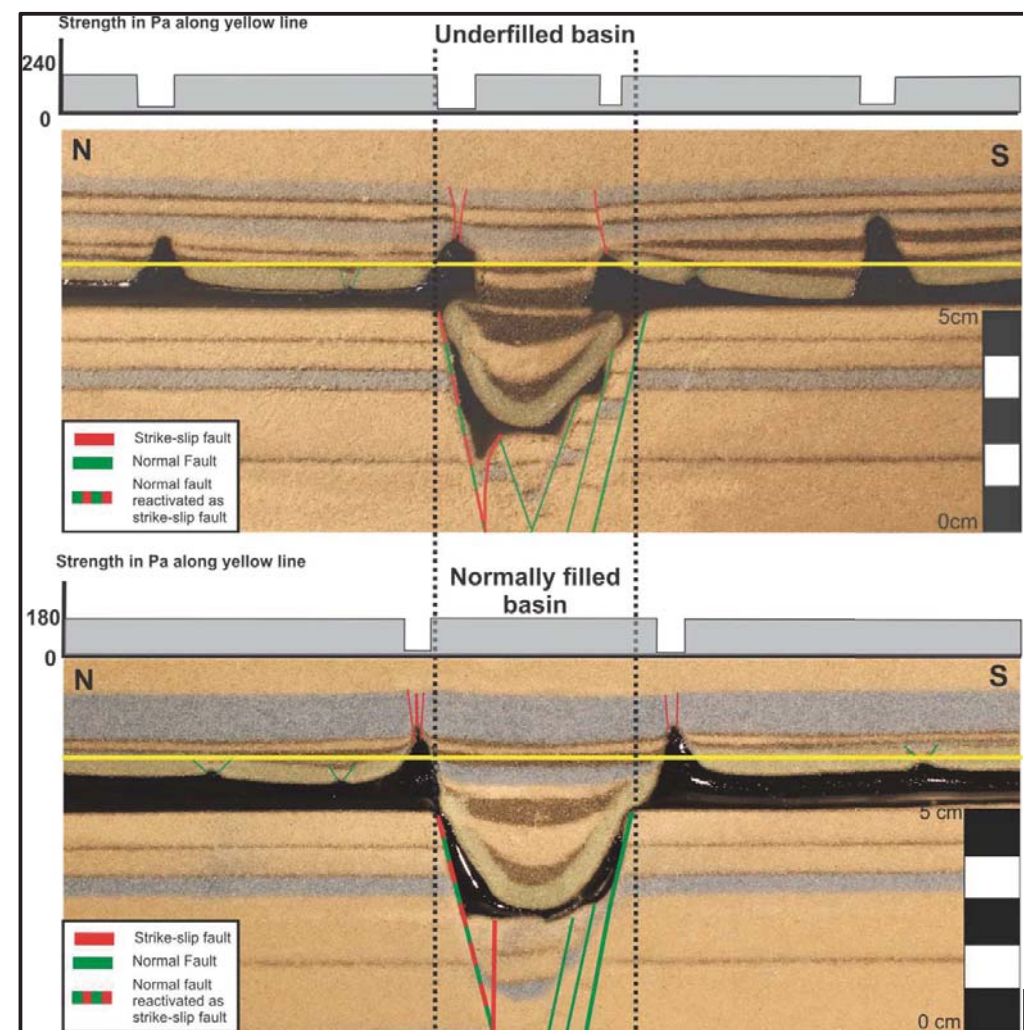


Fig. 90. Figure illustrating the lateral difference in strength between an underfilled graben with extruded putty (section 4.3) and a normally filled graben (section 3.2). The vertical dashed black lines intersect the top of the basement normal faults that bound that basement part of the graben. From these lines can be inferred that the brittle part of the sub putty graben is narrower for the underfilled basin than for the normally filled basin.

6. Integration and discussion

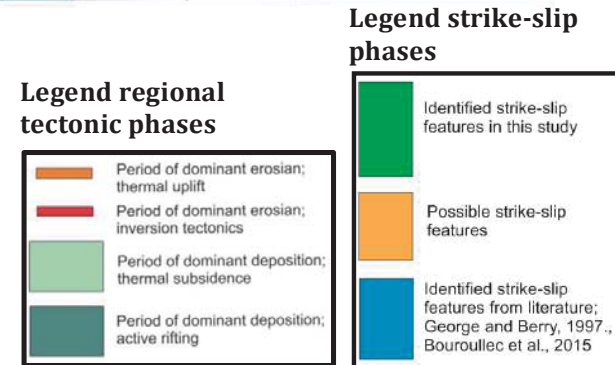
This study has provided better insights in several strike-slip movements that occurred in the Northern Dutch offshore in terms of timing, sense and amount of displacement and fault-salt interaction. In this section is discussed what could have caused the strike-slip motions that are observed in the Dutch Central Graben and Terschelling Basin (case study B-D) and to what extent the analogue models are a valid approximation for the observations regarding strike-slip movements in the northern Dutch Offshore.

6.1. Strike-slip motions in the Dutch offshore and analogue modelling

Strike-slip faulting has occurred during four time intervals in the northern Dutch offshore under regional extensional (Triassic, Jurassic and Lower Cretaceous) and compressional (Late Cretaceous) tectonics.



Fig. 91. Table that indicates the time period during which strike-slip movements have been observed (in green and from literature in blue) expected (in orange).



When the model of Kley et al., (2008b) (section2.4) is applied to the Dutch subsurface, one would expect that the Hantum Fault Zone and the Rifgronden Fault Zone accommodated dextral strike-slip motions during the Middle and Upper Triassic, thereby functioning as a transform fault zone to accommodate movements that resulted from active rifting in the Dutch Central Graben and the Lower Saxony Basin (Fig. 92). Evidence for these dextral movements were indeed found on the HFZ and RFZ in this study (Case Study D).

According to the model from Kley et al., (2008b), strike-slip motions could also have occurred during the Upper Jurassic and Early Cretaceous along preformed N-S trending basement faults that bound the Dutch Central Graben (Fig. 91 and Fig. 92). During this time, the N-S trending faults that bound the Dutch Central Graben could have functioned as an (oblique) transform fault zone that accommodated motions that resulted from active rifting in the Terschelling Basin and the Tail End Graben towards the north of the Dutch Central Graben (Fig. 93). According to the model from Kley et al., (2008b), these (oblique) strike-slip movements would have been sinistral. No evidence for these strike-slip faults was found in this study, although it has to be emphasized that the seismic resolution is insufficient underneath the Zechstein salt in the Dutch Central Graben to find direct evidence of these motions.

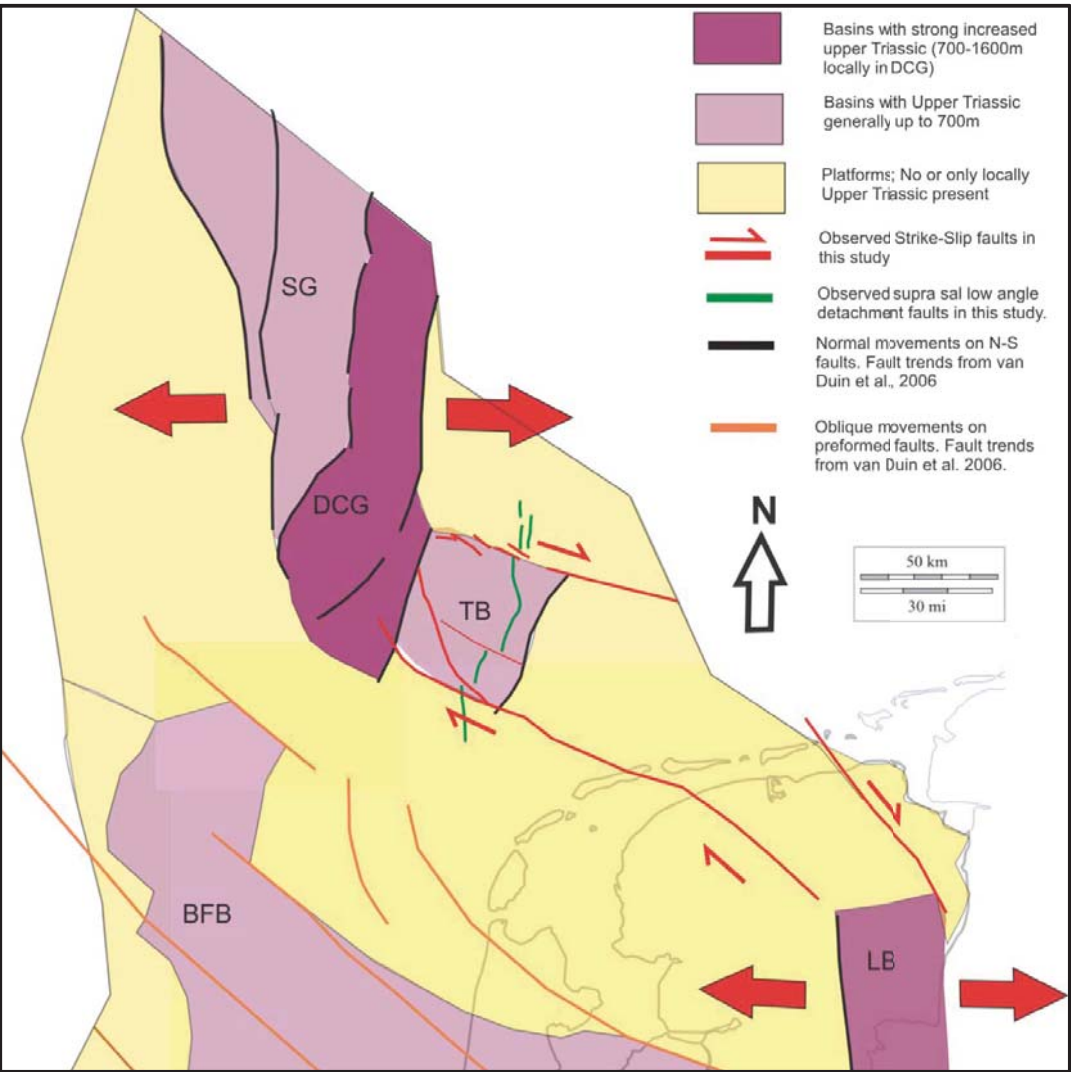


Fig. 92. Schematic map showing the geological setting of the Dutch subsurface during the Middle and Late Triassic. Abbreviations; BFB Broad Fourteens Basin, DCG Dutch Central Graben, LB Lower Saxony Basin, SG Step Graben, TB Terschelling Basin. Source for thickness distribution; Southern Permian Basin atlas.

Analogue models on the other hand have shown that strike-slip movements on (preformed) basement faults are redistributed by the overlying salt, thereby decoupling the supra-salt deformation pattern from the subsalt deformation pattern. Movements are preferentially transmitted and accommodated by salt diapirs as the supra salt interval is at its weakest here. The reason for this is twofold; 1) A package of salt becomes weaker with increasing salt thickness. 2) The overburden becomes weaker with decreasing sediment thickness. If sediments overlie salt diapirs or salt walls, strike-slip motions are transmitted via these salt structures into the overburden. Hence, basement induced strike-slip faults could preferentially be observed above diapirs. The reason that these faults are not observed above diapirs in the Dutch Central Graben and Terschelling Basin could be due to Mid-Kimmerian uplift and Late Cretaceous – Early Paleogene inversion and subsequent erosion. Surely, Mid-Kimmerian erosion has removed the entire Lower Jurassic as well as significant parts of the Upper Triassic in the Terschelling Basin, while Late Cretaceous – Early Paleogene inversion has removed large parts of the Upper Jurassic and Lower Cretaceous sediments in the Dutch Central Graben. Additionally, where the Upper Jurassic and Lower Cretaceous strata have been preserved in the Dutch Central Graben, renewed activity along salt walls and diapirs during Late Cretaceous – Early Paleogene inversion could have erased the evidence of strike-slip motions on preformed basement faults.

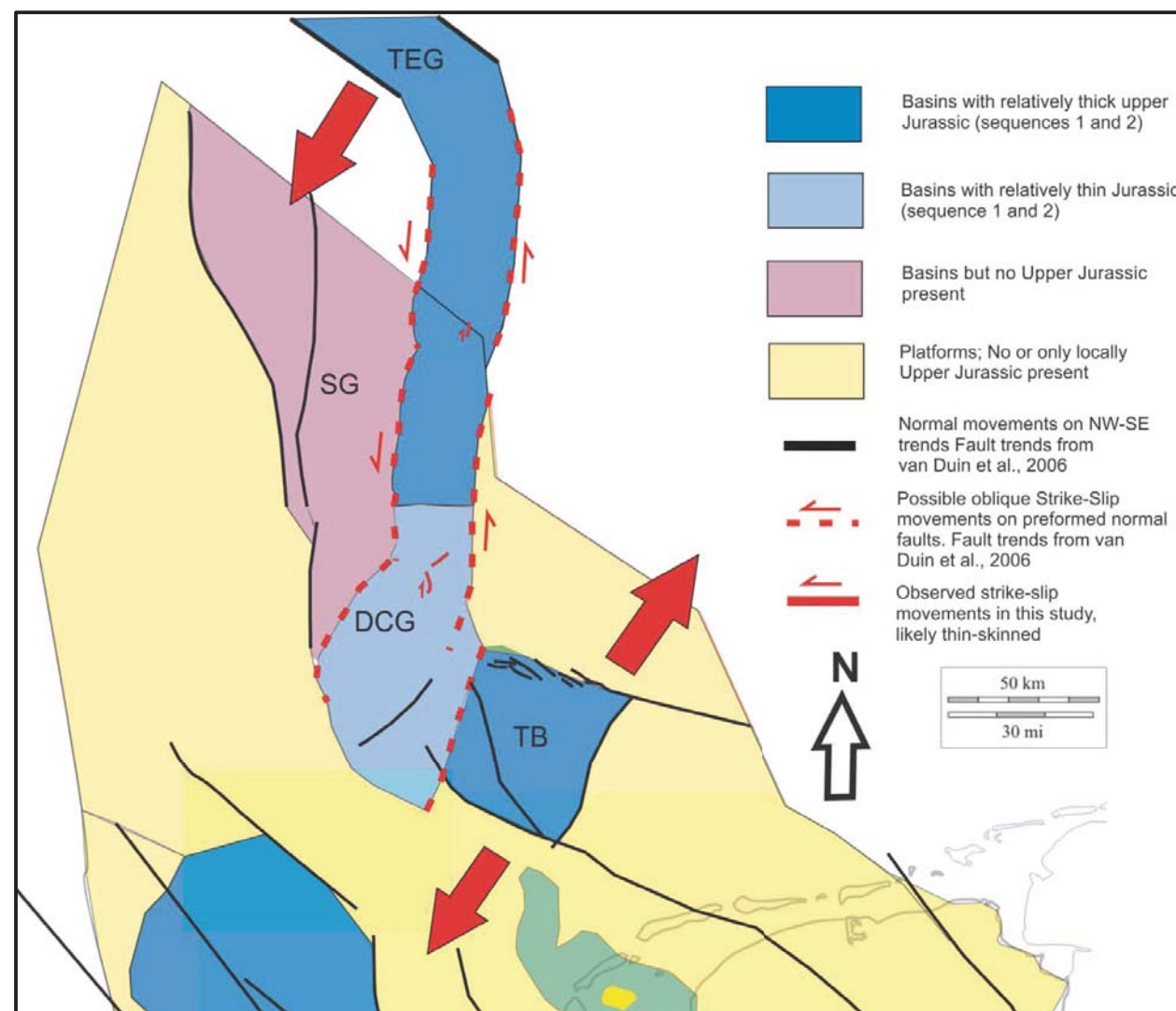


Fig. 93. Schematic map showing the geological setting of the Dutch subsurface during the Upper Jurassic (Sequence 2 and 3). Abbreviations; DCG Dutch Central Graben, SG Step Graben, TB Terschelling Basin, TEG Tail End Graben. Source for thickness distribution; Southern Permian Basin atlas.

6.2. The origin of the observed strike-slip movements in the Dutch Central Graben

Thin-skinned vs. thick skinned

The observed strike-slip motions that are present in the Dutch Central Graben are located in the central parts of the basin. These motions are rather subtle; in the order of 700 to 2500m. The Late-Jurassic to Early Cretaceous timing of Faults F1b and F1c corresponds to a change in regional extension direction from approximately E-W towards NE-SW. As suggested by Kley et al., 2008b, this might have led to an (oblique) reactivation of preformed N-S trending faults. However, whether or not the observed supra salt strike-slip faults are induced by strike-slip movements on basement faults is difficult to say with certainty due to the resolution of the seismic data at this depth. The Zechstein salt surely seems thick enough in the entire part of the Dutch Central Graben to cause decoupling of the supra-salt with respect to the sub-salt interval. The analogue models described in this report have shown that when strike-slip motions occurred along basement faults, a small part of this motion is accommodated in the central part of the basin by several small faults, despite the increased mechanical strength of this part of the model. The amount of strike-slip that is accommodated in the central part of the basin seems to be controlled by the width of the basin as defined by the outline of the silicon putty walls. Hence, the strike-slip motions observed in the B18 and F11 blocks might have been caused by underlying basement strike-slip features.

Alternatively the strike-slip motions are purely thin skinned and accommodate differential motions during the Late Jurassic to Early Cretaceous on basement normal faults. In this scenario, the decoupling of the salt causes the local stress field above the salt to deviate from the stress field below the salt, which might have been purely extensional (fig. 94). Additionally, a component of gravitational gliding probably enhanced the strike slip-movements, as is indicated by the general northward deepening of the Dutch Central graben. The slightly curved geometry of faults F1b and F1c, favours the latter scenario, as basement strike-slip faults usually tend to be straighter, as is for example the case for the faults of FG1 on the western platform areas, described in case study A. Additionally, according to the model described by Kley et al., 2008, strike-slip motions on preformed basement faults would have been sinistral instead of dextral. Hence, it is suggested that F1b and F1c don't provide evidence for strike-slip movements on preformed N-S basement faults.

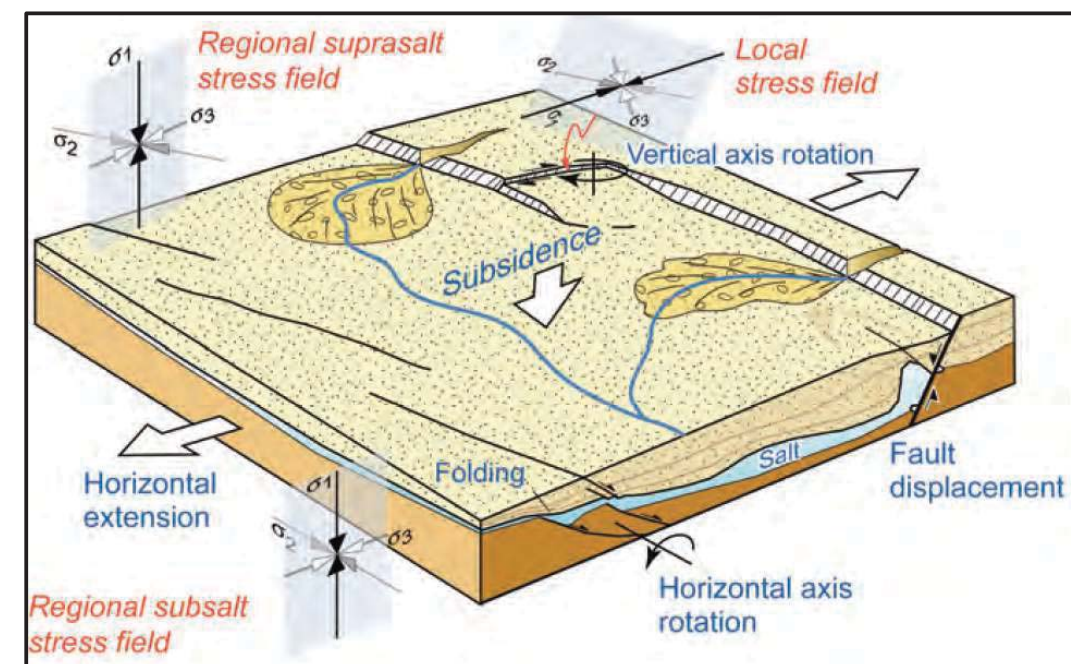


Fig. 94. Sketch that indicates how the local supra salt stress field can deviated from the regional stress field due to the presence of a salt layer. Figure from Kley et al., 2008

Regional structural evolution of the Central part of the Dutch Central Graben

An interpretation of the structural evolution of the area around fault F1c for the thin-skinned scenario is indicated in figures 95 and 96. According to this scenario, which is believed to be the most likely one, the first salt activity started during the Middle Triassic in response to normal movements along N-S oriented basement faults. Salt in this area reached the active piercing stage and evolved into the passive stage during the Late Triassic to Early Jurassic. When the regional stress regime changed towards NE-SW, new normal faults developed above the Zechstein salt (indicated in blue in fig. 96). It is likely that these thin skinned normal movements on ENE-WSW oriented faults are caused by normal movements on basement faults. However, it is hard to recognise these sub-salt faults in the seismic data. For sure, if new NW-SE basement faults developed, displacements were more subtle and not as large as during the Triassic along N-S trending basement faults. Additionally, also a component of gravitational spreading is likely to be involved, which is supported by the observation that NW-SE supra salt strike-slip faults all dip towards the N/NNE. Movements along these supra salt faults were not uniform throughout the basin, likely due to differential movements on basement faults, but certainly also due to the presence of salt walls and diapirs which had divided the brittle Mesozoic supra salt interval into several compartments, as they are laterally enclosed by salt walls in multiple areas. The differential motions between these compartments are primarily accommodated by the weak salt structures, as is shown by the analogue models. However, because salt walls don't fully enclose the different compartments, movements are transferred in the brittle interval in those places where the salt structures are absent (fig. 96). This scenario would explain both the curved geometry of fault F1c, as well as the different strike of fault F4c because fault F4c would transfer the motion between diapir B and the salt wall towards the northeast of diapir B in this scenario. Additionally, the interaction of the strike-slip faults F1c and F4c with salt diapir B, caused rotation of this diapir and likely also a component of compression on this diapir due to left stepping of the strike-slip fault.

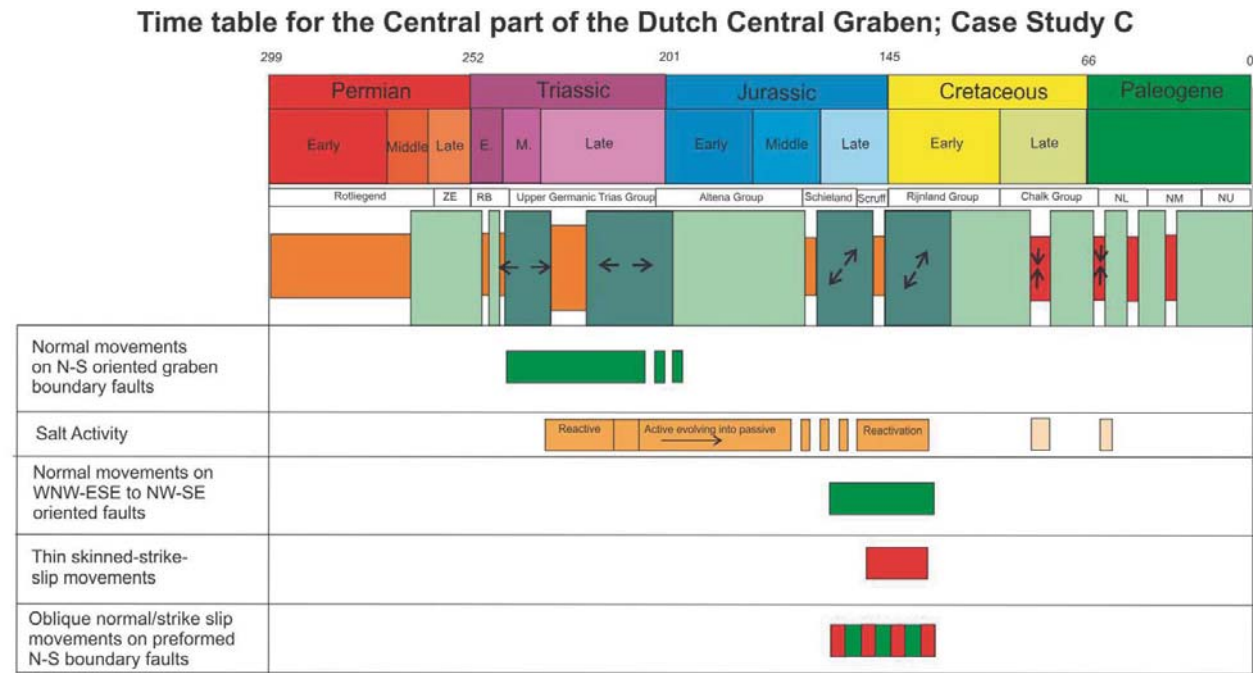


Fig. 95. Diagram indicating the time of activity for the main structural elements in the Central part of the Dutch Central Graben, as described in case study C.

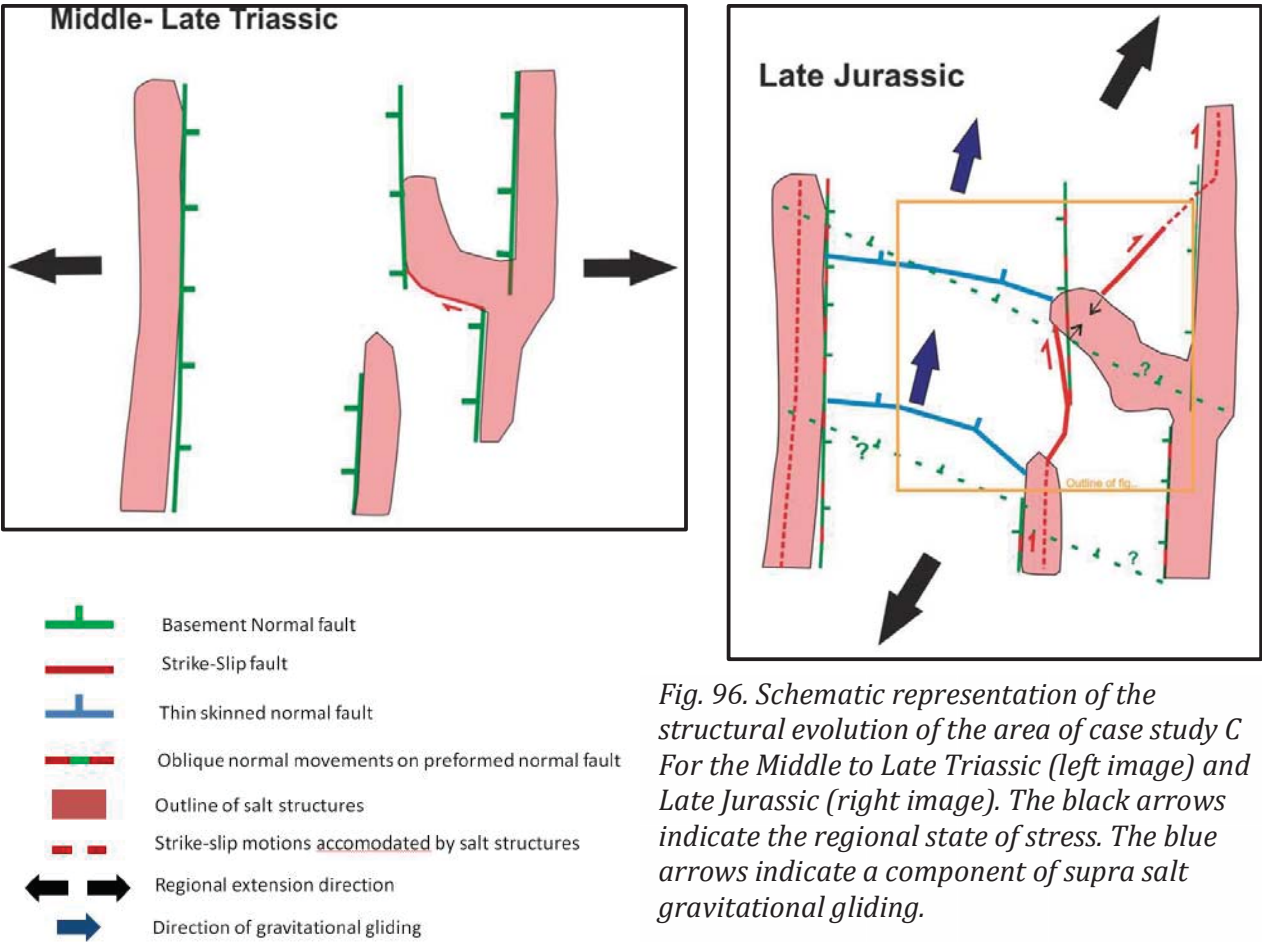


Fig. 96. Schematic representation of the structural evolution of the area of case study C. For the Middle to Late Triassic (left image) and Late Jurassic (right image). The black arrows indicate the regional state of stress. The blue arrows indicate a component of supra salt gravitational gliding.

6.3 Strike-Slip motions in the Terschelling Basin and at the Schill Grund High

Thin-skinned motions

The thin skinned strike-slip motions that are present in the Triassic interval of the Terschelling Basin and at the Schill Grund High are likely caused by differential motions on sub-salt basement faults (fig. 94), to some extent similar to the strike-slip motions in the Upper Jurassic in the Dutch central Graben. However, there are some differences as the supra salt interval in the Terschelling basin was much thinner during the Upper Triassic, than the supra salt interval in the Dutch Central Graben during the Upper Jurassic. Additionally, salt structures were in an early stage of development in the Terschelling Basin during the Middle and Upper Triassic, as E-W extension during the Triassic triggered the first motions of Zechstein salt in the Terschelling Basin. Most salt structures in this area reached the piercing stage during deposition of the Late Triassic Keuper formation. This means that during the time of E-W extension and accompanied strike-slip motions, Zechstein salt was abundantly present to act as weak zones to accommodate for the differential motions (Fig. 97). In the Dutch Central graben, during the Upper Jurassic, salt structures were much more mature and salt walls and diapirs were generally already established. Hence differential motions on basement faults also had to be accommodated by the brittle supra-salt overburden in the absence of salt (Fig. 97), as is described in case study C.

Thick skinned motions

The stepping geometry of the N-S trending Middle to Late Triassic Low angle detachment fault zone over the WNW-ESE trending Hantum and Rifgrunden fault zone has been interpreted as evidence for post Early Triassic dextral strike-slip faulting along these fault zones. The fact that strike-slip motions occurred along the RFZ fault zone is furthermore supported by its en echelon geometry of fault segments. This is the first time that dextral displacements along these fault zones

have been estimated and that evidence is adduced that significant dextral faulting occurred along these fault zones during the Mesozoic. Dextral motions along the HFZ and RFZ correspond with the regional model for the Permian Basin area as proposed by Kley et al., 2008. Hence, it is suggested that the HFZ and to some extent the RFZ functioned as dextral transform fault zones to compensate for movements related to the opening of the Dutch Central Graben and to some extent the Lower Saxony Basin. As part of these dextral movements, the Terschelling Basin as a whole seems to have been dextrally sheared, explaining the deviating NNE-SSW trend that is displayed by the low angle detachment fault zone, the salt walls and the shape of the Lower Triassic compartments.

Regional Structural evolution of the Terschelling Basin

A time table for the Terschelling basin, indicating the activity of the main groups of structural features, is shown in Fig. 98. Three stages of the interpreted structural evolution can be found in Fig. 99. First, during the Late Early Triassic (Fig. 99), activity started on N-S oriented basement faults bounding the Dutch Central Graben and probably on smaller N-S oriented basement faults underlying the Terschelling Basin. Extension accommodated by these faults was transmitted via the Zechstein salt into the Lower Triassic overburden, leading to the formation of initially N-S trending low angle detachment faults. In the Terschelling Basin, this E-W extension was enhanced by a westward component of gravity gliding, indicated by the overall westward deepening of the Terschelling Basin. Thin skinned extension triggered also the ascent of salt during the Middle-Triassic in the Terschelling Basin, where most salt structures reached the active piercing stage during the Upper Triassic. Differential motions along basement faults and due to differences in gravitational gliding, caused strike-slip motions, linking the motions between two segments of low angle detachment faults. These motions were accommodated by the salt which was abundantly present. After the initiation of activity on the low angle detachment faults, thick skinned dextral displacements commenced on the HFZ and RFZ, linking regional extension between the Dutch Central Graben and the Lower Saxony Basin. The dextral motions along the HFZ and RFZ dextrally offsetted the low angle detachment faults (fig. 99). Additionally, they caused overall shearing of the Terschelling Basin. The low angle detachment faults and dextral motions along the RFZ and HFZ most likely occurred simultaneously during the further period of E-W extension. Towards the Late Jurassic, when the direction of regional extension had changed, strike-slip motions no longer took place on the RFZ and HFZ. In contrast, they were activated in a normal way, thereby opening the Terschelling Basin (fig. 99). Finally, during the Late Cretaceous and Paleogene inversion pulses, the RFZ and HFZ underwent minor inversion.

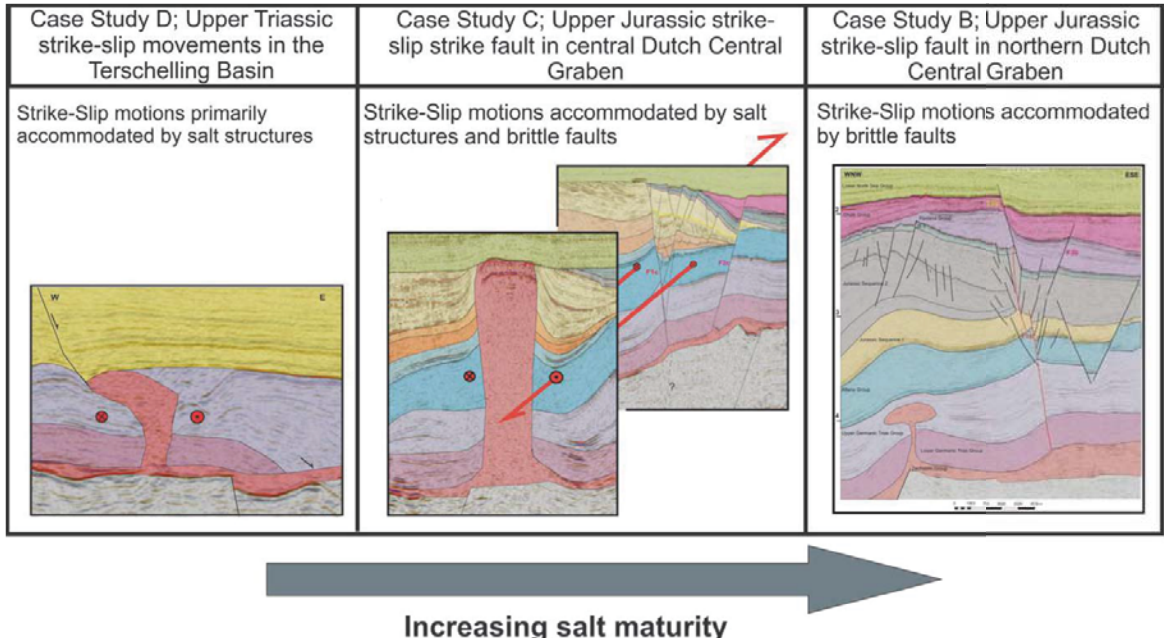


Fig. 97. Figure illustrating how the structural style of deformation of supra salt strike-slip movements depends on the presence of salt structures, which tend to be less abundant with increasing salt maturity.

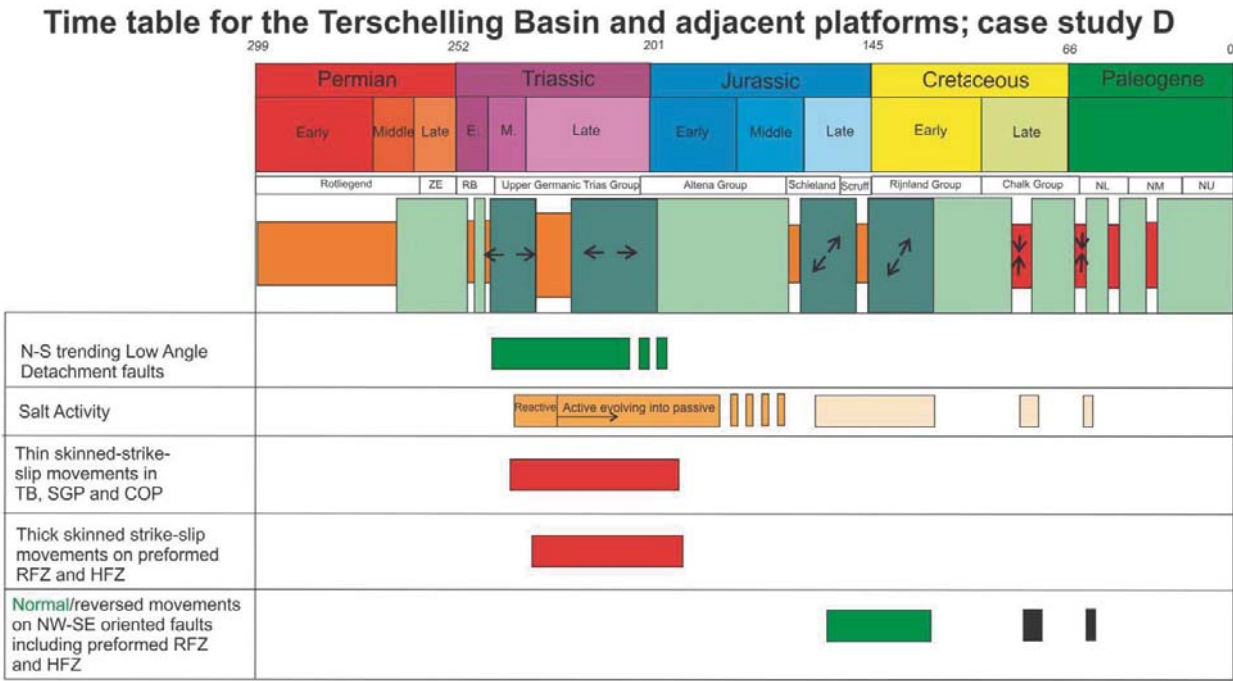


Fig. 98. Diagram indicating the time of activity for the main structural elements the Terschelling Basin and adjacent platforms, as described in case study D.

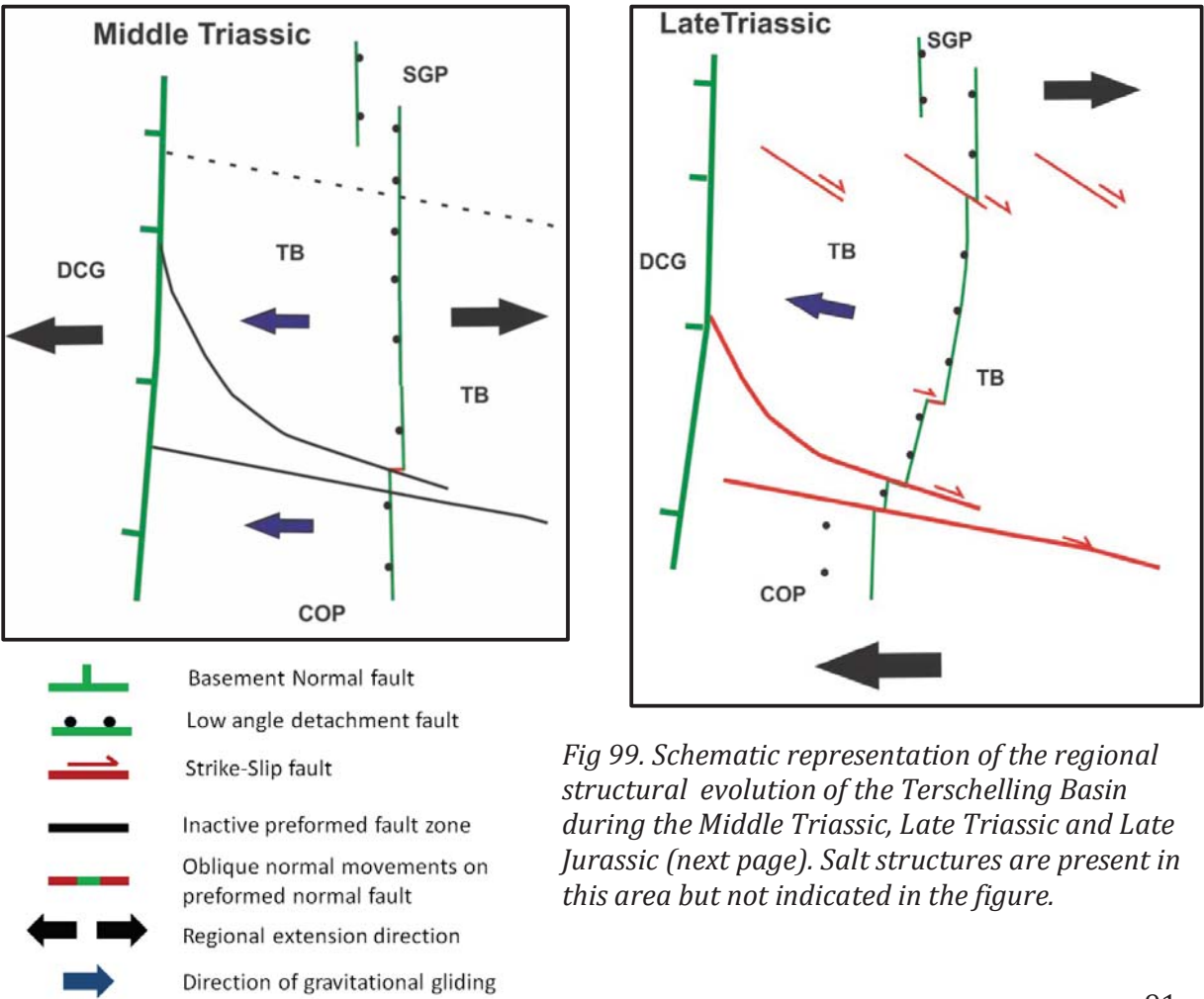
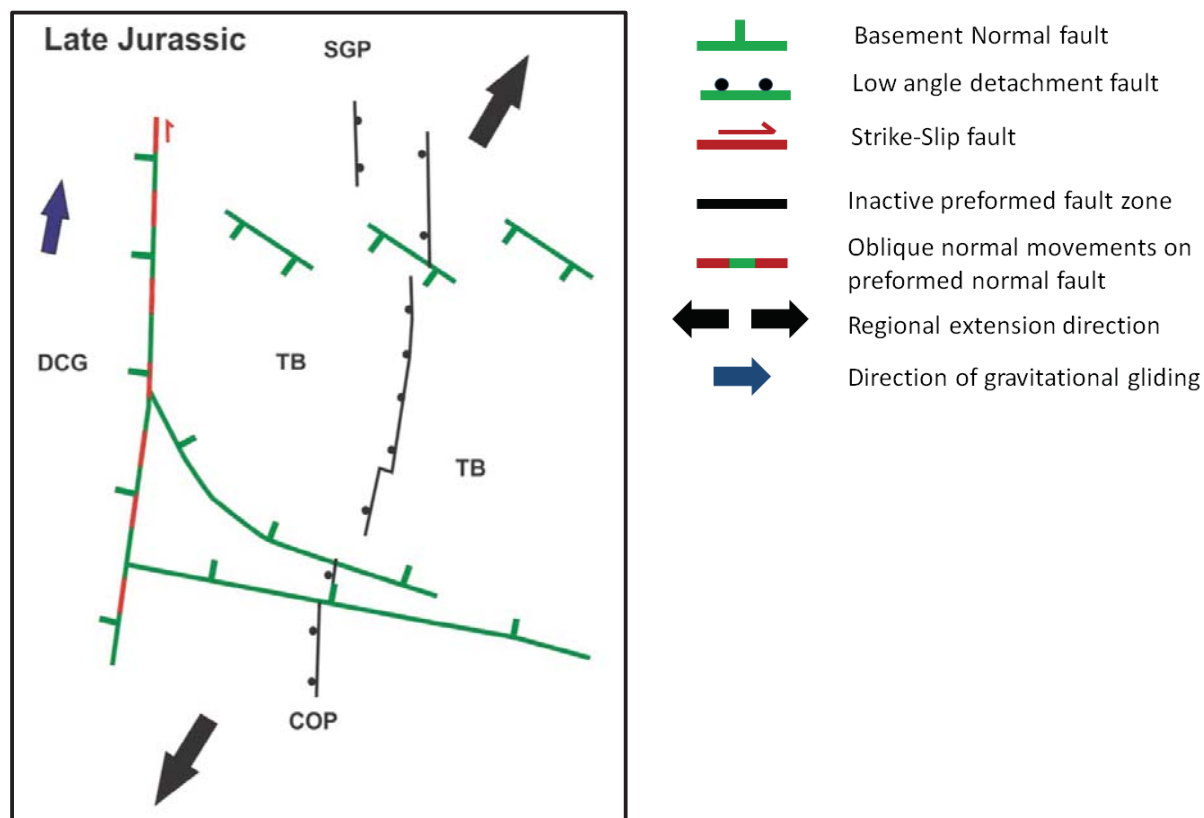


Fig 99. Schematic representation of the regional structural evolution of the Terschelling Basin during the Middle Triassic, Late Triassic and Late Jurassic (next page). Salt structures are present in this area but not indicated in the figure.



6.4. Natural analogies and comparison with other studies

Because of its rotation, the shape of salt diapir B (case study C) looks a bit like a rotated sigma clast in a sheared metamorphic rock (Fig. 100). Additionally, a striking-resemblance between diapir B and a diapir in the Great Kavir in northern Iran is present (Fig. 101). The diapir in northern Iran also shows the curved geometry of strike-slip faults upon the approach of the diapir. This rotation is also observed in analogue models performed by Dooley et al., (2012) (Fig. 11). Overall, the development of the area around case study C shows some analogy to the areas in the West African Passive margin (fig. 102). In this area, gravitational gliding towards the Atlantic has caused normal faulting in the higher part of the margin towards the continent and thrust faulting in the lower Atlantic part due to the presence of a salt layer, which acts as a decollement. Rates of gravitational gliding of the supra salt overburden were not the same everywhere so differential motions occurred between different blocks. These differential motions between the different blocks then led to strike-slip motions, which in analogy to the Dutch offshore and analogue modelling, are preferentially accommodated by salt structures. Additionally, the brittle interval in-between salt structures also has to accommodate these strike-slip motions, thereby linking the salt structures. However, the stronger component of gravitational gliding in the west African margin, has presumable caused larger supra-salt strike-slip motions, than in the Dutch Central Graben.

The Triassic compartments in the Terschelling Basin, which are surrounded on multiple sides by salt walls show an analogy with Cenozoic minibasins in the Gulf of Mexico. In this area, salt or salt welds that surround the minibasins primarily accommodate differential motions between adjacent minibasins (Fig. 103).

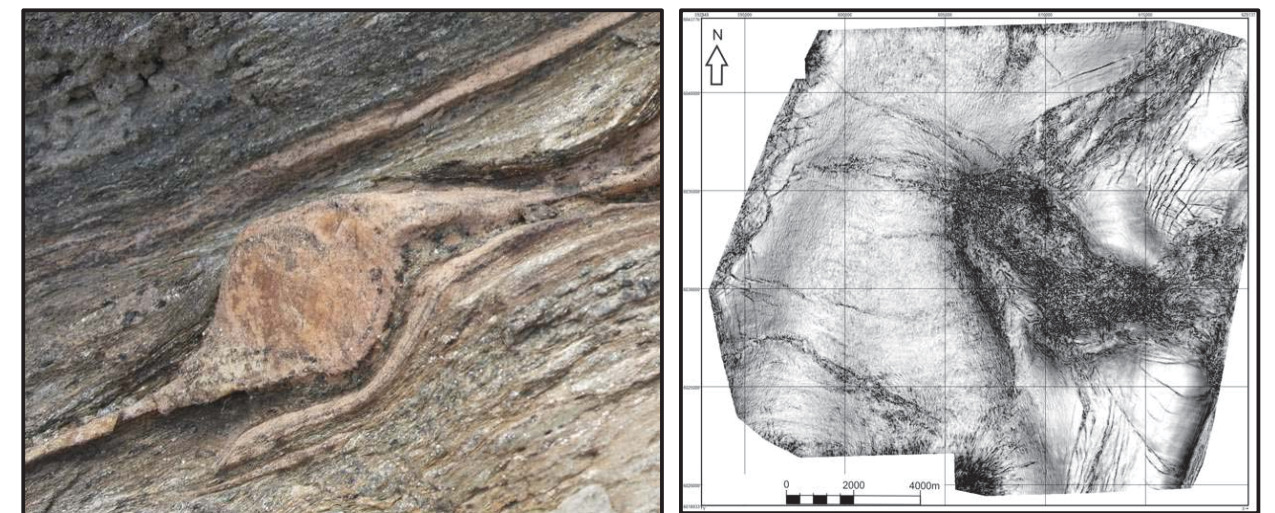


Fig. 100. The shape of salt diapir B discussed in case study C (right figure) shows geometrical similarities to a dextrally sheared sigma clast metamorphic shear zone (left figure). Left figure from Johanna Sommer; the art in science.

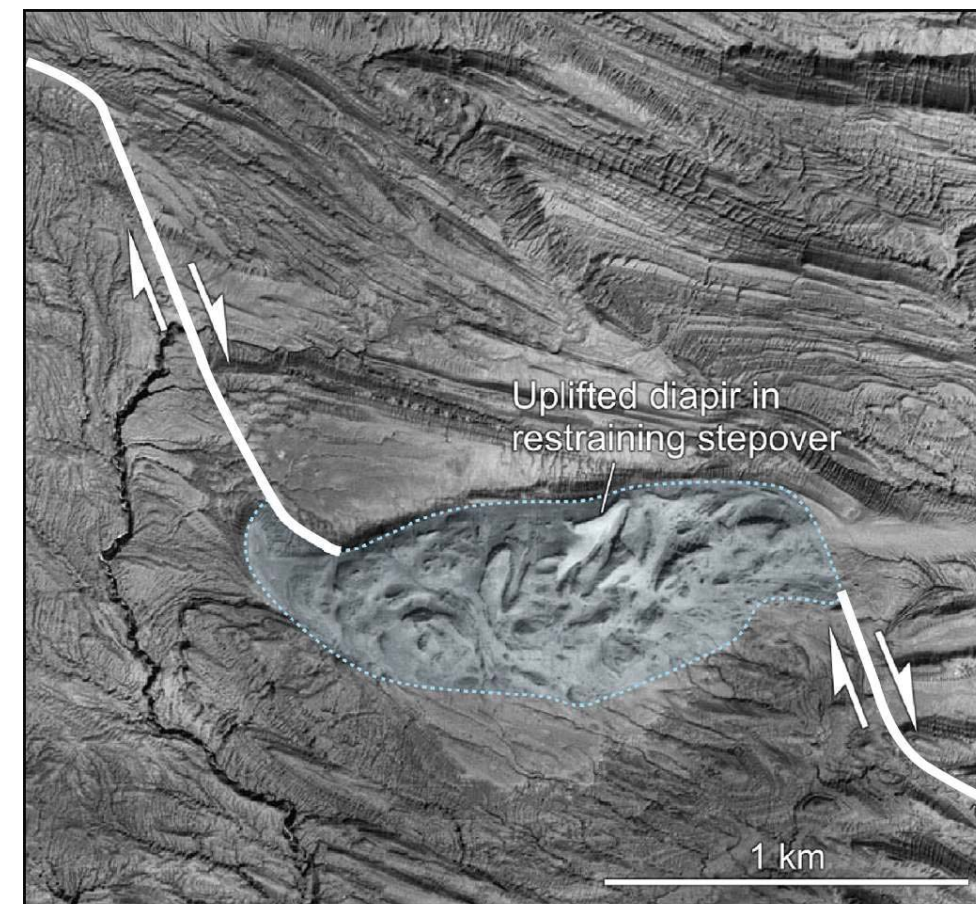


Fig. 101. Dextral strike-slip interaction with a salt diapir in the Great Kavir in northern Iran. The left stepping of the dextral strike-slip fault causes a restraining bend to develop over the diapir and causes localised compression, uplift as well as rotation of the salt diapir. Note the similarity between this diapir and diapir B in case study C (Fig. 100). Figure from Dooley and Schreurs, 2012.

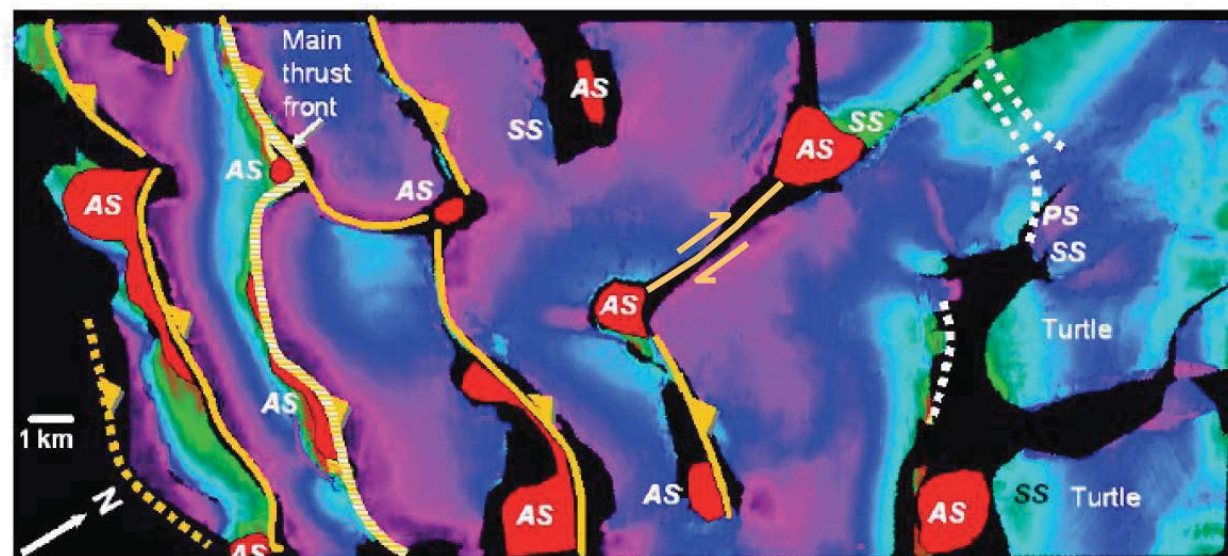


Fig. 102. Part of the west African margin before the country of Gabon, note that differential motions between different blocks are accommodated by salt structures (indicated in red) and brittle strike-slip faults that link these salt structures. Figure from Hudec and Jackson, 2004

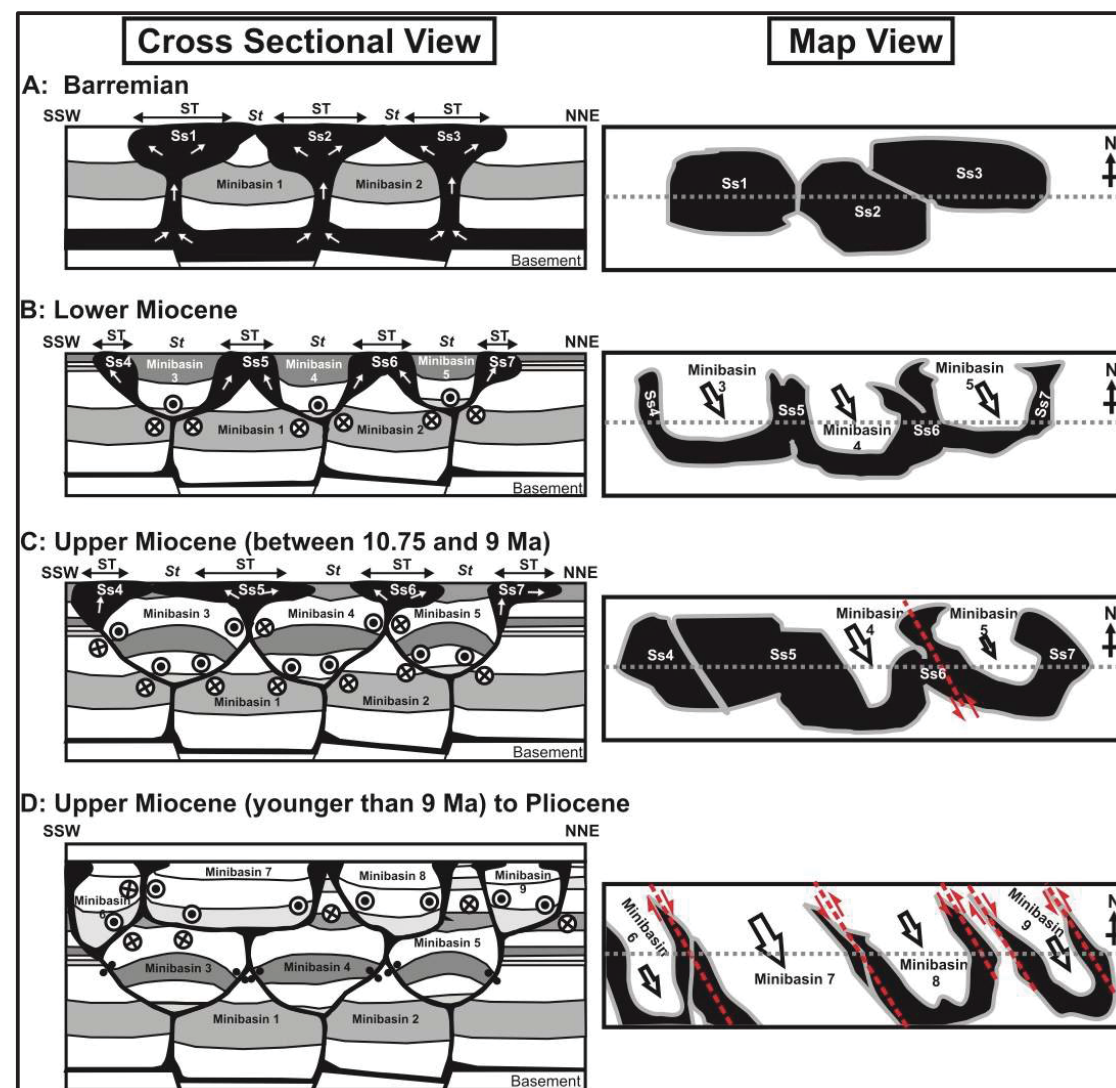


Fig. 103. Schematic figure showing the structural development of a complex of stacking minibasins. Differential motions between adjacent minibasins are accommodated via lateral motions along salt walls and salt welds. Fig. from bouroullec et al., 2016 in press.

7. Implications of strike-slip movements for hydrocarbon exploration

A proper understanding of strike-slip movements is of vital importance to assess all the components of a possible working hydrocarbon system. These components are; the presence of a structural trap, the presence of a seal and the occurrence of charge from deeper source rocks. A good structural trap related to strike-slip faulting can form due to the upward widening of the fault pattern, in combination with the tilting of fault blocks inside a strike-slip fault zone. An example of a working structural trap related to strike-slip faulting in the Dutch subsurface is the Pijnacker oil field, where oil is trapped in a positive flower structure (Racero-Baena and Drake, 1996). Additionally, strike-slip movements influence the reservoir quality on both side of the faults zone as strike-slip movements cause different blocks to move laterally with respect to each other. This means that in a rapidly changing depositional environment, such as during the Upper Jurassic in the Dutch Central Graben, reservoir qualities can differ significantly on one side of the strike-slip fault with respect to the other side of the strike-slip fault in the same stratigraphic interval. This is the case for instance, when material of a deeper part of the basin is brought laterally next to a more proximal part of the basin due to post-depositional strike-slip faulting. The influence of syn-depositional strike-slip faulting is poorly understood. But also here, it has to be taking into account that different rock types and different rock properties might be encountered on both sides of the fault, in the same stratigraphic interval. A good example of this, is the lateral stacking of alluvial fans along NW-SE striking Permian strike-slip faults as was observed by George and Berry (1997). Concerning the possibility of charge from sub salt source rocks, it is important that windows in the salt provide fluid conduits along which hydrocarbons can migrate. Hence, the question whether supra-salt strike-slip faults are triggered by sub salt basement strike-slip faults is of importance as a linked fault system could provide a fluid conduit along which hydrocarbons can migrate. However, this doesn't seem the case in the Dutch Central Graben, as supra salt strike-slip faults are likely purely thin skinned. However, charge could also originate from the supra salt Posidonia shale source rock in the Dutch Central graben.

8. Conclusions

The most important conclusions of this study are summarized below by answering the key questions that were addressed in this study.

Where are Mesozoic strike-slip faults located in the northern Dutch offshore and what is the timing, sense of displacement and amount of displacement?

Several Mesozoic strike-slip faults are present in the Northern Dutch offshore, both on the platform areas as well as in the basins (Fig. 20). The main conclusions in terms of amount- and sense of displacement, timing and fault salt relations are listed below per structural element and can also be found in Table 3 for individual faults and fault families.

- **Strike-slip faults on the western Platform areas**

A Group of SW-NE to WSW-ENE trending Late Cretaceous to Early Paleogene dextral strike-slip faults offsets and partly reactivates older fault trends, thereby forming pop-up and pull-apart structures. Offsets on individual strike-slip faults are in the order of 500-900m. The exact cause of these faults is uncertain but it is suggested that an approximate E-W directed ridge push force has played an imported role in the formation of these strike-slip faults.

- **Strike-slip faults in the Dutch Central Graben**

Several Late Jurassic/Early Cretaceous isolated strike-slip faults are present in the Dutch Central Graben. These faults are characterised by a curved strike that changes between approximately NW-SE to NE-SW. Estimated offsets on individual strike-slip faults range between 900 and 2500m.

- **Strike-slip faults in the Terschelling Basin and on the adjacent Schill Grund- and Central Offshore platforms**

Post Early Triassic and Pre- Late Jurassic dextral strike-slip movements have occurred on the preformed Hantum fault zone and Rifgronden fault zone. Dextral strike-slip movements on the Hantum Fault zone are estimated to be in the order of 5 à 6km. Dextral strike-slip movements on the Rifgronden Fault zone are estimated to be in the order of 2 à 3km. Strike-slip movements on basement faults also occur within the Terschelling Basin itself, accommodating differential movements for the overall dextral shearing of the basin. Thin skinned supra salt strike-slip motions occur both in the Terschelling Basin as well as on the adjacent platforms. These motions are primarily accommodated by salt walls and displacements are in the order of 1 à 2km.

Are the identified strike-slip faults in the salt controlled basins linked to deeper rooted basement faults and how are strike-slip motions on subsalt preformed basement faults distributed into the supra salt interval?

Analogue models show that subsalt strike-slip motions on inherited basement faults are transmitted into the supra salt overburden via the areas where the salt walls are highest, as this is the mechanically weakest part of the rock column.

Dutch Central Graben

- In accordance with the analogue models, the observed strike-slip movements in the Dutch Central Graben seem to be primarily accommodated by salt walls. Brittle strike-slip motions only occur in places where salt walls are absent to transfer motions between two salt structures. However, no evidence was found for strike-slip motions on

preformed N-S trending basement faults that bound the Dutch Central Graben. Instead, the strike-slip movements that were observed in the Dutch Central Graben are likely caused by differential motions on sub-salt normal faults, possibly enhanced by gravitational gliding.

Terschelling Basin

- Dextral basement strike-slip movements were accommodated in the Middle and Upper Triassic by the Hantum and Rifgronden Fault zones. Additionally the different Triassic compartments in the Terschelling Basin have moved laterally with respect to each other, where motions were primarily accommodated by the salt walls. To what extent these complex motions are caused by deeper rooted strike-slip faults is unclear. It is suggested that smaller strike-slip movements in the Terschelling Basin are purely thin skinned and originate from differential movements on sub salt normal faults, likely enhanced by a component of gravitational gliding. Larger strike slip movements are likely caused by deeper strike-slip basement faults.

Personal note

Unravelling the characteristics of a strike-slip fault in structurally complex basins such as the Dutch Central Graben and the Terschelling Basin is not straightforward. Analogue modelling has been helpful in unravelling some of the basic mechanisms regarding the distribution of strike-slip faults in a salt dominated basin. However analogue modelling is only a first order approximation for the complexity of nature and can't be used to model specific structures that have been affected by multiple deformation phases. Instead, a detailed structural analysis by making use of various thickness maps and attribute maps is a good way to gain more insight into the characteristics of specific faults. However, it has to be emphasized that estimated displacements from lateral offsets of older structures and thickness maps don't necessarily provide the original amount of displacement caused by strike-slip motions, as younger deformation phases may have reactivated the structure.

9. Recommendations for future work

- The analogue models described in this study consisted of an extensional phase, followed by a resting phase and finally a strike-slip phase. Hence, the models were used to study the distribution of strike-slip movements on inherited basement faults into the overburden of a mature salt basin. In the Terschelling basin on the other hand, strike-slip motions predate the main opening of the basin in the Upper Jurassic and Lower Cretaceous. Hence, during the time that the strike-slip motions took place (Middle and Upper Triassic), the salt structures were less mature. This means that the salt structures were less developed and that the basal salt layer was much thicker. Analogue models could be used to test the influence of a basement strike-slip fault on a thick but rather homogeneous upper crustal weak layer and a thin overburden.
- The analogue models described in this study show that strike-slip movements on a preformed sub-salt basement fault are primarily transmitted via the silicon putty walls. This led to the formation of strike-slip faults above the silicon putty walls in the brittle cover. Such supra salt wall strike-slip faults have not been observed in the seismic interpretation part of this study. It might very well be possible that evidence of these strike-slip faults is removed by later uplift and erosion or due to later reactivation of salt structures. However, it might be possible that there are some salt structures in the Dutch Central Graben that are overlain by Upper Jurassic and/or Cretaceous rocks and that have been relatively stable during Late Cretaceous inversion. If these strata are preserved above salt structures in the Dutch Central Graben, it would be interesting to see if they were affected by supra salt wall strike-slip faults. Additionally, such supra salt wall flower structures could provide structural traps for hydrocarbon accumulations.
- The analogue models 3 and 4 indicate that the amount of supra salt strike-slip movements in the graben depends on the distance between the salt walls on either side of the graben when sub-salt strike-slip movements occur on a preformed basement fault. It would be interesting to test this in a more quantitative way by performing multiple experiments with varying distance between the two opposing salt walls and better understand the relation between the width of the basin as defined by the salt walls, and the amount of strike-slip deformation that is accommodated by strike-slip faults in the graben.
- The seismic sections that are shown in this study are in seconds two way travel time (TWTT). Additionally, the isopach maps created in this study are also in second TWTT. Because seismic velocities differ with depth and with rock type, some intervals may appear thicker on a seismic line than others. Hence, a good velocity model, allowing the conversion from time to depth would considerably increase the reliability of the interpretations.
- Several strike-slip faults in the northern Dutch offshore have been identified in this study and a detailed structural analysis of some of these faults has led to a better understanding in terms of timing, fault salt interaction and sense- and amount of displacement. However, it is highly likely that there remain more unidentified structures that have accommodated strike-slip movements. Similar to this study, future studies could be devoted to gain more insight in the structural development of additional strike-slip features in the Netherlands. These studies could provide valuable information about the geological history of the Dutch offshore and for future hydrocarbon exploration. Additionally, when more strike-slip features are identified, larger trends could become visible, which could lead to an overall better understanding of the geological evolution of the Northern Dutch offshore.

10. Acknowledgements

First of all, I would like to thank TNO for providing me with the opportunity to perform my MSc. Research at their research institute and allowing me to work on an interesting and challenging topic for six months. I enjoyed working in the international, informal and yet very informative atmosphere of TNO and for this I would like to thank all the people that work at TNO.

A special word of thanks to my supervisors; Jeroen Smit and Renaud Bouroullec for their help throughout the project. To you I say: “Thank you for giving me this opportunity and thank you for sharing your expertise and ideas with me. I hope you can forgive me my occasional stubbornness. I’ve really appreciated your involvement in the project; which was manifested by many discussions, but also by eating a pizza after a long day in the lab, or *fruit des mer* after a day in the field”. Special thanks also to Dimitrios for providing me with the opportunity to work in the teclab at the UU. Additionally, I would like to thank all the people who were working at the Teclab of the UU, especially Bram Scheffer and Dagmar Smit. Their models provide valuable contributions to the understanding of salt behaviour under extensional and strike-slip conditions. At TNO, I would also like to thank Mart Zipp for his help with the seismic data and Geert de Bruin for sharing his expertise on the OpendTect Software. At EBN, special thanks to Marten ter Borgh for pointing out the presence of the SW-NE striking strike-slip faults on the western platforms, which were described in case study A of this study.

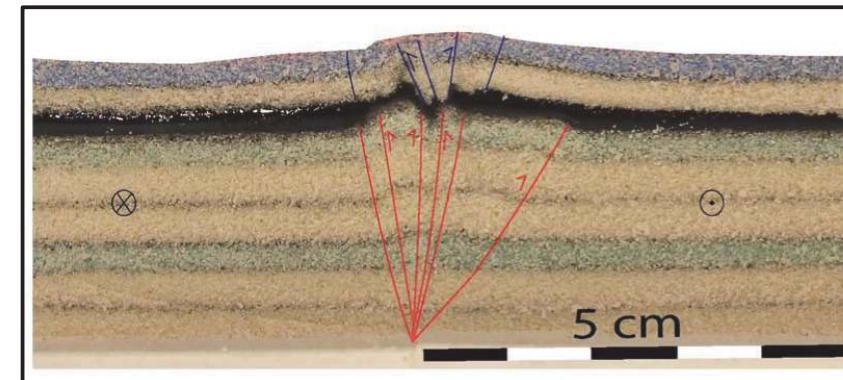
11. References

- Arthaud, F. and P. Matte 1977. Late Paleozoic strike-slip faulting in southern Europe and northern Africa: result of a right-lateral shear zone between the Appalachian and the Urals. Geological Society of America Bulletin, v. 88, p. 1305-1320.
- Bouroullec, R., G. de Bruin., Geel, Munsterman, D., K. Verreusel, R.M.C.H., 2015 TNO Focus Project
- Brun, J.P., 2009; Mauduit, T.P. O., 2009., Salt Roller: Structure and kinematics from analogue modeling., Journal of marine and petroleum geology, 26, 249-258
- Brun, J.P., 2002., Deformation of the continental lithosphere: insights from brittle-ductile models., Geological Society Special Publication., V.200., p. 355-370
- Byerlee, J., 1978., Friction of rocks., Pure and Applied Geophysics, V.116., p.615-626
- Clausen, J.A., Gabrielsen, F.H., Reksnes, P.A., Nysaether, E., 1999., Development of intraformational (Oligocene-Miocene) faults in the northern North Sea: influence of remote stresses and doming of Fennoscandia., Journal of Structural Geology 21, 1457-1475
- Davy, P., Cobbold, P.R., 1991., Experiments on shortening of a 4-layer model of the continental lithosphere. Tectonophysics, V. 188, p.1-25
- De Jager, J., 2003., Inverted basins in the Netherlands, similarities and differences., Netherlands Journal of Geosciences/Geologie en Minbouw 82: 339-349
- De Jager, J., Geluk, M.C., 2007, Geological development. In; Wong, T.E., Batjes, D.A.J. and de Jager, J. (eds): Geology of the Netherlands. Royal Netherlands Academy of Arts and Sciences (KNAW), Amsterdam: 5-26
- De Jager, J., 2012., the discovery of the Fat Sand Play 9Solling Formation, Triassic), Northern Dutch offshore – a case of serendipity. Netherlands Journal of Geosciences., Vol. 91-4. P. 609-619
- Donato, J.A., Martindale, W. & Tully, M.C., 1983. Buried granites within the Mid North Sea High. Journal of the geological Society 140: 825-837
- Dooley, T.P., Jackson, M.P.A., Hudec, M.R., 2009., Inflation and deflation of deeply buried salt stocks during lateral shortening., Journal of Structural Geology. V. 31., p. 582-600
- Gast, R. & Gundlach, T. (2006): Permian strike slip and extensional tectonics in Lower Saxony, Germany. [Permi- sche Blattverschiebungs- und Dehnungstektonik in Niedersachsen, Deutschland.] – Z. dt. Ges. Geowiss., 157: 41–56, Stuttgart
- Geluk, M.C., 2005. Stratigraphy and tectonics of Permo-Triassic basins in the Netherlands and surrounding areas. PhD thesis, University of Utrecht: 171 pp.
- Geluk, M.C., Paar, W.A., Fokker, P.A., 2007., Salt, Geology of the Netherlands, royal Netherlands academy of Arts and Sciences., pp.283-294
- George, G.T., Berry, J.K., 1997., Permian (Upper Rotliegend) synsedimentary tectonics, basin development and paleogeography of the southern North Sea., Geological Society, London, Special Publications 1997; v. 123; p. 31-61
- Goetze, C., Evan, B., 1979., Stress and temperature in the bending lithosphere as constrained by experimental rock mechanics., geophysical journal of the royal astronomical society., V. 59., p. 463-478
- Harding, R., Huuse, M., 2015., Salt on the move: Multi stage evolution of salt diapirs in the Netherlands North Sea., Marine and Petroleum Geology, V.61, p.39-55
- Heybroek, P., 1974., Explanation to tectonic maps of the Netherlands., Geologie en Mijnbouw, V.53, p.43-50
- Hudec, M.R., Jackson, M.P.A., 2007., Terra infirma: Understanding salt tectonics., Earth Sciences Reviews, V. 82., p. 1-28
- Hubbert, M.K., 1937., Theory of scale models as applied to the study of geologic structures., Geological Society of America Bulletin, V.48, p.1459-1519
- Jackson, M.P.A. and Hudec, M.R. and, 2009., Interplay of basement tectonics, salt tectonics, and sedimentation in the Kwanza Basin, Angola., aapg
- Kley, J., Franzke, H.J., Jähne, C., Krawczyk, C., Lohr, T., Reicherter, K., Scheck-Wenderoth., Sippel, J., tanner, D., van Gent, H., On strain and stress regarding the Central European Basin System.
- Kombrink, H., 2008. The Carboniferous of the Netherlands and surrounding areas; a basin Analysis. Proefschrift.
- Kombrink, H., doornenbal, J.C., duin, E.J.T., Den Dulk, M., Van Gessel, S.F., Ten Veen, J.H. & Witmans, n., 2012. New insights into the geological structure of the Netherlands; results of a detailed mapping project. Netherlands Journal of Geosciences 91-4:419-446
- Kiersnowski, H., Buniak, A., 2006., Evolution of the Rotliegend Basin of northwestern Poland., Geological Quarterly, 2006, V50.p.119-138
- Mann, P., 2007., global catalogue, classification and tectonic origins of restraining- and releasing bends on active and ancient strike-slip fault systems., Geological Society, London, Special Publications, V.290,p13-142.
- Mart, Y. and Ross, D. A., 1987., Post-Miocene rifting and diapirism in the northern Red Sea., Mar. Geol. 74, 173-190.
- Munsterman, D.K., Verreussel, R.M.C.H., Mijnlief, H.F., Witmans, N., Kerstholt-Boegehold, S., 2012., Revision and update of the Callovian-Ryazanian Stratigraphic Nomenclature in the northern dutch Offshore, i.e. central Graben Subgroup and Scruff Group. Netherlands Journal of Geosciences-Geology en Mijnbouw, 91 (4): 555-590.
- Nalpas, T., Le Douaran, S., Brun, J.P., Unternehr, P., Richert, J.P., 1995., Inversion of the Broad Fourteens Basin (offshore Netherlands), a small-scale model investigation., Sedimentary Geology, V. 95, p.237-250
- Peeters, S.H.J., 2015., Towards better understanding of the highly overpressured Lower Triassic Bunter reservoir rocks in the Terschelling Basin., MSc. Intern project Utrecht University at EBN
- Pfiffner, O.A., Ramsay, J.G., 1982., Constraints on geological strain rates: Arguments from finite strain states of naturally deformed rocks., Journal of Geophysical Research., V. 87., p. 311-321
- Racero-Baena, A., and Drake, S.J., 1996, Structural style and reservoir development in the West Netherlands oil province in H.E. Rondeel, D.A.J. Batjes, and W.H. Nieuwenhuijs, eds., Geology of gas and oil under the Netherlands: Dordrecht, Kluwer Academic Publishers, p. 211-227.
- Remmelts, G., 1995 Fault-related salt tectonics in the Southern North Sea, the Netherlands., in: M.P.A. Jackson, D.G. Roberts, S. Snelson (Eds.), Salt tectonics: a global perspective, AAPG memoir. 65 (1995), pp. 261-272
- Scheffer, B., 2016., Analogue modeling of salt diapirism: Example of North-Sea Central Graben., BSc. Thesis Utrecht University
- Smit, D., 2016., Salt tectonics in strike-slip settings: application to the North Sea. BSc. Thesis Utrecht University.
- Smit, J.H.W., 2005., Brittle-Ductile coupling in thrust wedges and continental transforms. PhD thesis.
- Smit, J.H.W., Brun, J.P., Fort, X., Cloetingh, S., Ben-Avraham, Z., 2008a., Salt tectonics in pull-apart basins with application to the Dead Sea Basin., Tectonophysics. V. 449., P. 1-16
- Smit, J.H.W., Brun, J.P., Fort, X., Cloetingh, S., 2008b. Pull-apart basin formation and development in narrow transform zones., Tectonics, V 27 (6), TC6018
- Smit, J.H.W., J.D. van Wees and S. Cloetingh (in press), The Thor suture zone: From subduction to intraplate basin setting. Geology, DOI:10.1130/G37958.1
- Spiers, C.J., Schutjens, P.M.T.M., Brzesowsky, R.H., Liezenber, J.L., Zwart, H.J., 1990., Experimental determination of constitutive parameters governing creep of rocksalt by pressure solution., Geological Society Special Publication., V.54. p. 215-227
- Ten Veen, J.H., van Gessel, S.F., van Dulk, M., 2012., Thin- and thick-skinned salt tectonics in the Netherlands; a quantitative approach., Netherlands Journal of Geosciences, 91, v.4.
- Tusheim, F., 1960., Mechanism of salt migration in northern Germany: Association of Petroleum geologists Bulletin, V. 44, p. 1519-1540.

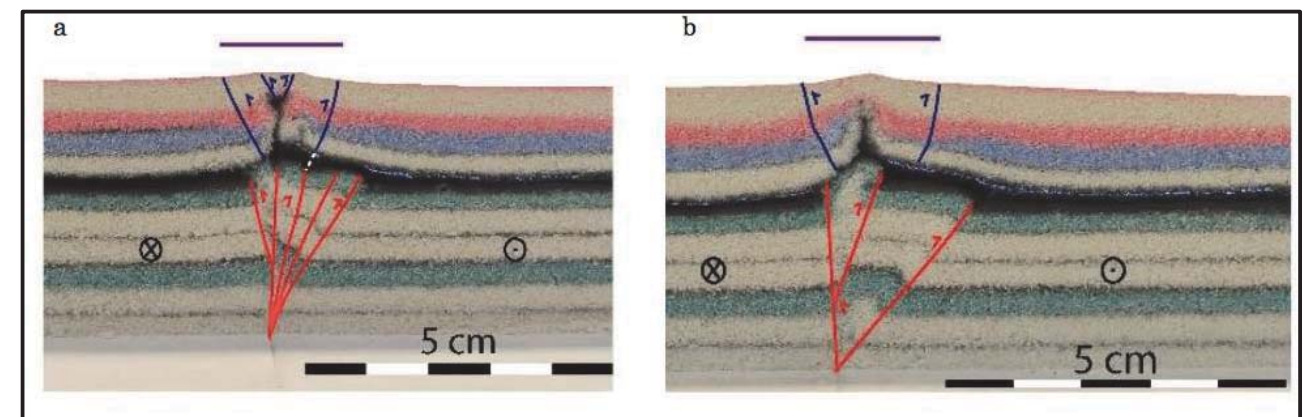
- Vagnes, E., Gabrielsen, R.H., Haremo, P., 1998., Late Cretaceous-Cenozoic intraplate contractional deformation at the Norwegian continental shelf: timing, magnitude and regional implications.
- Van Adrichem Boogaert, H.A. & Kouwe, W.F.P., 1993-1997. [Stratigraphic unit]. In: Stratigraphic Nomenclature of the Netherlands
- Van Duin, E.J.T., Doornenbal, J.C., Rijkers, R.H.B., Verbeek, J.W., Wong, Th.E., 2006., Subsurface structure of the Netherlands – Results of recent onshore and offshore mapping. Netherlands Journal of Geosciences Vol. 85-4. P. 245-276
- Van Keken, P.E., Spiers, C.J., van den Berg, A.P., Muzyert, E.J., 1993., The effective viscosity of rocksalt: implementation of steady-state creep laws in numerical models of salt diapirism., Tectonophysics., V. 225. p. 457-476.
- Verweij, J.M., Souto Carneiro Echternach, M., Witmans, N., 2009 - Terschelling Basin and southern Dutch Central Graben Burial history, temperature, source rock maturity and hydrocarbon generation - Area 2A TNO report - TNO-034-UT-2009-02065
- Van der Zwan, C.J., Spaak, P., 1992., Lower to Middle Triassic sequence stratigraphy and climatology of the Netherlands, a model., Palaeogeography, Paleoclimatology, Paleoecology, V.91, p.2277-290
- Van Wees, J.D., Cloetingh, S., 1996., 3D flexure and intraplate compression in the North Sea Basin., Tectonophysics, V. 266, p.343-359
- Van Wees, J.D., Stephenson, R.A., Ziegler, P.A., Bayer, U., Mccann, T., Dadlez, R., Gaupp, R., Narkiewicz, M., Bitzer, F., Scheck, M., On the origin of the Southern Permian Basin, Central Europe., Journal for Marine and Petroleum Geology, V.17, p.43-59.
- Van Wijhe, D.H., 1987; Structural evolution of inverted basins in the Dutch offshore., Tectonophysics, V. 137, p.171-219
- Van Winden, M., 2015., Salt tectonics in the northern Dutch offshore., MSc. thesis Utrecht University conducted at EBN and TNO.
- Vendeville, B.C. and Jackson, M.P.A., 1992., The rise of diapirs during thin-skinned extension.
- Weijermans, R., Schmeling, H., 1986., Scaling of Newtonian and non-Newtonian fluid dynamics without inertia for quantitative modelling of rock flow due to gravity (including concept of rheological similarity), Physics of the Earth and Planetary Interior., V. 43., p. 316-330
- Wessel, P., and Müller, R.D., 2007, Plate tectonics, in Schubert, G., and Watts, A.B., eds., Crust and Lithosphere Dynamics: Treatise on Geophysics, Volume 6: Elsevier, p. 49–98.
- Ziegler, P.A., 1990a. Geological Atlas of Western and Central Europe (2nd edition). Shell Internationale Petroleum Maatschappij B.V; Geological Society Publishing House (Bath): 239 pp.
- Ziegler, P.A., 1990b. Tectonic and paleogeographic development of the North Sea Rift system. In: Blundell, D.J. & Gibbs. (eds): Tectonic Evolution of the North Sea rifts. Oxford Science Publications (Oxford): 1-36

12. Appendix A

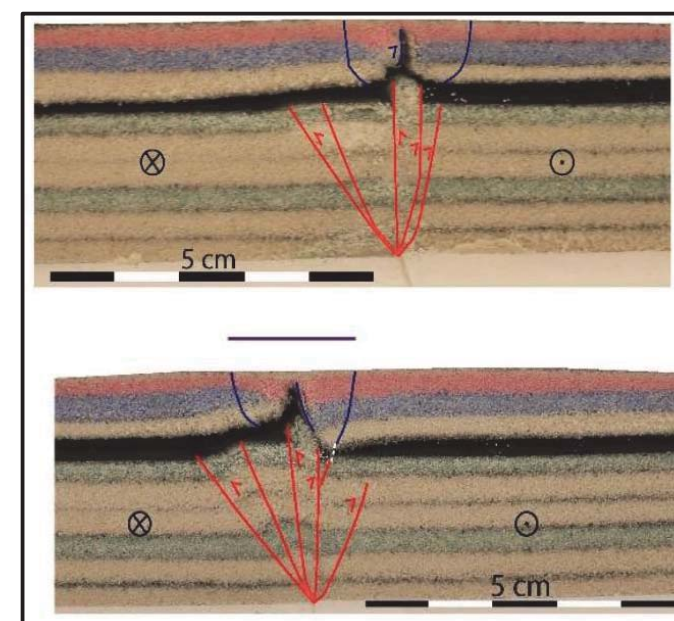
This appendix shows an impression of the work done by Dagmar Smit (BSc. Thesis 2016). Smit (2016) performed analogue models that investigated the role of strike-slip faulting on an initially uniform high weak layer of silicon putty. Smit (2016) i.a. found that the formation of sub salt pull-apart- and pop-up structures has a profound influence on the ascent of salt under strike-slip conditions. Additionally, the ascent of salt is enhanced when surface topography of the brittle overburden (created by the strike-slip deformation) is reduced by erosion. Additionally, sedimentation and a resting phase are of influence on the ascent of silicon putty.



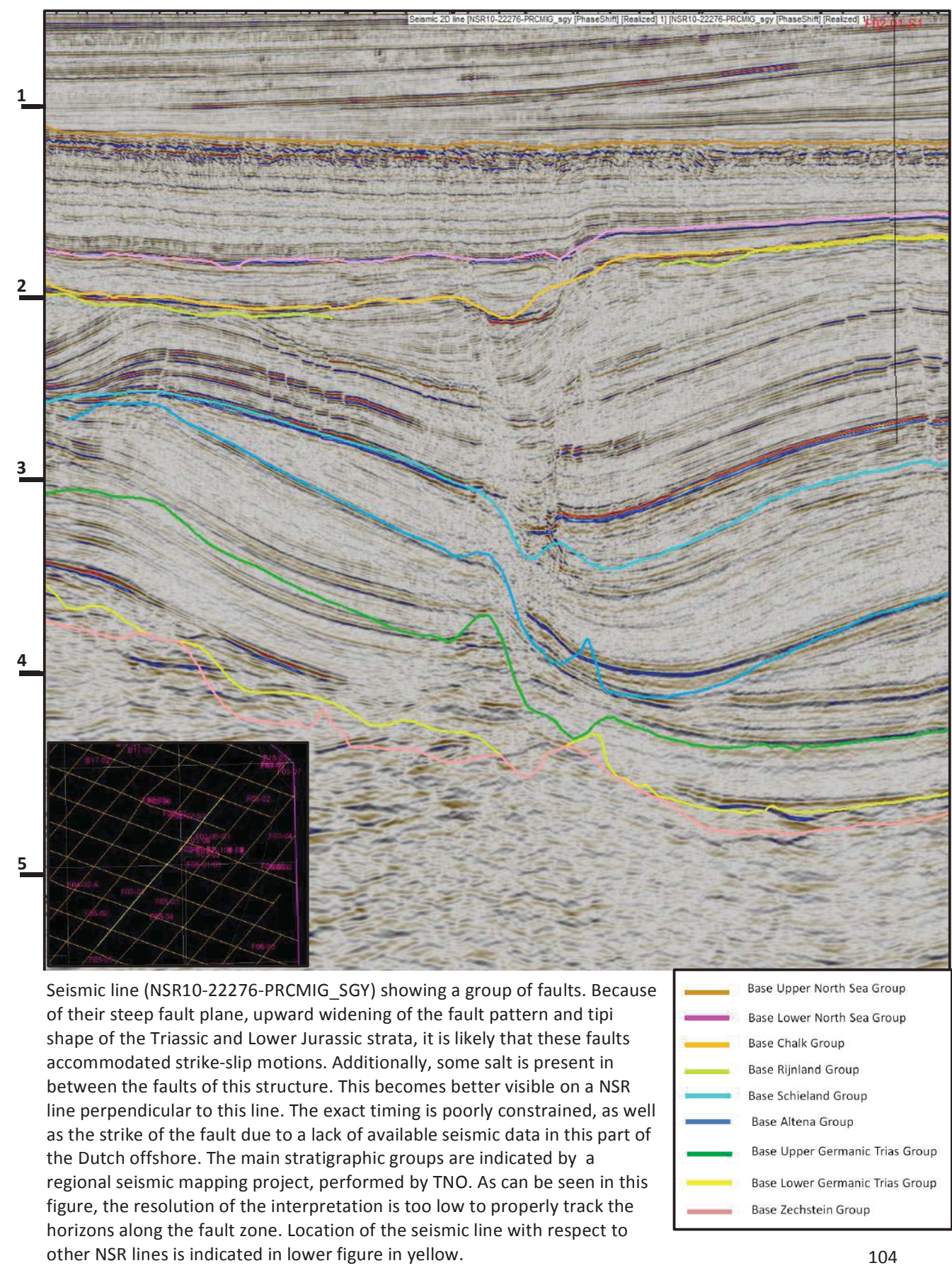
Left Figure; Cross-section through model 3 from Smit (2016), where the model underwent strike-slip faulting without erosion, resting and sedimentation. The ascent of silicon putty is limited, but some small appendix-like structures form in the putty. Figure from Smit (2016)



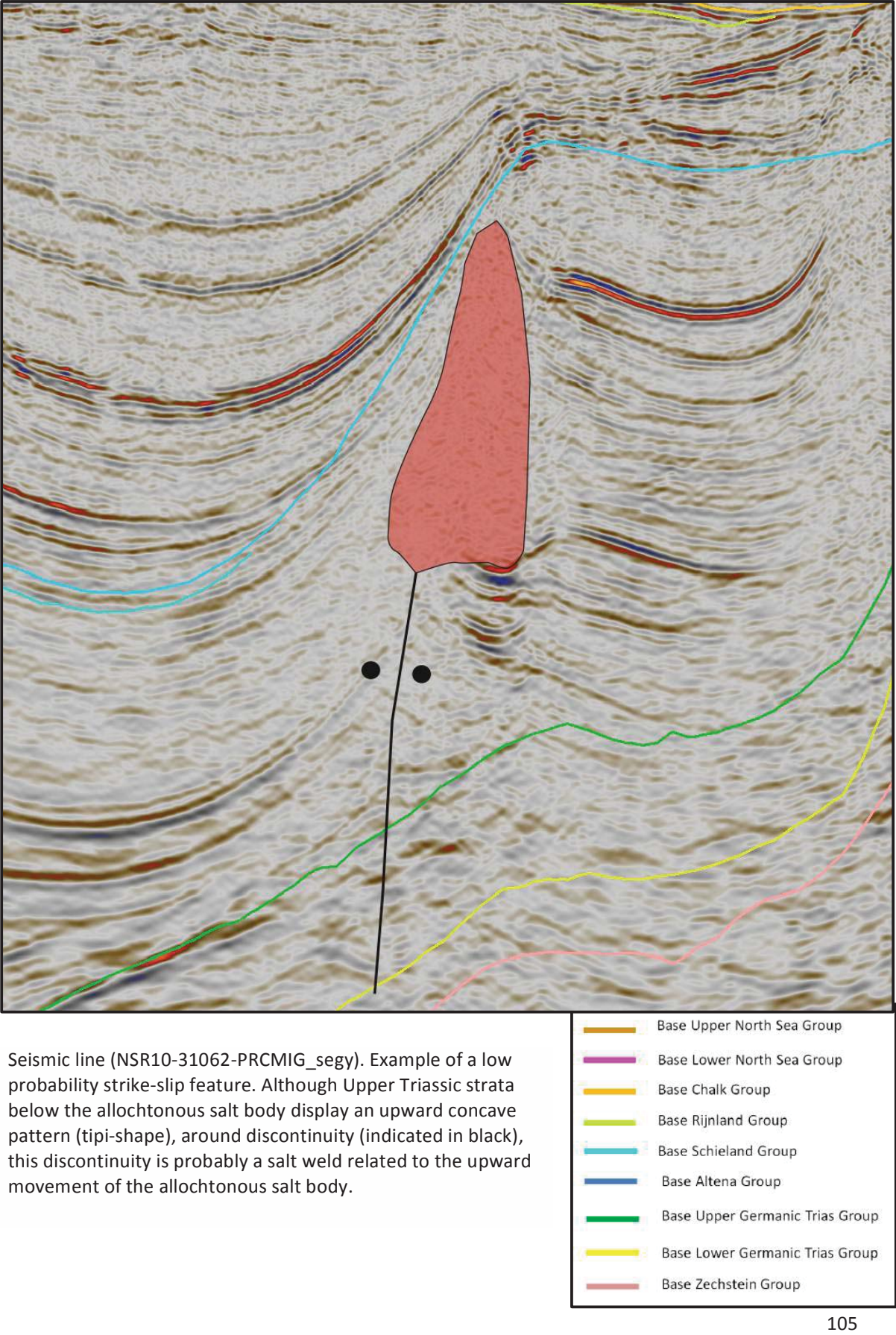
Upper two figures; Cross-section through model 6 from Smit (2016). Left two figures; Cross-sections through model 7 from Smit (2016). In both model 6 and 7, erosion and sedimentation were applied to the model. Additionally, a resting phase was applied to model 7. Note that the ascent of putty is stronger than in model 3. Also note that the salt structures are narrower and more angular than the salt structures that form under extension (Vendeville and Jackson, 1992; Scheffer, 2016). Figures from Smit (2016)



Appendix B



Appendix 2



Appendix D

This appendix shows an impression of the work done by Bram Scheffer (BSc. Thesis 2016). Scheffer (2016) performed analogue models that investigated the role of syn-kinematic sedimentation and different deformation rates on the ascent of silicon putty. Smit (2016) i.a. found that syn-kinematic sedimentation has a profound influence on the ascent of salt under extensional conditions. Additionally, a lower deformation rate tends to form more mature salt structures.

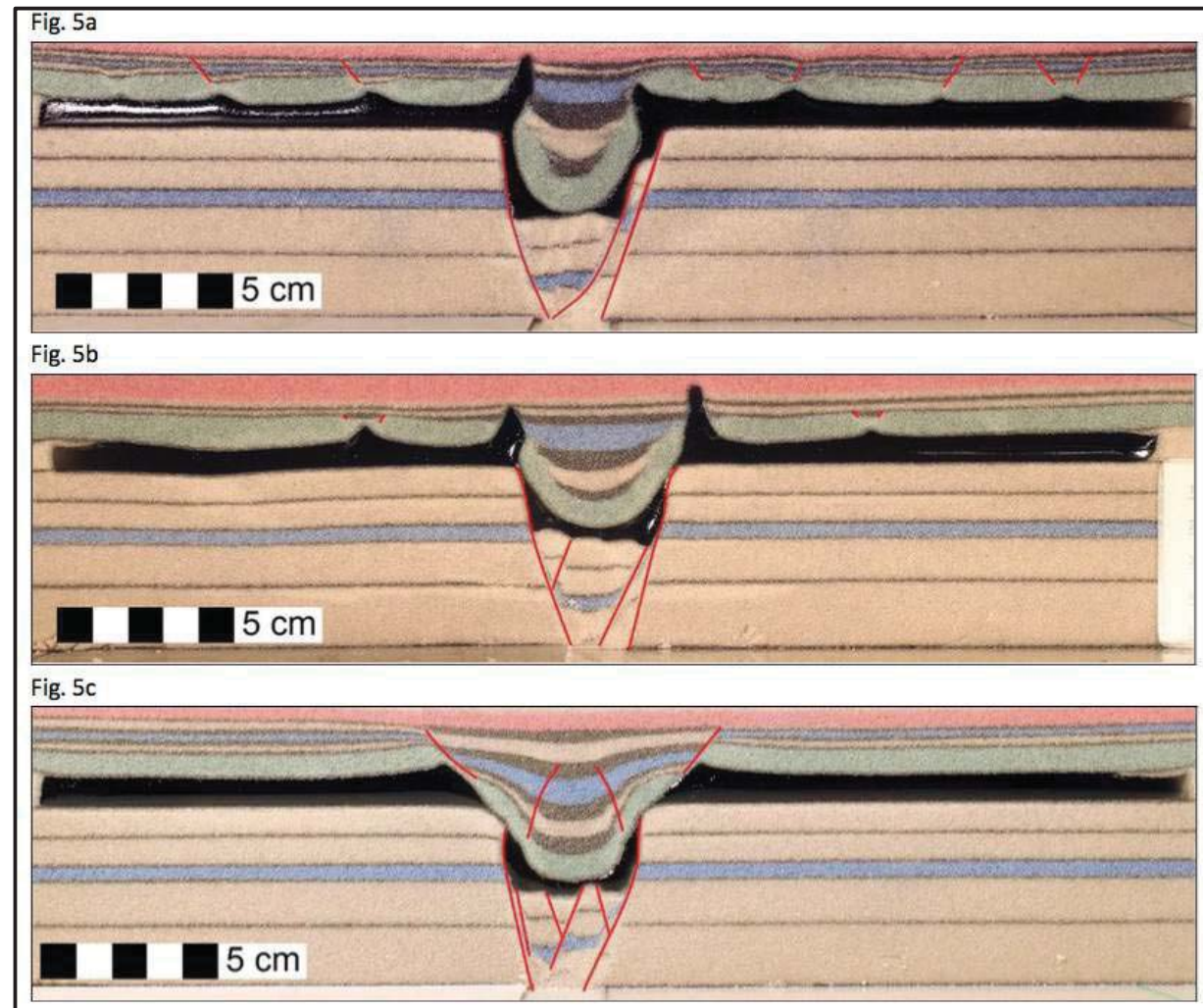

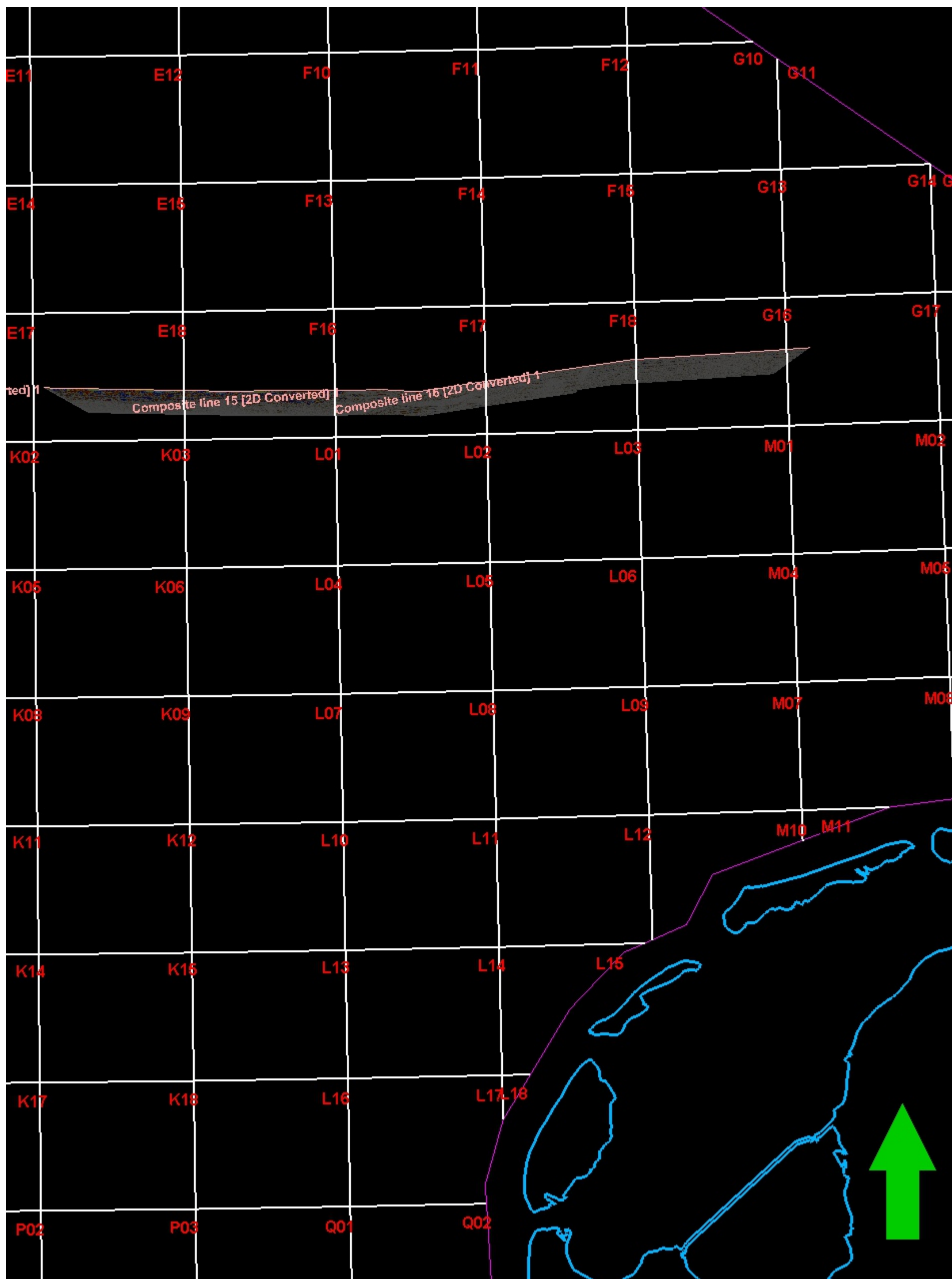
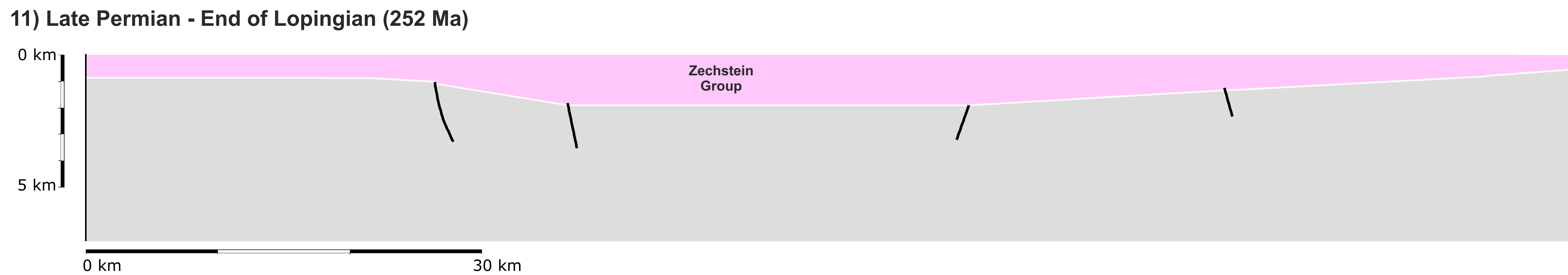
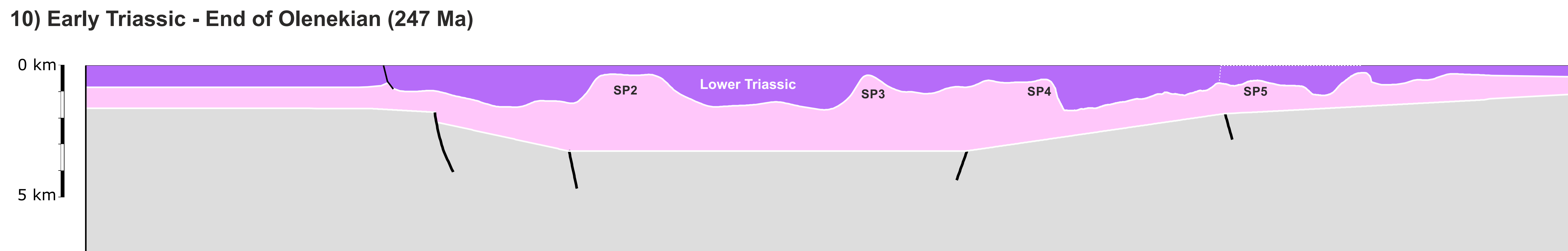
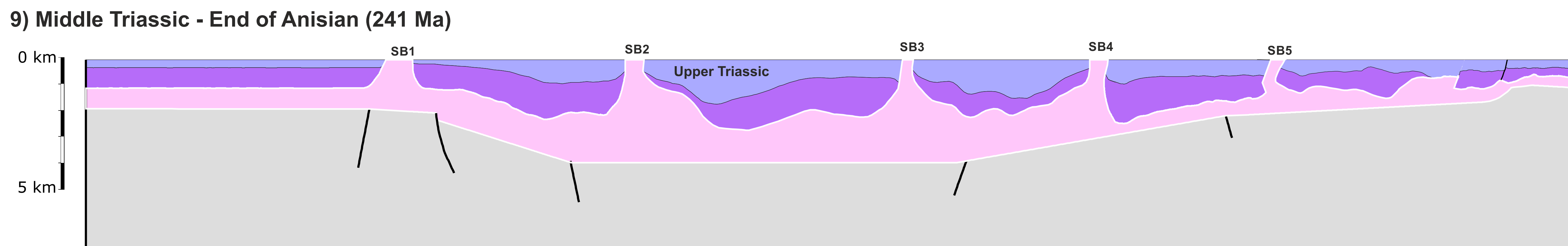
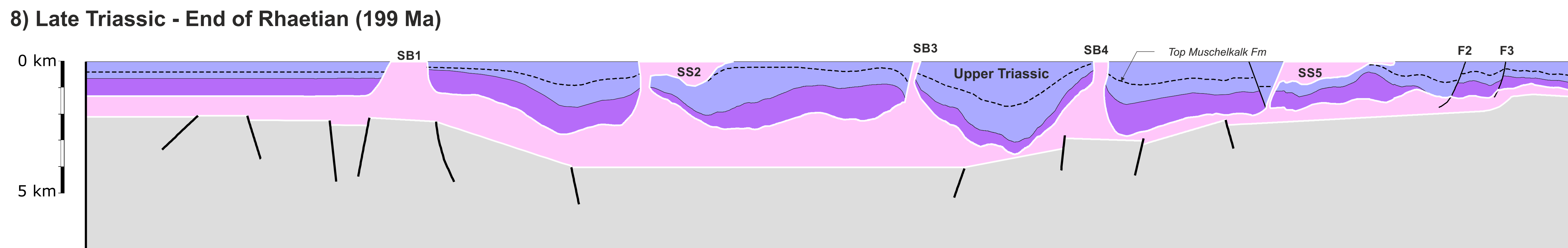
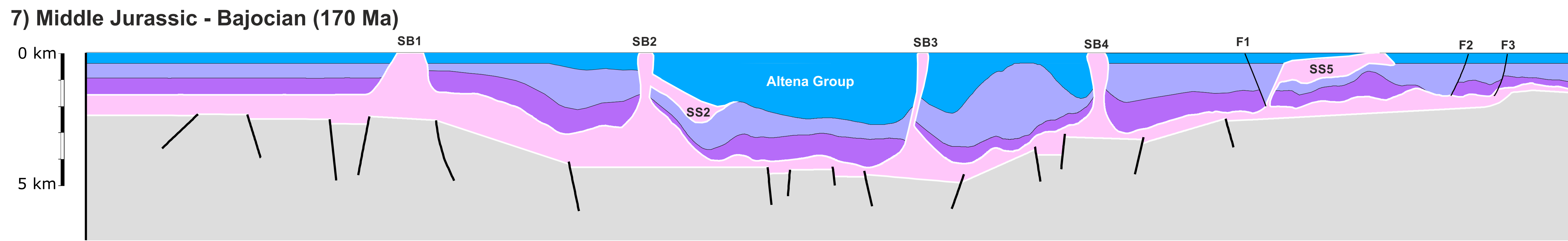
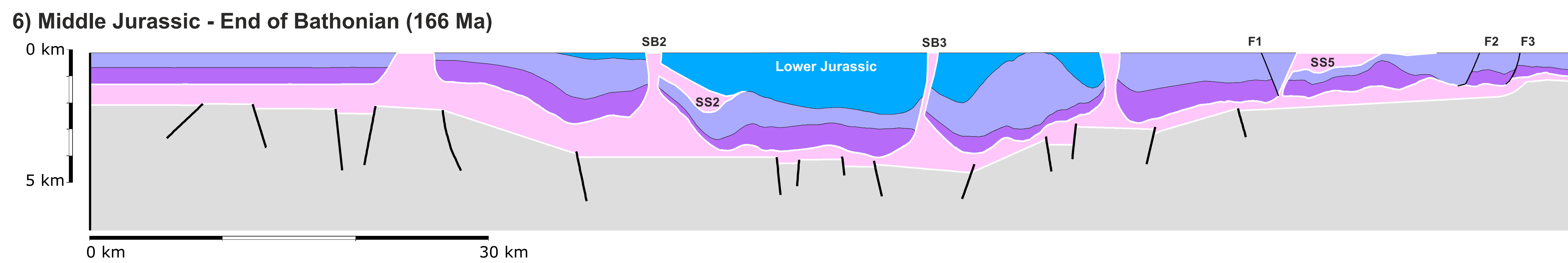
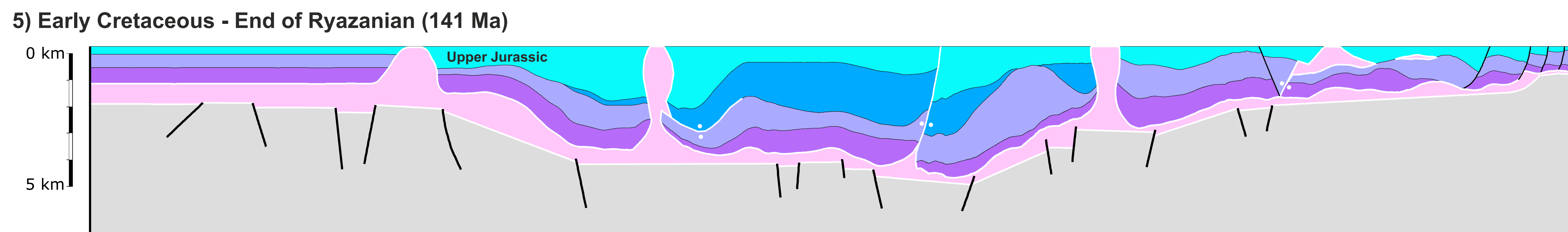
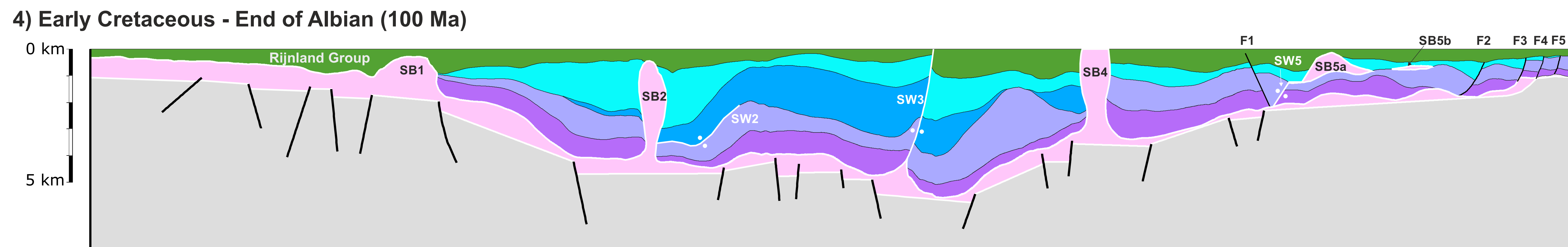
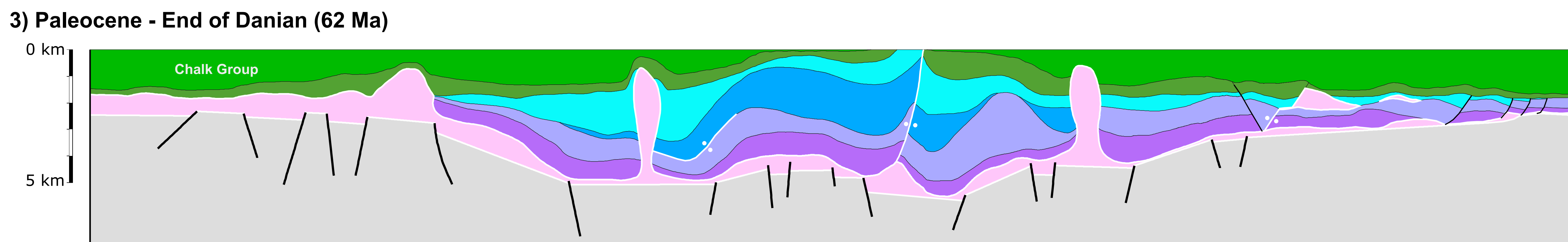
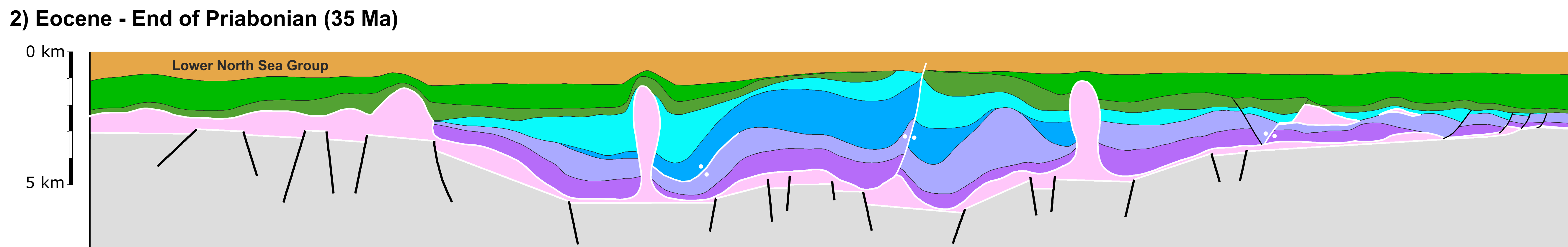
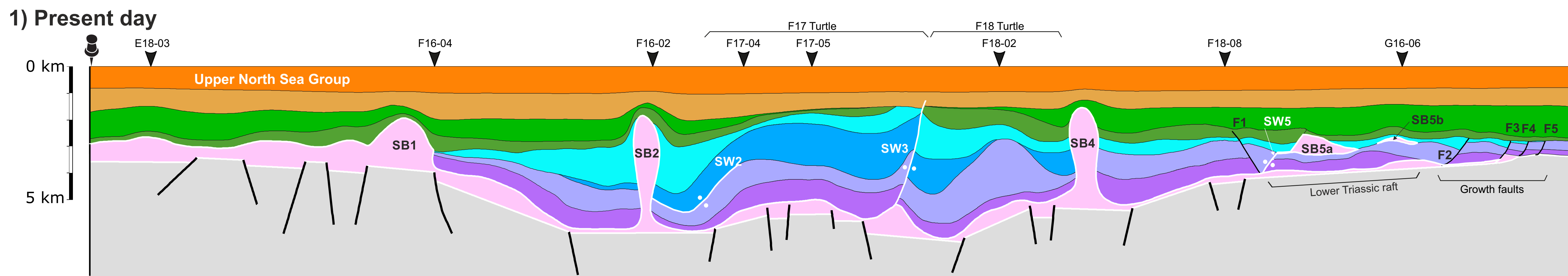
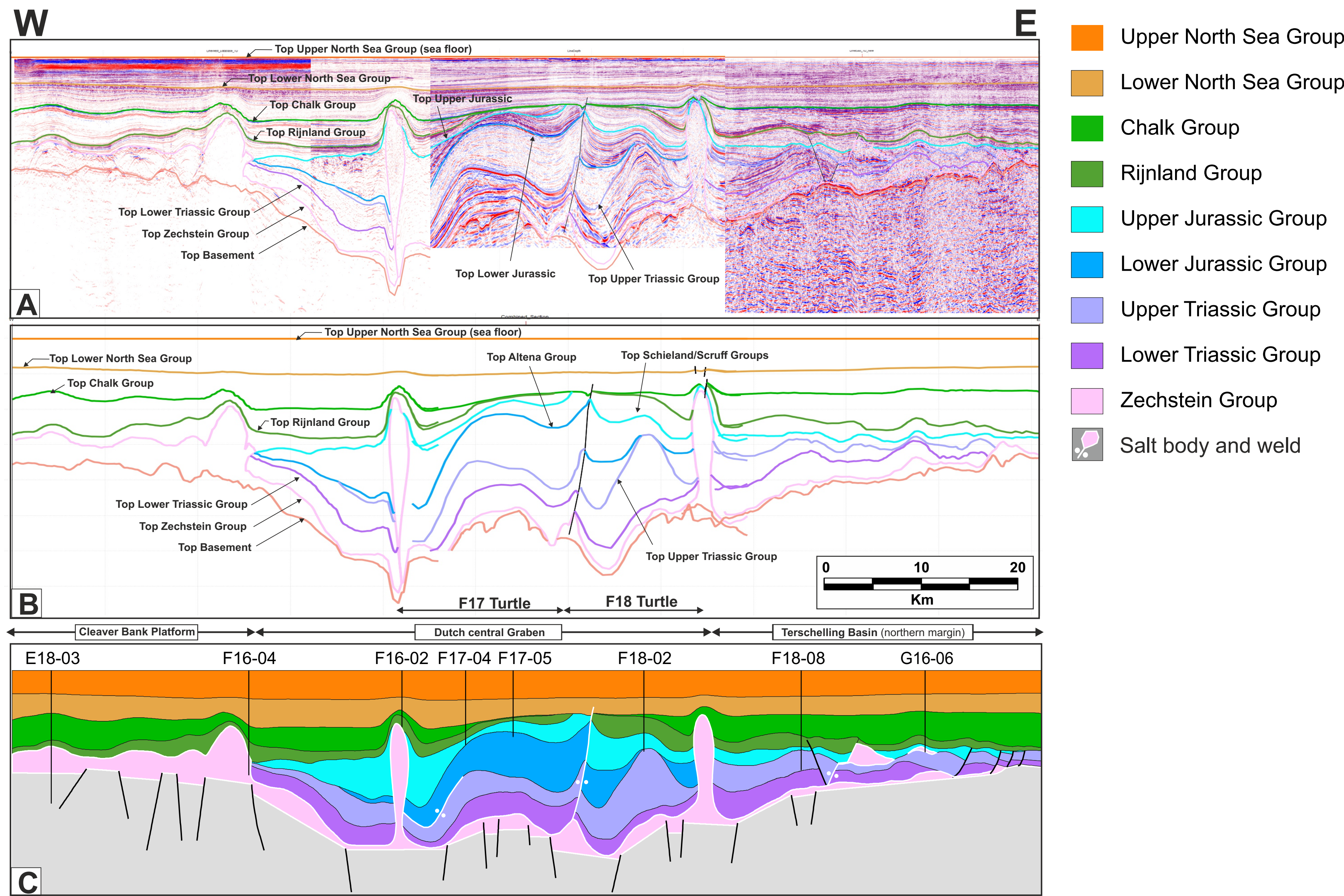


Figure showing the influence of syn-kinematic sedimentation on the ascent of silicon putty with varying amounts of sedimentation. In the top figure, sedimentation rates were less than the subsidence rate of the graben. In the middle figure, sedimentation rates were approximately equal to the subsidence rate of the graben. In the bottom figure, sedimentation rates were higher than subsidence rate of the graben. *Figure from Scheffer, 2016.*

2D Structural reconstruction: Sterling F17/F18

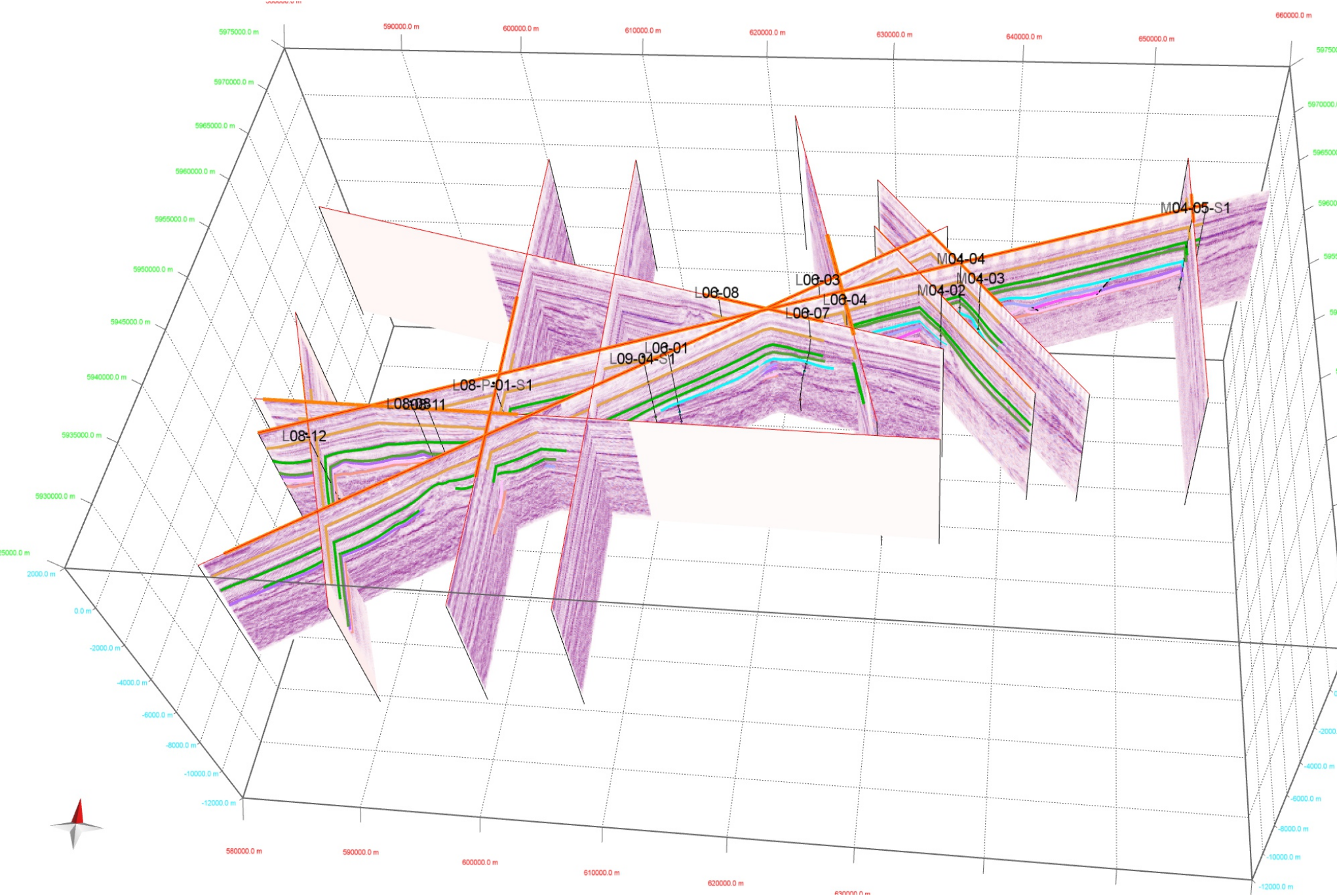
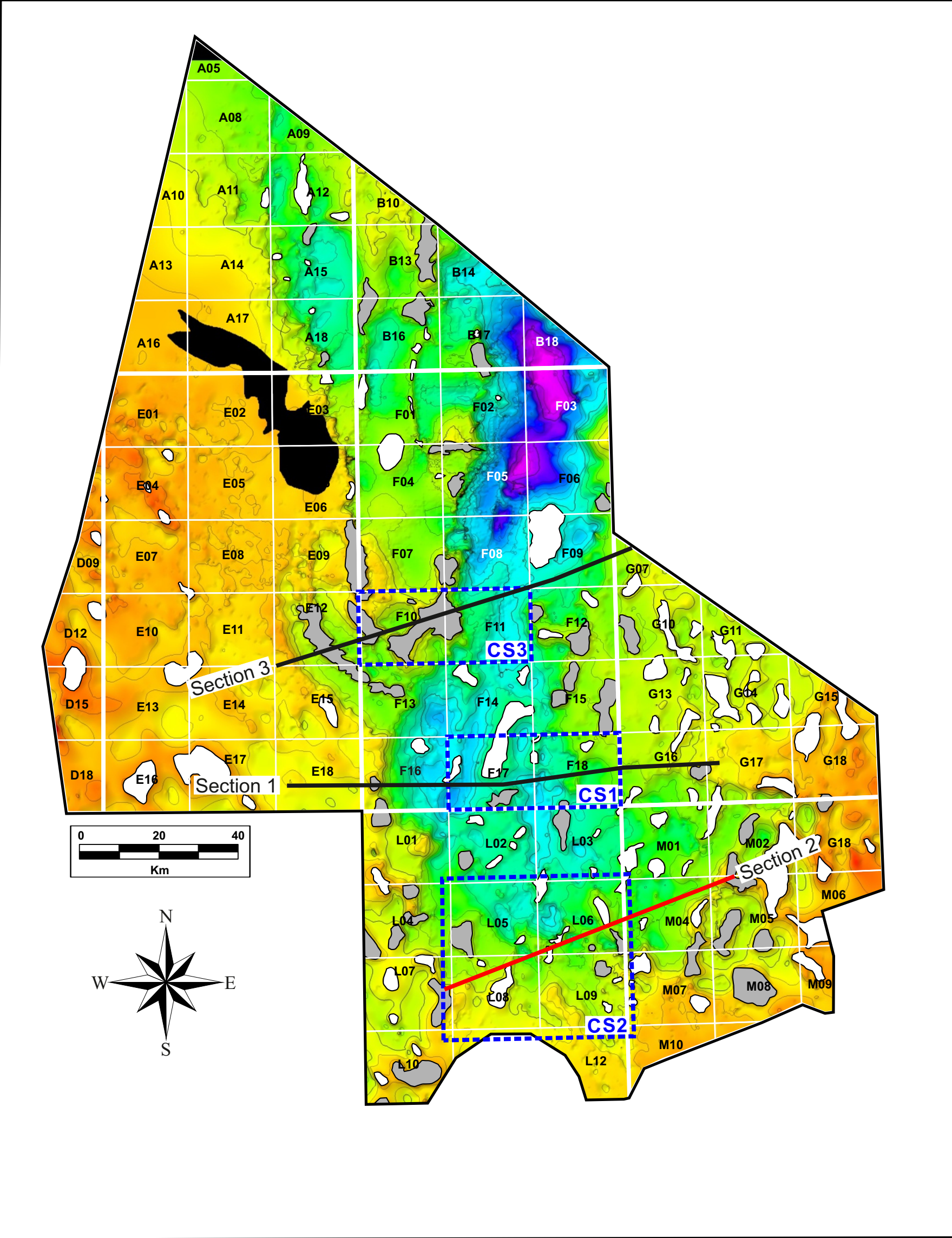
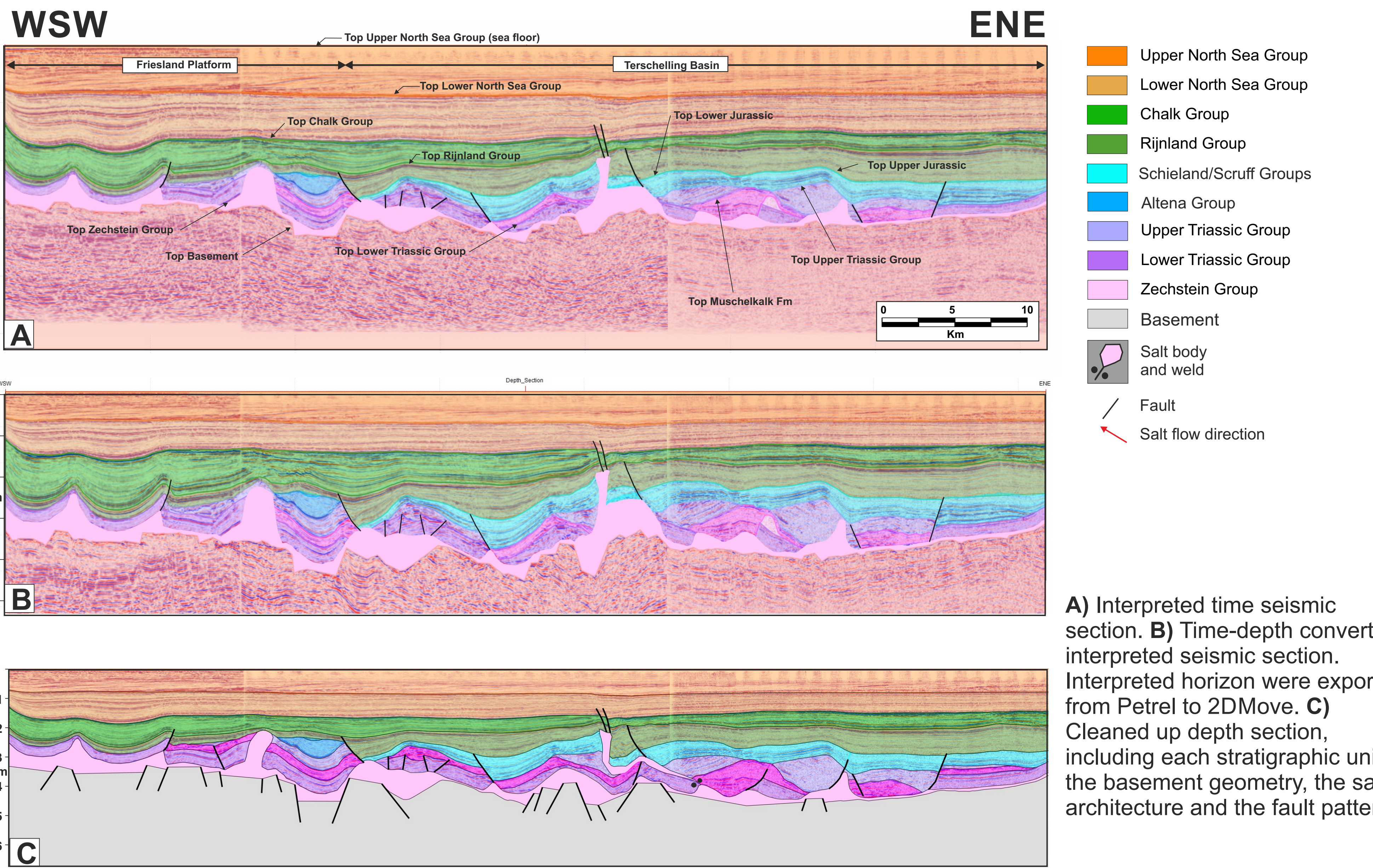
1. Interpret in  me domain
2. Convert to depth
3. Project to hybrid line
4. Clean up



Horizon	Lithology	Age	Interval	2DMOVE Model Lithology	Decompaction Factor (km ⁻¹)
Tertiary	Surface	0 Ma			
	North Sea Supergroup (NS)			50% Sand, 50% Shale	0.39
	Chalk Group (CK)			100% Chalk	0.71
	Rijnland Group (KN)			25% Sand, 50% Shale 25% Marl	0.45
	Schielland Group (SL)			50% Sand, 50% Shale	0.39
	Altena Group (AT)			25% Sand, 50% Shale 25% Marl	0.45
	Upper Germanic Trias Group (RN)			25% Sand, 50% Shale 25% Marl	0.45
	Lower Germanic Trias Group (RB)			70% Sand, 30% Shale	0.34
	Zechstein Group (ZE)			100% Salt	0.0
	Pre-Zechstein Basement (BSM)				0.0

Step nr.	Name	Step nr.	Name
1	Present	13	Lower Jurassic Erosion Restored
2	Upper North Sea Group Decompacted	14	Lower Jurassic Decompacted
3	Lower North Sea Group Unfolded	15	Upper Triassic Unfolded
4	Lower North Sea Group Decompacted	16	Upper Triassic Salt Stage Decompacted
5	Chalk Group Unfolded	17	Inter-Upper Triassic Decompacted
6	Chalk Group Decompacted	18	Inter-Upper Triassic Unfolded
7	Rijnland Group Unfolded	19	Lower Triassic Decompacted
8	Rijnland Group Decompacted	20	Lower Triassic Unfolded
9	Upper Jurassic Erosion Restored	21	Lower Triassic Erosion Restored
10	Upper Jurassic Unfolded	22	Salt Unloaded
11	Upper Jurassic Decompacted	23	Salt Unfolded
12	Lower Jurassic Unfolded		

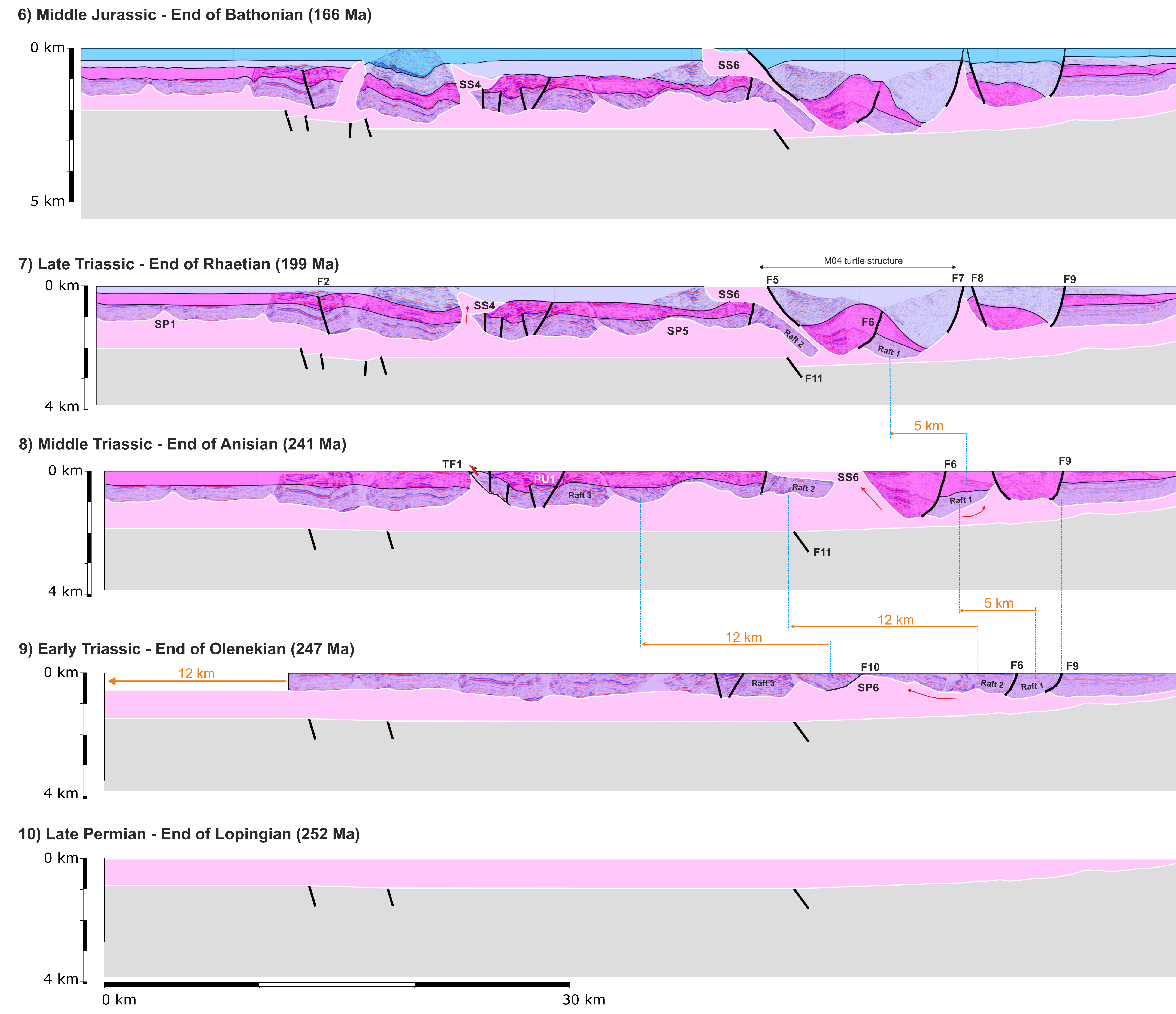
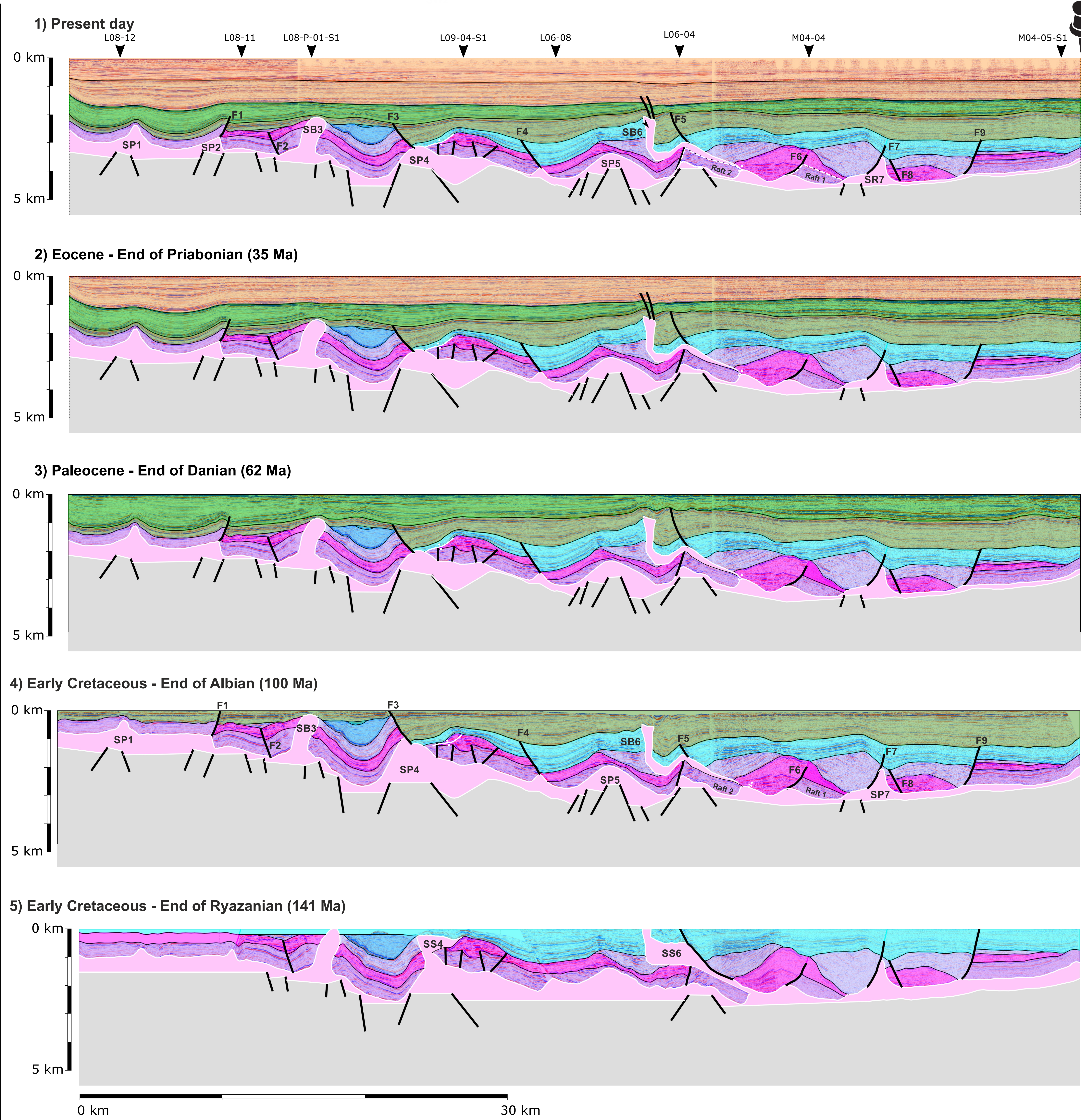
2D Structural reconstruction: Wintershall L06/L08



Horizon	Lithology	Age	Interval	2DMOVE Model Lithology	Decompaction Factor (km ⁻¹)
Surface		0 Ma			
North Sea Supergroup (NS)				50% Sand, 50% Shale	0.39
60 Ma					
Chalk Group (CK)				100% Chalk	0.71
97 Ma					
Rijnland Group (KN)				25% Sand, 50% Shale 25% Marl	0.45
134 Ma					
Schieland Group (SL)				50% Sand, 50%Shale	0.39
155 Ma					
Altena Group (AT)				25% Sand, 50% Shale 25% Marl	0.45
212 Ma					
Upper Germanic Trias Group (RN)				25% Sand, 50% Shale 25% Marl	0.45
241 Ma					
Middle Germanic Trias Group				70% Sand, 30%Shale	0.34
251 Ma					
Lower Germanic Trias Group (RB)				70% Sand, 30%Shale	0.34
258 Ma					
Zechstein Group (ZE)				100% Salt	0.0
258 Ma					
Pre-Zechstein Basement (BSM)					0.0

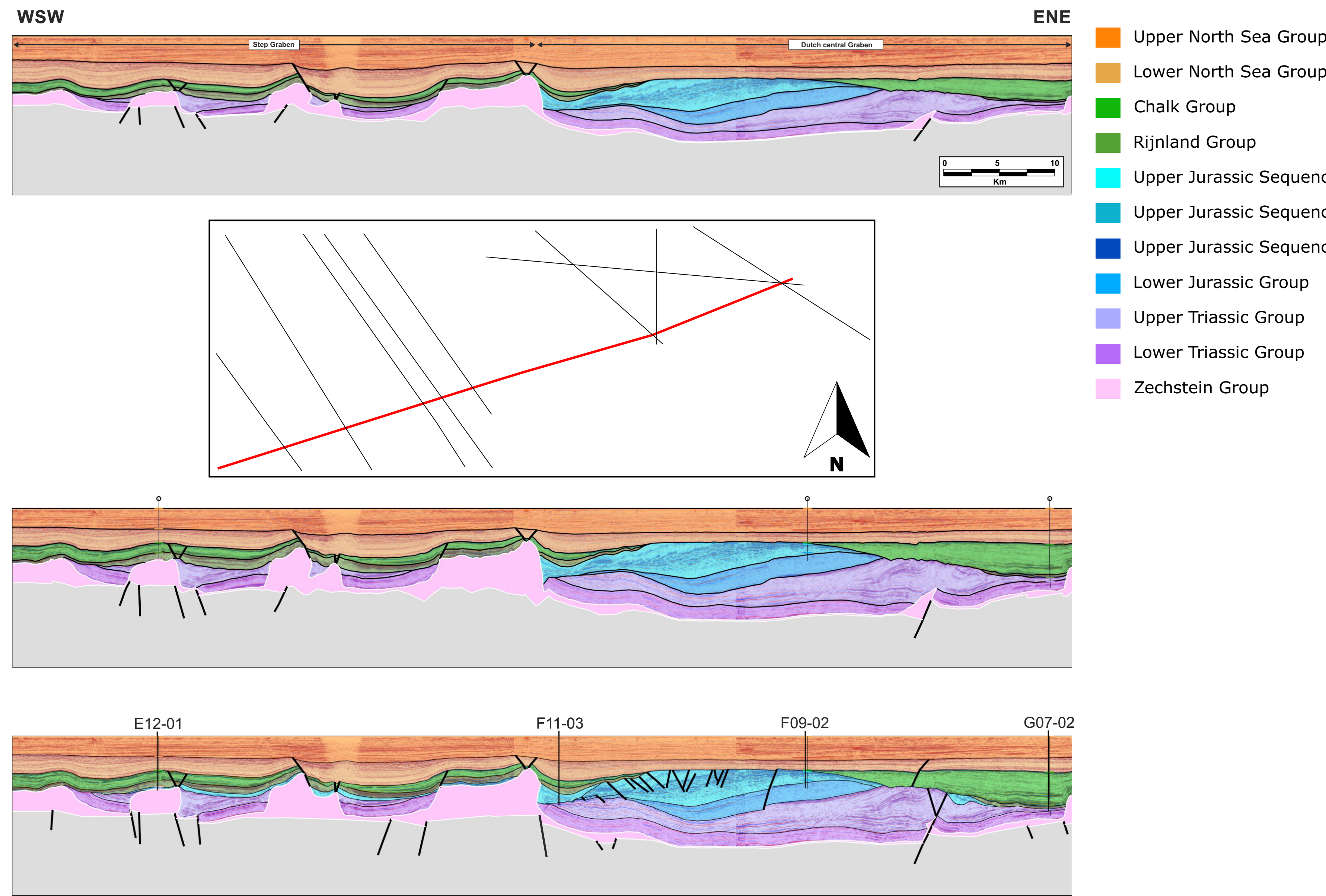
Local unconformity
Regional unconformity

Step nr.	Name	Step nr.	Name
1	Present	18	Upper Jurassic Decompacked
2	Lower North Sea Group Unfolded	19	Lower Jurassic Erosion Restored
3	Lower North Sea Group Unfolded	20	Lower Jurassic Erosion Restored
4	Lower North Sea Group Basement Adjusted	21	Lower Jurassic Basement Adjusted
5	Lower North Sea Group Decompacked	22	Lower Jurassic Decompacked Step 1
6	Chalk Group - Fault 1 Restored	23	Lower Jurassic Decompacked Step 2
7	Chalk Group - Fault 2 Restored	24	Upper Triassic Unfolded
8	Chalk Group Unfolded	25	Upper Triassic Unfolded Smoothed
9	Chalk Group Basement Adjusted	26	Upper Triassic Decompacked Step 1
10	Chalk Group Decompacked	27	Upper Triassic Decompacked Step 2
11	Rijnland Group Erosion Restored	28	Middle Upper Triassic Unfolded
12	Rijnland Group - Fault 3 Restored	29	Middle Upper Triassic Unfolded Tilted
13	Rijnland Group Unfolded	30	Middle Triassic Decompacked
14	Rijnland Group Decompacked	31	Lower Triassic Unfolded Step 1
15	Upper Jurassic Erosion Restored	32	Lower Triassic Unfolded Step 2
16	Upper Jurassic Unfolded	33	Lower Triassic Unfolded Step 3
17	Upper Jurassic Basement Adjusted	34	Salt Unfolded

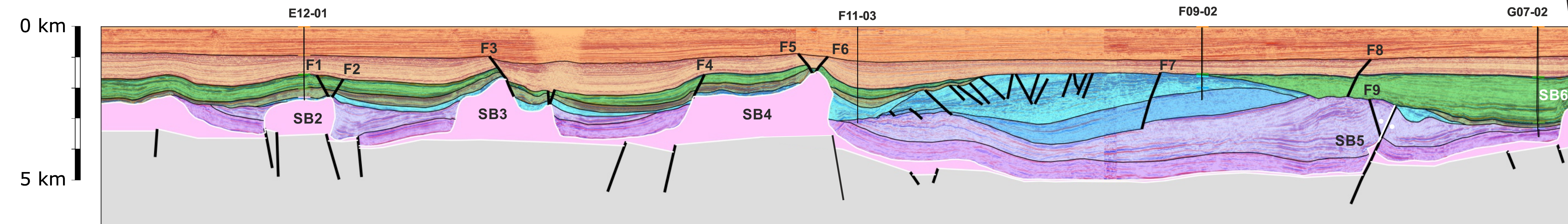


2D Structural reconstruction: EBN F10/F11

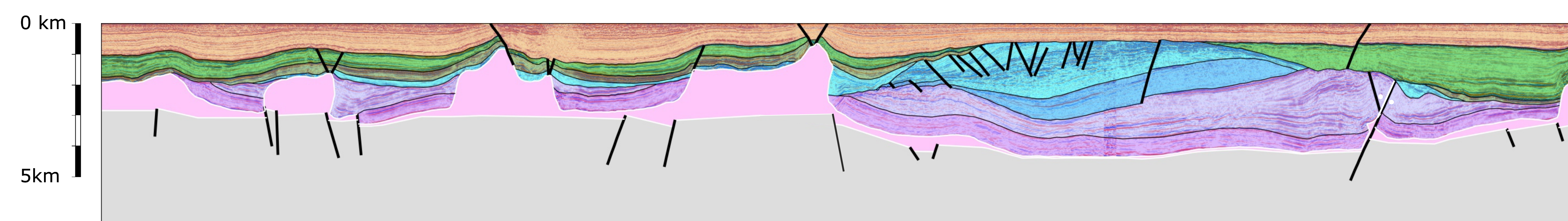
1. Interpret in time domain
2. Use nearby wells and extra 2D lines for time-depth conversion
3. Convert to depth
4. Clean up



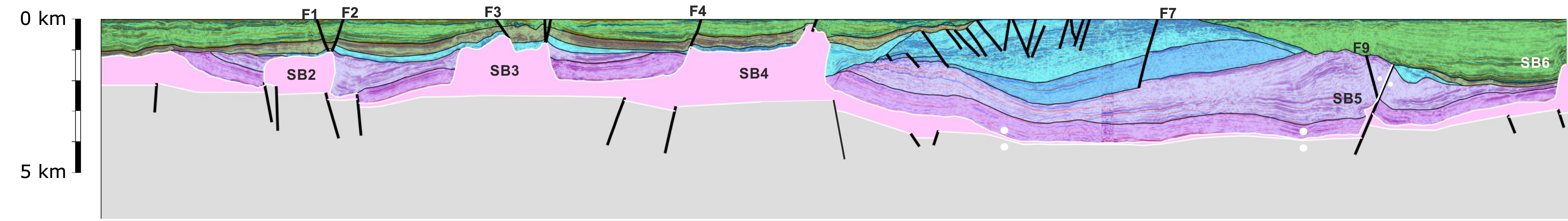
1A) Present day



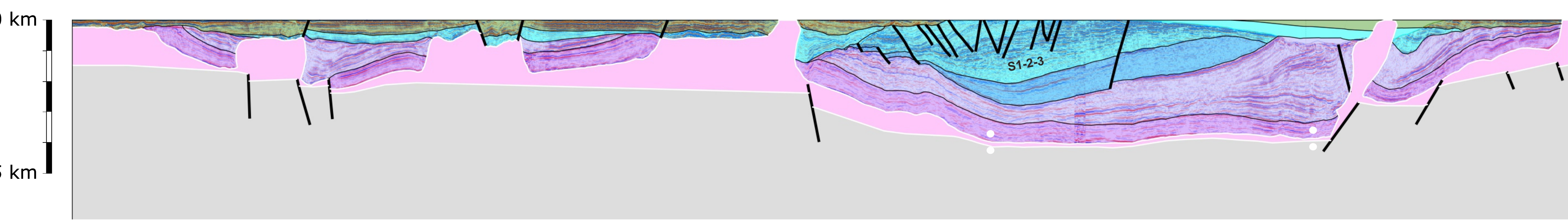
2A) Eocene - End of Priabonian (35 Ma)



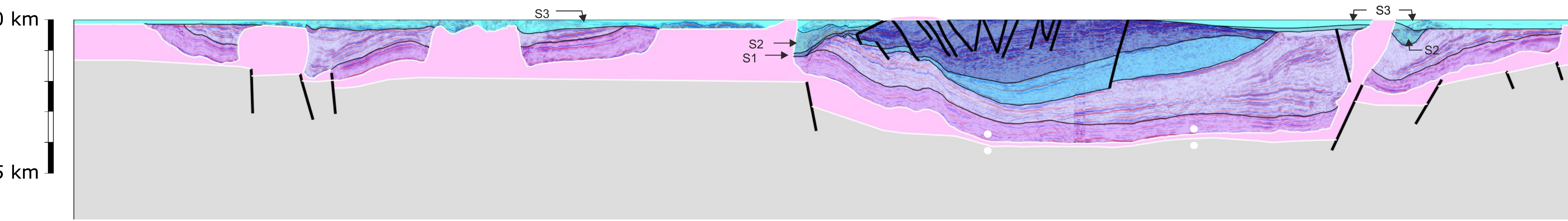
3A) Paleocene - End of Danian (62 Ma)



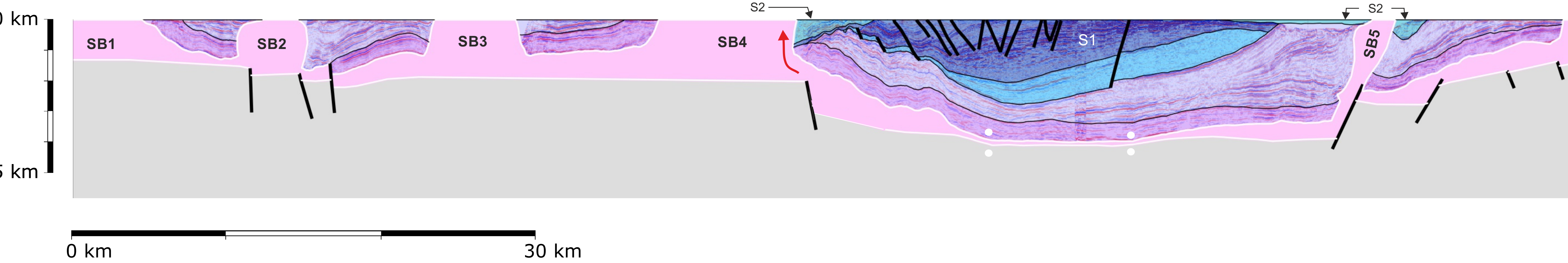
4A) Early Cretaceous - End of Albian (100 Ma)



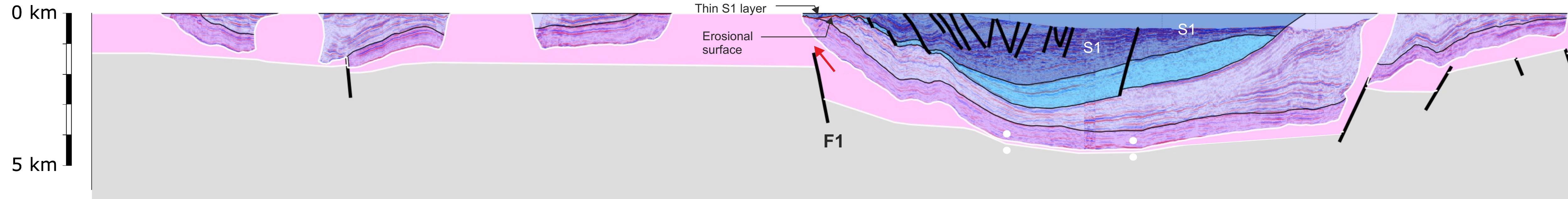
5A) Early Cretaceous - End of Ryazanian (141 Ma) - End of Scruff Group deposition



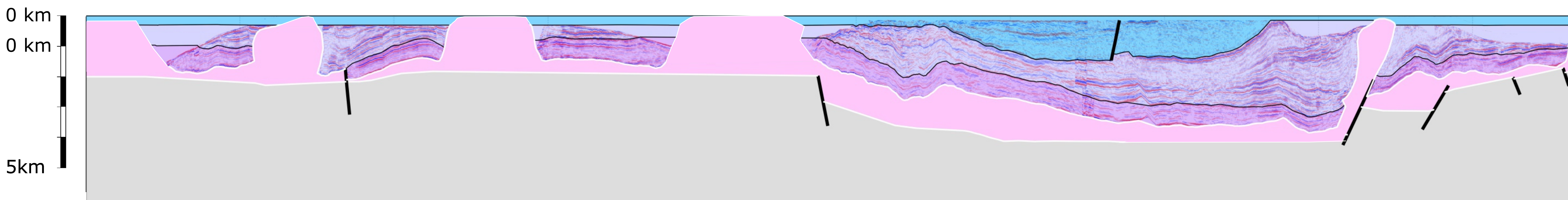
6A) Late Jurassic - Middle Volgian (146 Ma) - End of Schieland Group deposition (Sequence 2)



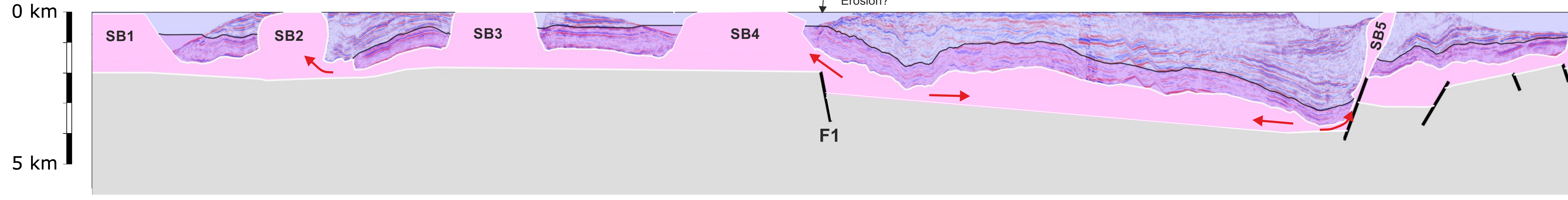
7A) Late Jurassic - Middle Volgian (156 Ma) - End of Middle - Late Jurassic Sequence 1 deposition



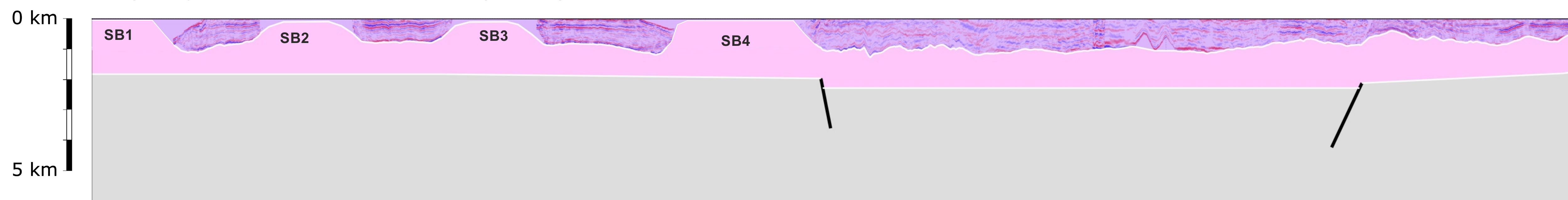
8A) Middle Jurassic - End of Bathonian (166 Ma)



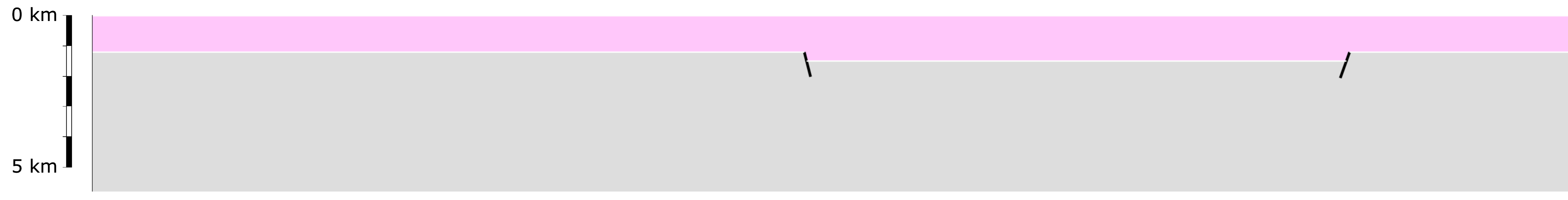
9A) Late Triassic - End of Rhaetian (199 Ma)



10A) Early Triassic - End of Olenekian (247 Ma)



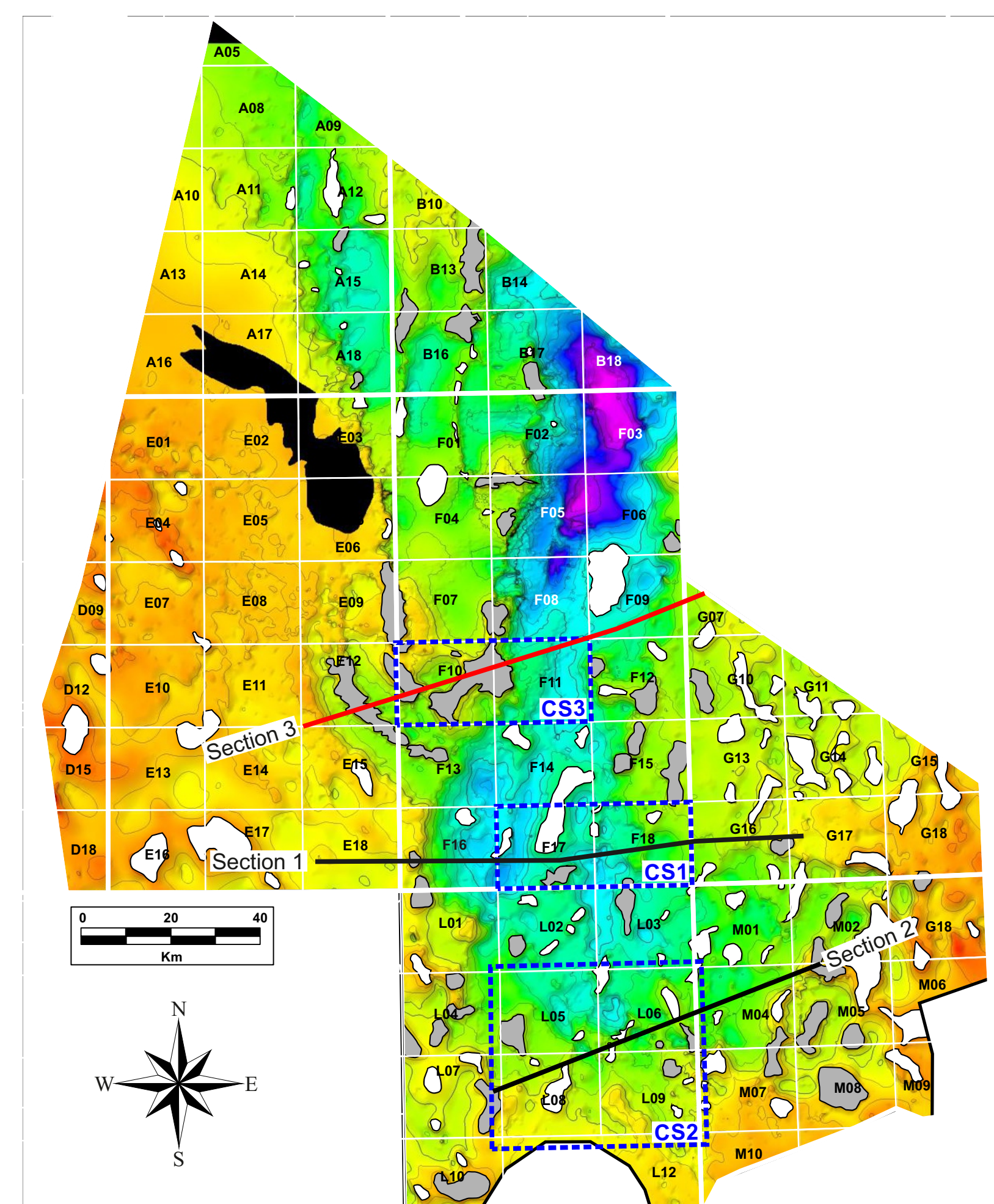
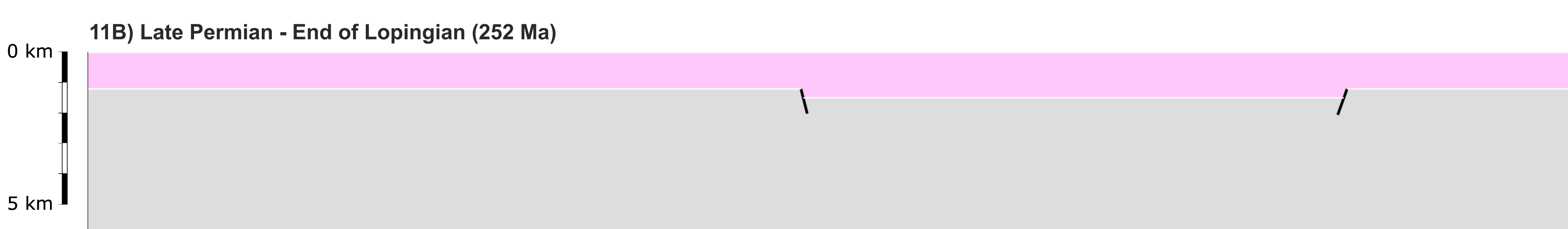
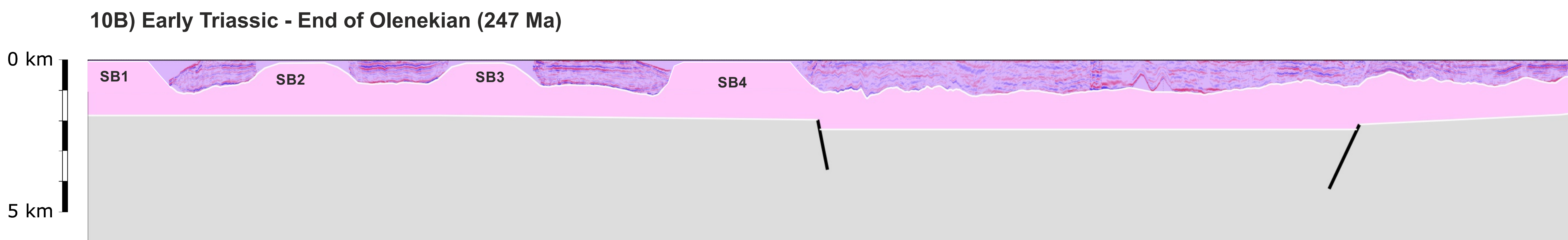
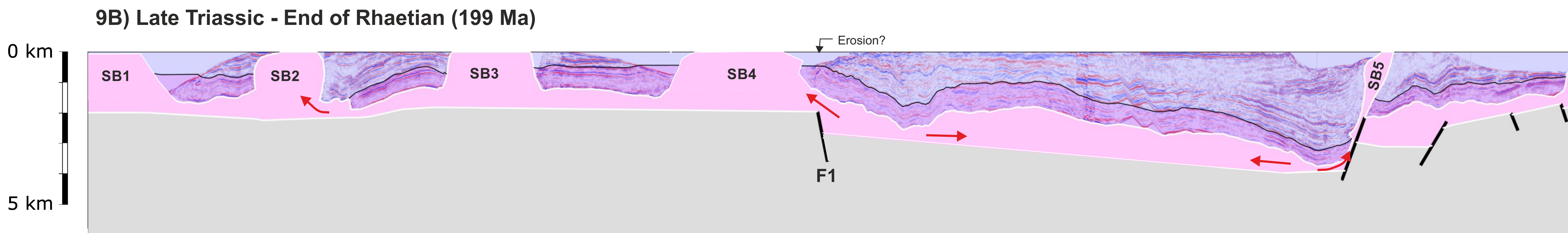
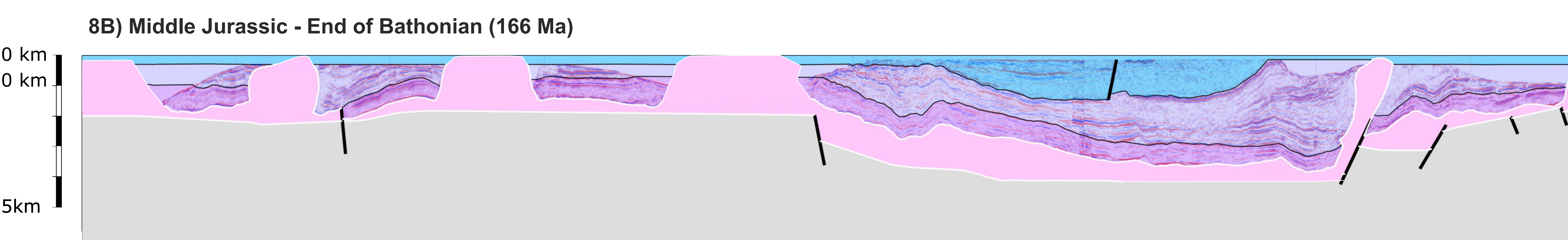
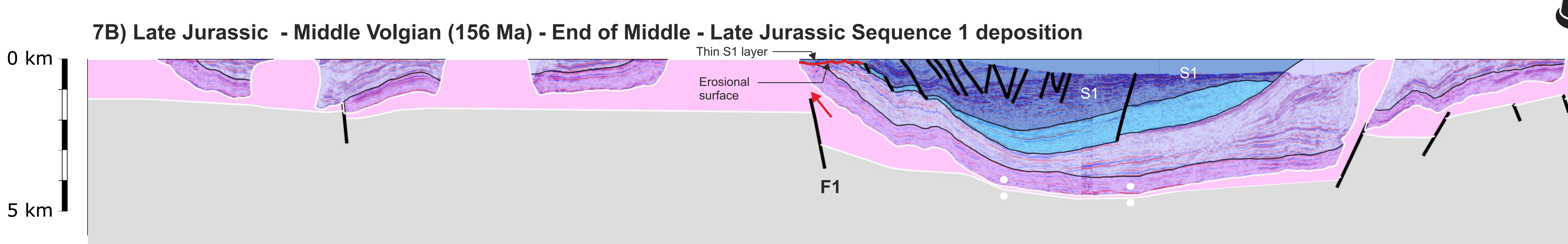
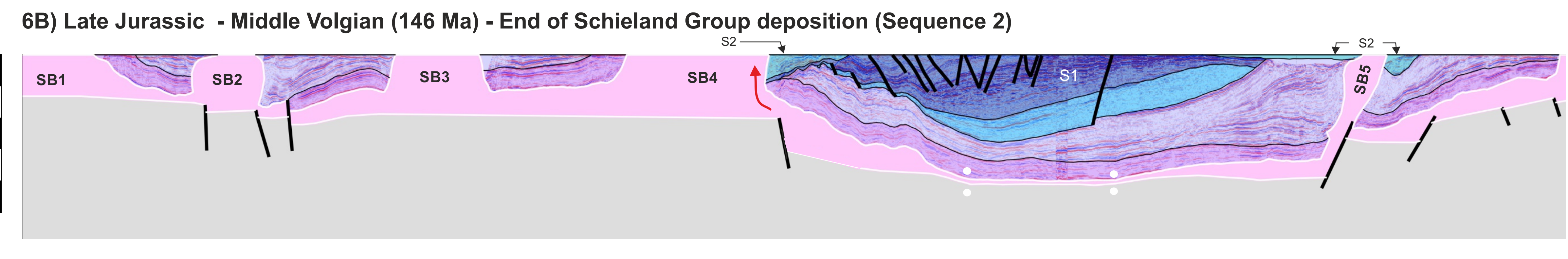
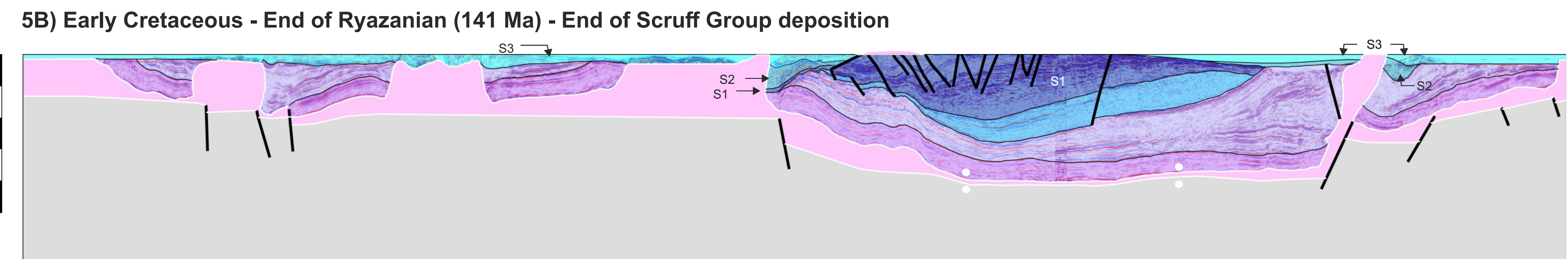
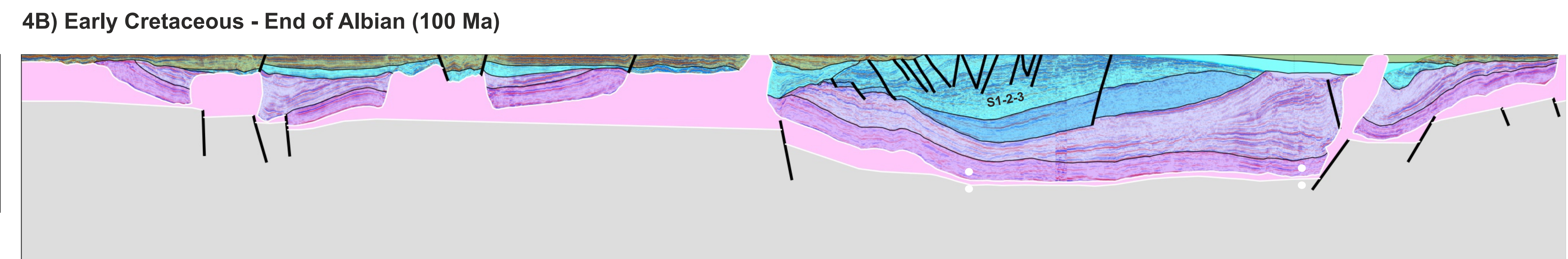
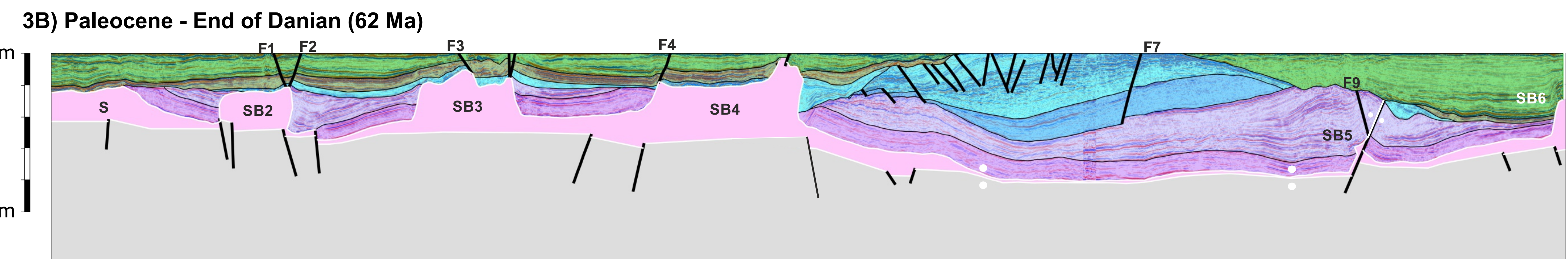
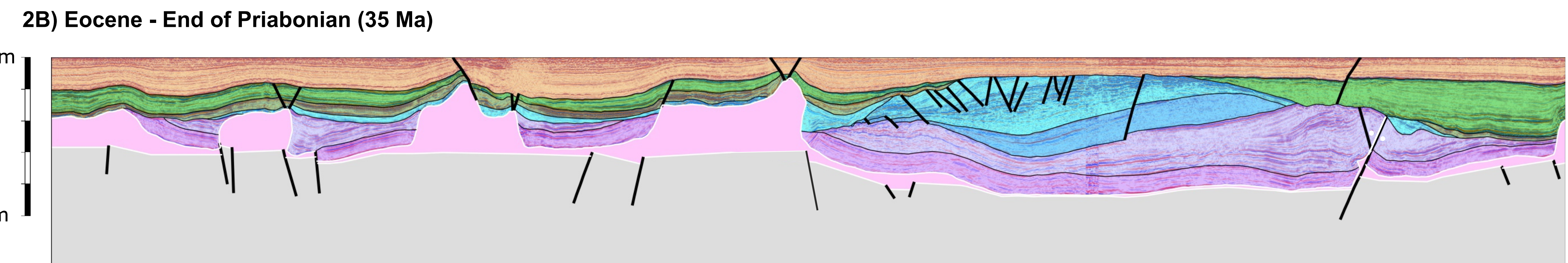
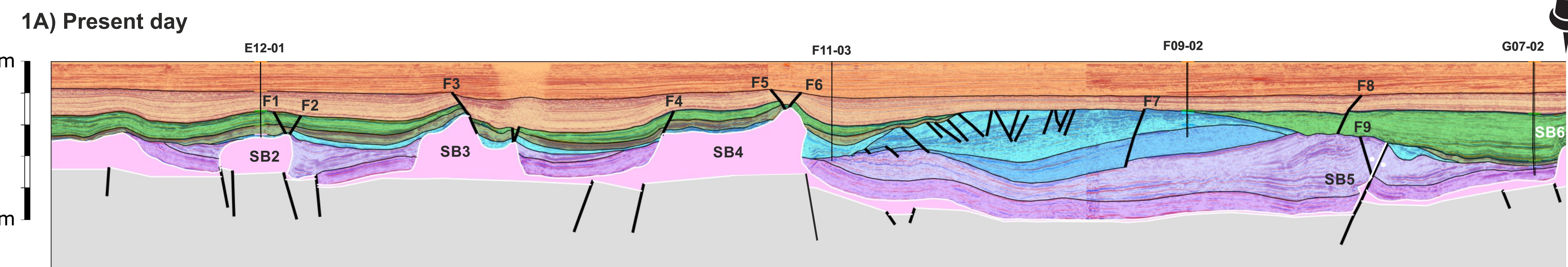
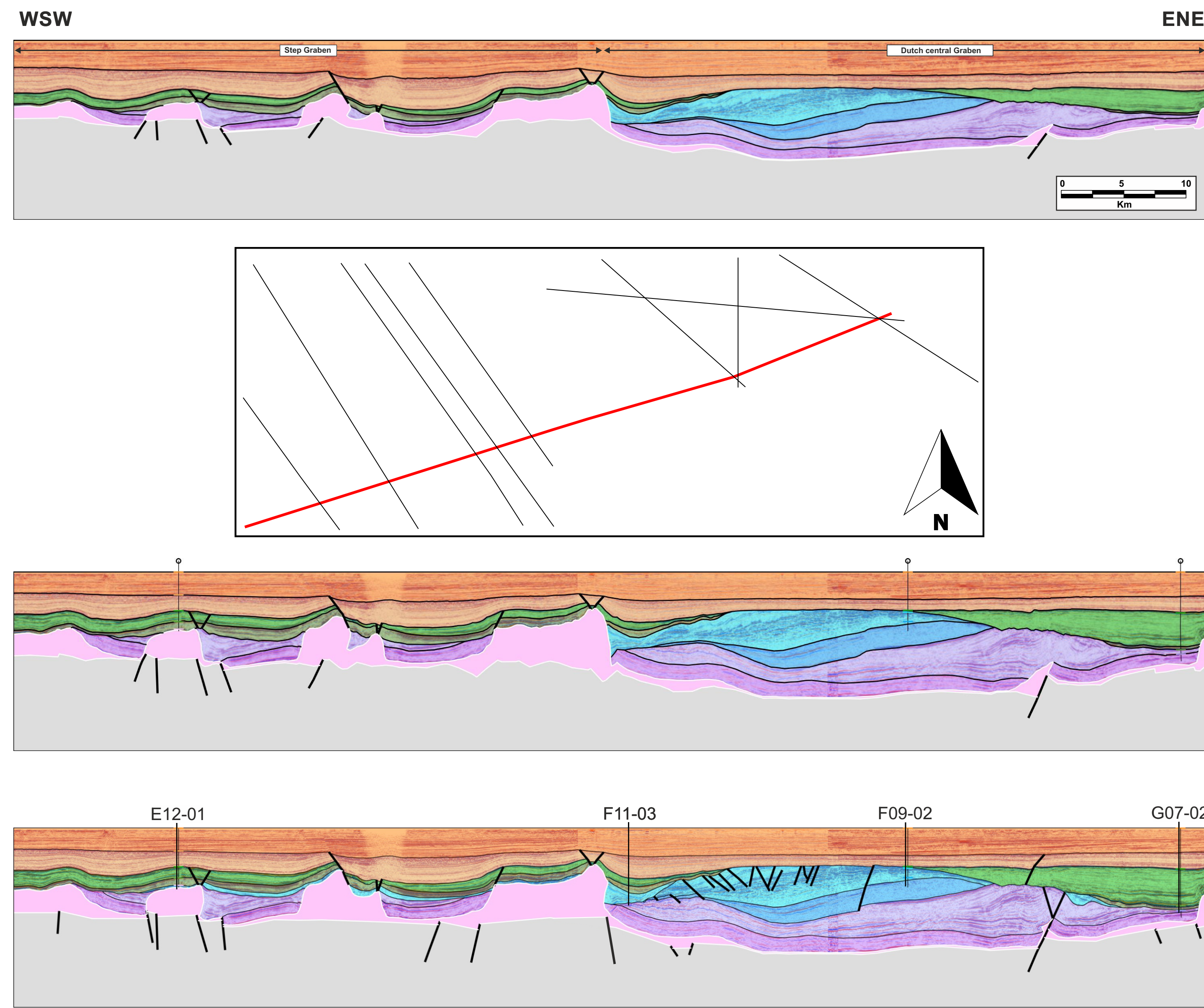
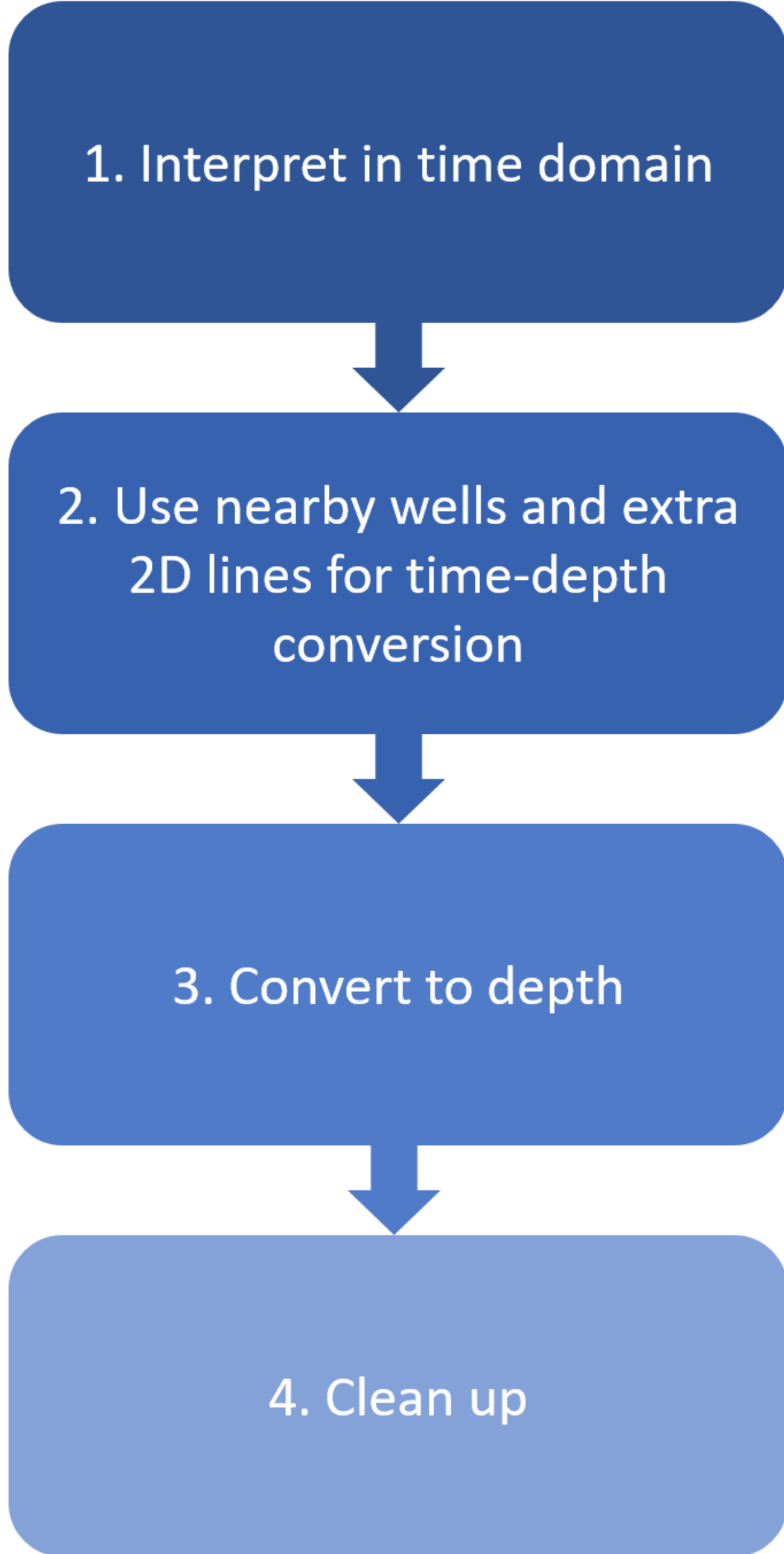
11A) Late Permian - End of Lopingian (252 Ma)



Horizon	Lithology	Age	Interval	2DMOVE Model Lithology	Decompaction Factor (km ⁻¹)
Surface		0 Ma			
Tertiary					
North Sea Supergroup (NS)		60 Ma		50% Sand, 50% Shale	0.39
Chalk Group (CK)		97 Ma		100% Chalk	0.71
Rijnland Group (KN)		134 Ma		25% Sand, 50% Shale 25% Marl	0.45
Schieland Group (SL)		155 Ma		50% Sand, 50% Shale	0.39
Altena Group (AT)		212 Ma		25% Sand, 50% Shale 25% Marl	0.45
Upper Germanic Trias Group (RN)		241 Ma		25% Sand, 50% Shale 25% Marl	0.45
Middle Germanic Trias Group		251 Ma		70% Sand, 30% Shale	0.34
Lower Germanic Trias Group (RB)		258 Ma		100% Salt	0.0
Zechstein Group (ZE)					
Pre-Zechstein Basement (BSM)					

Step nr.	Name	Step nr.	Name
1	Present	14	Upper Jurassic Sequences Interpreted
2	Upper North Sea Group Decompacted	15	Upper Jurassic Sequence 3 Decompacted
3	Upper North Sea Group Fault Restored	16	Upper Jurassic Sequence 2 Unfolded
4	Lower North Sea Group Unfolded	17	Upper Jurassic Sequence 2 Decompacted
5	Lower North Sea Group Basement Restored	18	Upper Jurassic Sequence 1 Unfolded
6	Lower North Sea Group Decompacted	19	Upper Jurassic Sequence 1 Decompacted
7	Chalk Group Unfolded	20	Lower Jurassic Unfolded Stage I
8	Chalk Group Basement Restored	21	Lower Jurassic Unfolded Stage II
9	Chalk Group Decompacted	22	Upper Triassic Unfolded
10	Rijnland Group Unfolded	23	Upper Triassic Decompacted
11	Rijnland Group Decompacted	24	Upper Triassic Unfolded
12	Upper Jurassic Erosion Restored	25	Initial (Salt unfolded)
13	Upper Jurassic Unfolded		

2D Structural reconstruction: EBN F10/F11



Horizon	Lithology	Age	Interval	2DMOVE Model Lithology	Decompaction Factor (km ⁻¹)
Surface		0 Ma			
North Sea Supergroup (NS)				50% Sand, 50% Shale	0.39
Chalk Group (CK)		97 Ma		100% Chalk	0.71
Rijnland Group (KN)		134 Ma		25% Sand, 50% Shale 25% Marl	0.45
Schieland Group (SL)		155 Ma		50% Sand, 50%Shale	0.39
Altena Group (AT)		212 Ma		25% Sand, 50% Shale 25% Marl	0.45
Upper Germanic Trias Group (RN)		241 Ma		25% Sand, 50% Shale 25% Marl	0.45
Middle Germanic Trias Group					
Lower Germanic Trias Group (RB)		251 Ma		70% Sand, 30%Shale	0.34
Zechstein Group (ZE)		258 Ma		100% Salt	0.0
Pre-Zechstein Basement (BSM)					0.0

Step nr.	Name	Step nr.	Name
1	Present	14	Upper Jurassic Sequences Interpreted
2	Upper North Sea Group Decompacted	15	Upper Jurassic Sequence 3 Decompacted
3	Upper North Sea Group Fault Restored	16	Upper Jurassic Sequence 2 Unfolded
4	Lower North Sea Group Unfolded	17	Upper Jurassic Sequence 2 Decompacted
5	Lower North Sea Group Basement Restored	18	Upper Jurassic Sequence 1 Unfolded
6	Lower North Sea Group Decompacted	19	Upper Jurassic Sequence 1 Decompacted
7	Chalk Group Unfolded	20	Lower Jurassic Unfolded Stage I
8	Chalk Group Basement Restored	21	Lower Jurassic Unfolded Stage II
9	Chalk Group Decompacted	22	Upper Triassic Unfolded
10	Rijnland Group Unfolded	23	Upper Triassic Decompacted
11	Rijnland Group Decompacted	24	Upper Triassic Unfolded
12	Upper Jurassic Erosion Restored	25	Initial (Salt unfolded)
13	Upper Jurassic Unfolded		

